TU Delft

Delft University of Technology

Thermal Rocket Propulsion

Version 2.10

Zandbergen, B.T.C.

Publication date
2025

Document Version
Final published version

Citation (APA)
Zandbergen, B. T. C. (2025). Thermal Rocket Propulsion: Version 2.10. (2.10 ed.) Delft University of Technology.

Important note
To cite this publication, please use the final published version (if applicable).
Please check the document version above.

Copyright
Other than for strictly personal use, it is not permitted to download, forward or distribute the text or part of it, without the consent of the author(s) and/or copyright holder(s), unless the work is under an open content license such as Creative Commons.

Takedown policy
Please contact us and provide details if you believe this document breaches copyrights.
We will remove access to the work immediately and investigate your claim.

This work is downloaded from Delft University of Technology.
For technical reasons the number of authors shown on this cover page is limited to a maximum of 10.

Course AE4S01

Thermal Rocket Propulsion (version 2.10)

17 September 2025

Faculty of Aerospace Engineering

B.T.C. Zandbergen

TU Delft Delft University of Technology

Foreword

Rocket propulsion (ae4s01) is a 7-week advanced course on rocket propulsion totalling 28 lecture hours of 45 min each. The course is offered at Delft University of Technology (TU-Delft), Faculty of Aerospace Engineering (LR), to students who have successfully followed the faculty's undergraduate program. The course has a workload of 120 hours and earns students 4 ECTS (European Credit Transfer System) points.

The course is a direct continuation of the introductory lectures on rocket propulsion given in the first year of the faculty's curriculum as part of the course "Aerospace Design and System Engineering Elements I" and in the second year as part of the course "Propulsion and power". It is considered of interest to students specializing in launch vehicle and spacecraft technology, but also to students who are interested in using rocket propulsion for aeronautical applications, like for sounding rockets, missiles, and rocket assisted take-off.

The course aims to provide students with the essential knowledge and insight needed to perform system engineering of thermal rocket systems. At the start of the lectures, the students should at least have a working knowledge of mathematics (differential equations, and statistics), thermo-dynamics of fluid flow (Poison equations, enthalpy, entropy), aerodynamics (including both sub- and supersonic and viscid and in-viscid flow), materials, structures (mostly strength and life of thin shell structures), and systems engineering.

The current document has been written to support the teachings. In this work the following topics are dealt with:

- Rocket propulsion fundamentals: A recap of rocket propulsion applications; Rocket propulsion requirements; The rocket equation; Types of rockets
- Thermal rocket propulsion fundamentals: Important performance parameters including amongst others thrust, impulse, specific impulse, volumetric specific impulse; Dimensioning and sizing rules for rocket systems.
- Ideal thermal rocket: Ideal performances, con-di nozzles, nozzle dimensions, overexpansion, underexpansion, optimum thrust, characteristic velocity and thrust coefficient, and quality factors.
- Nozzle design: Types of nozzles, nozzle profile, nozzle divergence, nozzle length, effect of nozzle profile on performance, nozzle structure and materials.
- Propellants and propellant properties: Chemical and non-chemical thermal propellants; Important properties for propellant selection.
- Chemical equilibrium calculations (introduction to program for calculation of chemical equilibrium gas composition and gas properties); Molar mass, specific heat ratio and adiabatic flame temperature calculation for gas mixtures (based on known reaction equation).Chemical equilibrium flow, frozen flow, and chemical kinetics (1/3 law of Coats, Bray approximation).
- Heat transfer: Convection, radiation and conduction,
- Cooling: Thermal insulation, ablation, radiative, film, dump and regenerative cooling; Comparison of cooling methods.
- Liquid rocket engine combustor design: Liquid injection, operating pressure, chamber pressure drop, characteristic length, chamber wall thickness estimation, chamber mass estimation.
- (Quasi) steady state internal ballistics solid and hybrid motors: Solid regression, grain shape, operating pressure, necessary condition(s) for

stable operation, pressure sensitivity for initial temperature and change in 'Klemmung', and local conditions (flow velocity, pressure, etc.).
    - Storage & distribution of liquids: Blow down & regulated systems, pressurant mass, pressurant storage, turbopumps, motor cycles, turbine drive gas mass flow.
    - Ignition: Types of igniters, igniter propellants, igniter energy and pressure, ignition duration
    - Motor controls: Thrust magnitude control, thrust vector control, expansion ratio control, mixture ratio control.

The last two topics are capita selecta for the AE4S01 course.

This document also provides for a range of problems for exercising upon. Problem answers have been collected in a separate section in this document.

Other useful literature to further the understanding of the design of thermal rocket propulsion systems include:

- "Rocket Propulsion Elements", by G.P. Sutton and O. Biblarz published by John Wiley & Sons Inc. In this book the basic principles of rocket propulsion are discussed as well as liquid rocket engines, solid rocket motors, electric propulsion, including sections on design of thrust chambers, engine structures, turbo-pumps, thrust vector control, and plume signatures, and with applications to launch vehicles, space flight, satellite flight, and missiles.
- Space Propulsion Analysis and Design, by R.W. Humble, G.N. Henry, W.J. Larson, McGraw-Hill Publishers: A really good book if you are into propulsion engineering. It is simply written but has depth for those who need the equations. It gives some good historical guidelines of what has worked in the past so that you don't stray too far. It introduces the reader to the basic thermodynamics of fluid flow and of thermo-chemical reactions and provides separate chapters on the dimensioning and sizing of solid, liquid, and hybrid rocket systems but also nuclear and electrical rocket systems. The methods presented not only allow for performance prediction, but also for preliminary sizing with respect to system mass and size.

Version 2.10 differs from the previous version in that:

- Several small data tables have been added in text to better illustrate the variations in important design/performance parameter values. Most notable changes have been made in chapters 3, 4, 6, 9, 11,14, 16, and 17.
- Some problems in the problems sections at the end of a chapter have been updated to make them clearer or have been replaced by others.
- Answers to problems posed at the end of each chapter have been added to ensure that readers without access to the TU-Delft online digital exercise environment also can check the outcome of the analysis performed.
- Errata list (version 2.09) has been worked in.
- Contents list is now visible in the contents side bar.
- Various relationships for mass estimation of solid rocket motors have been updated.
- References have been added, and others have been updated.
- Total page count has increased from 514 to 535.

Contents

Foreword		**iii**
Contents		**v**
1.	**Rocket Propulsion Fundamentals (a recap)**	**1**
2.	**Sizing Fundamentals (a recap)**	**19**
3.	**Thrust and Specific Impulse**	**31**
4.	**Ideal Thermal Rocket Motor**	**39**
5.	**Nozzle Design**	**67**
6.	**Propellants and Propellant Properties**	**97**
7.	**Thermo-Chemistry**	**113**
8.	**Heat Transfer and Cooling**	**155**
9.	**Cold gas thruster design**	**197**
10.	**LRE Combustor Design**	**217**
11.	**Solid Rocket Combustor Design**	**255**
12.	**Hybrid Rocket Combustor Design**	**287**
13.	**Mass estimation/scaling of engines and motors**	**305**
14.	**Liquid Propellant Storage**	**321**
15.	**Liquid Propellant Feeding**	**351**
16.	**Ignition**	**399**
17.	**Motor Controls**	**427**
Glossary		**453**
Answers to problems		**457**
Appendices		**467**

Rocket propulsion fundamentals

Contents

Symbols 2

1 General 3

2 Rocket equation 4

3 General steps in rocket system design (a design framework) 6

4 Rocket applications 7

5 Rocket system requirements 10

6 Important performance parameters 11

7 Types of rockets 16

8 Problems 17

References 18

Copyright notice:

The figures 3 and 4 are printed with courtesy to ESA.

Tables 1 and 2 have been taken from: Rocket propulsion Elements", by G.P. Sutton.

Symbols

Roman

A	Acceleration
C_T	Specific propellant consumption
F	Thrust
g_o	Gravitational acceleration at sea level
I	Impulse
I_{sp}	(Gravimetric) specific impulse
I_{ssp}	System specific impulse
m	Mass flow rate
M	Mass
P	Power
R	Vehicle empty-to-total mass ratio
t	Time
v	Flight velocity
w	Exhaust velocity
W	Weight

Greek

Δ	Increment or change
η	Efficiency
ρ	Propellant mass density

Subscripts

f	Refers to conditions at end of burn
j	Rocket exhaust jet or beam
p	Propellant
pros	Propulsion system
R	Rocket
T	Thrust
W	Power source

1 General

Propulsion[1] is usually associated with changing the momentum[2] of a body via a (propulsive) force, more commonly referred to as thrust, acting on this body (action = reaction) during some time. However, propulsion may also be associated with the generation of a propulsive force to counteract a disturbance force, thereby preventing any change in motion to occur. The propulsive force needed may vary in direction and/or magnitude.

In general, to generate thrust, a machine or device is needed. Such a machine or device is generally referred to as the propulsion system.

There are various ways of generating a propulsive force. Consider for instance walking, bird flight, driving, and sailing. The way we change momentum depends on the environment (land, water, air and space) we are in. For example, in case of land propulsion, we may use wheels to generate the propulsive force through friction when in direct contact with the solid earth. On the other hand, when moving over water, we may use the interaction of the wind with a sail to generate thrust.

For aerospace vehicles, an important means of propulsion is jet propulsion, which acts through the generation of a high velocity exhaust jet. Two types of jet propulsion are generally distinguished:

- The direct reaction systems and indirect reaction systems, which depend for their action on variation of the momentum of some external medium. In the case of direct reaction systems, the change in momentum of the external medium is purely obtained via energy addition to some medium, like air, ingested. Typical examples of this type of propulsion are a ramjet, and a turbojet. In the case of indirect reaction systems, the change in momentum is obtained via an engine and a propeller.
- The pure reaction systems, in which the propulsive effort or thrust is obtained by variation of the momentum of the system itself. These systems do not depend on some external medium to produce the reaction effort. Rockets are systems of this type.

In rocket systems, the propulsive force (thrust) is generated by expelling mass (initially stored in the vehicle) from the vehicle at a high velocity. It differs from other engines in that it carries the mass to be expelled internally, therefore it will work in the vacuum of space as well as within the Earth's atmosphere.

To clarify the difference between direct and pure reaction systems further, an overview of important characteristics is presented in Table 1. The overview shows that rockets offer a much higher thrust-to-weight (T/W) ratio. This allows installing the same thrust but at lower mass consequences for the total vehicle, which in turn allows for higher acceleration rates. Given the difference in T/W of almost a factor 25, this would allow for up to 25 times higher acceleration rates. Another advantage is an increased thrust density, i.e. thrust per unit of frontal area of the engine. The difference of about a factor 3 in thrust density would allow for the same thrust, but with a strongly reduced frontal area (also a factor 3), thereby limiting the vehicle drag. A third and very important advantage for space applications is that, because the rocket takes the mass to be expelled within, it can also operate in the vacuum of space or at very high altitude. A fourth advantage is that the thrust is independent of altitude, flight velocity and air temperature, whereas for jet propulsion, the thrust strongly depends on altitude, flight velocity and air temperature. A fifth advantage is that the flight velocity can be much greater than the velocity of the jet exhaust. In contrast, the flight velocity attained with turbojets is limited to maximum 1-1.5 km/s. A major disadvantage of rocket propulsion compared to jet propulsion is the high specific fuel (or

[1] The word propulsion is derived from two Latin words: ‘pro’ meaning before or forwards and ‘pellere’ meaning to drive. Its meaning is to push forward or drive an object forward.

[2] The (linear) momentum of a body is defined as the product of its mass times its velocity. It basically relates to linear motion. Analogous we have angular momentum as a measure for rotational motion. The angular momentum of a rigid object is defined as the product of the moment of inertia and the angular velocity.

rather propellant[3]) consumption leading to a large propellant mass to be carried on board of the vehicle. The main reason for this is that the rocket has to carry both the fuel and the oxidizer, needed to burn the fuel, on board of the vehicle. For air-breathing jet propulsion, the oxidizer is taken from the surrounding air.

Table 1: Rocket advantages over turbojet propulsion

Feature	Rocket engine or rocket motor	Turbojet engine
T/W, typical	75:1	5:1
Specific fuel/propellant consumption	0,8-1,4 kg/(Nhr)	0,05-0,15 kg/(Nhr)
Thrust density	375000 N/m^2	125000 N/m^2
Thrust versus altitude	Nearly constant	Decreases with increasing altitude
Thrust versus flight velocity	Nearly constant	Decreases with increasing flight velocity
Thrust versus air temperature	Constant	Decreases with increasing air temperature
Flight velocity versus exhaust velocity	Unrelated; flight velocity can be greater	Flight velocity always less than exhaust velocity
Altitude limitation	None; suited to space travel	14-17 km

Adapted from: Rocket Propulsion Elements

2 Rocket equation

A change in momentum ΔI of a body can be determined from:

$$\Delta I = \int d(M \cdot v) \tag{2-1}$$

- M: body mass
- v: velocity of body.

Vice versa, we can use the above relationship to determine the change in momentum needed to accomplish a certain velocity change.

In case mass is constant, we obtain:

$$I = M \cdot \Delta v \tag{2-2}$$

The change in momentum is accomplished by an external force F (not necessarily constant) which operates on the vehicle for a certain time t_a.(action time):

$$\int_0^{t_a} F \cdot dt = \int d(M \cdot v) \tag{2-3}$$

In case of a non-constant system mass, analysis leads to the 'rocket equation' also referred to as 'Tsiolkovsky equation', which trades exhaust velocity against rocket mass fraction or rocket mass.

To derive the rocket equation, we consider a rocket with an instantaneous mass M traveling at an instantaneous velocity v and expelling mass ΔM at a constant velocity w relative to the vehicle, see Figure 1. Assume no external forces (gravity, drag, etc.) are acting up on the vehicle.

[3] A chemical rocket propellant generally consists of a fuel and an oxidizer.

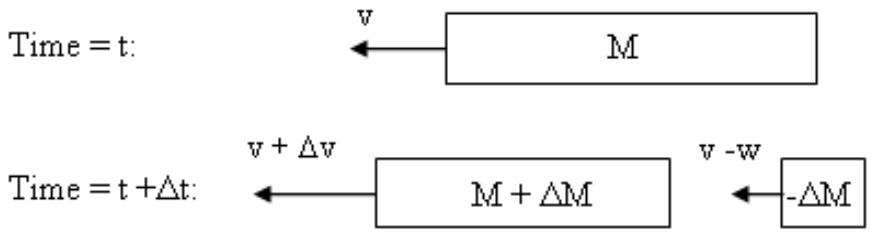

Figure 1: Rocket propulsion principle

Momentum at time t is:

$$I_t = M \cdot v \tag{2-4}$$

Idem at time t + Δt:

$$I_{t+\Delta t} = (M + \Delta M) \cdot (v + \Delta v) - \Delta M \cdot (v - w) \tag{2-5}$$

Since there are no external forces working upon the rocket, it follows that the change in momentum is equal to zero.

It follows for the momentum balance:

$$M \cdot v = (M + \Delta M) \cdot (v + \Delta v) - \Delta M \cdot (v - w) \tag{2-6}$$

Elaboration gives (neglecting terms of second order small):

$$M \cdot \Delta v + \Delta M \cdot w = 0 \tag{2-7}$$

For an infinitesimal change in velocity, we get:

$$M \cdot dv = -dM \cdot w \tag{2-8}$$

Separation of variables and integrating both sides leads to the rocket equation:

$$\Delta v = w \ln(M_o/M)$$

$$(\Delta v)_e = w \ln(R) \tag{2-9}$$

With:

- M_o = initial mass
- M = instantaneous mass
- Δv = Velocity change (follows from orbit analysis)
- R = M_o/M_f; M_f = final vehicle mass. It includes payload mass, structure subsystem mass, propulsion subsystem mass as well as the mass of all the other subsystems and the mass of propellants remaining in the vehicle. In practice, empty mass differs from dry mass in that empty mass also includes residual propellant mass (if any).

From this equation, we learn that to achieve certain change in flight velocity using rocket propulsion, it is best to expel the mass at the highest velocity possible. This way the empty mass and initial mass are closest, hence limiting the amount of mass to be expelled overboard. This is illustrated in Figure 2.

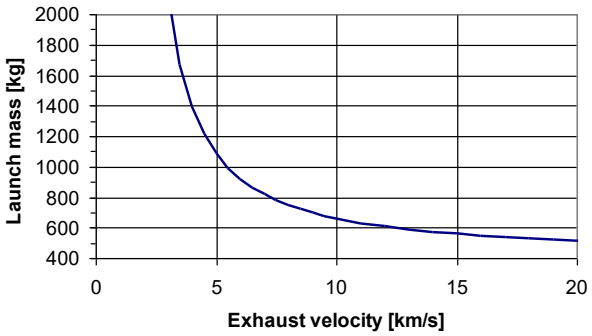

Figure 2: Results from rocket equation for vehicle with empty mass of 400 kg and mission characteristic velocity of 5000 m/s

It is noted though that in the above presented result, we have assumed that we can select the exhaust velocity without any consequence for the mass of the rocket system and hence for the vehicle carrying the rocket whatsoever. It will later be shown that this is not the case.

3 A design framework

From earlier designs, it follows that the design of any system, and hence also the design of a thermal rocket system, usually goes through several design steps. In this work we will distinguish 7 steps, which we will refer to as the basic steps of design or the design framework. In this section, these 7 steps will be introduced and shortly explained.

1. Define the problem/need of the system to be designed. In this step we consider the function(s) that need to be fulfilled by the system to be designed. For a propulsion system this would mean to produce thrust over a certain period as well as establishing the needs for thrust control (magnitude and/or direction).

2. Establish requirements[4]: This step is about establishing or defining the singular needs to be fulfilled both in terms of functional performance. In addition, as it is important that a function is performed in a sustainable way also other requirements are defined that allow ensuring a sustainable way. Such requirements may relate to mass, size, life (not necessarily identical to operation time), cost, reliability, maintainability, safety, etc.

3. Set up design options: In this step, design options are generated. Both historical options as well as break-through (innovative) options may be considered.

4. Analyse the design options: In this step design models are used to determine how well the design fulfils the requirements, i.e. its performances. The design models generally used are models that allow for investigating the effect of the various design options on the functional performances as well as other performance parameters, like mass, size, life, cost, reliability, maintainability, safety, etc. Depending on the design phase, such models may vary from very simple and user-friendly to highly sophisticated and complex models.

5. Compare the design options: This generally means that the design options are compared to each other in terms of how well they satisfy the requirements.

6. Make choice: A ranking of the design options is made and the 'best' concept(s) are considered for the next phase of development. Unfeasible options, i.e. options that do not fulfil the requirements are in principle discarded. Sometimes

[4] A requirement is a singular documented need (functional, physical) that a product (or process) needs to satisfy.

more than 1 option is retained. Also, successful elements of other options may be selected for inclusion in the best concepts.

7. Evaluate and/or Iterate. In this final step, the outcome is evaluated and if necessary, more detailed design with more detailed design analysis is specified.

Note that the first letters of the 7 steps make up the acronym DESACME that helps to remember these essential steps.

4 Rocket applications

Practical uses of rocket systems as weapons of war, commerce and the peaceful exploration of space are discussed to provide insight in the important propulsive performances needed to allow a vehicle or other system to function properly.

An important category of application of rocket systems is to propel space launch vehicles, where we require high flight velocities (more than 7.8 km/s), operation at high flight altitudes well above 14-17 km and high thrust levels to overcome gravity. Important tasks are to provide propulsion for accelerated flight (ascent flight), re-entry flight (braking), and flight sustenance, but also for attitude control as well as for stage separation and propellant settling.

For illustration, the European Ariane 5 space rocket launch vehicle can lift a payload of about 40 ton into a low Earth orbit or 6.8 ton payload into geostationary transfer orbit. To do so, the launcher has 3 stages; a large core stage (main stage) with attached to it two booster rockets and a smaller core stage on top of the main one. The two large booster rockets assist the core stage during the initial launch phase, which takes about 130 s. After burn-out of the two boosters, they are separated from the main core stage, which continues the ascent flight. After burn-out of the main core stage after about 590 s in flight, this stage is separated, and the second core stage takes over bringing the payload to its intended launch orbit. Total vehicle mass at lift-off is about 746 ton of which 642 ton is propellant. The main stage is powered by a single rocket engine, which provides for thrust, and yaw and pitch control. This engine produces 1145 kN of vacuum thrust and has a nominal burn time of 590 s. Total stage mass is ~170 tons and maximum propellant mass is ~155 tons (130 tons oxidizer and 25 tons fuel). Stage length and diameter are 29 m and 5.4 m, respectively.

Figure 3: Ariane 5 launch vehicle (Courtesy ESA/ESTEC)

The large booster rockets each provide thrust for about 130 s. During this time each booster provides a total impulse of 4.6×10^8 Ns. Thrust at lift-off is 5.5 MN, which reduces to about 4.0 MN at 35-55s to minimize aerodynamic loads. Maximum thrust is ~6 MN. The thrust tails off after 75 s to limit maximum launcher acceleration down to 3.5 g_o. The 2nd core stage is propelled by a single rocket engine (Aestus) producing 27.5 kN of thrust. Total propellant mass is 9. 7 tons stored in 4 propellant tanks. The EPS stage is spin stabilised. Its attitude control system consists of six thrusters that deliver a thrust of 400 N each. Of these 6 thrusters two are used for spin-up and two for spin-down. The remaining two are to allow tilting the spin axis.

A second important category is for spacecraft applications, where we require propulsion for orbit transfer, orbit acquisition / trim, repositioning, de-orbit, plane changes, etc. This requires not only high flight velocities (of the order of several km/s), but also to achieve this

high flight velocity in a vacuum environment. In addition, spacecraft may use rocket propulsion for:

- Orbit stabilisation or “station keeping” to compensate for disturbing forces like drag, solar wind, etc.
- Attitude control to perform 3-axis or spin stabilisation, to change the attitude of the S/C or to compensate for disturbing torques e.g. precession of spin axis
- Other: Spin-up/down, discharging/unloading of reaction or momentum wheels (typically every few days), stage separation, propellant settling to compact the bubbling propellant inside the tank, etc.

The next figure shows some features of a rocket propulsion system on a specific spacecraft.

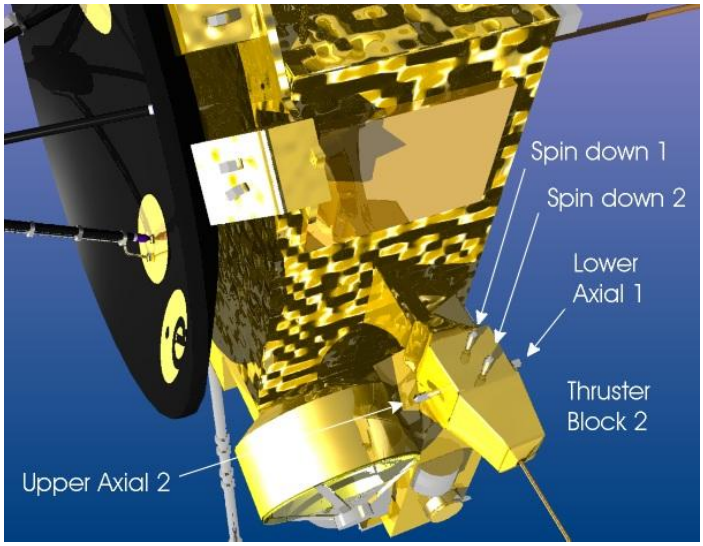

Figure 4: Ulysses rocket system features (courtesy ESA/ESTEC)

The system includes eight rocket motors that provide spin control and axial and radial delta v control. In addition, it includes a propellant storage tank and the pipes and valves necessary to regulate propellant flow from the tank to the thrusters. Instrumentation includes pressure transducers and temperature sensors. The tank is a titanium alloy shell containing hydrazine and nitrogen pressure gas separated by a membrane. Total tank volume is about 45 liters. Filters are included to filter the propellant flowing to the thruster blocks.

A third important category of application is to propel rocket weapons, like missiles and anti-tank weapons. The main purpose of using rocket propulsion in these systems is to attain high flight velocities in a very short time. For this it has to deliver a high thrust to reaching the high flight velocity quickly. Once at speed, thrust may be reduced greatly thereby allowing to maintain the high velocity (by compensating for drag) or even to allow for a reduction in flight speed (due to air drag and/or gravity).

Other rocket applications can be found in:

- Sounding rockets
- Amateur rockets
- Ejection seats
- Rocket assisted take off (JATO or Jet Assisted Take Off): Actually, a rocket that is used to give heavy military transport planes an extra "push" for taking off from short airfields.
- Race cars: The world's first rocket car, the RAK2 was unveiled in 1928 by Opel. On May 23, 1928, the RAK2 was unveiled to a crowd of 3,000 people in Berlin, Germany. The car * without an engine or gears * was powered by 24 rockets and 120 kilograms of explosives. Driven by Fritz von Opel, the grandson of Opel founder Adam Opel, the crowd watched the car reach a high speed of 230 kilometres per

hour in two kilometres. Rocket powered quarter mile race cars were the fastest type of racetrack vehicle ever built. Those cars had so much 'direct thrust' power that they could beat any conventional or jet powered racer from point A to point B, known as elapsed time. The miles per hour shown at the end of a run are interesting, but inconsequential. However, a car called 'VANISHING POINT' was reputed to have been driven at well over 640 kmph (400 mph) in the quarter mile.

- Gas-generators: Micro gas generators are used as air-bag inflators. Other generators can be used to drive or start up a gas turbine

All rocket propelled vehicles are equipped with one or more rockets (referred to as primary propulsion system) that allow(s) for adjusting the linear momentum. Some vehicles also have rockets (referred to as secondary propulsion system) that allow for 3-axis or spin stabilisation. The table 2 provides an overview of typical characteristics for a number of primary and secondary propulsion applications.

Table 2: Characteristics of some rocket propulsion applications (adapted from [Sutton])

Application	Thrust Profile	Typical Duration	Maximum Acceleration
Large space launch vehicle booster	Nearly constant thrust	2-8 min	2-6 g
Antiaircraft or antimissile missile	High thrust boost, decreasing thrust sustain phase	2-75 sec each	Up to 100 g
Spacecraft orbit maneuvers	Restartable	Up to 10 min cumulative duration	0,2-6 g
Air launched guided missile	High thrust boost phase with low thrust or decreasing thrust for sustain phase	Boost: 2-5 sec Sustain: 10-30 sec	Up to 25 g
Variable range military ballistic missile - surface launched	Same as above	Up to 2 min each stage	Up to 10 g
Spacecraft attitude control - large vehicles	Many restarts (up to 60.000)	Up to 1 hr cumulative duration	Less than 0,1 g
Spacecraft attitude control - small vehicles	Same as above	Up to 20 min	Same as above
Reusable main engines for space shuttle	Variable thrust, many flights with same engine	8 min, over 7 hr cumulative	Up to 4 g
Lunar landing	10:1 thrust variation	4 min	Several g
Weather sounding rocket	Single burn period - often decreasing thrust	5-50 sec	Up to 15 g
Antitank	Single burn period	0,2-3 sec	Up to 20 g

Besides providing for the necessary thrust, these systems also bring some side effects. For example, for Ariane 5, the propulsion system:

- Increases mass: To bring about 7 ton of payload into orbit, we require a giant rocket. Ariane 5 consists for about 80% of propellant (642 ton out of a total of 746 ton) and a structure to contain the propellant and to resist the launch loads.
- Increases size (volume): To store 642 ton of propellant requires a large volume. For instance, to store 642 ton of water requires 642 m^3 which comes down to a cylinder of length 50 m and diameter 4 m. For the Ariane 5 using liquid hydrogen and liquid oxygen, the density of the propellant is about 4 times lower than for water, so the effect is even more prominent.
- Increases cost: Ariane 5 propulsion system makes up about 50-70% of total launch cost. The latter stands at about 120 million Euros.
- Decreases reliability: 59% of all launch failures are caused by the propulsion system.
- Effects schedule: Initial development of Ariane 5 started in 1984 with actual development starting in 1987. First flight took place in 2000.
- Effects operations: To launch Ariane 5, a launch base is required in a remote place (Kourou). Launch preparations take about 1 month including preparing and mating of the various launcher stages and the payload in special buildings and the transfer to

the actual launch site on a big crawler, where the launcher is fuelled up, ready for count down.
- Etc.

For spacecraft we typically find that about 30% of spacecraft mass, 17% of all on-orbit spacecraft failures, and 5-8% of spacecraft cost are due to the propulsion subsystem.

5 Rocket system requirements

Each of the applications mentioned in the previous section requires different performances of the rocket system. Typical requirements stemming from the various applications include requirements which define 'how well' the propulsive tasks must be performed, i.e. the propulsive requirements. These are typically specified in terms of:

- Number and type of maneuvers. Typical maneuvers include boost, flight sustenance, trajectory/orbit correction (e.g. drag compensation), slew, 3-axis control, spin control, etc.
- Size of maneuvers for spacecraft, typically given in required velocity change or Δv: For typical values of Δv for several space propulsion tasks, see propulsion web site or [Fortescue and Stark].
- Acceleration level (if needed as a function of time): Acceleration generally is bound to minimum and maximum values:
  - Minimum acceleration is required e.g. to compensate for disturbing forces (e.g. gravity, solar radiation, atmospheric drag), limit gravitational losses (see section on "Launch vehicle trajectories"), and to limit flight duration. Typical minimum values for launchers are 1.2 – 1.3 g_o. For satellites using an impulsive shot approach, the thrust duration shall not exceed about 3% of the flight duration. For example, the typical duration of a LEO-GEO Hohman transfer orbit is about 5½ hour. This then limits the thrust duration at perigee to maximum about 10 minutes for a velocity change of the order of 2.46 km/s. For a 1000 kg satellite, this requires a minimum acceleration of 4.1 m/s^2. Minimum value is needed to allow reaching the final vehicle velocity within a limited time;
  - Maximum acceleration is of importance e.g. to limit structural mass, to limit the loads on the crew of a manned vehicle and for micro-gravitation research. Typical maximum accelerations are:
    - Launchers: 4-6 g_o.
    - Sounding rockets: up to 15 g_o.
    - Micro-gravitation research: 10^{-4} - 10^{-5} g_o.

  From acceleration levels, we typically derive requirements concerning thrust magnitude. These requirements may be different for different flight phases (boost phase, sustain phase).
- Minimum impulse bits, i.e. smallest change in momentum required to allow for e.g. fine attitude and orbit control of spacecraft.
- Cycle life, i.e. a number representing the number of on/off cycles or re-ignitions that the system must be capable of.
- Pulse duty cycle: Duration of a pulse versus time in between two pulses. This parameter is usually expressed as a percentage (%).
- Etc.

To fulfill the propulsive requirements should be the goal of any propulsion system to be designed. However, when doing so, it is also important that we do this at the lowest possible "expense", i.e. to allow for a sustainable design. This generally leads to a whole range of other requirements, which may include requirements w.r.t.:

- Mass. It is obvious that the mass of the rocket system shall be as low as possible as in that case the payload mass is maximized.
- Size. The payload envelope of the launcher selected dictates the size of the spacecraft. Hence, it also restricts the size of the rocket system. A small rocket system may allow selecting a smaller and hence cheaper launch vehicle.
- Electrical power usage. The more power a rocket system uses the more power is needed from the power supply system. This then increases the mass and the size of this vehicle subsystem.

- Configuration requirements that concern e.g. the mounting of the thruster. For example, to provide full 3-axis control, we need to be able to produce a torque about each of the 3 (perpendicular) axes. This may require different thrusters to stop/start the rotational motion. Other configuration requirements may concern the mounting of the thrusters. For example, it may be required that the thruster is canted to direct the hot exhaust away from the spacecraft.
- Storage life and operational life. Launcher missions are typically short duration missions that do not require long operation times (a few minutes). Deep space missions on the other hand may require long operation times of several hours just to prevent too high acceleration loads. Since deep space missions take several years to accomplish, storage life for rocket systems may also be of the order of years.
- Reliability or the probability that a system functions successfully over a specific time.
- Safety (hazardousness): Common hazards that should be safeguarded against are corrosion, fire, and explosion/detonation: Class 1.1 is catastrophic failure which evidences detonation, and class 1.3 is catastrophic failure which evidences fire and explosion, not detonation), and health hazards (toxicity of propellants).
- Working environment: On ground, in space or other.
- Still other, like constraints with respect to cost, structural loads, thrust misalignment; thrust off-set, thrust magnitude accuracy, development time, environmental load, maximum/minimum operation/storage temperature, etc.

The next table gives some specific requirements as used to initiate the design of the Ariane 5 booster rockets.

Table 3: Ariane 5 booster rocket requirements (IAF-85-173)

Parameter	Value
Total impulse capability	4.6×10^8 Ns
Thrust	Lift-off thrust 5.5 MN. Reduced thrust of about 4.0 MN at 35-55s to minimize aerodynamic loads. Thrust tail-off after 75 s to limit maximum acceleration to 3.5 g.
TVC capability	Yes, to limit the effects of thrust imbalance
Reliability	High (man-rated mission)
Cost	Low recurrent (manufacturing/production) cost
Transportability	Segmented design to allow transportation from Europe to Kourou
Length	Limited to allow attachment to core stage
Number of missions	1

6 Important performance parameters

In this section, several important performance parameters used in the foregoing and later chapters will be defined and shortly discussed.

6.1 Rocket thrust

An important parameter is the thrust delivered, as it determines the acceleration that can be achieved.

From the momentum balance eq. (2-6) an expression can be obtained for rocket thrust. Dividing the momentum balance by Δt and taking the limit for $\Delta t \to 0$ gives:

$$\lim_{\Delta t \to 0} M \cdot \frac{\Delta v}{\Delta t} + \frac{\Delta M}{\Delta t} \cdot w = M \cdot \frac{dv}{dt} - m \cdot w = 0 \tag{6-1}$$

Here m is mass flow rate (m = -dM/dt).

Rewriting the equation (6-1) gives:

$$M \cdot \frac{dv}{dt} = m \cdot w \tag{6-2}$$

This equation resembles the classical 2nd law of Newton:

$$M \cdot \frac{dv}{dt} = F \tag{6-3}$$

With:

$$F = m \cdot w \tag{6-4}$$

We now refer to the force F as the thrust force (hereafter shortly referred to as *thrust*). It is defined as the product of mass flow rate m and exhaust velocity w (relative to the vehicle).

Some missions require that the thrust is controllable for example to allow reducing acceleration loads towards the end of the flight, when the propellant tanks are almost empty. Good measures for thrust control capability of a rocket system are:

- Throttling capability or Thrust Magnitude Control (TMC): The capability to control/change the thrust of an individual rocket motor given as a 'percentage' (%) of nominal thrust. For example, a throttling capability of 50% means that the thrust can be reduced to 50% of its nominal value.
- Thrust Vector Control (TVC): The capability to change the thrust direction for an individual rocket motor expressed in 'degrees' (deg). Three rotation directions can be distinguished usually taken relative to the nominal position of a suitable body axis system. The rotations are 1 about the nozzle axis (roll direction), 1 up and down (pitch direction), and 1 left and right (yaw direction).

6.2 Specific propellant consumption

As for jet engines, it may be wise to consider the propellant consumption per unit of thrust produced. This is usually referred to as specific propellant consumption. However, since mass flow may change during the mission, it is better to use some average specific propellant consumption (C_T) defined as the ratio of propellant mass consumed and total impulse delivered:

$$C_T = \frac{M_p}{\int_o^{t_a} F \cdot dt} \tag{6-5}$$

It is typically expressed in kg/Nhr (see e.g. Table 1 in 'Rocket Propulsion Fundamentals'). For constant mass flow, it follows:

$$C_T = \frac{M_p}{\int_o^{t_a} F \cdot dt} = \frac{1}{w} \tag{6-6}$$

Hence to reduce specific propellant consumption, we should strive for high exhaust velocity.

6.3 Action time

Once we know the total impulse to be delivered by a rocket system and the thrust, the action time of the system can be determined from:

$$\int_0^{t_a} F \cdot dt = \int d(M \cdot v) \tag{6-7}$$

In case of a constant thrust and (expellant/propellant) mass flow rate, it follows:

$$t_a = M_p \Big/ m \tag{6-8}$$

With M_p is total expellant/propellant mass (from eq. (2-9)):

$$M_p = M_e \cdot \left(e^{(\Delta v / w)} - 1\right) = M_o \cdot \left(1 - e^{-(\Delta v / w)}\right) \tag{6-9}$$

So propellant mass and action time can be determined when either initial or empty mass of the vehicle is known.

In case of a constant acceleration (a), operation time can simply be determined from:

$$t_a = \Delta v \Big/ a \tag{6-10}$$

6.4 Total impulse

By exerting a thrust on an object (spacecraft, missile, etc.) a rocket system causes the object to change its momentum. The longer the rocket system thrusts, the larger the change in momentum of the body accomplished. The product of force and the period over which the force is applied is referred to as the impulse (I):

$$I = \int_0^{t_a} F \cdot dt = \int_0^{t_a} m \cdot w \cdot dt \tag{6-11}$$

For constant exhaust velocity, it follows:

$$I = w \cdot \int_0^{t_a} m \cdot dt \tag{6-12}$$

In case the action time is taken to be sum of all time periods that the rocket is active, we find for the total impulse delivered by the rocket propulsion system:

$$I_{tot} = F \cdot t_a = M_p \cdot w \tag{6-13}$$

Hence, the *total impulse* (I_{tot}) or total change in momentum that can be accomplished by a rocket system follows from propellant mass and exhaust velocity.

To increase the total impulse delivered by a rocket propulsion system, we must either increase the thrust or the action time. From eq. (6-13) it than follows that either the propellant mass (M_p) or the velocity (w) at which this mass is expelled must increase.

6.5 System (gravimetric) specific impulse

The best propulsion system is generally that system which delivers the requested total impulse for the lowest propulsion system mass. An important (not much used) measure of the quality of the propulsion system is the system specific impulse defined as the impulse delivered per unit propulsion system weight:

$$I_{ssp} = \frac{I}{W_{ps}} = \frac{I}{M_{ps} \cdot g_o} \tag{6-14}$$

With:

- M_{ps}: propulsion system mass which includes both the mass of the propulsion hardware and the propellant mass.
- W_{ps}: propulsion system weight.
- g_o: gravitational acceleration at sea level.

System specific impulse is typically expressed in seconds[5]; The higher the system specific impulse, the better the performance of the system. Note that if we use the system specific impulse to select the best propulsion system, we assume that changing the propulsion system has a negligible effect on vehicle mass.

6.6 Propellant (gravimetric) specific impulse

Another, much more used[6], performance parameter is the *specific impulse*. It is a measure of how much impulse is produced divided by the (propellant) weight that the rocket spends:

$$I_{sp} = \frac{I}{W_p} = \frac{\int_0^{t_a} F \cdot dt}{g_o \cdot \int_0^{t_a} m \cdot dt} \tag{6-15}$$

The higher the specific impulse, typically expressed in seconds, the less mass needs to be expelled to produce a given amount of thrust, so the less massive the rocket must be. Again, we note that some rocket scientists divide by mass instead by weight thereby expressing specific impulse in meters/second rather than in seconds.

At constant mass flow and exhaust velocity, we find:

$$I_{sp} = \frac{\int_0^{t_a} F \cdot dt}{g_o \cdot \int_0^{t_a} m \cdot dt} = \frac{m \cdot w \cdot t_a}{m \cdot t_a \cdot g_o} = \frac{w}{g_o} \tag{6-16}$$

This shows that to maximize the specific impulse, we should strive for maximum exhaust velocity. This is the same result as follows from the rocket equation. It differs from the system specific impulse in that the effect of a change in propulsion system dry mass (total system mass minus propellant mass) is neglected.

---

[5] Some rocket scientists define the specific impulse as total impulse divided by mass (not weight). In that case, specific impulse is expressed in meters/second.

[6] Specific impulse is much more used than system specific impulse, because most rocket systems used today are chemical rockets. Characteristic for chemical rockets is that propellant mass forms most of the system mass. In addition, we find that differences in dry mass for the various chemical systems exist, but in most cases are not significant.

Comparing eq. (6-6) and (6-16), we find that the specific impulse is identical to the reciprocal value of the average specific propellant consumption (C_T):

$$I_{sp} = \frac{1}{C_T \cdot g_o} \tag{6-17}$$

This shows that maximizing specific impulse is identical to minimizing the specific propellant consumption.

6.7 Volumetric specific impulse

A good measure for the size of a rocket system is the *volumetric specific impulse* (I_ρ). It is defined as the total impulse delivered per unit of propellant volume:

$$I_\rho = \frac{F \cdot t}{V_p \cdot g_o} = \rho \cdot I_{sp} \tag{6-18}$$

The higher I_ρ, the smaller the propellant storage and hence the spacecraft; High volumetric specific impulse requires high specific impulse and a dense propellant. Nowadays, the volumetric specific impulse is not used very often. Rather one uses simply propellant density.

6.8 Input power, jet power and energy

The power contained in the jet of a rocket motor is referred to as jet power. It sometimes is also referred to as beam power or thrust power (ESA). *Jet power* (P_J) is defined as the kinetic power in the jet. It is related to rocket thrust and exhaust velocity by an expression of the form:

$$P_J = 1/2 \cdot F \cdot w = 1/2 \cdot m \cdot w^2 \tag{6-19}$$

Rockets require high power. For example, a rocket with a thrust of 100 N and an exhaust velocity of 3000 m/s already has a beam power of 150 kW.

The efficiency with which the thruster converts input power into jet power is indicated by the *thrust efficiency* (η_T). It is defined as the total jet power divided by the total power provided by the power source (P_W):

$$\eta_T = \frac{P_J}{P_W} \tag{6-20}$$

The higher the thrust efficiency, the less power is needed by the propulsion system to produce a certain jet power. This parameter is of special interest when designing rocket systems with a separate power system, like an electrical or nuclear power system, providing the power needed to propel the spacecraft.

Taking thrust and exhaust velocity constant in time (constant mass flow), it follows for the total amount of energy required:

$$E = \frac{1/2 \cdot F \cdot t_a \cdot w}{\eta} = \frac{1/2 \cdot M_p \cdot w^2}{\eta} \tag{6-21}$$

The mechanical power provided by the rocket is given by:

$$P_{mech} = F \cdot v = m \cdot w \cdot v \tag{6-22}$$

Here v is the rocket's (instantaneous) flight velocity. Notice that the mechanical power provided increases with flight velocity.

The power provided by the rocket should be transferred into mechanical power. A measure of how efficient this occurs is given by the rocket efficiency. It can be calculated from:

$$\eta_R = \frac{F \cdot v}{\frac{1}{2} \cdot m \cdot (v - w)^2 + F \cdot v} \tag{6-23}$$

Here the term (v-w) gives the absolute velocity with which the jet is exhausted. So the first term in the denominator is the absolute kinetic power in the exhaust jet. It can be shown that the rocket efficiency has a maximum value when flight velocity equals the relative jet velocity. It can also be shown that even at high flight velocity (much higher than the (relative) jet velocity) efficiency remains in excess of 0% (unlike for e.g. air-breathing jet engines).

6.9 Pulse related parameters

The final performance parameters introduced here all relate to the pulse characteristics (on/off switching) of a rocket system. We mention:

- Impulse bit: Change in momentum per pulse.
- Minimum impulse bit: Smallest achievable impulse bit.
- Duty cycle: Nominal (single) burn time of a motor expressed in 'second' (s).
- Cycle life: Number representing the number of on/off cycles that a pulsed thruster can operate.
- Pulse duty cycle: Duration of a pulse versus time in between two pulses expressed as a 'percentage' (%).
- Thrust rise time: Time it takes for the system to go from zero thrust to full thrust.
- Thrust tail off time: Time it takes for the system to go from full thrust to zero thrust.

7 Types of rockets

Various types of rocket systems are distinguished based on how the expelled mass is accelerated to a high velocity:

a) Thermal acceleration, in which the enthalpy of the expellant is increased and converted into a high velocity jet via a nozzle.
b) Electro-static acceleration, in which thrust is derived from the direct acceleration of positively, charged propellant ions or colloids by an electric field.
c) Electro-dynamic acceleration, in which crossed electric and magnetic fields induce a Lorentz force in plasma.

The various methods lead to differences in attainable exhaust velocity and thrust levels, see tables 4 and 5 taken in part from [Fortescue and Stark, 2003]:

Table 4: Typical attainable exhaust velocities

Propulsion type	Exhaust velocity (km/s)
Thermal	1 – 20
Electro-static	5 – 100
Electro-dynamic	5 – 100

Table 5: Typical attainable thrust levels

Propulsion type	Thrust acceleration (g_o)
Thermal	0.1-10
Electro-static and electro-dynamic	10^{-3}-10^{-5}

From these tables, we learn that thermal acceleration allows for limited exhaust velocity, but also for high thrust levels. In contrast, electro-static and electro-dynamic acceleration allows for high exhaust velocity but limited thrust levels. Furthermore, the electro-static and electro-dynamic devices are much more complex to engineer than thermal systems. It is because of the relative simplicity of thermal rockets, and their high thrust levels that thermal rockets are the main type of rocket system in use for both space and earth applications including space launcher applications. Over time, it is expected that slowly electro-static and electro-dynamic devices will take over some space applications now performed by thermal systems. We mention drag compensation, and ultra-fine attitude control, but also deep space travel.

8 Problems

1) Which of the following statements are correct?

- Mission characteristic velocity is independent of the thrust with which the mission is conducted
- A high specific impulse means a high rocket exhaust velocity
- Propulsion means to push forward or drive an object forward
- A high specific impulse is good for limiting the on-board propellant mass
- For space propulsion we always need to expel mass initially stored on board the spacecraft
- The amount of propellant that needs to be stored on board a spacecraft is independent of the chosen thrust level

2) A (perigee) kick stage is being designed to boost a satellite from LEO to GEO with a maximum acceleration of $1g_o$. The ΔV is 1.83 km/s. You have selected for this kick stage a rocket system capable of expelling mass at a velocity w of 3000 m/s. The empty mass of the stage including payload is 1000 kg. What mass of propellant (M_p) should be loaded into this stage? Determine also maximum achievable thrust (F_{max}), minimum operation time (t_{min}) and total impulse (I_{tot}). You should consider both constant and variable thrust operation.

3) Same question as in problem 2, but now in case the mass is expelled at a constant velocity of 8,000 m/s.

4) From literature, we learn that the Ariane 5 main stage has a flight operation time of 600 s. It is estimated that during this time the stage produces a (flight) average thrust of 1000 kN with a (flight) average specific impulse of 400 s. Stage dry mass is 12000 kg. You are asked to determine for this system: exhaust velocity (w), jet power (P_j), total impulse (I), propellant mass flow rate (m) and total mass (M_p) and volume (V_p) of the propellant carried on board of the Ariane 5 main stage as well as stage thrust-to-weight (T/W) ratio at take-off, stage dry mass to total stage mass ratio (α) and system specific impulse (I_{ssp}). For propellant density, you may use a value of 333 kg/m^3.

5) According to [Humble], the following characteristics apply to the USA developed Nerva 2 thermo-nuclear rocket engine:

- Thrust: 334.061 kN
- Specific impulse: 825 s
- Burn time: 1200 s
- Thermal input power: 1570 MW
- Engine mass: 10138 kg

Calculate for this engine:

a) Jet power.
b) total impulse.
c) propellant mass flow rate.
d) thrust efficiency.
e) engine thrust-to-weight ratio (assume Earth Sea-level conditions).

6) In case we replace the single HM60 engine of the Ariane 5 cryogenic main stage introduced in problem 4 by 3 Nerva 2 engines as defined in problem 5, and given that the velocity increment delivered by the stage remains constant, and that only engine mass (not storage mass) and propellant mass are affected, calculate:

a) New total propellant mass to be carried on board of the main stage

b) Propellant volume in case the density of the liquid hydrogen is 70 kg/m^3.

References

1) Fortescue P, and Stark J., Spacecraft systems engineering, 3rd edition, Chapter 6.1, Chapter 6.2 (introductory part only), and Chapter 6.4 (introductory part and section 6.4.2).

2) Sutton G.P., Rocket Propulsion Elements, 7th edition, John Wiley & Sons Inc., 2007.

3) Timnat Y.M., and van der Laan F.H., Chemical Rocket Propulsion, Delft University of Technology, Delft, The Netherlands, 1985.

4) IAF-85-173, 1985.

5) Humble R.W., Henry G.N., and Larson W.J., Space Propulsion Analysis and Design, revised edition, ISBN 0-07-031320-2, McGraw-Hill, 1995.

System sizing fundamentals

Contents

Symbols 20

1 General lay-out of rocket systems and classification 21

2 Design analysis framework of rocket propulsions systems 22

3 Rocket system mass breakdown (some definitions) 22

4 Sizing fundamentals (a first analysis) 23

5 Rocket staging 28

6 Problems 29

Literature 30

Symbols

Roman

g_o	Gravitational acceleration at sea level
I	Impulse
I_{sp}	(Gravimetric) specific impulse
I_{ssp}	System specific impulse
I_{tot}	Total impulse
m	Mass flow
M	Mass
P	Power
t	Time
v	Flight velocity
V	Volume
w	Exhaust velocity

Greek

α	Mass fraction
$1/\alpha_W$	Specific power
Δ	Increment or change
$1/\varepsilon$	Specific energy
η	Thrust efficiency
ρ	Propellant mass density

Subscripts

dry	Refers to rocket system excluding propellants
f	Refers to conditions at end of burn
F	Feed system
in	Input
j	Rocket exhaust jet or beam
net	Net
o	Initial conditions
opt	Optimum
p	Propellant
ps	Propulsion system
s	Vehicle system excluding propulsion system and propellant
S	Propellant storage subsystem
T	Thrust generating subsystem
W	Power or energy subsystem

1 General lay-out of rocket systems and classification

The major components of any rocket system and therefore also thermal rocket system are (Figure 1):

a) Expellant or propellant, which forms the mass to be expelled.
b) Thrust generating (thruster) or accelerator system wherein the propellant is accelerated to a high exhaust velocity.
c) Feed and storage system that stores the expellant prior to its use and feeds the expellant to the (set of) accelerator(s).
d) Energy or power source that provides the energy/power necessary for thrust generation.
e) Control system that controls the working of the rocket and allows for adjusting the thrust of the accelerator(s).
f) Frame to hold the components.

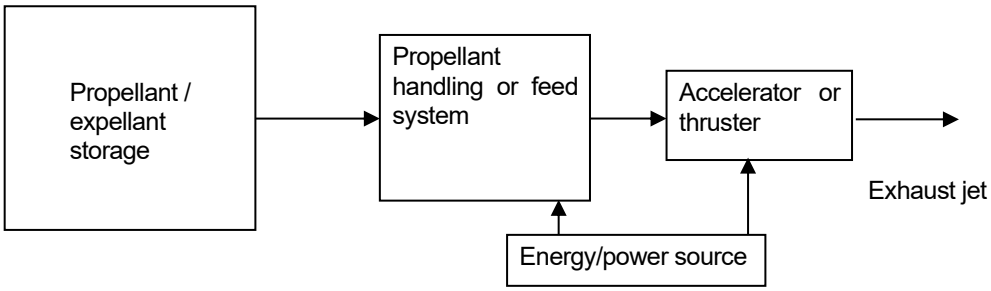

Figure 1: Rocket system schematic

An important distinction in thermal rockets is after the type of energy source used and how this is converted into useful energy. We distinguish systems that:

a) Carry the energy source within (internal energy source), like chemical rockets and nuclear rockets
b) Obtain the energy from an external energy source like the Sun or from a controlled remote laser or microwave source.

Internal energy rocket systems of course are much more independent from their environment than external energy rocket systems, but may suffer from a high mass, since also the energy source must be carried. On the other hand, even when not carrying the energy source on board, we should consider that the on-board energy collection and conversion system may contribute heavily to the rocket mass. An overview of the various thermal rockets distinguished is given in Figure 2.

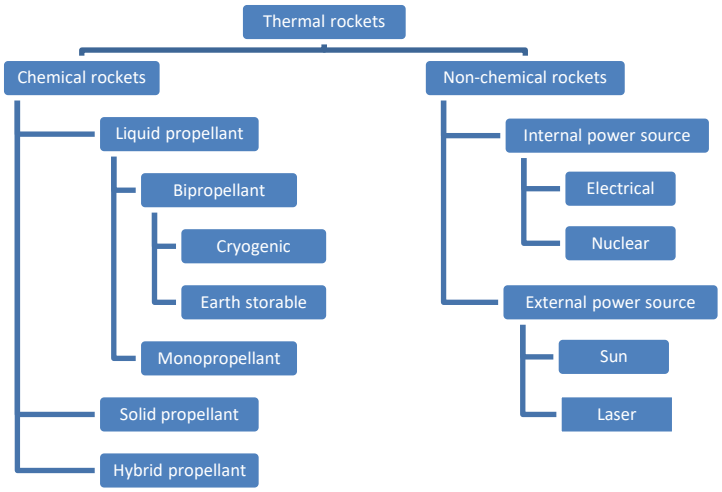

Figure 2: Thermal rocket types

The different energy sources used lead to differences in exhaust velocity and thrust acceleration levels.

2 Design analysis framework of rocket propulsions systems

In an earlier chapter we have introduced the general design framework consisting of 7 steps (DESACME). An important step in this framework is the design analysis to be performed. Below a next framework is given specifically for the design analysis of rocket propulsion systems. Focus in this framework is first on the dimensioning and sizing of the system as to realize the required performances. Only if performance requirements can be met, it makes sense to perform other analysis. The general design analysis framework advocated here also consists of 7 steps.

1. Select type of propulsion system based on attainable I_{sp} levels using historical data
2. Determine propellant mass (see chapter on rocket propulsion fundamentals), select thrust level and thrust time in agreement with (vehicle) acceleration limitations
3. Correct propellant mass for propellant remaining[1]
4. Dimension and size system for performance[2]
5. Check if the system fulfills performance requirements as well as mass and size constraints. If not, start all over
6. Perform cost, reliability, maintainability, etc. analysis
7. Check performances. If it is not OK modify the design otherwise prepare for next step in the design

3 Rocket system mass breakdown (some definitions)

A rocket propelled system includes next to the propulsion system also other elements like a structural system, a thermal system, an avionics system, and an electrical power system. Hereafter, we focus on the mass of the rocket propulsion system only and will neglect the effects of a change in propulsion system mass on the mass of the other vehicle systems.

The mass of a rocket propulsion system usually is divided into the propellant mass and the system dry mass:

$$M_{ps} = M_p + \left(M_{ps}\right)_{dry} \tag{2.1}$$

System dry mass sometimes is also referred to as inert mass. This mass is composed of the mass contributions of the individual system components, see the previous section:

$$\left(M_{ps}\right)_{dry} = M_T + M_W + M_F + M_S \tag{2.2}$$

With:

- M_T: Mass of thrust generating subsystem
- M_W: Mass of power subsystem[3]
- M_F: Mass of propellant feed subsystem
- M_S: Mass of propellant storage subsystem

To express the significance of the dry mass on total rocket system mass we use the net mass fraction. This fraction is defined by the ratio of rocket system dry mass to total rocket system mass.

$$\alpha_{net} = \frac{\left(M_{ps}\right)_{dry}}{M_{ps}} \tag{2.3}$$

[1] In most rocket propelled systems some non-usable propellant shall be considered. This can vary from roughly 0.5% to several percent of total propellant mass.

[2] Dimensioning and sizing can be done in many ways using analysis methods that range from simple to complex and highly detailed.

[3] Power subsystem is only considered part of propulsion system in case a separate power source is needed for propulsion.

The significance of the propellant mass is given by the propellant mass fraction[4], which gives the ratio of propellant mass to total motor mass:

$$\alpha_p = \frac{M_p}{M_{ps}} \tag{2.4}$$

Another important characteristic is the dry mass to propellant mass ratio α:

$$\alpha = \frac{\left(M_{ps}\right)_{dry}}{M_p} \tag{2.5}$$

Note that since $M_{ps} = M_p + \left(M_{ps}\right)_{dry}$:

$$\alpha = \frac{\alpha_{net}}{\alpha_p} \quad \wedge \quad \alpha_{net} = 1 - \alpha_p \tag{2.6}$$

Table 1 gives an overview of typical ranges for the net mass fraction of chemical systems.

Table 1: Typical net mass fractions for specific chemical rocket propelled systems

System	Net mass fraction
Solid rockets	
- Upper stage motors	0.05-0.12
- Booster stages	0.115-0.167
Liquid rockets	
- Cryogenic rocket stages	0.06-0.2
- Storable propellant rocket stages	0.05-0.35
- Satellite AOCS systems	
○ Regulated systems	0.02-0.15
○ Blow-down systems	0.10-0.35

Typical net mass fractions of rocket systems with separate energy/power source can be deduced from Table 1. It is noted though that values should not be considered as set in stone as developments continue.

4 Sizing fundamentals (a first analysis)

In this section we discuss sizing fundamentals of chemical systems (with integrated power-plant) and systems[5] with a separate power-plant.

From the rocket equation, we have learned that when the propulsion system dry mass is negligibly small; we should strive for maximum exhaust velocity. However, the dry mass of the propulsion system is usually not negligibly small, see the previous section.

To determine the effect of dry system mass on propellant mass, we will discuss two different cases, being systems for which the dry system mass scales linearly with expellant mass in section 4.1 and systems with a separate power-plant in section 4.2. Some more general cases are touched upon in section 4.3.

4.1 Dry mass linearly dependent on expellant mass

For solid rocket motors, we find that dry mass varies about linearly with propellant mass, see Figure 3:

[4] The term weight factor is used in [van der Laan and Timnat]. However, currently, the term mass fraction is more common.

[5] The word system is used in this text to denote the rocket propulsion system, i.e. also referred to as the rocket, only and not for example the spacecraft or space launcher in full.

$$\alpha = \frac{\left(M_{ps}\right)_{dry}}{M_p} = \text{constant} \tag{3.1}$$

The equation indicated in the figure relates motor dry mass (indicated as y) to propellant mass (indicated as x). From this equation, we find α = 0.1585.

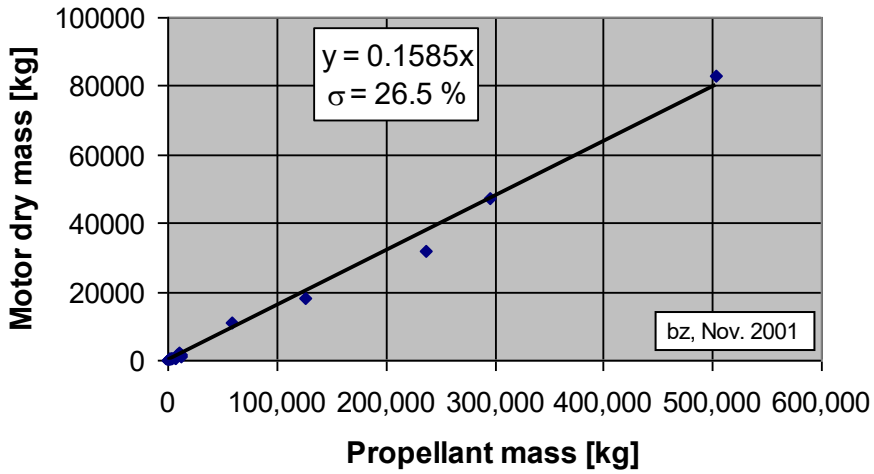

Figure 3: Dry mass to propellant mass solid rocket motors/stages

The linear relation can be explained by that for solid rocket motors next to the propellant mass the mass of the casing, which holds the propellant, and the liner that lines the propellant on the outside together make up most of the dry system mass. This is illustrated in table 2 for the minuteman solid rocket motor. It can be argued that both the mass of the casing and the liner scale with the amount of propellant.

Table 2: Mass characteristics first stage Minuteman missile [Sutton]

Mass	[kg]
Total mass	22929
Total inert	2141
Mass at burnout	1934
Propellant	20789
Motor Case	1160
Nozzle	402
Insulation	428
Liner	68
Igniter	12
Miscellaneous	71

In Figure 3, we have also indicated the standard deviation about the estimate as an indication of the accuracy of the relationship. As such, it explains in part for the range indicated in Table 1 for solid rocket motors.

To evaluate the effect of dry system mass on the total propellant mass needed, we substitute this linear relation between dry mass and propellant mass in the rocket equation. This gives:

$$\Delta V = w \cdot \ln\left(\frac{M_o}{M_f}\right)$$
$$\Delta V = w \cdot \ln\left(\frac{M_f + M_p}{M_f}\right) \tag{3.2}$$

And:

$$M_p = M_e \cdot \left(e^{\frac{\Delta v}{w}} - 1 \right) = \left(M_s + \left(M_{ps} \right)_{dry} \right) \cdot \left(e^{\frac{\Delta v}{w}} - 1 \right)$$

$$M_p = \left(M_s + \alpha M_p \right) \cdot \left(e^{\frac{\Delta v}{w}} - 1 \right) = \frac{M_s}{\left(1 - \alpha \cdot \left(e^{\frac{\Delta v}{w}} - 1 \right) \right)} \cdot \left(e^{\frac{\Delta v}{w}} - 1 \right) \qquad (3.3)$$

Here M_o is total vehicle mass at start, M_e is empty vehicle mass, and M_s is vehicle dry mass minus dry mass of the propulsion system:

$$M_s = M_f - \left(M_{ps} \right)_{dry} \qquad (3.4)$$

In the next figure some results are given for a representative vehicle and a mission characteristic at two different net mass fractions.

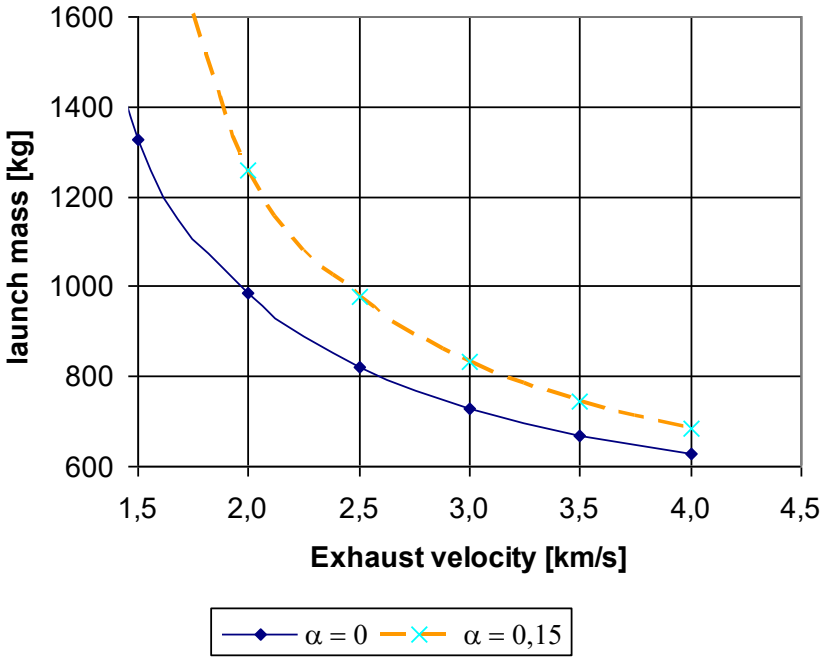

Figure 4: Vehicle (launch) mass versus exhaust velocity for two values of the net mass fraction (empty vehicle mass is 400 kg, mission characteristic velocity is 1800 m/s).

The figure shows that with increasing net mass fraction also the launch mass increases. This is mainly due to a higher propellant load. The mass of the propulsion system itself should be discounted from the empty vehicle mass. The figure also shows that when we have a linear relation between the dry mass of the propulsion system and the propellant mass, we still should strive to maximize the exhaust velocity.

4.2 Dry mass linearly dependent on power output power source

From the next table, it might be argued that for thermal rockets using a separate energy/power source the dry mass of the propulsion subsystem is dominated by the mass of the power source:

$$\left(M_{ps} \right)_{dry} \approx M_W \qquad (3.5)$$

Table 3: Typical mass data of rocket propelled vehicles using propulsion module with separate power system [Bos], [Zandbergen]

Vehicle Mass [kg]	Payload Mass [kg]	Propulsion type	Thrust	Action time	Propulsion Module/Stage Dry Mass[1] [kg]	Power System[2] Mass [kg]	Propellant Mass [kg]
12500	2500	Solar-Thermal	1 kN	days	890	720	8000 (e)
21850	5990	Nuclear-electric	10 N	> 1000 hr	9860	7385	5040
4346	1135	Solar-electric	3.2 N	> 1000 hr	1849	1420	1041
42600	17000	Solar-electric	31.3 N	200 days	17420	8201	8248

1) The Propulsion Module includes the arrays, Power Management and Distribution (PMAD), structures, mechanisms, avionics, auxiliary propulsion system, and payload interface.
2) Part of propulsion module/stage mass.

In case we assume that the mass of power source scales linearly with the power output of this source:

$$M_w = \alpha_w \cdot P_w \tag{3.6}$$

With:

- $1/\alpha_W$ = specific power (W/kg) or α_W is inverse specific power (kg/W)
- P_W = power output from power source

The linear dependency of power source mass with power is evident in case of using solar energy. This is because solar panel or solar collector area increases with increasing power. In case of using nuclear energy, this assumption is less evident, and one could reason that the mass of the energy source scales with the amount of energy instead of power. However, in practice again power is the dimensioning parameter. This is mostly because the mass of the energy source itself is negligible compared to the mass of the power conversion system needed to convert nuclear power into useful power. The latter again scales with power. Typical specific power values are given in the next table.

Table 4: Typical specific power values [Zandbergen]

Type of power system	Specific power
Thermal:	
- Radioisotope	25-170 W_t/kg
- Nuclear-thermal	300-4000 kW_t/kg
- Solar collector-receiver at 1 AU	200-2000 W_t/kg
Electrical:	
- Photo-voltaic array	10-40 W_e/kg
- Photo-voltaic system (incl. batteries)	7-12 W_e/kg
- Nuclear-electric	2.5-100 W_e/kg

Power output required from the power source can be related to jet power[6]:

$$P_w = \frac{P_j}{\eta} \tag{3.7}$$

With η is thrust efficiency, and P_j is jet power given by:

$$P_j = \frac{1}{2} \cdot F \cdot w = \frac{1}{2} \cdot m \cdot w^2 \tag{3.8}$$

[6] Notice that we assume that power output from the power source is identical to the input power of the thrust generating system. In practice, this is rarely the case.

Substitution of equation for the mass of the energy source gives for the system specific impulse:

$$I_{ssp} = \frac{I}{W} = \frac{F \cdot t}{\left(M_p + \alpha_W \cdot P_W\right) \cdot g_o} = \frac{m \cdot w \cdot t}{\left(m \cdot t + \frac{\alpha_W \cdot m \cdot w^2}{2\eta}\right) \cdot g_o} \tag{3.9}$$

Reworking gives:

$$I_{ssp} = \frac{w/g_o}{\left(1 + \frac{\alpha_W \cdot w^2}{2\eta t}\right)} = \frac{w/g_o}{1 + \varepsilon w^2} \tag{3.10}$$

With ε is specific mass of the energy source (expressed in kg/J); $1/\varepsilon$ is specific energy of the energy source (J/kg).

Next figure gives specific impulse as a function of exhaust velocity for two different values of specific mass of the energy source.

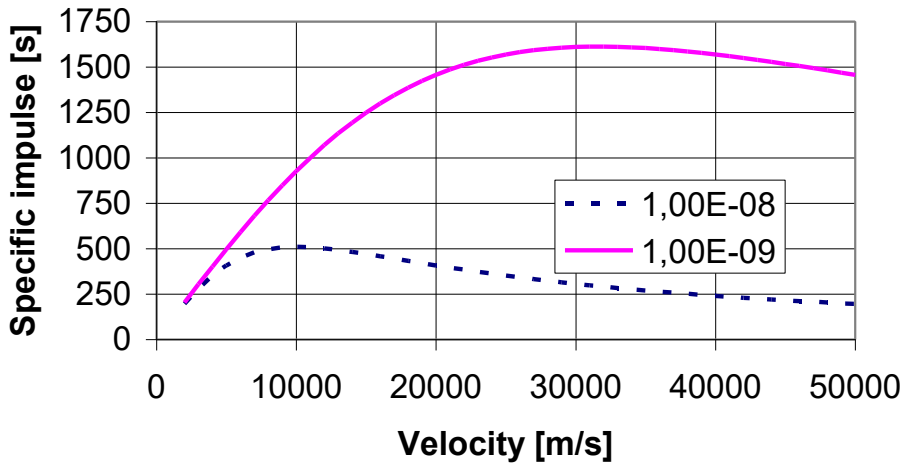

Figure 5: Optimum exhaust velocity for two different values of specific mass of energy source

From this figure, we learn that in this case specific impulse has some optimum value. The exhaust velocity at which this optimum occurs is referred to as the optimum exhaust velocity. This velocity depends on amongst others mission duration, specific power of power source, and thrust efficiency.

The value of the optimum exhaust velocity can be found by differentiating the specific impulse equation to exhaust velocity and setting the result equal to zero. This gives:

$$\frac{dI_{ssp}}{dw} = 0 = \frac{1/g_o \cdot (1 + \varepsilon w^2) - 2\varepsilon w \cdot (w/g_o)}{(1 + \varepsilon w^2)^2} \tag{3.11}$$

$$0 = 1/g_o \cdot (1 + \varepsilon w^2) - 2\varepsilon w \cdot (w/g_o) = 1 - \varepsilon w^2 \tag{3.12}$$

$$w_{opt} = \sqrt{1/\varepsilon} \tag{3.13}$$

For instance, in the case of $\varepsilon = 10^{-8}$ kg/J, we find that $w_{opt} = 10$ km/s and for $\varepsilon = 10^{-9}$ kg/J, $w_{opt} = 31.6$ km/s.

For the propellant mass, we find:

$$\Delta V = w \cdot \ln\left(\frac{M_o}{M_e}\right)$$
$$\Delta V = w \cdot \ln\left(\frac{M_e + M_p}{M_e}\right) \tag{3.14}$$

$$M_p = M_e \cdot \left(e^{\frac{\Delta v}{w}} - 1\right) = \left(M_s + \left(M_{prop}\right)_{dry}\right) \cdot \left(e^{\frac{\Delta v}{w}} - 1\right)$$
$$M_p = \left(M_s + M_W\right) \cdot \left(e^{\frac{\Delta v}{w}} - 1\right) = \frac{M_s}{\left(1 - \frac{w^2}{w_{opt}^{\ 2}} \cdot \left(e^{\frac{\Delta v}{w}} - 1\right)\right)} \cdot \left(e^{\frac{\Delta v}{w}} - 1\right) \tag{3.15}$$

The latter relationship also holds in case we are unable to select the optimum exhaust velocity, for example through technical constraints.

For the mass of the power source, we find:

$$M_W = \frac{w^2}{w_{opt}^{\ 2}} \cdot M_p \tag{3.16}$$

From the above equation, it follows for $w = w_{opt}$: $M_W = M_p$.

As a final remark, we note that in case we use (excess) power from an already present power source, for example for providing power to the payload once arrived at its operational orbit, we can omit the design of the power source from our considerations, and we should again strive for the highest feasible velocity.

4.3 Other (more general) cases

In the two foregoing sections we have performed sizing using simplifying assumptions. However, it almost never is as simple as assumed in the preceding two sections. For instance, dry mass of rocket systems may also be considered as a part mass that depends on propellant mass (not necessarily in a linear way) and a part mass that is independent of propellant mass. Also, the dry mass of an advanced rocket system not only depends on the mass of the power-plant but may also depend on the mass of the propellant storage system, the feed system and the thrust system itself. In all these cases, an analytical solution may not be easily obtained, and one may need to resort to using computer-based methods.

5 Rocket staging

See ADSEE I (AE1222-II) lecture notes on Launch Vehicle Design and Sizing.

6 Problems

1) Collect and list for at least 5 clearly different types of rocket propulsion systems, see Figure 2, available data on attainable thrust level, I_{sp} level, propulsion system (not only engine) mass, and propellant mass with proper referencing. Include at least 1 non-chemical rocket propulsion system and 1 non-thermal rocket propulsion system.

2) You are designing a rocket (propulsion) system capable of transferring a satellite from LEO to GEO. The mission characteristic velocity change (Δv) is 3.94 km/s and the dry mass of the satellite (excluding the rocket system) is 1000 kg.

a) In case we select an exhaust velocity of 3000 m/s, calculate for this mission:

i. The mass of propellant that should be loaded into the rocket in case the dry mass of the rocket system is 100 kg.

ii. Propellant mass and dry mass of the rocket system in case the dry mass of the rocket system linearly depends on propellant mass (α = 0.096).

iii. Propellant mass and dry mass of the rocket system in case the propulsion system inert (dry) mass (indicated by y) of the rocket system is given by the following relationship (x is propellant mass in kg): y = 0.0348 x + 58.152.

b) In case we select a rocket system equipped with a power source with a specific mass of 100 W/kg, an operational life of 1000 hours, and thrusters with a thrust efficiency of 0.7, calculate for this system:

i. Optimum exhaust velocity.

ii. Propellant mass and rocket system dry mass (based on power subsystem mass only) in case we select an exhaust velocity equal to the optimum exhaust velocity.

iii. Idem in case we select an exhaust velocity equal to 1.5 times the optimum exhaust velocity

3) Some designers argue that a linear relation exists between the propulsion system dry mass and propellant mass. Using the mass data for specific bipropellant RCS systems as given in the table below, you are asked to determine the slope (and when applicable) the y-intercept (y = system dry mass) of the linear relation that fits best. Discuss whether you agree with the assumption of a linear relationship or not (consider e.g. the assumption that system dry mass is independent of, or solely dependent on propellant mass).

Table: Mass characteristics of specific bipropellant RCS systems [Gale]

Satellite	System dry mass [kg]	Total propellant mass [kg]	Pressurant mass [kg]	Tank mass [kg]	Pressurant tank mass [kg]	Miscellaneous mass [kg]
DFS	74.5	773	2	40.0	13.8	20.7
Eurostar	105.335	996	N.A.	61.6	15.8	27.9
Eutelsat-2	103.3	1064	N.A.	57.7	15.8	29.8
Inmarsat-2	88.6	760	N.A.	49.4	15.7	23.5
Italsat	106.3	866	N.A.	62.0	16.8	27.5
Olympus	116.8	1722	N.A.	49.4	39.1	28.2

4) Consider the design of a two-stage[7] rocket that should be capable of delivering a velocity increment of 9.8 km/s to a payload of mass 5 tons. For this rocket we have selected a propulsion system capable of delivering an effective exhaust velocity of 3750 m/s (constant with altitude). In addition, we assume that both stages have a structural coefficient of 0.1. Determine for this vehicle the minimum launch mass needed to bring this payload into orbit.

Hint: Consider how total velocity increment is to be distributed over the two sub-rockets.

Literature

1) Bos R., Conceptual System Design of a Solar Electric Propulsion Stage for Earth-Moon Cargo Transfer Missions, MSc thesis report, TU-Delft, 2013.

2) Fortescue P., Stark J., and Swinerd G., Spacecraft systems engineering, 3rd edition, Chapter 6.4 (introductory part and sections 6.4.1 and 7.2.3).

3) Gale D., Williams C. Pope J., Gaydon S., Holl P., Bibliography of liquid propellant propulsion systems of European Spacecraft, Study note: SN/ESA-P/001/89/BAe, British Aerospace, January 1990.

4) Sutton G.P., Rocket Propulsion Elements, 7th edition, John Wiley & Sons Inc.

5) Zandbergen, B.T.C., ADSEE I, Part: Spacecraft bus Design and sizing, January 2020.

[7] Single stage rocket:
For a single stage launcher, we find a mass ratio of 13.64.

$13.64 = M_o/M_e$
$M_o - M_e = M_F$
$M_e = M_s + M_p$

$M_e/M_o = M_s/M_o + M_p/M_o$

Filling in numbers gives: $1/13.64 = 0.1 + 5000/M_o \rightarrow M_o =$ No realistic solution possible (only when structural mass ratio is much lower a solution might be possible. Take 5%, we get $5000/M_o = 0.0233 \rightarrow M_o = 214.5$ ton

Thrust and Specific Impulse of a Thermal Rocket Motor

Contents

1 Introduction 33

2 Thrust 33

3 Specific impulse 37

4 Problems 37

Literature 37

Symbols

The symbols are arranged alphabetically; Roman symbols first, followed by Greek. The used subscripts are given at the end of the list.

Roman

A	Area
D	Drag
F	Thrust
g_o	Gravitational acceleration at sea level
I_{sp}	Specific impulse
m	Mass flow rate
p	Pressure
R	Pressure force on rocket
S	Surface
U	Flow velocity
x, y, z	Coordinates in Cartesian system

Greek

ρ	Mass density

Subscripts

a	Refers to atmospheric conditions
e	Refers to conditions in nozzle exit
exp	Experimental value
eq	Equivalent
i	Internal surface of rocket thrust chamber
u	External surface of rocket

1 Introduction

The function of a thermal rocket engine system is to generate thrust thereby converting thermal energy into kinetic energy of the jet exhaust. A simple example of such a thermal rocket engine is a balloon. When you blow up a balloon and let it go it will fly all over the room (until running out of air). It is the air molecules flowing out the nozzle of the balloon that generate a thrust force.

In the previous chapter a simple expression has been derived for the rocket thrust in a vacuum environment. In this section, we will consider the thrust generation process in a thermal rocket in more detail and the effect of the pressure environment on thrust.

2 Thrust

Earlier, an expression has been derived for the rocket thrust purely based on the exchange of (linear) momentum. Since a rocket motor may be subject to a pressure environment and because pressure forces are acting on the gas in the chamber, we should investigate the effect of these pressure forces on rocket thrust. In this section, we will derive an equation showing the thrust of a thermal rocket motor to include not only a component depending on the exchange of linear momentum, but also a pressure component.

Consider a steadily operating rocket travelling through the atmosphere at a certain velocity. At the back of the rocket a high velocity gas jet leaves the rocket. Figure 1 presents a schematic picture of the rocket. The outer surface of the rocket is indicated by S_u, and the surface enveloping the gaseous body in the chamber and nozzle is called S_i. The nozzle exit area, i.e. the surface of the nozzle where the flow comes out, is indicated by A_e. The pressure of the gas flow at the nozzle exit is indicated by p_e, the density by ρ_e and the exhaust velocity by U_e. We furthermore assume that the injection flow velocity of the propellants as well as friction effects are negligibly small.

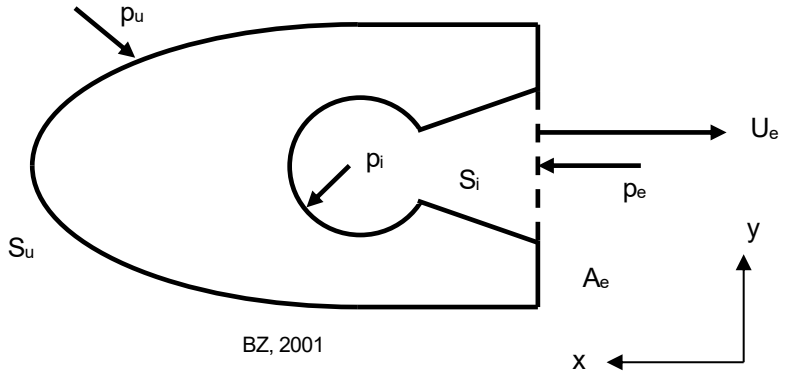

Figure 1: Pressure forces on rocket

Now we determine the resulting force R_x on the rocket by integration of internal and external pressures in the x-direction:

$$R_x = \left[\int_{S_i} p_i \cdot dS_i - \int_{S_u} p_u \cdot dS_u \right]_x \qquad (2\text{-}1)$$

When p_a is the constant ambient pressure, the integral of p_a over S_u and S_i is zero:

$$\oint p_a \cdot dS = \int_{S_i} p_a \cdot dS_i - \int_{S_u} p_a \cdot dS_u = 0 \tag{2-2}$$

Subtracting (2-2) from (2-1):

$$R_x = \left[\int_{S_i} (p_i - p_a) \cdot dS_i - \int_{S_u} (p_u - p_a) \cdot dS_u \right]_x \tag{2-3}$$

Consider now the body of gas inside the combustion chamber and nozzle. The net force on the gas in the chamber is the sum of the reactions from the chamber walls and of the reaction of the absolute gas pressure at the exit. These two reactions are opposed. The law of conservation of momentum dictates that the net force on the gas equals the momentum flux out of the chamber.

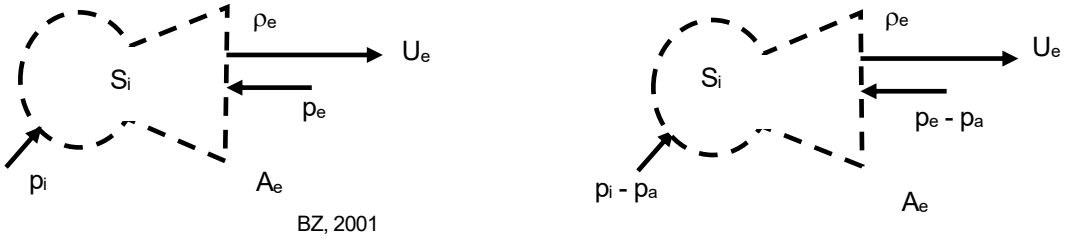

Figure 2: Pressure forces on gaseous body inside chamber and nozzle

Neglecting the momentum connected with the injection of propellant into the combustion chamber, we find:

$$\int_{S_i} (p_i - p_a) \cdot dS_i = \int_{A_e} \rho_e (U_e)^2 \cdot dA_e + \int_{A_e} (p_e - p_a) \cdot dA_e$$

$$\int_{S_i} (p_i - p_a) \cdot dS_i - \int_{A_e} (p_e - p_a) \cdot dA_e = \int_{A_e} \rho_e (U_e)^2 \cdot dA_e \tag{2-4}$$

For a first analysis, we assume that pressure, density and exhaust velocity in the nozzle exit are constant in magnitude and the flow of gases through the exit plane is one-dimensional. It follows:

$$\int_{S_i} (p_i - p_a) \cdot dS_i = m \cdot U_e + (p_e - p_a) \cdot A_e \tag{2-5}$$

Here m indicates the amount of expelled gas per unit time, i.e. the mass flow rate ($m = \rho_e U_e A_e$).

Next, combining (2-3) and (2-5) yields:

$$R_x = m \cdot U_e + (p_e - p_a) \cdot A_e - \left[\int_{S_u} (p_u - p_a) \cdot dS_u \right]_x \tag{2-6}$$

From this expression we obtain an expression for the drag D and the thrust F with R_x = F - D:

$$D = \left[\int_{S_u} (p_u - p_a) \cdot dS_u \right]_x \tag{2-7}$$

$$F = m \cdot U_e + (p_e - p_a) \cdot A_e \tag{2-8}$$

The equation (2-8) hereafter is shortly referred to as the "rocket thrust equation". It shows that for a thermal rocket engine next to a thrust related to the transport of linear momentum through the nozzle exit $m \cdot U_e$, hence the term “momentum thrust”, there is also a pressure related term $(p_e - p_a) \cdot A_e$ referred to as “pressure thrust”. It depends on the difference between the pressure p_e at the nozzle exit and the ambient pressure p_a and can be positive (under-expansion), zero (optimum expansion) or negative (over-expansion).

We will now show that since the mass flow remains constant throughout the nozzle maximum thrust is reached in case optimum expansion (pressure thrust is zero) can be achieved. For this we take the derivative of the thrust equation:

$$dF = m \cdot dU_e + (p_e - p_a) \cdot dA_e + A_e \cdot dp_e \tag{2-9}$$

According to the law of conservation of linear momentum:

$$m \cdot dU = -A \cdot dp \tag{2-10}$$

Combining (2-10) with (2-9) leaves:

$$\frac{dF}{dA_e} = p_e - p_a \tag{2-11}$$

To reach maximum thrust, we want the change in thrust with nozzle exit area to be zero. (2-11) shows us that this is achieved if $p_e = p_a$. The rocket nozzle design, which permits the expansion of the propellant product to the pressure that is exactly equal to the pressure of the surrounding fluid, is referred to as the “nozzle with optimum expansion ratio” or ”adapted” nozzle.

For an adapted nozzle equation, the thrust equation reduces to:

$$F = m \cdot U_e \tag{2-12}$$

As in practice, it is not always possible to achieve optimum expansion, we strive to keep the pressure thrust small compared to the momentum thrust. Because of this, it is common practice to define an equivalent velocity U_{eq} which takes the effect of the pressure thrust into account:

$$U_{eq} \equiv U_e + \frac{p_e - p_a}{m} \cdot A_e \tag{2-13}$$

This gives us the same simple equation we found for the adapted nozzle, except that the exhaust velocity is replaced by the equivalent velocity:

$$F = m \cdot U_{eq} \tag{2-14}$$

The importance of the equivalent velocity U_{eq} is that it allows us to write the rocket thrust as the product of mass flow m and velocity U_{eq}. It now becomes possible to use Tsiolkovsky's equation, i.e. the rocket equation, again to calculate the propellant mass.

Thrust at altitude

From the thrust equation, we learn that the thrust depends on the ambient pressure. In case mass flow rate, exhaust velocity, nozzle exit pressure and nozzle exit area are constant[1], and since the ambient pressure diminishes with increasing altitude, see Table 1, we find that the thrust increases when the vehicle is propelled at a higher altitude.

Table 1: Altitude (geometric) versus pressure (International Standard Atmosphere)

Altitude (km)	Pressure (bar)
0	1.013250
5	0.540482
10	0.265000
15	0.121118
20	0.055000
30	0.012000
40	0.003000
50	0.000800
60	0.000200
70	0.000060
80	0.000010
90	0.000002
100	0.000000

In Figure 3 the variation of the thrust and specific impulse with altitude is given for a specific rocket engine.

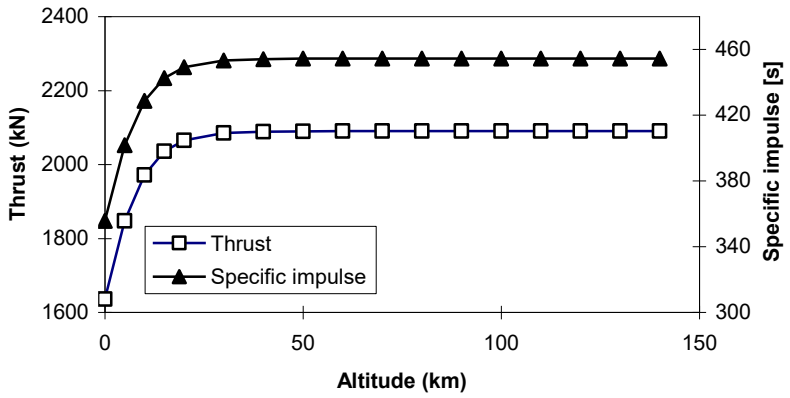

Figure 3: Altitude performance of the Space Shuttle Main Engine

[1] The assumption of constant mass flow rate, exhaust velocity, nozzle exit pressure and exit area holds for all rocket motors provided that the motor settings remain constant. Some further explanation will be given later when discussing the flow in the nozzle.

Effect of flight velocity

The rocket thrust equation shows that the thrust of a rocket essentially is independent of flight velocity. This in contrast to e.g. air-breathing jet engines, where thrust decreases with increasing flight velocity.

3 Specific impulse

Earlier we have defined the specific impulse as a measure for the performance of a rocket propulsion system. For a steadily operating thermal rocket it follows:

$$I_{sp} = \frac{U_{eq}}{g_o} \tag{3-1}$$

Since for a thermal rocket the equivalent velocity varies with altitude, we find that also the specific impulse of the rocket varies with altitude, see Figure 3. It is because of this altitude dependence why when giving specific impulse (and/or thrust) values for a rocket one should always add the pressure altitude for which the value given holds.

4 Problems

1) The following data are given for a rocket engine:
   - Thrust is 175 N at sea level (1 bar atmospheric pressure)
   - Propellant mass flow rate is 80 gram/s (determined by propellant feed system)
   - Nozzle exit diameter is 2.5 cm (determined by nozzle shape)
   - Nozzle exit pressure is 0.5 bar (determined by nozzle shape and propellant properties only)

   You are asked to determine for this motor:
   a. Gas exhaust velocity
   b. Engine thrust in space
   c. Effective exhaust velocity at sea level and in space

2) For the Ariane 5 Vulcain I[2] rocket engine, the following data are obtained from literature:
   - Vacuum thrust: 1075 kN
   - Vacuum specific impulse: 430 s
   - Diameter nozzle exit: 1.76 m

   You are asked to determine for this engine thrust and specific impulse at sea level as well as @ 10 km altitude. You may take atmospheric pressure at sea level and at 10 km altitude equal to 1 bar and 0.265 bar respectively.

Literature

1) Laan F.H. van der, and Timnat Y.M., Chemical Rocket Propulsion, TU-Delft, Department of Aerospace Engineering, April 1985.

2) Huzel K.K., and Huang D.H., Design of Liquid Propellant Rocket Engines, 2nd edition, NASA SP-125, 1971.

3) Sutton G.P., Rocket Propulsion Elements, 7th edition, John Wiley & Sons Inc.

[2] This rocket engine is also referred to as HM-60.

- This page is intentionally left blank -

Ideal Rocket Motor

Contents

Symbols 40

1 Introduction 41

2 Important Assumptions 41

3 Exhaust Velocity 42

4 Nozzle Shape 46

5 Critical Conditions 48

6 Critical Mass Flow 50

7 Nozzle Area Ratio 51

8 Characteristic Parameters 53

9 Quality Factors 57

10 Example 62

11 Problems 64

Literature 66

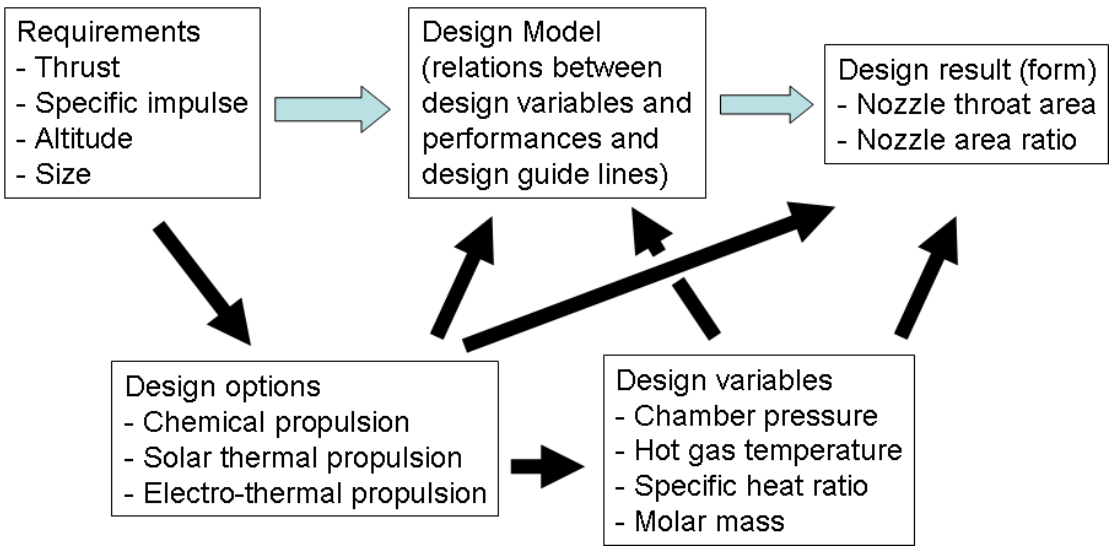

Symbols

The symbols are arranged alphabetically; Roman symbols first, followed by Greek. The used subscripts are given at the end of the list.

Roman

a	Velocity of sound
A	Area
c*	Characteristic velocity
c_p	Specific heat at constant pressure
C_p	Molar heat capacity at constant pressure
c_v	Specific heat at constant volume
C_V	Molar heat capacity at constant volume
C_A	Area (contraction) coefficient
C_d	Discharge coefficient
C_F	Thrust coefficient
C_ρ	Density coefficient
C_T	Specific propellant consumption
C_v	Velocity coefficient
E	Energy
F	Thrust
g_o	Gravitational acceleration at sea level
h	Enthalpy
I_{sp}	Specific impulse
m	Mass flow
M	Mach number
p	Pressure
R	Mass ratio, specific gas constant
R_A	Absolute gas constant
Re	Reynolds number
t	Time
T	Temperature
U	Flow velocity
x, y, z	Coordinates in Cartesian system

Greek

Δ	Increment or change
γ	Specific heat ratio
Γ	Vandenkerckhove constant
ξ	Quality factor
μ	Dynamic viscosity
M	Molar mass
ρ	Mass density

Subscripts

a	Refers to atmospheric conditions
c	Combustion chamber conditions
e	Refers to conditions in nozzle exit
eq	Equivalent
id	Value following from ideal rocket motor theory
L	Limit
max	Maximum
o	Initial conditions
p	Propellant
real	Real value
t	Throat
tot	Total conditions

1 Introduction

In an earlier chapter a relation has been derived showing that the thrust of a thermal rocket motor includes a momentum and a pressure term and an effective exhaust velocity has been defined. From the rocket equation it follows that it is advantageous to strive for a high (effective) exhaust velocity of the jet. In a balloon, the air molecules are accelerated to a high velocity because of the pressure difference between the air in the balloon and the atmosphere. The energy needed to generate the high velocity exhaust jet is taken from the air molecules. The higher the energy contained in the gas the higher the exhaust velocity. In practical rocketry, the high-pressure gases in the rocket motor are produced by heating solids, liquids, or gases to a high temperature via e.g. chemical and/or electrical means. In this chapter, we first introduce some assumptions which hold for what is commonly known as an "Ideal Rocket Motor" and show how these allow us to relate change in pressure, temperature and thermal energy over the nozzle to the exhaust velocity, i.e. change in velocity of the gas flow using basic laws of mechanics and thermodynamics. In addition, using the same simplifying assumptions, we introduce theory that allows us to relate exhaust velocity and thrust with size and shape of the nozzle. This latter theory is sometimes referred to as "ideal nozzle theory". Finally, we will show that ideal rocket motor theory allows for a reasonable approximation of the performances of a real/actual rocket motor and introduce some correction factors that allow for improving our estimates still further.

2 Important Assumptions

The most important assumptions are:

- The exhaust gases are homogeneous and have a constant composition. As in many solid propellant rockets metal powder is added, which is expelled in solid or liquid state, the combustion gases are not always homogeneous. As the temperature decreases when the gases are expanded through the nozzle, the chemical equilibrium changes and thus the composition of the gases varies.
- The gas or gas mixture expelled obeys the ideal gas law. The ideal gas law, or universal gas equation, is an equation of state of an ideal gas. It relates the pressure p of a gas with the volume V it occupies, the number to moles of the gas n, and the gas temperature[1]. The ideal gas law is valid for ideal gases[2] only. Real gases obey this equation only approximately, but its validity increases as the density of the gas tends to zero.

---

[1] The ideal gas law can be expressed with the 'Universal Gas Constant' R_A:

$$p \cdot V = n \cdot R_A \cdot T$$

The value of R_A is independent of the particular gas and is the same for all "perfect" gases. Its value is 8.314472 J/(mol-K). It can also be expressed with the 'individual' or 'specific gas constant' R:

$$p \cdot V = m \cdot R \cdot T \qquad \text{or} \qquad \frac{p}{\rho} = R \cdot T$$

The specific gas constant depends on the gas and is related to the molar mass of the expellant according to:

$$R = \frac{R_A}{M}$$

Here M is molar mass of the expellant, i.e. the mass of 1 mole of the expellant usually expressed in gram/mol. 1 mole typically contains 6.022 x 10^{23} (Avogadro's number) molecules.

[2] Ideal gas - a hypothetical gas with molecules of negligible size that exert no intermolecular forces.

- The heat capacity of the gas or mixture of gases expelled is constant. In practice the heat capacity depends on the temperature and composition of the expelled matter and neither of them is constant.
- The flow through the nozzle is one-dimensional, steady and isentropic. Only with a specially shaped nozzle, the flow can be made one-dimensional. During motor start-up and stop the gas flow is not steady. Though relatively small, there is some heat exchange with the surroundings causing the flow not to be isentropic.

3 Exhaust Velocity

In this section, an expression for the flow velocity in a rocket nozzle is derived using the first law of thermodynamics.

For any system, energy transfer is associated with mass and energy crossing the system boundaries. For any thermodynamic system energy includes kinetic energy, potential energy, internal energy and flow energy as well as heat and work processes.

The first law of thermodynamics states:

Energy can neither be created nor destroyed, only altered in form.

This leads to the energy balance: all energies into the system are equal to all energies leaving the system plus the change in storage of the energy within the system. In equation form:

$$\sum E_{in} = \sum E_{out} + \sum E_{stor} \tag{3-1}$$

Applying the energy balance to the gases[3] flowing through the nozzle, we may omit the storage term as for steadily operating nozzles there is no change in the energy contained. In general, also no heat is transferred to and from the flow in the nozzle (adiabatic flow), the flow performs no work, and the change in potential energy is neglected. In that case the energy balance reduces to:

$$h + \frac{1}{2} \cdot U^2 = \text{constant} = h_{tot} \tag{3-2}$$

In this equation h is specific enthalpy (sum of internal energy and flow energy[4]), U is flow velocity and $1/2 \cdot U^2$ is the specific kinetic energy of the moving gases. The specific enthalpy is usually expressed in J/kg, and U in m/s. This equation is valid along a streamline[5] in the nozzle.

For ideal gases the specific enthalpy is equal to the product of the (constant) specific heat and the absolute temperature:

$$c_p \cdot T_c + \frac{1}{2} \cdot U_c{}^2 = c_p \cdot T + \frac{1}{2} \cdot U^2 = c_p \cdot T_{tot} \tag{3-3}$$

Here index c is used to denote the combustion chamber. T is temperature of the gas at some place in the nozzle. T_{tot} and h_{tot} are the total temperature and total enthalpy, as the index “tot’ refers to the so-called “total” or “stagnation conditions”, where the flow has been brought to a rest (U = 0) by means of an isentropic process. An isentropic

[3] For steady state liquid flow, it can be shown that the energy balance reduces to Bernoulli's theorem for the restrictive case that the flow is isentropic (no heat flow and no energy dissipation by friction) and mass density remains constant (no work performed).
[4] Pressure times specific volume – work.
[5] A streamline is a path traced out by a mass-less particle as it moves with the flow.

expansion into vacuum would cause the temperature to decrease until 0 K is reached and the enthalpy term disappears. The velocity that could be attained in this way is called the "limiting velocity" U_L.

$$U_L = \sqrt{2 \cdot c_p \cdot T_{tot}} \tag{3-4}$$

As we assume an isentropic flow, we may use the Poisson relations (of which a derivation is given in appendix II):

$$\left(\frac{T}{T_c}\right) = \left(\frac{p}{p_c}\right)^{\left(\frac{\gamma-1}{\gamma}\right)} = \left(\frac{\rho}{\rho_c}\right)^{(\gamma-1)} \tag{3-5}$$

The velocity of sound is independent of pressure. It is defined as:

$$a = \sqrt{\gamma \cdot R \cdot T} \tag{3-6}$$

In (3-5) and (3-6) γ is the ratio of specific heats[6]:

$$\gamma = c_p/c_v. \tag{3-7}$$

R is the specific gas constant given by (see also footnote 1):

$$R = \frac{R_A}{M} = c_p - c_v \tag{3-8}$$

The specific heat ratio and specific gas constant or the molar mass depend on the gas composition.

Finally, we introduce the Mach number. It is a dimensionless flow parameter, defined as the ratio of the flow velocity and the velocity of sound:

$$M = \frac{U}{a} \tag{3-9}$$

If we assume the velocity of the reactants inside the combustion chamber to be zero, equation (3-3) changes into:

$$c_p \cdot T_c = c_p \cdot T + \frac{1}{2} \cdot U^2 \tag{3-10}$$

From (3-10) an expression for the flow velocity in the nozzle can be found as a function of the local temperature T:

$$U = \sqrt{2 \cdot c_p \cdot (T_c - T)} \tag{3-11}$$

---

[6] Physically, the value of γ relates to the degrees of freedom N of the gas particles:

$$\gamma = \frac{N+2}{N}$$

More degrees of freedom reduce the value of γ. For a mono-atomic gas N =3 (3 translations of the centre of mass). For a diatomic gas N = 5 (adding two rotational directions of the molecule about the centre of mass). For more complex molecules N increases further as then also vibrations should be considered.

Using the expression for the specific heat ratio and (3-8) this can be written as:

$$U = \sqrt{2 \cdot \frac{\gamma}{\gamma - 1} \cdot \frac{R_A}{M} \cdot T_c \cdot \left(1 - \frac{T}{T_c}\right)} \tag{3-12}$$

From this relation, we learn that for a given chamber temperature and constant mean molecular weight of the expellant; the flow velocity is a function of the local temperature only (or with the Poisson relation, of the local pressure or density only).

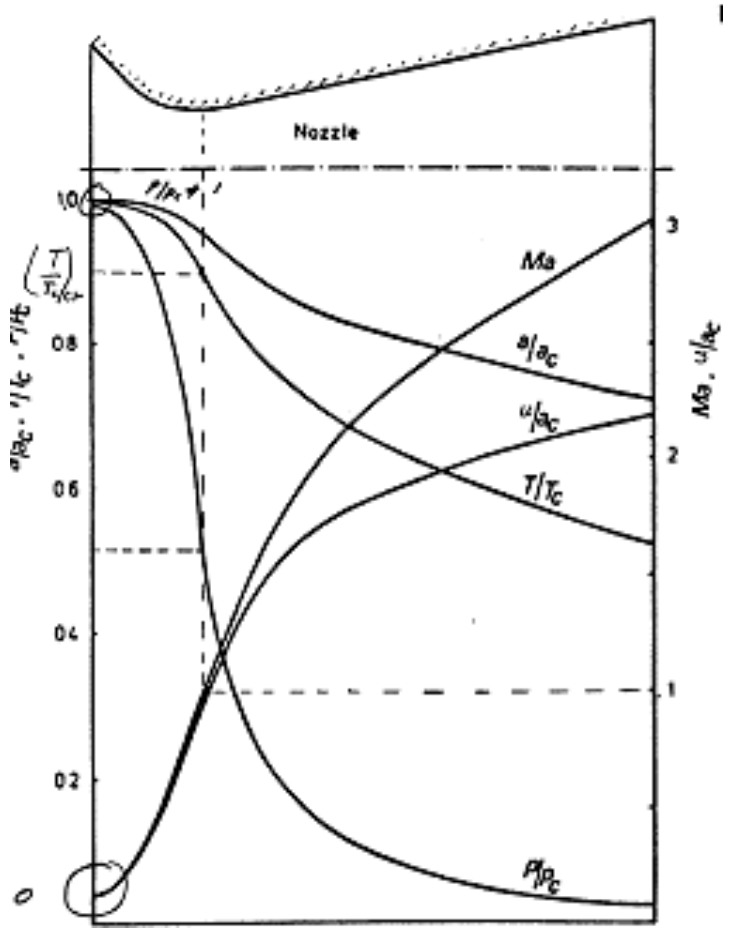

Figure 1: Pressure, temperature, velocity of sound, fluid velocity and Mach number versus nozzle length.

Figure 1 shows that the temperature decreases as the gases expand in the diverging part of the nozzle (this will be derived later). Therefore, the flow velocity increases, as can be understood from (3-12). As the expansion is assumed to be isentropic, the Poisson equations can be applied. Now the flow velocity can be written as:

$$U = \sqrt{2 \cdot \frac{\gamma}{\gamma - 1} \cdot \frac{R_A}{M} \cdot T_c \cdot \left(1 - \left(\frac{p}{p_c}\right)^{\left(\frac{\gamma-1}{\gamma}\right)}\right)} \tag{3-13}$$

Of special interest is the velocity at the exit of the nozzle, known as the exhaust velocity:

$$U_e = \sqrt{2 \cdot \frac{\gamma}{\gamma - 1} \cdot \frac{R_A}{M} \cdot T_c \cdot \left(1 - \left(\frac{p_e}{p_c} \right)^{\left(\frac{\gamma - 1}{\gamma} \right)} \right)} \qquad (3\text{-}14)$$

The exhaust velocity gives an important contribution to the thrust and to the equivalent velocity and therefore also to the I_{sp}.

From (3-14) we can learn how the various physical quantities affect the exhaust velocity. If the pressure ratio decreases, the whole term in brackets in (3-14) will increase as the exponent $(\gamma - 1)/\gamma$ is positive.

To study the effect of the specific heat ratio and the pressure ratio, we define the dimensionless exhaust velocity:

$$(U_e)_{dim} = \frac{U_e}{\sqrt{\frac{R_A}{M} \cdot T_c}}$$

In Figure 2 this dimensionless exhaust velocity is plotted as a function of the pressure ratio. The figure shows a strong increase of the exhaust velocity for pressure ratios up to 50. At higher pressure ratios the exhaust velocity still increases but much more slowly.

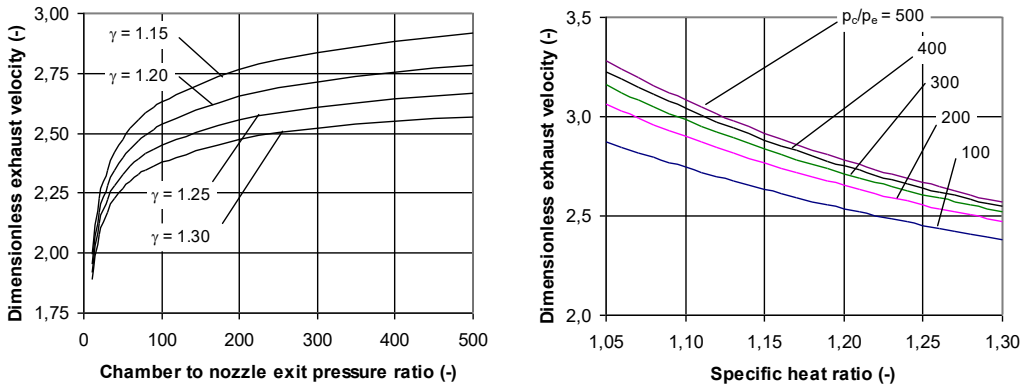

Figure 2: Dimensionless exhaust velocity as a function of pressure ratio and the specific heat ratio.

In current rocket motors, chamber pressures of up to 200 bars are used. At higher chamber pressures, construction problems arise. The exhaust pressure p_e depends strongly on the nozzle geometry.

Another important parameter which affects the exhaust velocity is the chamber temperature T_c. (3-14) shows that U_e is proportional to the square root of T_c. Though a high value of T_c is desirable from this point of view, a limit on the temperature should be set for two reasons:

- High temperatures may cause a weakening of the chamber wall, which may end up in a catastrophic failure. To allow increasing the chamber temperature, most rocket motors are equipped with either cooling or some means of thermal insulation.
- High temperatures may lead to dissociation of the gas (or mixture of gases). Dissociation requires energy, leaving less energy to be converted into kinetic energy of the expellant.

There is also an influence of the specific heat ratio γ on the exhaust velocity. Usually changes in γ are small (in between 1.15 and 1.3 for chemical rocket motors); as can be seen from Figure 2 the influence of γ on U_e is not strong.

Finally, (3-14) shows the influence of the mean molar mass M on U_e. A small value of M results in a relatively large exhaust velocity. This is one of the reasons for the use of hydrogen as a rocket propellant.

As already said, an adiabatic expansion to vacuum would lead to the highest possible exhaust velocity, called the 'limiting velocity'. Equation (3-14) can be written in the form:

$$U_L = \sqrt{2 \cdot \frac{\gamma}{\gamma - 1} \cdot \frac{R_A}{M} \cdot T_c} \qquad (3\text{-}15)$$

Using) the exhaust velocity can be written as:

$$U_e = U_L \cdot \sqrt{\left(1 - \left(\frac{p_e}{p_c}\right)^{\left(\frac{\gamma-1}{\gamma}\right)}\right)} \qquad (3\text{-}16)$$

In Figure 3 the ratio of exhaust velocity to limiting velocity (U_e/U_L) is given as a function of p_c/p_e for various values of γ.

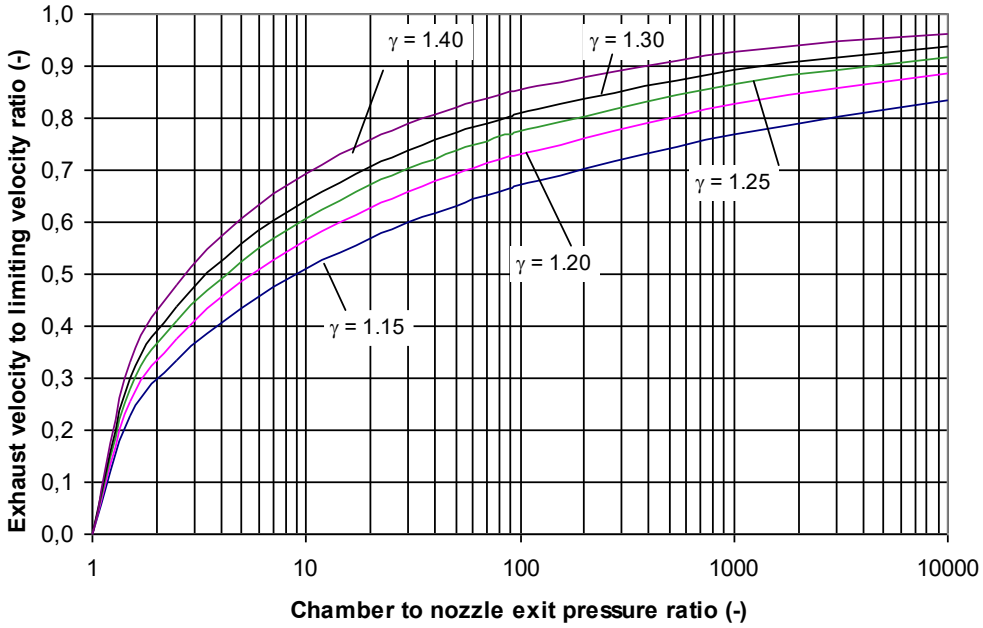

Figure 3: Velocity ratio versus pressure ratio

The figure shows that for pressure ratios more than 1000, the exhaust velocity is already about 80% of the theoretical maximum (i.e. the limiting velocity).

4 Nozzle Shape

As we have seen in the previous section, velocity U increases when temperature T decreases. As T, p, and ρ are linked by the Poisson relations, this means p and ρ also

have to decrease through the nozzle, see Figure 1. This process of decreasing pressure has already silently been assumed as we talked about “expansion” of the flow through the nozzle.

As already said, it is our objective to obtain a high exhaust velocity. In other words, we want to accelerate the expellant. This acceleration can only be accomplished by applying force to the gas flow. The reaction force from the gas on the engine walls is called the thrust. To find an equation which elicits the shape of the nozzle, we have to study the relation between the change in area dA and the change in gas velocity dU. For this, we use the principle of conservation of matter in a steady flow process also referred to as the “continuity equation”.

In mathematical form the continuity equation can be written as:

$$m = \rho \cdot U \cdot A \tag{4-1}$$

As the gas mass flow rate m is constant through the nozzle, the total derivative of the continuity equation is zero:

$$\begin{aligned} &m = \text{constant} \Leftrightarrow dm = 0 \\ &d(\rho \cdot U \cdot A) = UA \cdot d\rho + \rho A \cdot dU + \rho U \cdot dA = 0 \end{aligned} \tag{4-2}$$

Here A is area of cross section of the flow channel, or more specific the nozzle.

Dividing (4-2) by the continuity equation yields:

$$\frac{d\rho}{\rho} + \frac{dU}{U} + \frac{dA}{A} = 0 \tag{4-3}$$

For an incompressible medium, we find that the change in density by definition is zero. This then shows that for an incompressible medium to increase the flow velocity, the area should decrease. In reality, all media are to some extent compressible. However, there are several flow cases that can be modeled as incompressible, without detrimental loss of accuracy. This is the case for the flow of homogeneous liquids as well as for the flow of gases at velocities M < 0.3.

For compressible flow, we need to introduce a relation that allows for obtaining the change in density. For this, we use Poisson relation relating density to temperature (T = constant $\rho^{\gamma-1}$) and the energy equation relating temperature to flow velocity. It follows:

$$dT = (\gamma - 1) \cdot C \cdot \frac{\rho^{(\gamma-1)}}{\rho} d\rho = (\gamma - 1) \cdot \frac{T}{\rho} d\rho \tag{4-4}$$

The energy equation is known as:

$$c_p \cdot T + \frac{1}{2} \cdot U^2 = \frac{\gamma \cdot R}{\gamma - 1} \cdot T + \frac{1}{2} \cdot U^2 = \text{constant} \tag{4-5}$$

Taking the derivative yields:

$$\frac{\gamma \cdot R}{\gamma - 1} \cdot dT + U \cdot dU = 0 \tag{4-6}$$

Substituting (4-4) into (4-6) yields:

$$\frac{\gamma \cdot R \cdot T}{\rho} \cdot d\rho = a^2 \cdot \frac{d\rho}{\rho} = -UdU \tag{4-7}$$

From this equation $d\rho/\rho$ can be expressed in terms of the flow velocity U and the velocity of sound a. Using the definition of the Mach number M = U/a and substituting $d\rho/\rho$ into (4-3) yields:

$$\left(1 - M^2\right) \cdot \frac{dU}{U} = -\frac{dA}{A} \tag{4-8}$$

Now we have again found a relation between the velocity increment of the fluid and the change in cross-sectional area of the flow section. The relation shows that for M < 1 (subsonic flow) an increase in velocity should be accompanied by a decrease in cross-sectional area of the flow channel (the channel converges). For M >1 (supersonic flow) we find that to increase the flow velocity, the cross-sectional area should increase (the channel diverges). At M = 1 (sonic flow), we find that the change in area is zero. Going from subsonic to supersonic flow, we find that at M = 1, the cross-sectional area of the flow channel is at a minimum. This minimum is commonly referred to as the “throat’ of the flow channel.

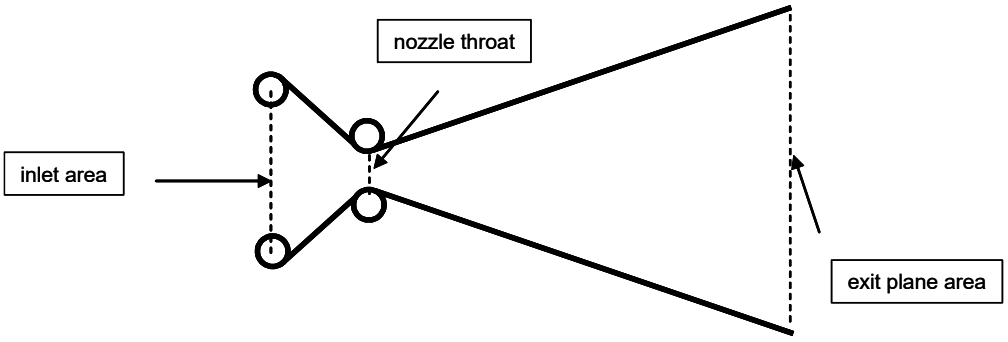

Figure 4: Nozzle shape

5 Critical Conditions

It has already been observed that the existence of a throat inside the nozzle does not necessarily lead to a sonic flow in the throat and a supersonic flow in the divergent part of the nozzle. For the flow to become sonic, certain conditions must be fulfilled. These are known as the ‘critical conditions’.

A certain ratio between the pressure in the throat and the chamber pressure must exist to bring about a sonic flow in the throat. If this ratio is reached, corresponding ratios can be found for the temperature and density by applying Poisson’s equations. These ratios are called the ‘critical ratios’.

First an expression for the mass flow per unit area is derived and with the use of this expression the critical pressure ratio is found.

From the continuity equation we know that:

$$\frac{m}{A} = \rho \cdot U \tag{5-1}$$

Substitution of the flow velocity U (3-13) into (5-1) yields:

$$\frac{m}{A} = \rho \cdot \sqrt{\frac{2\gamma}{\gamma - 1} \cdot R \cdot T_c \cdot \left(1 - \left(\frac{p}{p_c}\right)^{\left(\frac{\gamma-1}{\gamma}\right)}\right)} \tag{5-2}$$

Using the Poisson equation (3-5) gives:

$$\frac{m}{A} = \frac{p_c}{\sqrt{R \cdot T_c}} \cdot \sqrt{\frac{2\gamma}{\gamma - 1} \cdot \left(\frac{p}{p_c}\right)^{\left(\frac{2}{\gamma}\right)} \left(1 - \left(\frac{p}{p_c}\right)^{\left(\frac{\gamma-1}{\gamma}\right)}\right)} \tag{5-3}$$

Figure 5 shows the dimensionless mass flow per unit area as a function of the pressure ratio. As can be seen, m/A becomes zero for two values of p: p = 0 and p = p_c and reaches an extreme value somewhere for 0 < p < p_c.

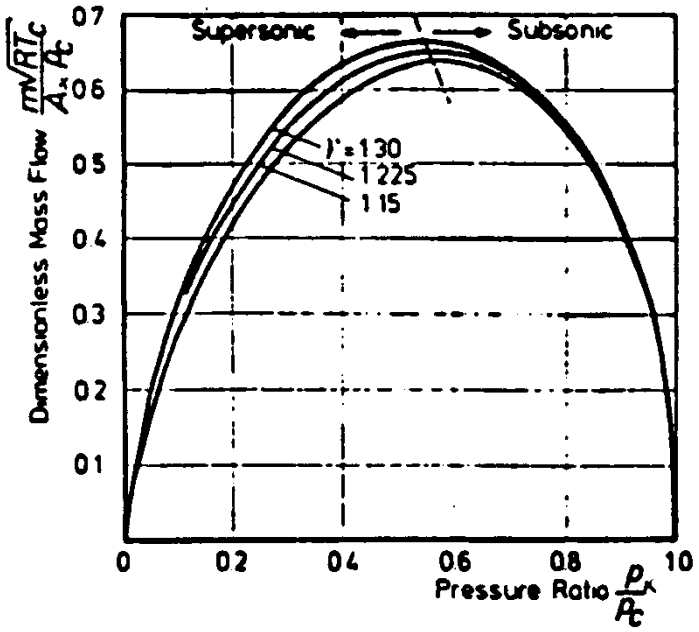

Figure 5: Dimensionless mass flow per unit area versus pressure ratio for a convergent-divergent nozzle [Timnat and van der Laan].

This extreme value is a maximum and can be found by differentiating (5-3) with respect to p/p_c and setting the result equal to zero. The result of this derivation is:

$$\left(\frac{p_t}{p_c}\right)_{cr} = \left(\frac{2}{\gamma + 1}\right)^{\left(\frac{\gamma}{\gamma-1}\right)} \tag{5-4}$$

As m is constant and A gets its minimal value at the throat, the maximum value of m/A is found in the throat. Therefore, the pressure p in (5-4) is the pressure in the throat and the pressure ratio is the critical pressure ratio. By applying Poisson's equations, we can also find the critical temperature ratio and the critical density ratio.

$$\left(\frac{T_t}{T_c}\right)_{cr} = \left(\frac{2}{\gamma + 1}\right) \tag{5-5}$$

$$\left(\frac{\rho_t}{\rho_c}\right)_{cr} = \left(\frac{2}{\gamma+1}\right)^{\left(\frac{1}{\gamma-1}\right)} \tag{5-6}$$

Substitution of (5-5) into the velocity equation yields:

$$U_t = \sqrt{2\cdot\frac{\gamma}{\gamma-1}\cdot R\cdot T_t\cdot\left(\frac{T_c}{T_t}-1\right)} = \sqrt{2\cdot\frac{\gamma}{\gamma-1}\cdot R\cdot T_t\cdot\left(\frac{\gamma+1}{2}-1\right)}$$
$$U_t = \sqrt{\frac{2\gamma}{\gamma-1}\cdot R\cdot T_t\cdot\left(\frac{\gamma-1}{2}\right)} = \sqrt{\gamma\cdot R\cdot T_t} = a_t \tag{5-7}$$

So, the throat velocity U_t is always equal to the local acoustic velocity for nozzles in which critical conditions prevail. Care must be taken that the chamber pressure never drops below the value at which the critical pressure ratio given in (5-4) cannot be reached. The velocity of sound is equal to the velocity of propagation of a pressure wave within the medium, sound being essentially a type of pressure wave. If therefore sonic velocity is reached at any point within a steady flow system, it is impossible for a pressure disturbance to travel upstream past the location of sonic or supersonic velocity. Any disturbance of the flow downstream of the nozzle throat section will have no influence on the flow at the throat section or upstream of the throat section, provided that this disturbance does not raise the downstream pressure above its critical value. Changing the exit pressure has no effect on the throat velocity or the flow rate in the nozzle. (It should be noted, however, that propagation of disturbances upstream through the subsonic part of the boundary layer is still possible).

6 Critical Mass Flow

We will now derive an expression for the mass flow through the nozzle at which the nozzle flow becomes supersonic.

The continuity equation applied at the throat is given by:

$$m = \rho_t\cdot A_t\cdot U_t = \rho_t\cdot A_t\cdot a_t = \rho_c\cdot a_c\cdot\left(\frac{a_t}{a_c}\right)\cdot\left(\frac{\rho_t}{\rho_c}\right)\cdot A_t \tag{6-1}$$

Using Poisson's equation and the critical conditions, we get:

$$\left(\frac{\rho_t}{\rho_c}\right) = \left(\frac{T_t}{T_c}\right)^{\left(\frac{1}{\gamma-1}\right)} = \left(\frac{2}{\gamma+1}\right)^{\left(\frac{1}{\gamma-1}\right)} \tag{6-2}$$

And:

$$\left(\frac{a_t}{a_c}\right) = \left(\frac{T_t}{T_c}\right)^{\left(\frac{1}{2}\right)} = \left(\frac{2}{\gamma+1}\right)^{\left(\frac{1}{2}\right)} \tag{6-3}$$

Substitution of (6-2) and (6-3) into (6-1) yields:

$$m = \rho_c \cdot a_c \cdot A_t \cdot \left(\frac{2}{\gamma+1}\right)^{\left(\frac{\gamma+1}{2(\gamma-1)}\right)}$$

$$m = \frac{p_c}{R \cdot T_c} \cdot \sqrt{\gamma \cdot R \cdot T_c} \cdot A_t \cdot \left(\frac{2}{\gamma+1}\right)^{\left(\frac{\gamma+1}{2(\gamma-1)}\right)} \quad (6\text{-}4)$$

With use of the "Vandenkerckhove function" defined as:

$$\Gamma = \sqrt{\gamma} \cdot \left(\frac{2}{\gamma+1}\right)^{\left(\frac{\gamma+1}{2(\gamma-1)}\right)} \quad (6\text{-}5)$$

We get:

$$m = \frac{\Gamma \cdot p_c \cdot A_t}{\sqrt{R \cdot T_c}} \quad (6\text{-}6)$$

We find that the mass flow through the nozzle is proportional to the chamber pressure and the area of the sonic surface (throat) and inversely proportional to the square root of the chamber temperature.

Useful values of the Vandenkerckhove function are given in the next table.

Table 1: Useful values of Vandenkerckhove function

γ	Γ	γ	Γ
1.05	0.6177	1.31	0.6691
1.10	0.6284	1.32	0.6709
1.11	0.6304	1.33	0.6726
1.12	0.6325	1.34	0.6744
1.13	0.6346	1.35	0.6761
1.14	0.6366	1.36	0.6779
1.15	0.6386	1.37	0.6796
1.16	0.6406	1.38	0.6813
1.17	0.6426	1.39	0.6830
1.18	0.6446	1.40	0.6847
1.19	0.6466	1.41	0.6864
1.20	0.6485	1.42	0.6881
1.21	0.6505	1.43	0.6897
1.22	0.6524	1.44	0.6914
1.23	0.6543	1.45	0.6930
1.24	0.6562	1.50	0.7011
1.25	0.6581	1.55	0.7089
1.26	0.6599	1.60	0.7164
1.27	0.6618	1.65	0.7238
1.28	0.6636		
1.29	0.6654		
1.30	0.6673		

7 Nozzle Area Ratio

The nozzle has two important areas:

1. Exit area A_e
2. Throat area A_t

We will derive a relation between the local pressure ratio p/p_c and the expansion ratio A/A_t. As this will be a general expression, the substitution of $A = A_e$ and $p = p_e$ gives the relation between A_e/A_t and p_e/p_t. From (6-6) we know that the mass flow through the nozzle is proportional to the chamber pressure p_c, and the throat area and inversely proportional to the square root of the combustion chamber temperature T_c. Substitution into the expression for the mass flow per unit area given by:

$$\frac{m}{A} = \frac{p_c}{\sqrt{R \cdot T_c}} \cdot \sqrt{\frac{2\gamma}{\gamma - 1} \cdot \left(\frac{p}{p_c}\right)^{\left(\frac{2}{\gamma}\right)} \left(1 - \left(\frac{p}{p_c}\right)^{\left(\frac{\gamma-1}{\gamma}\right)}\right)} \tag{7-1}$$

Yields:

$$\frac{A}{A_t} = \frac{\Gamma}{\sqrt{\frac{2\gamma}{\gamma - 1} \cdot \left(\frac{p}{p_c}\right)^{\left(\frac{2}{\gamma}\right)} \left(1 - \left(\frac{p}{p_c}\right)^{\left(\frac{\gamma-1}{\gamma}\right)}\right)}} \tag{7-2}$$

When we take $A = A_e$ and $p = p_e$, (7-2) changes into:

$$\frac{A_e}{A_t} = \frac{\Gamma}{\sqrt{\frac{2\gamma}{\gamma - 1} \cdot \left(\frac{p_e}{p_c}\right)^{\left(\frac{2}{\gamma}\right)} \left(1 - \left(\frac{p_e}{p_c}\right)^{\left(\frac{\gamma-1}{\gamma}\right)}\right)}} \tag{7-3}$$

The variation of area ratio with pressure ratio is illustrated in Figure 6.

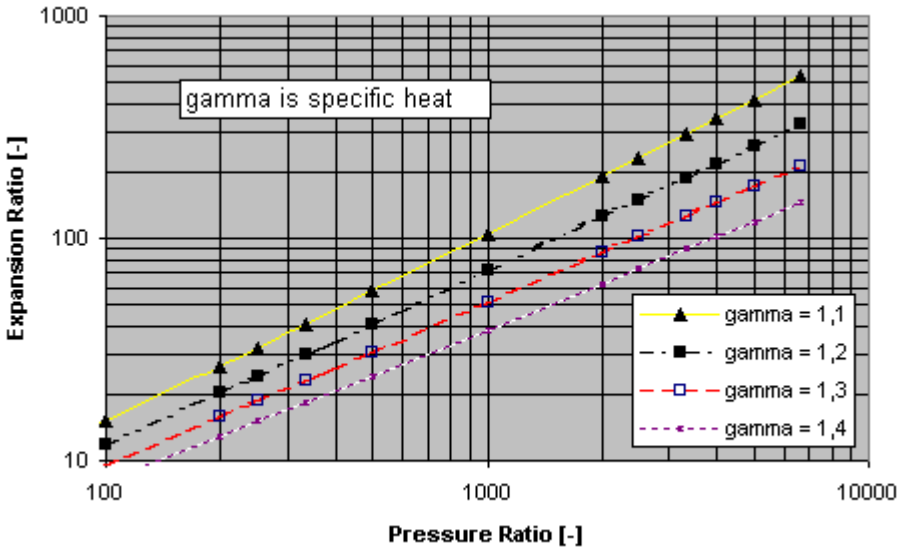

Figure 6: Variation of area ratio with pressure ratio.

The figure shows that to obtain a high-pressure ratio (or a large pressure drop) we should strive for a nozzle with a high expansion ratio.

It is instructive to show that this equation can also be derived in a different way. When we use the continuity equation applied at the throat and at the exit area, we find:

$$\rho_e \cdot A_e \cdot U_e = \rho_t \cdot A_t \cdot U_t \tag{7-4}$$

Reworking gives:

$$\frac{A_e}{A_t} = \frac{\rho_t \cdot U_t}{\rho_e \cdot U_e} = \frac{\rho_t}{\rho_c} \cdot \frac{a_t}{a_c} \cdot \frac{\rho_c}{\rho_e} \cdot \frac{a_c}{U_e} \tag{7-5}$$

Here U_t is a_t is used.

With the critical density and temperature ratio:

$$\frac{\rho_t}{\rho_c} = \left(\frac{2}{\gamma+1}\right)^{\left(\frac{1}{\gamma-1}\right)} \quad \text{and} \quad \frac{a_t}{a_c} = \sqrt{\frac{T_t}{T_c}} = \left(\frac{2}{\gamma+1}\right)^{\left(\frac{1}{2}\right)} \tag{7-6}$$

And with the use of the Poisson equation, we get:

$$\frac{A_e}{A_t} = \left(\frac{2}{\gamma+1}\right)^{\left(\frac{1}{\gamma-1}\right)} \cdot \left(\frac{2}{\gamma+1}\right)^{\left(\frac{1}{2}\right)} \cdot \left(\frac{p_c}{p_e}\right)^{\left(\frac{1}{\gamma}\right)} \cdot \frac{\sqrt{\gamma \cdot R \cdot T_c}}{U_e} \tag{7-7}$$

Using the definition of Γ and the expression (3-14) we again find (7-3).

8 Characteristic Parameters

In the preceding sections, we have shown the influence of such factors as temperature, molar mass of the gases and expansion ratio on the specific impulse. In this section we introduce two characteristic parameters, the thrust coefficient C_F and characteristic velocity c* (pronounced cee-star), that allow us to determine the contribution of the gas expansion in the nozzle and the energetic content of the expellant on the specific impulse separately, according to:

$$I_{sp} = C_F \cdot c^* / g_o \tag{8-1}$$

8.1 Thrust Coefficient

The thrust coefficient determines the amplification of the thrust due to the gas expansion in the rocket nozzle as compared to the thrust that would be exerted if the chamber pressure acted over the throat area only, and if there were no chamber flow:

$$C_F = \frac{F}{p_c \cdot A_t} \tag{8-2}$$

With the earlier derived thrust equation and substitution of the expression for the critical mass flow (6-6) and the flow velocity (3-14), we get:

$$C_F = \Gamma \cdot \sqrt{\frac{2\gamma}{\gamma-1} \cdot \left(1 - \left(\frac{p_e}{p_c}\right)^{\left(\frac{\gamma-1}{\gamma}\right)}\right)} + \left(\frac{p_e}{p_c} - \frac{p_a}{p_c}\right) \cdot \frac{A_e}{A_t} \qquad (8\text{-}3)$$

In case of ideal expansion, i.e. $p_e = p_a$, the thrust coefficient reduces to:

$$C_F{}^o = \Gamma \cdot \sqrt{\frac{2\gamma}{\gamma-1} \cdot \left(1 - \left(\frac{p_e}{p_c}\right)^{\left(\frac{\gamma-1}{\gamma}\right)}\right)} \qquad (8\text{-}4)$$

$C_F{}^o$ is called the "characteristic thrust coefficient". It mainly depends on the pressure ratio, i.e. the area ratio. In Table 2 the variation of characteristic thrust coefficient with pressure ratio is tabulated.

Table 2: Variation of characteristic thrust coefficient with pressure ratio and specific heat ratio.

	γ = 1.15	γ = 1.20	γ = 1.25	γ = 1.30	γ = 1.35	γ = 1.40
p_e/p_c	$C_F{}^o$	$C_F{}^o$	$C_F{}^o$	$C_F{}^o$	$C_F{}^o$	$C_F{}^o$
0.5000	0.7353	0.7421	0.7488	0.7552	0.7616	0.7679
0.2500	1.0171	1.0204	1.0241	1.0279	1.0319	1.0360
0.1000	1.2738	1.2683	1.2642	1.2612	1.2591	1.2578
0.0500	1.4223	1.4084	1.3972	1.3877	1.3801	1.3739
0.0300	1.5151	1.4946	1.4775	1.4631	1.4512	1.4411
0.0200	1.5810	1.5549	1.5331	1.5147	1.4992	1.4862
0.0100	1.6805	1.6445	1.6145	1.5892	1.5678	1.5497
0.0050	1.7665	1.7205	1.6823	1.6500	1.6229	1.5999
0.0020	1.8637	1.8043	1.7554	1.7144	1.6801	1.6511
0.0010	1.9271	1.8577	1.8009	1.7536	1.7142	1.6811
0.0005	1.9833	1.9040	1.8395	1.7863	1.7422	1.7053
0.0003	2.0206	1.9342	1.8644	1.8070	1.7596	1.7201
0.0001	2.0911	1.9899	1.9091	1.8434	1.7897	1.7452
0.0000	2.5008	2.2466	2.0811	1.9644	1.8780	1.8116

From this table, we learn that the characteristic thrust coefficient increases with pressure ratio and is maximum for $p_e = 0$ (expansion to vacuum).

Using the expression for the characteristic thrust coefficient, the thrust coefficient can now be written as the sum of the former and a term which depends on the ambient pressure, chamber pressure and the pressure ratio p_e/p_c. (It is shown later that A_e/A_t depends on p_e/p_c only).

$$C_F = C_F{}^o + \left(\frac{p_e}{p_c} - \frac{p_a}{p_c}\right) \cdot \frac{A_e}{A_t} \qquad (8\text{-}5)$$

In Figure 7 thrust coefficient C_F and characteristic thrust coefficient $C_F{}^o$ (line of ideal expansion) are plotted versus the expansion ratio A_e/A_t.

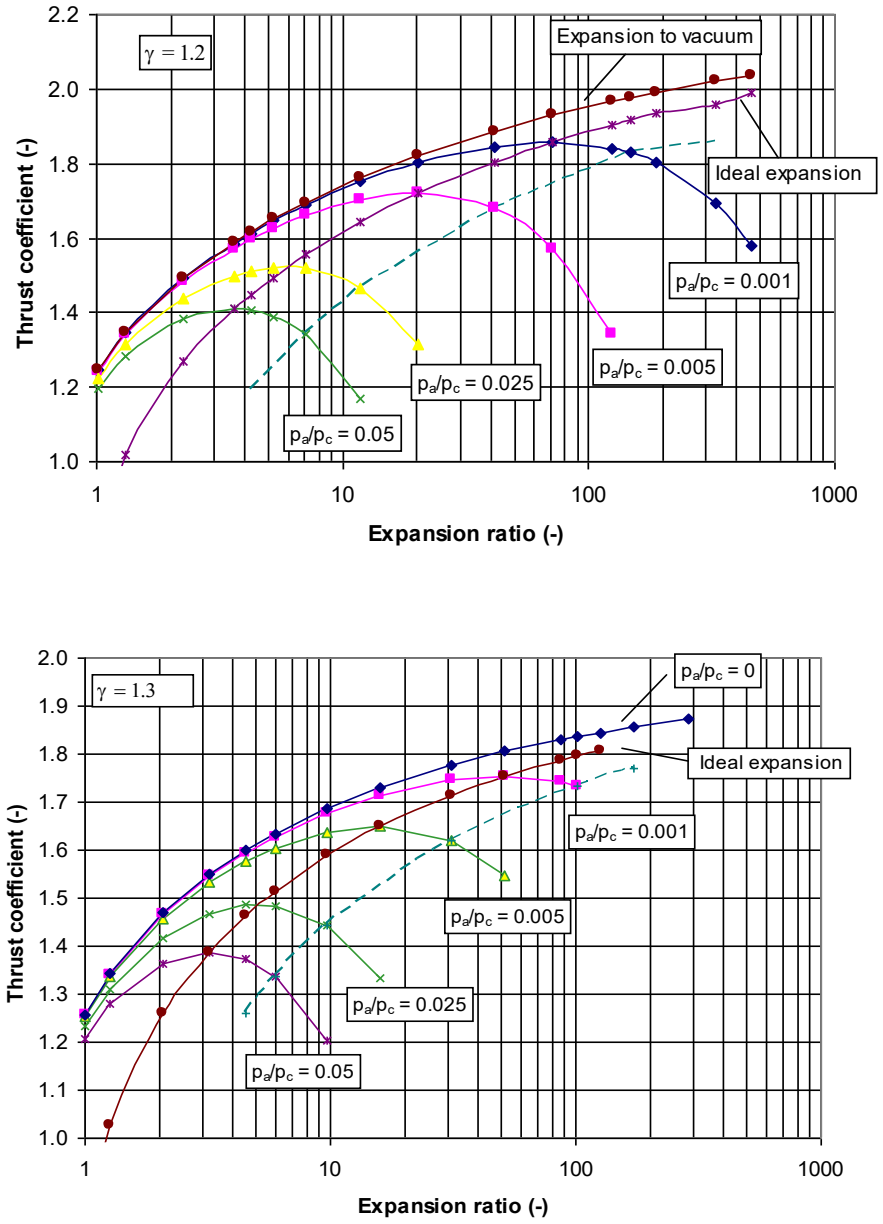

Figure 7: Thrust coefficient versus expansion ratio for various ambient to chamber pressure (p_e/p_a) ratios for two different values of specific heat ratio.

The figure shows that for a given ambient pressure to chamber pressure ratio, the thrust coefficient, and hence also the thrust, is maximum in case $p_e = p_a$. In the figure we have also indicated a dotted line which indicates above what expansion ratio separation starts to occur, see for further information on flow separation, the next chapter ("Nozzle design"). According to [Sutton], after flow separation takes place, thrust and thrust coefficient do not increase with further increasing area ratio.

Combining the definition of the characteristic thrust coefficient with (7-3) yields for the area ratio:

$$\frac{A_e}{A_t} = \frac{\Gamma^2}{\left(\frac{p_e}{p_c}\right)^{\left(\frac{1}{\gamma}\right)} \cdot C_F{}^o} \tag{8-6}$$

This relationship is usually expressed in tables or in a graphical way.

The maximum thrust coefficient $(C_F)_{max}$ can be found by taking the derivative of (8-3) with respect to the pressure ratio and setting the result equal to zero:

$$\frac{dC_F}{d\left(p_e / p_c\right)} = 0 \tag{8-7}$$

As this is rather cumbersome and the result is the same as for the derivation of maximum thrust as in the previous chapter, we will leave this for the reader to explore for himself.

8.2 Characteristic Velocity

Earlier, we showed that the mass flow through the nozzle is given by (6-6). Now we define the characteristic velocity c*:

$$c^* = \frac{1}{\Gamma} \cdot \sqrt{R \cdot T_c} \tag{8-8}$$

This equation shows c* to be dependent on the temperature T_c to which the expelled gases are heated, the mean molecular weight M ($R = R_A/M$) of the expelled gases and the ratio γ between the specific heat capacities c_p and c_v. So, c* is a property that reflects the energy level of the propellants available for propulsion purposes. The characteristic velocity, as distinct from the specific impulse, is independent of the pressure ratio.

Introducing the above expression for the characteristic velocity into (6-6) leads to a simple equation for the mass flow:

$$m = \frac{p_c \cdot A_t}{c^*} \tag{8-9}$$

Now c* is also given by:

$$c^* = \frac{p_c \cdot A_t}{m} \tag{8-10}$$

As all variables in the right part of (8-10) can be measured in a static test, the experimental value of c* can be determined. It can be compared with the theoretical (or ideal) value of c* calculated with (8-8). The ratio of these two values is an indication of the efficiency of the combustion process. It can also be shown that the characteristic velocity is proportional to the limiting velocity U_L as defined in (3-15):

$$c^* = \frac{U_L}{\Gamma \cdot \sqrt{\frac{2\gamma}{\gamma - 1}}} \tag{8-11}$$

8.3 Relation between specific impulse and characteristic parameters

Combining the definition of C_F in (8-2) and c* given in (8-10) yields:

$$F = m \cdot C_F \cdot c^* \tag{8-12}$$

Now the specific impulse or equivalent velocity can be written as:

$$I_{sp} = U_{eq} / g_o = C_F \cdot c^* / g_o \tag{8-13}$$

In both the equivalent velocity and in C_F, the dependence on the ambient pressure is considered.

For the adapted nozzle holds:

$$I_{sp} = U_e / g_o = C_F^{\,o} \cdot c^* / g_o \tag{8-14}$$

As c* only depends on the propellant, it is a constant for a given motor. The dependence of exhaust velocity on pressure ratio is known from (3-13).

9 Quality Factors

The real performance (thrust and specific impulse) of a thermal rocket motor generally differs from the ideal performance predicted using ideal rocket theory (IRT). This is mainly attributed to the ideal rocket motor assumptions having only limited validity. For instance, in a real rocket motor we also must consider heat transfer from or to the expanding gas flow in the motor, non-ideal gas behavior, heterogeneous[7] fluid flow, non-axial flow, flow separation, friction, shock waves, chemical reactions, etc.

To bridge the gap between the performance as follows from ideal rocket theory and the real performance one may introduce corrections factors. For this, we may write the thrust of an ideal rocket motor using (8-12). The same relation can also be used for the thrust of a real rocket motor; however, we should realize that the value of mass flow rate, thrust coefficient and characteristic velocity of the real motor may be quite different from those of the ideal motor. We write:

$$F_{id} = m_{id} \times C_{F,id} \times c^*_{id} = m_{id} \times I_{sp,\,id} \tag{9-1}$$

And:

$$F_{real} = m_{real} \times C_{F,\,real} \times c^*_{real} = m_{real} \times I_{sp,\,real} \tag{9-2}$$

Here we use the subscripts “id” and “real” to denote ideal and real rocket motor values, respectively.

Using the above relations, we can now define 5 quality (correction) factors (generally denoted with ξ and expressed as Xi) that tell how well a real rocket motor compares to an ideal rocket motor and/or that can be used to estimate real values from ideal rocket performances for similar rocket engines. We obtain:

$$F_{real} = \xi_F F_{id} = C_d\, m_{id} \times \xi_n C_{F,id} \times \xi_c c^*_{id} = C_d\, m_{id} \times \xi_s\, I_{sp,id} \tag{9-3}$$

[7] Heterogeneous fluid is a fluid within which the density varies from point to point.

The quality[8] factors (or correction factors) are defined as:

- Motor or thrust quality factor:

$$\xi_F = \frac{F_{real}}{F_{id}} = C_d \xi_n \xi_c \tag{9-4}$$

- Discharge coefficient[9]:

$$C_d = \frac{m_{real}}{m_{id}} \tag{9-5}$$

- Nozzle flow quality:

$$\xi_n = \frac{C_{F,\,real}}{C_{F,\,id}} \tag{9-6}$$

- Combustion or heating quality[10,9]:

$$\xi_c = \frac{c^*_{real}}{c^*_{id}} \tag{9-7}$$

- I_{sp} or propellant consumption quality

$$\xi_s = \frac{I_{sp,\,real}}{I_{sp,\,id}} = \xi_n \, \xi_c \tag{9-8}$$

So, it essentially comes down to determining the above defined quality factors to learn how a real rocket motor compares to an ideal one and/or how to correct ideal rocket performance to obtain real performance of a similar[11] engine. This will be the subject of the remainder of this section. Two methods will be distinguished, being 1) from experimental data or 2) from theoretical or simulated data produced using more complex theory than IRT.

1) <u>From experimental data</u>

The most obvious way is by obtaining experimental data on thrust and mass flow rate at various working pressures of the engine. For each working pressure then the quality factors can be obtained, and it can be determined whether real performance is close or not. If not, corrective actions (design changes) may be considered to the motor as a whole or its main components to improve quality.

---

[8] Quality factor sometimes is referred to as efficiency. In this work though we prefer the use of quality factor as efficiency is more commonly related to energy usage. It also prevents for any confusion between thrust quality and thrust efficiency (earlier defined as jet power/input power).

[9] The ratio of real mass flow rate to ideal mass flow rate depends on both discharge coefficient and combustion efficiency, according to:

$$\frac{m_{real}}{m_{id}} = \frac{C_d}{\xi_c}$$

So when using the discharge coefficient as defined in (9-5), this is under the condition that combustion efficiency is unity and when using (9-7), this is under the condition that discharge coefficient is unity.

[10] Combustion quality is used in relation to chemical rocket motors, whereas heating quality is preferred in case of non-chemical thermal rocket motors.

[11] What is meant by a “similar” engine is still to be defined. One way of defining similarity is by stating that a similar engine has identical quality under similar operating conditions as the engine from which the quality factors have been obtained. This is not a very scientific definition, but it indicates a way of proving similarity.

Two approaches are commonly used depending on whether the engine is operating at a high throat Reynolds number (Re > 100,000)[12] or at a low throat Reynolds number (Re < 22,000). At intermediate Reynolds numbers, it depends on the value of the discharge coefficient whether one opts for the high or low Reynolds number approach. Both the high and low Reynolds number approach will be discussed hereafter.

Quality factors for high throat Reynolds number rocket motors

At high throat Reynolds number, the flow in the rocket motor is generally highly turbulent with limited friction effects. Under these conditions, we generally find that the experimental and ideal (from IRT) mass flow rate differ less than 1-2%, see for instance the work of [Szaniszlo]. Under these conditions, it is usually assumed that the actual and theoretical mass flow rates are identical, meaning the discharge coefficient equals unity[13]:

$$m_{real} = m_{id} = m \tag{9-9}$$

In that case, we obtain:

$$F_{real} = \xi_F F_{id} = m \times \xi_n C_{F,id} \times \xi_c c^*_{id} = m \times \xi_{sp} I_{sp,id} = \xi_s m I_{sp,id} \tag{9-10}$$

Rearranging above relation gives:

$$\xi_F F_{id} = \xi_n \xi_c \left(m C_{F,id} c^*_{id}\right) = \xi_s m I_{sp,id} \tag{9-11}$$

From this relation we find for rocket motors at high throat Reynolds number that:

$$\xi_F = \xi_s = \xi_n \xi_c \tag{9-12}$$

It follows that for an engine operating at high throat Reynolds number trust quality equals I_{sp} quality. Both in turn relate to the combustion quality and nozzle quality.

For large rocket motors the quality factors can now be determined from measuring (real) thrust and mass flow rate and pressure, provided that for this motor information is available on the nozzle geometry only using the earlier definition of c* and/or thrust coefficient. We use (9-6), where $C_{F,real}$ is obtained from:

$$C_{F,real} = \frac{F_{real}}{p_c A_t} \tag{9-13}$$

And $C_{F,id}$ is obtained from relation (8-3).

Combustion quality may be determined from (9-7), where:

(9-14)

[12] Re is defined here as.

$$\mathrm{Re} = \frac{\rho \cdot a \cdot D}{\mu} = \frac{4 \cdot m}{\pi \cdot \mu \cdot D}$$

With a being the velocity of sound, μ the dynamic viscosity of the expanding medium, and D the nozzle diameter all taken at the nozzle throat.

[13] [Sutton] has noted that, for high Reynolds number chemical rocket motors, it is quite possible to find a discharge coefficient higher than 1 (up to about 1.15). However, this is not because of a blocking effect in the nozzle, but because of a reduced combustion quality, as in that case, the actual mass flow rate must be higher than the theoretical mass flow rate to realize a given combustion chamber pressure. [Ahmad] in 2001, performed CFD analysis to compute effective nozzle discharge coefficients for subscale sharp-edged converging/diverging nozzles at moderate (but not low) throat Reynolds number for NASA. Computed discharge coefficients ranged from 0.88 to 0.97.

And theoretical value for c* is determined using (8-8).

Typical ranges reported for the quality factors of high Reynold number chemical rocket motors have been taken from the work of [Sutton] and [Huzel] and are given in next table.

Table 3: Typical value range for quality factors of high Reynolds number chemical rocket motors (discharge coefficient is assumed equal to 1)

	[Sutton]	[Huzel]
Nozzle quality	0.92-0.96	0.92-1.00
Combustion quality	0.85-0.98	0.87-1.03
Motor (or I_{sp}) quality	0.8-0.9	0.85-0.98

The table shows that all qualities are close to 1, indicating that real performances are close to ideal performances, but not exactly equal. The table also shows that in practice, there is a range of values that is considered reasonable. In general, when a value is obtained on the low side, the designer may decide to improve the design of the rocket motor. For instance, low motor quality may be because of low nozzle quality or low combustion quality. In turn, low nozzle quality may be due to flow separation, shocks and/or excessive boundary layer growth in the nozzle divergent. Improvements may then be sought by changing the nozzle design, see later. On the other hand, a low combustion quality indicates the occurrence of rough combustion and/or unstable conditions in the motor that may require modifications in chamber pressure, the injector design and/or the combustion chamber [Barrère].

The table also shows there is a difference in the values reported by Sutton and Huzel. The reason for this is not given, but it is considered that this is due to differences in the calculation of the properties of the hot gas in the combustion chamber (frozen flow conditions or chemical equilibrium or somewhere in between, see chapter on chemistry). Another reason may be because the types of engines (solid, liquid, hybrids) used for determining the quality factors differ.

Quality factors for low throat Reynolds number rocket motors

At low throat Reynolds numbers (Re < 100,000), the flow in the rocket motor tends to be highly laminar leading to a thick boundary layer in the nozzle throat, which causes (partial) flow blockage. Because of this blocking effect the real mass flow rate may be substantially lower than for an ideal rocket motor and the discharge coefficient can no longer be assumed to equal unity.

Following [Sheshagiri] the discharge coefficient is written as:

$$C_d = C_\rho C_v C_A \tag{9-15}$$

Where C_ρ, C_v and C_A are referred to as the density coefficient, the velocity coefficient and the area contraction coefficient, respectively. The first two can be combined in a mass flux coefficient given by the effective mass flux (mass flow per unit of cross-sectional area) divided by the mass flux as follows from IRT:

$$C_{\rho v} = \frac{(\rho v)_{eff}}{(\rho v)_{id}} \tag{9-16}$$

In most rocket motors, this mass flux coefficient will not be appreciably different from unity except in nozzles with a sharp nozzle throat region (see chapter on nozzle design), or in nozzles where real gas effects, like compressibility and specific heat strongly dependent on temperature, cannot be neglected or when considering very high temperature jets in which chemical changes such as dissociation and recombination occur (see later chapter on chemistry).

The area contraction coefficient (also simply referred to as area coefficient) gives the reduction of the effective flow area with respect to the geometric one (perpendicular to the flow), and is calculated as:

$$C_A = \frac{A_{t,\,eff}}{A_t} \tag{9-17}$$

This part of the relation is primarily because of the blocking effect that results from a boundary layer. With decreasing Reynolds number, the reduction of the effective area increases.

For low throat Reynolds rocket motors, it is mostly the area coefficient that is quite different from 1. Hence at low Reynolds number also the discharge coefficient can differ significantly from 1. In [Johnson], results are shown for cold gas flow through a critical nozzle over a throat Reynolds number[14] range of 2,000-22,000 for Hydrogen, Nitrogen, Carbon dioxide and Argon. Discharge factors reported are down to about 0.92 depending on the gas used and the throat Reynolds number. In [Grisnik] values of the discharge coefficient of supercritical nozzles are reported using unheated Hydrogen and Nitrogen as propellant for different nozzle shapes (conical, bell, trumpet, etc.). Values are reported for a throat Reynolds number range of 500 – 9,000. Results show discharge coefficients as low as 0.8 with lowest values reported at lowest throat Reynolds number. Results also indicate an effect of the nozzle shape with a maximum difference of 12%. It is noted that in the work of Grisnik, it is not clear whether the throat Reynolds number is based on the ideal mass flow rate or the real mass flow rate. Also, it is unclear whether Grisnik uses the local dynamic viscosity or the dynamic viscosity at stagnation conditions. Next to Grisnik and Johnson, various other researchers have investigated the discharge coefficient in relation to a range of variables including nozzle cross-sectional shape, roughness, etc. This is left for further study when needed.

In the following text, we will discuss how to determine the quality factors for low-Reynolds number motors.

The discharge coefficient of a low (throat) Reynolds motor can be determined based on information on the ideal mass flow rate and the real mass flow rate. Next, assuming that the effect of the area coefficient is dominant in the determination of the discharge coefficient and hence setting the mass flux coefficient equal to 1, we obtain:

$$C_d = C_{\rho v} C_A \overset{C_{\rho v} = 1}{\Longrightarrow} C_d = C_A = \frac{A_{t,eff}}{A_t} \tag{9-18}$$

Above relation shows that by determining the discharge coefficient one also obtains a relation between the (geometric) throat area and the effective throat area.

The nozzle quality now is again calculated using the expression (9-6). However, some modifications are necessary when calculating the real and ideal values of the thrust coefficient. The real value is calculated from:

$$C_{F,real} = \frac{F_{real}}{p_c\, A_{t,real}} \overset{C_{\rho v}=1}{\Longrightarrow} C_{F,real} = \frac{F_{real}}{p_c\, A_{t,eff}} = \frac{F_{real}}{p_c\, C_d\, A_t} \tag{9-19}$$

And the theoretical value of the thrust coefficient is again determined using relation (8-3).

[14] Instead of using the dynamic viscosity in the nozzle throat, Johnson uses the dynamic viscosity at stagnation conditions.

Similarly, we can determine the c* quality using relation (9-7). The experimental value shall be determined using:

$$c^*_{real} = \frac{p_c A_{t,real}}{m_{real}} \overset{C_{pv}=1}{\Longrightarrow} c^*_{real} = \frac{p_c A_{t,eff}}{m_{real}} = \frac{p_c C_d A_t}{C_d m_{id}} = \frac{p_c A_t}{m_{id}} \tag{9-20}$$

The ideal characteristic velocity is again determined using relation (8-8). Comparing (9-20) and (8-8), it is clear that c* is not affected and hence c* quality is equal to unity.

Note that when Cd is set equal to unity essentially the same relations should be obtained as for the high-Reynolds number motors.

2) <u>From theoretical analysis using fundamental principles</u>

An alternative method to determine the necessary corrections factors is by using theoretical models that allow modelling the effects of non-ideal flow in a rocket motor based on fundamental principles. Such a method is considered appropriate in case validated models that allow determining these quality factors are available. Typical such theoretical models will be discussed in some later chapters in the present work. It should be realized though that an important drawback of using theory to estimate correction factors is that even advanced theoretical methods usually are based on several simplifying assumptions and without having access to actual data, it is difficult to know which assumptions can be realistically made.

10 Example

In the example presented in this section, we will use Ideal rocket Theory (IRT) to calculate various characteristics of the LR91-11 rocket motor, used in the 2nd stage of the Titan 4 space launch vehicle.

For this motor it is known from literature that it uses a liquid bipropellant consisting of nitrogen tetroxide (N_2O_4) and Aerozine 50[15] (A-50) at a (mass) mixture ratio of 1.86. Also known are a nozzle expansion ratio (ε) of 49.2, a diameter of the nozzle exit (D_e) of 1.6 m and a chamber pressure (p_c) of 5.93 MPa. Assuming chemical equilibrium (see a later chapter) gives the following properties of the hot gases produced in the chamber:

- Chamber temperature (T_c): 3,267K
- Specific heat ratio (γ) of the combustion gases: 1.2176
- Gas constant (R) of the combustion gases: 375.3 J/(kg·K).

We will describe the calculation of the following parameters based on the use of IRT:

- Altitude at which the nozzle reaches optimal expansion.
- Limit exhaust velocity, ideal exhaust velocity, and Mach number and temperature in nozzle exit.
- Nozzle throat diameter (d*), mass flow rate (m), and the ideal thrust (F) at the optimal altitude.

a) To determine the altitude at which the nozzle reaches optimum expansion, we first use the Saint Venant equation to determine the pressure ratio. With γ = 1.2176 and Γ = 0.652 follows:

$$\varepsilon = \frac{0.652}{\sqrt{\frac{2(1.2176)}{1.2176-1}\cdot\left(\frac{p_e}{p_c}\right)^{\left(\frac{2}{1.2176}\right)}\left(1-\left(\frac{p_e}{p_c}\right)^{\left(\frac{1.2176-1}{1.2176}\right)}\right)}}$$

[15] Aerozine 50 is a 50/50 mixture of hydrazine (N_2H_4) and unsymmetrical dimethyl hydrazine ($C_2H_8N_2$), also called UDMH.

This equation can be solved for p_e/p_c, by either a trial-and-error method (iterating) or a numerical method. It follows:

$$\frac{p_e}{p_c} = 1.49E-3 \text{ or } \frac{p_c}{p_e} = 670$$

We find two solutions, including a sub- and a supersonic one. Here we will use the supersonic one as it is considered that we are in the divergent part of the nozzle.

Using the pressure ratio and the given chamber pressure, we find for the pressure in the nozzle exit:

$$p_a = p_e = \frac{5.92 \times 10^6 \text{ Pa}}{670} = 8836 \text{ Pa} \quad \text{or} \quad 8.84 \text{ kPa}$$

According to the International Standard Atmosphere (ISA), an atmospheric pressure of 8.84 kPa corresponds with an altitude of about 16.9 km.

b) To determine the limit exhaust velocity and ideal exhaust velocity we use:

$$(v_e)_{\text{lim}} = \sqrt{\frac{2\gamma}{\gamma - 1} \cdot R \cdot T_c} = \sqrt{\frac{2(1.2176)}{1.2176 - 1} \cdot (375.3 J/kg - K)(3267 K)} = 3704 \ m/s$$

and:

$$v_e = (v_e)_{\text{lim}} \cdot \sqrt{\left[1 - \left(\frac{p_e}{p_c}\right)^{\left(\frac{\gamma-1}{\gamma}\right)}\right]} = (3704 \text{ m/s})(0.829) = 3071 \text{ m/s}$$

Where we have used the pressure ratio as calculated under (a).

Temperature in the nozzle exit is determined using Poisson. It follows:

$$\frac{T_e}{T_c} = \left(\frac{p_e}{p_c}\right)^{\frac{\gamma-1}{\gamma}} = 0.313 \text{ ; with } T_c = 3267\text{K, follows } T_e = 1023 \text{ K}$$

Mach number in the nozzle exit is determined using:

$$\frac{T_c}{T_e} = \frac{1}{0.313} = 3.195 = \left(1 + \frac{1.2176 - 1}{2} \cdot M_e^2\right)$$

It follows: Me = 4.49.

c) Nozzle throat diameter (d*) can be obtained from the area ratio and the exit diameter (D_e).

$$A_e = \frac{\pi d_e^2}{4} = \frac{\pi (1.6 \text{ m})^2}{4} = 2.011 \text{m}^2$$

$$A^* = \frac{A^*}{A_e} A_e = \frac{2.011 \text{m}^2}{49.0} = 0.041 \text{m}^2$$

$$d^* = \sqrt{\frac{4 A^*}{\pi}} = 0.228 \text{ m}$$

It follows for the mass flow rate (m):

$$m = \frac{\Gamma\, p_c\, A^*}{\sqrt{R\, T_c}}$$
$$= \frac{\left(5.93 \times 10^6 \text{ Pa} \right)\left(0.041 \text{m}^2 \right)\left(0.6518 \right)}{\sqrt{\left(375.3 \frac{\text{J}}{\text{kg·K}} \right)\left(3{,}267 \text{ K} \right)}} = 143.1 \frac{\text{kg}}{\text{s}}$$

Finally, the thrust can be calculated using:

$$F_T = m\, v_e + \left(p_e - p_a \right) A_e$$

For optimum expansion follows:

$$F_T = \left(143.1 \text{kg/s}\right)\left(3071.2\right)$$
$$F_T = 4.395 \times 10^5 \text{ N} \quad \text{or} \quad 439.5 \text{ kN}$$

We find that the LR91-11 motor according to IRT achieves a thrust of 439.5 kN at its optimal altitude of 16.9 km. At sea level, we obtain a thrust of 254 kN and in vacuum 457 kN.

Using the calculated values of thrust and the mass flow rate (143.1 kg/s) also the specific impulse can be determined. It follows:

- I_{sp} @ sea level: 180.7 s
- I_{sp} @ 16.9 km: 313.2 s
- I_{sp} @ vacuum: 325.8 s

It is now also possible to determine nozzle and combustion quality using actual thrust and specific impulse values for this engine (see e.g. Wikipedia). A warning though is at its place as the properties of the hot gas in the combustion chamber have been guessed and may be off from actual values. Still, the exercise is nice to perform.

11 Problems

1) The following data are given for an ideal rocket engine: Propellant mass flow rate m = 0.1 kg/s, chamber pressure p_c = 5 bar; chamber temperature T_c = 2500 K, molar mass M = 2 kg/kmol (Hydrogen gas), ideal gas specific heat ratio γ = 1.40, nozzle expansion area ratio ε = 100. Flow Mach number at nozzle inlet M_i = 0.2. Determine the following parameters at nozzle inlet, nozzle throat, nozzle location x characterised by A_x/A_t = 20, and nozzle exit:
   - Static pressures (p_i, p_t, p_x, and p_e).
   - Flow temperatures.
   - Flow velocities.
   - Flow Mach numbers.
   - Flow areas.

2) You are member of a team designing a thermal rocket engine with the following performances:
   - Vacuum thrust: 1000 kN
   - Vacuum specific impulse: 370 ± 2 sec.

The team is considering the use of liquid oxygen and kerosene as the propellant combination and has selected for this combination a combustion chamber pressure of 100 bar. Flame temperature, molar mass and specific heat ratio for the liquid oxygen and kerosene combination at this pressure are equal to 3264 K, 21, and 1.146, respectively. Under the assumption that the rocket motor behaves as an ideal rocket motor, you are asked to determine using ideal rocket motor theory:

- Thrust coefficient C_F.
- Nozzle throat area A_t.
- Nozzle exit area A_e.
- Nozzle geometric expansion (area) ratio ε.
- Nozzle pressure ratio p_c/p_e, and
- Nozzle exit pressure p_e.

3) You are designing a resistojet for use on board of the International Space Station (ISS). For this engine you intend to use carbon dioxide, a waste product on board of the ISS, as propellant to save propellant mass. The required thrust for this engine is 10 N. The following data are given: chamber pressure p_c = 20 bar; molar mass M = 44 kg/kmol (carbon-dioxide gas), ideal gas specific heat ratio γ = 1.181, nozzle expansion area ratio ε = 60, and vacuum specific impulse I_{sp} = 120 s. Determine for this engine using ideal rocket motor theory:
   - Thrust coefficient C_F.
   - Required c*.
   - Required chamber temperature T_c.
   - Required power input P_{in} in case the heating of the carbon dioxide takes place at constant pressure. You may assume a temperature independent specific heat at constant pressure of carbon dioxide c_p = 1234 J/kg/K and an initial temperature of the carbon dioxide of 300 K.

4) Assume a thrust chamber of an ideal rocket motor in which m = 193.6 kg/s; p_c = 68.9 bar; T_c = 3633 K; M = 22.67; γ = 1.20; and ε = 12. Determine the following:
   - Theoretical c*
   - Theoretical C_F at sea level and in space
   - Theoretical I_{sp} at sea level and in space
   - Actual c*, if c* correction factor is 0.97
   - Actual C_F at sea level and in space, if sea level C_F correction factor is 0.983
   - Actual specific impulse at sea level and in space

5) For the Vulcain 2 rocket engine, given in figure (successor to the HM-60 or Vulcain 1) the following data is obtained from web page [Wikipedia]:
   - Vacuum thrust: 1359 [kN]
   - Vacuum specific impulse: 429 [s]
   - Chamber pressure: 117.3 [bar]
   - Expansion ratio: 58.2
   - Nozzle exit diameter: 2.09 [m]
   - Hot gas temperature: 3553.9 [K]
   - Molar mass: 13.689 [kg/kmol]
   - Specific heat ratio: 1.1422

Figure 8: Vulcain 2 motor used on Ariane 5

Of the above data, the first 5 have been measured in practice. The remaining data have been determined theoretically.

Determine for this rocket engine:
   a) The combustion quality
   b) The nozzle quality
   c) The motor quality / velocity correction factor.

Literature

1) Ahmad, R.A., Discharge Coefficients and Heat Transfer for Axisymmetric Supersonic Nozzles, November 2001, in Heat Transfer Engineering 22(6):40-61, DOI: 10.1080/014576301317048424.

2) Laan F.H. van der, and Timnat Y.M., Chemical Rocket Propulsion, TU-Delft, Department of Aerospace Engineering, April 1985.

3) Barrère M., Jaumotte A., Fraeijs de Veubeke B., Vandenkerkchove J., Rocket Propulsion, Elsevier Publishing company, 1960.

4) Grisnik S.P., Smith, T.A. and Saltz, L.E., Experimental Study of LOW Reynolds Number Nozzles, NASA TM-89858, AIAA-87-0992, 1987.

5) Huzel K.K., and Huang D.H., Design of Liquid Propellant Rocket Engines, 2nd edition, NASA SP-125, 1971.

6) Johnson A.N., Espina P.I., Mattingly G.E., Wright J.D., and Merkle C.L., Numerical characterization of the discharge coefficient in critical nozzles, NCSL Symposium, session 4E, 1998.

7) Sheshagiri Hebbar K., Sridhara K. and Paranjpe P.A., Performance of Conical Jet Nozzles in Terms of Discharge Coefficient, J. of the Aeronautical Society of India, Vol. 22, No.1, February 1970.

8) Sutton G.P., Rocket Propulsion Elements, 9th edition, John Wiley & Sons Inc., 2017.

9) Szaniszlo A.J., Experimental and analytical sonic nozzle discharge coefficients for Reynolds numbers up to 8 x 10^6, NASA TN D-7848, January 1975.

Web pages

1. https://en.wikipedia.org/wiki/Vulcain.

Nozzle design

Contents

Nozzle design 67

Contents 67

Symbols 68

1 Introduction 69

2 Some types of nozzles 69

3 Nozzle shape selection 70

4 Nozzle profile 71

5 Nozzle length 73

6 Non-adapted nozzles 76

7 Effect of nozzle profile/shape on performance 78

8 Nozzle structure 90

9 Nozzle materials 92

Problems 93

References 94

For further study 95

Nozzle design framework

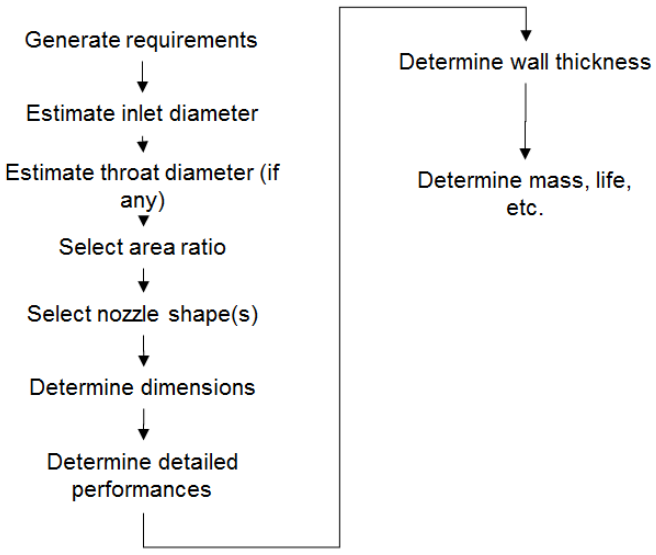

Symbols

The symbols are arranged alphabetically; Roman symbols first, followed by Greek. The used subscripts are given at the end of the list.

Roman

A	Area
C_F	Thrust coefficient
D	Diameter
F	Thrust
j	Safety factor
L	Length
m	Mass flow
R	Radius
r_u	Throat longitudinal radius
r_a	Nozzle contraction radius
p	Pressure
t	Wall thickness
T	Temperature
x, y, z	Coordinates in Cartesian system

Greek

α	Exit cone half angle (conical nozzle)
β	Contraction half angle
ε	Exit cone expansion ratio, loss factor
θ	Nozzle contour angle
σ	Stress

Subscripts

a	Atmospheric
c	Combustion chamber conditions
con	Convergent nozzle section
e	Refers to conditions in nozzle exit
t	Throat
$\perp$	Perpendicular

Acronyms

E-D	Expansion-deflection
TMC	Thrust magnitude control
TVC	Thrust vector control
SITVC	Secondary injection TVC
MITVC	Mechanical interference TVC
SRM	Solid rocket motor

1 Introduction

The nozzle is the component of a rocket that produces thrust. This is accomplished by converting the thermal energy of the hot chamber gases into kinetic energy and directing that energy along the nozzle's axis. Nozzles come in many different sizes and shapes and make up a large part (roughly 20-35%) of engine/motor mass, see e.g. annex I. In addition, they form an important source of catastrophic motor/engine failures, especially in case of complex nozzles that are to endure high heat loads.

According to ideal rocket motor theory, the performance of a nozzle is primarily determined by its expansion ratio. Using ideal rocket motor theory nozzle throat diameter and nozzle exit diameter can be determined. The diameter of the subsonic inlet side of the nozzle is usually determined by some key dimension, such as the volume needed for combustion, dimensions of a solid or hybrid propellant grain, dimensions of heater element, limitations to flow velocity, etc. Practice shows that ideal rocket theory is quite adequate for a first estimate within 92 - 100% of theory.

Various nozzle shapes exist that allow obtaining the required expansion ratio within a limited nozzle length. Depending on the detailed shape, the nozzle may be easy to manufacture, small size, low cost or have a slightly higher performance, e.g. due to limited flow divergence or improved altitude compensation capabilities. Hereafter, we will discuss nozzle design in more detail, thereby considering various nozzle types. We will discuss both selection of nozzle type as well as the design of the nozzle profile and the determination of the effect of nozzle shape on performance. Next the flow through a non-adapted nozzle is dealt with. Finally, we discuss typical nozzle materials and nozzle wall lay-outs. For an overview of the design framework see this chapter's title page. For more details on the structural design of rocket nozzles, see later in this work.

2 Some types of nozzles

The following three main nozzle types are distinguished (Figure 1):

Conical nozzles
The simplest nozzle is a conical nozzle. It has a conical divergent part, which is characterized by the cone half-angle α. It usually lies between 12 and 18 degrees.

Bell shaped or contoured nozzle
The geometry of the contoured nozzle closely resembles a bell shape, hence the designation bell nozzle. It has a high angle expansion section (30°-60°) right behind the throat; this is followed by a gradual reversal of nozzle contour slope so that at the nozzle exit the divergence angle is reduced. Depending on the divergence angle, we refer to the nozzle as ideal or truncated.

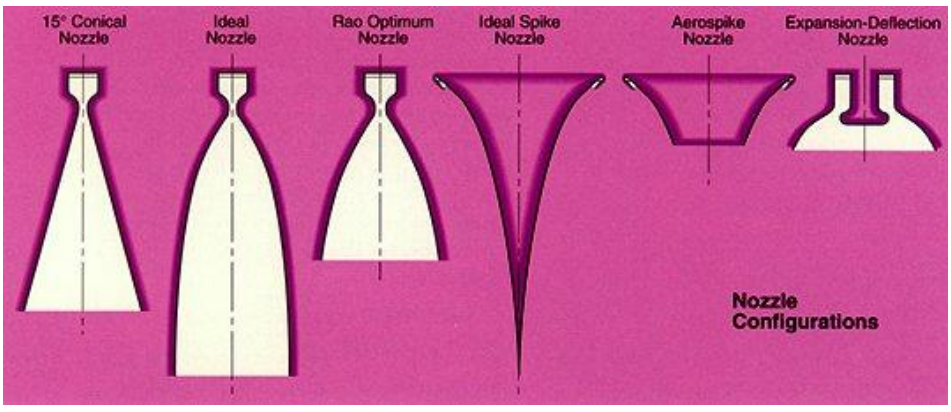

Figure 1: Typical nozzle shapes

Plug nozzles

A plug nozzle has a centre body “plug” which blocks the flow from what would be the centre portion of a “traditional” nozzle. The nozzle profile is like that of the bell or contoured nozzle. The exhaust gasses experience a relative fast expansion outside the throat, accompanied by expansion waves, followed by a redirection of the flow accompanied by compression effects. Two types of plug nozzles exist:

- Radial in-flow: The first major variety of plug nozzles is the radial in-flow type, exemplified by the spike nozzle. This nozzle type has received strong attention for application on aerospace planes like the US X33 vehicle, mainly because of its altitude compensating features.
- Radial out-flow nozzles: The second major variety of annular nozzle is the radial out-flow nozzle. This nozzle type was the subject of much research in the late 1960s and early 1970s. Example of this type is the expansion-deflection (E-D) nozzle.

Both types of plug nozzles have a jet geometry which is essentially open on one side, allowing for altitude compensation. Hence this type of nozzle is sometimes also referred to as "altitude-compensating" nozzle. Like the bell nozzle, plug nozzles are usually also of a truncated design.

3 Nozzle shape selection

The main task of the nozzle is to guide the expansion of the flow to a high exhaust velocity. Preferably, it should do so at minimum expense in terms of cost, mass, size, manufacturing time, etc.

Nozzle performance as we have seen earlier mainly depends on the nozzle area ratio. So the main issue is here to select the nozzle shape that offers lowest mass, shortest length, etc. for identical area ratio. In the remainder of this section, we will discuss the various nozzle shapes with regard to amongst others length, mass, complexity and cost.

The conical nozzle is the simplest nozzle type and offers ease of fabrication and hence low cost. Disadvantage is that losses due to flow divergence can be appreciable and that a relatively long nozzle is necessary to achieve a given area ratio. Long nozzles are heavy, take much space and cause friction and heat transfer to be relatively high.

Bell nozzles allow for a significant reduction in flow divergence (essentially down to zero divergence). For an ideal nozzle, however, this leads to an excessively long nozzle with the associated disadvantages. It is for this reason that bell nozzles are truncated. Of course, this is at the expense of a somewhat higher divergence angle at the nozzle exit (up to 8°) [Huzel].

The annular nozzle also allows for reduced flow divergence and reduced length compared to the conical nozzle. Compared to the bell nozzle, it offers in addition better altitude compensation, which leads to an increase in performance at lower altitudes for identical area ratio. Altitude compensation is dealt with in some more detail in the section titled “Non-adapted nozzles”. However, the special shape of the nozzle and especially the heat loads on the plug make this nozzle the most complex one and hence costly.

In Figure 2 a size comparison of optimal cone, bell, and radial nozzles is given for identical conditions (area ratio, thrust coefficient). The figure clearly shows that the conical nozzle shape leads to the longest nozzle. It also shows that the E-D nozzle allows for a major reduction in nozzle length, but at the expense of a substantial increase in diameter.

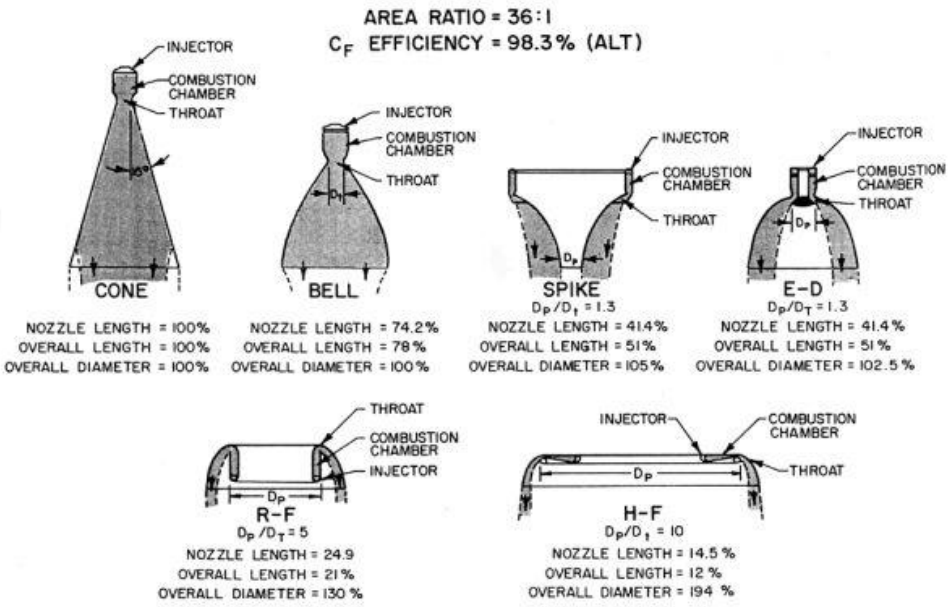

Figure 2: Size comparison of different nozzle shapes, E-D = expansion deflection, R-F = return flow, and H-F = horizontal flow [Huzel and Huang, 1967]

In practice, we find that conical nozzles are mostly used on most military rockets and on small space rocket motors. Bell nozzles are used in case high performance in terms of specific impulse is of utmost importance. Typical applications are the Space Shuttle Main Engine, Ariane 5 Vulcain engine, Delta 4 RS68 engine, and Atlas RD180 engine. Plug nozzles are the least employed of those discussed due to their enormous complexity. Interest in plug nozzles is mostly for use on aerospace planes, where altitude compensation is a premium. Figure 3 shows some typical nozzles considered.

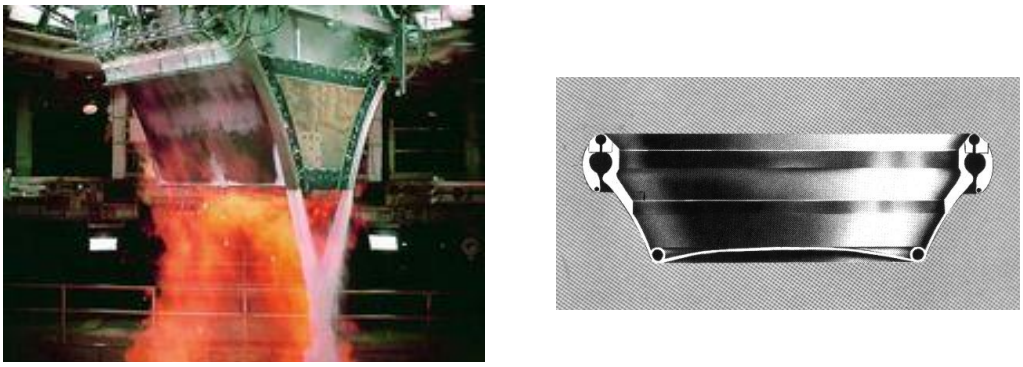

Figure 3: Linear aerospike (left) and annular aerospike nozzle

The Russian RD-0126/Yastreb engine is one of the first engines equipped with an E-D nozzle. The first test was conducted in August 1998. The engine can deliver 39.24-kN and a specific impulse of 476 seconds while burning liquid oxygen and hydrogen. So far, no other applications are known.

4 Nozzle profile

4.1 Profile of nozzle contraction

The design of the convergent part of the nozzle is mostly aimed at reducing pressure losses due to the flow contraction, see section on liquid injection. To limit the pressure loss, we use a nicely rounded and smooth convergent such that the flow remains

attached. In that case a discharge coefficient close to 1.0 can be realized. Measured discharge coefficient for nozzle throat assemblies is in the range 0.94 to 0.98. ISO 5167 gives values for flow with high Reynolds Numbers through venturis of 0.980 to 0.995, depending on the roughness of the convergent section.

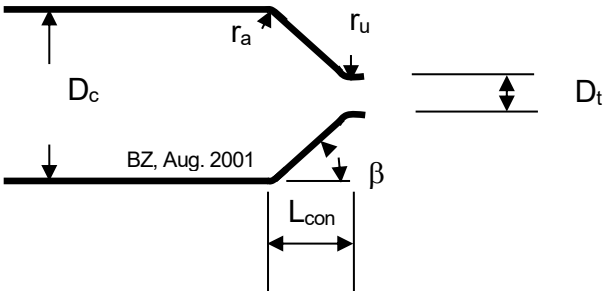

Figure 4: Schematic of chamber convergent

Contraction half angle (β), throat longitudinal radius (r_u) and contraction radius (r_a) are usually determined based on considerations with respect to motor length, and pressure loss. The shorter the convergent is the lower the motor mass and the higher the pressure loss. Typical values are [NASA (a), (b)]:

- $r_u/R_t = 0.5 – 1.5$
- $r_a/D_c < 0.5$
- $\beta = 30 – 60$ degrees

Here D_t is throat diameter, R_t is throat radius and D_c is chamber diameter.

4.2 Conical divergent

Important parameters in the definition of the geometry of a conical nozzle (Figure 5) are the nozzle divergence half angle θ, the throat radius R_t, the throat longitudinal radius R_u, the nozzle length L, the nozzle expansion ratio ε, and the radius of the nozzle exit R_e.

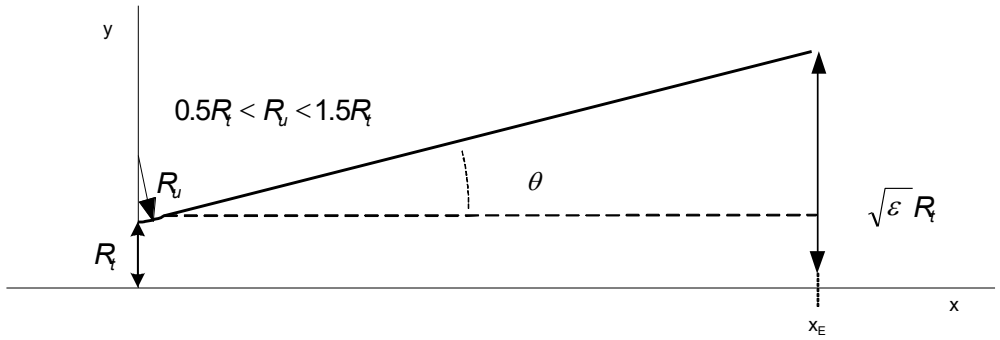

Figure 5: Conical divergent profile

Various literature sources among which [Sutton], and [Huzel] report that the optimum conical nozzle has a wall divergence half angle in between 12° - 18° and a throat longitudinal radius in between 0.5 R_t and 1.5 R_t.

4.3 Contoured or Bell shaped divergent

The geometry of the contoured nozzle closely resembles a bell shape, hence the designation bell shape nozzle. It has a high angle expansion section (30°-60°) right behind the throat; this is followed by a gradual reversal of nozzle contour slope so that at the nozzle exit the divergence angle is reduced (values down to 8° seem feasible) [Huzel]. The large divergence immediately behind the throat is permissible because the high relative pressure and the rapid expansion do not cause separation in this region. The reversal of the contour slope causes a redirection of the flow and thus some compression waves. In an efficiently shaped contoured nozzle, the expansion waves from the nozzle throat region coincide with the effects of the compression and redirection of the flow in the centre section of the diverging nozzle section.
Important parameters in the definition of the geometry of a bell nozzle (Figure 6) are again the throat radius R_t, the throat longitudinal radius R_u, the nozzle length L, the

nozzle expansion ratio ε, and the radius of the nozzle exit R_e. In addition, we use the nozzle throat divergence half angle θ_p and the nozzle exit divergence half angle θ_e.

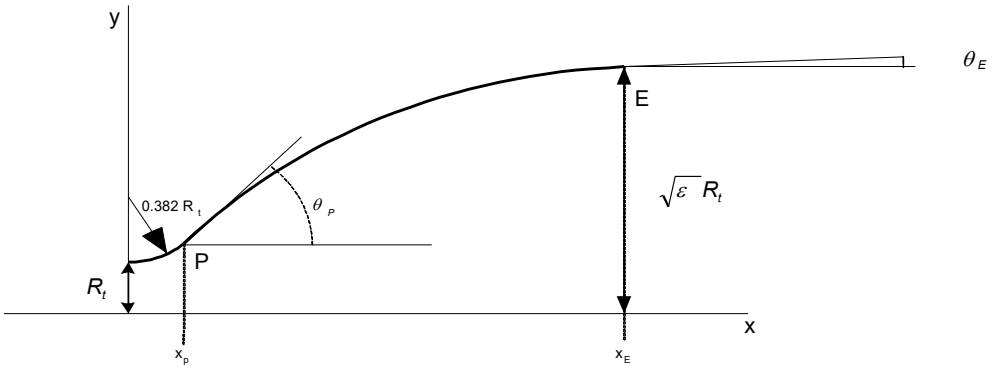

Figure 6: Bell nozzle profile

According to [Huzel] the circular part after the throat can be approximated using a radius of 0.382 R_t.

5 Nozzle length

In this section we will provide a method that allows for estimating nozzle length for the conical and bell nozzle for a given expansion ratio and nozzle throat radius (determined using ideal rocket motor theory) and compare the results. As design variables, we consider the throat longitudinal radius, the divergence half angle right (conical nozzle) and the divergence half angle right after the throat and at the nozzle exit (bell). We will use an orthogonal axis system (x, y) with the point of origin taken in the throat and the x-axis taken along the nozzle axis of symmetry and the positive y-axis in an upward direction.

5.1 Length of conical nozzle (divergent part only)

The point where the conical part intersects with the throat region (determined by the throat longitudinal radius and the requirement that the transition from throat to divergent is smooth) can be determined using:

$$x_P = R_u \cdot \sin\theta \tag{0.1}$$

$$y_P = R_t + (1 - \cos\theta) \cdot R_u \tag{0.2}$$

Hence, the position of point P is known once we have selected the nozzle divergence half angle and the throat longitudinal radius.

The length of the nozzle divergent L follows from the value of x_E. This value can be calculated using [Huzel]:

$$x_E = \frac{\left(\sqrt{\varepsilon} - 1\right) \cdot R_t + R_u \cdot (\sec\theta - 1)}{\tan\theta} = \frac{\left(\sqrt{\varepsilon} - 1\right) \cdot R_t + R_u \cdot (1/\cos\theta - 1)}{\tan\theta} \tag{0.3}$$

The y-coordinate of the nozzle exit follows from:

$$y_E = \sqrt{\varepsilon} \cdot R_t = R_e \tag{0.4}$$

5.2 Length of Bell nozzle (divergent part only)

Like for the conical nozzle, the point where the contoured nozzle intersects with the throat region, again determined by the throat longitudinal radius and the requirement that the transition from throat to divergent is smooth, can be determined using (see also Figure 7):

$$x_P = 0.382 \cdot R_t \cdot \sin\theta_P \tag{0.5}$$

$$y_P = R_t + (1 - \cos\theta_P) \cdot 0.382 \cdot R_t = 1.382 \cdot R_t - 0.382 \cdot R_t \cdot \cos\theta_P \tag{0.6}$$

From the point P on the nozzle shape can be approximated by a parabola [Rao, 1960], [Huzel].

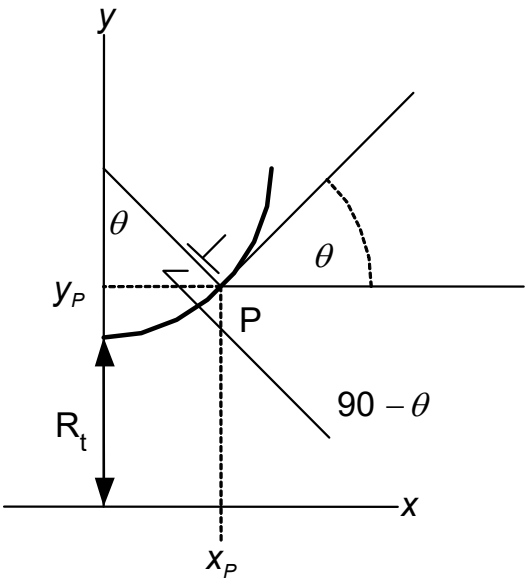

Figure 7: Bell nozzle throat contour

The following equation is valid:

$$x = ay^2 + by + c \tag{0.7}$$

Here the x-axis is taken to be the axis of symmetry of the parabola (x in longitudinal direction) with the y-coordinate essentially giving the radius of the nozzle at the location x.

We should solve for the unknowns a, b, c, to find the equation of the parabola that goes through the point P and E. Here we consider the case that point P is known as well as the angle of the tangents in the points P and E (initial angle of parabola and final angle of parabola). Using the solution found, the length of the nozzle is computed based on a given nozzle exit radius (y_E).

To solve for the unknowns a, b, c we need a system of three independent equations in the three unknowns.

One equation follows from that the equation (0.7) should go through the point P:

$$x_P = a{y_P}^2 + by_P + c \tag{0.8}$$

Two more relations can be found using the known angle of the tangent in the points P and E:

$$x_P' = 2ay_P + b = \tan\left(\pi/2 - \theta_P\right) \tag{0.9}$$

$$x_E' = 2ay_E + b = \tan\left(\pi/2 - \theta_E\right) \tag{0.10}$$

This gives a system of three equations in the three unknowns a, b, and c that can be solved. Notice that y_E (the length of the divergent part of the nozzle) is considered to be known.

Solving for a, b and c

Equations (0.9) and (0.10) allow solving for a:

$$\Rightarrow a = \frac{\tan\left(\pi/2 - \theta_E\right) - \tan\left(\pi/2 - \theta_P\right)}{2 \cdot (y_E - y_P)} \tag{0.11}$$

Substitution of (0.6) and (0.11) in (0.9) than allows finding a solution for b:

$$\Rightarrow b = \tan\left(\pi/2 - \theta_P\right) - 2 \cdot \frac{\tan\left(\pi/2 - \theta_E\right) - \tan\left(\pi/2 - \theta_P\right)}{2 \cdot (y_E - y_P)} \cdot Y_P \tag{0.12}$$

Substitution of (0.5), (0.6) and the now known a and b in (0.8) gives for c:

$$\Rightarrow c = x_P - a \cdot y_P^2 - b \cdot y_P \tag{0.13}$$

Solving for nozzle length x_E

With a, b and c known, the equation for the parabolic approximation (0.7) is determined, thereby allowing for determining x_E using.

$$\boxed{x_E = a y_E^2 + b y_E + c} \tag{0.14}$$

It is mentioned here that the parabolic relation used in this section allows demonstrating the use of such a relation for the design of a near optimum thrust bell nozzle. It already allows for quite a decent approximation. As an alternative, one may also start with the general quadratic equation in 2 variables. In its general form, it reads: $ax^2 + bxy + cy^2 + dx + ey + f = 0$. This relation has 6 unknowns (a to f). However, setting c equal to 1 and limiting the solutions to parabola type only ($b^2 - 4ac = 0$), a parabola relation results that allows considering all 4 boundary conditions (and not only 3 as are employed in the simple analysis presented earlier). *For even more accurate calculations of the contour use can be made of the method of characteristics (MoC), see section 7.4. Of course, the MoC can also be used to check the presence of shocks in the nozzle.*

5.3 Length comparison

In this section the length of a conical and contoured nozzle are compared for various expansion ratios up to 100 and a nozzle throat radius of 0.1 m. The conical nozzle selected has a divergence half angle of 15°, and a nozzle longitudinal throat radius of 0.5 R_t. Two bell nozzles have been selected. The first one (bell nozzle 1) has a divergence half angle right after the throat of 30° and of 5° at the exit. For the second one (bell nozzle 2) the divergence half angle right after the throat is increased to 45°. The results are given in Figure 8.

The figure shows that the bell nozzle is substantially shorter than the conical nozzle. The bell nozzle with a 30° half angle right after the throat has a length 80% of the length of the conical nozzle. In case of increasing the half angle to 45° the length decreases even further. A major issue, however, remains if the flow can be expanded over such a high angle without too many losses.

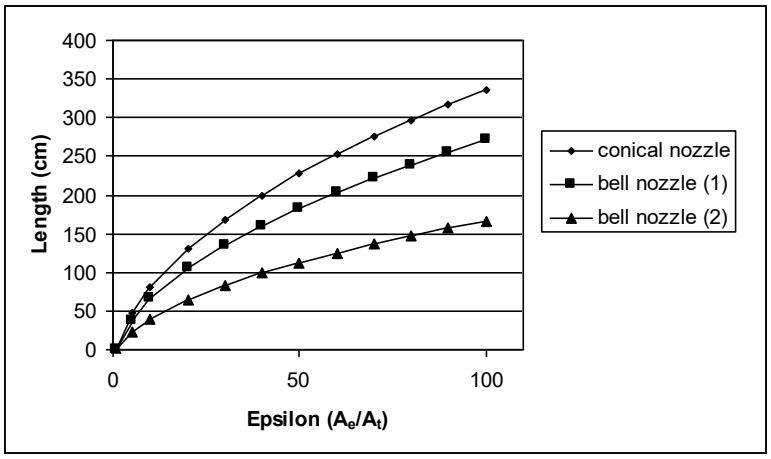

Figure 8: Nozzle length comparison

6 Non-adapted nozzles

Nozzle performance (thrust coefficient) is optimum in case exit pressure p_e equals (is adapted to) ambient pressure p_a. In that case we refer to the nozzle as an 'adapted nozzle'. In case exit pressure p_e differs from ambient pressure p_a, we refer to the nozzle as a 'non-adapted nozzle'. In practice, all rockets used in space (vacuum) experience non-adapted flow else they should be equipped with an infinitely long (and heavy) nozzle. Also, space launcher rocket engines will experience non-adapted flow during most of the ascent flight. This is because the atmospheric pressure decreases with altitude, whereas nozzle exit pressure usually remains constant. How non-adapted flow influences performance is discussed in some detail below.

6.1 Under-expansion

When the ambient pressure is lower than the exit pressure, further expansion is still possible downstream of the exit section. In that case we deal with an 'under-expanded nozzle'. The flow downstream of the exit area is shown in Figure 9. The expansion continues through a system of expansion waves. The free-jet boundaries form a succession of wedge-shaped expansions and contractions. The flow through the nozzle is given by the isentropic supersonic flow solution.

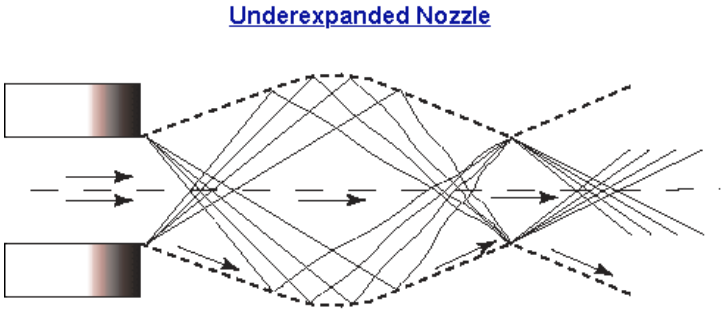

Figure 9: Flow pattern of an under-expanded nozzle

6.2 Over-expansion

In case ambient pressure is higher than exit pressure, we deal with an 'over-expanded nozzle'. Three essentially different flow-patterns can result, which will be discussed separately here. In each case we refer to Figure 10, where the pressure ratio p/p_c is given as a function of the distance from the nozzle entrance. The lines drawn in this picture denote the pressure ratios for certain conditions discussed in the text.

As can be seen, all pressure ratios take the value of one ($p = p_c$) at the nozzle entrance (left side of the picture). At the right side, the lines drawn end somewhere between zero and one. The regimes we distinguish are:

a. $p_c \geq p_a \geq (p_a)_1$
For $p_a = p_c$, the ambient pressure is equal to the pressure inside the combustion chamber. No flow passes through the nozzle. The rocket motor is not operational. Now consider that we lower p_a, while keeping p_c constant (notice that we can also consider increasing p_c, while keeping p_a constant. If $p_a > (p_a)_1$, sonic speed is never reached at any point along the nozzle and the latter operates as a Venturi tube (curve a).
When $p_a = (p_a)_1$, the flow just becomes sonic at the throat. The critical pressure ratio is reached. Just behind the throat the flow becomes subsonic again. No shock waves occur. Curve b shows the change of pressure ratio throughout the nozzle for this type of flow. Notice that up to this point, the pressure in the nozzle exit is always equal to the atmospheric pressure, since in subsonic flow no pressure discontinuity can be maintained.

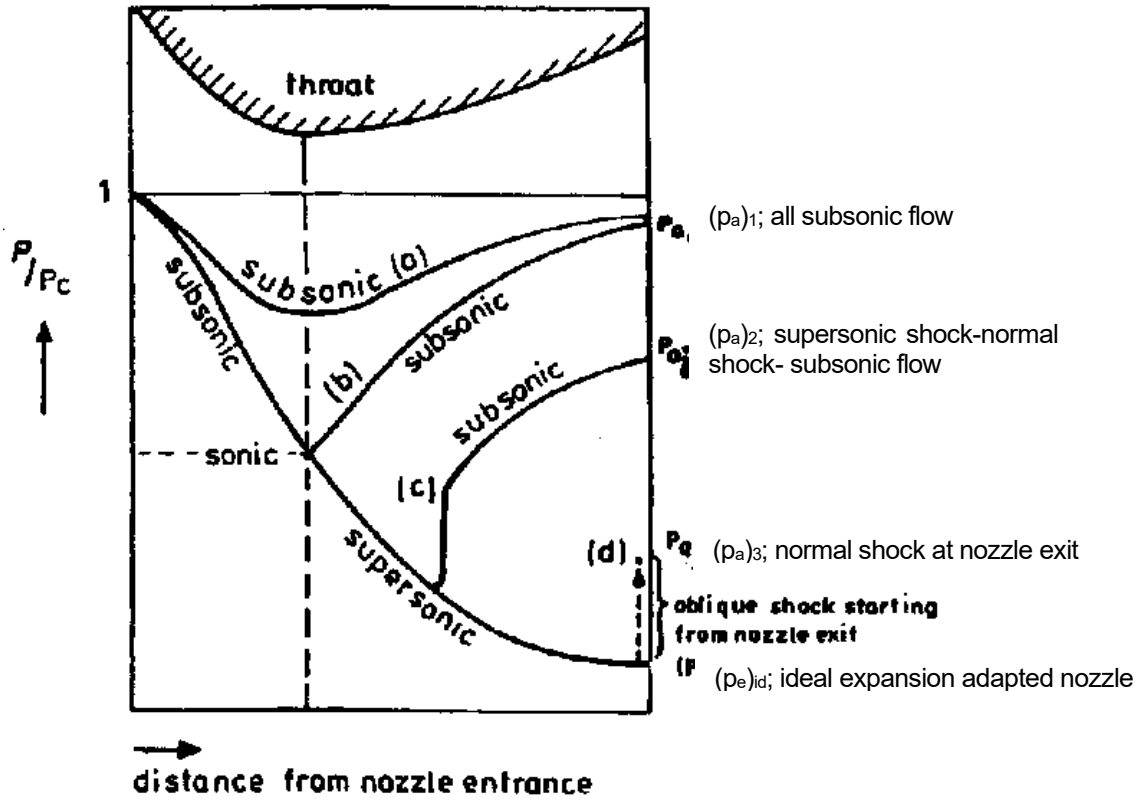

Figure 10: Effect of atmospheric pressure on over-expanded nozzle flow

b. $(p_a)_1 > p_a \geq (p_a)_3$
If $p_a < (p_a)_1$, supersonic flow in a part of the divergent section of the nozzle is possible. Somewhere between the throat and the nozzle exit a normal shock will occur and the flow becomes subsonic. The place inside the nozzle where this

shock occurs depends on the value of the ambient pressure p_a only (for given p_c). If p_a is high and close to $(p_a)_1$, the shock occurs close to the throat section and with decreasing value of p_a, the normal shock wave moves towards the nozzle exit, which is reached for $p_a = (p_a)_3$. The occurrence of a normal shock wave is a way for the flow to adapt itself to the external pressure, given the shape of the nozzle and the total pressure inside the chamber. After the shock, a subsonic compression takes place such that the exit pressure equals the ambient pressure $(p_a)_2$ (curve c). Both the supersonic flow between the shock wave and the nozzle exit, obey the four mentioned basic laws. The subsonic and supersonic solutions meet at the plane of the normal shock wave.

c. $(p_a)_3 > p_a > p_e$
If the ambient pressure p_a is lower than the pressure $(p_a)_3$ at which a normal shock occurs at the nozzle exit, the flow in the nozzle will be fully supersonic. The ambient pressure p_a is higher than the free jet pressure p_e. The exhaust gas is compressed by an oblique shock which originates at the nozzle exit. The pressure recovery from p_e back to p_a takes place outside the nozzle through two oblique shock waves which meet on the nozzle axis, are refracted and then reflected on the free jet boundaries as shown in Figure 11.

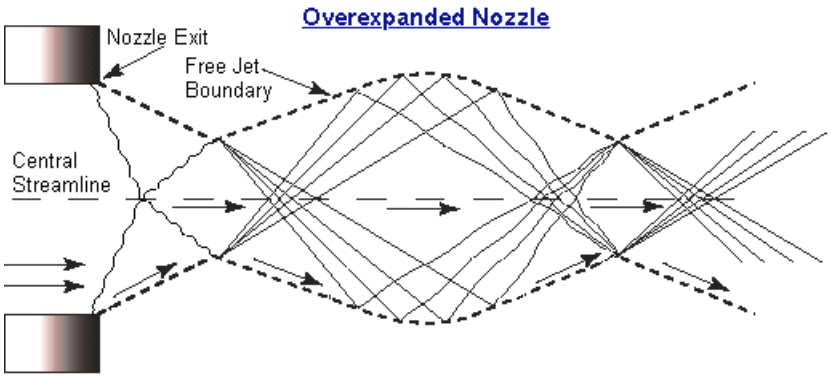

Figure 11: Flow pattern of an over-expanded nozzle

7 Effect of nozzle profile/shape on performance

In this section the effect of the nozzle profile on the performance of the nozzle is determined using simple modelling methods. We will discuss the effect of flow divergence, boundary layer formation and heat transfer. Other effects like a non-circular nozzle cross-section, wall roughness will only be touched upon briefly.

7.1 Flow divergence

Until now we assumed the exhaust velocity of the flow to be parallel to the nozzle axis. For practical nozzles, this leads to an overestimation of nozzle performance. In this section we will introduce a refinement of the earlier introduced purely 1-dimensional model to allow for considering flow divergence. This method will be derived for a conical nozzle, as the method in that case is simple. Following the derivation of the correction factor for a conical nozzle, we will also present a correction factor for a bell type of nozzle derived from experimental data.

7.1.1 Conical nozzle

We consider a conical nozzle, Figure 12. All streamlines are assumed to originate at the apex, T, of the diverging cone. We assume surfaces of constant properties to exist (constant pressure, density and temperature, constant velocity and constant composition

of the combustion products); they will be sections of spheres with their centre in T. The surface of constant properties existing at the nozzle exit is referred to as A_s.

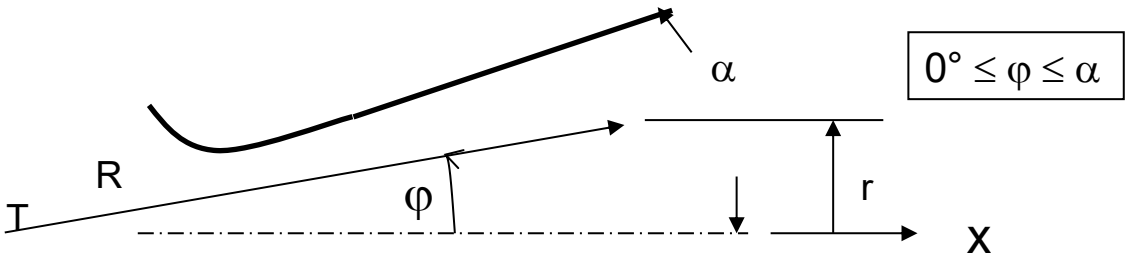

Figure 12: Conical nozzle flow

The exhaust velocity U_e is pointing in the radial direction, normal to the surface A_s. We consider the balance of forces in the x-direction on the system enclosed by the control surface. Because of symmetry reasons forces in the y-direction cancel out:

$$F_x = \int U_x \cdot dm + \int \left[(p_e - p_a) \cdot dA_s \right]_x \tag{0.15}$$

The first term of the right-hand side is the impulse- or momentum-thrust; the second term is the pressure-thrust. Note that again the impulse connected with the injection of the propellants into the chamber is neglected.

With: $U_x = U_e \cdot \cos\varphi$ and: $dm = \rho_e \cdot U_e \cdot 2\pi r \cdot R \cdot d\varphi = 2\pi \cdot R^2 \cdot \rho_e \cdot U_e \cdot \sin\varphi \, d\varphi$

It follows for the impulse term:

$$\int U_x \cdot dm = 2\pi \cdot R^2 \cdot \rho_e \cdot U_e{}^2 \cdot \int_0^{\alpha} \sin\varphi \cdot \cos\varphi \, d\varphi \tag{0.16}$$

Integrating the impulse term gives:

$$\int U_x \cdot dm = 2\pi \cdot R^2 \cdot \rho_e \cdot U_e{}^2 \cdot \left(\frac{1 - \cos^2\alpha}{2} \right) \tag{0.17}$$

The mass flow m through the nozzle can be determined by integrating dm over A_s:

$$\begin{aligned} m &= 2\pi \cdot R^2 \cdot \rho_e \cdot U_e \cdot \int_0^{\alpha} \sin\varphi \, d\varphi \\ m &= 2\pi \cdot R^2 \cdot \rho_e \cdot U_e \cdot (1 - \cos\alpha) \end{aligned} \tag{0.18}$$

We find for the impulse term:

$$\begin{aligned} \int U_x \cdot dm &= 2\pi \cdot R^2 \cdot \rho_e \cdot U_e{}^2 \cdot \int_0^{\alpha} \sin\phi \cdot \cos\phi \, d\phi \\ &= 2\pi \cdot R^2 \cdot \rho_e \cdot U_e{}^2 \cdot \left(\frac{1 - \cos^2\alpha}{2} \right) \\ &= \frac{1 + \cos\alpha}{2} \cdot m \cdot U_e = \lambda \cdot m \cdot U_e \end{aligned} \tag{0.19}$$

The contribution of the pressure thrust is found by:

$$\int\left[\left(p_e - p_a\right)\cdot dA_s\right]_x = \int_0^{\alpha}\left[\left(p_e - p_a\right)\cdot 2\pi\cdot R^2\cdot\sin\varphi\cdot\cos\varphi\right]\cdot d\varphi$$
$$= \left(p_e - p_a\right)\cdot 2\pi\cdot R^2\cdot\frac{\sin^2\alpha}{2} \qquad (0.20)$$
$$= \left(p_e - p_a\right)\cdot\pi\cdot r_e^{\,2} = \left(p_e - p_a\right)\cdot A_e$$

This shows that the contribution of the pressure thrust in the case of flow divergence does not change with respect to its contribution in the ideal case (no flow divergence).Substitution of (0.19) and (0.20) in (0.15) yields:

$$F_x = \frac{1+\cos\alpha}{2}\cdot m\cdot U_e + \left(p_e - p_a\right)\cdot A_e = \lambda\cdot m\cdot U_e + \left(p_e - p_a\right)\cdot A_e \qquad (0.21)$$

The parameter λ is usually called the thrust correction factor due to flow divergence. For a conical nozzle with α equal to 15°, λ has a value of 0.983 and a decrease of the impulse-thrust of 1.7% is found. For α equal to 10° this is 0.8% and for α equal to 20° this is 3%. The loss in thrust due to sideward components of the exhaust velocity is called the divergence loss ε_{div}. It is written as:

$$\varepsilon_{div} = 1 - \left(\frac{1+\cos\alpha}{2}\right) = 0.5\cdot\left(1-\cos\alpha\right) \qquad (0.22)$$

7.1.2 Bell nozzle

An empirically obtained expression valid for bell-type nozzles is taken from [AGARD-AR-230]:

$$\varepsilon_{div} = 0.5\cdot\left[1-\cos\left(\frac{\alpha+\theta_{ex}}{2}\right)\right] \qquad (0.23)$$

With θ_{ex} is nozzle divergence half angle at nozzle exit and α is nozzle divergence angle of conical nozzle that fits inside the bell contour.

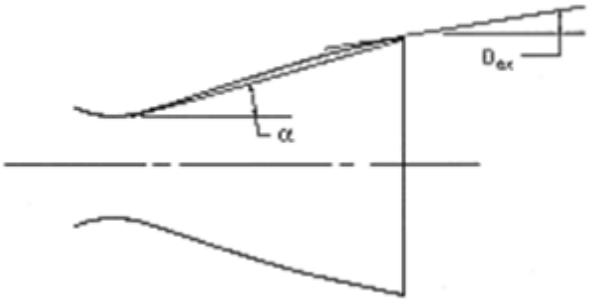

Figure 13: Bell nozzle contour with determining angles for flow divergence [AR-230].

For a bell nozzle with α equal to 20° and θ_{ex} equal to 6°, we find ε = 0.0128 or 1.3%, which compares well with a conical nozzle with the same half cone angle.

7.2 Boundary layer

Because of viscous effects a boundary layer builds up in the nozzle. This boundary layer will reduce the performance of the nozzle due to the flow losing momentum and because the undisturbed flow will be displaced over some distance. Another effect is that because of the boundary layer a subsonic flow exists close to the wall. This means that

disturbances can propagate from the nozzle exit toward the throat and may lead to flow separation. These effects are discussed in some detail below. A further major importance of the boundary layer development is its influence on the heat transfer to the nozzle walls. This is discussed in the section on heat transfer. First though we present some basic knowledge pertinent to boundary layers.

7.2.1 Boundary layer fundamentals

When a flow passes over an external surface or runs through a pipe section, it usually experiences friction drag, which causes a boundary layer to form. In the boundary layer, the flow velocity decreases from the velocity in the undisturbed flow to essentially zero. This is depicted in Figure 14 for both external and internal flow.

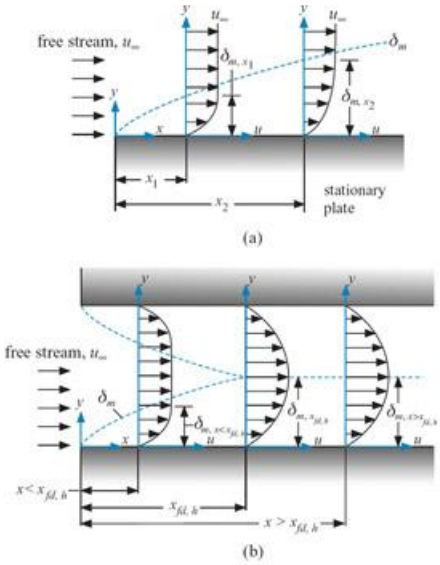

Figure 14: (a) Laminar external flow over a flat plate, and (b) laminar internal flow between two parallel plates

Top figure shows a boundary layer being formed and growing in size with increasing distance travelled along the plate. Bottom figure shows same process until the two boundary layers (top and bottom wall) meet. The distance where the two meet is referred to as the entrance length. Thereafter, the flow is referred to as fully developed. The following parameters are commonly used to communicate the properties of boundary layers:

- **Boundary layer thickness** δ: The thickness of the boundary layer is usually taken as the distance across a boundary layer from the wall to a point where the velocity reaches a value of 0.99 times the velocity of the undisturbed flow.
- **Skin friction coefficient** c_f or C_f is a kind of drag coefficient. It is related to the shear stress in the flow.
- **Displacement thickness** δ^* is hypothetical thickness over which the external in-viscid flow is displaced by the presence of the boundary layer.
- **Momentum thickness** θ is hypothetical thickness of boundary layer taken at free stream conditions, representing the loss of momentum occurring in the boundary layer.

Many investigations, both of a practical and theoretical nature, have been performed with as purpose to determine the effects of friction for both internal and external flow. A good reference in this sense is the work of [Schlichting], but many other good references exist.

From these investigations, it is found that the amount of friction experienced by the flow depends on the velocity difference between the flow and the wall and the fluid viscosity as well as on how chaotic the flow is. If the flow is nicely layered, we refer to the flow as laminar flow, if the flow is chaotic, we refer to the flow as turbulent. A parameter found to be very useful in expressing the effects of friction is the Reynolds number Re. It is a

dimensionless number that gives a measure of the ratio of inertial forces to viscous forces and can be determined using:

$$Re = \frac{\rho \cdot v \cdot L}{\mu} \tag{0.24}$$

Here:

- v is mean (internal flow) or undisturbed (external flow) fluid velocity
- L is a characteristic linear dimension (travelled length of fluid or hydraulic radius)
- μ is dynamic viscosity of the fluid
- ρ is mass density of the fluid

In general, the flow tends to be laminar at low flow velocities and high dynamic viscosity and turbulent at high flow velocities and low dynamic viscosity.

Properties of boundary layers under varying conditions (Reynolds number, expanding flow, etc.) have been determined for many simple geometries and are documented in many different handbooks. For example, the next table gives properties for the flow over a flat plate. Notice that skin friction coefficient is here given as variable with the distance x. In some works, it may also be given as an average over some length. Also notice that the Reynolds number used is based on using the distance x travelled along the flat plate starting at the leading edge (x = 0). For Reynolds number based on distance x below about 500,000, the flow is usually considered as laminar. At higher values, the flow is either in transition or fully turbulent.

Table 1: Summary of expressions for laminar and turbulent boundary layers on a smooth flat plate aligned parallel to a uniform stream [Stern]

		(a)	(b)
Property	Laminar	Turbulent(†)	Turbulent(‡)
Boundary layer thickness	$\frac{\delta}{x} = \frac{4.91}{\sqrt{Re_x}}$	$\frac{\delta}{x} \cong \frac{0.16}{(Re_x)^{1/7}}$	$\frac{\delta}{x} \cong \frac{0.38}{(Re_x)^{1/5}}$
Displacement thickness	$\frac{\delta^*}{x} = \frac{1.72}{\sqrt{Re_x}}$	$\frac{\delta^*}{x} \cong \frac{0.020}{(Re_x)^{1/7}}$	$\frac{\delta^*}{x} \cong \frac{0.048}{(Re_x)^{1/5}}$
Momentum thickness	$\frac{\theta}{x} = \frac{0.664}{\sqrt{Re_x}}$	$\frac{\theta}{x} \cong \frac{0.016}{(Re_x)^{1/7}}$	$\frac{\theta}{x} \cong \frac{0.037}{(Re_x)^{1/5}}$
Local skin friction coefficient	$C_{f,x} = \frac{0.664}{\sqrt{Re_x}}$	$C_{f,x} \cong \frac{0.027}{(Re_x)^{1/7}}$	$C_{f,x} \cong \frac{0.059}{(Re_x)^{1/5}}$

* Laminar values are exact and are listed to three significant digits, but turbulent values are listed to only two significant digits due to the large uncertainty affiliated with all turbulent flow fields.

† Obtained from one-seventh-power law.

‡ Obtained from one-seventh-power law combined with empirical data for turbulent flow through smooth pipes.

Handbooks also provide for relations for more complex geometries. For cases where handbooks do not offer a solution, one generally uses Computer Fluid Dynamics (CFD). In this work, we will mainly stick to readily available expressions as it allows for gaining better insight.

7.2.2 Boundary layer formation in rocket nozzles (first observations)

All rocket nozzles do experience the formation of a boundary layer. For some nozzles this effect is large and for others limited. This is mainly governed by the Reynolds number. For rocket nozzles, the Reynolds number is usually determined using the throat diameter as the characteristic dimension. It follows:

$$Re_t = \rho_t \, v_t \, D_t / \mu_t \tag{0.25}$$

Where gas density, velocity and dynamic viscosity are all taken at the free stream conditions in the nozzle throat. For throat Reynolds numbers more than 100,000, we typically find that the boundary layer effect is mostly limited to the nozzle divergent and hence effect is mostly seen in the nozzle quality factor. Below a throat Reynolds number of 100,000 also boundary layer effects should be expected in the nozzle throat, where the presence of the boundary layer reduces the flow area available to the flow, thereby affecting the discharge (quality) factor. See later sections for further information.

7.2.3 Momentum loss

The boundary layer affects the rocket thrust directly through the skin friction on the nozzle wall. This skin friction has an axial component, which must be subtracted from the thrust. The effect of the boundary layer on the thrust can be determined from the momentum loss thickness of the boundary layer using:

$$\Delta F = \left(\rho_e \cdot u_e \cdot 2\pi \cdot R_e \cdot \theta_e\right) \cdot u_e \tag{0.26}$$

Here ρ is flow density, u is flow velocity, R is nozzle radius, and θ is momentum loss thickness. The subscript 'e' refers to the conditions in the nozzle exit. Of these flow density and flow velocity may be determined using ideal rocket theory (given nozzle shape).

For the determination of the momentum loss thickness, many different approaches exist including the use of CFD. Here though we will describe a simple (but slightly inaccurate) method, wherein it is considered that the nozzle essentially resembles a flat plate aligned parallel to a uniform stream. The advantage of this method is that it allows for a clearer insight in the various parameters that affect the boundary layer. It assumes that the boundary layer only starts developing in the nozzle divergent, which defines the nozzle throat as the leading edge of the flat plate. The length of the nozzle measured along the contour then defines the length of the flat plate.

To determine the momentum loss thickness in the nozzle exit, we can use the relations as shown in Table 1. We only must determine whether the boundary layer is laminar or turbulent or whether it makes a transition from laminar to turbulent. To not overcomplicate the matter, we can start by assuming that the flow is either fully laminar or turbulent. Another complicating factor is that the relations are valid for constant conditions (velocity, density) along the flat plate. However, in a nozzle, these conditions vary strongly. To account for these strongly varying conditions, it is considered determining the momentum loss thickness first using the conditions (mass density, flow velocity and temperature) in the nozzle throat as the (constant) free stream conditions and second using the conditions in the nozzle exit as the (constant) free stream conditions. The actual momentum loss thickness can then be determined as an average value of the two[1]. A third complicating factor is the compressibility of the flow.

According to [Schlichting] effects of compressibility for turbulent flow can be modelled using the Reference Temperature Approach (RTA). In this approach, the friction coefficient for compressible flow is determined based on the friction coefficient for incompressible flow by using a Reference Temperature Approach (RTA). We write:

$$c_f = c_{f,i} \cdot \frac{\rho_f}{\rho_o} \tag{0.27}$$

Where:

- c_f = skin friction coefficient compressible flow
- $c_{f,i}$ = skin friction coefficient incompressible flow at reference temperature
- ρ_o = mass density undisturbed flow (just outside boundary layer)
- ρ_f = mass density at reference temperature

[1] A slightly more accurate approach may to distinguish stations along the nozzle contour in flow direction and to use a piece-wise constant approximation (in between stations) to determine the properties of the boundary layer, thereby focussing on the growth in momentum thickness and/or displacement thickness between two stations.

The challenge remaining is in selecting the right reference (or film) temperature. One approach is to select some kind of average temperature over the boundary layer. Neglecting the effect of high velocity flow, this would come down to $T_f = (T_o + T_w)/2$, where the subscript 'f' refers to the film, 'o' to the undisturbed conditions outside the boundary layer and 'w' to the conditions at the wall. However, in case of high velocity flow (Mach number more than about 0.3), one must also consider that because of the reduced speed in the boundary layer, the temperature in the boundary layer increases from the static temperature just outside the boundary layer to a value close to the total temperature of the flow. The following expression has been taken from the work of [Wong]:

$$T_f = T_o \left(\frac{T_w/T_o + 1}{2} + 0.22 \, \frac{\gamma-1}{2} \, M^2 \right) \tag{0.28}$$

Notice that from the above relation it is found that for M = 0, the film temperature is exactly an average of T_o and T_w. Also note that with increasing Mach number, the film temperature increases.

Next, assuming that dynamic viscosity is linearly dependent on temperature, pressure across the boundary layer in direction perpendicular to the wall is constant, and that the fluid behaves as an ideal gas, it can be shown that:

$$c_f = c_{f,i} \left(\frac{T_w/T_o + 1}{2} + 0.22 \frac{\gamma-1}{2} M^2 \right)^{-0.6} \tag{0.29}$$

Here M is the Mach number in the flow, γ is specific heat ratio of the fluid, T_w is fluid temperature at wall, and T_o is fluid temperature just outside the boundary layer. This relation provides hence insight in how flow Mach number and temperature do affect the friction coefficient and hence the momentum loss thickness. Such a relation can then be used as a starting point for experimental research and sometimes gives surprisingly good results.

Above-described method allows for determining the momentum loss thickness, be it that it does require some simplifying assumptions. Still, it is considered that such an approach allows for a first estimate as well as insight in the main determining parameters. In case though that reality is quite different because of e.g. rough nozzle, and reacting flow, one usually needs to resort to CFD or experiments to obtain more proper values.

7.2.4 Reduction in nozzle area ratio

The presence of a boundary layer slightly alters the free-stream characteristics. This is because in the boundary layer, the flow velocity is much lower than in the core flow. Hence, the boundary layer cannot contain the same amount of gas as when the boundary layer is not existent and it will result in a displacement of the core flow with a certain distance, i.e. the displacement thickness, δ^*. At high throat Reynolds number (Re_t > 100,000) there is little to no effect of the boundary layer on the nozzle throat and the effect is limited to the nozzle divergent only. This means that at the nozzle throat the displacement thickness is essentially negligible, whereas at the nozzle exit, the displacement thickness is maximum. Once displacement thickness is known, the effective area ratio at a distance x along the nozzle can be determined from:

$$\frac{A_{x,eff}}{A_x} = \left(\frac{R_{x,eff}}{R_x} \right)^2 \cong 1\text{-}2\frac{\delta_x^*}{R_x} \tag{0.30}$$

Where it is assumed that the displacement thickness δ_x^* at a location x is much smaller than the radius (R_x) of the nozzle cross-section perpendicular to the flow at that location.

To provide a first estimate of the displacement distance in the nozzle a similar approach as used for the momentum loss thickness can be used. This is left for the reader to work out for him/herself.

7.2.5 Example calculation flat plate

Consider a smooth flat plate of length 2 m aligned parallel to a uniform fluid stream. Mass density of fluid stream is given as 1.225 kg/m^3 and flow velocity is 1500 m/s. Dynamic viscosity of fluid is 12.5E-6 Pa-s. In addition are given:

- Flow temperature: 1000 K.
- Specific heat ratio: 1.4.
- Molar mass of fluid: 28 gram/mol.
- Plate temperature: 298 K.

All parameters are considered constant along the flat plate.

At trailing edge of plate (x = 2 m), we find for the Reynolds number:

$$\mathrm{Re}=\frac{\rho\, v\, x}{\mu}=294\mathrm{E}6$$

This high a value points in the direction of a turbulent boundary layer. So, taking the boundary layer as fully turbulent, but incompressible, gives for the friction coefficient:

$$c_{f,i}=\frac{0.0592}{(\mathrm{Re}_{x=2\ m})^{0.2}}=\frac{0.0592}{(294\mathrm{E}6)^{0.2}}=1.20$$

Momentum loss and displacement thickness are:

$$\theta = 0.625 \times c_{f,i} \times x = 0.625 \times 1.20 \text{ x } 2 \text{ m} = 1.50 \text{ mm}$$

$$\delta^* = 1.29\ \theta = 1.29 \times 1.50 \text{ mm} = 1.93 \text{ mm}$$

Correcting for compressibility effects using (7-15), we obtain:
Mach number: $M = v / (\gamma RT)^{0.5} = 1500 \text{ m/s} / 645 \text{ m/s} = 2.33$

$$c_f = c_{f,i}\left(\frac{T_w/T_o+1}{2}+0.22\frac{\gamma-1}{2}M^2\right)^{-0.6} = c_{f,i}\left(\frac{298/1000+1}{2}+0.22\frac{1.4-1}{2}2.33^2\right)^{-0.6}$$

Which gives:

$$c_f = c_{f,i} \times 1.078 = 1.30$$

It now follows:

$$\theta = 0.625 \times 1.30 \times 2 \text{ m} = 1.63 \text{ mm}$$

$$\delta^* = 1.29\ \theta = 2.10 \text{ mm}$$

Hence, we find that compressibility leads to a slight increase in momentum loss and displacement thickness. Even when considering compressibility, the boundary layer is quite thin. This is because of the high Reynolds number of the flow. For lower Reynolds numbers (usually found in low thrust nozzles), the effect of the boundary layer may be much more pronounced.

7.2.6 Effect on thrust coefficient

To determine the effect of the boundary layer on nozzle quality, we can also conduct experiments at different Reynolds numbers and nozzle area ratio. This approach is e.g. demonstrated by [Spisz], who found:

$$C_F = C_{F,i} - C_{F,vis} \tag{0.31}$$

$$C_{F,vis} = 17.6e^{\frac{0.0032\,A_e}{A_t}}/\sqrt{0.773\,Re_t} \quad ; 2000 \le Ret \le 10000 \tag{0.32}$$

Here $C_{F,i}$ is thrust coefficient that results without viscous losses, $C_{F,vis}$ is effect of boundary layer on thrust coefficient, C_F = thrust coefficient corrected for viscous effects and Re_t is determined using nozzle wall temperature as representative temperature for determining fluid properties. Some typical results are provided in next table for a fixed area ratio.

Table 2: Effect of viscosity on thrust coefficient in relation to throat Reynolds number at a nozzle area ratio of 10.

Re_t	$C_{F,vis}$
1,000	0.65361
10,000	0.20669
100,000	0.06536
1,000,000	0.02067
10,000,000	0.00654

Results in the above table clearly shows that the effect of the boundary layer is most pronounced at low Reynolds number. From the relation, we furthermore learn that the effect becomes more pronounced for larger area ratios. This is because in that case the nozzle tends to become longer, which leads to an increase in boundary layer thickness.

7.2.7 Reduction in nozzle throat area

At low Reynolds numbers, the effect of the boundary layer on the nozzle throat area increases and can no longer be neglected. This typically happens when the Reynolds number in the nozzle throat is below about 100,000. Because of the increased presence of the boundary layer (increased boundary layer displacement thickness), the effective area for the flow reduces. This gives rise to flow blockage in nozzle throat and hence, the actual mass flow rate becomes lower than the one expected based on the geometric throat area. The performance reduction due to these effects may be accounted for in terms of the earlier introduced empirical discharge coefficient, C_d:

$$C_d = \frac{m_{real}}{m_{ideal}} \tag{0.33}$$

[Tang and Fenn] have shown that for adiabatic flow (cold gases) in smooth nozzles of circular cross-section the discharge coefficient found from experiments is well correlated by the following analytical relation obtained for a choked axi-symmetric nozzle with reasonable throat contour (not too sharp):

$$C_d = 1 - \left(\frac{\gamma+1}{2}\right)^{3/4}\left\{\frac{-2.128}{\gamma+1}+3.266\right\}R^{-0.5}+0.9428\,\frac{(\gamma-1)(\gamma+2)}{(\gamma+1)^{0.5}}R^{-1} \tag{0.34}$$

in which γ is specific heat ratio of gas (constant), R is a modified throat Reynolds number given by:

$$R = Re_t\left(\frac{R^*}{R_t}\right)^{0.5}, \tag{0.35}$$

Here R^*/R_t is nozzle throat radius divided by radius of throat curvature (nozzle throat contour). Notice that with increasing value of R^*/R_t the sharpness of the throat contour reduces.

Next table shows typical value of discharge coefficient thereby demonstrating that the effect of the discharge factor becomes pronounced at throat Reynolds numbers below about 100,000 as indicated earlier. Results also show that the effect of the specific heat ratio is limited.

Table 3: Nozzle discharge coefficients ($R^* = R_t$) calculated using the relation of Tang and Fenn for two values of the specific heat ratio.

Re_t	C_d ($\gamma = 1.2$)	C_d ($\gamma = 1.4$)
10^6	0.9975	0.9975
10^5	0.9922	0.9921
10^4	0.9753	0.9752
10^3	0.9223	0.9221
10^2	0.7686	0.7592
10	0.2962	0.2953

Another (non-analytical) approach is to use computer Fluid Dynamics to estimate the discharge factor for flow through supercritical nozzles. This approach was followed by [Johnson] who applied this method to cold gas flow through a critical nozzle over a throat Reynolds number[2] range of 2,000-22,000 for Hydrogen, Nitrogen, Carbon dioxide and Argon as the cold gas. Discharge factors reported are down to about 0.92 depending on the gas used and the throat Reynolds number. Johnson also showed that C_d scales about linearly with the inverse of the ideal throat Reynolds number to the power ½. A figure showing part of the results of Johnson can be found in the chapter on cold gas thrusters.

Next to the parameters identified above, there are more parameters that effect the discharge coefficient, like the length of the nozzle convergent, the angle of the convergent, effect of compressibility, surface roughness, nozzle shape (conical, bell, trumpet, etc.) the cross-sectional shape of the nozzle and so on. In the chapter on cold gas thrusters some of these aspects are discussed in more detail. However, there is still room for further study.

Note that in case of a chemical rocket engine, due to a reduced combustion quality, the actual mass flow rate will be higher than the theoretical mass flow rate to realize a certain pressure. This effect, however, should be strictly separated from the blocking effect of the boundary layer (affecting the effective nozzle throat cross-sectional area) as considered in this section.

7.2.8 Flow separation

Because of the boundary layer a subsonic flow exists close to the nozzle wall. Hence a disturbance can propagate from the nozzle exit toward the throat. In the case of overexpansion where shock waves exist at the nozzle exit, this shock wave may propagate upstream and cause flow separation, Figure 15; it generally happens for p_e/p_a between 0.25 and 0.35 [Barrère]. The actual location where the boundary layer detaches depends on the surface roughness of the nozzle wall, the detailed shape of the nozzle and the viscosity of the exhaust gases. The oblique shocks do not necessarily have to be symmetric. In case they are not, the thrust vector is misaligned, and a dangerous situation may appear. It is therefore important to avoid separation and oblique shock waves inside the nozzle, also because this is often accomplished by non-steady flow phenomena. The most simple and classical criterion for flow separation was formulated by Summerfield et al and is purely based on extensive experiments from conical nozzles in the late 1940s. The Summerfield criterion stipulates that the pressure ratio p_e/p_a should never be allowed to drop below 0.35-0.45. Schmucker in 1973 published the following empirical criterion:

[2] Instead of using the dynamic viscosity in the nozzle throat, Johnson uses the dynamic viscosity at stagnation conditions.

$$\frac{p_e}{p_a} = \left(1.88 \cdot M_e - 1\right)^{-0.64} \tag{0.36}$$

It is an improvement over the Summerfield criterion as it accounts for the increase in separation pressure ratio with Mach number as found in practice. However, even so, agreement with actual results is sometimes rather poor.

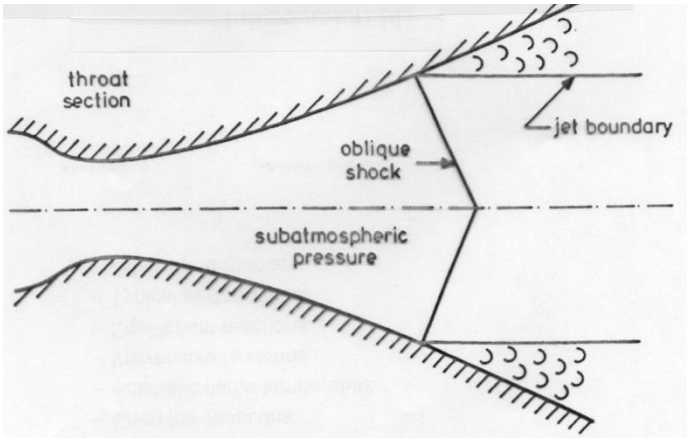

Figure 15: Separation and oblique shock wave in a nozzle due to over-expansion

In the next figure [Stark] compares actual data obtained for a cold gas thruster using nitrogen as propellant to the Schmucker criterion (dotted line).

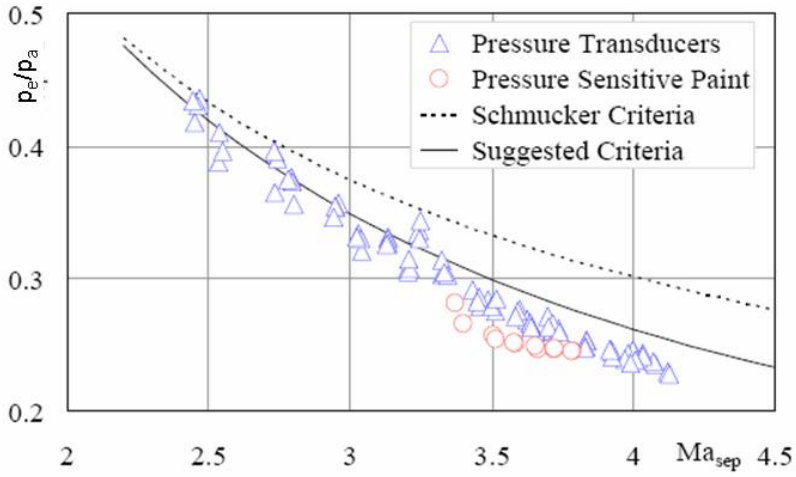

Figure 16: Comparison of flow separation data with some criteria

Results show that for high Mach numbers, the Schmucker criterion tends to give a conservative estimate for flow separation, with the solid line represented by:

$$\frac{p_e}{p_a} = \frac{\pi}{3\left(Ma\right)_{sep}} \tag{0.37}$$

allowing for a better estimation of the pressure where flow separation occurs.

Summarizing, we find Summerfield the easiest to apply criterion but leading to a conservative design. For a less conservative design the Schmucker criterion might be applied and in case even the latter is considered too conservative, the Stark criterion might be considered, although in that case it could turn out that we still might face flow separation, necessitating some expensive re-design.

In Figure 17 the expansion behaviour of the bell and plug nozzle is compared.

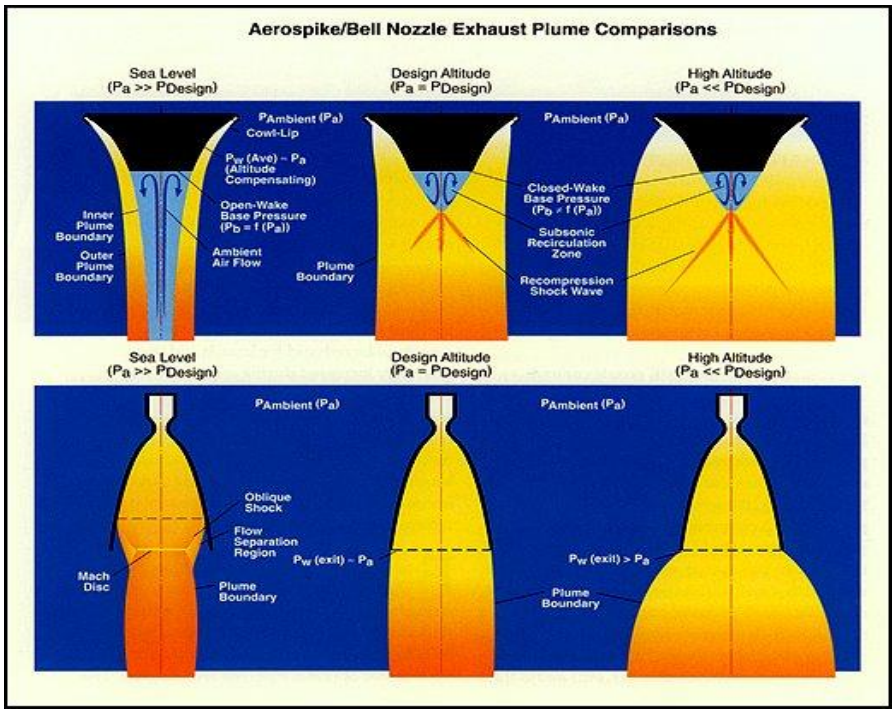

Figure 17: Comparison of expansion behaviour (courtesy Boeing Rocketdyne)

The figure shows that the behaviour of bell and plug nozzle is comparable at design altitude and at high altitude. At low altitude, we find that the bell nozzle is much more prone to flow separation than the plug nozzle. This is the reason behind the improved altitude compensation capabilities of the plug nozzle.

7.3 Effect of heat transfer

In the nozzle heat is transferred from the hot exhaust gases to the relatively cool nozzle wall. This will cause a decrease in flow enthalpy and hence exhaust velocity. The extent of this effect will depend on the specific nozzle shape, and the local heat flux. How the heat flux depends on the nozzle shape is treated in the chapter on heat transfer. For now, we assume that the heat transferred per unit time and per unit of nozzle surface is known.

Assuming steady state conditions, the total amount of heat transferred per unit of time follows from:

$$\dot{Q} = \iint q(S) \cdot dS \tag{0.38}$$

Here q is the heat transferred per unit of area and per unit of time and S is the surface area of the nozzle.

In case of a constant heat flux, we find:

$$\dot{Q} = q \cdot S \tag{0.39}$$

Hence, the heat flow from the hot gases to the wall depends on the heat flux, and the surface area S.

To estimate the effect of cooling on the exhaust velocity and hence the impulse-thrust we propose to use as a first approximation:

$$\delta_{cooling} = 50 \cdot \left(1 - \frac{v_{ideal\ with\ loss}}{v_{ideal}} \right) \% \qquad (0.40)$$

Where the velocities are calculated using ideal rocket theory, with the velocity in the numerator calculated using a value for the enthalpy corrected for the heat loss.

7.4 Improved modelling

Up to now, we have discussed a very simple one-dimensional flow method that allows us to determine a reasonably good approximation of nozzle performance. To improve theoretical predictions, we have also introduced several corrections to the thrust. A problem is that this model does not allow for considering the detailed shape of the nozzle. It also does not allow for calculating the performance of plug-type and scarfed[3] nozzles.

To allow for improved modelling, we must resort to computational fluid dynamics (CFD). In CFD, we try to solve the governing partial differential equations of fluid flow (see Navier-Stokes equations) with numbers and advancing these numbers in space and/or time to obtain a numerical description of the flow field of interest. For nozzle design, nowadays several numerical methods are available.

A relatively simple method allowing for considering the detailed shape of the nozzle including plug-type and scarfed nozzles is the “Method of Characteristics” (MOC). This method was first applied for the design supersonic nozzles by RAO in 1958 [RAO]. The problem considered was to determine wall contours that would transform a uniform or source flow usually at Mach number of unity to a uniform shock-free flow at some higher Mach number. Since then, various applications of MOC to the design of supersonic nozzles have been made and various computer-based tools have been developed. For example, at TU-Delft [Ablij] developed a computer code “Nozzle” allowing for the design and performance prediction of bell and conical nozzles. This code was later adapted by [Beenen] for analyzing single expansion ramp nozzles (SERN’s). A drawback of MOC-based methods is that their application is limited to the supersonic region of the nozzle, requires assuming a shape for the sonic line in the nozzle throat, and does not readily allow for considering the varying gas properties in the nozzle.

More detailed and complex methods use finite difference techniques to calculate the flow properties in the nozzle. These methods are very calculation intensive, but nowadays standard.

8 Nozzle structure

The structure of the nozzle essentially is a thin shell structure. This structure is subject to high heat loads and pressure loads with typical nozzle inlet pressures and gas temperatures ranging from a few bars up to 200 bar (e.g. SSME) and a few hundred K up to several thousand K. To cope with these extreme conditions, a more complicated structure may result, allowing for cooling / thermal insulation. For instance, some liquid rocket engines have a double wall through which a coolant flows to cool the nozzle structure, whereas SRM nozzle walls typically are covered by a flame liner to protect the wall from heating up. Further complications to the structure result from the need to interface with the combustion/heater chamber and may also result from provisions necessary to allow for thrust control (see later section).

Figure 18 provides a cross-sectional view of two typical wall nozzles used in solid propellant rocket motors. They both have a metallic shell (Titanium/aluminium/steel) covered by some ablator or insulator that protects the shell from excessive heating and a throat insert. Under certain conditions, it is possible to use a simplified structure e.g.

[3] A scarfed nozzle is an axi-symmetric nozzle that has been cut at an angle to allow the engine to fit in some envelope.

consisting of a shell and a throat insert (no insulator or ablator) but rather a material like Tungsten that can withstand high temperatures (sometimes more than 3000 K). More recently, structural wall materials include next to metallic materials other materials like plastics, glass-, silicon- and carbon-phenolics and carbon/carbon.

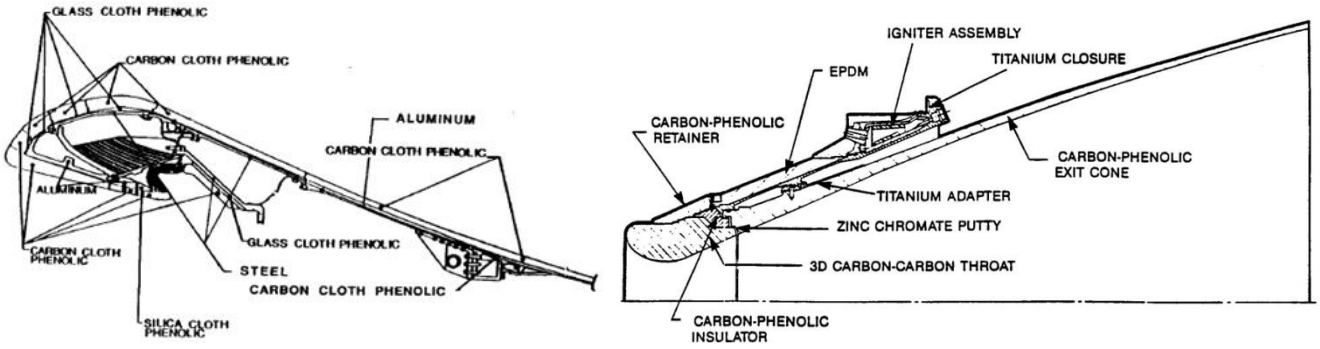

Figure 18: SRM nozzle wall structure

Nozzles for radiation-cooled rockets are mostly of a single wall design, where the structural material can carry both the heat and pressure loads. Usually, a coating is applied to protect the material from oxidation. No other insulation is necessary.

For nozzles of liquid rocket engines that are subject to high heat loads we typically use a "double wall" design. This allows for efficient removal of excess heat either through film, dump or regenerative cooling. In case of low nozzle pressures, low heat flux and low coolant pressure requirements a simple double wall design consisting of two concentric shells can be used. For higher heat flows, "tubular wall" designs are used. For example, the nozzle of the HM-60 is made up of 1,800 meters of thin-walled welded tubes (4 x 4 mm, 0.4 mm thickness) allowing coolant to flow through (see entry on cooling). The tubes are spirally wound, enabling the forming of any bell-shape desired. Overall length of the nozzle is 1.8 m, with an inlet diameter of 0.59 m an exit diameter of 1.76 m, and an expansion ratio of 45:1. The use of tubular walls is by far the most widely used design approach for the nozzle used in large rocket engines including also the Japanese LE5, and the USA H-1, J-2, F-1, and RS-27 rocket engines.

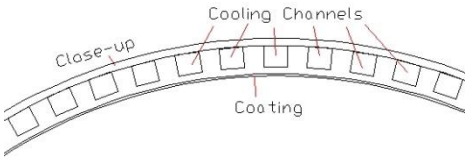

Figure 19: Example of channel wall of liquid rocket engine

To cope with high heat flows, ”channel-wall" designs are used. These are so named because the coolant flows through rectangular channels, which are machined or formed into a hot gas liner fabricated from a high-conductivity material, see Figure 19. The figure shows that the wall consists of three layers: a coating, the slotted high-conductivity material, and the close-up. These three layers can be different materials or the same.

The structural design of the nozzle is quite complex. A first step is the materials selection, see the next section. A second step is to perform a design from a thermo-mechanical point of view, i.e. computation of the stresses due to the combined pressure and thermal loading, to calculate the thickness of the elements making up the nozzle wall. Thermal loading needs to be considered because of the huge temperature difference along the nozzle with a very high temperature at the combustor end and a much lower temperature at the nozzle exit. Also, we should reckon with a significant difference in temperature over the thickness of the nozzle wall which is furthermore complicated in case we need to use a cryogenic coolant. Another factor adding to the complexity is in case the nozzle wall is composed of different materials, like thermal insulation materials, heat exchanger

materials, ablator materials and/or coatings that expand differently than the structural material. This can lead to additional stresses in the nozzle wall.

A very first approach to perform such a design is to use thin shell theory to compute the stresses in the material based on pressure loading only and then determine the nozzle wall thickness thereby applying appropriate safety margins. This is explained in some detail in the chapter on “Design of thin shell structures”. Large nozzles typically employ a nozzle wall of a tapered design. This can be easily understood when considering that nozzle pressure drops significantly (sometimes up to a factor 1000-10000), whereas the change in diameter is limited to a factor of ~20. For smaller nozzles this tapering is less obvious as walls may be so thin that this leads to very costly production.

To allow for a proper calculation of the wall thickness, we should not only consider the pressure in the nozzle but also the temperature of the material. These can be determined using the earlier presented 1D isentropic flow model in combination with heat transfer models (still to be discussed), thereby considering the cooling properties of the materials used. More details on nozzles of LRE and SRM can be obtained from [NASA (a) and (b)].

9 Nozzle materials

A typical double wall of a liquid rocket motor is shown in Figure 19. As stated before, it consists of three layers: a coating which protects the underlying material from oxidation (corrosion), a high-conductivity material that transfers the heat to a coolant, and the structural material providing strength. Structural material used in such engines includes Inconel (some kind of nickel alloy), stainless steel or titanium. High-conductivity materials used include pure copper or copper alloys, like NARloy Z. A typical coating material is silicide (e.g. SiO_2) or alumina (Al_2O_3).

Two specific solid rocket motor nozzles were already shown in Figure 18. They both consist of a metallic shell covered on the flame side by tape wrapped phenolics that ablate (erode) during operation. This way the phenolic material protects the structural shell from excessive temperatures. This thermal or flame line can be quite heavy. From a study by [Nickens] it was reported for a 260-inch (6.60 m) diameter solid rocket motor a nozzle mass of 21.7 tons of which the structural mass was only 4.43 tons with the remainder being made up by the thermal liner and insulation layers covering the nozzle structure. More modern designs focus on using materials that can withstand higher temperatures and or erode/ablate less to limit the nozzle mass. To limit the ablation is also considered important to preserve the shape (including nozzle throat area and nozzle area ratio) of the nozzle.

Depending on the function a material fulfils, the following main classes of nozzle materials can be distinguished: structural materials; thermal conductors, thermal insulators, ablative (erodible) materials and coatings. The choice of material for each of these functions depends on considerations concerning strength, density, corrosiveness[4], fatigue resistance, brittleness, etc.

The structural material we choose generally depends on the maximum operating temperature to which it will be exposed to.
Up to 500 K, the most used structural materials are aluminium alloys and fiberglass-resin composites, both of which have high-strength-to-weight ratios, are light in weight, easily fabricated, have good corrosion resistance, and are reasonable in cost. High strength steels are used when major considerations are high strength in thin sections, or operation at the higher end of the temperature range.
In the temperature range 500 – 1000 K titanium alloy or Inconel may be used. Both are high-strength low-density metallic alloys. In the temperature range 900 – 1400 K we must

[4] Material compatibility with a propellant is classified sequentially from Class 1 materials, which exhibit virtually no reaction with the propellant, to Class 4 materials, which react strongly with the propellant.

resort to the use of cobalt-based alloys, like Haynes 25, or Haynes 188. Cobalt based alloys are readily worked and can be age hardened. A major drawback, however, is their relatively high density and their sensitivity to oxidation and corrosion at elevated temperatures, which necessitates the use of a coating.
At temperatures more than 1300 K refractory metals like rhenium, molybdenum, columbium (Niobium) and alloys of these elements are to be used as the structural material. To protect this material against oxidation usually a silicide coating is used. However, also other coatings are possible. More recently, one is considering the use of ceramic-matrix carbon as the structural material as this requires no coating and is equally capable of attaining high temperatures.

Typical properties of some of the materials mentioned in the foregoing have been collected in Annex K of this work.

Problems

1) Nozzle selection

Generate a table wherein you present an overview of the advantages and disadvantages of the various nozzle shapes with respect to amongst others nozzle size, performance, complexity, cost and design heritage.

2) Conical nozzle design

You are designing a conical nozzle for a hydrogen-oxygen rocket motor with a vacuum thrust of 1 MN and a vacuum specific impulse of 450 s. You have selected the following design conditions:

- Chamber pressure of 110 bar
- Mass mixture ratio of 5
- Specific heat ratio: 1.15
- Flame temperature: 3400 K
- Molar mass: 11.8 kg/kmol

You are asked to determine:

a. Length of nozzle exit cone. Given are an exit cone half angle of 18 degrees, a contraction angle of 30 degrees, and a throat longitudinal radius of 1 time the radius of the throat cross-sectional area.
b. Nozzle wall structural thickness at nozzle throat and exit using D6AC steel as the main structural material and assuming that internal pressure loading is the dimensioning load. Furthermore, you may assume that insulation is present that keeps the material at room temperature. See annex L for the analysis of thin-shell structures.

3) Contoured nozzle design

You are in the process of designing a nozzle for a large rocket motor. You have selected as baseline a conical nozzle that has the following dimensions:

- Throat radius: 0.115 m
- Exit radius: 0.78 m
- Divergence half angle: 18 deg
- Throat longitudinal radius; 1 x throat radius

You are asked to determine a comparable bell nozzle contour with a nozzle length divergent part being 85% of that of the conical nozzle assuming that the bell nozzle contour can be approximated as a parabola.

4) Performance loss conical nozzle

Consider the conical nozzle defined in problem 2. Given are a wall temperature of 500 K and a dynamic viscosity of 53 μPa-s. You are asked to calculate:

- Loss factor due to flow divergence.
- Loss factor due to viscous effects (without considering any reduction in nozzle area ratio).
- Loss factor resulting from the reduction in nozzle area ratio (consider the displacement thickness of the boundary layer).

In addition, you are asked to determine if for this nozzle flow separation occurs. If so, would you try to circumvent this problem or not (explain, do not calculate).

References

1. AGARD, Performance of rocket motors with metallized propellants, AGARD Advisory Report, AR-230, 1986.

2. Barrère M., Jaumotte A., Fraeijs de Veubeke B., Vandenkerkchove J., Rocket Propulsion, Elsevier Publishing company, 1960.

3. Huzel D.K. and Huang D.H., Design of Liquid Propellant Rocket Engines, NASA SP-126, NASA, Washington, D.C., 1971.

4. Johnson A.N., Espina P.I., Mattingly G.E., Wright J.D., and Merkle C.L., Numerical characterization of the discharge coefficient in critical nozzles, NCSL Symposium, session 4E, 1998.

5. NASA (a), Solid Rocket Motor Nozzles, NASA SP-8115, 1975.

6. NASA (b), Liquid Rocket Engine Nozzles, NASA SP-8120, 1976.

7. Nickens T.L., Sutton J.L., Erickson L.H., Sottosanti P.C. Thrust Vector Control Study for Large Rocket Motor Applications, Thiokol, NASA CR 114223, April 1970.

8. RAO G.V.R., Exhaust Nozzle Contour for Optimum Flight, Jet Propulsion 28, No. 6, 1958.

9. RAO G.V.R., Approximation of Optimum Thrust Nozzle Contour", ARS Journal, Vol. 30, No. 6, p. 561, 1960.

10. Schlichting H., Boundary Layer Theory, McGraw-Hill, Inc, 1979.

11. Schmucker R.; Flow processes in overexpanding nozzles of chemical rocket engines (in German), report TB-7, -10, -14, Technical University Munich, 1973.

12. Spisz et al, Thrust coefficients of low-thrust nozzles, NASA TN-D3056, 1965.

13. Stark R.H., Flow Separation in Rocket Nozzles: A simple criteria, German Aerospace Center, Lampoldshausen, Germany.

14. Sutton G.P., Rocket Propulsion Elements, 9th ed., John Wiley & Sons, Inc., 2017.

15. Stern F., Fluid Mechanics (class notes), University of Iowa, 1999.

16. Tang S.P. and Fenn J.B., Experimental Determination of the Discharge Coefficients for Critical Flow through an Axisymmetric Nozzle, AIAA Journal Vol. 16, No.1, January 1978.

17. Wong H.Y., Handbook of Essential Formulae and Data on Heat Transfer for Engineers, Longman Group UK, London, 1977.

For further study

1. Performance losses in Low-Reynolds-Number Nozzles, J Spacecraft, vol.5, no. 9,1968.

2. Beenen A.J.R., Single Expansion Ramp Nozzle analysis, TU-Delft, LR thesis work, August 1996.

3. Ablij H., Nozzle profile determination using the Method of Characteristics, TU-Delft, LR thesis work, ….

4. Meerbeeck W.B.A., Zandbergen B.T.C., and Souverein, L., A Procedure for Altitude Optimization of Parabolic Nozzle Contours Considering Thrust, Weight and Size, 5th European Conference for Aeronautics and Space Sciences (EUCASS), Munchen, Germany, DOI: 10.13140/RG.2.1.1118.0006, July 2013.

- This page is intentionally left blank -

Propellants and Propellant Properties

Contents

Contents....97

1 Introduction....98

2 Liquid propellants....98

3 Solid Propellants....99

4 Hybrid propellants....100

5 Non-chemical propellants....100

6 Important properties for propellant selection....100

References....111

For further reading....111

1 Introduction

The most important class of rocket propellants today is formed by the class of “chemical propellants”. Chemical propellants are characterized by that they carry the energy required for the heating of the propellant within. A chemical propellant is formed by associating a fuel with an oxidizer that under certain conditions react thereby releasing chemical energy. Fuel constituents are in general atoms of hydrogen, lithium, beryllium, boron, carbon, sodium, magnesium, aluminium and silicon. Oxidizer constituents include atoms like those of oxygen, chlorine, and fluorine. Thus, the term chemical propellant embraces all the active components, and it is possible to compile Figure 1. A second class is formed by the “non-chemical propellants”. These propellants are characterized by that a separate energy source, like a nuclear or electrical power source or the Sun, is required to heat the propellant to a high temperature. Theoretically, any substance can be used as a propellant in a thermal rocket motor, but there are certain other qualities necessary for the proper working of a propellant, which may serve as criteria for rejecting some and considering others. These qualities include such factors as price, availability, storability, handling properties, toxicity, specific weight, available experience, etc.

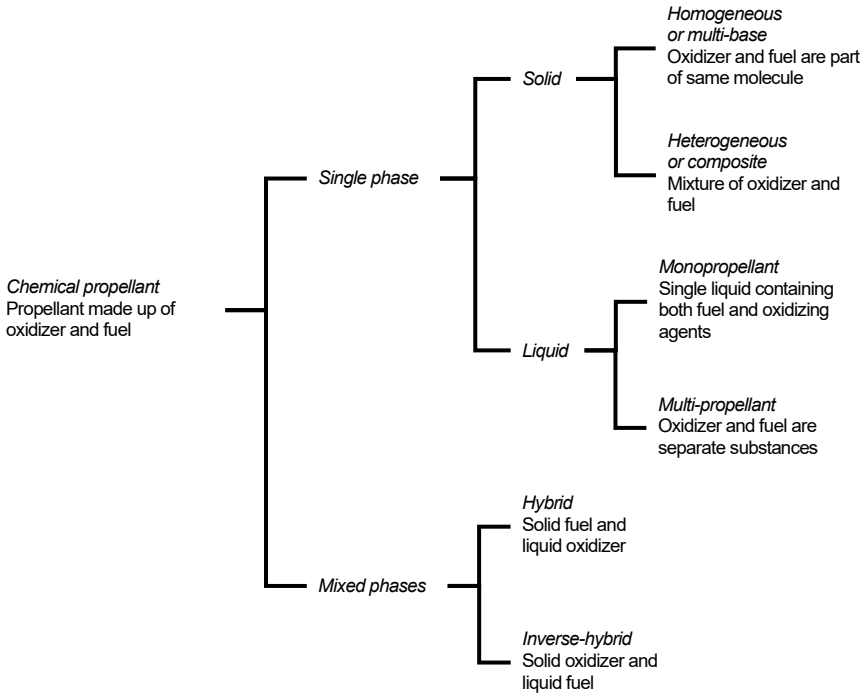

Figure 1: Overview of chemical propellant types [Timnat].

In the next few sections, we discuss the various types of propellants in some more detail.

2 Liquid propellants

A liquid propellant is characterized by that it is stored in the liquid state.

An important group of liquid propellants are the “monopropellants”. A monopropellant contains both the oxidizer and fuel, either in one molecule (called a simple monopropellant, like hydrazine, hydrogen test peroxide and methyl-nitrate) or as a mixture (called a composite monopropellant, like nitric acid with amyl-acetate). An advantage of a monopropellant propulsion system is that only one propellant tank and a single feed system is required. The monopropellant of choice today is hydrazine

offering a vacuum specific impulse as high as 230 s. Hydrogen test peroxide (HTP) sometimes is considered in case cost is an issue, but its vacuum specific impulse is limited to about 150 s. For monopropellants, usually a catalyst is required to ensure the proper decomposition of the monopropellant. For hydrazine, amongst others Shell 405 is used as a catalyst. It basically consists of finely divided iridium on an aluminium oxide support. Iridium is present to the extent of 30% of the total catalyst mass. For HTP, silver wire cloth and silver-plated nickel screen are used as catalyst. The nickel-based silver-plated screen increases temperature capability compared to silver wire cloth.

An even more important group are the "bipropellants". These consist of a separate fuel and oxidizer, which react exothermally when mixed. Because of the violent reaction occurring upon mixing, bipropellants require separate tanks for the oxidizer and the fuel for storage. For bipropellants, the mixture ratio of the fuel and oxidizer is an important parameter for realizing high specific impulse.

3 Solid Propellants

In a solid (chemical) propellant the fuel and oxidizer are stored in a condensed, solid state of matter.

An important class of solid propellants are the "homogeneous" propellants. In these propellants, the fuel and oxidizer belong to the same molecule, as for instance in nitrocellulose. Homogeneous propellants can be further subdivided into single, double, and triple base propellants. A typical single base propellant is the earlier mentioned nitrocellulose. It is a white fibrous material and is also referred to as guncotton. A classic example of a double base-propellant is the mixture of nitrocellulose and nitro-glycerine. The latter is an oily liquid. When mixed, the two form a colloidal solution; hence they are sometimes also referred to as colloidal propellant. Usually, plasticizers are added to enhance the mechanical properties. Double base propellants can be extruded, cast or pressed into shape.

Another important class of solid propellant is formed by the "heterogeneous" or "composite propellants". These consist of a separate fuel and oxidizer usually blended in some initially liquid plastic or rubbery binder material. After mixing, the mixture is cured to a hard rubbery state (usually at an elevated temperature). Curing can be done before propellant loading into the rocket motor, or the mixture can be cast (poured) into the motor case. Both oxidizer and metal fuel are usually added in the form of small particles which are a few to a several hundred microns in diameter. The fuel is mostly aluminum and the binder a hydrocarbon polymer[1], like polyurethane or polybutadiene. Typical polybutadiene currently used is hydroxyl terminated polybutadiene (HTPB), whereas in older designs carboxyl terminated polybutadiene (CTPB) or poly-butadiene acrylonitrile (PBAN) were used. HTPB based propellants offer better mechanical properties and processing compared to CTPB and PBAN based propellants. As oxidizer, usually an organic salt is used like ammonium perchlorate (AP), ammonium nitrate (AN), or potassium-perchlorate. A special composite propellant worth mentioning is black powder or gunpowder. It is the 'traditional' model rocket motor propellant. It uses charcoal as fuel and potassium nitrate and sulphur as oxidizers. Sometimes wax is added as binder material. Another propellant used in amateur rocketry is "rocket candy", which is based on a mixture of sorbitol (or some other sugar) and potassium nitrate.

A third class of solid propellant is formed by the Composite Modified Double Base (CMDB) propellants. These basically form a class in between the first two, where the polymerizable binder has been replaced by e.g. nitrocellulose.

[1] In the past, asphalt or tar has been used as binder.

Some additional information on solid propellants and their composition can be found on: TU Delft: Solid rocket propellants and their properties.Information on “Rocket candy” propellant may be obtained from [Olde].

4 Hybrid propellants

A “hybrid propellant” typically consists of a solid fuel and a liquid (or gaseous) oxidizer. Early hybrid propellants are liquid oxygen and colloidal benzene or laughing gas (N_2O) oxidiser and coal fuel. Later hybrid propellants used amine fuel and nitric acid oxidiser or poly-butadiene fuel and nitric acid oxidiser. Today, the solid fuels used are like the binders used in composite solid propellants. Sometimes metals like Aluminium (Al) or Boron (B) are added as fuel to increase the energy available from combustion. Oxidizers used in hybrid rocket are either gaseous or liquid. Typical oxidizers include HTP, NTO and Nitrous Oxide (NO) also referred to as laughing gas. In case of a hybrid rocket using a solid oxidizer; we tend to speak of an “inverse-hybrid propellant”.

5 Non-chemical propellants

Non-chemical propellants are mostly used in cold gas-, resistojet-, arcjet, and solar/laser-thermal propelled systems and usually require a separate energy source, like a nuclear or electrical power source or the Sun or a laser, to allow for thrust generation. For cold gas propelled systems, the energy used for thrust generation is fully contained in the gas and no separate energy source is needed. For thermal non-chemical propellants amongst others a low energy requirement for the heating of the propellant is important. Next to the energy required for heating, it is important that the propellant offers low molar mass and low specific heat ratio. The latter two allow for maximizing the exhaust velocity. Again, next to the above qualities, other qualities, like price, availability, storability and available experience are important to consider for propellant selection. Typical non-chemical propellants include Hydrogen, Helium, Ammonia, Nitrogen, Carbon-dioxide Methane, Water (or steam), and Argon.

6 Important properties for propellant selection

An important parameter for the selection of chemical propellants is the specific impulse. In case of non-chemical rockets, we have next to the specific impulse also the energy needed to heat the propellant to a certain temperature. The lower the energy needed, the less energy needs to be produced, leading to a low mass of the energy source. Besides specific impulse and energy needed (non-chemical systems) there are certain other qualities, which may serve as criteria for rejecting some and considering other propellants. Typical such qualities are state of aggregation, density, mechanical properties, toxicity, detonation risk, handling qualities, storage qualities (or storability), plume signature[2], price, availability, and available experience. A summary table of typical propellant properties of importance for propellant selection is given in Table 1. In this section some of these properties are discussed in detail. The numbers mentioned in the text are considered typical values for space applications. By no means should these values be interpreted as extremes. Additional data may be obtained from [Kit].

[2] Rocket exhaust plumes can be observed by either radiation or smoke. Rocket plume radiation may be in the infrared, visible, ultra-violet and the microwave band wavelengths.

6.1 Performance

An important performance parameter of both chemical and non-chemical thermal propellants is the specific impulse[3], i.e. the total impulse delivered per unit of propellant weight. For chemical systems this is the most important performance parameter. For non-chemical systems, next to specific impulse, we should also consider the power needed to heat up the propellant flow as this greatly determines the mass of the energy system. In the next two sections we will provide some detailed data.

Table 1: List of important properties for propellant selection

Category	Parameter
Propulsive Performance	Molar mass, specific heat ratio, temperature
Heating properties	Enthalpy, specific heat, heat of vaporisation
Storability	Density, coefficient of cubical expansion, freezing point, boiling point, vapour pressure, stability
Mechanical properties (solids only)	Yield and ultimate stress, elasticity, etc.
Cooling qualities	Heat of vaporisation, specific heat, thermal conductivity
Handling qualities	Explosiveness, toxicity, corrosiveness
Other properties	Price

6.1.1 Chemical propellants

High-energy bipropellants offer a sea level specific impulse in the range 270-360 s. High performance solid propellants are more limited, offering a sea level specific impulse in the range 210-265 s. Hybrid propellants offer a specific impulse in the range 230-270 s, which is similar to those obtainable with liquid bipropellants (apart from the very high performing ones, like liquid oxygen – liquid hydrogen). Liquid monopropellants offer a specific impulse in the range 160-190 s. Further information can be obtained from next two tables.

[3] The specific impulse can be used as a comparative measure for rocket propellants only if we compare specific impulse values at a fixed altitude and a fixed combustion pressure. As such, the specific impulse then is a good measure for the combined effect of changes in flame temperature, molar mass and specific heat ratio for the different propellants. Some detailed information on how these latter three properties vary with composition can be obtained from: Propellant Combustion Charts and TU Delft: Solid rocket propellants and their properties. How such information is obtained is tackled in a later chapter in this work on the thermochemistry of rocket propellants.

Table 2: Specific impulse of specific liquid chemical propellants at 69 bar chamber pressure and ideal expansion to 1 bar

Propellant combinations	I_{sp} Range (sec)
Low-energy monopropellants:	160 to 190
- Hydrazine	
- Ethylene oxide	
- Hydrogen peroxide	
High-energy monopropellants:	190 to 230
- Nitromethane	
Low-energy bipropellants:	200 to 230
- Perchloryl fluoride-Available fuel	
- Analine-Acid	
- JP-4-Acid	
- Hydrogen peroxide-JP-4	
Medium-energy bipropellants:	230 to 260
- Hydrazine-Acid	
- Ammonia-Nitrogen tetroxide	
High-energy bipropellants:	250 to 270
- Liquid oxygen-JP-4	
- Liquid oxygen-Alcohol	
- Hydrazine-Chlorine trifluoride	
Very high-energy bipropellants:	270 to 330
- Liquid oxygen and fluorine-JP-4	
- Liquid oxygen and ozone-JP-4	
- Liquid oxygen-Hydrazine	
Super high-energy bipropellants:	300 to 385
- Fluorine-Hydrogen	
- Fluorine-Ammonia	
- Ozone-Hydrogen	
- Fluorine-Diborane	

Table 3: Specific impulse of specific solid chemical propellants at 69 bar chamber pressure and ideal expansion to 1 bar

Propellant combinations	I_{sp} Range (sec)
Potassium perchlorate:	
Thiokol or asphalt	170 to 210
Ammonium perchlorate:	
Thiokol	170 to 210
Rubber	170 to 210
Polyurethane	210 to 250
Nitropolymer	210 to 250
Ammonium nitrate:	
Polyester	170 to 210
Rubber	170 to 210
Nitropolymer	210 to 250
Double base	170 to 220
Composite modified double base	230 to 250
Boron metal components and oxidant	200 to 250
Lithium metal components and oxidant	200 to 250
Aluminium metal components and oxidant	200 to 250
Magnesium metal components and oxidant	200 to250
Perfluoro-type propellants	250 and above

The solid propellants up to the composite modified double base propellants are classical rocket/missile propellants consisting of a solid oxidizer and a hydrocarbon binder fuel. The metal components with oxidant (e.g. ammonium perchlorate, potassium perchlorate, ammonium nitrate, or potassium nitrate) are pyrotechnic powder or pelletized solid propellants for instance used in pyrotechnic igniters, see later chapter on igniters. These demonstrate the advantage of using metals as fuel. Combining these metals with a hydrocarbon binder and a solid oxidizer leads to the more modern solid rocket propellants used for instance for space rockets.

6.1.2 Non-chemical propellants

Cold gas propellants

All substances in the gaseous state and or which can be easily vaporized can be used as cold gas propellant. A range of cold gas propellants and their performances in terms of specific impulse are given in the next table.

Table 4: Cold gas molar mass (M)and specific impulse (I_{sp}) values [Nguyen]

Propellant	Symbol	M [g/mol]	$I_{sp,t}$ [s] a)	$I_{sp,m}$ [s] a)
Hydrogen	H_2	2.0	296	272
Helium	He	4.0	179	165
Neon	Ne	20.4	82	75
Nitrogen	N_2	28.0	80	73
Argon	Ar	39.9	57	52
Krypton	Kr	83.8	39	37
Xeon	Xe	131.3	31	28
Chlorofluoromethane	CCl_2F_2	121	46 b)	37
Carbon tetrafluoride	CF_4	88	55	45
Methane	CH_4	16	114	105
Ammonia	NH_3	17	105	96
Nitrous oxide	N_2O	44	67 b)	61

a) At 25 °C. Assume expansion to zero pressure in the case of the theoretical value
b) At 38 °C and area ratio of 100

Difference between theoretical and measured specific impulse allows for determining motor quality. Motor quality is found to be in range 0.80-0.95. Lowest quality is for dichlorodifluoromethane. Highest quality is for Helium and Xenon.

Thermal propellants

In a non-chemical thermal rocket, a working fluid is heated to a high temperature after which it is expanded through a rocket nozzle to create thrust. Typical non-chemical thermal rocket propellants used today include hydrogen, helium, ammonia, nitrogen, and carbon dioxide. The next figure gives an overview of typical performances achievable for specific non-chemical propellants as a function of temperature.

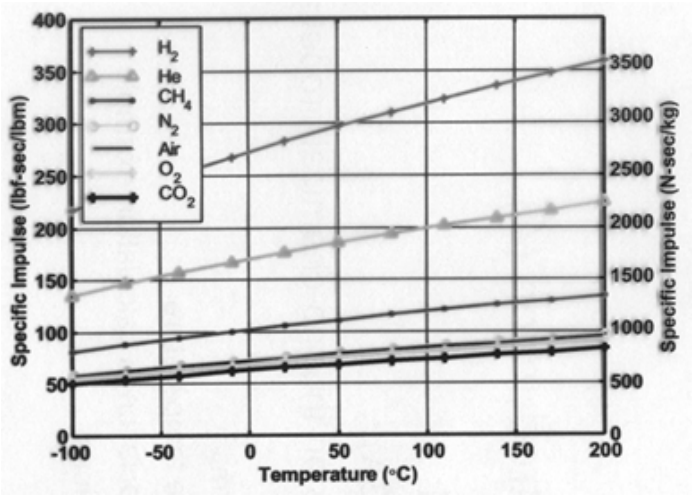

Figure 2: Theoretical specific impulse levels for specific non-chemical propellants as a function or propellant temperature (performances taken at 69 bar and assuming ideal expansion to sea level pressure).

Maximum specific impulse occurs for highest temperature feasible. Currently the state of technology allows for a maximum gas temperature of about 3000-3500 K, which gives a specific impulse of maximum about 900 s (about twice the value possible for the best performing chemical propellant) using hydrogen propellant. The second best

is helium, allowing for a maximum specific impulse of about 600-700 s. For ammonia (NH_3) the maximum specific impulse is in between 250-300 s, for nitrogen (N_2) in between 220 - 260 s and for carbon-dioxide (CO_2) in between 180-210 s.

However, energy is needed to heat up the propellant. To reduce the amount of energy required, and hence the mass of the energy subsystem, it is beneficial to have low specific heat. For rocket propellants that generally react at constant pressure, it is the specific heat at constant pressure that counts. Table 5 shows that hydrogen requires the most energy to heat up to a certain temperature and Xenon the least.

Table 5: Molar heat capacity and specific heat of some species (at room temperature and 1 bar pressure)

Specie	Formula	Molar heat capacity [J/mol-K]	Molar mass [kg/kmol]	Specific heat at constant pressure [kJ/kg-K]
Hydrogen	H_2	28.84	2	14.4
Helium	He	20.79	4	5.25
Nitrogen	N_2	29.12	28	1.04
Oxygen	O_2	29.36	32	0.920
Xenon	Xe	20.79	131.5	0.158

To solve this dilemma, one should strive to optimize the system specific impulse, see section “Sizing Fundamentals”.

6.2 Other properties

In this section several other qualities necessary for the proper working of a propellant are discussed. These qualities include storability, ignition properties, ballistic properties, handling properties, toxicity, and price.

6.2.1 Storability

Propellants need to be stored on board of the vehicle. Preferably propellants should remain in the intended state (gaseous, liquid or solid) over a reasonable range of temperature and pressure and be sufficiently stable and non-reactive with construction materials to permit storage in closed containers over longer periods of time without additional measures. Typical parameters of interest for storability hence include propellant density, freezing point, boiling point, vapour pressure, stability, and corrosiveness.

Mass density

Mass density depends on the specie and on the physical state of the propellant.

Gaseous species generally have low mass density, see next table, leading to a relatively large storage volume. Gas mass density can be increased by increasing the storage pressure. Today, typical storage pressures are up to 300-400 bar. The variation of gas mass density with temperature and pressure follows from the ideal gas law. More accurate results can be obtained in case also compressibility is considered, see later chapter on fluid storage, or by using tabulated data from e.g. [NIST].

Table 6: Mass density of some specific gases at two different pressures at 273 K [NIST].

Specie	Formula	Mass density (kg/m^3)	
		(@ 1 bar)	@ 241 bar
Hydrogen	H_2	0.090	18.45
Helium	He	0.179	37.83
Nitrogen	N_2	1.25	278.96
Oxygen	O_2	1.43	370.99
Carbon dioxide	CO_2	1.98	Liquefied

Liquid and solid species allow for higher mass density and hence lower storage volume, see Table 7 and Table 8.

Table 7: Mass density of some specific liquids used in liquid bipropellants @ room temperature unless indicated otherwise [NIST], [Sutton].

Compound	Density	Temperature
Alcohol (ethanol)	789 kg/m^3	
Liquid Oxygen	1141 kg/m^3	90.2 K
Nitrogen Tetroxide	1477 kg/m^3	
Liquid Hydrogen	70.9 kg/m^3	20.4 K
Liquid Nitrogen	806.1 kg/m^3	77.36 K
Liquid Methane	422.6 kg/m^3	111.5 K
Hydrogen Test Peroxide	1388 kg/m^3	
Hydrazine	1008.5 kg/m^3	
Mono Methyl Hydrazine	874 kg/m^3	
Dimethyl Hydrazine	791 kg/m^3	
Unsymmetrical Dimethyl Hydrazine	783 kg/m^3	
Dodecane (Kerosene)	745.7 kg/m^3	
Rocket Propellant-1 (RP-1)	733 kg/m^3	

Table 8: Mass density of some solids used in solid and hybrid propellants [Timnat & Korting]

Fuel	Average molecular formula [-]	Mass density [kg/m^3]	Molar mass [kg/kmol]
Plexiglas (PMMA)	$(C_5H_8O_2)_n$	1180	100
Polyethylene (PE)	$(C_2H_4)_n$	940	28
Polystyrene (PS)	$(C_8H_8)_n$	1050	104
HTPB	$(C_{10}H_{15.538}O_{0.073})_n$	930	138
PVC		1380	

For example, high-density solid propellants have a mass density in the range of 1500 – 1900 kg/m^3 compared to about 1000 – 1350 kg/m^3 for high-density storable liquid propellants. This compares favourably to the 280 - 375 kg/m^3 attainable for the high performing liquid oxygen – liquid hydrogen propellant. For hybrid propellants, it is possible to obtain a density in the range 1000 – 1200 kg/m^3. An important parameter for the determination of the mass density of a propellant is the mass mixture ratio (liquid bipropellants) of the propellant species or the detailed composition. The latter can be given in mass percentages, volume percentages, etc.

For most liquid and solid propellants, there is also a small effect of temperature on mass density to be considered. For instance, using [NIST] we learn that liquid hydrazine density varies from 1025.8 kg/m^3 at 273 K to 1004 kg/m^3 at 293k15 K and liquid hydrogen density from 71 kg/m^3 at 20.4 K to 76 kg/m^3 at 14 K. This change in mass density, will also affect the volume required for storage. The degree with which the volume of a substance (liquid/solid) changes with temperature is sometimes expressed using the coefficient of cubical (or thermal) expansion of the substance (β). It follows:

$$\Delta V = \beta \, \Delta T \, V$$

Where ΔT is the temperature change and V is volume. Values for the coefficient of cubical expansion for different species can be obtained from e.g. [Binas] as well as a range of other handbooks. For instance, alcohol has a mean coefficient of 1.1 x 10^{-3} per degree Kelvin over the range 293-373 K, for hydrogen peroxide, this is between 7.5 – 8.5 x 10^{-4} 1/K over the same range and for kerosene and hydrazine, both at room temperature, it is between 9.5-10 x 10^{-4} 1/K and 0.0001 1/K, respectively.

Freezing point

The physical state of specie depends on temperature and pressure, see Figure 3. Preference is to store propellant species at a pressure and temperature close to ambient conditions. This is well possible for a range of gaseous, liquid and solid species used in rocket propulsion. For example, solid propellants and solid fuels (in case of hybrid propellants) can be easily stored over longer periods of time of up to several years. Preferred storage temperature is in the range 0 to 45 °C with maximum relative humidity of 30-35%.

To increase the mass density of some species that are gaseous at standard conditions, we use liquefaction, where the propellants are cooled to a very low temperature. Such propellants are referred to as cryogenic propellants. Typical cryogenic propellant species are liquid oxygen (typically kept at ~91 K) and liquid hydrogen (kept at ~20 K). Cryogenic storage is advantageous for storage volume but poses a range of other problems. One example is the problem of boil-off[4]. To limit boil-off, the storage tank needs to be insulated. Another measure is that tanks are filled only a few hours before launch. Furthermore, a refrigerating circuit might be in place to cool the specie. Even so, cryogenic propellants are constantly evaporating so that measures must be taken to limit pressure build-up in the storage tanks. Another problem is that cryogenic propellants may cause ice to be formed on the tanks, leading to an increase in system mass and possible causing damage to the vehicle when breaking loose. Furthermore, pumps that operate at extremely low temperatures are difficult to design.

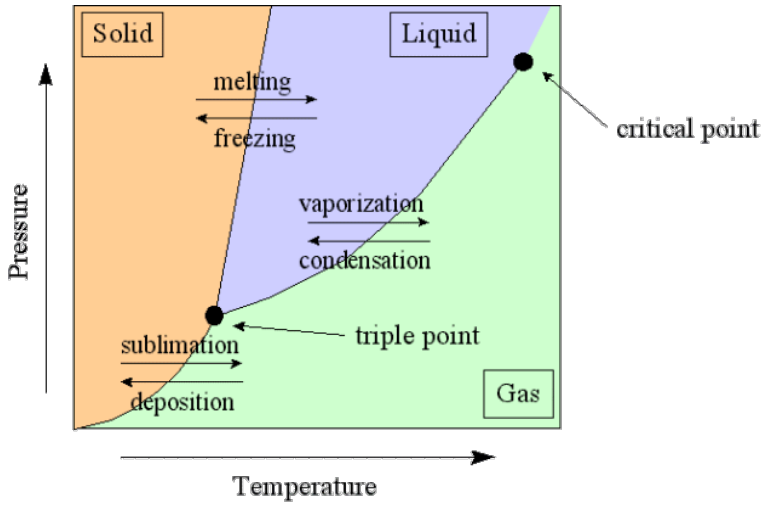

Figure 3: Phase diagram

Boiling point and vapour pressure

To limit vapour pressure and hence tank pressure, liquid species should have a high boiling point and/or a low vapour pressure over the temperature range of interest. In

[4] Boil-off is amount of specie that vaporizes in a liquid gas storage through external heating (ambient temperature). The gas is vented when the operating pressure is exceeded.

some applications it might be an advantage to have a high vapour pressure, as in that case no additional pressurization system might be necessary to ensure propellant feeding, see section on propellant feeding. Boiling point of some specific propellants can be obtained from Table 10.

Stability and corrosiveness

It is important that propellants are sufficiently stable and non-reactive with construction materials to permit storage in closed containers over longer periods of time without additional measures. This is especially important in case we use a monopropellant like hydrazine or hydrogen-peroxide. For instance, hydrogen-peroxide deteriorates at a rate of 1% per year, see Table 10.

6.2.2 Ignitability

Gaseous propellants are easiest to ignite. Next are liquid, hybrid and solid propellants of which the latter is the most difficult to ignites. Monopropellants have the advantage that they only need a catalyst to start the decomposition process. This means that no separate ignition system is required. Some bipropellants are self-igniting (hypergolic), like Unsymmetrical Di-Methyl Hydrazine (UDMH) with nitric acid. “Non-hypergolic” propellant systems require an independent ignition system and, in some cases, continuous ignition. Important characteristics include impetus, ignition delay time, stability (monopropellants). For further discussion of these properties, you are referred to the section on ignition of (chemical) rocket motors.

6.2.3 Ballistic properties

Ballistic properties are of importance with respect to the combustion of a propellant. These properties include amongst others burn or regression rate, temperature and pressure sensitivity of burn rate (solid propellant), fuel regression rate (hybrid propellant) and reaction time or characteristic chamber length (liquids). These properties are discussed in more details in the sections dealing with the internal ballistics of liquid, solid and hybrid propellant rocket motors.

6.2.4 Cooling and insulation properties

Solid propellants or solid fuels (in case of hybrid propellants) sometimes are used to insulate the chamber wall from the hot combustion gases. Insulation comes in part from low thermal conductivity of the propellant or fuel. More importantly, however, is that the heat flow to the wall is reduced because part of this heat is used to heat up and vaporise the (initially) solid propellant. Some liquid fuels, like hydrogen, alcohol, kerosene, mono-methyl-hydrazine, and methane, are used to cool the rocket motor, either through film, dump, regenerative, or transpiration cooling. The reason for using the fuel as coolant and not the oxidiser is because of the corrosiveness of the latter especially at elevated temperatures. More details on cooling (including insulation cooling and ablation cooling) can be found in the section on heat transfer and cooling.

6.2.5 Mechanical properties

Considered out of scope.

6.2.6 Safety and handling properties

Typical parameters important for safety and handling include explosiveness, fire hazard, toxicity, and corrosiveness. Essential health and safety information on chemicals can be obtained from International Chemical Safety Cards, see for example annex A. For illustration, hydrogen is considered extremely flammable. Many reactions may cause fire or explosion. Hydrogen may also lead to suffocation and in case of

handling cryogenic hydrogen; there is the danger of frost bite. Below some of the parameters of interest are discussed in some detail. A tabular overview of typical data for specific propellants can be obtained from Table 10.

Fire, explosion and detonation hazard

Most chemical fuels are considered fire hazardous or may give cause to explosions. For example, there have been accidents where liquid oxygen was spilled onto asphalt (a fuel), which caused an explosion when a truck was driven over the spill. The small amount of heat and pressure caused by the tire was enough to trigger an explosion in that concentration of oxygen. Solid rocket propellants are explosives by nature, i.e. a substance (or mixture of substances), which is capable, by chemical reaction, of producing gas at such a temperature and pressure as to cause damage to the surroundings. Once burning starts, it will be almost impossible to stop it. Solids also have potential for detonation[5]. The latter requires extensive safeguards during propellant manufacturing as well as launcher- and payload processing.

Toxicity and corrosiveness

Most liquid propellants, like fluorine, hydrazine, nitric acid, mono-methyl hydrazine, oxygen etc., are difficult to handle, because they are very toxic and/or corrosive. This requires special pre-cautions; see e.g. Figure 4. In contrast, solid propellants as well

as the solid component of hybrid propellants are relatively harmless in human contact. A measure for toxicity of propellants is the median lethal dose.[6]

Figure 4: Liquid propellant loading (ESA)

Environmental load[7]

The major exhaust products of various solid and liquid chemical propellants are shown in the table below. Typical concerns related to rocket exhaust products are toxicity, acid rain, Ozone depletion, and the 'Greenhouse effect'. Further information on the environmental effects of rocket exhaust products can be obtained from e.g. [R.R. Bennet, et al., 1992].

[5] **Detonation** This is a supersonic combustion wave. Detonations in gases propagate with velocities that range from 5 to 7 times the speed of sound in the reactants. For hydrocarbon fuels in air, the detonation velocity can be up to 1800 m/s. The ideal detonation speed, known as the **Chapman-Jouguet velocity**, is a function of the reactant composition, initial temperature and pressure.

[6] In toxicology, the **median lethal dose**, **LD_{50}** (abbreviation for "lethal dose, 50%"), **LC_{50}** (lethal concentration, 50%) or **LCt_{50}** is a measure of the lethal dose of a toxin, radiation, or pathogen. The value of LD_{50} for a substance is the dose required to kill half the members of a tested population after a specified test duration. LD_{50} figures are frequently used as a general indicator of a substance's acute toxicity.

[7] Global impact of rocket exhaust on stratospheric ozone concentration and ground level ultraviolet radiation is estimated at maximum 0,02%.

Table 9: Major exhaust products of some typical rocket propellants

Propellant system	Major exhaust products
Ammonium perchlorate/aluminium	HCL, H_2O, Al_2O_3, CO_2, N_2
Liquid Oxygen/liquid Hydrogen	H_2O
Liquid Oxygen/hydrocarbon	CO_2, hydrocarbons, H_2O
Nitrogen tetra-oxide / dimethylhydrazine	NO_x, CO_2, N_2

6.2.7 Price

Table 10 gives prices of some specific liquid propellants. Solid (HTPB/AP/Al) propellant cost (including casting) is about $ 5 - 40 per kg (2007) including casting, depending on the total quantity needed per year. Propellant cost usually is not a major factor of interest for liquid propellant rocket systems, as it forms only a small part of the total cost of the propulsion system. For solid propellant systems, the propellant cost is somewhat more important with for the Shuttle SRB an estimated contribution of 20% of the total booster cost [Calabro]. Propellant prices may differ with production scale and or order size. E.g. for UDMH engineering studies indicated a price of $ 1.00 per kg with large scale sustained production. But due to its toxic nature, production and transport costs soared in response to environmental regulations. By the 1980's NASA was paying $ 24.00 per kg.

Table 10: Liquid propellant properties [DESC]

Propellant	Use	Formula	Freezing point [K]	Boiling point [K]	Density [kg/m^3]	Stability	Handling	Storability	Materials compatibility	Cost[1)] [FY 2007 $/kg]
Hydrazine	Fuel, oxidiser, coolant	N_2H_4	273.2	386.2	1001 @ 293.15 K	Up to 422 K	Toxic & flammable	Good	Al, SS, Teflon, Kel-F, Polyethylene	106
95% Hydrogen peroxide	Fuel, oxidiser, coolant	H_2O_2	267.5	419.2	1414 @ 298.15 K	Unstable decomposition @ 423.7 K	Burns skin & flammable	Deteriorates at 1% per year	Al, SS, Teflon, Kel-F	10-11
Mono-methyl-hydrazine (MMH)	Fuel, coolant	$N_2H_3(CH_3)$	220.4	359.3	878 @ 293.15 K	Good	Toxic	Good	Al, SS, Teflon, Kel-F, Polyethylene	135
Nitrogen-tetroxide (NTO)	Oxidiser	N_2O_4	261.5	294.3	1440 @ 293.15 K	Function of temperature	Burns skin & toxic	Good when dry	Al, SS, Nickel alloy, Teflon	22
Rocket-Propellant 1 (RP-1)	Fuel, coolant	$CH_{1.97}$	<229.3	>445.4	800-820 @ 293.15 K	Auto-ignition @ 516.4 K	Flammable	Good	Al, steel. Nickel alloy, Cu, Teflon, Kel-F, Neoprene	3.5-10
Unsymmetrical-di-methyl-hydrazine (UDMH)	Fuel, coolant	$N_2H_2(CH_3)_2$	215.4	336.5	789 @ 293.15 K	Good		Good	Al, SS, Teflon	
Ammonia	Fuel, coolant	NH_3	195.4	239.8	683 @ BP	Good		Cryogenic	Al, steel, Teflon	
Liquid hydrogen	Fuel, coolant	H_2	13.9	20.4	71 @ BP	Good	Flammable	Cryogenic	Al, SS, Nickel alloy, Kel-F	1-5
Liquid oxygen	Oxidiser	O_2	54.3	90.1	1142 @ BP	Good	Good	Cryogenic	Al, SS, Nickel alloy, Cu, Teflon, Kel-F	0.13
Liquid methane	Fuel, coolant	CH_4	91	112	422.62 @ 111.5K			Cryogenic		3-4

BP = Boiling point; FY = Fiscal Year
Al = aluminium, SS = Stainless steel, Cu = Copper.

1) Prices tend to depend heavily on the quantity needed and the cost year. More up to date prices in relation to the quantity needed can be found here: Memorandum on Standard Prices for Aerospace Energy Category Items (2024)

References

1) Andrews, W.G., Haberman, E.G., Solids Virtues a Solid Bet, Aerospace America, June 1991.

2) Bennet, R.R., et al., Chemical Rockets and the Environment, Aerospace America, May 1991.

3) Calabro, M., Gizzi, E., "Launcher analysis and cost benefits", D1.2, 23 February 2018, Horizon 2020 project.

4) Huzel, K.K., et al, Design of liquid propellant rocket engines, 1971.

5) Kit and Evered, Rocket propellant data Handbook, The MacMillan Company, New York, 1960.

6) Nguyen, H.; Köhler J.; Stenmark, L.; The merits of cold gas micropropulsion in state-of-the-art space missions, IAC-02-S.2.07, 2002

7) NIST (National Institute of Standards and Technology), Chemistry webbook, DOI: https://doi.org/10.18434/T4D303

8) Olde, M.C., Potassium Nitrate Sorbitol Propellant; Experimental Investigation of Solid Propellant Characteristics, MSc thesis work, TU-Delft, 2019.

9) Sutton. G.P., Rocket Propulsion Elements, 6th edition, John Wiley & Sons, Inc. 1992.

10) SPIAG; Solid Rocket Motor Briefing, June 1999.

11) Timnat, Y.M., and Korting, P.A.O.G., Hybrid rocket motor experiments, TU-Delft, LR-452, February 1985.

12) Timnat, Y.M., and Laan, F. van der, "Chemical Rocket Propulsion", TU-Delft, LR, 1985.

13) DESC (US Defense Energy Support Centre, "Missile Fuels Standard Prices Effective Oct. 1, 2007.", Defense Energy Support Center, Virginia, July 2007. [Accessed 20/08/2020].

For further reading

1) "A new generation of solid propellants for space launchers", Acta Astronautica vol. 47, Nos. 2-9, pp. 103-112, 2000.

2) Lo, R. (1970). Advanced Chemical Rocket Propellants: On the Way from Theory to Hardware. In: Partel, G.A. (eds) Space Engineering. Astrophysics and Space Science Library, vol 15. Springer, Dordrecht. https://doi.org/10.1007/978-94-011-7551-7_12.

3) Werling L. et al, Research and Test Activities on Advanced Rocket Propellants at DLR's Institute of Space Propulsion in Lampoldshausen, 9TH European Conference for Aeronautics and Space Sciences (EUCASS), DOI: 10.13009/EUCASS2022-4540, 2022.

- This page is intentionally left blank -

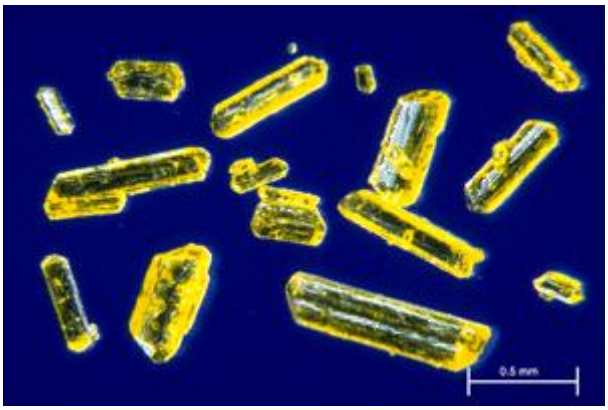

HNF crystals (courtesy APP)

$$3N_2H_4\ (l) \rightarrow\ 4NH_3\ +\ N_2 + \text{Energy}$$

Contents

Contents 113

List of symbols 115

1 Introduction 116

2 Chemical formula, mole, and molar mass 116

3 Energy/power needed for heating 119

4 Specific heat and specific heat ratio 124

5 Chemical reactions, mass balance, and mixture ratio 126

6 Heat of reaction and heat of formation 130

7 The adiabatic flame temperature 134

8 Chemical equilibrium 135

9 Propellant combustion characteristics and design charts 141

10 Effect of expansion in the nozzle 142

11 Computer tools 144

12 The effect of various parameters on performance 148

13 Problems 152

References 153

List of symbols

Roman

A	Compound
c_p	Specific heat capacity at constant pressure
C_p	Molar heat capacity at constant pressure
c_v	Specific heat capacity at constant volume
C_v	Molar heat capacity at constant volume
ER	Equivalence ratio
I_{sp}	Specific impulse
k	Reaction rate constant
K	Equilibrium constant
M	Mass
n	Number of moles of specific substance
N	Total number of moles in mixture
N_A	Avogadro's number
O/F	Mixture ratio
p	Pressure
Q	Heat
r	Reaction rate
R	Specific gas constant
R_A	Universal or absolute gas constant
S	Entropy
T	Temperature
U	Internal energy
H	Enthalpy
V	Volume
w	(true) exhaust velocity
W	Work

Greek

γ	Specific heat ratio
M	Molar mass
ρ	Mass density
ν	Stoichiometric coefficient

Superscripts

o	Refers to standard conditions (1 bar pressure and in a reference state, i.e. solid, liquid or gas)

Subscripts

av	Available
e	Refers to the final state
f	Formation
i	Refers to the various compounds in a mixture
mix	Mixture
o	Refers to the initial state
req	Required

1 Introduction

Today, many developments are taking place both in the development of new chemical propellants [d'Andrea], [Schöyer], [Gadiot], and [Mul] as well as in the development of (advanced) thermal rockets using either solar or nuclear energy to provide the energy to heat up the propellant. Main performance parameter is the specific impulse. Ideal rocket motor theory shows that specific impulse is nearly proportional to the (true) exhaust velocity[1] 'U':

$$w = \sqrt{\frac{2\gamma}{\gamma - 1} \cdot \frac{R_a}{M} \cdot T_c \cdot \left(1 - \left(\frac{p_e}{p_c} \right)^{\left(\gamma - 1 / \gamma \right)} \right)} \qquad (1.1)$$

From this relation we learn that it is desirable to have (see also section on ideal rocket motor):

- A high value of the temperature of the hot gases in the chamber 'T_c'. However, a major limitation to this temperature is the maximum temperature that can be withstood by the chamber wall and/or can be handled by the cooling system (if present).
- A low molar mass 'M'
- A large pressure drop 'p_e/p_c' over the nozzle
- A low value of the specific heat ratio 'γ'

It is the temperature of the hot gasses, the molar mass and the specific heat ratio that depends on the (chemical) propellant selected.

In case of using a separate energy source to heat up the propellants also the energy or power needed to heat up this propellant is of interest.

In the first part of this chapter, we shall consider the determination of molar mass, specific heat and specific heat ratio as well as the heat needed to heat up a (mixture of) substance(s) to the required temperature. In addition, we will consider thermo-chemical calculations that permit evaluation of the heat of reaction and the conditions in the chamber. More specific, the case of constant pressure, adiabatic combustion, forming a set of molecular products, in thermal and chemical equilibrium with each other will be treated. Second, attention will be paid to the evaluation of conditions inside the nozzle. The gaseous products and any condensed substances (liquid or solid) are expanded through a supersonic nozzle to a specific cross section, a specific exit pressure and against a specific ambient pressure. When expanding in the nozzle, the temperature of the hot gases drops, which may lead to a change in gas composition as well as in the gas properties with an accompanying change in exhaust velocity and hence specific impulse.

2 Chemical formula, mole, and molar mass

Chemical formula

In chemistry, distinct substances are usually referred to as chemical compounds or shortly compounds. The simplest substances into which ordinary matter can be divided using chemical means are the chemical elements. Today, over 100 different elements exist, see figure 1.

[1] In case of ideal expansion, specific impulse is directly related to the true exhaust velocity according to:

$$I_{sp} = w \cdot g_o$$

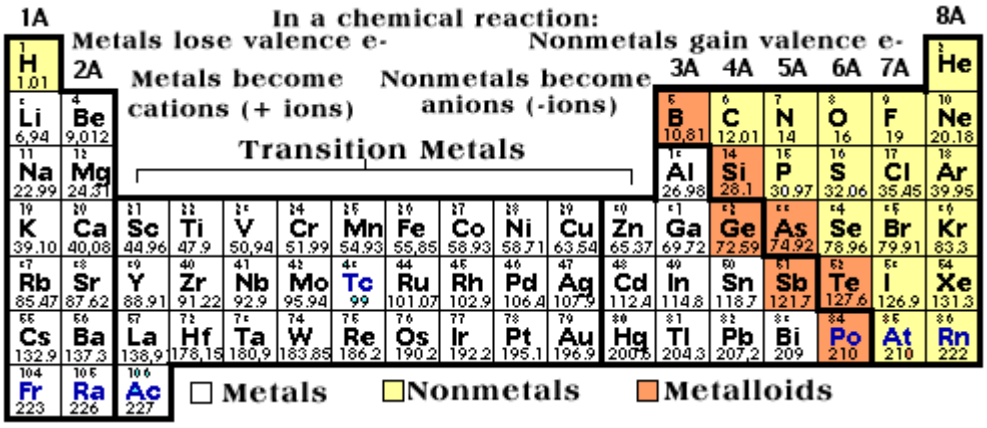

Figure 1: Periodic table of the elements [Bentor]

The smallest basic unit of a chemical element is an "atom". Atoms can be combined to form different chemical compounds (substances). The smallest particle of a substance that retains all the properties of the substance is referred to as “molecule”. For instance, we know that water can be formed by combining the elements hydrogen and oxygen, but the physical properties (like boiling point, and melting point) of water are completely different from the properties of its elements. The atoms that make up a compound and their ratio are usually represented by the compounds "chemical formula[2]" For instance, the chemical formula of nitric acid is written as HNO_3, which means that 1 molecule of nitric acid consists of 1 atom hydrogen (H), 1 atom nitrogen (N) and 3 atoms oxygen (O). The chemical formula of a great number of compounds can be obtained from handbooks on chemistry, like [CRC] or from the World Wide Web (www) like [NIST]. Table 1 gives chemical formula of specific propellant constituents. If the molecular formula of a compound is unknown, or if it has none, the compound is represented by its correct empirical formula. In an empirical formula we use the simplest (lowest) whole-number ratio of the elements that are present. For example, the molecular formula of benzene is C_6H_6, but the empirical formula is simply $(CH)_n$.

Table 1: Chemical formula and molecular mass of specific propellant constituents [NIST] and [CRC]

Substance	Acronym	Chemical formula	Molecular mass
Ammonia		NH_3	17.032
Ammonium nitrate	AN	NH_4NO_3	80.046
Ammonium perchlorate	AP	NH_4HClO_4	117.5
Carbon dioxide		CO_2	44.00
Hydrazine		N_2H_4	32.046
Hydrogen		H_2	2.016
Hydrogen peroxide		H_2O_2	34.016
Methane		CH_4	16.03
Monomethylhydrazine	MMH	CH_3NHNH_2	46.072
Nitric acid		HNO_3	63.016
Nitrogen		N_2	28.014
Nitrogen tetroxide	NTO	N_2O_4	92.016
Oxygen		O_2	32.000
Polyethylene	PE	$(C_2H_2)_n$	$(26.016)_n$
Unsymmetrical dimethylhydrazine	UDMH	$(CH_3)_2NHNH$	60.100

Molecular mass

The "relative molecular mass[3]" is the sum of the relative atomic masses of the atoms comprising a molecule, whereas the "atomic weight or relative atomic mass of an atom" is the average mass of an atom of an element, usually expressed in atomic mass units[4]. Typical values for the relative atomic mass of the chemical elements are

[2] Also referred to as molecular formula.
[3] Also referred to as molecular weight.
[4] One atomic mass unit (amu) is 1/12 the mass of a carbon-12 atom.

listed in many chemical textbooks, like [CRC], [Barrow], and [Binas]. Data can also be obtained from the worldwide web (www), like [NIST], and [Bentor].

To illustrate this method, we calculate the molecular mass of water, hydrazine, and aluminum-nitrate. The chemical formula of water is H_2O, of hydrazine N_2H_4, and of aluminum-nitrate $Al(NO_3)_3$. It follows for the molecular mass of these three substances:

- Water: 2 x 1.008 + 1 x 16.000 = 18.016
- Hydrazine: 2 x 14.007 + 4 x 1.008 = 32.046
- Aluminum-nitrate: 1 x 26.980 + 3 x 1 x 14.007 + 3 x 3 x 16.000 = 213.00

Values of the molecular mass of specific species are given in Table 1.

Mole, molar mass and number of moles

The “mole” is the standard unit in chemistry for communicating how much of a substance is present. According to the International Union of Pure and Applied Chemistry (IUPAC) the "mole" is the amount of substance of a system, which contains as many elementary entities as there are atoms in 0.012 kilogram of carbon-12. Measurements have shown that 6.022×10^{23} atoms are present in 12 grams of carbon-12. This number is so important in chemistry that it has a name. It is called "Avogadro's Number[5]" and has the symbol N_A. When the mole is used, the elementary entities must be specified and may be atoms, molecules, ions, electrons, other particles, or specified groups of such particles. The symbol for mole is "mol.”

"Molar mass" is the mass in grams of one mole of a substance. It has the symbol ‘M’ and as unit grams per mole. The symbol for grams/mole is ‘g/mol’. One way to determine the molar mass of a substance is to calculate the molecular weight based on the chemical formula of the chemical compound and stick the unit "g/mol" after the number. For instance, the molar mass of water, hydrazine, and aluminum-nitrate is, 18, 32, and 213 g/mol, respectively.
The number of moles ’n’ present in a certain mass ‘M’ of a substance follows by dividing this mass by the molar mass of this substance:

$$n = \frac{M}{\mathrm{M}} \tag{2.1}$$

For example, 100 gram of hydrogen with an average molar mass of 2 g/mol (rounded value) equals 50 moles.

One way of measuring number of moles directly without knowing a molar mass is by using the ideal gas equation along with pressure ‘p’, temperature ‘T’, and volume ‘V’ observations.

$$p \cdot V = n \cdot R_A \cdot T \tag{2.2}$$

With ‘R_A‘ is universal gas constant (R_A = 8.314 J/(mol-K)). Vice versa, we can find that one mole of an ideal gas occupies 22.4 litres at standard conditions (1 atmosphere and 273 K).

The substitution of the number of moles relationship in the ideal gas equation, allows us to rework this relationship to provide us with a relationship that allows us to directly find the molar mass, without knowing the number of moles present:

[5] Avogadro’s number is named so in honour of Amedeo Avogadro, an Italian chemist, who in 1811, made a critical contribution (recognized only in 1860 after his death), which helped greatly with the measurement of atomic masses.

$$M = \frac{\rho \cdot R_A \cdot T}{p} \tag{2.3}$$

For instance, consider a 10 l container filled with 100 g of pure gas at a pressure of 10 bars and a temperature of 10 °C. Based on the gas volume and the mass of the gas, we find a gas density of 10 kg/m^3. Using the ideal gas law, we find for the molar mass:

$$M = \frac{\rho \cdot R_A \cdot T}{p} = \frac{10 \cdot 8314.32 \cdot 283{,}15}{1\,E+6} = 23.5\ g/mol \tag{2.4}$$

This method can also be used in case the composition of the exhaust (the substances presents and their chemical formula) of a rocket is not known. In that case, the above method provides us with the "mean molar mass" of the exhaust gases. However, in practice, this is not as simple as it may seem, and we rather use other methods to determine the (mean) molar mass of the exhaust gases.

One such method is by determining an (number) "average molar mass" based upon the mass of the gas mixture divided by the number of moles in the mixture:

$$M = \frac{\sum_i n_i \cdot M_i}{\sum_i n_i} \tag{2.5}$$

The subscript 'i' refers to the different substances present in the gas mixture and 'n' to the number of moles. How we determine the composition of the gas mixture and the molar quantities will be dealt with later.

Mole fraction

The "mole fraction" of a substance gives the fraction of the total number of moles in a mixture due to one component of the mixture (n_i/N with $N = \Sigma n_i$). For example, the mole fraction of substance A in a mixture of A and B means the number of moles of A divided by the number of moles of A plus the number of moles of B.

3 Energy/power needed for heating

To heat up a substance, like in thermal rocket motors, a certain amount of energy is required. To calculate this energy change, we use the first law of thermodynamics, which is essentially the law of conservation of energy, i.e. the total energy of the system plus the surroundings is constant. Writing the first law in internal energy form for 1 mole of matter[6], we get:

$$\delta Q = dU + \delta W \tag{3.1}$$

[6] The first law holds independent of how much of a substance is present. However, the value of e.g. the internal energy depends on how much substance is present, i.e. it is an extensive variable. An extensive variable can be made into an "intensive" variable, i.e. a variable that does not depend on how much substance is present, in two ways:

- Divide by the mass present in the system. The result is a property that is normalized by the mass. We add the term *specific* to indicate that we've divided by the mass.
- Divide by the number of moles present in the system. The result is a property that is normalized by the number of moles present. We add the term *molar specific* to indicate we've divided by the number of moles.

Standard is to use uppercase letters in case of using the mole as the standard quantity of matter; In case of using the kilogram as the standard quantity lowercase letters are used, for example 'U' for molar specific internal energy and 'u' for specific internal energy.

Here the symbol 'Q' refers to the heat change, 'U' to the change in internal energy[7] and 'W' to the work performed and 'd' and 'δ'indicate that we consider an infinitesimal change in the state of the system. The symbol 'd' furthermore indicates that internal energy is a state function. This means that for a particular state of a system internal energy has some particular value. The symbol 'δ' furthermore refers to a path function. This is a parameter, which varies in magnitude depending upon how conversion from one state to another is achieved. In case we only consider work done due to the system contracting or expanding against the confining pressure, we can write:

$$\delta W = p \cdot dV \tag{3.2}$$

$$\delta Q = dU + p \cdot dV \tag{3.3}$$

With 'V' is volume and 'p' is pressure.

To calculate the energy change, it is convenient to consider two conditions that are special and occur frequently: (1) the volume of the system is kept constant, and (2) the pressure on the system is held constant. The latter situation, for example, is that existing for reactions or other processes carried out in containers open to the atmosphere.

For a constant-volume process, no 'p V' work is done and we obtain:

$$\delta Q = dU \tag{3.4}$$

Constant-pressure processes are different in that generally the volume of the system changes and work is done on or by the surroundings. Introducing a new energy term called the enthalpy defined by:

$$H = U + p \cdot V \tag{3.5}$$

It follows for the first law (in enthalpy form):

$$\delta Q = dH - V \cdot dp \tag{3.6}$$

Since a rocket motor is open to the atmosphere, the heating of the propellants inside it can be considered a constant pressure process. In that case, the last term on the right hand side in the first law in enthalpy form vanishes. If the index o is used to indicate the state before the reaction and index e to indicate the state after the reaction, integration of the first law shows that:

$$Q = H_e - H_o = \Delta H \tag{3.7}$$

The change in enthalpy (and internal energy) or relative enthalpy can be determined by measuring the heat needed to raise the temperature of a certain amount of a substance from an initial state to a final state. These kinds of measurements can be made using a calorimeter. A "'calorimeter" is an apparatus used to measure the change in enthalpy or internal energy of a substance. Two types can be distinguished:

- Solution calorimeter - An insulated container, open to the atmosphere, used to measure heat change at constant pressure, see figure 5-2. A weighed sample of a substance at a certain temperature is placed in the calorimeter. A certain mass of hot water and a given temperature is added. From the temperature that results the specific heat of the substance is determined (based on the known specific heat of water.

[7] Internal energy depends on contributions due to translational motion of the molecules, rotational motion, vibrations and electrons (of metallic crystals).

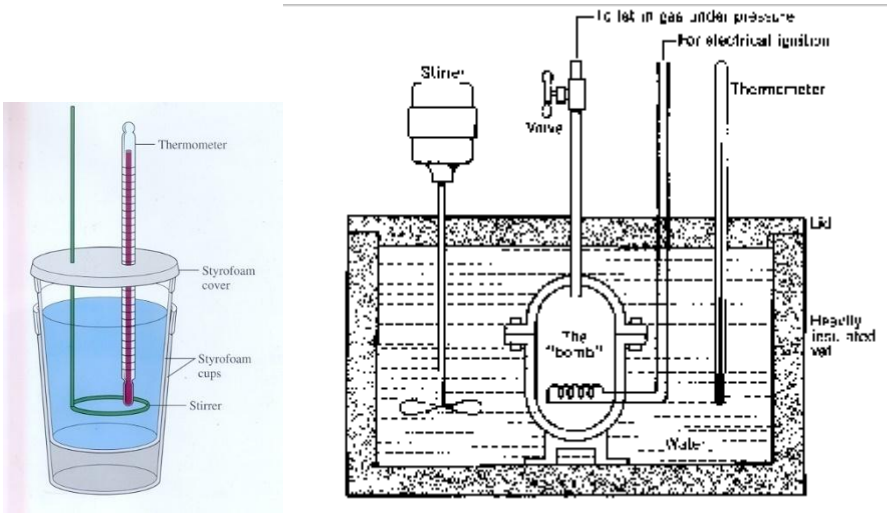

Figure 2: Schematic solution calorimeter (left) and bomb calorimeter (right)

- Bomb calorimeter - A sealed, insulated apparatus used to measure heat change at constant volume. A weighed sample of a substance is placed inside a closed vessel surrounded by water. The vessel then is filled with oxygen under a pressure of about 30 bars. A fine wire heated by an electric current is used to start the reaction. The heat liberated is determined by measuring the temperature rise of the water around the calorimeter. Of course, bomb and water should be carefully insulated from the surroundings, see also figure 5-2.

An important problem with respect to enthalpy measurements is that we can only measure changes in the enthalpy of the system and have no way to determine the absolute enthalpy. It is for this reason that we select 298,15 K (or 25 ^{o}C), which is slightly above normal room temperature, as reference temperature. Since the enthalpy change furthermore depends on pressure and the amount of the substance considered, scientists have agreed upon a standard reference set of conditions, i.e. “standard conditions”. These conditions refer to 1 mole of a substance and 1 bar pressure and have been chosen so that experiments can be done easily. Results are documented in amongst others [JANAF], [CODATA]. A useful "on-line" source of data is [NIST][8].

Table 2: Gas phase relative enthalpy of some species [JANAF]

T (K)	$[H^{\circ}_T - H^{\circ}_{298,15}]_{nitrogen}$ (kJ/mol)	$[H^{\circ}_T - H^{\circ}_{298,15}]_{hydrogen}$ (KJ/mol)
0	-8.670	-8.467
100	-5.768	-5.468
1300	31.503	29.918
1400	34.936	33.082
1500	38.405	36.290
1600	41.904	39.541
1700	45.429	42.835
1800	48.978	46.169

The superscript ‘^{o}’ is used to indicate that the enthalpy is taken at standard conditions.

Rocket propulsion engineers generally use gas phase relative enthalpy data because of the nature of the rocket exhaust. For an ideal gas, it can be shown that enthalpy is a function of temperature only (no pressure effect). In that case, we can calculate the total energy required for heating (or cooling) ‘Q_{req}’ using:

[8] Values will differ between various publications, depending on which set of past experiments were used to compile the reference source used by the author. The different values tend to be fairly close. It is recommended to use the JANAF-NIST values and not try to make these differences be an issue.

$$Q_{req} = n \cdot \Delta H = n \cdot \Delta H^{o} = n \cdot \left(H^{o}_{T} - H^{o}_{298.15} \right) \tag{3.8}$$

And in case of a mixture of gases:

$$Q_{req} = \sum_{i} \left(n \cdot \Delta H \right)_{i} \tag{3.9}$$

Here 'i' refers to the various substances present in the mixture.
The temperature dependence is often approximated using:

$$H^{o}_{T} - H^{o}_{298.15} = A \cdot T + B \cdot \frac{T^{2}}{2} + C \cdot \frac{T^{3}}{3} + D \cdot \frac{T^{4}}{4} - \frac{E}{T} + F \tag{3.10}$$

To calculate the required energy, it is of course possible to use (mass) specific values instead of molar specific values.

To convert molar specific enthalpy to (mass) specific enthalpy, we simply divide the molar specific enthalpy by the molar mass:

$$\Delta h = \frac{\Delta H}{M} \tag{3.11}$$

Using specific enthalpy, the required heat simply follows from the multiplication of the specific heat of the substance and its mass 'M':

$$Q_{req} = \sum_{i} M_{i} \cdot \Delta h_{i} \tag{3.12}$$

Phase transition

- When heating a substance, we must consider possible phase changes of this substance. For instance, ice melts to give liquid water. Liquid water boils to give water vapour, which is a gas. The phases present in a one-component system at various pressures and temperatures can conveniently be presented on a pressure versus temperature plot, see fig. 3.

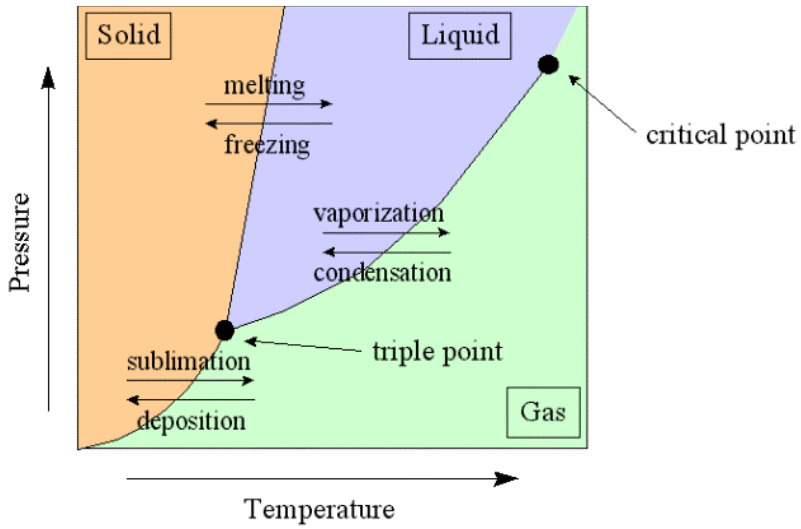

Figure 3: Representative one-component phase diagram

From this figure, we learn that the temperature at which melting/freezing, vaporization/condensation and sublimation/deposition occurs depends on pressure. In addition, two special points occur:

- Critical point: Point where the densities of liquid and vapour become equal and the interface between the two vanishes. Above this point, only one phase can exist. For instance, above the critical temperature, we cannot liquefy a gas independent of how high the pressure is.

Triple point: The temperature and pressure at which solid, liquid, and vapour phases of a particular substance coexist in equilibrium.

Transitions between solid, liquid, and gaseous phases typically involve large amounts of energy compared to the specific heat. We distinguish:

- Heat of fusion (h_{fus}) - the heat absorbed by a solid per unit mass when it melts to give the same amount of liquid at the same temperature and pressure.
- Heat of sublimation (h_{sub}) - the heat absorbed by a solid per unit mass when it sublimes to give the same amount of vapor at constant temperature and pressure.
- Heat of vaporization (h_{vap}) - the heat absorbed by a liquid per unit mass when it is changed to give the same amount of vapor at constant temperature and pressure.

Next table gives the boiling points and the heat of vaporization of specific substances used in rocket propulsion.

Table 3: Normal boiling point (at 1 atmosphere pressure) and heat of vaporization of specific substances

Substance	Boiling point (K)	Boiling point (°C)	Heat of vaporization (kJ/kg)
Helium	4.2	-268.93	20.9
Hydrogen	20.36	-252.89	452
Nitrogen	77.3	-195.81	201
Argon	87.2	-185.95	162.8
Oxygen	90.2	-182.97	213
Methane	111.7	-161.45	577.4
Carbon dioxide	194.65	-78.5	571.3
Ammonia	239.7	-33.45	1368
Ethyl alcohol	351	78	854

To vaporize a liquid (mixture) of mass M, the heat needed is given by:

$$Q_{req} = \sum_i \left(M \cdot h_{vap}\right)_i = \sum_i \left(n \cdot H_{vap}\right)_i \qquad (3.13)$$

Here the subscript 'i' again indicates the various substances in the mixture.

The heat of vaporization at conditions different from the above normal conditions can be determined based on that enthalpy is a state function. For example, the heat of vaporization of ammonia at 300 K should equal the heat of vaporization at 239.7 K (see table) plus the enthalpy change to heat up the vaporized ammonia to 300 K, see [JANAF] or [NIST] minus the enthalpy change to heat up the liquid ammonia from 239.7 K to 300 K [NIST].

Other high temperature effects

At high temperatures, such as that which occurs in rocket motors, compounds partially break up into electrically neutral fractions, called radicals. This process is called *dissociation*. For example, at 3000 K, the degree of dissociation of hydrogen is in the range 0.5 – 10%, depending on the pressure, whereas at 4000 K it is even in the range of 5 - 65% [Zandbergen, 1995]. Dissociation is highly endothermic and may cause the flame temperature to drop. On the other hand, the molar mass of the mixture will also decrease. For a more in-depth treatment, see the section on chemical propellants hereafter.

At temperatures above about 4000 K even ionization may occur. However, since thermal rockets temperatures are limited to below 4000 K, ionization will not be treated here.

Example calculations

Example 1: Heating without phase transition

Problem: You are designing a small thermal rocket engine using gaseous nitrogen (stored at 298.15 K) as propellant. You have selected a mass flow rate of 0.1 kg/s and a hot gas temperature of 1500 K. Calculate for this rocket the thermal power needed to heat the nitrogen propellant to 1500 K.

Solution: Using the Table 2, we find that the change in enthalpy required to heat up 1 mol of nitrogen from the initial temperature of 298.15 K to 1500 K is 38.34 kJ. Using the molar mass of nitrogen, we find that the flow rate in moles/second equals 100/28 = 3.57 mol/s. It follows that per second we must add at least 137 kJ of energy. This gives for the power input a value of 137 kW.

Example 2: Heating with phase transition

Problem: Consider the same rocket engine as in example 1, but now you store the nitrogen on board in the liquid phase. Calculate again the thermal power needed to heat the nitrogen propellant to 1500 K and determine the increase in required power compared to the value found in example 1.

Solution: The main difference is that we have to consider that the nitrogen is stored in the liquid phase. We will assume here that the nitrogen is stored at a temperature just below the boiling point (77.3 K). The next step is to determine the heat required to vaporize nitrogen. Using the heat of vaporization given in Table 3, we find that to vaporize 100 grams of nitrogen per second requires 20.1 kW of power. Next, we calculate the relative enthalpy to heat the vaporized nitrogen from 77.3 K to 298.15 K. From Table 2, and using linear interpolation, we find that the change in enthalpy required to heat the nitrogen gas from 77.3 K to 298.15 K is about 6.43 kJ/mol. Considering that every second 3.57 moles flow through the rocket, this gives a power requirement of 23.9 kW. To this we still must add the power needed to heat the nitrogen from 298.15 K to 1500 K, which is 137 kW (see example 1). The total power then adds up to 181 kW (20.1+23.9 + 137). This is an increase in required power of more than 30%.

Example 3: Heat change at constant volume from known data on heat change at constant pressure

Problem: Calculate the heat change at constant volume for the vaporisation of water at 373 K (100 °C) under 1 bar pressure. You may use for the heat change to vaporise 1 mole of water at 1 bar pressure a value of 40.70 kJ mol^{-1}.

Solution: Heat change at constant pressure can be calculated from heat change at constant volume and vice versa using:

$$\Delta H = \Delta E + p \cdot \Delta V \tag{3.14}$$

The heat change to vaporise 1 mole of water at 1 bar pressure is 40.70 kJ mol^{-1} and since this is a heat change at constant pressure, it follows: ΔH = 40.70 kJ mol^{-1}. Also, at constant pressure where $\Delta V = V_{H2O}(g) - V_{H2O}(l) \approx V_{H2O}(g)$ = 22.4 x 373 / 273 l (if H_2O vapour behaves ideally) so that $\Delta E = \Delta H - p\ \Delta V = 40.70 \times 10^3 - 101.25 \times 10^3 \times 22.4 \times 10^{-3} \times 373 / 273 = 40.70 \times 10^3 - 3100$ J= 37.6 kJ.

4 Specific heat and specific heat ratio

Specific heat

Heat capacity of a substance essentially is the energy needed to raise the temperature of this substance by 1°C. More important is the specific heat of the substance. This is

the heat capacity either per unit mass or per mole. Specific heat of substance depends on heating conditions:

- c_v is specific heat at constant volume, I.e. the amount of heat needed to raise the temperature of a substance by 1°C at constant volume conditions.
- c_p is specific heat at constant pressure, I.e. the amount of heat needed to raise the temperature of a substance by 1°C at constant pressure conditions.

Molar heat capacity - The energy needed to raise the temperature of 1 mol of a substance by 1 C, usually in units of J/mol- C. To obtain molar heat capacity, multiply specific heat by molar mass.

The molar heat capacity at constant pressure and volume are strongly related to the energy content of a molecule. It can be derived that monatomic gases have low specific heat, and polyatomic molecules have high specific heats, see Table 4.

Table 4: Molar heat capacity of specific substances at 298,15 K and 1 bar pressure

Element or compound	C_p^o J/(mol.K)
H_2 (g)	28.84
He (g)	20.79
Xe (g)	20.79
N_2 (g)	29.12
O_2 (g)	29.36
Ar (g)	20.79
Ne (g)	20.79

Specific heat at constant pressure and specific enthalpy are related by:

$$dh = c_p \cdot dT \quad \text{or} \quad dH = C_p \cdot dT \tag{4.1}$$

It follows that just like enthalpy; specific heat at constant pressure depends on temperature only. Some typical values are shown in the table below.

Table 5: Specific heat at constant pressure of specific species (gaseous state) at four different temperatures [NIST].

	C_p^o (J/(mol-K)			
Compound	298.15 K	1000 K	2000 K	3000 K
Hydrogen	28.8	30.1	34.3	38.9
Nitrogen	29.1	32.6	36.0	37.7
Oxygen	29.4	34.7	37.7	41.4
Water	-	41.3	51.2	55.7
Carbon dioxide	37.1	54.4	60.2	63.2

This temperature dependence for the specific heat is often approximated using:

$$C_p^o = A + B \cdot T + C \cdot T^2 + D \cdot T^3 + \frac{E}{T^2} \tag{4.2}$$

For a mixture of gases, an (number) average specific heat can be determined based upon the specific heat of the gas mixture divided by the number of molecules in the mixture:

$$C_p = \frac{\sum_i n_i \cdot C_{pi}}{\sum_i n_i} \tag{4.3}$$

Specific heat ratio
Specific heat ratio follows from:

$$\gamma = C_p / C_v = c_p / c_v \tag{4.4}$$

Specific heat at constant volume can be determined using:

$$R_A = C_p - C_v \quad \text{or} \quad R = \frac{R_A}{M} = c_p - c_v \tag{4.5}$$

A large value of the ratio of specific heats implies low values for the specific heats at constant pressure and volume. It can be shown that monatomic gases not only have low specific heats, but also a high specific heat ratio. For polyatomic molecules the opposite is true. Hence for rocket applications, main interest is on monatomic or diatomic gases rather than on polyatomic gases. Example calculations are given in the next section and the section on "Chemical equilibrium".

5 Chemical reactions, mass balance, and mixture ratio

In a chemical reaction, a transformation of substances takes place to form one or more new substances with completely different properties. For instance consider the transformation of hydrogen when mixed with oxygen to water. The substances that undergo the reaction process are called the “reactants”, and the substances that result from the combustion process “products”.

Chemical reaction equation
A chemical reaction equation is a formal statement that describes a chemical reaction. It is written in the basic form:

$$\text{Reactants} \rightarrow \text{Products} \tag{5.1}$$

For example, consider the reaction of methane with oxygen:

$$\text{Methane} + \text{Oxygen} \rightarrow \text{Carbon Dioxide} + \text{Water}$$

This equation states that methane reacts with oxygen to form carbon dioxide and water. The distinct substances in a reaction equation are usually referred to as chemical compounds. Typically, we write the reaction equation using the chemical formula of the substances. For example, the reaction of methane with oxygen forming carbon dioxide and water may be written as:

$$CH_4 + O_2 \rightarrow CO_2 + H_2O \tag{5.2}$$

Chemical reaction equations not only tell us what substances are reacting and what substances are produced, but they also tell us in what ratio the substances react or are produced. For example, the chemical reaction $2H_2 + O_2 \rightarrow 2H_2O$ can be translated into words as "two molecules of hydrogen plus one molecule of oxygen react to form two molecules of water" or when expressed in moles "two mol of hydrogen plus one mol of oxygen react to form two mol of water".

If we denote the reactants by A_i and the products by A_j, and if n_i and n_j refer to the number of molecules or moles, a chemical reaction can be expressed in general form as:

$$\sum n_i \cdot A_i \rightarrow \sum n_j \cdot A_j \tag{5.3}$$

Mass balance

In a chemical reaction matter is neither created nor destroyed. This is usually referred to as the mass or atom balance law and means that all the atoms present among the reactants (the left side of the equation) must be accounted for among the products (the right side). A chemical equation in which all atoms are accounted for is referred to as a 'balanced equation". Chemical equations do not come already balanced. This must be done before the equation can be used in a chemically meaningful way. Let's take a simple unbalanced equation and try to balance it. Consider again the reaction of methane with oxygen:

$$a \cdot CH_4 + b \cdot O_2 \rightarrow c \cdot CO_2 + d \cdot H_2O \tag{5.4}$$

For the equation to be correct both sides should have equal amounts of atoms. Since in the above equation, we have 3 different atoms, we have 3 atom balances:

- C: a x C = c x C
- H: a x 4H = d x 2H
- O: b x 2O = c x 2O + d x O

Since it is about ratio's, we can select e.g. 'a' as the independent number. Setting 'a' equal to 1, we get:

$$CH_4 + 2O_2 \rightarrow CO_2 + 2H_2O \tag{5.5}$$

Thermo-chemical equation

A thermo-chemical equation is a balanced chemical equation that specifies a value for the change in energy that occurs. Since for energy changes the physical stated of the reactants and products are important, this state is also indicated in the equation. If a reactant is solid (s) is placed after the formula, if gaseous we use (g) and if liquid we use (l). Depending on the state of the reactants and products, we distinguish two types of reactions:

- "Heterogeneous reaction" - a reaction in which not all of the chemical compounds are in the same phase.
- "Homogeneous reaction" - a reaction in which all the chemical compounds are in the same phase.

In chemical rocket motors mostly, a heterogeneous reaction occurs.

Reactant mixture ratio

In chemical rocket motors, the reactants are usually clear. The ratio in which they react is referred to as the (reactant) "mixture ratio". The mixture ratio 'r' can be determined on a mass basis or on a molar (volume) basis. In case of a bipropellant, i.e. a propellant consisting of a separate fuel and oxidizer, the mixture ratio based on mass follows from:

$$O/F = {M_{ox}}/{M_f} \tag{5.6}$$

Here M_{ox} is the oxidizer mass and M_f is the fuel mass. The volumetric mixture ratio in that case follows from:

$$(O/F)_{vol} = {V_{ox}}/{V_f} = O/F \cdot {\rho_f}/{\rho_{ox}} \tag{5.7}$$

Here ρ refers to the density of the fuel (subscript 'f') and the oxidizer (subscript 'ox'), respectively. For example, for the Space Shuttle main engine, propellant is supplied from the 47 m tall external tank at a rate of about 178,000 litres per minute of liquid hydrogen and 64,000 litres per minute of liquid oxygen. This indicates a volumetric (or molar) mixture ratio of 0.36:1 and a mass mixture ratio of 5.6:1[9] for the shuttle's main engines.

[9] Mass density of liquid oxygen is taken equal to 1140 kg/m^3 and for hydrogen 73,8 kg/m^3.

In chemical rocket propulsion, the mixture ratio is a very important design parameter, as it not only influences the resulting flame temperature and the properties of the jet exhaust, but also determines the volume needed to store the propellants. These issues will be dealt with in more detail later.

Compounds produced

In chemical rocket motors, the reactants are usually clear. What compounds are produced is not always clear. This is determined by amongst others the valence or oxidation number of the atoms involved. Atoms in a molecule are bound together by electron pairs. These are called bonding pairs. More than one set of bonding pairs of electrons may bind any two atoms together (multiple bonding). The combining behaviour of atoms is described by their valence or oxidation number(s):

- Metals, which commonly donate electrons and form compounds in which they exist in the positive state, are assigned positive oxidation numbers.
- Non-metals, which commonly accept electrons and form compounds in which they exist in the negative state, are assigned negative oxidation numbers.

By balancing these integral valence numbers in a known compound, the relative proportions of the elements present can be accounted for. For example, hydrogen with a valence of +1, oxygen with a valence of –2, nitrogen +3, and carbon +4 may combine to form H_2O, CO_2, and N_2O_3, which indicate the relative numbers of atoms of these elements in compounds, which they form with each other. Some elements can have several different oxidation states. For example, hydrogen and oxygen can have a valence of +1 and –1, iron +2 or +3, and chlorine can have a valence of -1, +1, +3, +5, and +7, depending on the type of compound in which it occurs. Valence numbers can be obtained from for instance [CRC], and [Binas]. In principle, all compounds that can be formed based on the valence numbers may exist. In that case, the mass balance principle does not allow for solving the reaction equation. Fortunately, the compounds with the highest oxidation number are the most stable and especially at low temperatures allow for a reasonable first guess. At higher temperatures, we have to resort to other theoretical methods, see section on chemical equilibrium hereafter, or to measure[10] the composition of the substances formed.

Types of reaction

In chemical rocket motors energy can be gained from the combination of two or more elements forming a complex compound (composition) or by breaking down a single compound into simpler compounds (decomposition).

Synthesis (composition):

Two or more elements or compounds may combine to form a more complex compound. The basic form is: A + B → AB.

Examples:

- Hydrogen with oxygen: $2H_2(g) + O_2(g) \rightarrow 2H_2O(l)$
- Magnesium with oxygen: $2Mg(s) + O_2(g) \rightarrow 2MgO(s)$
- Carbon with oxygen: $C(s) + O_2(g) \rightarrow CO_2(g)$
- Diborane with oxygen: $B_2H_6(g) + 3O_2(g) \rightarrow B_2O_3 + 3H_2O(g)$
- Hydrogen with fluorine: $H_2(g) + F_2(g) \rightarrow 2HF(l)$

Combustion (of hydrocarbons):

A reaction wherein one or more hydrocarbons are burned with oxygen is usually referred to as a combustion reaction. When a hydrocarbon is burned with sufficient oxygen supply, the products are always carbon dioxide and water vapor. We refer to this as ‘complete combustion’. If the supply of oxygen is low or restricted, then carbon monoxide will be produced (‘incomplete combustion’).

[10] The composition of a gas mixture can be measured using mass spectrography. The foremost technical problem though is the sampling procedure, especially when taking a sample in the nozzle exhaust.

Examples:
- Combustion of methane: $CH_4(g) + 2O_2(g) \rightarrow CO_2(g) + 2H_2O(g)$
- Combustion of butane: $2C_4H_{10}(g) + 13O_2(g) \rightarrow 8CO_2(g) + 10H_2O(g)$

Complete combustion means the reductor attains the higher oxidation number. In incomplete combustion the lower oxidation number is attained.

Decomposition:
A single compound breaks down into its component parts or simpler compounds. The basic form of the reaction is: $AB \rightarrow A + B$

Examples:
- Decomposition of water: $2H_2O \rightarrow 2H_2 + O_2$
- Decomposition of hydrazine: $2N_2H_4 \rightarrow 4NH_3 + N_2$
- Decomposition of hydrogen peroxide: $2H_2O_2 \rightarrow 2H_2O + O_2$

The latter two reactions are interesting for rocket propulsion as they produce a lot of energy.

Stoichiometric mixture and equivalence ratio
A typical combustion reaction for a rocket might include kerosene and liquid oxygen:

$$C_{12}H_{26} + 12.5 \cdot O_2 \rightarrow 12 \cdot CO + 13 \cdot H_2O \tag{5.8}$$

The above reaction is called a stoichiometric reaction. That is, the reaction is complete such that there is just enough O_2 present to react with all $C_{12}H_{26}$.

If n_r and n_p take such values that it is possible in principle for all reactants to disappear and form products, n_r and n_p are called “stoichiometric coefficients”, which will be indicated by (ν_r, ν_p). The reactant mixture ratio in that case is referred to as the “stoichiometric mixture ratio”.

The “equivalence ratio” (ER) is defined as the ratio of the actual mixture ratio to the stoichiometric mixture ratio:

$$ER = (O/F)/(O/F)_{st} \tag{5.9}$$

There are three possible conditions for the equivalence ratio:
1. ER < 1: Fuel rich mixture. Combustion is incomplete. Some fuel remains.
2. ER = 1: Stoichiometric mixture. Fuel and oxidizer are used up completely.
3. ER > 1: Fuel lean mixture. There is excess oxidizer.

Example:

Let us consider the reaction of hydrazine and nitrogen tetroxide forming water, and nitrogen at a temperature of 3000 K. We are mixing the hydrazine and nitrogen tetroxide (NTO) in the mass mixture ratio of 1.4375 : 1. Since the molar mass of hydrazine and NTO is 32 and 92, respectively and the given O/F mass mixture ratio, we find that for every 32 gram of hydrazine we have 46 gram of NTO or on every mole of hydrazine, we have 0.5 mole of NTO. Using the mass balance, this gives:

$$2N_2H_4 + 1 \cdot N_2O_4 \rightarrow 4H_2O + 3N_2 \tag{5.10}$$

In the next table, we have collected the known molar mass, molar quantities and specific heats of the products taken from [NIST]. Using these data, we find for the average molar mass of the product mixture (4 x 18 + 3 x 28)/7 = 22.29 gram/mol.

Substance	n_j	M_j	$n_j \cdot M_j$	$C_{p_j}^{3000K}$	$n_j \cdot C_{p_j}$
(-)	(-)	(gram/mol)	(-)	(J/K/mol)	(J/K)
H_2O	4	18	72	58,2	232.8
N_2	3	28	84	37,7	113.1
	N = 7		Sum = 156		Sum = 345.9

The value of γ can be calculated once the specific heat at constant pressure and volume are known. C_p follows from:

$$C_p = \frac{\sum_j n_j \cdot C_{pj}}{\sum_j n_j} = \frac{345.9}{7} = 49.4 \ \ J/mol \tag{5.11}$$

C_v follows from:

$$C_v = C_p - R_A = 49.4 - 8.3 = 41.1 \ J/mol \tag{5.12}$$

It now follows for the specific heat ratio:

$$\gamma = \frac{C_p}{C_v} = \frac{49.4}{41.1} = 1.20 \tag{5.13}$$

6 Heat of reaction and heat of formation

An important parameter for a chemical rocket propellant is the amount of energy that is liberated in the reaction, i.e. the “heat of reaction”, as it greatly determines the resulting temperature of the reactants. It is defined as the change in enthalpy occurring when products are formed from reactants. This change of enthalpy may be either positive or negative, depending on whether the reaction is endothermic (absorbs heat) or exothermic (gives out heat). For combustion types of reactions (reaction involving oxygen), the heat of reaction is also referred to as the “heat of combustion”.

To determine the heat of reaction for constant pressure processed, we use again the first law of thermodynamics written in enthalpy form:

$$Q = H_e - H_o = \Delta H \tag{6.1}$$

For chemical reactions, ΔH is referred to as "heat of reaction". A positive change means that energy is absorbed during the reaction ("endothermic" reaction) and a negative change means that energy is released during the reaction ("exothermic" reaction). If the reaction is reversed, then the sign of ΔH is also reversed.

Heat of reaction can be determined by measurement for instance using the earlier introduced bomb calorimeter or solution calorimeter. Since the bomb calorimeter is a closed vessel, it essentially is a constant volume apparatus, and the heat of reaction is equal to the change in internal energy. The enthalpy change than follows from:

$$\Delta H = \Delta U + \Delta(p \cdot V) = \Delta U + R_A \cdot T \cdot \Delta n_g \tag{6.2}$$

Three factors can affect the heat of reaction:
- The concentrations of the reactants and the products
- The temperature of the system
- The partial pressure

For determining the heat of reaction, chemical scientists have agreed that the heat of reaction is related to 1 mol of product. Furthermore, they have agreed upon a standard

reference set of conditions for temperature and pressure, being 298.15 K (or 25 °C), and 1 bar.

Only a very few of a great many possible chemical reactions are such that their heats of reaction can be accurately determined directly under all conditions. For this to be possible, the reaction must be fast, complete and clean. In other cases, we must resort to theoretical methods to calculate the energy change associated with chemical reactions. For this, we use Hess's Law, but first we will introduce the "standard heat of formation".

Standard heat of formation

The "standard heat of formation", indicated by '$\Delta_f H°$', is defined as the heat of reaction for the formation of one mole of a substance from its elements in their standard state. We take the standard state for a solid or a liquid as its most stable state at a given temperature and at a pressure of 1 bar. For gases, we take the standard state as the ideal gas condition at a given temperature and a pressure of 1 bar. It then follows that the standard enthalpy of formation of an element in its standard state is zero because it has not been formed from something else. Usually, a subscript is added to the heat of formation to indicate the temperature at which the reaction takes place. In addition, we add an indication of the state (g, l or s, for gas, liquid or solid) of the substance formed. For an example, see hereafter.

For a great many compounds, the heat of formation at various temperatures has been determined and tabulated in handbooks, like [CRC], JANAF], and [CODATA] or on the world-wide web, like [NIST].

Hereafter, we will mainly use the heat of formation at 298,15 K as this allows for adding the heat of formation and the relative enthalpy to determine the total enthalpy change when next to a reaction also heating/cooling is involved. This is explained later in more detail.

For example, the standard heat of formation for water (H_2O) is the enthalpy change for the following reaction:

$$H_2\ (g) + 1/2 O_2\ (g) \rightarrow H_2O\ (l) \quad \Delta_f H^\circ = -285.83\ \text{kJ/mol} \tag{6.3}$$

Notes:

- Elemental source of oxygen is O_2 and not O because O_2 is the stable form of oxygen at 25 °C and 1 bar, likewise with H_2;
- Why are the molar quantities for hydrogen and oxygen “1” and "1/2", respectively? The heat of reaction is based on the formation of 1 mol of product. Thus, $\Delta_f H°$ values are reported as kJ / mole of the substance produced.
- The heat of formation is negative, because heat is liberated.

In case water vapour is formed, the heat of formation is:

$$\Delta_f H^\circ\ [H_2O, g] = -241.826\ \text{kJ/mol} \tag{6.4}$$

We find a lower heat of formation for water vapour than for liquid water. This is because to go from liquid water to water vapour requires energy.

The formation of one-atomic oxygen from O_2 requires heat.

$$\Delta_f H^\circ\ [O, g] = 249.173\ \text{kJ/mol} \tag{6.5}$$

One should be aware of that the heat of formation differs depending on the standard conditions used[11].

Hess's law

If a reaction is carried out in a series of steps, ΔH for the reaction will be equal to the sum of the enthalpy changes for the individual steps.

This law allows us to **calculate** ΔH for a reaction from listed ΔH values of **other reactions** (i.e. you can avoid having to do an experiment).

Simply stated, the ΔH^o for a reaction = summation of the heats of formation of the products minus the summation of the heats of formation of the reactants:

$$\Delta H = \sum_p \left[n \cdot \Delta_f H^o \right]_p - \sum_r \left[n \cdot \Delta_f H^o \right]_r \tag{6.6}$$

Here the subscript 'p' refers to the products of the reaction, and 'r' the reactants.

As an example of the use of tabulated standard state enthalpies, consider the combustion reaction of methane at 298,15 K and 1 bar to form gaseous carbon dioxide and liquid water:

$$CH_4\ (g) + 2O_2\ (g) \rightarrow CO_2\ (g) + 2H_2O\ (l) \tag{6.7}$$

This reaction can be thought of as occurring in two steps. In the first step methane and oxygen are decomposed into their elements, where we take the elements in their standard state at given (standard) conditions. The standard reference state for a solid or a liquid is its most stable state at a given temperature and at a pressure of 1 bar. For gases, it is convenient to take the standard reference state as the ideal gas condition at a certain temperature (usually 0 K or 298,15 K) and a pressure of 1 bar.

$$CH_4\ (g) \rightarrow C\ (s) + 2H_2\ (g) \tag{6.8}$$

$$\Delta_f H^o = -74.87\ \text{kJ/mol} \tag{6.9}$$

$$O_2\ (g) \rightarrow O_2\ (g)\ \text{(elemental form)} \tag{6.10}$$

In the second step the elements react to form gaseous carbon dioxide and water vapour:

$$C\ (s) + O_2\ (g) \rightarrow CO_2\ (g) \tag{6.11}$$

$$\Delta_f H^o = -393.51\ \text{kJ/mol} \tag{6.12}$$

$$H_2\ (g) + \frac{1}{2} \cdot O_2\ (g) \rightarrow H_2O\ (l) \tag{6.13}$$

$$\Delta_f H^o = -285.83\ \text{kJ/mol} \tag{6.14}$$

Using Hess's law, we find for the heat of combustion of methane:

$$\Delta H = \left[-393.51 + 2 \cdot (-285.83) \right]_p - \left[1 \cdot (0) + 1 \cdot (-74.87) \right]_r \tag{6.15}$$

$$\Delta H = -890.3\ \text{kJ/mol} \tag{6.16}$$

Table 6 shows the heat of combustion of some typical fuels.

[11] In case we take 0 K as reference temperature, the heat of formation of water is -239,0788 kJ/mol, and of monatomic oxygen 251,1619 kJ/mol.

Table 6: Enthalpies of combustion at 25 °C and 1 bar [Barrow]. Products are carbon dioxide (g) and water (l).

	kJ/mol		kJ/mol
H_2	285.84		
C (s)	393.51	n-butane (g)	2878.51
CH_4 (g)	890.35	Ethylene (g)	1410.97
C_2H_6 (g)	1559.88	Acetylene (g)	1299.63
C_3H_8 (g)	2220.07	Ethanol (l)	1366.95

Propellant composition

In a chemical reaction essentially an oxidation process occurs, representing a transfer of electrons between a reductor (fuel) and an oxidizer. For a large energy release, the oxidizers should be of high electro-negativity and the fuel molecules should be highly electropositive. It is for this reason that oxidizer constituents include mainly atoms like those of oxygen, chlorine, and fluorine, whilst the fuel constituents are in general atoms of hydrogen, lithium, beryllium, boron, carbon, sodium, magnesium, aluminium and silicon. Figure 4 shows the available energy for a number of elements when mixed in the stoichiometric ratio with oxygen.

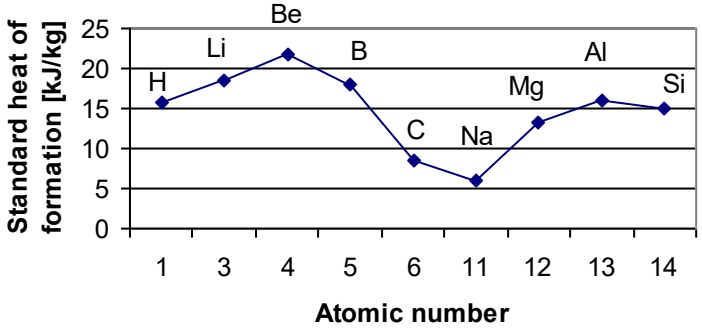

Figure 4: Available energy of the light elements associated with oxygen (stoichiometric mixture and elements taken at the standard temperature of 298.15 K). Indicated are periods in the periodic system of the elements

Thermodynamic data

Investigating the thermodynamics of reactions can be fraught with problems, not least of which is the lack of available heat of formation data. Thermodynamic data on common substances can be obtained from for instance [CODATA], [JANAF] or [CRC]. Useful "on-line" source of data is available at [NIST]. Unfortunately, in rocket motors sometimes also not so common substances are used of which it is difficult to obtain data.

Examples

Example 1: Heat of combustion of propane

The reaction equation for the complete combustion of propane is:

$$C_3H_8\ (g) + 5O_2\ (g) \rightarrow 3CO_2\ (g) + 4H_2O\ (l) \qquad (6.17)$$

We start with the reactants, decompose them into elements, and rearrange the elements to form products. The overall enthalpy change is the enthalpy change for each step.

Decomposing into elements (note O_2 is already elemental, so we concern ourselves with C_3H_8):

$$C_3H_8\ (g) \rightarrow 3C\ (s) + 4H_2\ (g) \qquad (6.18)$$

$$\Delta H_1 = -\Delta_f H^o\ [C_3H_8\ (g)] \tag{6.19}$$

Now form CO_2 and H_2O from their elements:

$$3C\ (s) + 3O_2\ (g) \rightarrow 3CO_2\ (g) \tag{6.20}$$

$$\Delta H_2 = 3\Delta_f H^o\ [CO_2\ (g)] \tag{6.21}$$

$$4H_2\ (g) + 2O_2\ (g) \rightarrow 4H_2O\ (l) \tag{6.22}$$

$$\Delta H_3 = 4\Delta_f H^o\ [H_2O\ (l)] \tag{6.23}$$

Look up values of the heat of formation using [NIST] and add:

$$\Delta H_c = (3 \cdot -393.51 + 4 \cdot -285.83) - (1 \cdot -104.7 + 0) = -2219.2\ \text{kJ} \tag{6.24}$$

This value agrees nicely with the value given in Table 6 The slight difference is attributed to small differences in the data used.

Example 2: Hydrazine decomposition
Consider the following decomposition reaction of hydrazine

$$3N_2H_4\ (l) \rightarrow 4NH_3\ + N_2 + Q_1 \tag{6.25}$$

This equation states that three mol of hydrazine decomposes to form four mol of ammonia and one mol of nitrogen. This also means that 96 kg of hydrazine react to form 68 kg of ammonia and 28 kg of nitrogen.

Decomposing hydrazine into its elements, we get:

$$3N_2H_4\ (l) \rightarrow 3N_2\ (g) + 6H_2\ (g) \tag{6.26}$$

$$\Delta H_1 = -3\Delta_f H^o\ [N_2H_4\ (l)] \tag{6.27}$$

Now form NH_3 from its elements (nitrogen is already an element):

$$2N_2\ (g) + 6H_2\ (g) \rightarrow 4NH_3\ (g) \tag{6.28}$$

$$\Delta H_2 = 4\Delta_f H^o\ [NH_3\ (g)] \tag{6.29}$$

Look up values of the heat of formation using [CRC] and add:

$$\Delta H_c = (4 \cdot -45{,}90 + 1 \cdot 0) - (3 \cdot -50{,}626 + 0) = -335{,}5\ \text{kJ} \tag{6.30}$$

It follows the decomposition of hydrazine to ammonia and nitrogen is exothermic to the extent of 112 kJ/mole of hydrazine.

Example 3: Heat of reaction for the reaction between hydrogen and fluorine[12]

$$H_2\ (g) + F_2\ (g) \rightarrow 2HF\ (g) \tag{6.31}$$

$$\Delta H_c = (2 \cdot -272.546) - (1 \cdot 0 + 1 \cdot 0) \tag{6.32}$$

The reaction releases energy and is exothermic:

$$\Delta H_c = -545.092\ \text{kJ} \tag{6.33}$$

7 The adiabatic flame temperature

In a chemical rocket motor, the heat of reaction is used to heat up the reaction products to a high temperature. If all heat of reaction is used to heat up the reaction products, the resulting temperature is called the "Adiabatic flame temperature". In reality, of course one should consider losses associated with heat transfer to the surroundings. However, experience shows that in rocket motors the adiabatic flame

[12] NASA considered this as a chemical propellant for rocket boosters.

temperature is a reasonable first approximation for the temperature of the combustion gases. This is, because the heat transfer to the walls of the combustion chamber is negligible compared to the net heat released in the reaction.

To calculate the adiabatic flame temperature, we use the energy balance. This balance states that the energy needed to raise the temperature of the substances present in the reaction, is equal to the energy released by the forming of new chemical bonds between the products minus the energy needed to destruct the chemical bonds between the reactants. The values of the energy concerned with these chemical bonds are expressed by the "heats of formation", which have been discussed in the previous section.

The heat that is released by the chemical reaction is called the "available heat". It is the difference between the heat of formation of the products and the heat of formation of the reactants. For exothermic processes like the chemical reaction taking place inside a combustion chamber, this difference will be positive. If for instance the chemical reaction equation is given by:

$$\sum n_i \cdot A_i \rightarrow \sum n_j \cdot A_j \tag{7.1}$$

The available heat can be expressed by as:

$$Q_{av} = \sum_{i=1}^{n} n_i \cdot \left(\Delta H_f^\circ\right)_i - \sum_{j=1}^{m} n_j \cdot \left(\Delta H_f^\circ\right)_j \tag{7.2}$$

As the reaction takes place at a temperature, which is different from the temperature at which fuel and oxygen are stored in the rocket, heat is required to raise the temperature to the final temperature, i.e. the chamber temperature T_c.
As the pressure in the combustion chamber is considered constant, this required heat can be calculated from:

$$Q_{req} = \sum_{j=1}^{m} n_j \cdot \int_{298,15}^{T_c} \left(C_p\right)_j \cdot dT \tag{7.3}$$

The required heat is equal to the sum of the amounts of heat required to raise each quantity of reaction product to the temperature level T_c. As these quantities are expressed in the number of moles of each compound involved, the integral in each term is multiplied with its corresponding factor n_j. The integral of the specific heats of the substances over the temperature range considered can also be written in the familiar form:

$$Q_{req} = \sum_{j=1}^{m} n_j \cdot \left(H^\circ_{T_c} - H^\circ_{298,15}\right)_j \tag{7.4}$$

In case rocket propellants are stored at a temperature different from 298,15 K., like liquid hydrogen and liquid oxygen, one must add to the required heat the heat needed to vaporize the liquids and to heat up to the liquids to 298,15 K.

8 Chemical equilibrium

As stated before, at high temperatures compounds partially will break up into radicals. The inverse reaction*, that may take the overhand in the nozzle is also possible and is called* recombination. In that case, the reaction really involves two reactions. There is a "forward" reaction and a mirror image "reverse" reaction:

$$H_2\ (g) + F_2\ (g) \rightarrow 2HF\ (g) \text{ forward} \tag{8.1}$$
$$H_2\ (g) + F_2\ (g) \leftarrow 2HF\ (g) \text{ reverse} \tag{8.2}$$

In case also the reverse reaction occurs; we call this type of reaction “reversible”. If the transformation of the products back into the reactants is not possible, the reaction is called “irreversible”. Irreversible reactions are generally characterized by that at least one of the reactants is consumed completely. An equilibrium chemical reaction is indicated by replacing the single arrow ‘$\rightarrow$’ with the double arrow ‘$\Leftrightarrow$’.
In reversible chemical reactions, the reactants are initially the only molecules around. They react to form products. The quantity of the reactants dwindles and the forward reaction slows down. The product amounts increase at the same time the reactants are disappearing. These products "decompose" to form reactants. The rate for this reverse reaction increases as the amount of product grows. Ultimately there comes a time when the forward reaction rate and the reverse reaction rates are equal, see Fig. 5. The mixture is at “chemical equilibrium”. For any reaction at chemical equilibrium, the reactants are being transformed into products at the same rate as the products are being reverted into the reactants.

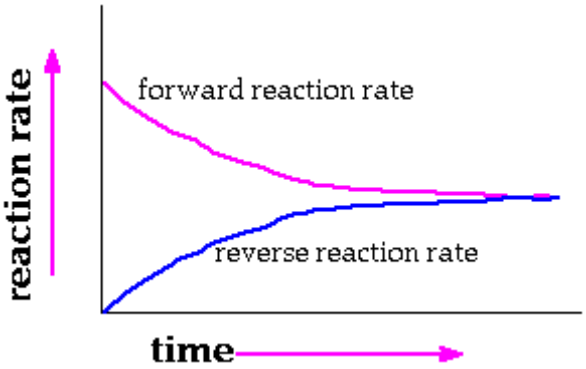

Figure 5: Reaction rate

To calculate chemical equilibrium, we can consider the reaction rate of chemical reactions[13]. The rate of a chemical reaction is proportional to the product of the concentrations of the reactants. For any general reaction:

$$A + B \Leftrightarrow 2C + D \tag{8.3}$$

The rate law expression for the forward reaction is:

$$r_f = k_f\ [A] \cdot [B] \tag{8.4}$$

and for the backward reaction:

$$r_b = k_b\ [C] \cdot [C] \cdot [D] = k_b\ [C]^2 \cdot [D] \tag{8.5}$$

Where [X] represents the activity of substance X, i.e. the reactive amount of substance X per unit volume (the concentration), and k is a constant of proportionality known as the rate constant. The latter is not affected by concentration and only depends on temperature.

For ideal gases we can use the partial pressure of the gas as the measure of the activity of the gas[14]. In that case, the rate of the forward reaction is k_f times p(A) times p(B) and of the reverse reaction k_b times $p(C)^2$ times p(D).

[13] Another approach, more favoured today, is to minimize the change in (Gibbs) free energy, see annex B.
[14] When using the partial pressure are the measure of the activity of the gas, we use the ideal gas law to convert the equilibrium constant expressed in concentrations (number of moles n per unit volume) to partial pressures. Notice that in that case also a different value for the equilibrium constant results. In other words, the value of the equilibrium constant expressed in partial pressures is different from the value of this constant when expressed in concentrations.

Then at equilibrium k_f p(A) p(B) = k_b p(C)^2 p(D), so that we can now define the equilibrium constant based on partial pressures 'K_p' as the ratio of the rate constants (k_f /k_b), where the activities of the products (right hand side of the equation) appear in the numerator and the activities of the reactants (left hand side of the equation) in the denominator:

$$K_p = \frac{k_f}{k_p} = p(C)^2 \cdot \frac{p(D)}{(p(A) \cdot p(B))} \tag{8.6}$$

In general, this can be written as:

$$K_p = \frac{\prod_j p_j^{n_j}}{\prod_i p_i^{m_i}} \tag{8.7}$$

Here the subscript 'i' refers to the reactants and 'j' to the products.

The following example of a reversible reaction is considered:

$$H_2 + 1/2 O_2 \Leftrightarrow H_2O \tag{8.8}$$

For perfect gases, the equilibrium constant K_p for this relation is expressed as a function of the respective partial pressures:

$$K_p = \frac{p_{H_2O}}{p_{H_2} \cdot (p_{O_2})^{1/2}} \tag{8.9}$$

And in molar quantities, see annex B:

Values for the equilibrium constant can be obtained once the equilibrium conditions at a certain temperature are known. Like the reaction rate constants, the numerical value of K_p depends on the temperature only.

$$K_p = \frac{n_{H_2O}}{n_{H_2} \cdot (n_{O_2})^{1/2}} \cdot \left(\frac{p}{N}\right)^{-1/2} \tag{8.10}$$

Notice that the value for the equilibrium constant depends on how the equilibrium equation is written. In this work we will use the JANAF convention wherein the equilibrium constant is based on the formation of 1 mol product from its elements. The equilibrium constant also depends on the units used for pressure. Typically, pressure is expressed in bar or in atmosphere, depending on the source of data used.

Using tabulated values on K (K= K(T)), we can determine equilibrium composition. Typical such tabulated values can be obtained from [JANAF].
For reactions involving liquids and solids, as well as gases, the liquids and solids are not included in the equilibrium expression.

The iterative solution process
The set of equations, which consists of the energy balance, the mass balance for the several elements, and the expressions for the reaction constants, can be solved, giving the adiabatic flame temperature and the mixture ratios of the reaction products.

One approach is to perform the required algebra necessary to obtain **one equation in one unknown**, and to solve the equation, as follows:
- If the highest power is one: use rearrangement and ordinary algebra.
- If the highest power is two: rearrange the equation into standard quadratic form and use the quadratic formula. Discard any negative root.

- If the highest power is three or more: either solve the equation by successive approximations (the brute force method) or go back to a previous step and make reasonable simplifying assumptions to obtain an equation no more complex than a quadratic.

In case the nature of the set of equations does not allow a straightforward algebraic solution, iterative methods must be used (method of successive approximations). First an intermediate simplified system is introduced, which provides a reasonable first approximation. This can for example be accomplished by leaving out some of the less important compounds in the equations. The corrective terms representing the other substances are introduced afterwards. Next, one assumes a value of the adiabatic temperature and calculates the molar fractions. Now the available and the required heat at the assumed temperature can be calculated. If the available heat exceeds the required heat, the adiabatic flame temperature is higher than assumed. If the opposite is true, then the adiabatic flame temperature is lower than was assumed. If the difference between required heat and available heat is acceptable, the iterative process can be stopped. If not, the value of the guessed temperature has to be adjusted once more, and another step is necessary.

Example

Problem: Calculate the adiabatic flame temperature of (gaseous) H_2 and O_2 at a pressure of 20.69 bars and an initial temperature of 25 °C. It is to be expected that the temperature is high enough to cause dissociation.

Solution:
The reaction equation is given by:

$$\begin{aligned} 2H_2 + 1O_2 \rightarrow n_{H_2O}\ H_2O + n_{H_2}\ H_2 + n_{O_2}\ O_2 + n_H\ H \\ + n_O\ O + n_{OH}\ OH + Q_{av} \end{aligned} \tag{8.11}$$

Here Q_{av} is zero (definition of adiabatic flame temperature). Essentially this then gives us 7 unknowns (molar quantities of the 6 products and the adiabatic flame temperature).

To solve these 7 unknowns, we have two equations resulting from the mass balance for hydrogen and oxygen atoms:

$$\text{H: } 4 = 2n_{H_2O} + 2n_{H_2} + n_H + n_{OH} \tag{8.12}$$

$$\text{O: } 2 = n_{H_2O} + 2n_{O_2} + n_O + n_{OH} \tag{8.13}$$

There are six different types of products of which two are the same as the reactants. So four chemical reactions at equilibrium must be considered:

$$H_2 + 1/2\,O_2 \Leftrightarrow H_2O \tag{8.14}$$

$$1/2\,H_2 + 1/2\,O_2 \Leftrightarrow OH \tag{8.15}$$

$$1/2\,H_2 \Leftrightarrow H \tag{8.16}$$

$$1/2\,O_2 \Leftrightarrow O \tag{8.17}$$

The four equilibrium constants of these reactions form a further four equations, making a total of 6 (independent) equations. The four equilibrium constants can be expressed in terms of partial pressure or in terms of molar fractions:

$$\left(K_p\right)_{H_2O} = \frac{n_{H_2O}}{n_{H_2} \cdot \left(n_{O_2}\right)^{1/2}} \cdot \left(\frac{p}{N}\right)^{-1/2} \Rightarrow \frac{n_{H_2O}}{n_{H_2} \cdot \left(n_{O_2}\right)^{1/2}} = \left(K_p\right)_{H_2O} \cdot \left(\frac{p}{N}\right)^{1/2} \tag{8.18}$$

$$\left(K_p\right)_H = \frac{n_H}{\left(n_{H_2}\right)^{1/2}} \cdot \left(\frac{p}{N}\right)^{1/2} \Rightarrow \frac{n_H}{\left(n_{H_2}\right)^{1/2}} = \left(K_p\right)_H \cdot \left(\frac{p}{N}\right)^{-1/2} \tag{8.19}$$

$$\left(K_p\right)_O = \frac{n_O}{\left(n_{O_2}\right)^{1/2}} \cdot \left(\frac{p}{N}\right)^{1/2} \Rightarrow \frac{n_O}{\left(n_{O_2}\right)^{1/2}} = \left(K_p\right)_O \cdot \left(\frac{p}{N}\right)^{-1/2} \tag{8.20}$$

$$\left(K_p\right)_{OH} = \frac{n_{OH}}{\left(n_{H_2}\right)^{1/2} \cdot \left(n_{O_2}\right)^{1/2}} \Rightarrow \frac{n_{OH}}{\left(n_{H_2}\right)^{1/2} \cdot \left(n_{O_2}\right)^{1/2}} = \left(K_p\right)_{OH} \tag{8.21}$$

With:

$$N = \sum_j n_j \tag{8.22}$$

A seventh equation follows from the energy balance, which gives:

$$Q_{av} = Q_{req} \tag{8.23}$$

$$\sum_{i=1}^{m} n_i \cdot \left(\Delta H_f^\circ\right)_i - \sum_{j=1}^{k} n_j \cdot \left(\Delta H_f^\circ\right)_j = \sum_{j=1}^{k} n_j \cdot \left(H^\circ_{T_c} - H^\circ_{298,15}\right)_j \tag{8.24}$$

This then completes the set of equations needed to solve for the unknowns. Using the previously described solution approach, we now assume a value of N. The stoichiometric equation shows that two moles of hydrogen and one mole of oxygen yield two moles of water. This gives an initial value for N of 2. If the temperature of combustion is assumed to be 3500 K, the values of the equilibrium constants can be found from [JANAF]. It follows:

$$H_2O: \quad \log K_f = 0.713 \quad \rightarrow \quad K_f = 5.164 \tag{8.25}$$

$$H: \quad \log K_f = -0.228 \quad \rightarrow \quad K_f = 0.592 \tag{8.26}$$

$$O: \quad \log K_f = -0.307 \quad \rightarrow \quad K_f = 0.493 \tag{8.27}$$

$$OH: \quad \log K_f = 0.160 \quad \rightarrow \quad K_f = 1.445 \tag{8.28}$$

Substitution of the known values, i.e. the molar quantity of water, the equilibrium constants and of p (in bar) and N gives the following result:

$$\frac{n_O}{\left(n_{O_2}\right)^{1/2}} = \left(K_p\right)_O \cdot \left(\frac{p}{N}\right)^{-1/2} = 0.493 \cdot \left(\frac{20.69}{2}\right)^{-1/2} = 0.153 \tag{8.29}$$

$$\frac{n_H}{\left(n_{H_2}\right)^{1/2}} = \left(K_p\right)_H \cdot \left(\frac{p}{N}\right)^{-1/2} = 0.592 \cdot \left(\frac{20.69}{2}\right)^{-1/2} = 0.184 \tag{8.30}$$

$$\frac{n_{OH}}{\left(n_{H_2}\right)^{1/2} \cdot \left(n_{O_2}\right)^{1/2}} = \left(K_p\right)_{OH} = 1.445 \tag{8.31}$$

$$\frac{n_{H_2O}}{n_{H_2} \cdot \left(n_{O_2}\right)^{1/2}} = \left(K_p\right)_{H_2O} \cdot \left(\frac{p}{N}\right)^{1/2} = 5.164 \cdot \left(\frac{20.69}{2}\right)^{1/2} = 16.609 \tag{8.32}$$

This set of equations can be solved. Put molar quantity of hydrogen = x and molar quantity of oxygen as y. it follows:

$$n_H = 0.184 \cdot x^{1/2} \tag{8.33}$$

$$n_O = 0.153 \cdot y^{1/2} \tag{8.34}$$

$$n_{OH} = 1.455 \cdot x^{1/2} \cdot y^{1/2} \tag{8.35}$$

$$n_{H_2O} = 16.609 \cdot x \cdot y^{1/2} \tag{8.36}$$

Substitution of these values into the mass balance for hydrogen yields:

$$4 = 33.218 \cdot x \cdot y^{1/2} + 1.455 \cdot x^{1/2} \cdot y^{1/2} + 2 \cdot x + 0.184 \cdot x^{1/2} \tag{8.37}$$

Solving for y gives:

$$y = \left(\frac{4 - 2 \cdot x - 0.184 \cdot x^{1/2}}{33.218 \cdot x + 1.455 \cdot x^{1/2}} \right)^2 \tag{8.38}$$

With the use of the mass balance for oxygen, one gets an algebraic equation for x (i.e. the molar quantity of hydrogen):

$$\begin{aligned} 2 = &\left(4 - 2 \cdot x - 0.184 \cdot x^{1/2}\right) \cdot \frac{16.609 \cdot x + 1.455 \cdot x^{1/2} + 0.153}{33.218 \cdot x + 1.455 \cdot x^{1/2}} \\ &+ 2 \cdot \left(\frac{4 - 2 \cdot x - 0.184 \cdot x^{1/2}}{33.218 \cdot x + 1.455 \cdot x^{1/2}} \right)^2 \end{aligned} \tag{8.39}$$

After solving this, one obtains for the molar quantity of (molecular) hydrogen x = 0.302 and the molecular quantity of (molecular) oxygen y = 0.093. Now the other molar fractions can be found by substitution of x and y:

$$n_H = 0.184 \cdot x^{1/2} = 0.184 \cdot 0.302^{1/2} = 0.101 \tag{8.40}$$

$$n_O = 0.153 \cdot y^{1/2} = 0.153 \cdot 0.093^{1/2} = 0.047 \tag{8.41}$$

$$n_{OH} = 1.455 \cdot x^{1/2} \cdot y^{1/2} = 1.455 \cdot 0.302^{1/2} \cdot 0.093^{1/2} = 0.244 \tag{8.42}$$

$$n_{H_2O} = 16.609 \cdot x \cdot y^{1/2} = 16.609 \cdot 0.302 \cdot 0.093^{1/2} = 1.530 \tag{8.43}$$

The total number of moles of the products is equal to 2.317, which is slightly higher than the assumed value of 2. If the calculation given above is carried out once more with this value of N the values found for the molar quantities of the products turn out to be about the same as given here. Now the available heat and required heat can be calculated, see the table below.

Table 7: Enthalpies and heats of formation for a given product composition

Substance	n_j	n_j/N	ΔH_f^o	$n_j \cdot \Delta H_f^o$	$H^o_T - H^o_{298,15}$	$n_j \cdot \left(H^o_T - H^o_{298,15}\right)$
(-)	(-)	(%)	(kJ/mol)	(kJ)	(kJ/mol)	(kJ)
O_2	0.093	4.0	0	0	118.165	10.989
H_2	0.302	13.0	0	0	107.555	32.482
O	0.047	2.0	249.173	11.711	67.079	3.153
H	0.101	4.4	217.999	22.018	66.554	6.722
OH	0.244	10.5	38.987	9.513	108.119	26.381
H_2O	1.530	66.0	-241.826	-369.994	154.768	236.795
	N = 2.317			Sum = -326.752		Sum = 316.522

In this example, we see that the available heat is equal to 326.752 kJ and the required heat is equal to 316.522 kJ. Apparently, the true combustion temperature is somewhat higher than 3500 K.

Taking 3500 K as the final temperature, we can use the known product composition at this temperature to determine the mean molar mass of the exhaust gases and the specific heat ratio, see next table.

Table 8: Specific heat and molar mass for a given product composition

Substance	n_j	n_j/N	$n_j \cdot M_j$	$C_{p_j}^{3500K}$	$n_j \cdot C_{p_j}$
(-)	(-)	(%)	(-)	(J/K/mol)	(J/K)
O_2	0.093	4.0	2.97	40.716	3.787
H_2	0.302	13.0	0.61	38.149	11.521
O	0.047	2.0	0.75	21.092	0.991
H	0.101	4.4	0.10	20.786	2.099
OH	0.244	10.5	4.15	37.376	9.120
H_2O	1.530	66.0	27.54	57.058	87.299
	N = 2.317		Sum = 36.12		Sum = 114.817

The values for the specific heat of the products and molar mass of the products have been taken from [JANAF].

The mean molecular mass of the combustion products is equal to:

$$M = \frac{\sum_j n_j \cdot M_j}{\sum_j n_j} = \frac{36.12}{2.317} = 15.6 \quad \text{gram/mol} \tag{8.44}$$

The value of γ can be calculated once the specific heat at constant pressure and volume are known. C_p follows from:

$$C_p = \frac{\sum_j n_j \cdot C_{pj}}{\sum_j n_j} = \frac{114.817}{2.317} = 49.554 \ \text{J/mol} \tag{8.45}$$

C_v follows from:

$$C_v = C_p - R_A = 49.554 - 8.314 = 41.24 \ \text{J/mol} \tag{8.46}$$

It now follows for the specific heat ratio

$$\gamma = \frac{C_p}{C_v} = \frac{49.554}{41.24} = 1.120 \tag{8.47}$$

This was a sample calculation; in actual rockets hydrogen and oxygen are used as liquids at temperatures of 20.4 and 90.2 K, respectively. This means that also heat is required to vaporize the liquids and to heat the gases formed to the starting temperature of 298.15 K assumed in this example. This means that in that case the temperature of 3500 assumed is too high and a further iteration is required.

9 Propellant combustion characteristics and design charts

Important combustion characteristics of rocket propellants are combustion temperature and molar mass and specific heat ratio of the combustion gases. These parameters largely depend on the propellant constituents, their (mass or volume) ratio and the combustion pressure. For a range of liquid bipropellants [Braeunig] presents 4 graphs, which can be used to estimate (1) the optimum mixture ratio of the combustion reactants, (2) the adiabatic flame temperature of the combustion reaction, (3) the average molecular weight of the combustion products, and (4) the specific heat ratio of the combustion products. The same can be done for hybrid propellants. For metallized solid propellants this is also possible, except that usually there are more parameters needed to describe the effect of different mixture ratios.

10 Effect of expansion in the nozzle

The gaseous products and any condensed substances (liquid or solid) are expanded through a supersonic nozzle to a specific cross section, a specific exit pressure and against a specific ambient pressure. Earlier we assumed that the gas properties in the nozzle are constant. We call this case "constant properties flow". In practice, because of decreasing temperature and pressure in the nozzle, the composition of the combustion gases may change.

Two cases are generally considered being “frozen flow” (FF) and “chemical equilibrium flow” (CEF). In the FF case, the reactions in the nozzle are slow compared to the expansion and hence the composition does not change. As of the change in pressure, though, the properties of the flow will vary. This is different from the constant properties flow earlier mentioned as the latter has both constant composition and properties throughout the nozzle. In the CEF case, the time needed for the reactions is short compared to the expansion time and hence the composition will vary as well as the properties of the exhaust gas (molar mass and specific heat ratio) of the exhaust gas.

An even better estimation of real-world performance is obtained by assuming the chemical substances are in chemical equilibrium up to the throat of the engine, whereas thereafter they are assumed to be "frozen" (no further chemical reactions). This is referred to as “Bray’s approximation” and mimics behaviour in real world engines - at the throat; there is a sharp drop in temperature, which slows chemical reactions, and a sharp increase in the velocity of the gas, which reduces residence time (the quicker the gas is expelled from the engine, the less time there is for chemical reactions to go to completion). The transition point can usually be approximated by a single point, the freezing point, where the equilibrium flow changes into a frozen flow, see fig. 6. Of course, this freezing point may be chosen at another suitable location in the nozzle.

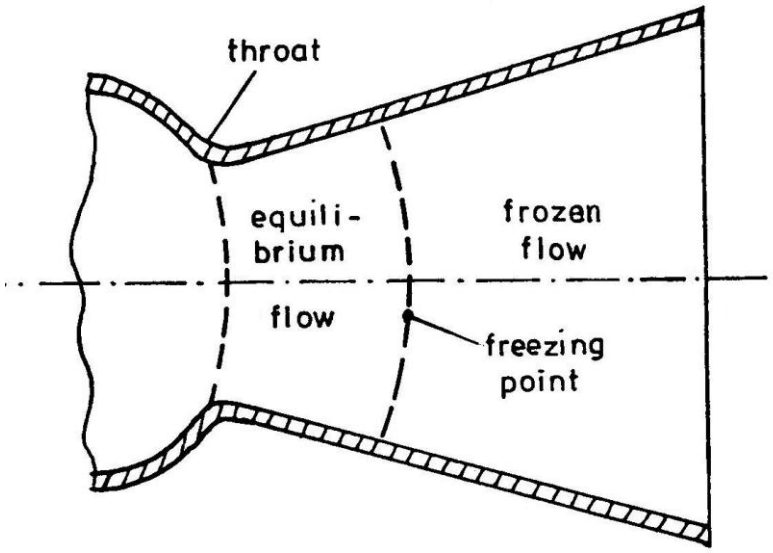

Figure 6: Equilibrium flow and frozen flow regions

Frozen flow (FF)

If the velocity of the exhaust gases inside the chamber is assumed to be zero, then the velocity of these gases at the exit of the nozzle can be found from the change of enthalpy of the reaction products between the chamber and the nozzle exit[15]:

$$\frac{1}{2}M \cdot w_e^{\,2} = \frac{1}{N} \cdot \sum_j n_j \cdot \left[H_{T_c} - H_{T_e} \right]_j \tag{10.1}$$

Here, 'j' refers to the various reaction products in the combustion chamber and exhaust (constant composition).

If one assumes the flow to be isentropic, then

$$S_{T_x}^{\,p_x} = S_{T_c}^{\,p_c} \tag{10.2}$$

Here x refers to an arbitrary location in the nozzle.

With (see annex B):

$$S_T^{\,p} = \frac{1}{N} \sum_j n_j \cdot \left[S_T^{\,p} \right]_j \tag{10.3}$$

$$S_T^{\,p} = \frac{1}{N} \sum_j n_j \cdot \left[S_T^{\,o} \right]_j - \frac{R_A}{N} \cdot \left(N \cdot \ln\left(\frac{p}{p_0} \right) + \sum_i n_j \cdot \ln\left(\frac{n_j}{N} \right) \right) \tag{10.4}$$

The first term represents the entropy of the reactant mixture at the temperature T and standard atmospheric pressure. The second term relates to the actual pressure p (in bar) and the third to the molar quantities of the different species present in the mixture.

If a frozen flow is assumed throughout the nozzle, no reaction takes place and the composition of the reactants does not change between the chamber and the nozzle exit. So:

$$\sum_j n_j \cdot \left[S_{T_c}^{\,o} - S_{T_e}^{\,o} \right]_j - R_A \cdot N \cdot \ln\left(\frac{p_c}{p_e} \right) = 0 \tag{10.5}$$

For given chamber pressure, the chamber temperature and composition of the combustion gases can be calculated as explained before. For given exit pressure, one must assume the temperature in the nozzle exit. Values for the entropy for the substances can be obtained from for instance [JANAF]. Substitution of all known variables into the entropy equation will have to show that this equation is satisfied. If not, one must correct the assumed exit temperature, etcetera. If nozzle exit temperature is known, the exhaust velocity can be obtained using the earlier given velocity equation.

Chemical Equilibrium flow (CEF)

In case one assumes an equilibrium flow throughout the nozzle the mathematical treatment of the flow becomes more complicated, as the composition changes constantly due to the changing temperature. We write the conservation of energy of a fixed mass, chosen as the mass of one mole of combustion products in the chamber.

[15] For 1 kg of reaction products, we can also write:

$$\frac{1}{2} w_e^{\,2} = \sum_j \left[h_{T_c} - h_{T_e} \right]_j$$

$$\frac{1}{2}\cdot w_e^{\,2} = \frac{\sum_j n_j \cdot \left[H_{T_c}\right]_j}{\sum_{ji} n_j \cdot M_c} - \frac{\sum_{j'} n_{j'} \cdot \left[H_{T_e}\right]_{j'}}{\sum_{j'} n_{j'} \cdot M_e} \qquad (10.6)$$

M_c is the mass of one mole of products inside the chamber, while M_e is the mass of one mole of products at the exit plane of the nozzle. As the composition of the gases has changed, between the chamber and the exit, a prime is used to denote the different substances and molar quantities at the exit.

The constant entropy condition is given by:

$$S_{T_c}^{\,p_c} = \frac{1}{N_e}\cdot\sum_{j'=1} n_{j'}\cdot\left(\left[S_{T_e}^{\,o}\right]_{j'} - R_A\cdot\left[\ln\left(p_e\right)+\ln\left(n_{j'}/N'_e\right)\right]\right) \qquad (10.7)$$

Here N_e is the number of moles at the nozzle exit.

To calculate the value of temperature, molar mass and molar quantities in the nozzle exit is quite like the one discussed in the previous sections of this chapter and of which an example is given earlier. This type of calculations can best be run on a computer and various software tools have been developed in this field, see the next section.

11 Computer tools

Several tools are available that help the designer to quickly assess the thermochemistry of a propellant. Three of such tools are GASEQ (developed by C. Morley, United Kingdom) [Morley], RPA or RPA-Lite[16] (Rocket Propulsion Analysis tool developed by A. Ponomarenko), and NASA CEA2 (version 2 of NASA Glenn's computer program Chemical Equilibrium with Applications) originally developed by [Gordon and McBride].

Gaseq is a chemical equilibrium program, primarily for gas phase combustion. It allows for solving several different types of problem, including:

- Composition at a defined temperature and pressure
- Adiabatic temperature and composition at constant pressure
- Composition at a defined temperature and at constant volume
- Adiabatic temperature and composition at constant volume
- Adiabatic compression and expansion
- Equilibrium constant calculations
- Shock calculations

Gaseq runs under Windows 3.1 (usable in Windows 95, Windows 7 and Windows 10) and requires vbrun300.dll in the gaseq, windows or windows\system directory. Gaseq is freeware software and can be obtained via the World Wide Web.

CEA2 and RPA (or RPA-Lite) both allow for solving the same types of problems as for Gaseq. However, a major advantage of these tools over Gaseq is that they also allow for combustion calculations for several common rocket propellants. Data on these propellants are included in a database that comes with the program. A further advantage is that both tools allow for calculating the specific impulse of rocket engines. In more detail, CEA2 and RPA/RPA-Lite calculate the chamber and throat conditions as well as the conditions and specific impulse for any specified expansion condition (area ratio or pressure ratio). Input data that must be specified by you (the user) include data on the propellants to be burned in the engine, their proportions, the chamber pressure, and the expansion ratio(s) or exhaust pressure(s). When you specify propellants, their characteristics (density, molecular weight, heat of formation etc.) are looked up from the data stored in the propellant library. Other menu items

[16] RPA-Lite is a freeware version of the RPA tool.

allow you to change how the program does the calculations (you can ask for "frozen flow" rather than "shifting equilibrium" calculations). Both CEA2 and RPA/RPA-Lite allow for using SI units. Like Gaseq, both CEA2 and RPA-Lite are freely available from the web.

Table 9, Table 10, and Table 11 present sample outputs as produced using CEA2.

Table 9 shows the CEA2 output for the same problem as worked out in the example in the reader in the section dealing entitled **Chemical equilibrium**. The output is obtained by selecting first the option rocket performance and next frozen flow. As inputs are used an O/F (mass) ratio of 8 with both propellants in the gaseous state at 298,15 K (25 °C) and a chamber pressure of 20,69 bar. In addition, we omitted in CEA all products other than the ones considered in the example. Note that this omitting of products is not feasible in RPA-Lite (and maybe also not in RPA).

Table 9: CEA calculated adiabatic flame temperature and hot gas properties of gaseous hydrogen and oxygen at a pressure of 20,69 bar; Initial propellant temperature (at injection) is 298 K.

```
          THEORETICAL ROCKET PERFORMANCE ASSUMING FROZEN COMPOSITION

             REACTANT                    WT FRACTION      ENERGY      TEMP
                                         (SEE NOTE)     KJ/KG-MOL      K
FUEL        H2                           1.0000000         0.000    298.150
OXIDANT     O2                           1.0000000         0.000    298.150

O/F=    8.00000  %FUEL= 11.111111  R,EQ.RATIO= 0.992085  PHI,EQ.RATIO= 0.992

                CHAMBER   THROAT     EXIT
Pinf/P            1.0000   1.7735   85.070
P, BAR            20.690   11.666  0.24321
T, K             3494.54  3175.03  1576.17
RHO, KG/CU M    1.1075 0 6.8734-1 2.8865-2
H, KJ/KG          0.00000 -1020.74 -5787.75
U, KJ/KG         -1868.09 -2718.02 -6630.33
G, KJ/KG         -57737.4 -53479.2 -31829.6
S, KJ/(KG)(K)     16.5222  16.5222  16.5222

M, (1/n)          15.554   15.554   15.554
Cp, KJ/(KG)(K)    3.2174   3.1707   2.7052
GAMMAs            1.1993   1.2028   1.2463
SON VEL,M/SEC     1496.8   1428.8   1024.7
MACH NUMBER        0.000    1.000    3.320

PERFORMANCE PARAMETERS

Ae/At                      1.0000   10.000
CSTAR, M/SEC               2106.8   2106.8
CF                         0.6782   1.6149
Ivac, M/SEC                2616.7   3649.9
Isp, M/SEC                 1428.8   3402.3

MOLE FRACTIONS

*H              0.04644   *H2             0.13077   H2O             0.64683
*O              0.02172   *OH             0.11291   *O2             0.04133

 * THERMODYNAMIC PROPERTIES FITTED TO 20000.K
```

Comparing the outputs obtained with CEA and the results from the example mentioned earlier, we learn that the difference in combustion temperature is quite limited. In the example, we also obtain a molar mass of 15.6 gram/mol, a specific heat at constant pressure of 54.394 J/mol or 3486.8 kJ/(kg –K) and a specific heat ratio of 1.18. The latter two are only slightly different from the parameter values in the combustion chamber as given by CEA and can be explained from a slightly different composition of the product mixture.

Differences in the results are attributed to small differences in thermodynamic data and/or rounding applied in the example worked out in the reader.

Table 10 presents the output as determined for the reaction of liquid hydrogen with liquid fluorine at a molar mixture ratio of 5:1 and a chamber pressure of 30 bars.

Table 10: Sample output from CEA for a liquid hydrogen – liquid fluorine mixture at a molar mixture ratio of 5:1 and a chamber pressure of 30 bars (frozen chemistry calculations).

```
        THERMODYNAMIC EQUILIBRIUM COMBUSTION PROPERTIES AT ASSIGNED PRESSURES

        CASE = LH2-LF2

                 REACTANT          WT FRACTION         ENERGY             TEMP
                                   (SEE NOTE)          KJ/KG-MOL           K
        OXIDANT     F2(L)          1.0000000          -13091.000         85.020
        FUEL        H2(L)          1.0000000          -9012.000          20.270

        O/F=  3.76230    %FUEL=  20.998257    R,EQ.RATIO=  5.009899    PHI,EQ.RATIO=
5.009899

        THERMODYNAMIC PROPERTIES

        P, BAR             30.000
        T, K               2739.12
        RHO, KG/CU M       1.0497 0
        H, KJ/KG           -1210.91
        G, KJ/KG           -66836.3
        S, KJ/(KG)(K)      23.9586

        M, (1/n)           7.969
        Cp, KJ/(KG)(K)     5.5717
        GAMMAs             1.2550
        SON VEL,M/SEC      1893.9

        MOLE FRACTIONS

        *F        0.00002
        *H        0.00976
        *HF       0.33013
        *H2      0.65949
```

The results given in Table 10 have been verified by manual calculation [Zandbergen, 2003]. The results are found to be in good agreement, see below table.

Table 11: Verification of CEA results by manual calculations

Parameter	CEA result	Manual calculation result
Chamber temperature [K]	2739.12	2739
Molar mass [gram/mol]	7.969	7.96
Specific heat ratio [-]	1.2550	1.299
Mole fractions		
F	0.00002	0.000
H	0.00976	0.012
HF	0.33013	0.331
H_2	0.65949	0.657
H_2F_2	0.00061	Not included

Largest difference is for specific heat ratio and molar fraction of H. The latter is attributed to calculation inaccuracies (rounding errors) in the manual calculation. The former is because in the manual calculation it is assumed that after reaching equilibrium the composition is frozen, whereas the CEA results are for equilibrium conditions in the chamber (reactions are still ongoing).

Table 12 presents typical outputs for an NTO-MMH mixture with an equal number of moles of NTO and MMH that react at a pressure of 100 psia (6.9 bar) and subsequently expand in a nozzle with an area ratio of 100. Additional data shown in the table include amongst others specific impulse and thrust coefficient. Furthermore, the evolution of these parameters through the nozzle is given. The result on gas composition (chemical equilibrium flow) clearly shows that the number of radicals in the mixture decreases toward the nozzle exit due to the decreasing nozzle temperature.

Table 12: Sample output from CEA2 for an NTO-MMH mixture with an equal number of moles of NTO and MMH (chemical equilibrium flow assumption)

```
        THEORETICAL ROCKET PERFORMANCE ASSUMING EQUILIBRIUM
        COMPOSITION DURING EXPANSION FROM INFINITE AREA COMBUSTOR

 Pin =   100.1 PSIA

           REACTANT                    WT FRACTION      ENERGY      TEMP
                                        (SEE NOTE)     KJ/KG-MOL      K
FUEL       CH6N2(L)                     1.0000000     54200.000    298.150
OXIDANT    N2O4(L)                      1.0000000    -17549.000    298.150

 O/F= 1.99710  %FUEL= 33.365587  R,EQ.RATIO= 1.250015  PHI,EQ.RATIO= 1.250015

                CHAMBER   THROAT     EXIT
 Pinf/P           1.0000   1.7298  1577.67
 P, BAR           6.9000   3.9888  0.00437
 T, K            3131.55  2975.33  1000.69
 RHO, KG/CU M   5.7726-1 3.5571-1 1.2097-3
 H, KJ/KG         265.43  -369.15 -5221.21
 G, KJ/KG       -38379.3 -37086.0 -17570.2
 S, KJ/(KG)(K)   12.3404  12.3404  12.3404

 M, (1/n)         21.783   22.061   23.014
 Cp, KJ/(KG)(K)   6.3964   5.8874   1.8021
 GAMMAs           1.1322   1.1318   1.2507
 SON VEL,M/SEC    1163.3   1126.6    672.5
 MACH NUMBER       0.000    1.000    4.926

 PERFORMANCE PARAMETERS

 Ae/At                     1.0000   100.00
 CSTAR, M/SEC              1721.9   1721.9
 CF                        0.6543   1.9238
 Ivac, M/SEC               2122.0   3421.7
 Isp, M/SEC                1126.6   3312.6

 MOLE FRACTIONS

 *CO             0.10568  0.10198  0.03370
 *CO2            0.05208  0.05778  0.13297
 *H              0.02691  0.02171  0.00000
 HO2             0.00002  0.00001  0.00000
 *H2             0.09209  0.08761  0.13298
 H2O             0.34764  0.36486  0.36702
 *N              0.00001  0.00000  0.00000
 *NO             0.00751  0.00550  0.00000
 *N2             0.31174  0.31677  0.33333
 *O              0.00653  0.00446  0.00000
 *OH             0.04014  0.03194  0.00000
 *O2                                       0.00966      0.00736      0.00000
```

Explanation of terms
Cp is specific heat
GAMMA is specific heat ratio
SON VEL is velocity of sound
HF gives heat of formation of the substances involved
CSTAR is characteristic velocity
CHAMBER refers to chamber conditions
THROAT refers to throat conditions
EXIT refers to conditions at nozzle exit
Ae/At: Geometric expansion ratio
Ivac: Specific impulse in vacuum
ISP: Specific impulse at sea level
CF: Thrust coefficient

12 The effect of various parameters on performance

In Fig. 7, the theoretical properties of liquid oxygen and liquid hydrogen propellants are shown. Flame temperature, characteristic velocity, mean molecular mass and specific heat ratio are plotted versus the oxidizer-to-fuel mass mixture ratio. The stoichiometric mixture ratio is about 8, giving the highest combustion temperature, but not the highest characteristic velocity. The highest characteristic velocity is reached for a mixture ratio of about 3, because at this mixture ratio the mean molar mass is lower. In practice for these motors, it is often desirable to operate at a "fuel-rich" mixture ratio as in that case, we have a non-oxidizing environment.

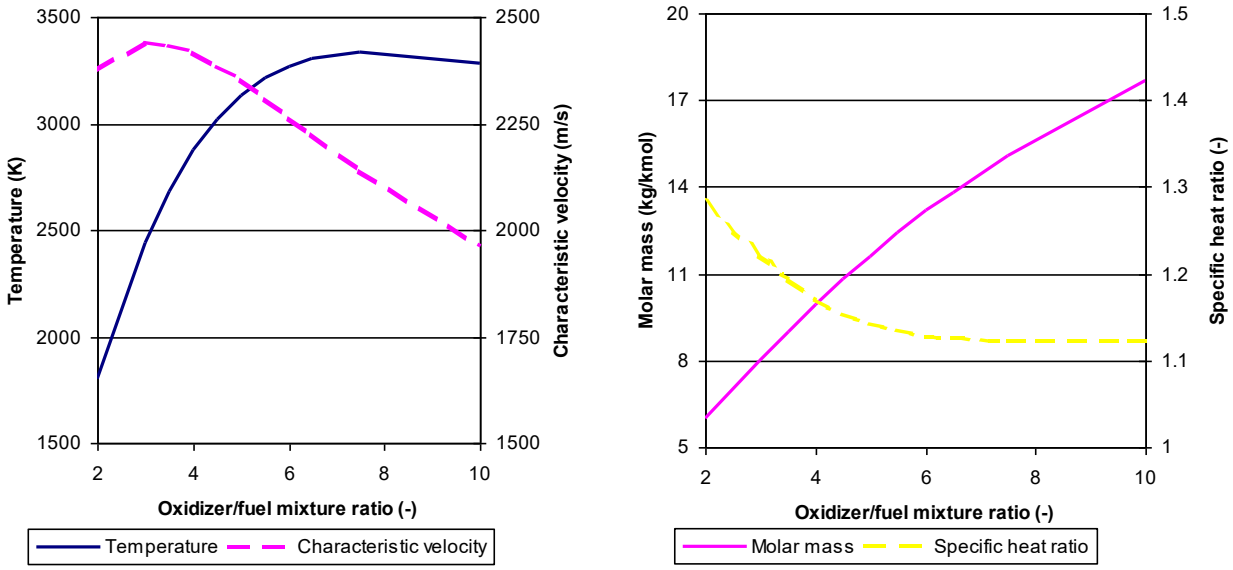

Figure 7: Theoretical chamber properties of liquid oxygen/liquid hydrogen as a function of mass mixture ratio (chamber pressure is 10 bar).

Table 13 shows the value of the temperature, the characteristic velocity, the mean molar mass, and the ratio of specific heats for NTO-MMH as a function of mixture ratio. One can see that both temperature and characteristic velocity peak at a mass mixture ratio markedly different from that for liquid oxygen and liquid hydrogen. [SSE] provides an overview of theoretical properties of several other common propellants.

Table 13: Theoretical chamber properties of NTO-MMH as a function of mass mixture ratio (chamber pressure is 10 bar).

Mixture ratio	Flame temperature	Molar mass	Specific heat Ratio	Characteristic velocity
(-)	(K)	(kg/kmol)	(-)	(m/s)
1.0	2355.9	16.7	1.252	1644.8
1.2	2654.0	18.0	1.217	1698.7
1.4	2878,5	19.2	1.186	1728.8
1.6	3033.5	20.2	1.161	1743.6
1.8	3126.8	21.1	1.144	1741.4
2.0	3178.8	21.9	1.135	1728.,4
2.1	3183.2	22.2	1.132	1719.,5
2.2	3187.5	22.5	1.13	1710.3
2.3	3187.2	22.9	1.129	1695.7
2.4	3183.2	23.1	1.129	1687.3
2.5	3176.4	23.4	1.128	1675.2
3.0	3117.5	24.5	1.129	1621.4

In Figure 8 the influence of the pressure on the combustion temperature and on the molar mass is shown for MMH-NTO. Both flame temperature and molar mass increase with increasing pressure. This is because at higher pressures, there is less dissociation.

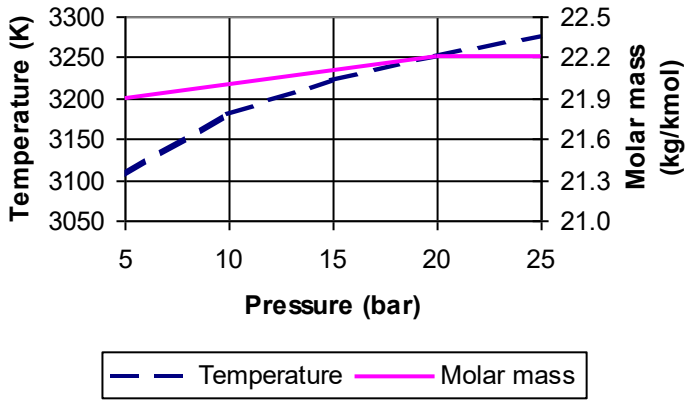

Figure 8: Theoretical effect of pressure on the combustion of NTO and MMH (mass mixture ratio of 2.05)

In the next table, some theoretically determined values for the specific impulse of a liquid hydrogen - liquid oxygen rocket are given at different equivalence ratios for a chamber pressure of 41.37 bar and ideal expansion to 1 bar. Results indicate that specific impulse values for constant properties flow (CPF) and chemical equilibrium flow (CEF) are substantially higher than for frozen flow (FF), especially at high temperature (ER close to 1). The higher performance for CPF is because the specific heat ratio is assumed constant[17], whereas for FF the specific heat ratio increases with decreasing nozzle temperature. For CEF, this is because recombination occurs and hence more chemical energy is released in the flow. This effect is most strongly felt at high combustion temperatures.
CPF and CEF tend to give overly optimistic values, in that in practical engines the exhaust process is so quick that some energy releasing processes in the exhaust aren't fast enough, and the actual exhaust products are not in chemical equilibrium.

Table 14: Specific impulse (s) liquid hydrogen-liquid oxygen rocket at different equivalence ratios (ER) for a chamber pressure of 41.37 bar and ideal expansion to 1 bar.

ER	0.25	0.50	1.00	2.00	4.00
CPF	363.6	380.0	341.3	272.6	207.5
FF	359.6	369.7	325.3	261.0	203.1
CEF	359.6	374.5	342.5	271.1	204.7

Calculated exhaust gas composition is shown in Table 15. For a NTO-MMH mixture assuming both frozen and chemical equilibrium flow conditions at two pressure conditions.

[17] To determine the performance for CPF (Constant Properties Flow) the hot gas conditions in the combustion chamber should be known. Two options exist; For option 1, the properties of the hot gas in the chamber are determined based on the option of chemical equilibrium conditions, whereas for option 2, the propellant composition is considered frozen. Both options give same molar mass and flame temperature, but option 1 provides for a higher specific heat ratio and hence a higher performance. The latter option has been used for determining the results given in the table. Note that the choice between option 1 and 2 is still open and has to be determined using experiments or further analysis.

Table 15: Calculated nozzle exit gas composition in moles per 100 grams of exhaust gases for frozen flow and chemical equilibrium flow conditions at two chamber pressures (fixed mass mixture ratio of 2.05 and nozzle area ratio of 83.

Compound	CEF		FF	
	10 bar	20 bar	10 bar	20 bar
H	0	0	0.111	0.093
H_2	0.484	0.488	0.385	0.371
H_2O	1.651	1.647	1.605	1.633
O	0	0	0.031	0.025
O_2	0	0	0.051	0.043
OH	0	0	0.180	0.167
NO	0	0	0.040	0.040
N_2	1.442	1.442	1.422	1.422
CO	0.152	0.148	0.459	0.453
CO_2	0.559	0.563	0.252	0.258

The results show the effect of pressure on composition both under CEF and FF conditions. The results also show that when assuming CEF recombination occurs in the nozzle as opposed to FF, where the composition essentially remains the same as in the combustion chamber. This leads to a substantial reduction in for instance carbon monoxide. Also, nitrogen monoxide is no longer present in the exhaust. In reality, the exhaust composition will be somewhere in between that of CEF and FF.

In fig. 9, theoretically determined values for specific impulse and the heat (per kg) required for heating up the propellant to a certain temperature are given for the thermal propellants hydrogen and nitrogen.

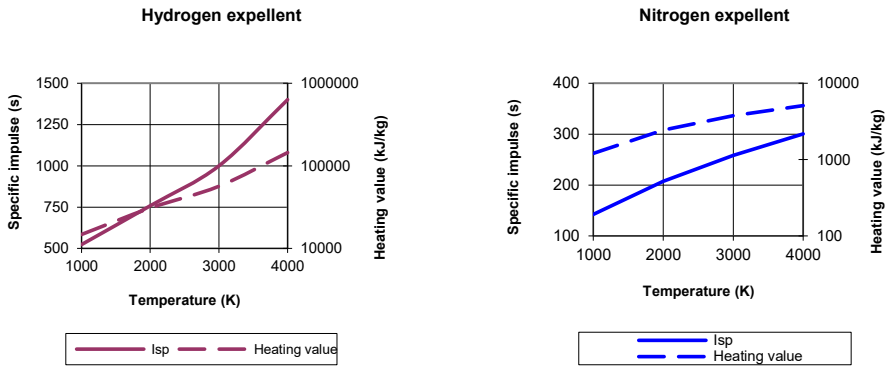

Figure 9: Theoretically determined optimum specific impulse of liquid hydrogen (left) and liquid nitrogen (right) at 1 MPa chamber pressure and expansion to an area ratio of 100 (calculated assuming chemical equilibrium flow).

Results indicate the high specific impulse attainable with liquid hydrogen, depending on the allowable chamber temperature. The figure also shows the much higher energy (power) need to heat up 1 kg of hydrogen compared to 1 kg of nitrogen.

The real world

According to [Sutton], experimental values for the specific impulse of chemical rocket motors are, in general, 3-12% lower than those calculated by the chemical equilibrium flow method. Only a portion of this correction (1-4%) is due to combustion efficiencies caused by incomplete combustion, and non-uniform mixture ratio across the injector. The remainder is attributed to nozzle inefficiencies due to nozzle friction and the use of propellants for purposes other than thrust (such as film cooling, powering turbo-pumps and providing tank ullage gas).

In figure 10 the I_{sp} is given as function of the fuel percentage for hydrogen-oxygen and JP4 (some kind of kerosene)-oxygen. For the first propellant the equilibrium flow is the best approximation while for the second propellant the frozen flow is the best approximation.

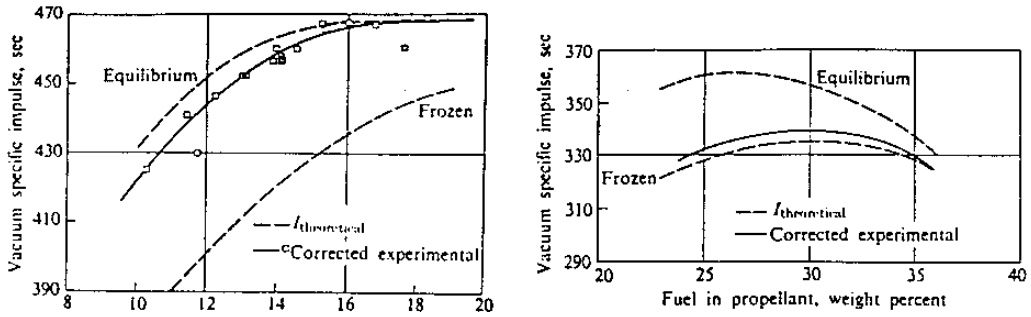

Figure 10: Corrected specific impulse of hydrogen-oxygen (left) and JP4 -oxygen (right) rocket [Olson]

[Dunn] compared the theoretical results calculated using "frozen at throat" conditions (Bray approximation) with performance data taken from specification sheets, see the table below.

Table 16: Comparison of theoretically determined and actual values for specific impulse

Engine	Condition	O/F mass mixture ratio (-)	Chamber pressure (MPa)	Nozzle area expansion ratio (-)	Real I_{sp} (s)	Calculated I_{sp} using Bray approximation (s)	Real to calculated I_{sp} (%)
F1	Sea level	2.27	6.77	16	265	281.5	94.1
RS-27	Sea level	2.24	4.84	8	262.5	279.3	93.9
H1	Sea level	2.23	4.83	8	263	279.1	94.2
MA5-booster	Sea level	2.25	4.41	8	259.1	276.0	93.9
MA5-sustainer	Sea level	2.27	5.07	25	220.4	239.5	92.0
J2	Vacuum	5.5	5.26	27.5	425	434.4	97.8
SSME	Vacuum	6	22.5	77.5	453.5	452.9	100.4

The F1, RS-27, and H1 engines are LOX/kerosene engines designed as first stage engines for boosters. All are slightly over-expanded at sea level. The MA5 engine uses the same propellants, but is a three-chamber engine, with two boost chambers and nozzles designed for sea level operation, and 1 sustainer chamber and nozzle designed for high altitude efficiency. At sea level, the booster engines are slightly over-expanded, while the sustainer is very badly over-expanded, to a point where there is probably flow separation in the nozzle. All the kerosene engines have a real-world I_{sp} which is about 92 to 94% of the theoretical I_{sp} calculated using "frozen at throat" assumptions.
The J2 and SSME burn hydrogen and oxygen and are optimized for vacuum operation (although the SSME also operates in the over-expanded condition at take-off). Actual I_{sp} is about 98% to within a fraction of a percent of the results of a "frozen at throat" I_{sp} calculation.

13 Problems

1. You are designing a small thermal rocket engine using liquid hydrogen (stored at just below 20.36 K) as propellant. You have selected a mass flow rate of 0.05 kg/s and a hot gas temperature of 2000 K. Calculate for this rocket the thermal power needed to heat the hydrogen propellant to 2000 K.

2. The heat of evaporation of propane at the normal boiling point (-42.0 ^{o}C @ 1 atm.) is 15,7 kJ/mol. Given is that the average heat capacity for liquid propane is 109 J/(mol-K) over the temperature range between the normal boiling point (at 1 bar) and 298.15 K. Enthalpy of heating of gaseous propane can be found in the NIST chemistry webbook. Calculate the heat of evaporation of propane at 298.15 K at the vapour pressure. Hint: Use Hess's law.

3. Balance the following reaction equations:

$$H_2O_2 \rightarrow \ldots O_2 + \ldots H_2O$$
$$2N_2H_4 \rightarrow \ldots NH_3 + \ldots N_2$$
$$H_2 + \ldots O_2 \rightarrow \ldots H_2O$$
$$H_2 + 2O_2 \rightarrow \ldots H_2O + \ldots O_2$$
$$CH_4 + \ldots O_2 \rightarrow \ldots CO_2 + \ldots H_2O$$
$$N_2H_4 + N_2O_4 \rightarrow \ldots NH_3 + \ldots NO_2 + \ldots N_2$$
$$C_{12} + H_{26} + \ldots O_2 \rightarrow 12CO + \ldots H_2O$$

4. Consider the reaction of acetic acid with sodium bicarbonate as given below:

$$1\ CH_3COOH + 1\ NaHCO_3 \rightarrow 1\ NaCH_3COO + 1\ CO_2 + 1\ H_2O$$

   Determine for this balanced reaction equation:
   - The mass mixture ratio of acetic acid versus sodium bicarbonate.
   - The volume the carbon dioxide formed will have in the gaseous state at 1 bar and 273 K. Idem at 293 K

   In case we consider the reaction of vinegar (5% mass solution of acetic acid in water), calculate the amount of vinegar needed to allow complete reaction between the acetic acid and 7 grams of sodium bicarbonate.

5. Use the NIST Chemistry WebBook to look up the standard heat of formation for the following substances: Hydrogen (l), Hydrogen peroxide (l), Oxygen (l), Methane (l), Oxygen (g), and Methane (g).

6. Determine for the hydrogen peroxide reaction (assuming water (l) and oxygen (g) as the reaction products), the heat of reaction. Clearly indicate whether this is an endothermic or exothermic reaction.

7. Calculate the adiabatic flame temperature of a mixture of liquid hydrogen and liquid oxygen (oxidizer-to-fuel mass mixture ratio of 5) at a pressure of 100 bar using chemical equilibrium theory. Reactant temperature for liquid hydrogen may be taken equal to 20.27 K and for liquid oxygen 90.18 K. Outline all calculation steps clearly.

8. Calculate the entropy of a gas mixture consisting of 0.5 mol water, 0.1 mol hydrogen, and 0.05 mol OH at a temperature of 2500 K and a pressure of 20 x 10^5 N/m^2.

9. Use RPA-Lite to calculate the theoretical specific impulse of a rocket engine using a mixture of MMH and NTO (mass mixture ratio of 1.65) at a chamber pressure of 20 bar and a nozzle area ratio of 150 assuming constant properties, equilibrium and frozen flow conditions, respectively. Also determine the specific impulse using Coats' law. You may assume standard initial conditions for the reactants.

References

1) *D'Andrea, B., Lillo, F., Faure, A., and Perut, C.,* A new generation of solid propellants for space launchers", Acta Astronautica vol. 47, Nos. 2-9, pp. 103-112, 2000.

2) *Barrow, G.M.,* Physical Chemistry, International student edition, 4th ed., McGraw-Hill, 1979.

3) *Bentor*, Y., Online interactive periodic table of the elements: http://www.chemicalelements.com/

4) *Binas,* Physics Handbook, 3rd ed., Wolters Noordhof, 1996.

5) *CRC,* Handbook of Chemistry and Physics, 60th Edition, CRC Press, Boca Raton, 1980.

6) *Dunn, B.,* README file for Air Force Specific Impulse Program, November 2001.

7) Gordon S., McBride B., Computer Program for Calculation of Complex Chemical Equilibrium Compositions, Rocket Performance, Incident and Reflected Shocks, and Chapman-Jouguet Detonations, NASA SP-271, 1971.

8) *JANAF,* NIST-JANAF Thermochemical Tables, Fourth edition, Journal of Physical and Chemical Reference Data, Monograph 9, 1998.

9) *NIST*, Online thermochemical tables: http://webbook.nist.gov/chemistry.

10) *Cox, J. D., Wagman, D. D., and Medvedev, V. A.*, CODATA Key Values for Thermodynamics, Hemisphere Publishing Corp., New York, 1989.

11) *Gadiot, G.M.H.J.L., Mul, J.M., Lit, P.J. van, and Korting, P.A.O.G.,* Hydrazinium Nitroformate and its use as oxidizer in High Performance Solid Propellants.

12) *Mul, J.M., Korting, P.A.O.G., and Schöyer, H.F.R.,* Search for New Storable High-Performance Propellants, AIAA-88-3354, 1988.

13) *Morley, C.,* A Chemical Equilibrium Program for Windows: http://www.c.morley.ukgateway.net/gseqmain.htm

14) *Olson, W.T.,* Recombination and Condensation Processes in High Area Ratio Nozzles, J. Amer. Rocket Soc., 32, 5, May 1962, Pages 672-680.

15) *Schöyer, H.F.R.,* Some New European Developments in Chemical Propulsion, ESA Bulletin, No. 66.

16) *Sutton, G.P.,* Rocket Propulsion Elements, 6th ed., John Wiley and Sons, Inc. 1992.

17) *Zandbergen, B.T.C.,* The degree of dissociation of hydrogen, fluorine, oxygen, hydrogen-fluorine and water at various temperatures and pressures (in Dutch), Technical note 10040, LR memorandum M-701, TU-Delft, 1995.

18) *Zandbergen, B.T.C.,* Chemical reactions with dissociation; Example calculation using the method of 'successive approximations", Technical note 10008, TU-Delft, faculty of Aerospace Engineering, 2003.

This page is intentionally left empty

Heat transfer in rocket motors

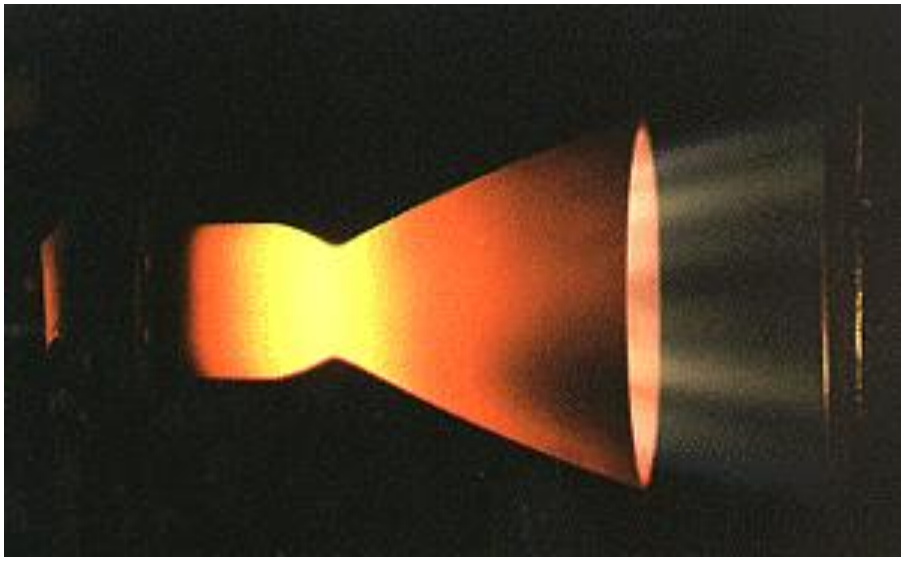

B.T.C. Zandbergen

Contents

Contents 156

1 Introduction: Heat transfer in rocket motors 159

2 Heat transfer (fundamentals of) 159

2.1 Radiation heat transfer 160

2.2 Heat transfer through conduction 165

2.3 Heat transfer through convection 167

3 Hot-gas side heat transfer 174

3.1 Convection 175

3.2 Net rate of radiation 180

3.3 Conduction 182

3.4 Heat transfer measurements 183

4 Cooling of rocket motors (fundamentals) 183

4.1 Un-cooled motors 183

4.2 Heat-Sink Cooling 183

4.3 Insulation 184

4.4 Ablation cooling 185

4.5 Radiation cooling 187

4.6 Film cooling 189

4.7 Dump and regenerative cooling 190

4.8 Transpiration or sweat cooling 192

4.9 Comparison of cooling methods 192

5 Analysis tools 193

6 Problems 194

References 195

List of symbols:

Roman

a	Constant in convective heat transfer calculations
A	Cross-sectional area
c	Specific heat
c^*	Characteristic velocity
c_f	Local friction coefficient
c_p	Specific heat at constant pressure
D	Diameter
D^*	Throat diameter
F	Monochromatic hemispherical emissive power
G	Mass flux (mass flow rate divided by cross-sectional area)
h	Heat transfer coefficient
H_{abl}	Heat of ablation
k	Thermal conductivity constant
L	Thickness, length
m	Mass flow
M_o	Mach number undisturbed flow
Nu	Nusselt number
p	Pressure
Pr	Prandtl number
Q	Heat transfer rate of the slab or shell
q	Heat flow per unit surface area or heat flux
r	Recovery factor
r	Radius
r_c	Radius of curvature of throat section
R	Radius
R_T	Thermal resistance
Re	Reynolds number
S	Total hemispherical emissive power
St	Stanton number
T	Temperature
T_o	Static temperature of undisturbed flow
T_o	Stagnation (total) temperature
T_r	Reference temperature
$T_{w,g}$	Temperature of hot gas at wall
v	Flow velocity
x	x-ordinate
y	y-ordinate

Greek

α	Absorptivity
$\partial./\partial x$	Gradient along x-ordinate
Δ	Difference
ε	Emissivity
φ	Factor defined in SB correlations
γ	Specific heat ratio
λ	Wavelength
μ	Dynamic viscosity
ρ	Reflection coefficient, density
τ	Transmission coefficient

Subscripts

ad	Adiabatic
b	Bulk
f	Film
g	Gas
s	Surface
sur	Surroundings
w	Wall

Constants

h	Planck's constant (6,6256 x 10^{-34} W/s^2)
c	Velocity of light in vacuum (2,998 x 10^{-8} m/s)
k	Boltzmann's constant (1,3805 x 10^{-23} W.s/K)
σ	Stefan Boltzmann constant (5,6705 x 10^{-8} W/(m^2K^4))

1 Introduction: Heat transfer in rocket motors

In this chapter methods are presented that allow for the determination of the heat transfer in rocket motor systems.

Heat transfer in rocket motors is typically about one order in magnitude higher than the heat transfer in a jet engine. This can be easily understood, when we consider that hot gas temperatures in a jet engine are limited to about 1400-1600 K, whereas such temperatures in rocket motors may range up to 4500 K. On the other hand, most rocket motors only burn for a short time, whereas jet engines may burn for hours. Even so, the heat transfer from the hot gas flow to the wall of the motor may affect the strength of the materials of which it is made, see also chapter on structural design, and hence some means of cooling may be required. Such a cooling system adds mass and complexity to the system.

Other reasons to understand heat transfer and cooling are

- Maximize heating of propellants in case of laser-, solar-, and electro-thermal propulsion.
- Limit energy losses. Heat transfer means a loss of energy and hence a reduction in performance.
- Limit unwanted heat flows to e.g. surrounding systems. Heat transfer can cause expansion of propellants and/or structural materials, which might lead to unwanted stresses causing structural failure.
- Preserve propellant phase (liquid, solid). For example, in case of cryogenic propellants, heat transfer from the surroundings to the propellant can cause significant boil off. In practice this is why loading of cryogenic propellants continues until shortly before the start of the rocket and why cryogenic tanks are covered with thermal insulation.
- Etc.

In this chapter attention will be given to the fundamentals of heat transfer. Second heat transfer from the hot gas to the thrust chamber wall is discussed. Finally, several cooling methods are discussed.

2 Heat transfer (fundamentals of)

Heat transfer deals with transfer of thermal energy from a medium with high temperature to a medium with low temperature. The amount of heat transferred per unit time is usually referred to as heat transfer rate ‘Q’ and is expressed in (J/s or W). In case we consider the heat flow per unit surface area ‘A’, we refer to this as the heat flux ‘q’ and is expressed in (J/(s-m^2) or W/m^2):

$$q = \frac{Q}{A} \tag{2.1}$$

Heat transfer, next to work transfer, is one of two types of energy interactions that are accounted for in the first law of thermodynamics. For a closed system:

$$Q = \frac{dE}{dt} + W \tag{2.2}$$

Here Q (rate of heat transfer) and W denote the sum of all the heat and work transfer interactions experienced by the closed system.

Different modes of heat transfer exist, each governed by its own physical principle:

- Radiation heat transfer
- Conductive heat transfer
- Convective heat transfer

Hereafter, the three types of heat transfer are dealt with in more detail.

2.1 Radiation heat transfer

All species (solids, liquids and gases) emanate thermal radiation. “Thermal radiation” is energy emitted by matter in the form of electromagnetic waves at a finite temperature. It usually results from changes in the electron configuration of the atoms or molecules. Most of the heat emitted at temperatures below 6000K is infra-red radiation. Hence, thermal radiation is sometimes referred to as infra-red radiation. The wavelength band for infra-red radiation is 0,7 – 100 μm. Besides emitting thermal energy, a body also may receive thermal energy from its surroundings. The difference between the two represents the net heat transfer. Hereafter, we will deal with determining both the amount of thermal radiation emitted by a body as well as received.

2.1.1 Thermal emission

To describe thermal radiation, we generally use an ideal radiator, referred to as a “black body”. More specific, a black body is a body for which the following holds:

- Intensity of the radiation emitted is equal in all directions. We speak of a diffuse emitter.
- Intensity of the radiation emitted at wavelength λ is governed by Planck’s law[1]:

$$I(\lambda) = \frac{2hc^2}{\lambda^5} \cdot \frac{1}{e^{hc/\lambda kT} - 1} \tag{2.3}$$

It essentially gives the intensity of monochromatic radiation (also referred to as spectral radiance) in watts per unit wavelength, unit area and unit solid angle[2] (W/(m^2-m-sr)). Figure 1 gives typical values of spectral radiance at 4 different temperatures.

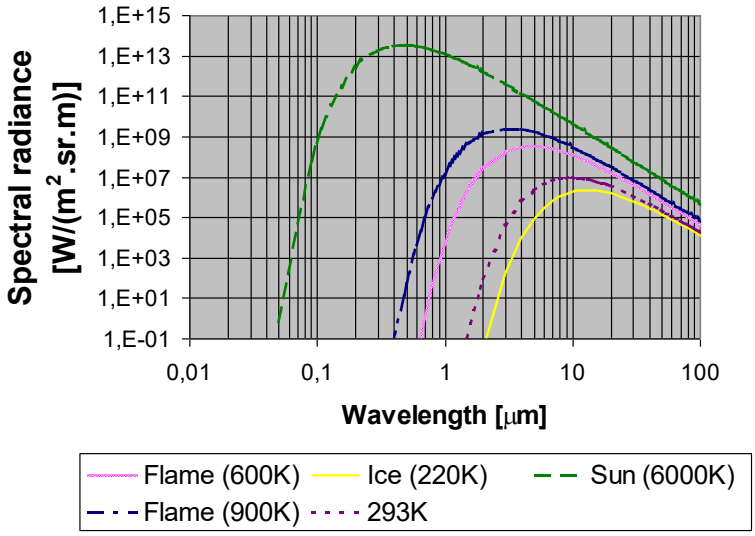

Figure 1: Effects of wavelength and temperature on monochromatic intensity.

The wavelength of maximum emission can be found by differentiating Planck's law with respect to wavelength and putting the result equal to zero:

$$\lambda_{max} = b/T \ [\mu m] \tag{2.4}$$

This result is known as Wien's displacement law where T is absolute temperature and b is a constant of proportionality called *Wien's displacement constant*, equal to 2.897771955...×10^{-3} m·K.

[1] Planck’s law has been earlier discussed in several undergraduate lectures on thermal control, and Earth Observation.
2 Solid angle ω is the area A on a spherical surface divided by the square of the radius of the sphere it is expressed in steradian (sr): 1 sr = (180/π)^2 deg^2.

The monochromatic hemispherical emissive power, also referred to as spectral irradiance, follows by multiplication of the intensity with π.

$$\Phi(\lambda) = \frac{2\pi hc^2}{\lambda^5} \cdot \frac{1}{e^{hc/\lambda kT} - 1} \tag{2.5}$$

Here h is Planck's constant (6.6256 x 10^{-34} J-s), c is velocity of light in vacuum, k is Boltzmann's constant (1.381 x 10^{-23} J/K), and T is temperature (K).

- The total emitted power (in W/m^2) over the whole spectrum into a hemisphere is governed by Stefan Boltzmann's law[3]:

$$S = \sigma T^4 \tag{2.6}$$

With σ is Stefan Boltzmann constant: 5.6705 x 10^{-8} W/(m^2K^4).

A black body radiator is a highly theoretical case, which in practice rarely exists. However, in many practical cases the body behaves as a diffuse grey body. This is a body for which the total radiation emitted is given by the following equation:

$$q = \varepsilon \cdot \sigma \cdot T^4 \tag{2.7}$$

Where 'q' = heat flux (W/m^2), and $\varepsilon = \varepsilon(T)$; ε = emissivity constant ($0 < \varepsilon < 1$).

The emissivity constant indicates how efficiently the surface emits radiation relative to an ideal radiator or blackbody ($\varepsilon = 1$). There are two main ways to measure emissivity: calorimetric or radiometric. In the calorimetric method emissivity is evaluated in terms of heat lost or gained by the material. Only total hemispherical emissivity is measured, i.e. the thermal radiation is measured over all wavelengths and angles. A classical method for measuring a metal would be to pass a current through a thin strip specimen situated in vacuum. In the central isothermal section of the strip there will be a known area and temperature losing heat by radiation. To keep the temperature steady, this heat loss must be balanced by electrical heating of power. A common radiometric method is to measure the thermal radiation from the object using an infrared-measuring instrument and then comparing it to radiation from a blackbody at the same temperature. Results indicate that the emission coefficient of solids and liquids depends on the material, the surface treatment or roughness, the wavelength and the temperature of the material. Dependence of emissivity is usually weak, see Table 1.

Table 1: Emission coefficient for specific materials [PBNA]

Material	T (in °C)	Emissivity
Aluminum:		
Non-oxidized	100	0.03
Non-oxidized	500	0.06
Oxidized	200	0.11
Oxidized	600	0.19
Stainless steel:		
Polished	100	0.22
Polished	425	0.45
Iron (roughly polished)	100	0.17
Carbon (coal)	20	0.952
Graphite	100-500	0.76-0.71
Black paint		
Shining	40	0.90
Matted	40	0.97
Mercury	0	0.09
Liquid water	0-40	0.95

[3] Verify that Stefan Boltzmann's law can be obtained by integration of Planck's radiation formula in terms of monochromatic hemispherical power from $\lambda = 0$ to $\lambda = \infty$.

Emissivity of gases is slightly more complicated. Especially at low temperature gases only radiate in distinctive wavebands and hence it is not possible to use the “grey body analysis”. At high temperatures, these wavebands broaden, and it becomes possible to use the grey body analysis. Important radiating gases are carbon dioxide, water, carbon monoxide, and ammonia. Thermal emission of gases depends on gas temperature 'T_g', partial pressure 'p_x', thickness of the gas 'L', and total pressure 'p':

$$\varepsilon_g = f\left(T_g,\, p_x \cdot L,\, p\right) \tag{2.8}$$

$$L = 3.6 \cdot \frac{V}{S} \tag{2.9}$$

Here ‘V’ is volume occupied by gas and ‘S’ is surface area of volume occupied.

The function f describing the emissivity of a gas is usually reported graphically by the following two types of figures. When the mixture pressure is equal to 1 atm., the emissivity of water is simply the emissivity indicated in the figure 2. If the total pressure of the mixture differs from 1 atm, the emissivity should be multiplied with a pressure correction factor, see also figure 2.

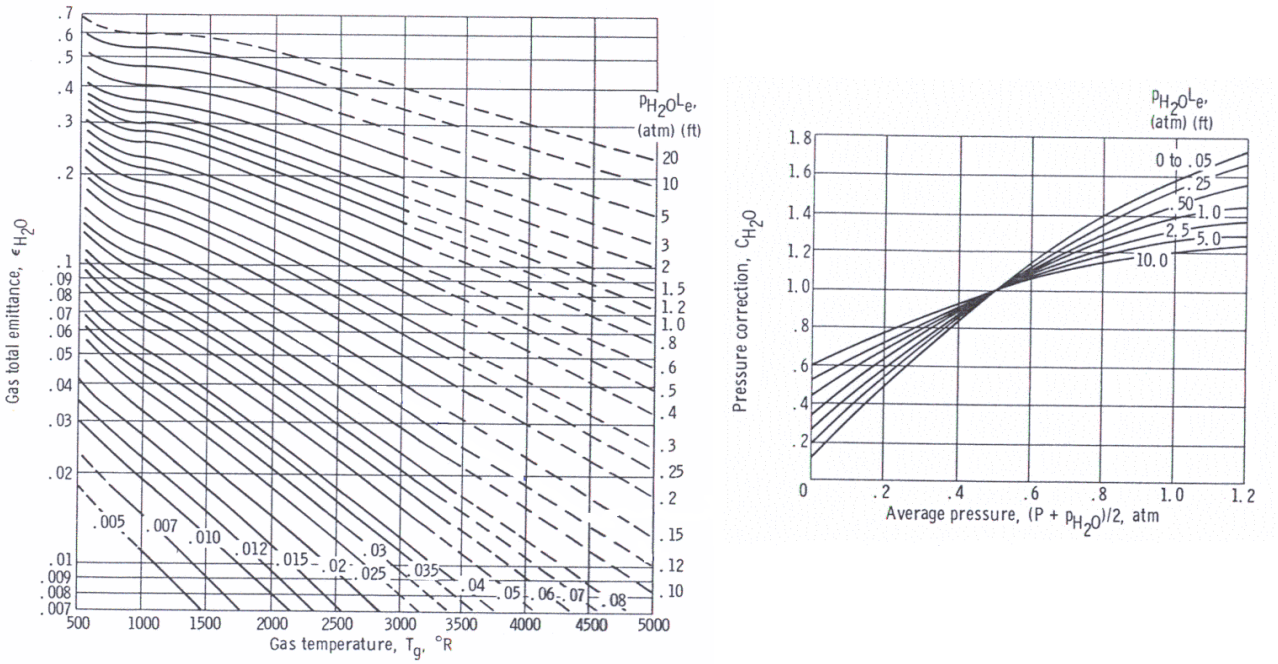

Figure 2: Emissivity of water vapour at a mixture pressure of 1 atm (left) and pressure correction factor (right) [Siegel].

Graphs for various radiating gases can be found in amongst others Heat Transmission by W.H. McAdams, 3rd Edition, McGraw-Hill, 1954 in a chapter contributed by H.C. Hottel.

Emissivity of gases with only one radiating component can be simply calculated using the type of graphs illustrated in figure 2. In case more radiating components are present, we will use the sum of the emissivity of the radiating components. In practice, emissivity for such a mixture will be smaller as we must adjust for the overlap of wave bands of the emitting constituents, but this is considered beyond the scope of the present treatment.

2.1.2 Radiation received

Just as a body emits energy, it also receives radiation from its surroundings. Three things can happen to the radiation received:

- A fraction is absorbed by the body
- A second fraction is reflected toward the space that can be seen by the reflecting surface
- A third fraction passes right through the body and exits through the other side.

Conservation of energy dictates:

$$\alpha + r + \tau = 1 \tag{2.10}$$

In words, absorption 'α' plus reflection 'r' plus transmission 'τ' must sum to unity. In case there is zero transmission, we refer to the surface as opaque. If in addition, reflection is also zero, we refer to this body as a grey body.

In contrast to radiation emission, which reduces the thermal energy of matter, absorption increases it. Rate of energy absorbed per unit surface area is defined as:

$$q_{abs} = \alpha \cdot q_{received} \tag{2.11}$$

Here α is absorption constant. Its value is in the range $0 < \alpha < 1$. Generally, the absorption factor is determined from Kirchhoff's law. This law states that for some specific known temperature and wavelength the emission coefficient and the absorption coefficient are equal ($\alpha = \varepsilon$).

2.1.3 Net energy transfer

Since a body both emits and receives thermal radiation, the net energy transfer is the thing that counts. Assume an area A_1, which radiates with spectral intensity I_1. The flux received by an area A_2, see figure 3, is given by:

$$\Phi_{1\to 2} = I_1 \cdot (A_1)_n \cdot \frac{(A_2)_n}{r^2} = I_1 \cdot A_1 \cdot \cos(\theta_1) \cdot \frac{A_2 \cdot \cos(\theta_2)}{r^2} \tag{2.12}$$

With r is distance, θ is angle between line connecting the two surfaces and the normal on to the area.

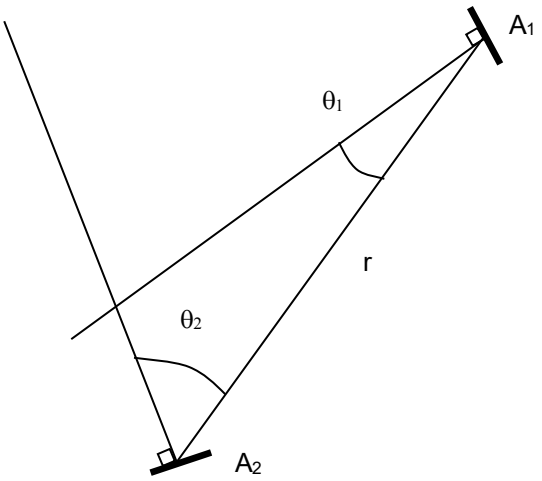

Figure 3: Radiation geometries

Vice versa, we can compute the flux received by surface 1 from surface 2. It follows for the net heat transfer to the body 1:

$$\Phi_{1\to 2} - \Phi_{2\to 1} = (I_1 - I_2) \cdot \frac{\cos(\theta_1) \cdot \cos(\theta_2)}{r^2} \cdot A_1 \cdot A_2 \tag{2.13}$$

Following Bejan, we write this equation in terms of the total hemispherical emissive powers associated with the respective temperatures of area 1 and 2:

$$q_{1-2} = \sigma \cdot \left(T_1^4 - T_2^4\right) \cdot \frac{\cos(\theta_1) \cdot \cos(\theta_2)}{\pi r^2} \cdot A_1 \cdot A_2 \tag{2.14}$$

The finite size surfaces 1 and 2 communicate through a very large number of infinite small area pairs of the kind analyzed until now. The net heat transfer rate from area 1 to 2 can be obtained by integrating the net heat transfer rate between two infinite small pairs over the two finite areas of surfaces 1 and 2:

$$q_{1-2} = \sigma \cdot \left(T_1^4 - T_2^4\right) \cdot \int_{A_1} \int_{A_2} \frac{\cos(\theta_1) \cdot \cos(\theta_2)}{\pi r^2} \cdot dA_1 \cdot dA_2 \tag{2.15}$$

We generally write the double integral with the product $A_1 F_{12}$, in which the dimensionless factor F_{12} is the "geometric view factor" based on A1:

$$q_{1-2} = \sigma \cdot \left(T_1^4 - T_2^4\right) \cdot F_{12} \cdot A_1 \tag{2.16}$$

Hence, to determine the net heat transferred by radiation between two surfaces, it all comes down to the determination of the respective surface temperatures, as well as the determination of the product $A_1 F_{12}$. The value of the geometric view factor is a purely geometric factor, one that depends only on the sizes, orientations, and relative position of the two surfaces. Values for this geometric view factor for several different configurations can be obtained from handbooks. A useful website providing simple relations for the calculation of the geometric view factor for various configurations is maintained by John R. Howell of University of Texas at Austin.

To determine one view factor from knowledge of the other, the following two relations are important [Bejan].

Reciprocity rule:

$$A_1 \cdot F_{1-2} = A_2 \cdot F_{2-1} \tag{2.17}$$

Summation rule:

$$\sum_{j=1}^{n} F_{ij} = 1 \tag{2.18}$$

This rule follows from the conservation requirement that all the radiation leaving surface i be intercepted by the enclosure surfaces.

2.1.4 Net energy transfer (multiple reflections)

In case of non-black bodies part of the radiation falling on to the body is absorbed and part is reflected. In that case the net energy transferred from body 1 to 2 equals:

$$Q_{1\text{-}2} = \varepsilon_1 \cdot A_1 \cdot B_{12} \cdot \sigma \cdot (T_1^4 - T_2^4) \tag{2.19}$$

B_{12} = ratio of radiation emitted by A_1 and absorbed by A_2 inclusive reflections versus total radiation emitted by A_1. B_{12} = is referred to as Gebhart factor, or radiation exchange factor between surface 1 and 2.

For an enclosure of n surfaces we must consider exchange factors with each of the surfaces. A general expression for the Gebhart factor is given below:

$$B_{ij} = F_{ij}\varepsilon_j + \sum_{k=1}^{n} (1 - \varepsilon_k)\, F_{ik} B_{kj} \qquad \varepsilon_i \cdot A_i \cdot B_{ij} = \varepsilon_j \cdot A_j \cdot B_{ji} = R_{ij}\ (m^2) \tag{2.20}$$

The sum of Gebhart factors from a surface must be 1 (incl. j = i):

$$\sum_j B_{ij} = 1 \tag{2.21}$$

2.2 Heat transfer through conduction

Conduction takes place in stationary mediums such as solids, liquids, and gases due to a temperature gradient. Heat flows through thermally conductive materials by a process generally known as 'gradient transport'. It depends on three quantities: the conductivity of the material, the cross-sectional area of the material, and the spatial gradient of temperature. Conductive heat transfer is mathematically best described by Fourier's law, which quantifies the conduction process as a rate equation in three dimensions. The discussion hereafter will be limited to uni-directional conduction, i.e. conduction in one direction only.

For a one-dimensional plane, the time rate of energy at which energy enters the system by conduction through a plane with unit area is:

$$q_x = -k \cdot \frac{\partial T}{\partial x} \tag{2.22}$$

With:

- q_x = (W/m^2) heat flux
- k = (W/m-K) thermal conductivity constant
- $\partial T / \partial x$ = temperature gradient

From this relationship, we learn that the larger the conductivity, and/or the temperature gradient the faster the heat flows. The minus sign shows that heat transfer takes place in the direction of decreasing temperature. The thermal conductivity is a measure of how efficiently a material conducts heat or how fast heat travels through it. It depends on the material used; some materials allow heat to move quickly through them (conductors), some others allow heat to move very slowly through them (insulators). Among all materials, diamonds have the best conduction coefficient. Also, metals are good or respectable conductors. Non-metallic materials in general are weak conductors. Conductivity for specific materials is given in the table 2. A temperature dependence of conductivity is also illustrated in the table.

Table 2: Thermal conductivity of some materials [Weast] and [PBNA]

Material	Temperature (K)	Conductivity (W/m/K)
Al	293	210
Copper	293	389
Steel	290	45.3
	373	44.8
Stainless Steel	293	17.3
Snow (compact)	293	0.21
Calcium Silicate	293	0.0548
Phenolic	293	0.0332
Fiberglass	293	0.04
Polystyrene	293	0.0288
Hydrogen-peroxide	293	0.54
Ethanol	293	0.14
Methanol	293	0.21
Water	273	0.598
	293	0.600
	573	0.681
Air	273	0.0242
	293	0.0260
	573	0.0430

The coefficient of conductivity can be determined from measurement. One way is to heat one end of an insulated bar to a constant temperature and to have the other in a fluid cooled heat sink. The latter is used both to regulate and to measure the heat transferred. Based on the known heat transfer and the dimensions of the bar, the coefficient of conductivity follows.

The conduction equation can be derived using the first law of thermo-dynamics for closed systems:

$$\dot{q} = \frac{de}{dt} + \dot{w} \tag{2.23}$$

Here de is change in internal energy (per unit area) given by:

$$de = c \cdot dT \cdot \Delta x \cdot \rho \tag{2.24}$$

Since there is no internal heat generation, $\dot{w}$ can be set equal to zero. The net rate of heat transfer follows from:

$$\begin{aligned} q \text{ (in W/m}^2) &= q_{x+\Delta x} - q_x = q_x + \frac{\partial q_x}{\partial x}\Delta x - q_x \\ q &= \frac{\partial q_x}{\partial x}\Delta x = \frac{\partial -k \cdot \partial T / \partial x}{\partial x}\Delta x \end{aligned} \tag{2.25}$$

When taking k constant:

$$q = -k \cdot \frac{\partial \partial T / \partial x}{\partial x} \cdot \Delta x = -k \cdot \frac{\partial^2 T}{\partial x^2} \cdot \Delta x \tag{2.26}$$

For steady state conditions, see figure, where temperatures at surface of material are constant, this gives:

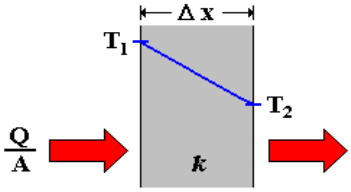

$$\frac{\partial^2 T}{\partial x^2} = 0 \Rightarrow \frac{\partial T}{\partial x} = \text{constant} \Rightarrow$$
$$T_2 - T_1 = -k \cdot \Delta x \tag{2.27}$$

For a bar with length L in the direction of the temperature difference, this gives (omitting the minus sign from now on the premises that heat always flows from high temperature to low temperature):

$$q_x = \frac{k}{L} \cdot \Delta T \tag{2.28}$$

The total heat transfer rate that crosses the bar is simply:

$$\dot{Q} = \frac{kA}{L}\Delta T = \frac{\Delta T}{R_T} \tag{2.29}$$

The factor L/(kA) can be seen as a resistance (like in electricity), hence the term thermal resistance (R_T). With Q is heating rate, q the heat flux, T the temperature, L the thickness of the slab or shell, k the thermal conductivity of the conducting material, A the cross-sectional area normal to the heat transfer direction, and R_T the thermal resistance.

Below comparable expressions for steady-state unidirectional conduction are given for cylindrical and spherical geometries:

- Cylindrical shell of length L, inside radius r_i and outside radius r_o:

$$\dot{Q}_r = \frac{2\pi \cdot k \cdot L}{\ln\left(\frac{r_o}{r_i}\right)} \cdot (T_i - T_o) \tag{2.30}$$

$$R_T = \frac{\ln\left(\frac{r_o}{r_i}\right)}{2\pi \cdot k \cdot L} \tag{2.31}$$

- Sphere with inside radius R_i and outside radius R_o:

$$\dot{Q}_R = \frac{4\pi \cdot k \cdot R_i \cdot R_o}{(R_o - R_i)} \cdot (T_i - T_o) \tag{2.32}$$

$$R_T = \frac{(R_o - R_i)}{4\pi \cdot k \cdot R_i \cdot R_o} \tag{2.33}$$

The thermal resistance concept is particularly useful when estimating the heat transfer through a composite wall, see next figure. In such a wall sheets of different material are used. Consider for instance a structural material covered by a thermal insulator. Each sheet has its own thermal resistance. The resistance of the two layers together can be determined by simple addition of the resistance of the individual layers.

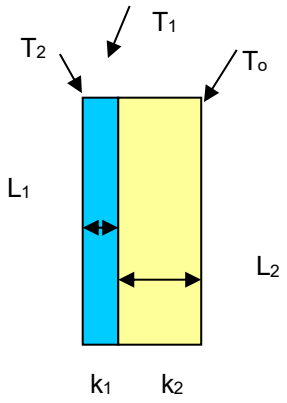

$$\dot{Q}_x = \frac{\Delta T}{R_T} = \frac{\Delta T}{R_{T_1} + R_{T_2}} = \frac{\Delta T}{L_1 / k_1 \cdot A + L_2 / k_2 \cdot A} \tag{2.34}$$

Figure 4: Composite wall

2.3 Heat transfer through convection

"Convection" is energy transfer between a solid surface and an adjacent moving gas or liquid, i.e. the transport of heat by a moving fluid (liquid or gas). It basically results from a combination of diffusion or molecular motion within the fluid and the bulk or macroscopic motion of the fluid.

Two classes of convection[4] are distinguished according to the nature of the flow:

1. Forced convection: flow induced by external means, such as pump, a fan, or wind.
2. Natural convection: induced by buoyancy forces due to density differences caused by temperature variations in the fluid and to gravitational forces. Consider e.g. the heating of a room by convector plates.

[4] When heat conducts into a static fluid it leads to a local volumetric expansion. As a result of gravity-induced pressure gradients, the expanded fluid parcel becomes buoyant and displaces, thereby transporting heat by fluid motion (i.e. convection) in addition to conduction. Such heat-induced fluid motion in initially static fluids is known as free convection. For cases where the fluid is already in motion, heat conducted into the fluid will be transported away chiefly by fluid convection. These cases, known as forced convection, require a pressure gradient to drive the fluid motion, as opposed to a gravity gradient to induce motion through buoyancy.

Hereafter, we will first discuss Newton's law of cooling for applications wherein the fluid properties can be considered constant. We will introduce the Stanton/Nusselt number as a dimensionless number characteristic for convective heat transfer as well as the Reynolds analogy and the modified Reynolds analogy for the estimation of the Stanton number. Next, we will discuss the effects of a high temperature difference on heat transfer and finally, we introduce the case of high-Mach number flow. Because in rocket motors we have mostly forced convection, we will limit ourselves to this class. However, much of what we will discuss is also applicable to free convection, be it that in the calculation of the Stanton/Nusselt number other parameters become important.

2.3.1 Newton's law of cooling

Newton's law of cooling gives for the heat transfer per unit of time and unit of surface by convection (convective heat flux) from the system to the fluid:

$$q_\alpha = h_\alpha \cdot (T_s - T_r) \tag{2.35}$$

Where:

- q_α = convective heat flux (W/m^2)
- h_α = convective heat transfer coefficient (W/m^{2}K); The heat transfer coefficient, h_α, is an empirical parameter that encompasses the nature of the fluid flow pattern near the surface, the fluid properties, and the surface geometry (flat wall, inside tube, outside curved surface).
- T_s = surface or wall temperature (K)
- T_r = fluid reference temperature (K)

Once the coefficient of convective heat transfer is known, we can determine the effect of a change in surface and/or fluid reference temperature on the heat transferred by convection, assuming that the heat transfer coefficient is independent from changes in those two temperatures.

Typical coefficients of convective heat transfer, in W/(m^2.K), are [Bejan]:

- Gases, 1 atmosphere, forced convection: 10-200
- Gases, 200 atmosphere, forced convection: 200-1000
- Organic liquids (like kerosene), forced convection: 100-1000
- Water (forced flow): 580-2300
- Boiling water: 11600

For $T_r = T_s$ obviously no energy is transferred, which explains that T_r is also referred to as the adiabatic wall temperature. For $T_r > T_s$ energy is transferred from the fluid to the surface (surface is heated), and vice versa for $T_r < T_s$ (surface is cooled).

Attention is drawn to that Newton's law of cooling can be used to determine the heat transferred locally (both T_s and T_r vary in flow direction) or an average over a surface or pipe section. In the latter case some average value for T_s and T_r are used.

2.3.2 Coefficient of heat transfer

There are two ways of determining heat transfer coefficients: Via the Nusselt number or the Stanton number.

Nusselt number

The Nusselt number Nu is the classical form used for the calculation of the heat transferred by convection. It is the ratio of heat transferred by convection compared to that which would be transferred by conduction alone. In formula form:

$$Nu = \frac{h_\alpha \cdot \Delta T}{k \cdot \Delta T / x} = \frac{h_\alpha}{k / x} \tag{2.36}$$

Where k is thermal conductivity constant, see for typical values the table 2, and x is a characteristic dimension, e.g. for internal pipe flows the (hydraulic) pipe diameter.

Nu is a dimensionless number. If Nu = 1, we have pure conduction. Values of Nu larger than 1 mean that heat transfer is enhanced by convection.

If Nu is known, the film coefficient at different value of conductivity and/or characteristic dimension can be determined from:

$$h_\alpha = Nu \cdot k / x \tag{2.37}$$

Stanton number

A more recent method is to use the Stanton number St. Like Nu it is a dimensionless number. It is defined as the ratio of heat transferred by convection compared to the total heat contained in the fluid flow. The latter is also referred to at the thermal capacity of the fluid. For gases St can be written as:

$$St = \frac{q_\alpha}{\rho \cdot v \cdot c_p \cdot (T_s - T_r)} = \frac{h_\alpha \cdot (T_s - T_r)}{\rho \cdot v \cdot c_p \cdot (T_s - T_r)} = \frac{h_\alpha}{\rho \cdot v \cdot c_p} \tag{2.38}$$

Here ρ is fluid density, v is fluid velocity, and c_p is specific heat of the fluid at constant pressure. For flat plate or external flows, these characteristics are usually taken at the free stream conditions. For pipe flows, we use the bulk properties. For liquids the specific heat at constant pressure is simply replaced by the specific heat 'c'. There is plenty of literature about methods to measure or calculate the density and flow velocity of fluids see for instance [Anderson]. Specific heat has already been dealt with in the section on 'Thermo-chemistry'. Values for a great variety of gases and liquids can be found in various handbooks, like [Weast]. Values for some specific species are summarised in table 3.

On the other hand, when St is known, the film coefficient for different values of mass density, flow velocity and specific heat can be determined from:

$$h_\alpha = St \cdot \rho \cdot v \cdot c_p \tag{2.39}$$

The use of St has found favour over the Nusselt number because of the ease in which it can be obtained from experimental data as well as because of the direct relation that exists between St and the friction factor, see hereafter.

Relation between St and Nu

Since the heat transferred by convection can be predicted using either Stanton or Nusselt, a relation must exist between the two. Analysis shows that Nu can be related to St via the dimensionless Reynolds[5] number Re and the also dimensionless Prandtl[6] number Pr :

$$Nu = St \cdot Pr \cdot Re \tag{2.40}$$

Hence Nu can be derived from St and vice versa.

[5] The Reynolds number gives the ratio of the inertial forces to the viscous forces.

[6] The Prandtl number has been treated extensively in the aerodynamics lectures. It basically is a measure for how well momentum transfer between flow and wall relates to heat transfer (heat conduction) between flow and wall.

2.3.3 Theoretical predictions of the Stanton number

For rocket motors, the determination of St from experimental data is quite complicated and expensive. Also, in the early design stages no such data might be available. These are two reasons to use a more theoretical approach to obtain an estimate on the amount of heat transferred by convection.

Under specific conditions (no external pressure gradient and Prandtl number equal to one), it can be shown that momentum and heat transfer are related. This relation is given by the “Reynolds analogy”. Since the Reynolds analogy relates heat transfer and fluid friction, it has greater utility than other expressions for the heat-transfer coefficient.

To determine an expression for St, generally a distinction is made between external and internal flow configurations.

External flow
For external flow, the Reynolds analogy is usually written as:

$$St = \frac{c_f}{2} \tag{2.41}$$

The Reynolds analogy allows us to estimate the Stanton number based on known information on the local skin friction coefficient ‘c_f’. From aerodynamics, [Anderson] we know already that the skin friction coefficient depends on the specific geometry considered, the Reynolds number, and on the type of flow (laminar or turbulent) and the surface roughness (turbulent flows only). Information on the friction coefficient of various types of flows can be obtained from handbooks like [Wong], and [Anderson]. Some specific relations for incompressible flow over a flat plate are given in annex C.

In general, we find that the friction coefficient depends on the earlier introduced Reynolds number Re:

$$c_f = f(Re) \tag{2.42}$$

Where:

$$Re_x = \frac{\rho \cdot v \cdot x}{\mu} \tag{2.43}$$

With x a characteristic dimension of the flat plate. For average heat flux estimations, this dimension is usually taken equal to the length L of the flat plate. The Reynolds number in this case is indicated as Re_L.

Which relation is to be used also depends on the type of flow (laminar or turbulent). This again depends on the Reynolds number based on the plate length ‘L’. In case the Reynolds number is below some critical value, the flow is laminar. Above this value the flow is generally considered turbulent.

The dynamic viscosity μ as occurs in the Reynolds number is essentially a measure of the resistance to flow of a fluid under an applied force [Anderson]. It can be determined from measurements using dynamic instruments, either rotating (shearing) or oscillating or calculated from the measured pressure drop that results for a flow through a tube of a certain length and diameter. Values of dynamic viscosity for many substances can be obtained from handbooks like [Weast]. For illustration, the next table gives dynamic viscosity of several species.

Table 3: Dynamic viscosity for specific liquids [Weast] and [PBNA]

Liquid substance	Temperature [°C]	μ [Centipoise[7]]	c [kJ/(kg-K)]
Hydrogen-peroxide	0	1.85	
	20	1-1.4	
Methanol		0.7	2.50
Ethanol		1.7	2.44
Water	20	1.00	4.18
	40	0.65	4.18
	100	0.28	4.18

Typical values of viscosity for typical rocket engine products are in the range of 1-2 x 10^{-5} kg/(m-s) at 400 K up to about 9 x 10^{-5} kg/(m-s) at 3000 K. The impact of pressure is usually minor (less than about 10%).

The temperature influence on dynamic viscosity can be determined from:

$$\mu = \mu_o \cdot \left(\frac{T}{T_o} \right)^{\omega} \tag{2.44}$$

Where

- μ = viscosity at input temperature T
- μ_o = reference viscosity at reference temperature T_o
- T = input temperature
- T_o = reference temperature
- ω = exponent (typically in the range 0.5-1; For air, ω is about 0.7)

For mixtures, the calculation of dynamic viscosity can be quite complex. A simple but less accurate method is to use a mass-weighted mixing rule (also known as Graham's rule) of the respective pure component data {Davidson]:

$$\mu = \sum x_i \cdot \mu_i \tag{2.45}$$

Here x refers to the mass fraction and 'i' refers to the various constituents (for example from chemical equilibrium calculations) in the gas mixture. Notice that the above relation is only correct in case the sum of the mass fractions equals 1. If not, the result obtained using the above relation should be divided by the sum of mass fractions of the species involved. A slightly more complex rule is Wilke's Mixture rule, but this is considered beyond the scope of the present text.

Pipe flow

For internal or pipe flow, the Reynolds analogy is conveniently written as:

$$St = \frac{f_F}{2} = \frac{f_{DB}}{8} \tag{2.46}$$

With f_F is Fanning friction factor, and f_{DB} is Darcy-Weisbach friction factor: $f_{Darcy} = 4\ f_{Fanning}$. Some specific relations for the Darcy-Weisbach friction factor for flow in circular pipes are given in Annex C. Typical values for the friction factor for straight circular pipe flow can be obtained from the Moody diagram, see chapter on Liquid propellant feed system design, section 5.4. In the same section also, a relation is provided that allows for considering the effect of surface roughness.

[7] 1 centipoise = 10^{-3} Pa.s or 1 centipoise is equal to 0,001 Newton second per square metre.

Like for flow over a flat plate, we generally find that the friction coefficient depends on the Reynolds number Re:

$$f = f(Re) \tag{2.47}$$

For pipe flows, the Reynolds number is based on the pipe diameter as the characteristic length, the bulk fluid density, and the bulk velocity. The latter two can be related using:

$$\rho \cdot v = {}^{m}\!/_{A} = G \tag{2.48}$$

With G is mass flux.

Typical values of the Darcy-Weisbach friction factor are in the range 0.05-0.005. The region of Reynolds numbers in between laminar and turbulent flow $2320 < Re_D < 10.000$ is also referred to as transition flow region.

Non-circular pipes
As a good engineering approximation, the frictional loss in non-circular pipes is about the same as in circular pipes, provided we use the hydraulic diameter D_h as the characteristic length:

$$D_h = {}^{4 \cdot A}\!/_{P} \tag{2.49}$$

Here 'A' is the cross-sectional area and 'P' is the wetted perimeter. Note that $D_h = D$ for a circular pipe. Note also that this is valid for both laminar and turbulent flow. In laminar flow the error is ±40% and for turbulent flow the error is ±10%.

Entrance length
The relationships given for the friction factor in pipe flows hold for fully developed flow. In general, we must consider that in the first part of the pipe flow the velocity distribution varies with downstream distance. This part is referred to as the entrance length. Downstream of the entrance length is the region of fully developed flow, in which velocity profiles are independent of x. It is possible to predict the entrance length for laminar flow analytically [Langhaar]:

$$\frac{L_e}{D} = 0.058 Re_D \tag{2.50}$$

For turbulent flow the entrance length is given by:

$$\frac{L_e}{D} = 4.4 Re_D^{1.6} \tag{2.51}$$

Modified Reynolds analogy
The Reynolds analogy is valid for Prandtl = 1. In case Pr is not equal (or close) to one [Bejan] advises to use the modified Reynolds analogy according to Colburn. For external flows, it follows:

$$St = \frac{c_f}{2} \cdot Pr^{-2/3} \tag{2.52}$$

For internal flows:

$$St = \frac{f_F}{2} \cdot Pr^{-2/3} \tag{2.53}$$

Prandtl can be determined using (see lectures on aerodynamics):

$$Pr = \frac{\mu \cdot c_p}{k} \tag{2.54}$$

Hence, to verify the value of the Prandtl number, we need information on dynamic viscosity 'μ', specific heat, 'c' or 'c_p' for gases and thermal conductivity 'k' of the fluid under consideration.

For gases, we may approximate the Prandtl number using:

$$Pr \approx \frac{4\gamma}{9\gamma - 5} \tag{2.55}$$

The product of the Stanton number and the two-thirds power of the Prandtl number is generally referred to as the **Colburn *j* factor.**

When using the modified Reynolds analogy, the maximum deviation between experimental data and predicted values according to [Bejan] may be of the order 40%, which signifies the importance of experiments to verify the accurateness of the theory used for the conditions considered.

2.3.4 Expressions for Stanton and/or Nusselt

Over the years many (semi-empirical) expressions for convective heat transfer have been developed for many different body shapes, and flow situations with either isothermal wall or uniform heat flux. Typical expressions found for Nu are given in Annex D. Generally we find:

$$St = f(Re,Pr) \tag{2.56}$$

$$Nu = f(Re,Pr) \tag{2.57}$$

2.3.5 High temperature effects

The friction and heat transfer results summarized in the foregoing section are based on the assumption of constant fluid properties. For applications in which the temperature variation experienced by the fluid is large compared to the absolute temperature level of the fluid, the fluid properties needed for the calculation of the Stanton number should be adapted for temperature effects. A typical adaptation in case the temperature of the fluid differs much from the temperature of the wall is to evaluate all fluid properties needed for the determination of the Stanton number at the film temperature.

$$T_f = \frac{T + T_w}{2} \tag{2.58}$$

With T is temperature of undisturbed flow or average fluid bulk temperature and T_w is wall temperature.

2.3.6 High-Mach number effects

At high Mach numbers, we should also consider the increase in temperature that results when the velocity of the flow is reduced from the free flow temperature down to zero at the wall. In this case, we calculate the convective heat transfer using:

$$q_\alpha = h'_\alpha \cdot (h_{ad} - h_w) \tag{2.59}$$

With h'_α is a modified coefficient of convective heat transfer, h_{ad} is enthalpy of flow at wall in case the velocity is adiabatically reduced to zero and h_w is enthalpy of fluid at the wall temperature. Neglecting temperature effects on specific heat in a direction normal to the wall, it follows again:

$$St = \frac{q_\alpha}{\rho \cdot v \cdot c_p \cdot (T_{ad} - T_w)} = \frac{h_\alpha}{\rho \cdot v \cdot c_p} \tag{2.60}$$

The adiabatic wall temperature, i.e. wall temperature for zero heat flow) is defined as:

$$T_r = \left(T_w\right)_{ad} = T_o \cdot \left(1 + r \cdot \frac{\gamma - 1}{2} \cdot M_o^{\,2}\right) \tag{2.61}$$

With:

- r = recovery factor
- γ = specific heat ratio
- T_o = static temperature of undisturbed flow
- M_o = Mach number undisturbed flow

The recovery factor depends on the Prandtl number 'Pr', which determines the ratio of the viscous effects and the conductivity in the flow. For laminar boundary layers, we find:

$$r = Pr^{1/2} \tag{2.62}$$

For turbulent boundary layers an experimental relationship holds:

$$r = Pr^{1/3} \tag{2.63}$$

In general, we find for the recovery factor a value slightly below 1 (r < 1).

In case of constant specific heat, Stanton can again be determined using the modified Reynolds analogy and expressions for the skin friction coefficient and friction factor, except that the fluid properties needed for the computation of the Stanton number need to be evaluated at the film temperature. The latter in turn is corrected to also take into account Mach number effects:

$$T_f = T\left[\frac{1 + T_w/T}{2} + 0.22 \cdot \frac{\gamma - 1}{2} \cdot M_o^{\,2}\right] \tag{2.64}$$

Since in most cases the Prandtl number and the specific heat of the gas are only weakly dependent on temperature, we find that the Stanton number for high-mach number flow can be determined based on the Stanton number for incompressible flow (here indicated using the subscript 'o') using [Ziebland]:

$$St = St_o \cdot \left[\frac{\mu}{\mu_f}\right]^{-b} \cdot \left[\frac{\rho_f}{\rho}\right]^{1-b} = St_o \cdot \left[\frac{T}{T_f}\right]^{1-b\cdot(1+\omega)} \tag{2.65}$$

In this relationship, -b is the exponent indicating the dependence of St_o on the Reynolds number, and ω is an exponent indicating the dependence of the viscosity on temperature, see earlier. Furthermore, we have assumed that the pressure does not change over the boundary layer in a direction normal to the wall. This gives (using the ideal gas law):

$$\left[\frac{\rho_f}{\rho}\right] = \left[\frac{T}{T_f}\right] \tag{2.66}$$

3 Hot-gas side heat transfer

Convection is the most dominant form of heat transfer in rocket motors. However, in some thermal rocket motors, radiation heat transfer from the hot gases to the thrust chamber wall can amount to about 20-25 % [Timnat and van der Laan] or 30-40% of total heat transfer. Especially for solid rocket motors that have solid particles in the hot gas flow the contribution of radiation to the total heat transfer can be high.

3.1 Convection

The convective heat transfer can be found using Newton's law of cooling in a slightly modified form:

$$q_\alpha = h_\alpha \cdot (T_r - T_s) \tag{3.1}$$

Here we have adapted Newton's law of cooling for application to rocket motors, where generally the temperature of the gas flow is higher than the surface temperature, and for high gas flow velocity applications (M>0.3), where the fluid temperature changes significantly due to stagnation effects (hence fluid reference 'T_r' and not fluid temperature).

In rocket motors, the surface temperature is usually determined from the maximum wall temperature that still allows for sufficient strength of the chamber wall. The fluid reference temperature in the combustion chamber is usually set equal to the chamber temperature. In the nozzle, the fluid reference temperature is set equal to the adiabatic wall temperature discussed earlier with the specific heat ratio, static temperature and Mach number based on the conditions at the location considered. The latter can for example be determined using ideal rocket motor theory.

Various semi-empirical methods are available for the calculation of the coefficient of convective heat transfer in rocket motors mostly based on the earlier discussed relationship between this coefficient and the Stanton number:

$$h_\alpha = \rho \cdot v \cdot c_p \cdot St \tag{3.2}$$

Typically, in rocket engines, the value of the Stanton number is around 0.002 [Ziebland].

[Cornelisse et al] determined a relationship for the coefficient of convective heat transfer in the combustion chamber using an experimental relationship for Stanton for turbulent flows in long slender pipes (credited to Colburn[8]) as a starting point:

$$St = a \cdot Re_D^{-1/5} \cdot Pr^{-2/3} \tag{3.3}$$

For the calculation of the coefficient of convective heat transfer in the combustion chamber up to about the nozzle throat Cornelisse et al use a = 0.023 (as follows from the original Colburn relationship) and the local chamber diameter 'D' as the characteristic length. Furthermore, they use as flow velocity the average flow velocity in the chamber, and the fluid properties are taken equal to the properties of the combustion gas in the combustion chamber at the chamber temperature:

$$h_\alpha = a \cdot \rho_c^{0,8} \cdot v_c^{0,8} \cdot (1/D_c)^{0,2} \cdot (k \cdot Pr^{0,33}/\mu^{0,8}) \tag{3.4}$$

With:

ρ_c Mass density of hot gas (mixture) in chamber
v_c Average flow velocity
D_c Diameter of chamber
k Thermal conductivity of hot gas in chamber
Pr Prandtl number of hot gas flow in chamber
μ Dynamic viscosity of hot gas in chamber

When using the ideal gas law to introduce the chamber pressure in the relationship for the coefficient of convective heat transfer, we find:

[8] The original expression of Colburn is based on the Nusselt number:

$$Nu = 0.023 \times Re_D^{4/5} \times Pr^{1/3}$$

The relation is valid for Re ≥ 10000, 0.6 ≤ Pr ≤ 160 and for pipes with length to diameter ratio equal or larger then 60, provided that temperature differences between flow and wall are moderate. Results show maximum deviation between experimental data and predictions under the conditions specified of about 20%.

$$h_\alpha = a \cdot p_c^{0.8} \cdot \left(\frac{v_c}{R \cdot T_c} \right)^{0.8} \cdot (1/D_c)^{0.2} \cdot \left(k \cdot Pr^{0.33} / \mu^{0.8} \right) \quad (3.5)$$

With:
p_c Pressure of hot gas (mixture) in chamber
R Specific gas constant
T_c Temperature of hot gas in chamber

Based on this relationship, Cornelisse et al conclude that, since velocity, diameter and gas properties do not vary much along the chamber, the coefficient of convective heat transfer is about proportional to the pressure to the power 0,8. Figure 5 shows how the heat fluxes in rocket motors have increased steadily over the years, which is mainly due to the increase in chamber pressure. Modern high-pressure rocket motors, like the Space shuttle main engine, encounter very high heat fluxes.

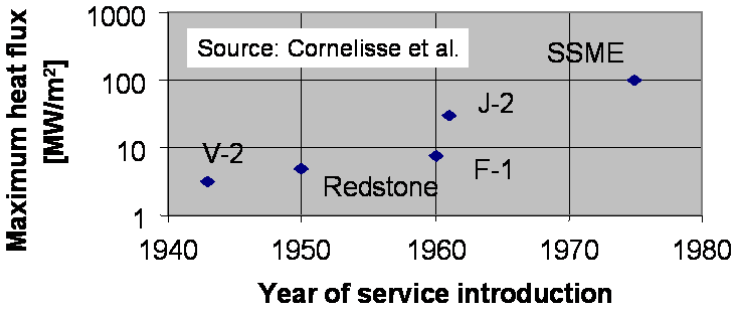

Figure 5: Heat flux in rocket motors has steadily increased over the years

Cornelisse et al furthermore show that the coefficient of convective heat transfer can also be written as:

$$h_\alpha = 1.213 \cdot a \cdot m^{0.8} \cdot \mu^{0.2} \cdot c_{p,g} \cdot Pr^{-2/3} \cdot D^{-1.8} \quad (3.6)$$

With $c_{p,g}$ is specific heat at constant pressure of hot gas and 'm' is mass flow. For a constant mass flow (given motor or motor setting) this shows that when variations in dynamic viscosity, specific heat and Prandtl are only small, the largest convective heat flux can be expected in the nozzle throat.

In the nozzle, from about 1 diameter downstream of the throat, Cornelisse et al use the same relation, but with a = 0.025-0.028. Unfortunately, they do not give any indication on the accuracy of the relations presented but based on that the Colburn relation used in their work as a starting point only provides reasonable results (maximum 20% difference between predicted and measured values) in case of moderate temperature differences, it is expected that uncertainty is at best ±20%.

Often used semi-empirical correlations for hot-gas side heat transfer in rocket motors are:

- Standard Bartz (SB) equation [Bartz]:

$$h_\alpha = \left(\frac{0.026}{D_t^{0.2}} \right) \cdot \left(\mu_o^{0.2} \cdot c_{p,g} / Pr^{0.6} \right) \cdot \left(\frac{p}{c^*} \right)^{0.8} \cdot \left(\frac{D_t}{r_c} \right)^{0.1} \cdot \left(\frac{D_t}{D} \right)^{1.8} \cdot \varphi \quad (3.7)$$

Where D_t/r_c allows for considering other nozzle throat contours and φ is correction factor for property variation across the boundary layer, given by:

$$\varphi = \frac{\left[1 + M^2 \cdot (\gamma - 1)/2 \right]^{-0.12}}{\left[0.5 + 0.5 \cdot (T_{w,g}/T_o) \cdot \left(1 + M^2 \cdot (\gamma - 1)/2 \right) \right]^{0.68}} \quad (3.8)$$

- Modified Bartz equation:

$$h_\alpha = 0.026 \cdot (G^{0.8} / D^{0.2}) \cdot \left(\mu_o{}^{0.2} \cdot c_{p,g} / Pr^{0.6}\right) \cdot \left(T_o / T_f\right)^{0.68} \quad (3.9)$$

With:

c^*	Characteristic velocity
D_t	Throat diameter
r_c	Radius of curvature of throat section
φ	Factor defined in SB correlations
γ	Specific heat ratio
M	Local Mach number
T_o	Stagnation (total) temperature
$T_{w,g}$	Temperature of hot gas at wall
G	Mass flux
T_f	Film temperature

The film temperature is taken from [Ziebland]:

$$T_f = 0.5 \cdot T_w + 0.28 \cdot T + 0.22 \cdot T_r \quad (3.10)$$

Here T_w is the wall temperature, T the static temperature in the flow and T_r the adiabatic wall temperature. Notice that the modified Bartz equation resembles the equation given by Cornelisse et al. The main differences are that in the Bartz equation the exponent indicating the dependence of the Stanton number on the Prandtl number is taken equal to –0.6 instead of –2/3, and that the variation of the gas properties with temperature over the boundary layer is considered using $\omega = 0.60$ (see relation 2.65).

Both the original and modified Bartz equation are considered valid for predicting convective heat flux in turbulent flow nozzles under the assumption that the boundary layer at the nozzle entrance is thin or almost non-existent. In case of a thick boundary layer, it is considered that heat flux may reduce by about 10%. It is also used to predict convective heat transfer in the chamber by taking this heat flux identical to the heat flux at the nozzle entrance. This gives a constant heat flux over the chamber. Though, the latter heat flux varies along the chamber and is expected to decrease towards the injector plate. It is also expected to vary in case of significant combustion pressure oscillations.

Example calculation of convective heat transfer (using modified Bartz)

In this example, we will calculate the convective heat transfer in a rocket motor with the following properties:

- *Propellant mass flow (m); 186.5 kg/s*
- *Combustion chamber pressure (p_c): 20 MPa*
- *Temperature of hot gases in combustion chamber (T_c): 3000 K*
- *Flow velocity in combustion chamber (v_c): 50 m/s*
- *Maximum allowable material temperature of chamber wall (T_w): 850 K*
- *Diameter of cylindrical chamber (D_c): 0.5 m*
- *Viscosity of gas mixture in combustion chamber ($\mu_c = \mu_o$): 6.62 x 10^{-5} kg/(m-s)*
- *Specific heat ratio (γ): 1.207*
- *Specific heat at constant pressure (C_p): 2045 J/(kg-K)*
- *Specific gas constant (R): 350.8 K /(kg-K)*

A) Convective heat flux in combustion chamber

The convective heat flux is calculated using modified Bartz relation:

$$q_\alpha = h_\alpha \cdot (T_c - T_w) \tag{3.11}$$

$$h_\alpha = a \cdot p_c^{0.8} \cdot \left(\frac{v_c}{R \cdot T_c}\right)^{0.8} \cdot 1/D_c^{0.2} \cdot \left(k \cdot Pr^{0.4} / \mu_o^{0.8}\right) \cdot \left(T_c / T_f\right)^{0.68} \tag{3.12}$$

In this relation a = 0.026, p_c = 200 x 10^5 N/m^2, and v_c is 50 m/s.

Prandtl is:

$$Pr \sim \frac{4\gamma}{9\gamma - 5} = \frac{4 \cdot 1{,}207}{9 \cdot 1.207 - 5} = 0.823 \tag{3.13}$$

The coefficient of thermal conductivity at chamber conditions is:

$$k = \frac{\mu_c \cdot c_{p,g}}{Pr} = \frac{6.62x10^{-5} \cdot 2045}{0.823} = 0.165 \text{ W/(m-K)} \tag{3.14}$$

The stagnation temperature is 3000 K and the film temperature in the chamber is:

$$T_f = \frac{T + T_w}{2} = \frac{3000 + 850}{2} = 1925 \text{ K} \tag{3.15}$$

Substitution of values gives for the coefficient of convective heat transfer:

$$\begin{aligned} h_c &= 0.026 \cdot (200x10^5)^{0.8} \cdot \left(\frac{50}{350.8 \cdot 3000}\right)^{0.8} \cdot \left(\frac{1}{0.5}\right)^{0.2} \\ &\cdot \left(\frac{0.165 \cdot 0.823^{0.4}}{(6.62x10^{-5})^{0.8}}\right)\left(\frac{3000}{1925}\right)^{0.68} = 3267 \text{ W/(m}^2\text{K)} \end{aligned} \tag{3.16}$$

This gives for the convective heat flux:

$$q_\alpha = h_\alpha \cdot (T_c - T_w) = 3267 \cdot (3000 - 850) = 7.02 \text{ MW/m}^2 \tag{3.17}$$

B) Nozzle throat region

To calculate the convective heat flux in the throat region, we use:

$$q_\alpha = h_\alpha \cdot \left((T_w)_{ad} - T_w\right) \tag{3.18}$$

Here we have taken the adiabatic wall temperature as the reference temperature.

$$\begin{aligned} T_r = (T_w)_{ad} &= T_o \cdot \left(1 + r \cdot \frac{\gamma - 1}{2} \cdot M_o^{\,2}\right) \\ &= 2719 \cdot \left(1 + 0.937 \cdot \frac{1.207 - 1}{2} \cdot (1)^2\right) = 2983 \text{ K} \end{aligned} \tag{3.19}$$

Here the static temperature in the throat is estimated using the Poison equation (ideal rocket motor).

$$T_o = \frac{2}{\gamma + 1} \cdot T_c = \frac{2}{1.207 + 1} \cdot 3000 = 2719 \text{ K} \tag{3.20}$$

The recovery factor is estimated assuming turbulent flow. Since for an ideal rocket motor Pr remains constant throughout the nozzle, it follows:

$$r = Pr^{1/3} = (0.823)^{1/3} = 0.937 \tag{3.21}$$

The convective heat transfer coefficient is again determined using the modified Bartz equation, but now expressed in terms of mass flow rate (same as was done by Cornelisse et al):

$$h_\alpha = 1.213 \cdot a \cdot m^{0.8} \cdot \mu_o^{0.2} \cdot c_{p,g} \cdot Pr^{-0.6} \cdot D^{-1,} \cdot (T_c / T_f)^{0.68} \tag{3.22}$$

With a = 0,026 and the throat diameter taken equal to 0,137 m. Substitution of values gives for the coefficient of convective heat transfer:

$$h_\alpha = 1.213 \cdot 0.026 \cdot (186.5)^{0.8} \cdot (6.62x10^{-5})^{0.2} \cdot 2045 \cdot (0.137)^{-1.8} \cdot (0.823)^{-0.6} \cdot (2983/1842)^{0.68} = 34.5 \text{ kW/m}^2\text{-K} \tag{3.23}$$

This gives for the convective heat flux:

$$q_\alpha = h_\alpha \cdot (T_r - T_s) = 34.5 \cdot (2983 - 850) = 73.5 \text{ MW/m}^2 \tag{3.24}$$

This result clearly shows the much higher heat transfer in the nozzle throat as compared to the combustion chamber. Note that the addition of the correction of the change in fluid temperature leads to an increase in heat flux with a factor of 1.37 as opposed to the case in which no such correction is made (compare equation 3.6 from Cornelisse et al and the Bartz equation as given in equation 3.22).

Summary overview

In the foregoing, we have dealt with convective heat transfer from the hot gas to the cold chamber wall in a rocket motor. We have shown based on some simple models that the heat flux in a rocket motor is determined primarily by the pressure and the local chamber diameter. Next, using the models presented, we have calculated the heat transfer in a fictitious rocket motor using the same inputs as Cornelisse et al. For the chamber, the results proved to be comparable. For the nozzle throat no such comparison was feasible as these data were not calculated by Cornelisse et al.

However, when dealing with the fundamentals of convective heat transfer, it was already stressed that most relations used are of a semi-empirical nature, with even for some much simpler flow situations possible deviation between theory and measurement of the order of 40%. The next figure, taken from the work of Sugathan et al, shows that for rocket motors this situation can be even worse.

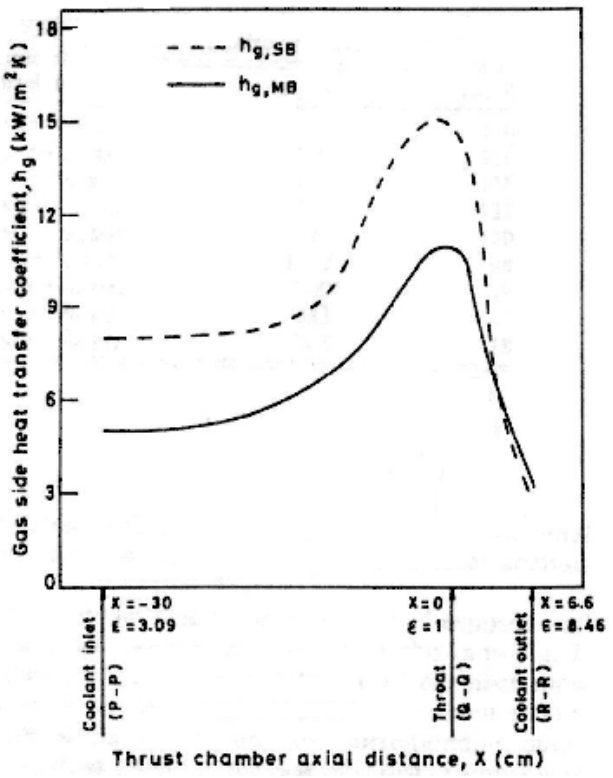

Figure 6: Comparison of several correlations for gas-side heat transfer in rocket motors (Adapted from [Sugathan]).

The large uncertainty is due to on the one hand the semi-empirical nature and on the other hand there is the continuing demand for simple, if only approximate model of the way convective heat transfer works. The method(s) presented by purpose are relatively simple and many complicating factors have been left out. We mention the effect of chemical reactions on fluid properties, accelerating flow on the boundary layer, injector geometry on mixing, etc. For this the reader is referred to the overview on heat transfer given by [Ziebland] as a starting point for further investigations.

3.2 Net rate of radiation

According to [Sutton] at low temperatures (below 800 K) radiation accounts only for a negligible portion of the total heat transfer in a rocket device. At higher temperature (between 1900-3900 K) radiation is believed to contribute between 5 and 35% of the heat transfer to the chamber walls.

The temperature of the chamber wall mainly depends on the net rate of radiation from the combustion products to the chamber wall. For rocket motors, the correct determination of this net rate of radiation is an extremely complex problem to which no satisfactory solution has yet been found.

In this section, a few cases are given that all deal with determining the net rate of radiation between the combustion gases and the chamber wall. In all cases, except one, it is assumed that the combustion products inside the chamber see only the chamber wall and nothing else and that the combustion products completely fill the motor. In addition, it is assumed that transmittance of the chamber wall is negligible. The cases differ in the assumption of the emission and absorption properties of the chamber wall and the combustion products. For clarity, hereafter, all parameters referring to the combustion products are given the index 1 and those referring to the chamber wall are given the index 2.

Black medium surrounded by a grey body
[Cornelisse et al] and [Timnat and Laan] consider the combustion products in the rocket motor as a radiating black body and the chamber as a grey body. The net rate of radiation from the hot gas to the chamber wall then follows from:

$$q_{1\to 2} = \alpha_2 \cdot \sigma \cdot T_1^4 - \varepsilon_2 \cdot \sigma \cdot T_2^4 \tag{3.25}$$

Assuming negligible differences[9] in the effect of a different temperature, we find:

$$q_{1\to 2} = \varepsilon_2 \cdot \sigma \cdot \left(T_1^4 - T_2^4\right) \tag{3.26}$$

Since most combustion gases tend to have low emissions, the case of a black medium surrounded by a grey body is considered of importance only in case of highly metallized hydrocarbon-based solid propellants.

Grey medium surrounded by a black body
Assuming the combustion products act as a grey body and that the chamber wall acts as a black body, the net rate of radiation heat transfer between the (diffuse) grey medium and the wall follows from:

$$q_{1\to 2} = \varepsilon_1 \cdot \sigma \cdot T_1^4 - \alpha_1 \cdot \sigma \cdot T_2^4 \tag{3.27}$$

In this relation, the absorptivity of the gases is taken different from the emissivity. This is because both depend on the spectrum of the incident radiation and the temperature of the radiating body. Since we have assumed a grey surface, we find that α and ε are

[9] Generally, the absorptivity of the wall differs from the emissivity of the wall, because of different temperatures of target surface and radiating grey body

independent of wavelength and only depend on temperature. Further assuming a diffuse-grey surface, the total hemispherical absorptivity of a surface of temperature T is equal to the total hemispherical emissivity of the same surface. In case, the temperature of the incident radiation does not differ substantially from that of the target surface, the absorptivity is equal to the emissivity of that surface ($\alpha = \varepsilon$). It follows:

$$q_{1\to 2} = \varepsilon_1 \cdot \sigma \cdot \left(T_1^4 - T_2^4\right) \tag{3.28}$$

However, this final approximation may not be valid when the incident radiation and the target surface have vastly different temperatures.

Grey medium surrounded by a grey body

For a grey medium surrounded by a grey body in thermal equilibrium or with negligible temperature differences, the net rate of radiation heat transfer from the medium to the body follows from Bejan [3]:

$$q_{1\to 2} = \frac{\sigma \cdot (T_1^4 - T_2^4)}{\frac{1}{\varepsilon_1} + \frac{1}{\varepsilon_2} - 1} \tag{3.29}$$

Where again we have assumed negligible effect of differences in temperature on absorptivity and emissivity (Kirchhoffs law). The above relation is identical to the relation that follows for two infinitely large parallel plates.

Other relations

[Barrère et al] give for the net heat transfer by radiation between the gas and the wall:

$$q_{1\to 2} = 0.5 \cdot (\varepsilon_2 + 1) \cdot \left(\varepsilon_1 \cdot \sigma \cdot T_1^4 - \alpha_1 \cdot \sigma \cdot T_2^4\right) \tag{3.30}$$

Here the first two terms represent an effective emissivity for the wall as deduced from the emissivity ε_2 when the wall is regarded as a grey body, and the temperature effect on absorptivity and emissivity of the combustion gases is taken into account.

[Ziebland et al] propose a relation of the form:

$$q_{1\to 2} = F \cdot \left(\bar{\varepsilon}_{1_c} \cdot \sigma \cdot T_1^4 - \bar{\varepsilon}_{1_w} \cdot \sigma \cdot T_2^4\right) \tag{3.31}$$

Where F is a view factor considering the detailed geometry of the motor and $\bar{\varepsilon}$ is an effective emissivity of the gas respectively at chamber temperature (index c) and wall temperature (index w). The inclusion of the view factor becomes especially important for the nozzle, as the nozzle also sees the outside world and hence can radiate some of the heat received to the outside world. For example, at the nozzle exit about half of the radiation produced is radiated into "space". This will cause a decrease in net radiative heat transfer to the nozzle wall as opposed to the case of full enclosure.

Hot gas emissivity

Practical values of hot gas emissivity for rocket propellants depend on the propellant composition and whether radiating constituents are present or not. Important contributing factors to radiation in rocket motors are heteropolar gases, such as water vapour and carbon dioxide (for IR) and ozone (for UV) and solid/liquid particles[10] in the hot gas flow. Typical values of emissivity for hydrogen-oxygen product mixture are 0.1-0.2 [Ziebland]. Typical values for metallized solid propellants can be much higher and may even approach 1.

[10] Al_2O_3 particles expelled from solid-propellant rocket motors may account for up to 50% of the mass flux at the nozzle exit.

3.3 Conduction

Generally, right after start of motor operation, both chamber and nozzle walls will start to heat up to a high temperature. Representative temperature responses are shown in the following figure for a high area ratio nozzle (highest area ratio indicates nozzle outlet). The figure shows that outer-wall temperature increases with time (non-steady heat conduction). The figure furthermore shows temperature differences in a direction along the nozzle indicating a multi-directional heat transfer problem.

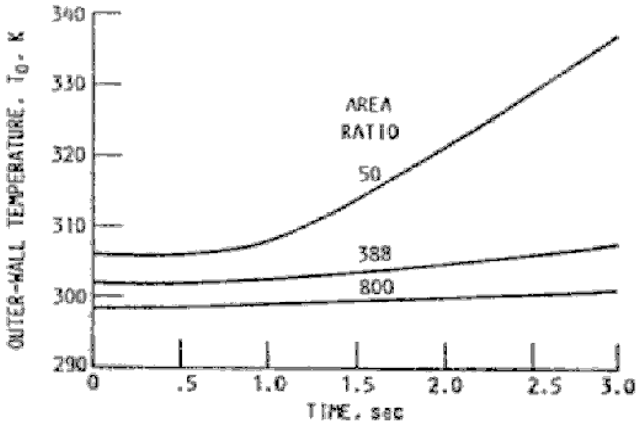

Figure 7: Measured outer-wall temperature time history for three thermocouple locations [Kacynski].

Since most rocket motors have an axis of rotational symmetry (the longitudinal axis), the general heat conduction equation is best analysed using a cylindrical coordinate system. For reasons of simplicity and because it is expected that temperature gradients across the nozzle wall are much larger than in a direction along the nozzle wall, we will neglect any conduction in the direction along the wall. The general heat conduction equation in case of constant material properties is written as:

$$\frac{1}{r}\cdot\frac{\partial}{\partial r}\left(r\cdot\frac{\partial T}{\partial r}\right)=\frac{1}{\alpha}\cdot\frac{\partial T}{\partial t} \tag{3.32}$$

With ‘r’ is radius, ‘T’ is temperature, ‘t’ is time, and ‘α‘ is diffusivity, which depends on thermal conductivity ‘k’, density ‘ρ’, and specific heat of the material ‘c’:

$$\alpha=\frac{k}{(\rho\cdot c)} \tag{3.33}$$

The steady state equation can be found in the section on heat transfer fundamentals.

In case of a thin shell, we may again use a Cartesian coordinate system but now attached to the inner/outer surface of the shell. The equation that governs the temperature variation across this thin shell is the one for unsteady unidirectional heat conduction with constant material properties, derived earlier.

$$\frac{\partial}{\partial x}\left(\frac{\partial T}{\partial x}\right)=\frac{1}{\alpha}\cdot\frac{\partial T}{\partial t} \tag{3.34}$$

With x measured in a direction across the wall.

3.4 Heat transfer measurements

Two techniques to determine the total amount of heat transferred common in rocket experiments are:

- "Heat-sink" method, wherein the combustion chamber and nozzle are made from a high-conductivity material, usually copper, in which a thermocouple to measure temperature is buried in the thick, un-cooled wall. During rocket operation, the high thermal conductivity of the copper keeps the inside wall from melting as the heat rapidly flows into the interior of the mass. This allows a rocket to operate for a few seconds and sometimes as long as 30 seconds. After the run, the temperature of the copper mass comes to equilibrium and by measuring this temperature; the total amount of heat absorbed can be calculated from the known mass and specific heat of the copper.
- "Water jacket" method wherein a jacket surrounds comparatively thin engine walls and a high-velocity water flow keeps the walls cool. The average heat transfer can be obtained by measuring the water flow and its temperature rise.

The latter method allows considering variations in time. In case we take measurements along the stream, it also allows for a location dependent heat transfer to be established. Both methods do not allow distinguishing between convection and radiation heat transfer as well as the effect of different materials (conductivity).

4 Cooling of rocket motors (fundamentals)

In most rocket motors some degree of cooling is needed to prevent weakening of the wall. If no adequate cooling of the heater chamber wall and nozzle wall is provided for, the temperature of the wall on the hot gas side may exceed the value at which the material melts or is oxidized. The local loss of material and the local heating weakens the wall so that the remaining material is inadequate to take the imposed load, leading to a malfunction of the motor and even to an explosion. To keep the wall temperature below critical limits, several methods of cooling were developed, which differ in cooling capacity and have different effects on mass, cost and complexity [Sutton], and [Broek]. Which type of cooling is best suited for a specific application depends on several factors, like the temperature of the gas flow, the operation time and the size and shape of the motor. In this section, several cooling methods are discussed in some detail.

4.1 Un-cooled motors

Especially when the heat transfer is low due to small dimensions of the rocket or short burning times, it may be permissible to take no special precautions to cool the chamber and nozzle walls. This can only be the case for some small solid propellant rockets used for military purposes. Of course, suitable materials must be selected.

To solve for heat transfer in an un-cooled motor, we essentially must solve the relation for heat transfer through conduction through the chamber walls, see section on fundamentals of conductive heat transfer.

4.2 Heat-Sink Cooling

In heat-sink cooling the non-cooled walls act essentially as a heat-sink by absorbing heat from the hot gases. Heat-sink cooling according to [Sutton] allows the use of a single-wall metal combustion chamber and nozzle offering a simple easy-to-make and inexpensive means of cooling.

The amount of heat absorbed depends on the heat capacity (c) of the material, the initial material temperature ($T_{initial}$), the melt temperature of the material (T_{melt}), and the mass (M) of the heat sink material. For a constant heat capacity, we find:

$$Q = M \cdot c \cdot (T_{melt} - T_{initial}) \tag{4.1}$$

Typical heat sink materials are Copper and mild steel, which offer not only a high heat capacity, and melting point, but also a high thermal conductivity to reduce the temperature gradient. Typical values are:

- Aluminum: 0.88 kJ/kg/K and 932 K
- Copper: 0.39 kJ/kg/K and 1356 K

Figure 8 gives the time it takes for a slab of copper to heat up to a certain temperature assuming a constant heat flux of 1 MW/m^2 and a uniform temperature (conduction goes to infinity) throughout the heat sink.

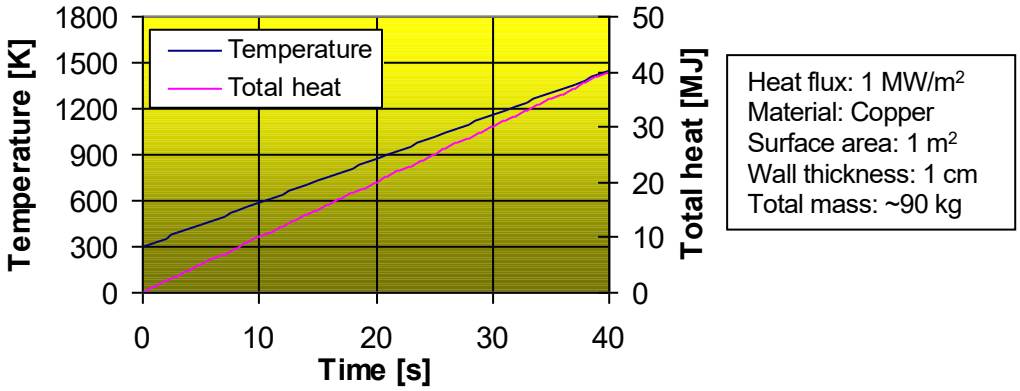

Figure 8: Thickness of heat sink

The figure shows that 90 kg of copper is heated to the melting temperature within 40 seconds.

In reality, the heat flux is likely to decrease with increasing temperature of the thruster material. It follows:

$$h_\alpha \cdot (T_f - T) \cdot A = M \cdot c \cdot {}^{dT}\!/_{dt} \tag{4.2}$$

With h_α is convective heat transfer coefficient, T_f is flame temperature, T is hot side wall temperature, A is contact area between hot gas and heat sink, M is mass of heat sink, c is specific heat of heat sink material, and t is time. Separation of variables and solving for T gives:

$$T = (T_o - T_f) \cdot e^{-\left({}^{h_\alpha \cdot A}\!/_{M \cdot c}\right) \cdot t} + T_f \tag{4.3}$$

Comparing the results obtained with this relationship with those shown in figure 6, we should find that in the former case the temperature of the heat sink material is always lower than when assuming a constant heat flux or that it takes longer for the heat sink material to reach a certain temperature. This is left for the reader to verify.

Heat sink cooling usually causes the chamber and nozzle wall to be thicker and heavier than necessary from the point of view of strength. Therefore, it is mostly used for rocket motors that are fired in a static test for testing and research purposes.

4.3 Insulation

If a low thermal conductivity material (insulator) is interposed between the hot gas flow and the load-carrying wall, the temperature of the wall can be reduced. In the ideal case, the temperature of the structural material remains essentially unchanged.

The working of insulation is illustrated in Figure 9 using paper and polyester as insulating materials. The figure shows that the addition of an insulating layer causes a less steep

rise in temperature for the structural material, thereby increasing the life of the material. Notice, that for an insulation material it is essential that the insulator temperature remains below its melting point.

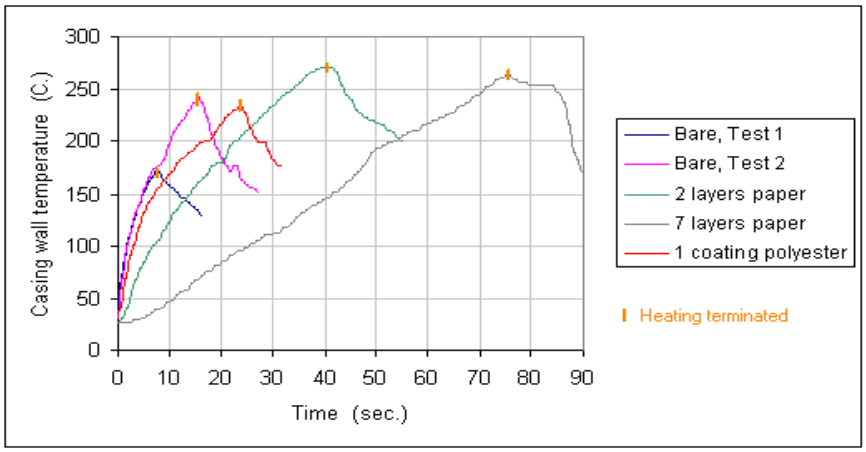

Figure 9: Results from heating tests using a 2100 K propane torch flame [Nakka]

Typical insulation materials are special paints, paper[11], rubber, pyrolytic graphite, polystyrene foam[12], ceramics, Silica, and Kevlar. In rocket motors, one may for instance apply a ceramic liner, special insulating paints or a plastic or rubber-like material bonded or glued to the wall. Important material properties include maximum use temperature and its thermal conductivity.

Sometimes insulating materials are used to form special inserts near hot regions like the throat. This is amongst others applied in some ablative cooled motors, see figure 10, as through these inserts, the throat dimensions remain unchanged. Typical materials used include tungsten, graphite, and ceramics. As the coefficients of thermal expansion of these materials may be different from the surrounding material, one must guard against high internal stresses.

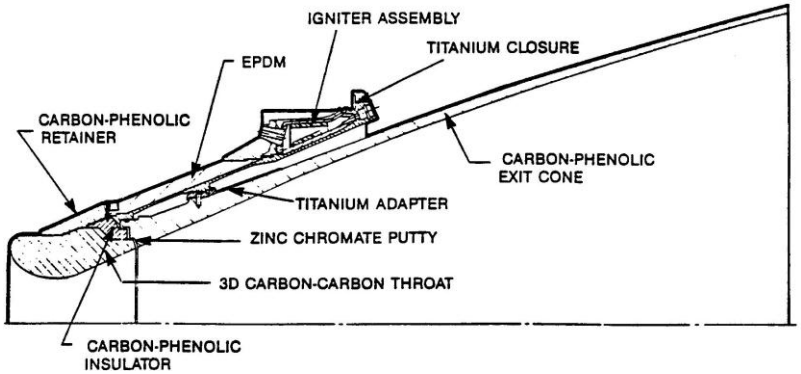

Figure 10: Nozzle design using throat insert and ablation cooled nozzle extension.

4.4 Ablation cooling

In ablation cooling the cooling effect is achieved by using special ablator materials that decompose endothermal and char away, thereby removing heat away from the surface, see Figure 11. The temperature of the structural material remains essentially unchanged.

[11] ZIRCAR Refractory Composites, Inc. offers a wide range of insulating refractory papers. These non-woven, non-asbestos, fibre-based products are engineered as thermal barrier materials for use in high temperature applications up to 1450°C. Thermal conductivity is in the range of 0.05-0.16 W/(m.K), and density is in the range 140-280 kg/m^3, both depending on temperature.

[12] Polystyrene foam is a/o used as insulation material for cryogenic tanks. Conductivity of polystyrene is in the range 0.025 – 0.040 W/(m.K).

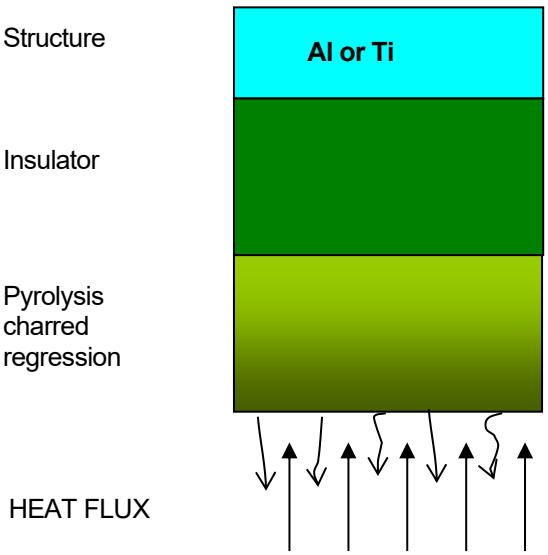

Figure 11: Principle of ablation cooling

Ablation cooling is used primarily, in short burn, liquid or solid propellant motors where a liquid coolant is not available. Ablation cooling is for example used on the Space Shuttle SRB's, where the aluminium structure is protected from the heat of the hot gases by a series of carbon-cloth phenolic rings. Ablation cooling is also used on the FASTRAC engine, which allows for the ablative layer to be replaced after flight to allow for use on the next flight, see figure 12.

The combustion chamber features an ablative cooling layer that decomposes as it absorbs the heat of combustion. The chamber is integrated with the main nozzle assembly into a unitised structure made of state-of-the-art ablative and refractory materials. High-performance silica-phenolic tape makes up the ablative liner, which is over wrapped with graphite-epoxy to form the complete chamber/nozzle assembly. The ablative behaviour of the liner is used to both cool and insulate the metal nozzle shell by resin boil-off and char layer formation.

Besides for rocket motors, ablative cooling has also been applied for the heat shield of Apollo, the Galileo probe and for the heat shield of the Japanese Hope vehicle. In addition, the ablation concept is used for Teflon propellant plasma thrusters (the initially solid Teflon is ablated to form a gaseous propellant) and for laser propelled vehicles.

Typical ablators are rubber, and composite materials utilising phenolic or epoxy resins reinforced with carbon, graphite or silica fibres. Important design parameters are the thickness of the ablation layer and the mass.

The modelling of ablation cooling involves transient heat transfer processes, reaction process at the surface, and decomposition processes within the solid. Details are discussed to some extent by [Ziebland]. Here only some essentials are dealt with.

The effect of ablation cooling on heat transfer can be explained from the theory of [Spalding] where the local skin friction coefficient under conditions of mass release is determined as given in equation (4.4) [13]

With $c_{f,o}$ is local skin friction coefficient for a turbulent boundary layer in absence of blowing and B is Spalding number you'll get the equation (4.5):

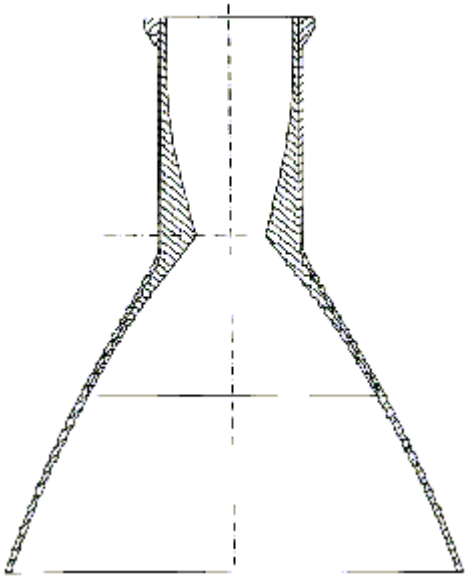

Figure 12: Schematic of ablation cooled thrust chamber

Here h_v is heat absorbed in gasifying unit mass of the ablator material and Δh_T is the difference in enthalpy of the hot gases at the wall and at the edge of the boundary layer (core flow). With increasing enthalpy difference and

[13] The same theory also applies in case of an evaporating liquid film, see film cooling and to the modelling of hybrid solid regression (see later), where the initially solid fuel enters the combustion chamber in a gaseous form.

decreasing enthalpy needed for evaporation of the ablator material, the amount of gas formed increases. The increasing mass flow entering the boundary layer will reduce the effect of friction on the boundary layer and hence also the heat transferred.

$$c_f = 1.2 \cdot c_{f,o} \cdot \ln(1+B) / B \tag{4.4}$$

$$B = \frac{\Delta h_T}{h_v} \tag{4.5}$$

The total heat transferred must balance with the total amount of material released:

$$Q = \rho \cdot r \cdot t \cdot S \cdot H_{abl} = M_{abl} \cdot H_{abl} \tag{4.6}$$

Here ρ is density of ablator material, r is rate of ablation, i.e. the rate with which the ablation material regresses in a direction perpendicular to the surface of the ablator material, t is thickness of ablator material, S is ablator surface, and H_{abl} is the heat of ablation.

Heat of ablation (in J/kg) is a measure of the effective heat capacity of an ablating material. It is determined by heat capacity, heat required for phase changes, and heat required for breaking up virgin material:

$$H_{abl} = H_{phase\ changes} + H_{pyrolysis} + \int c \cdot dT \tag{4.7}$$

Typical values are in the range 2000-3000 kJ/kg.

The following figure shows the required ablator mass as a function of heat input and time assuming a heat of ablation of 5000 kJ/kg and a mass density of the ablator material of 1900 kg/m^3.

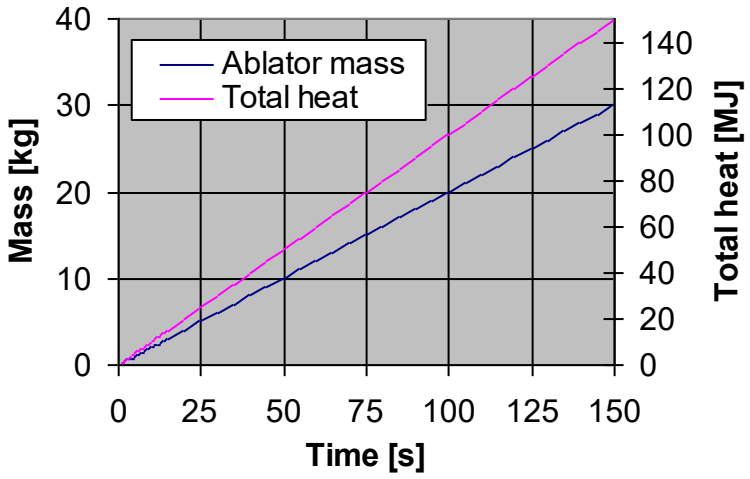

Figure 13: Ablator mass as a function of time

Results indicate that ablation cooling for a total heat input of 40 MJ requires an ablator mass of about 10 kg. Compare this with the 90 kg of copper required to allow for heat sink cooling at the same heat input.

4.5 Radiation cooling

Radiation cooling is based on the exchange of heat between the outer thrust chamber wall and its surroundings by means of radiation. In radiation-cooled motors, external

radiation losses from the wall material, see picture on cover, balance the heating from the combustion products, thereby allowing the chamber wall to operate in thermal equilibrium.

The basic theory of radiation cooling is simple. The heat radiated away from the hot wall surface will follow the Stefan-Boltzmann law $q = \varepsilon \sigma T^4$. For illustration, the next figure shows the heat flux due to radiation assuming a diffuse grey body freely radiating in space. The emission coefficient of the body has been set equal to 0.8. The latter value is considered fairly standard to obtain using suitable surface finishes.

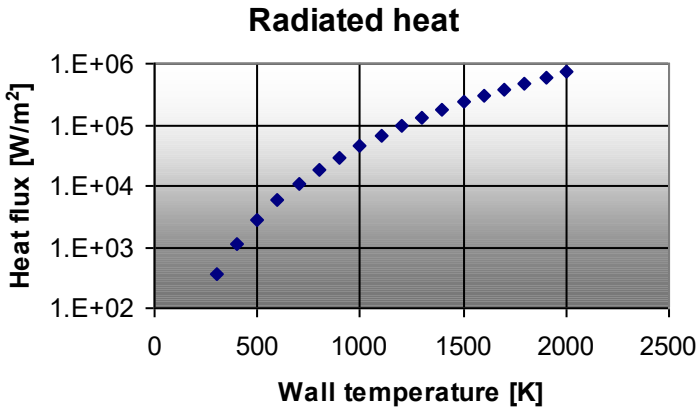

Figure 14: Radiation heat flux

From the results we find that to transfer 1 MW/m^2, which is moderate (see section on 'Heat transfer'), we already need a chamber wall temperature more than 2000 K. Unfortunately, stainless steels are only satisfactory up to 1200 K. At higher temperatures, we must resort to high temperature refractory[14] metals, including Tungsten, Rhenium, Tantalum, Molybdenum, Chromium, Vanadium and Niobium (also referred to as Columbium), and ceramic materials capable of withstanding temperatures up to about 2500 K, but with the disadvantage of a high mass density and the need of a coating to protect the refractory metal walls against oxidation. For typical material properties, see annex K. An example of a radiative cooled thruster can be found in Figure 15.

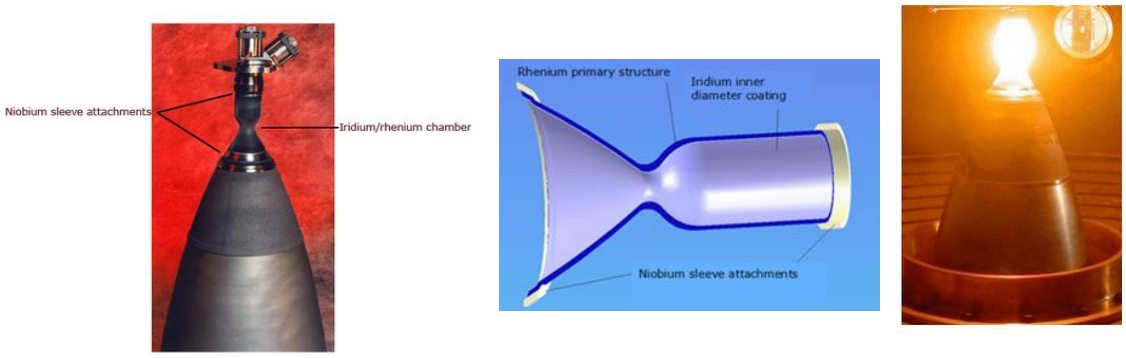

Figure 15: Example of a radiation cooled thruster. Left picture shows thruster under cold conditions, right picture shows thruster under hot conditions (notice the hot glowing chamber) and middle picture shows a schematic of the build-up of the motor. (courtesy Ultramet)

Radiation cooling is especially effective in outer space where the temperature of the environment is extremely low (~3K). Typical use of radiation cooling is in small thrusters, like in monopropellant engines, and for nozzle extensions of large rocket motors that operate at moderately high temperatures. At higher temperatures, radiation cooling may be combined with other methods that ensure low wall temperatures like film cooling or ablative cooling and insulation.

[14] Refractory metals are metals with a very high melting point above about 1900 °C).

4.6 Film cooling

In film cooling, a relatively cool gas or liquid film along the wall exposed to the hot combustion gases is produced to protect the structure of the chamber and the nozzle against the heat, see figure 15.

In film-cooled liquid rocket motors, the coolant liquid or gas is injected at several places along the wall, for example via slots in the wall, forming a blanket near the wall and reducing the boundary layer temperature, or extra fuel or oxidizer is injected in an annular zone, close to the chamber wall. Usually, fuel is injected instead of oxidizer to protect the wall material from oxidation and because generally the heat capacity of the fuel is higher than that of the oxidizer. Compared to regenerative and dump cooling, see hereafter, this allows for lower pressure drops and reduced mass of the thrust chamber.

In solid propellant rockets, film cooling can be accomplished by inserting a ring of very cool burning propellant upstream of the nozzle.

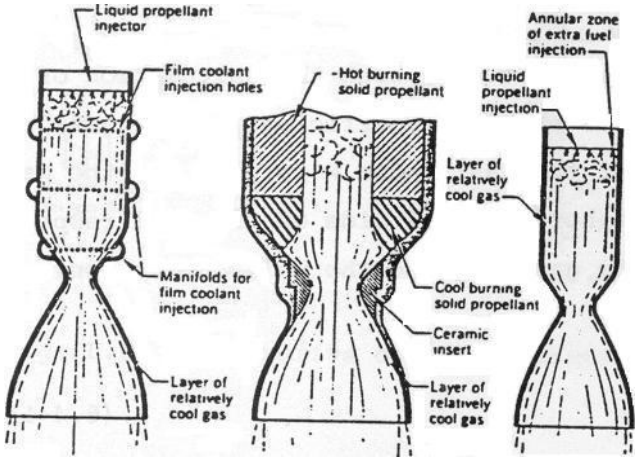

Figure 16: Three methods for forming a cool boundary layer [Sutton]

In case of a liquid film, the effect of film cooling on heat transfer may in part be explained from he theory of [Spalding] as discussed earlier when dealing with ablation cooling except that now h_v is heat needed to vaporize the film coolant liquid and Δh_T is the difference in enthalpy between the hot gasses in the core flow and close to the liquid film. Some further adaptation of the theory might be necessary since in the case of film cooling the film already has a velocity different from zero. A second aspect that must be considered when considering liquid film cooling is the heat transfer from the thin film to the chamber wall. This is left for the reader to explore.

In case of a gaseous film, [Ziebland] presents a method combining the results from Hatch and Papel and Stollery and El-Ehwany. The former assumed the film to be of uniform average temperature at any point downstream of the point of injection, and heat is transferred into the film at the same rate as to the wall in absence of film cooling. On the other hand, Stollery and El-Ehwany assumed that, downstream of the coolant injection slot, the film will tend to behave as an ordinary boundary layer with a similar velocity profile. For further information on this theory both in accelerating and non-accelerating flow, the reader is referred to [Ziebland].

Since, like for ablation cooling, the coolant material is consumed, new material must be provided for. Again, we find that the amount of film coolant material relates to the time the motor is operative, the heat transferred and the heat capacity and heat of vaporization of the coolant.

Generally, a performance penalty is associated with film cooling arising from the fact that the gases close to the wall are cooler than in the main stream.

4.7 Dump and regenerative cooling

Dump and/or regenerative cooling is often applied for large liquid propellant rockets in which either the fuel or the oxidizer, or both, is/are circulated through passages along motor wall to absorb the heat transferred through the wall.

Two types exist:

- Dump cooling where the hot coolant is dumped overboard through openings at the aft end of divergent nozzle.
- Regenerative cooling where coolant heat is used to raise the temperature of propellant.

The next figure shows a schematic of a rocket engine combining both dump and regenerative cooling.

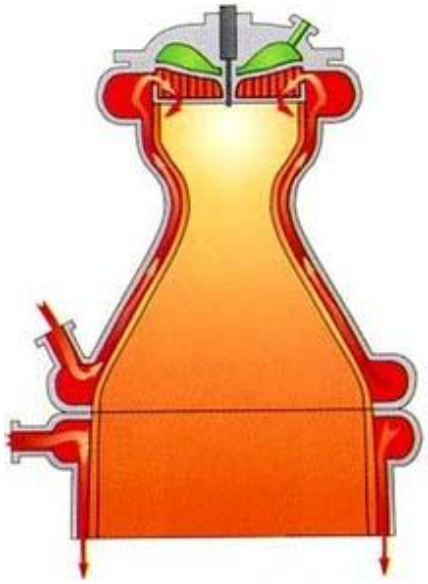

Figure 17: Schematic of regenerative cooled combustion chamber and dump cooled nozzle (courtesy Boeing)

The combination of a regenerative cooled combustion chamber and dump cooled nozzle is used in amongst others the Ariane 5 HM60 or Vulcain main engine.

Early combustor (thrust chamber) designs had low chamber pressure, low heat flux and low coolant pressure requirements, which could be satisfied by a simple "double wall chamber" design with regenerative and film cooling.
For higher heat flows, "tubular wall" combustion chambers are used. This is by far the most widely used design approach for the vast majority of large rocket engine applications. These chamber designs have been successfully used for amongst others the Ariane 5 HM-60, H-1, J-2, F-1, RS-27 rocket engines. For example, the dump-cooled nozzle extension of the European Vulcain rocket motor is made up of 1,800 meters of thin-walled welded tubes (456 tubes, 4 x 4 mm, 0,4 mm thickness) through which the coolant flows. The hydrogen coolant is tapped off of the main propellant mass flow. Coolant mass flow rate is about 6% of total hydrogen mass flow rate. The primary advantage of tubular wall combustion chambers is its light weight.

For still higher heat flows, like for the SSME, ”channel wall" combustors are used. These are so named because the hot gas wall cooling is accomplished by flowing coolant through rectangular channels, which are machined or formed into a hot gas liner fabricated from a high-conductivity material, such as copper or a copper alloy.
The amount of heat transferred can be calculated when we consider that both dump and regenerative cooling both essentially include a thin wall exposed on two sides to fluid motion, see example of channel wall. On one side of the wall, we have the hot combustion gases and on the other side the coolant flow.

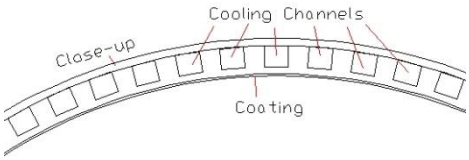

Figure 18: Example of channel wall

Figure shows that the wall of a regeneratively cooled rocket motor consists of three layers: a coating, the channel, and the close-up. These three layers can be different materials or the same material.

The heat exchange between the gas flow and the wall due to convection is given by:

$$(q_\alpha)_g = (h_\alpha)_g \cdot \left((T_w)_{ad} - (T_s)_g\right) \tag{4.8}$$

For a thin wall with thickness L, the heat flux through the wall is:

$$q_w = \frac{k}{L} \cdot \Delta T = \frac{k}{L} \cdot \left((T_s)_g - (T_s)_l\right) \tag{4.9}$$

The heat absorbed by the liquid is:

$$(q_\alpha)_l = (h_\alpha)_l \cdot \left((T_s)_l - T_b\right) \tag{4.10}$$

In these equations subscript ‘g’ refers to hot gas side, subscript ‘l’ to the coolant side of the wall and ‘b’ to the bulk of the coolant in a cross-section.

For steady heat transfer between gas flow, wall and cooling liquid, the heat flux is constant:

$$q = q_\alpha + q_r = q_w = (q_\alpha)_l \tag{4.11}$$

Combining the above equations yields

$$q = \frac{(T_w)_{ad} - T_b + q_r / (h_\alpha)_g}{\left(1/h_\alpha\right)_g + L/k + \left(1/h_\alpha\right)_c} \tag{4.12}$$

From this equation, the total heat exchange can be calculated. It is also possible to calculate the hot wall temperature and to verify if the maximum allowable wall temperature is not exceeded.

The various terms in the above heat transfer balance have been discussed before. Some specific correlations for coolant side heat transfer coefficient are given below [Taylor]:

- Sieder-Tate relation (turbulent flow regime):

$$h_\alpha = (0.025) \cdot \frac{k}{D} \cdot \left(Re^{0.8} \cdot Pr^{0.4}\right) \cdot \left(T_b / T_w\right)^{0.55} \tag{4.13}$$

- Hess & Kunz relation:

$$h_\alpha = (0.0208) \cdot \frac{k}{D} \cdot \left(Re^{0.8} \cdot Pr^{0.4}\right) \cdot \left(1 + 0.01457 \cdot \mu_w / \mu_b\right) \tag{4.14}$$

With:

- k = thermal conductivity of liquid
- D = diameter of cooling channel cross section
- Pr = Prandtl number
- T_b = bulk temperature of coolant, i.e. arithmetic mean of the fluid temperature at the entrance and the outlet.
- T_w = temperature of coolant at wall (I.e. surface temperature)

- Re = Reynolds number
- μ_w = dynamic viscosity of coolant at wall
- μ_b = dynamic viscosity of bulk of coolant

Sieder-Tate relation was first postulated by McCarthy and Wolf [McCarthy]. In this relation, all fluid properties are taken at the bulk temperature. The relation is valid for coolant temperatures at channel inlet in range 75 K to 311 K, for differences in bulk temperature versus wall temperature up to a factor 11 and for pressures in the range 2.2-90 bar and length to diameter ratios in the range 5-60.

Hess and Kunz relation has been developed for cooling using supercritical hydrogen. All properties are taken at the film reference temperature taken as:

$$T_f = T_b + 0.5(T_w - T_b)$$

More information can be obtained from [Taylor]. In this work various other relations can be found.

When the temperature of the hot gas wall exceeds the boiling point of the liquid coolant, small vapor bubbles may form in the liquid. This phenomenon is referred to as "nucleate boiling" and effectively increases the heat transfer because of flow turbulence and liquid vaporization. Unfortunately, this effect is difficult to control. For more information on boiling heat transfer, you are referred to the literature, e.g. [Rohsenow]. To prevent boiling, sometimes supercritical cooling is applied, where the pressure of the fluid is raised, and consequently also the boiling point. Supercritical cooling is for example applied in the case of hydrogen coolant. This allows for hydrogen to be heated up to a few 100 K up from about 20 K in the case of non-supercritical cooling (1 bar pressure).

From the above discussion, we may conclude that important coolant properties are thermal conductivity, specific heat, dynamic viscosity, and boiling temperature. Typical values for these properties for specific liquid propellants can be obtained from, for instance, the NIST chemistry webbook or the CRC handbook for chemistry and physics.

4.8 Transpiration or sweat cooling

Transpiration or sweat cooling is achieved by diffusing coolant through porous walls. It permits a uniform, continuous injection of fluid over the entire surface of the wall to be cooled, by using a porous wall material through which the propellant is fed. Aerojet in the past has conducted extensive research on transpiration cooling but encountered a series of new and worrisome material problems. For example, it was difficult to obtain porous materials of uniform permeability-but worse yet; the porous structure became clogged in unpredictable and non-uniform ways. These problems of manufacturing large chamber pieces of uniform porosity, variable thickness and complex shape today still requires considerable ingenuity.

4.9 Comparison of cooling methods

In an excellent overview on advanced cooling techniques for rocket engines [Sutton], Sutton et al compare fourteen basic methods and various combinations thereof for application in rocket engines with respect to the principal limitations, the likely heat transfer rates, means for extending the limits of the methods and principal applications. In the next table, some of their results are shortly summarized. For a more extensive overview, the reader is referred to the original work.

Table 4: Comparison of cooling methods [Sutton]

Method	Active/passive method	Cooling capacity kW/m^2	Other
Heat sink	Passive	80-11500	Short duration
Insulation	Passive	80-6500	No limitation to duration
Ablative	Passive	160-16000	Limited duration
Radiation	Passive	80-650	No limitation to duration
Film	Active	1600-160000	No limitation to duration. Danger of fluid leakage and clogging of fluid channels.
Transpiration	Active		No limitation to duration. Danger of fluid leakage and high danger of clogging of fluid channels.
Dump	Active		No limitation to duration. Danger of fluid leakage and clogging of fluid channels.
Regenerative	Active	1600-160000	No limitation to duration. Danger of fluid leakage and clogging of fluid channels.

In Table 4, a distinction is made between passive and active cooling. Passive cooling refers to systems that cool without relying on mechanical devices, like pumps and fans, which require additional energy. Active cooling methods are based on the use of mechanically driven pumps to transport the heat to the required spaces. Active cooling in rocket motors typically is by leading a liquid coolant along the hot chamber walls, thereby cooling the chamber walls. In general, passive cooling methods are cheaper and/or more reliable than active cooling methods.

5 Analysis tools

RTE
RTE is a computer based three-dimensional thermal analysis tool for re-generatively cooled rocket engine combustion chambers and nozzles. The program is in FORTRAN and uses GASP (GAS Properties) and CET (Chemical Equilibrium with Transport Properties) for evaluation of the coolant and hot gas properties, respectively. The inputs to this code consist of the composition of fuel/oxidant mixtures and flow rates, chamber pressure, coolant entrance temperature and pressure, dimensions of the engine, materials and number of nodes in different parts of the engine. The program allows temperature variations in axial, radial and circumferential directions and by implementing an iterative scheme, it provides a listing of nodal temperatures, rates of heat transfer, and hot gas and coolant thermal and transport properties. The fuel/oxidant mixture ratio can be varied along the thrust chamber. This feature allows the user to incorporate a non-equilibrium model or an energy release model for the hot-gas-side.

TEMPROFIL
TEMPROFIL [Geld] is a Pascal-coded computer program capable of calculating temperatures in thick-walled cylindrical geometries for a wide variety of boundary conditions, including fixed surface temperature, and heating through convection and/or thermal radiation. To allow the effect of solid fuel/propellant regression on the temperature profile considered, the location of the inner surface changes depending on the rate specified. The program also allows for taking into account temperature dependent material properties.

6 Problems

1) A heat rate of 300 kW is conducted through a section of copper material of cross-sectional area 1 m^2 and thickness 2.5 cm. Given is an inner (hot) surface temperature of 450 ^oC and a thermal conductivity of the wall material of 389 W/m-K. Determine:
   a. Outer surface temperature?
   b. Outer surface temperature in case the thermal conductivity of the material is 20 W/m-K?
   c. What happens if we select a material with a still lower thermal conductivity?

2) One surface of a 0.2 cm thick rocket combustion chamber wall of stainless steel is maintained at 700 K by the hot combustion gasses, while the opposite surface is exposed to a cooling fluid for which T = 400 K and h = 100 W/m^2-K. If the thermal conductivity of the steel is 40 W/m-K, what is the temperature of the surface adjoining the coolant in case of steady state heat transfer?

3) A cylindrical steel rocket chamber of 1.5 cm diameter and 2.5 cm length holds hot propellant gases with a temperature of 900 ^oC, an emissivity of 0.2 at 1200 K, and 0.1 at 600 K. Hot gas mass flow rate is 100 g/s, and chamber pressure is 20 bar. The maximum chamber wall temperature is set at 500 ^oC. The inside wall emissivity is 0.07 at 293 K, 0.14 at 593 K, and 0.23 at 1273 K.
   a. Calculate for this motor the net heat flux due to radiation from the hot combustion gases to the chamber wall in case you consider the combustion gases:
      i. A grey medium fully enclosed by a black surface.
      ii. A black body fully enclosed by a grey surface
      iii. A grey medium surrounded by a grey surface with α is ε (Kirchhoff's law applies).
   b. The wall emissivity of the steel material can be increased by oxidation to 0.74-0.87 over the temperature range 500 - 1400 K. Calculate the difference in net heat flux to the wall for the three cases considered

4) In a vertically oriented downward thrusting cylindrical thrust chamber of 0.5 m diameter, we have a 3000 K flame front of equal diameter at 0.1 m distance from the injector face. The emissivity of the flame front is 0.2. The injector face has a constant emissivity of 0.85 on both inside and outside surface and $\alpha = \varepsilon$. The cold fluid in between the flame front and the injector face does not emit or absorb radiation. There is no forced flow.
   a. What two modes of heat transfer may occur in this system? Justify your answer?
   b. What is the geometric view factor between the injector face and the flame front?
   c. What is the equilibrium temperature of the injector face in case we only consider radiative heat transfer between the two discs (you may neglect any effect of the sidewalls or of walls shielded by the flame front)?

5) A 5 mm thick cylindrical steel rocket chamber of 50 cm diameter and 100 cm length holds hot propellant gases with a temperature of 3000 K. Hot gas mass flow rate is 186.5 kg/s, and chamber pressure is 150 bar. Average molar mass of the hot gas is 23.7 kg/kmol, specific heat ratio is 1.207, and dynamic viscosity of the combustion gases in the combustion chamber is 6.62×10^{-5} Pa-s. The maximum material temperature is set at 550 ^oC. Calculate for this motor:
   a. The heat flux due to convection (hot gas side only) to the chamber wall at the maximum material temperature.
   b. Idem in the nozzle throat. You may estimate the throat diameter using ideal rocket motor theory.

6) For the same motor as discussed in the previous problem, you are asked to calculate the change in convective heat flux in case we use an evaporating water film with an initial temperature of 293 K to cool the wall.

7) You are designing a small un-cooled rocket motor with a burn time of 8 seconds. For this motor, you have selected stainless steel with a thermal conductivity of 40 W/m-K,

and a specific heat of 480 J/kg-K as the wall material. In addition, you have estimated a coefficient of convective heat transfer from the hot gases to the wall of 700 W/(m^2-K) and from the hot wall to the environment of 40 W/(m^2-K). The combustion chamber gases have a temperature of 2000 K. Heat transfer through radiation may be neglected. You are asked to calculate the material temperature as a function of time and location (across the wall) using 313 K (a hot day) as the initial material temperature and 5 mm as the wall thickness. You may neglect any temperature effect on material properties and coefficients of convective heat transfer as well as conduction in a direction along the wall.

8) You are designing a resistojet using hydrogen gas as propellant and an electrical heater for heating the propellant. This heater is designed as a hollow spiral tube with an internal and external tube diameter of 2.5 mm and 5 mm, respectively, and a spiral diameter of 5 cm through which the gaseous hydrogen flows. As heater temperature, you have selected 2000 K (uniform over the heater). The coefficient of convective heat transfer and the Nusselt number describing the heat transferred from this tube to the hot gas are independent of the distance x taken in stream-wise direction along the tube. The Nusselt number is given by $Nu = 0.023 * Pr^{0.4} * Re_D^{0.8} * (d_w/d_c)^{0.1}$ with d_w is internal diameter of tube and d_c is spiral diameter of tube. The fluid properties of the hydrogen gas are taken at the average gas temperature and include a specific heat of 0.029 kJ/(mol-K), a dynamic viscosity of 0.00892 centiPoise, and a thermal conductivity of 168.35 mW/(m-K). Flow velocity and gas density are also to be evaluated at the average gas temperature. The latter is calculated as an ordinary average of the highest and lowest value of temperature occurring in the tube. You are asked to calculate for this motor the length of the flow tube necessary to accomplish the heating of 0.1 g/s of hydrogen at 20 bar pressure to a temperature of 1500 K from an initial temperature of 298 K.

References

1) *Anderson J.D. jr.,* Fundamentals of Aerodynamics, McGraw-Hilll International Editions, 1991.

2) *Cornelisse J.W., Schöyer H.F.R., and Wakker K.F.,* Rocket Propulsion and Space Flight Dynamics, Pitman Publ. Ltd., London, 1979.

3) *Bartz D.R.*, Turbulent boundary layer heat transfer from rapidly accelerating flow of rocket combustion gases and of heated air, JPL, December 1963.

4) *Bejan A.,* Heat Transfer, John Wiley & Sons, Inc., ISBN 0-471-50290-1, 1993.

5) *Barrere M., Jaumotte A., Fraijes de Veubeke B., and Vandenkerckhove J.,* Rocket Propulsion, Elsevier Publishing Company, 1960.

6) *Broek M.J.R. van den,* Cooling concepts for ramjets and rocket motors, TU-Delft, January 1992.

7) *Broek M.J.R. van den,* Design of a cooling system for high temperature applications, Engineering thesis, TU-Delft/LR, December 1992.

8) *Davidson T.A.*, A simple and accurate model for calculating viscosity of gaseous mixtures, US department of the interior, Bureau of Mines, R19456, 1993.

9) *Geld, C.W.M. van der, Mies J.A.M.A., and Ramaprabhu R,* Numerical solutions of heat transfer problems in cylindrical geometries, M-564, TU-Delft, Faculty of Aerospace Engineering, Delft, The Netherlands, 1987.

10) *Kacynski K.J. Pavli A.J., and Smith T.A.,* Experimental evaluation of heat transfer on a 1030:1 Area Ratio Rocket Nozzle, AIAA-87-2070, 1987.

11) *Langhaar H.L., Journal of Applied Mechanics, vol. 64, A-55, 1942.*

12) *McCarthy, J. R. ; and Wolf, H.*, The Heat Transfer Characteristics of Gaseous Hydrogen and Helium. Res. Rep. 60-12, Rocketdyne Div., North American Aviation, Inc., Dec. 1980.

13) *Monachos engineering,* http://www.monachos.gr/eng/resources/thermo/conductivity.htm, Greece.

14) *Nakka R,* Experimental Rocketry Web Site *http://members.aol.com/ricbnakk/therm.html.*

15) *PBNA,* Polytechnical handbook (in dutch), 48th ed., ISBN 90-6228-266-0, 1998.

16) *RTE,* Rocket thermal Evaluation, 1999 version, http://www.johnsonrockets.com/rocketweb/rte.html

17) *Rohsenow W.M.,* "Boiling", in Handbook of Heat Transfer Fundamentals, ed. W.M. Rohsenow, J.P. Hartnet and E.N. Ganic, McGraw-Hill, New York, 1985.

18) *Sugathan N, Srinivasan K, and Srinivasa Murthy S.,* Comparison of Heat Transfer Correlations for Cryogenic Engine Thrust Chamber Design, J.Propulsion, vol.7, no.6, 1991.

19) *Sutton G.P., Wagner, G.R., and Seader J.D.,* Advanced cooling techniques for rocket engines, Astronautics and Aeronautics, January 1966.

20) Taylor, M.F., Correlation of local heat-transfer coefficients for single-phase Turbulent Flow of Hydrogen in tubes with temperature ratios to 23, Lewis research center, NASA TN-D-4332, January 1968.

21) *Timnat Y.M., and Laan F.H. van der,* Chemical Rocket Propulsion, TU-Delft, Faculty of Aerospace Engineering, Delft, The Netherlands, 1985

22) *Weast R. C. (Ed.). Handbook of Chemistry and Physics, 61st ed.,* Boca Raton, FL: CRC Press, 1981.

23) *Wong H.Y.,* Handbook on essential formulae and data on heat transfer for engineers, 1977.

24) *Ziebland H., and Parkinson R.C.,* Heat Transfer in Rocket Engines, AGARDograph no. 148, AGARD-AG-148-71

Cold/cool gas monopropellant thrusters

Contents

Cold gas monopropellant thrusters 197

Contents 198

List of symbols 199

1 Introduction 200

2 Workings and specifications of a cold gas thruster 201

3 Design framework 202

4 Thruster control valve 203

5 Plenum chamber design 203

5.1 Overall shape options 203

5.2 Operating pressure (from internal ballistics) 204

6 Plenum throat assembly design 205

7 Nozzle design 209

8 Start-up and thrust decay 210

9 Free molecular flow 212

10 Verification of performance 212

11 Design using CFD 213

12 Other design aspects 214

12.1 Material options 214

12.2 Thruster mass 214

12.3 Thruster service life 214

12.4 Still other design aspects 214

Problems 215

References 216

For further reading 216

Photos on cover: Courtesy Moog and Omnidea/RTG

List of symbols

Roman

A	Area
C_d	Discharge coefficient
D	Diameter
F	friction factor
L	Length
m	Mass flow
p	Pressure
Q	Volume flow rate
r	Radius
r_a	Contraction approach radius
r_u	Longitudinal throat radius
Re	Reynolds number
R	Specific gas constant
T	Temperature
v	Velocity
V	Volume

Greek

β	Contraction half angle
ρ	Density
ζ	Pressure loss coefficient
γ	Specific heat ratio
Γ	Vandenkerckhove constant or ideal flow coefficient
$\Gamma(\gamma_t)$	ideal flow coefficient based on conditions in throat
$\Gamma(\gamma_c)$	ideal flow coefficient based on conditions in chamber
Φ	factor correcting for real gas effects

Subscripts

c	Chamber or contraction
con	Convergent
e	Expansion
in	Inlet
plenum	Plenum
t	Throat

Superscripts

*	Characteristic parameter

1 Introduction

A cold/cool gas thruster (CGT) is a thrust producing device that uses the energy stored in a cold/cool high-pressure gas to produce thrust. Some typical cold gas thrusters are shown in next figure.

Figure 1: Specific cold gas thrusters (courtesy Moog)

A cold gas thruster is by design the simplest rocket thruster available for use. It is fed by a high-pressure gas which expands in a nozzle thereby producing thrust. In principle any gas can be used as propellant, but typical gases considered are:

- Gases: Hydrogen, Nitrogen, Helium, Xenon, Argon, Freon, and Methane
- Liquefied gases[1]: Butane, Propane, Sulfur hexafluoride (SF_6), Ammonia, and Carbon dioxide

Typical specific impulse levels are in range 40-250s, depending on the propellant used. Highest specific impulse is attained using a propellant with a low molar mass.

Other important design features include:

- Nonhazardous propellants reduce handling costs and safety requirements
- Low cost
- Reliable
- Pulsed operation: Tens of thousands of thrust cycles can easily be accomplished

Cold gas thrusters have been used on several spacecrafts including COS-B, Eureca, GRACE, GOCE, Cryosat, GAIA, ALMASat and CNAPS. Primary usage is for precise attitude and/or orbit control applications for which pulsed operation is key. Characteristics of some cold gas thrusters are provided in Table 1.

Table 1: Characteristics of specific cold gas thrusters using Nitrogen propellant [Zandbergen]

Engine	Manufacturer	Vacuum Thrust [N]	Vacuum Specific Impulse [s]	Cycle life [Cycles]	Engine Mass [kg]	Inlet Pressure [bar]	Envelope[4] [mm] (LxD)
PMT	Bradford	0.002[3]	>60		<0.175	2.5	41 x 65 x 51
VP-03-001	Moog-ISP	0.001	>70		< 0.300	1	87 x 16 x 91
SVT01	Moog-ISP	0.01-0.05	72	1,500,000	<0.06	1.5-2.5	Ø 16
58-125	Moog	0.0045	65		0.007		
	Marotta	0.05			0.07	6.9	
CGT1	DASA	0.02	67		0.120	7.0	64 (L)
	Sterer	1[2]	68	250,000	0.174	3.5	66 x 31
58-102	Moog	1.11		10,000	0.015	8.8-6.3	24.7 x 14.5
58-112	Moog	1.11		10,000	0.015	7.4-4.9	24.7 x 14.5
58-115	Moog	2.89			0.013		
58-113	Moog	3.33		10,000	0.015	8.8-6.3	24.7 x 14.5
58-103	Moog	5.55		10,000	0.015	8.8-6.3	24.7 x 14.5
50-673	Moog	44.5		5,000	0.231	10.5-4.9	87 x 80 x 64[1]
50-820	Moog	52					
58-126	Moog	266		10,000	0.181	10.5-4.9	70 x 63(e)

1) Thruster triad
2) A maximum thrust level of 10 Newton is possible, but at the expense of a higher inlet pressure
3) Using Xenon, this value is 50 milli-Newton with a specific impulse of 30 s
4) L is length, D is diameter, (e) means estimated

[1] **Liquefied gas** (sometimes referred to as **liquid gas**) is a gas that has been turned into a liquid by cooling or compressing it.

From the table, we learn that nitrogen CGTs are mainly of limited size with thrust of order mN to several hundred N. No larger thrusters or higher thrust CGTs could be found. Specific impulse is in range 65 to 77s with cycle life of up to 1,500,000 cycles.

In the following sections, we will discuss the design and sizing of cold gas thrusters in some detail. Important parameters in sizing a cold gas thruster include shape, size, mass, operating pressure, materials used, etc. For the discussion, we will consider the main elements of a cold gas thruster, being the thruster control valve with the plenum[2] or settling chamber and the nozzle separately.

2 Workings and specifications of a cold gas thruster

Figure 2 shows a schematic of a cold gas thruster with integrated control valve. The nozzle is directly mounted onto the outlet of the control valve thereby limiting the size of the plenum chamber. The control valve controls the thrust duration and allows for start/stop actuation. The internal volume of the valve makes up the plenum chamber of the thruster. The size of this volume should be carefully considered to realize a fast enough response time and short impulse bits. On the right, we find provisions for attaching the thruster to a spacecraft and a screwed connection allowing for connection to a feed system (side inlet), whereas the thruster on the left shows an inlet in line with the nozzle axis.

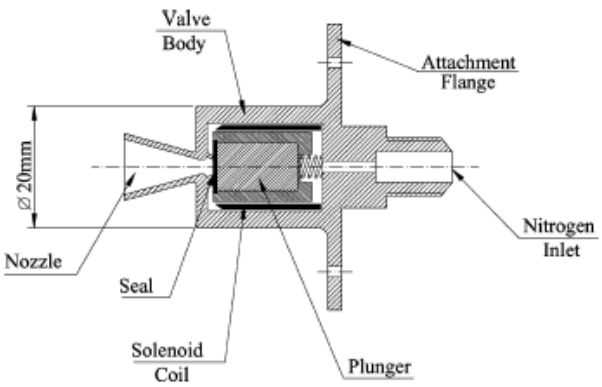

Source unknown

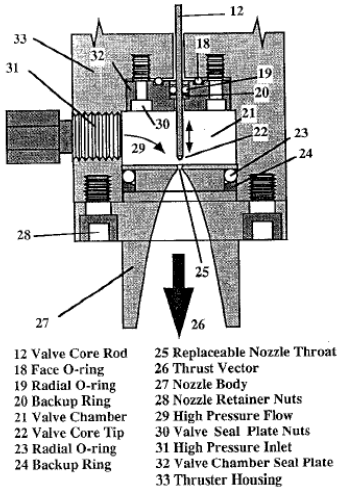

Fast Variable-Amplitude Cold Gas Thruster [Stone]

Figure 2: Cold gas thruster schematics

The control valve is essential to realize the cycle life and/or the minimum impulse bit. It typically is a solenoid valve which opens when power is on (energized) and closes when power is off. Figure 3 shows on left the de-energized position in which the valve is closed and there is no propellant flowing and hence no thrust generation. Upon actuating the solenoid coil, the plunger will move to the left (open position), see schematic on right, thereby allowing pressurized cold gas to flow in the thruster. When de-energizing, a spring pushes the valve back onto its seat thereby stopping the propellant flow. The use of a solenoid valve has as advantage that the valve closes automatically when a power failure occurs.

[2] A plenum chamber is a pressurised housing containing a gas or fluid at positive pressure (pressure higher than surroundings). One function of the plenum is to equalise pressure for more even distribution, because of irregular supply or demand.

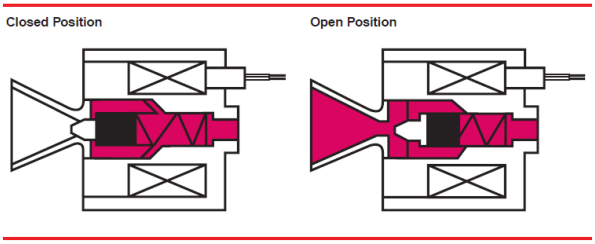

Figure 3: Propellant flow in cold gas thruster (schematic) [Moog]

Typical performance specifications of a cold gas thruster are shown in Table 2. It shows a thrust of 3.6 N at 14.8 bar at thruster inlet, with the latter indicated as the nominal operating pressure. Not indicated here is the temperature of the propellant gas. Most likely is that this is taken at room temperature (21 ^{o}C). The thruster can also operate at a different pressure level (and at different gas temperatures) but then thrust level will differ. Also given is a proof pressure of almost 76 bar, which shows the built in safety at normal operating conditions. Thruster response time is given as less than 4 ms, which means that in less than 4 ms after the valve is commanded to open full thrust is attained. Thermal capability indicates the range of temperatures over which the thruster can be operated and wetted materials, indicates the material used in contact with the propellant gas. Stainless steel is used to form amongst others the housing and the nozzle. Nylon is used as sealant material and the soft seat on which the valve rests to prevent gas leakage through the valve.

Table 2: Typical cold gas thruster performance and physical characteristics

Parameter	Value
Thrust:	3.6 N @ 14.8 bar
Pressures:	
Operating:	14.8 bar
Proof:	75.8 bar
Response time	< 4 ms
Cycle life	> 10,000
Mass	0.023 kg
Thermal Capability	-40^{o}C to +60^{o}C
Wetted materials:	Stainless steel, Nylon

3 Design framework

When designing a cold gas thruster, we are to produce a design output (baseline design) based on inputs while following some design process.

Design inputs consist of performance requirements including e.g. the propellant to work with, maximum and minimum thrust level, specific impulse, minimum response time, impulse bit, and number of cycles as well as a range of other requirements that stem from limitations concerning size, mass, electric power consumption, cost, life, reliability, safety (through defining appropriate safety factors), leakage, operating temperature, etc. Other inputs to the design are the design options available, i.e. different configurations that can do the job. In general, it is advised that the designer develops a database of historical designs and performances that allows for a quick sanity check on the requirements and allows for identifying design options.

Once the design inputs have been established, the design options can be selected, and the design analysis may start. In this analysis step the candidate options are analysed on how well they can fulfil the design requirements. Most important is to start with the

performance analysis. This is because if the performance requirements cannot be met, it does not make sense to perform other analysis, like a cost analysis, a life analysis, a reliability analysis and so on. The design analysis of a cold gas thruster is also the focus of this chapter. In the performance design analysis, we essentially go through the following steps:

1. Determine thruster mass flow rate from required thrust and specific impulse.
2. Select appropriate thruster control valve using information on specified propellant, mass flow rate, inlet pressure and response time.
3. Determine pressure drop over thruster valve and plenum and plenum (chamber) pressure.
4. Determine nozzle throat area and throat dimensions using IRT.
5. Design nozzle shape and estimate discharge coefficient and nozzle quality.
6. Design plenum chamber for appropriate response time.
7. Generate an overview of the design results.
8. Verify (check) design results against the requirements; where needed this can include verification by testing.
9. If necessary, iterate on the design.

Once the design converges to a feasible solution, other analysis can also commence.

Note that the above steps provide for a suggested approach only. Depending on available information, some steps can be omitted or combined.

4 Thruster control valve

As indicated earlier, this is typically a solenoid valve. Selecting the right valve is important to be able to realise the thruster requirements. We mention e.g. that the valve should be compatible with the working fluid, i.e. the propellant. Other important valve requirements are:

- Its working pressure and the associated margin of safety
- Its minimum response time, i.e. the minimum interval between the moment of activation of the valve until the pressure has fallen to 10% or risen to 90% of the nominal pressure; this is discussed in some detail in a later section on start-up and thrust decay
- the drop in pressure that results between the inlet and the plenum up to the point of entering the nozzle. The latter is discussed in some detail in the next section.

5 Plenum chamber design

5.1 Overall shape options

From reasons of easy manufacturing and to withstand high internal pressure inside the thruster, the plenum shape is kept very simple; being mostly of a cylindrical nature, see earlier illustrations. This cylindrical shape has the advantage of easy manufacturing. Important dimensions are diameter, length and the angle of the convergent, see Figure 4.

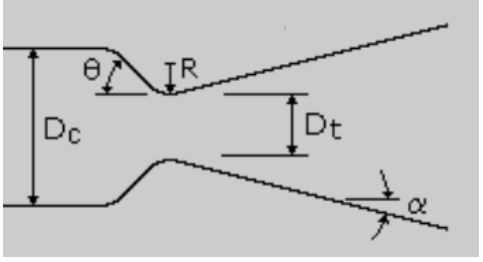

Figure 4: Important parameters defining CGT geometry

Values for the convergent half angle (θ) may range up to 90°, whereas the throat longitudinal radius (R_u) may be of order 2 times the radius of throat cross-sectional area. See later sections for more information on values for throat convergence angle and throat longitudinal radius.

5.2 Operating pressure (from internal ballistics)

During operation, mass enters the thruster via the thruster inlet. Via thruster inlet, the gas arrives in the plenum after which it enters the nozzle. On its way from thruster inlet to plenum inlet, the total pressure in the flow will drop because of frictional losses.

The pressure drop between the thruster inlet and plenum outlet/nozzle inlet is determined by the following relation:

$$\Delta p = \lambda \frac{l}{d} \rho \frac{v^2}{2} + \varsigma \rho \frac{v^2}{2} \tag{5-1}$$

Where λ is friction coefficient, ς (zeta) is coefficient of local head loss (depends on the exact design of the control valve), l is pipe length, d is pipe diameter, and ρ and v are density and velocity of fluid in the pipe. Note that the first term in above relation gives the pressure drop due to friction in the flow passage and the second term gives the pressure drop associated with restrictions or sudden changes in cross section. In general, one aims to keep this pressure drop as low as possible. This means that one should limit the flow velocity in the flow passage. This can be done by selecting a passage with a large cross-section, but this may increase the mass of the thruster. Another way is to limit the flow resistance. A guideline on how to set the flow velocity is given in a later chapter on fluid feed systems.

During operation gaseous propellant is fed from the tankage system to the thruster, whereas also mass leaves the combustor via the outlet. In case the two flows are in equilibrium, we say that stable operating conditions have been reached. In the remainder of this section, we are interested in a method to determine the chamber pressure under these equilibrium conditions and on how this equilibrium is attained.

Using the above relation on pressure drop and assuming that pressure drop is small compared to the overall pressure, we find that the inflow of mass into the plenum per unit time is proportional to the pressure difference over the plenum to the power 0.5. In practice, the exponent may be slightly different depending on the nature of the flow, so we write:

$$m_{in} = c_1 (p_{in} - p_c)^n \tag{5-2}$$

Here c_1 is a constant proportionality and the pressure drop is written as the difference between the pressure at the thruster inlet p_{in} and the chamber pressure p_c. Since n is unknown, this parameter usually needs to be determined from either detailed simulations or by testing. From testing also, the value of the proportionality constant c_1 can be determined.

Mass flow expelled through the nozzle is given by:

$$m_{out} = \frac{p_c A_t}{c*} \tag{5-3}$$

For a given thruster and propellant, throat cross-sectional area and c* can be considered constant and we may write:

$$m_{out} = c_2 p_c \ \ with \ \ c_2 = \frac{A_t}{c*} \tag{5-4}$$

Where c_2 is again a constant of proportionality, but different from c_1.

Equalizing the inflow and the outflow, gives the equilibrium pressure in the plenum. For n = 1 follows:

$$p_c = \frac{c_1}{(c_1 + c_2)} p_{in} \tag{5-5}$$

From this relation follows that, for n = 1, chamber pressure directly depends on the ratio of the two proportionality constants.

6 Plenum throat assembly design

The connection of the cold gas plenum/settling chamber to the nozzle is mostly through a convergent section. The design of this convergent as well as the divergent are important to limit boundary layer thickness in the nozzle throat and to limit performance loss. In addition, the approach volume adds to the plenum volume and hence effects the response time.

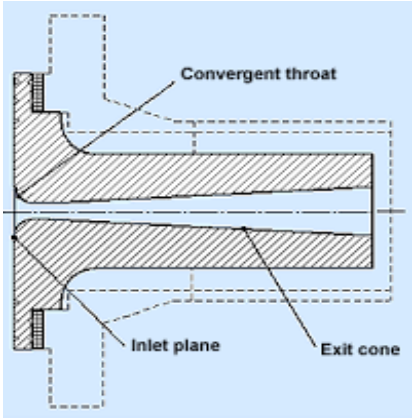

Figure 5: Profile of plenum throat assembly (mounting support represented by dotted lines)

Important design parameters have already been introduced in Figure 4. Some guidelines w.r.t. values to be selected can be obtained from Figure 6, be it that this figure shows a schematic of an optimized con-di flow channel used for flow measurement purposes.

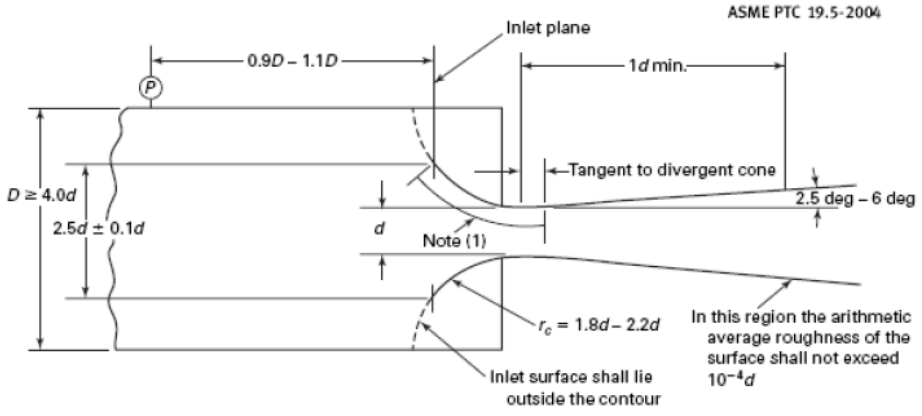

NOTE:
(1) In this region the surface shall not exceed $15 \times 10^{-6}d$ arithmetic average roughness and the contour shall no deviate from toroidal form by more than 0.001d.

Figure 6: Design of a venturi for mass flow rate determination [Stratford]

It shows a rounded approach of diameter in range 1.8-2.2 times the geometric throat diameter and specifies a wall surface roughness of the wall less than 10^{-4} times the throat diameter. The half angle of the divergent section in this case is chosen quite small as it allows for precise mass flow measurement. However, for practical cold gas nozzles, they

are chosen much larger as to reduce its length, thereby accepting a somewhat lower nozzle quality, see earlier chapter on nozzle design.

As a first step in the design of the plenum throat assembly, the throat diameter (or radius) should be determined. For this, use can be made of one-dimensional inviscid gas dynamics theory applied to an ideal compressible gas. According to this theory, the mass flow rate is a function of pressure and temperature at the upstream stagnation conditions, the diameter of nozzle throat and the ratio of specific heat of gas:

$$\mathrm{m}_{ideal} = \frac{\Gamma \, \mathrm{p}_c \, \mathrm{A}_t}{\sqrt{R \, T_c}} \tag{6-1}$$

Where:

m_{ideal}	ideal mass flow rate
Γ	Vandenkerckhove constant or ideal flow coefficient
p_c	total pressure in chamber
A_t	nozzle throat cross-sectional area
d_t	nozzle throat diameter
R	Specific gas constant
T_c	total temperature of propellant gas in thruster

Depending on the value of chamber pressure selected, the design mass flow rate and the cold gas properties and temperature, the cross-sectional area and hence the throat diameter can be determined.

Once the throat diameter is determined, the nozzle throat can be designed in some more detail.

In practice, however, these ideal conditions cannot be met all times. First, the flow through the nozzle is not one-dimensional and without friction. Second, the gas will not always act as an ideal gas. Especially in case of low thrust (< 100 mN) applications, corrections can be quite large as at these low thrust levels, i.e. low propellant mass flow rates, viscous effects tend to be large leading to a thick boundary layer in the nozzle throat and in the nozzle divergent. In that case, some special considerations need to be made thereby considering the presence of a boundary layer to allow for a proper design. Hereafter, we will discuss two of the more important effects, being real gas and viscous effects.

Real gas effects

For cold gas thrusters working at high pressures, compressibility or real gas effects may become important. In that case we should not use the ideal gas law, but instead:

$$\frac{p}{\rho} = ZRT \tag{6-2}$$

Here Z is denoted as the compressibility factor. At a given pressure and temperature, it gives the ratio between real and ideal mass density at standard conditions (22.4 liter per mol at 1 atm and 20 deg C.):

$$\mathrm{Z} = \rho_{\mathrm{real}} / \rho_{ideal} \tag{6-3}$$

Z = 1 refers to an ideal gas. Z>1 means that real density is larger than ideal density and hence the real volume taken up by a given mass of gas is less than in the ideal case. Z<1 means that the gas is denser than the gas in the ideal state.

Compressibility or real gas effects become especially important when operating conditions in the thruster are close to the critical conditions. For illustration, Table 4 gives compressibility factors and critical conditions for some typical cold gas propellants.
The table clearly shows that compressibility depends on the selected gas and reduces with reducing pressure (pressure moves away from critical pressure). This effect

can be modeled using [Amini]:

$$\mathrm{m}_{real} = (\mathrm{Z}_{plenum})^{-0.5} \times m_{ideal} \tag{6-4}$$

Here compressibility factor is determined in the plenum. Thus, in case compressibility in the plenum is more than 1, the real mass flow rate will be smaller than the ideal mass flow rate This also means that when determining the throat diameter for a given mass flow rate, the real diameter should be larger than the diameter resulting in the real case.

Table 3: Compressibility factor for some cold gas propellants at typical cold gas thruster operating conditions [Liley]

Gas	Crit. temperature (°C)	Crit. pressure (bar)	Compressibility factor (-)	
			@ 20 bar, 300 K	@ 10 bar, 300 K
Argon	-122	49	0.9884	0.9941
Hydrogen	-240	20	1.0117	1.0059
Methane	-83	46	0.9667	0.9830
Nitrogen	-147	33	0.9971	0.9983
Xenon	+17	58	0.8885	0.9465

Another effect associated with real gases is that specific heat of the gas varies with temperature and hence will vary depending on the location in the nozzle. A first estimate of this effect can be obtained using CEA.

Table 4: Change in value of isentropic coefficient from chamber to nozzle throat

Gas	Isentropic coefficient	
	Chamber @ 300 K	Nozzle throat
Argon	1.6667	1.6667
Hydrogen	1.4057	1.4166
Methane	1.3053	1.3192
Nitrogen	1.3996	1.3998
Xenon	1.6667	1.6667

To allow for correcting for variation of specific heat ratio and compressibility, the following relation is considered:

$$\mathrm{m}_{real} = (\mathrm{Z}_{plenum})^{-0.5} \frac{\Gamma(\gamma_t)}{\Gamma(\gamma_c)} \times m_{ideal} = \phi \times m_{ideal} \tag{6-5}$$

Where:
$\Gamma(\gamma_t)$ ideal flow coefficient based on conditions in throat
$\Gamma(\gamma_c)$ ideal flow coefficient based on chamber conditions (Vandenkerckhove parameter)
Φ factor correcting for real gas effects

[Johnson] provides measured values for the latter for various gases over a range of pressures (up to 100 bar). For nitrogen the real gas correction factor varies from 1 at low pressure to 1.07 at 100 bar depending on the temperature of the gas in the plenum/settling chamber. For hydrogen and helium, the factor varies from 1 at low pressure to ~0.98 at 100 bar pressure, again depending on the gas temperature in the plenum/settling chamber.

Discharge coefficient

The presence of a boundary layer and a radial pressure gradient will reduce the cross-sectional area available to the flow in the nozzle throat. This in general reduces the mass flow rate compared to the ideal mass flow rate of which the extent is given by the discharge coefficient (C_d). This coefficient was earlier discussed in the chapter on nozzle design, thereby introducing an analytical expression by Tang and Fenn, which allows to predict the discharge coefficient of a smooth nozzle with a not too sharp throat contour. A table was provided showing values obtained using the Tang and Fenn relationship for a gas with a specific heat ratio of 1.4 (hydrogen or nitrogen). You are reminded that results

showed that above a Reynolds number of 10,000, the effect on the discharge coefficient is limited to less than a few percent.

Results of [Wahlen, 1987], who performed experiments on various nozzles with various shapes (conical, bell, trumpet) and different divergence angles, area ratios for nitrogen and hydrogen propellant, confirm the earlier theoretical findings, including the pronounced effect at low (throat) Reynolds number.

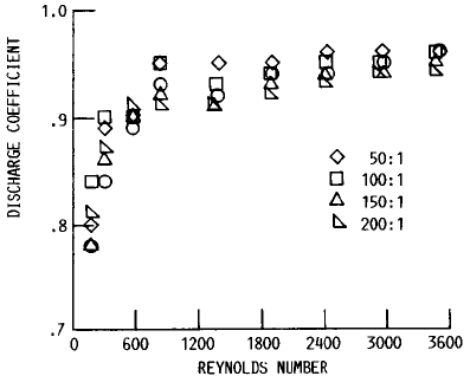

Figure 7: Discharge coefficient of conical nozzle with 20° divergence half angle versus throat Reynolds number using Hydrogen at room temperature as propellant [Wahlen]

[Johnson] investigated the effect of Reynolds number as well as the effect of different gases. Some results are shown in Figure 8.

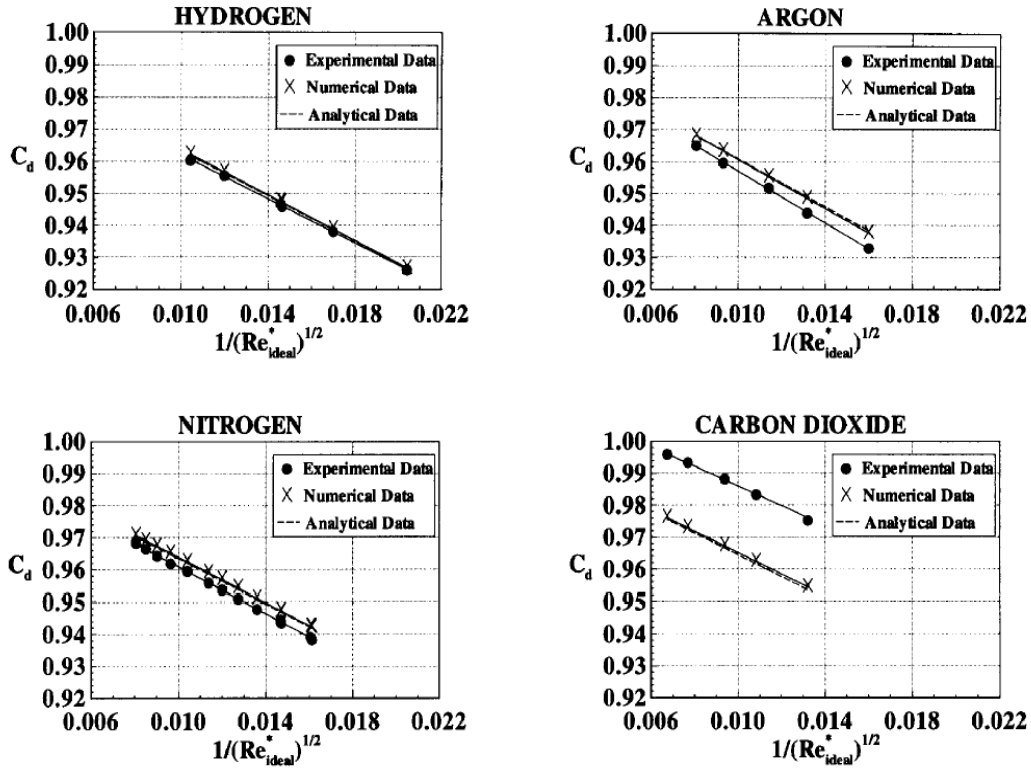

Figure 8: Nozzle discharge coefficient at low Reynolds number [Johnson]

The results clearly confirm that the discharge coefficient reduces with decreasing throat Reynolds number depending on the propellant gas used. The difference in the results for the different gases is partly explained from the effect of the specific heat ratio as follows from the analytical relation provided by Tang and Fenn and partly from real gas effects as is explained in the preceding section.

For very small nozzles, it is sometimes hard to realize a not too sharp throat region. This may influence the discharge coefficient as is illustrated in Figure 9. This figure shows results for the discharge coefficient obtained from numerical simulations using Helium (specific heat ratio is 1.667) as propellant. Clearly the results show a decrease in discharge coefficient with decreasing Reynolds number. More interestingly, we see also the effect of the detailed throat geometry (i.e. the sharpness) here given as the ratio of the longitudinal throat radius versus cross-sectional throat radius R_u/R_t. It follows that with decreasing throat longitudinal radius, at least down to a ratio of 2.0, the discharge coefficient increases. This would mean that up to this ratio a sharp throat section is beneficial for the discharge coefficient.

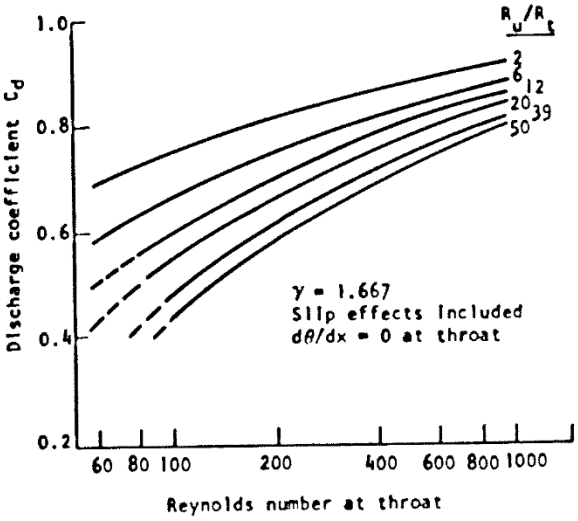

Figure 9: Nozzle discharge coefficient at very low Reynolds numbers using Helium propellant [NASA]

Summarizing, we can say that many parameters including convergence half angle, sharpness of throat, and surface roughness, affect the discharge coefficient. Several simple relationships exist that allow for determining the effect of these parameters, but to obtain improved insight, we need to have more detailed modelling using Computer Fluid Dynamics (CFD) and/or use experiments to verify the proper performance of the thruster.

7 Nozzle design

Typical nozzles used for cold gas thrusters are, like most rocket nozzles, of a conical-divergent design. Once the throat diameter is determined, nozzle exit area can be determined using ideal rocket theory (one-dimensional gas-dynamics theory). Next, we select the basic shape of the nozzle (conical or bell) and we determine the length of the nozzle.

In practice, the design must be corrected to consider losses due to non-ideal effects, including real gas effects, non-one-dimensional flow as well as viscous effects. This will lead to a lower value of the thrust coefficient. For instance, [Spisz] investigated this experimentally for a hydrogen thruster with a divergence half angle of 20 degree and different nozzle area ratios in range 25-150. Spisz found a 12% loss in thrust coefficient as compared to the one-dimensional isentropic thrust coefficient corrected for flow divergence at a Reynolds number of about 10,000 to almost 30% at a throat Reynolds number of 2,000.

[Wahlen] investigated the effect of different nozzle shapes (conical, bell, trumpet) on nozzle quality (referred to as nozzle efficiency in below figure) for both nitrogen and hydrogen propellant for throat Reynolds numbers in range 500-6000. Figure 10 gives a typical result found by Wahlen for a 15° conical nozzle using nitrogen propellant.

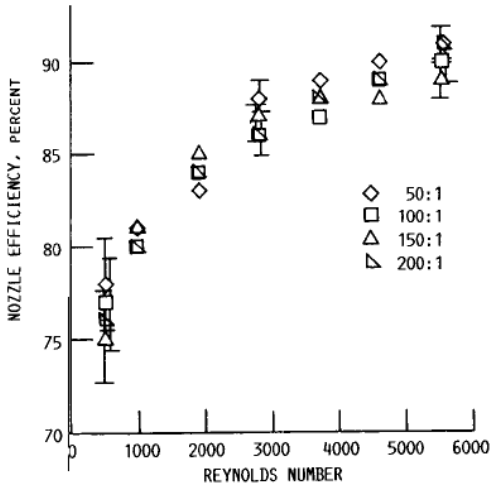

Figure 10: Nozzle efficiency of conical nozzle with 15° divergence half angle versus throat Reynolds number using cold nitrogen (room temperature) as propellant [Wahlen]

The results shown in figure confirm the strong dependency on throat Reynolds number and a weaker dependency on area ratio as was also found by Spisz, see earlier chapter on Nozzle design. Note that in the results of Wahlen the effects of non-one-dimensional flow are not separated from the viscous effects.

From our discussion, it should be clear that multiple parameters do affect the losses occurring in the nozzle. We mention throat Reynolds number, area ratio, surface roughness but also divergence half angle, nozzle shape and propellant. For a proper design, the effect of these parameters should be either known, or one should accept a reduced efficiency. How much this reduction is, should be established using either analytical methods, detailed numerical simulations or by testing, see also the earlier chapter on nozzle design.

8 Start-up and thrust decay

So far, we have not considered transient or time-dependent effects. In this section, we will discuss start-up and thrust decay of the thruster thereby showing the importance of keeping the plenum volume as small as possible. This is one of the reasons that often the nozzle is directly mounted on to the valve body.

During start-up, the flow rate -through the valve into the plenum exceeds that through the nozzle causing a pressure build up. Likewise, for thrust decay, the flow rate through the nozzle exceeds the flow rate in the plenum and hence the pressure will drop. A typical cycle is shown in Figure 11.

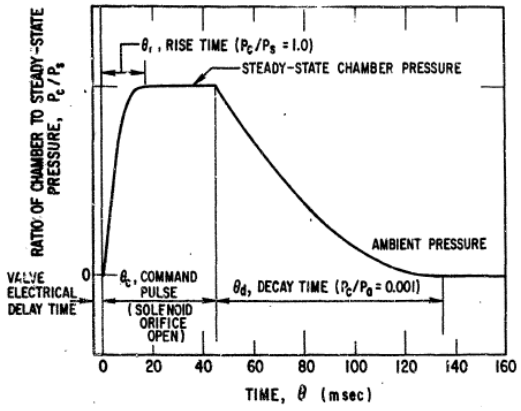

Figure 11: Typical pulse-pressure history [Greer]

For modelling, one can start with conservation of mass. It follows:

$$m_{in} = m_{out} + \frac{dM}{dt} \tag{8-1}$$

This equation essentially says that at any moment the mass flow entering the chamber should balance with the mass flow that is flowing out of the chamber and the accumulation of mass in the plenum itself.

With:

$$\frac{dM}{dt} = \frac{d\rho V_{plenum}}{dt} \tag{8-2}$$

And since plenum volume is constant:

$$\frac{dM}{dt} = V_{plenum}\frac{d\rho}{dt} \tag{8-3}$$

Using the ideal gas law and assuming homogeneous plenum conditions and isothermal condition, we obtain:

$$\frac{dM}{dt} = V_{plenum}\frac{d\rho}{dt} = \frac{V_{plenum}}{RT_c}\frac{dp_c}{dt} \tag{8-4}$$

Where:

V_{plenum}	Plenum volume
R	Specific gas constant
T_c	Temperature of cold gas in chamber (assumed constant)

Considering that inlet pressure is constant, we may also write:

$$\frac{dM}{dt} = \frac{V_{plenum}}{RT_c}\frac{d(p_{in} - p_c)}{dt} = \frac{V_{plenum}}{RT_c}\frac{d\Delta p}{dt} \tag{8-5}$$

Introducing a new proportionality constant $c_3 = V_{plenum}/RT$, it follows:

$$c_1(\Delta p)^n + c_2\Delta p + c_3\frac{d\Delta p}{dt} = c_2 p_{in} \tag{8-6}$$

Setting n equal to 1 (as an example) gives:

$$(c_1 + c_2)\Delta p + c_3\frac{d\Delta p}{dt} = c_2 p_{in} \tag{8-7}$$

After integration we obtain:

$$\Delta p(t) = constant\ e^{-\left(\frac{c_1+c_2}{c_3}\right)t} + \frac{c_2 p_{in}}{c_1 + c_2} \tag{8-8}$$

The integration constant introduced in above expression can be determined by setting Δp equal to p_{in} at time t = 0.

Figure 12 shows a typical output obtained using water vapor of temperature 550 K as propellant. Given are an inlet pressure of 5.0 bar, a chamber volume of 0.27 mm^3, a characteristic velocity of 754.4 m/s, and a throat area of 2.83E-9 m^2. Flow rate in and pressure drop are related using $m_{in} = 5E-9(p_{in} - p_c)^{0.5}$ where m_{in} is in kg/s and pressure difference is given in Pa.

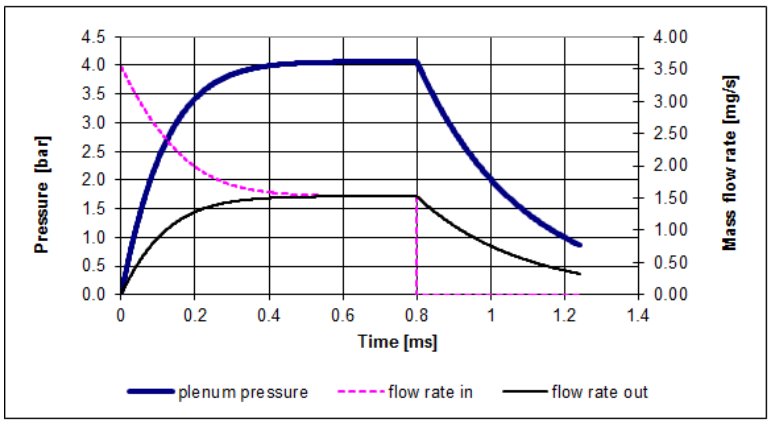

Figure 12: Pressure and mass flow rate history from start up to equilibrium operation

Also shown in the figure is the pressure decay that results after setting the inlet mass flow rate to zero at time t = 0.8 ms.

Next to the assumption of negligible ignition delay and no heat loss to the environment, it is also assumed there is no time delay on the opening of the thruster valve. With time delay in valve opening and closing, the start-up and decay are delayed.

9 Free molecular flow

At very low pressures and low thrust levels as considered for micro-thrusters with thrust in micro-Newton range, the flow does no longer behave as a continuum and the thruster performances can no longer be determined using ideal rocket theory. Rarefied flows are often characterized by Knudsen number K_n higher than 0.001. Below this value continuum flow is still applicable.

The Knudsen number is a dimensionless quantity defined as

$$K_n = {}^{\lambda}/_{l} \tag{9-1}$$

Where *l* is the characteristic length and *λ* is the molecular mean free path. The mean free path *λ* of a molecule in a rarefied gas is given by

$$\lambda = \frac{1}{\sqrt{2}\pi\sigma^2 n} \tag{9-2}$$

Where σ is the effective diameter of the molecule and n is the number density, i.e. the number of molecules per unit volume.

[La Torre] who performed an extensive numerical study on small thrusters with focus on nozzle performance, showed that for single nozzle thrusters with a thrust larger than 1 mN CFD simulations are found to be still accurate and could even be extended down to 0.1 mN. At still lower thrust levels La Torre concluded that the flow could no longer be dealt with as a continuum flow.

10 Verification of performance

To verify the proper design of the thruster two approaches are usually available, being 1) verification by testing and 2) verification by detailed (numerical) simulations. The first method in general leads to quite expensive testing which may take quite some time to prepare (test hardware needs to be produced, test facility needs to be reserved, specialised personnel is needed to operate the facility, etc.). The second clearly has the

advantage that it is cheaper and faster, provided that the tool has been shown to work correctly (has been validated).

The modelling of time dependent processes in the thruster needed to evaluate the design on stability and start-up behaviour cannot be accomplished with analytical tools. For this, computational solvers need to be used like Fluent, COMSOL etc. For flow computations and strength.

11 Design using CFD

Provided that we have a well validated code, we can use the code to investigate the effect of (small) variations on the design (parametric design).

For instance, [La Torre] investigated the effect of varying nozzle convergent and/or divergent half angle on nozzle efficiency as compared to the same nozzle but with inviscid flow. La Torre also investigated the effects of surface roughness on nozzle performance as well as the effects of further miniaturization.

[Krusharev] used CFD to allow selecting the best option from a range of nozzles considered, see Figure 13. All nozzles are of an axisymmetric design, except for nozzle 4, which is designed as a slit (2-D) nozzle with a slit length of 100 micro-meter. Nozzle 4 also has a slightly higher area ratio (32) than the other 3 (25).

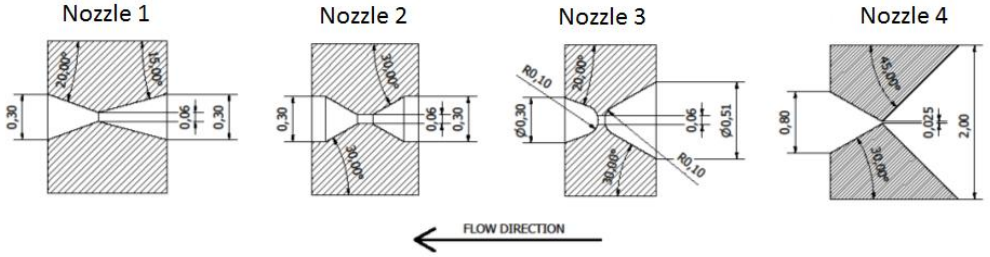

Figure 13: Candidate nozzles for a small cold gas (water vapour) thruster; Nozzles 1-3 are of an axisymmetric design, whereas nozzle 4 is of a linear (slit) design [Krusharev]

Next table shows CFD results obtained by [Krusharev] for the 4 different nozzles depicted above at two different chamber pressures. Results from one-dimensional (ideal rocket) theory have been added to allow determining the discharge coefficient and the thrust quality.

Table 5: CFD results for various nozzles using water vapour propellant of temperature 550 K; all nozzles have an exit-to-throat area ratio of 25 (except for nozzle 4) and expansion is to vacuum.

Water vapour 7 [Bar]					
Design	Nozzle 1	Nozzle 2	Nozzle 3	Nozzle 4	1-D
Mass Flow [mg/s]	2.65	2.43	2.18	2.28	2.62
Discharge coefficient [-]	1.010	0.926	0.831	0.869	1
Exhaust Velocity [m/s]	1147.7	1107.1	1069.6	970.9	1328.0
Thrust [mN]	3.04	2.69	2.33	2.22	3.48
Specific impulse [s]	117.0	112.9	109.0	99.0	135.4
Specific impulse quality (or efficiency) [-]	86.4%	83.3%	80.5%	73.1%	100%
Water vapour 5 [Bar]					
Design	Nozzle 1	Nozzle 2	Nozzle 3	Nozzle 4	1-D
Mass Flow [mg/s]	1.88	1.72	1.55	1.63	1.87
Discharge coefficient [-]	1.003	0.918	0.827	0.870	1
Exhaust Velocity [m/s]	1135.8	1092.8	1065.3	930.4	1328.0
Thrust [mN]	2.13	1.88	1.65	1.52	2.49
Specific impulse [s]	115.8	111.4	108.6	94.9	135.4
Specific impulse quality (or efficiency) [-]	85.5%	82.3%	80.2%	70.0%	100%

Results shown in table indicate nozzle 1 offers best performance. Nozzles 2 and 3 have slightly lower performance but can be more easily manufactures. Nozzle 4 shows worst performance even though it expands more.

Using CFD we can quickly select the more promising nozzle. This may help to limit the number of iterations needed in the design.

12 Other design aspects

In the previous sections, we focussed on the sizing needed to obtain the proper performance, i.e. discharge coefficient and thrust coefficient. However, when designing a cold gas thruster, next to performance, also other issues should be considered, like material options, mass, cost and operational life. In the next few paragraphs some of these aspects are considered in some detail.

12.1 Material options

Choice of chamber material depends on the use of the material (structural material, valve seat, etc.) and considerations concerning strength, density, corrosion resistance[3], fatigue resistance, brittleness, etc. For an explanation of these terms, you are referred to for instance material handbooks.

Table 6: CGT thruster materials

Thruster	Structural material	Valve seat	Ref
SAFER (58-118)	Stainless steel	Nylon	Moog
SVT01	Stainless 304L	EPDM Rubber/Silicone Rubber	Moog
2 lbf CGT	Stainless steel	Silicone rubber	Vacco
Vacco 5 N	Stainless steel	Kel-F (plastic)	Vacco
TG1	Stainless steel/Ti6Al4V	Vespel Sp	Omnidea/RTG

Material properties for a range of structural materials used in rocket design have been collected in annex K.

12.2 Thruster mass

Most cold gas thrusters essentially consist of a valve and a nozzle which are integrated into a single housing. To this we should add provisions for mounting of the thruster, and wiring.

Chamber mass can be estimated using thin shell theory. For this the reader is referred to chapter “Mass estimation”.

12.3 Thruster service life

A well-known phenomenon in the field of structural engineering is that repeated stressing of a material can cause failure, even when the applied stress is well below the yield stress. This is referred to as low cycle fatigue. For more information, see the chapter entitled “Design of thin shell structures”.

12.4 Still other design aspects

Besides mass and life also other parameters, like cost, reliability, and safety, are of importance to consider when designing a rocket thrust chamber.

[3] Material compatibility with a propellant is classified sequentially from Class 1 materials, which exhibit virtually no reaction with the propellant, to Class 4 materials, which react strongly with the propellant.

Thruster production and development costs depend on valve size, shape and lot acceptance testing. Production costs furthermore depend on quantity.

Typical thruster reliability data show a failure rate of 5.7×10^{-8} failures per hour. This gives a reliability of 0.995 over a 10-year life.

To estimate these characteristics for conceptual design purposes, it is advised to use either estimation by analogy of parametric estimation. For later stages, we can use either parametric, or engineering build up estimation. It is for the reasons of estimation that it is advised to develop a data base with actual (historic) values on the characteristics of interest and to the level of detail considered necessary.

Problems

1. Consider the design of a CGT using cold nitrogen gas (293 K) as propellant. It is specified that the thruster shall deliver a vacuum thrust of 5 mN and a vacuum specific impulse of 65 s. Given is that you select a design chamber (total) pressure of 5 bar at nozzle entrance.

   Using ideal rocket motor theory, determine for the above CGT:
   - Nozzle throat area,
   - Nozzle pressure ratio and minimum geometric expansion (area) ratio required.

2. Determine for the CGT specified in the previous problem the required nozzle throat area, nozzle pressure ratio and geometric expansion ratio, but now given a nozzle quality (correction) factor of 0.90[4] (90%; amongst others to account for flow divergence) and a nozzle discharge coefficient of 0.80 (80% to account for flow blockage).

   Generate a table that lists mass flow rate, nozzle throat area, nozzle pressure ratio and geometric expansion ratio for both the real (this problem) and the ideal rocket motor (problem 1).

3. Using nozzle dimensions as determined in problem 2, determine the dimensions of a conical nozzle with a divergence half angle of 20^o. Use convergent half angles of 45^o and 90^o with throat longitudinal radius 2 times the throat radius. Include a drawing showing the contour and the important nozzle dimensions.

4. Using IRT and Figure 8 and Figure 10, determine for the thruster discussed in problem above and at least one thruster from table 1 in this chapter the throat Reynolds number, the discharge coefficient and the nozzle efficiency when using cold nitrogen gas as propellant. Pick reasonable temperature and pressure value (motivate). Dynamic viscosity of nitrogen may be taken from NIST chemistry webbook or CRC Handbook of Chemistry and Physics.

5. Determine using IRT for a nitrogen CGT of thrust 2.5 mN and specific impulse 80 s the Knudsen number given a chamber pressure of 5 bar and a propellant temperature of 550 K and verify whether the thruster can be simulated using continuum flow techniques.

   Note that because of the elevated temperature, the thruster considered in this problem is not an actual cold gas thruster. Still, this problem has been added as part of the theory presented in this chapter also is important for the design of SMALL (low thrust) hot gas and chemical thrusters.

[4] Especially for throat Reynolds numbers below 1000, nozzle quality factor and discharge factor tend to reduce considerably, see this chapter as well as the chapter on nozzle design.

6. Consider the design of a CGT for vacuum operation. You select cold nitrogen gas as propellant. Nitrogen temperature is 293 K. The mass flow rate $\dot{m}$ through the thruster control valve has been calibrated using nitrogen gas. and relates to the drop in pressure (Δp) between thruster inlet and chamber outlet according to:

$$\dot{m} = 5\ (\Delta p)^n$$

Here $\dot{m}$ is in mg/s and Δp in bar.

You select a thruster inlet pressure of 5 bar (constant) and nozzle throat area of 7.92E-9 m^2.

a) Calculate for this motor equilibrium chamber pressure and mass flow rate for n = 0.5
b) Same question but now consider how this chamber pressure and mass flow rate vary with the exponent n (n in range 0.5-1.1; use step size 0.1).

References

1. Amini, A., Owen, I., The use of critical flow venturi nozzles with saturated wet steam, *Flow Meas. Instrum.,* Vol. 6, No. 1, pp. 41~17, 1995
2. Greer, H., Diep, D.J., Dynamic- Performance of Low Thrust Cold Gas Reaction Jets in a Vacuum, Aeorospace corporation, TR-669(6230-33)-1, August 1966.
3. Johnson. R.C., Real-gas effects in flow metering, NASA TM X-52965, May 1971.
4. Johnson, A.N., Espina, P.I., Mattingly, G.E., Wright, J.D. and Merklet, C.L., Numerical characterization of the discharge coefficient in critical nozzles, by, NCSL Workshop & Symposium, Session 4E, 1998.
5. Krusharev, I., Micro – Thruster Development; Propulsion System for the DelFFi Mission, MSc thesis, TU-Delft, The Netherlands, August 2015.
6. La Torre, F., Gas flow in miniaturized nozzles for micro-thrusters, PhD-thesis, TU-Delft, The Netherlands, 2011.
7. Liley, P.E., Thomson, F.H., Friend, D.G., Daubert, T.E., Buck, E., Physical and Chemical Data, McGraw Hill, 1999.
8. Massier, P.F., Back, L.H., Noel, M.B. and Saheli, F., Viscous effects on the flow of supersonic nozzles, AIAA J., Vol.8, No. 3, 605-607, 1970.
9. NASA. Liquid Rocket Engine Nozzles. NASA SP-8120, 1976.
10. Spisz, E.W., Brinich, P.F., Jack, J.R., Thrust coefficient of low-thrust nozzles, NASA TND-3056, 1965.
11. Stone, W.C., Fast Variable-Amplitude Cold Gas Thruster, Journal of Spacecraft and Rockets, Vol. 32, No. 2, March-April 1995.
12. Wahlen, M.V., Low Reynolds Number Nozzle Flow Study, NASA-TR-100130, July 1987.
13. Wang, C., Zandbergen, B.T.C., Cervone, A., Chu, J., Numerical Studies on Performance of Free Molecule Micro-Resistojet for CubeSats, 6th European Conference for Aeronautics and Space Sciences (EUCASS), 2015.
14. Zandbergen, B.T.C., Modern liquid propellant rocket engines; 2000 Outlook, Internal Publication, Delft University of Technology, Faculty of Aerospace Engineering, Delft, The Netherlands, March 2000.

For further reading

1. Makled, A.E., AL-Sanabawy, M. A., Bakr, M. A., Theoretical and Experimental Evaluation of Cold Gas System Components, Paper: ASAT-13-PP-23.

LRE combustor design

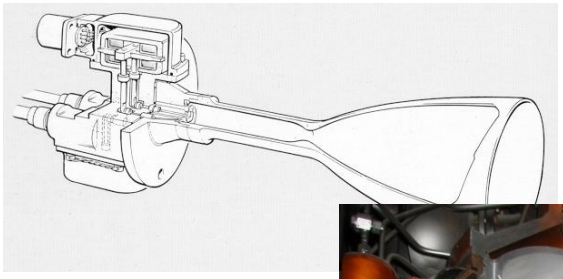

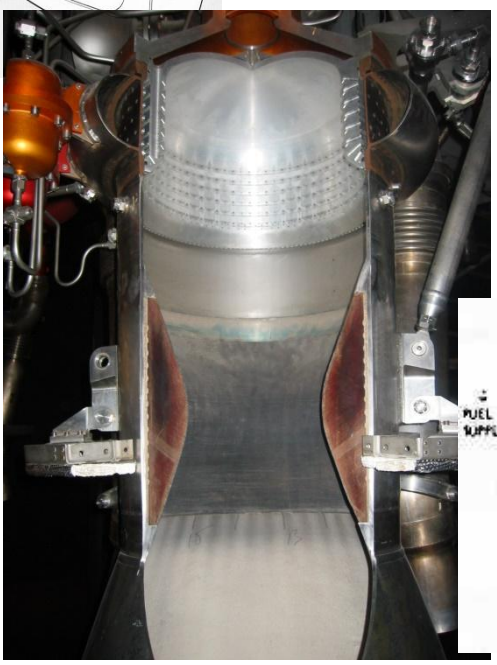

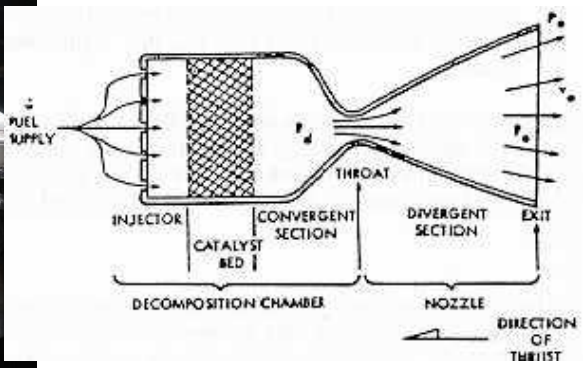

Contents

List of symbols 219

1 Introduction 220

2 Processes occurring in the combustor 221

3 Shape of the combustor 222

4 Main components 222

4.1 Injection system 223

4.2 Combustor tube 226

4.3 Catalyst bed 227

4.4 Chamber throat assembly 227

4.5 Chamber materials 227

5 Design and sizing of elements 228

5.1 Distributor 228

5.2 Injector and the injector elements 229

5.3 Combustion 241

5.4 Combustion stability 244

5.5 Pressure drop due to flow acceleration 245

5.6 Catalyst bed 246

5.7 Chamber throat assembly 247

5.8 Chamber material selection 247

5.9 Chamber wall thickness based on internal pressure 247

5.10 Chamber mass 248

5.11 Chamber service life 248

5.12 Other chamber characteristics 248

Example 249

Problems 251

References 253

For further reading 254

List of symbols

Roman

A	Area
C_d	Discharge coefficient
Dr	Surface regression rate
D	Diameter
H	Enthalpy
L	Length
m	Mass flow
M	Mach number
n	Number of injector holes
O/F	Oxidizer-to-fuel mass mixture ratio
p	Pressure
q	Heat flux
Q	Volume flow rate
r	Radius
r_a	Contraction approach radius
r_u	Longitudinal throat radius
R	Specific gas constant
S	Surface area
T	Temperature
v	Velocity
V	Volume

Greek

β	Contraction half angle
γ	Jet angle
λ	Vaporization rate contstant
ρ	Density
τ	Residence time
ζ	Pressure loss coefficient
Γ	Vandenkerckhove parameter

Subscripts

c	Chamber or contraction
con	Convergent
e	Expansion
f	Fuel or fluid
i	Injection
o	Oxidizer
t	Throat
vap	vaporization

Superscripts

*	Characteristic parameter

1 Introduction

A LRE rocket combustor or decomposition chamber essentially is a thin-walled vented pressure vessel in which the rocket propellant burns or decomposes to provide a hot high-pressure gas fit for expansion in a nozzle.

Figure 1 shows a schematic of a combustion chamber of a large liquid hydrogen-liquid oxygen rocket motor. It essentially consists of an injector and dome assembly, an igniter tube (central in the injector and dome) and a combustion chamber. The injector and dome assembly is located at the top of the chamber. The dome manifolds the liquid oxygen and serves as a mount for the igniter (middle top). The fuel is directed via the coolant manifold[1] and the double wall, providing regenerative cooling to the combustion chamber walls, and then to the injector. In the combustion chamber the two flows vaporize, mix and react creating the hot gas needed for thrust generation. A nozzle extension is bolted to the aft flange of the combustion chamber allowing for higher performance.

Figure 1: Schematic of large bipropellant rocket combustor (courtesy Boeing)

Figure 2 shows a typical monopropellant decomposition chamber. It uses a catalyst bed, placed inside the chamber and contained by retainer gauzes, to further propellant decomposition.

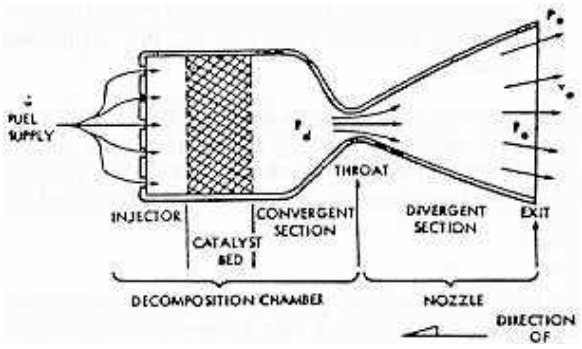

Figure 2: Monopropellant thruster schematic

The monopropellant enters the thruster via the propellant valve and is routed directly to the injector. The injector provides a proper distribution of the propellant over the catalyst bed. Under the action of the catalyst, the monopropellant decomposes thereby generating a hot gas mixture, which exits the chamber through the convergent/divergent nozzle, thereby generating thrust. Cooling of the chamber is by radiation cooling only.

The main performance requirement for a combustion or decomposition chamber is to achieve a high combustion quality, without unduly high mass and cost of the chamber. This we will discuss later in some more detail.

Table 1 provides characteristic data of some specific liquid rocket engine combustion chambers.

[1] A manifold is a chamber or pipe with a number of inlets or outlets used to collect or distribute a fluid.

Table 1: Characteristic data of some combustion chambers [McHugh], [Pouliquen], [Schoyer]

Parameter	Aestus (L5/L7)	LE-5	HM7B	HM60 (Vulcain 1)	ATE
Propellant	MMH/NTO	LH/LOX	LH/LOX	LH/LOX	MMH/NTO
Thrust [kN]	20/27.5	103	62.2	1113	20
Core flow O/F	2.1/2.05	5.5	5.14	5.9	2.32
Mass flow [kg/s]	6.37/8.76	28.3	13.86	258.4	5.81
Chamber pressure [bar]	10/10.4	36.8	35	109	90
Chamber mass [kg]		40.8	69	430	
Chamber diameter [mm]	180/-	240	180	415	119
Chamber length [mm]		351	283	426	178
Characteristic length [mm]		840	680	840	
Contraction ratio [-]		3.11	2.78	2.99	10
Injector type	Coaxial	Coaxial	Coaxial	Coaxial	
# of injector elements	96/132	208	90	516	
Injector pressure drop [bar]	<7-8	5.49 (f) / 12.15 (ox)	9.2 (f) / 11.1 (ox)	22.6 (f) / 26.5 (ox)	~15
Cooling	Regenerative	Regenerative	Regenerative	Regenerative	Regenerative
Type of wall	Milled channel wall	Brazed tubes	Milled channel wall	Milled channel wall	Milled channel wall
# of coolant channels		240	128	360	122
Coolant	MMH	Hydrogen	Hydrogen	Hydrogen	NTO
Material	Stainless steel liner with galvanized nickel closure	Nickel 200	Cu alloy inner layer with galvanized nickel closure	Cu alloy inner layer with galvanized nickel closure	Gold coated NARloy Z
Maximum chamber wall temperature [K]	750	900			770

The data provided in the table includes general information as motor identifier, propellants used and thrust level. Then some more specific data are provided. Most of the data will be covered in some detail in the following text.

2 Processes occurring in the combustor

Within an LRE combustor several processes occur, including fluid injection, vaporization, mixing (in case of bipropellants), ignition, and combustion. These processes are more or less subsequent to each other. This allows us to distinguish different zones in the combustor. Typically three major zones are distinguished, see Figure 3.

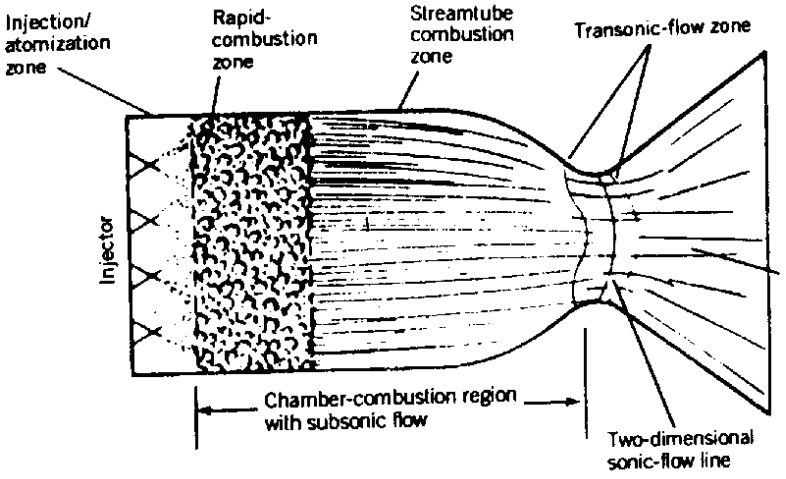

Figure 3: Combustion zones in a LRE combustor [Sutton]

Injection/Atomization Zone
The liquid propellants are injected into the combustion chamber via an injection system at velocities typically between 7 to 60 m/sec. When the liquid fuel and oxidizer are injected into the chamber the individual jets are broken up into small droplets. This region is relatively cold; however, heat transferred via radiation from the rapid combustion region causes most of the small droplets to vaporize. At this zone chemical reactions are occurring, but at a minimal level since the zone is relatively cool. Also, the region is heterogeneous, with fuel and oxidizer rich regions.

Rapid Combustion Zone
In this zone chemical reactions are fast due to the increasing temperature caused by the liberation of heat during the reaction. Any remaining droplets are vaporized, and the mixture is fairly homogeneous due to local turbulence and diffusion of gas species. The gas expands causing the specific volume of the mixture to increase and the gas begins to move axially with significant velocity. There is some transverse motion of the gas as high-burning-rate regions expand towards cooler low-burning-rate regions.

Stream Tube Combustion Zone
In this region chemical reactions continue but at a reduced rate. The axial velocity of the gas continues to increase (200 to 600 m/sec). Transverse convective flow decreases to almost zero and the flow forms small streamlines across which turbulent mixing is minimal.

In actuality, the boundaries of these zones are difficult to define and transition from one zone to the next is gradual. The length of the zones is heavily influenced by choice of propellants and the properties unique to them, the operating conditions (i.e. mixture ratio, chamber pressure, etc.), the injector design, the chamber geometry, and whether an catalyst is used or not. These aspects are dealt with in some more detail in the following sections.

3 Shape of the combustor

Because of the high pressure in LRE combustors, the shape is kept very simple, being mostly of a cylindrical or spherical nature, see Figure 4.

The cylindrical shape has the advantage of easy manufacturing, whereas the spherical shape yields a minimum surface area for a given volume. Other shapes include the pear-shape, which is found particularly in high-thrust rocket motors, and the tubular and conical shape. The latter are without a throat-section, which eases manufacturing.

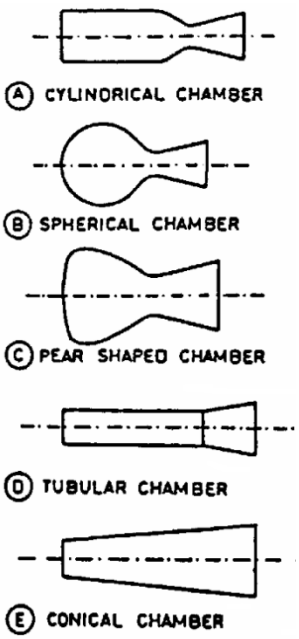

Figure 4: Geometry of combustion chamber with nozzle

4 Main components

In this section, the main components of the LRE combustor are discussed in some detail. We start with the injection system, followed by the combustor tube, and the chamber throat assembly. Some attention is also paid to the catalyst bed that is included for monopropellant LRE. A specific section provides information on the type of materials used in LRE combustors.

4.1 Injection system

Figure 5 shows the injection system of specific liquid propellant rocket motor using a mixture of Unsymmetrical dimethyl hydrazine (UDMH) and Hydrazine hydrate (UH25) as fuel and Nitrogen Tetroxide (NTO) as oxidizer. The liquid oxidizer enters the motor on top after which it flows through the oxidizer manifold to the cylindrical-shaped injector. The liquid fuel first flows into the fuel manifold. From this manifold it is fed into the combustor via the fuel injection holes.

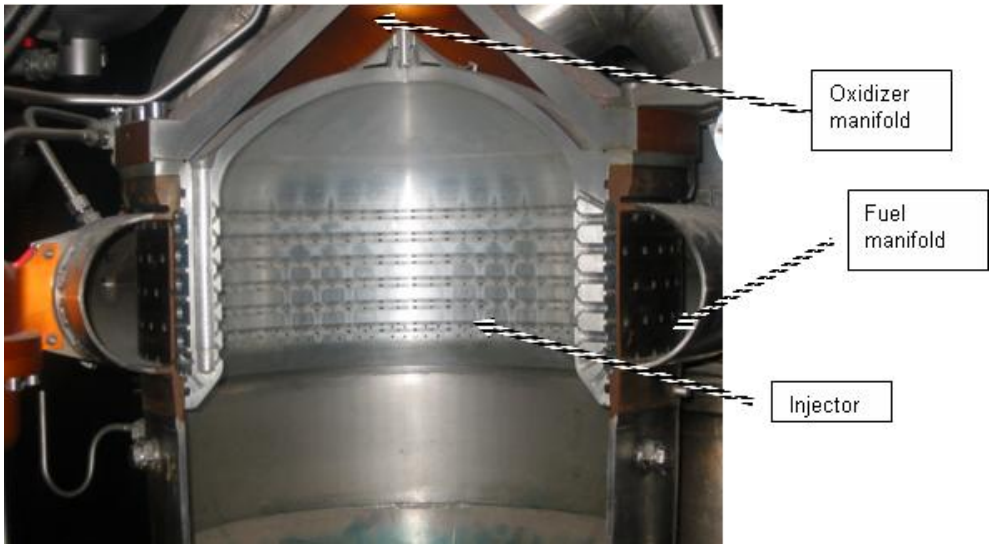

Figure 5: Injection system of a large liquid propellant rocket motor

The main function of the injection system is to ensure a suitable flow of the liquids allowing for smooth mixing, vaporization, ignition and chemical reaction, all at the proper mixture ratio. To ensure proper propellant injection, the injection system consists of a distributor and an injector. Hereafter these two components are discussed in some detail.

4.1.1 Distributor

A distributor is a manifold (an arrangement of piping/tubing) designed to evenly distribute the propellant flow over the injector orifices while (for bipropellant motors) ensuring a perfect sealing between the oxidizer and fuel tubes, see Figure 6 (left-hand figure).

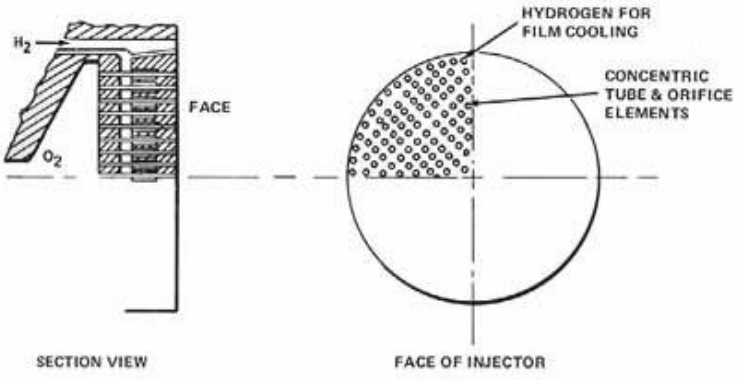

Figure 6: Schematic of distributor

4.1.2 Injector

An injector is a disk or cylinder containing many small perforations/openings/holes, which are usually referred to as orifices. Its purpose is to cause droplet formation/atomization and ensure even mixing and propellant distribution over the full cross-sectional area of the combustion chamber. This improves stability of the burning process and reduces oscillations.

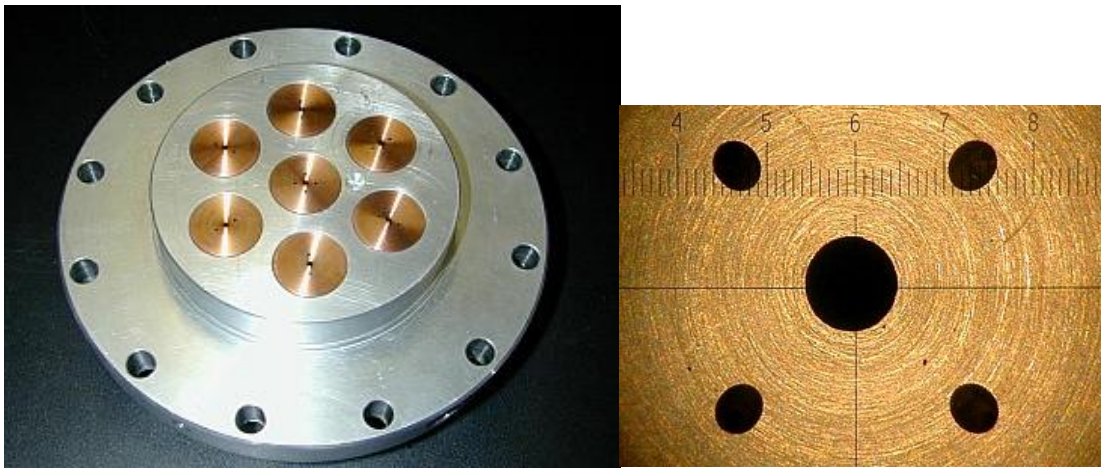

Figure 7: Injector plate (photo courtesy University of Basel)

Figure 7 shows several (7) inserts in the injector plate which each contain one large centre perforation and 4 smaller perforations in a circle about the centre perforation. This combination is referred to as an injector element. The surface of the injector plate facing the combustion is generally referred to as the injector face.

Injector pattern

Figures 4-6 show that the injector elements (or atomizers) are not arbitrarily distributed over the injector. Generally, a special pattern (arrangement) is used to allow for an even filling of the chamber, to distribute the heat loading over the full face of the injector plate and to allow for face cooling. One such pattern is a concentric pattern as shown in figures 5 and 6.

Types of injector elements

The simplest form of propellant injection into the chamber is achieved by a 'shower head' injector, see Figure 8 (middle). Mixing of the fuel and the oxidizer relies on turbulence and diffusion.

Another non-impinging type of injector is the spray nozzle in which conical, solid cone, hollow cone, or other type of spray sheet can be obtained. When a liquid hydrocarbon fuel is forced through a spray nozzle the resulting fuel droplets are easily mixed with gaseous oxygen and the resulting mixture readily vaporized and burned. Spray nozzles are especially attractive for the amateur builder, since several companies manufacture them commercially for oil burners and other applications.

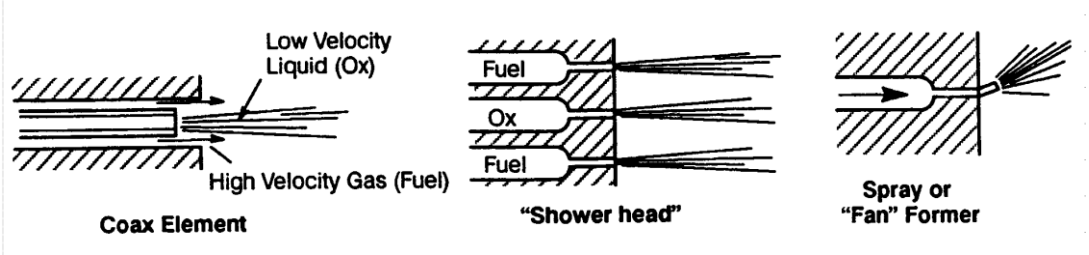

Figure 8: Schematic of non-impinging types of injectors

A third type of non-impinging injector is the coaxial element, see figure 5 (left hand side), where a low velocity liquid stream (oxidizer) is surrounded by a high velocity (fuel) gas jet. This type is used in many current designs of liquid hydrogen – liquid oxygen rocket engines, like the European Ariane 5 Aestus, Vinci, and Vulcain 1 and 2 rocket motors. Advantage is that the liquid hydrogen, which is also used as coolant, can be heated to a higher temperature before injection.

Besides non-impinging types of injectors, there are also many rockets that use an “impinging stream” type of injector. In this type of injector, the propellants are injected through a number of separate holes in such a manner that the fuel and oxidizer streams impinge upon each other. Impingement aids atomization of the liquids into droplets as well as to distribution and mixing. One type is the like-on-like impinging injector (Figure 9) where jets of the same fluid impinge, breaking the streams into droplets. Mixing is obtained by locating the impinging streams of fuel and oxidizer near each other so that the resulting droplets mix well. This type of injector was used in many liquid hydrogen-liquid oxygen rocket motors, like the Ariane 4 Viking engine.

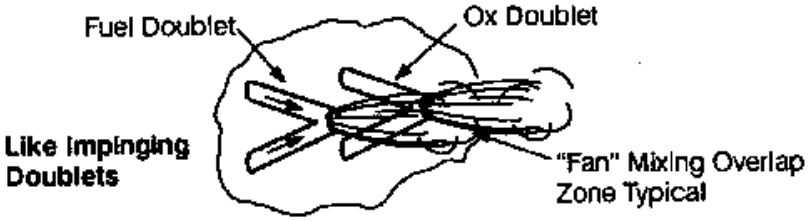

Figure 9: Like impinging superimposed injector configuration

A second type of impinging injector configuration uses jets of different fluids that impinge on each other (Figure 10). This is for example the case in most storable, bi-propellant, reaction control system thrusters. Depending on the thrust level, one or more multiple unlike doublet injectors are used. Below about 100 N a single doublet type of injector suffices [Kaiser Marquardt].

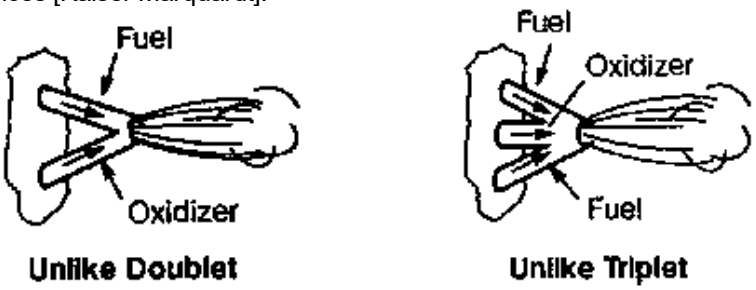

Figure 10: Unlike impinging injector configuration

Compared to the non-impinging type of injectors, the impinging type offers high combustion efficiency, but a higher heat load on the face plate. In addition, it is very sensitive to fabrication tolerances and hence brings high cost.

Recently investigations are concentrating on swirl injectors and swirl coaxial gas-liquid injectors that introduce a swirl component in the injector flow. This has been shown to enhance propellant mixing and thus improve engine performance.

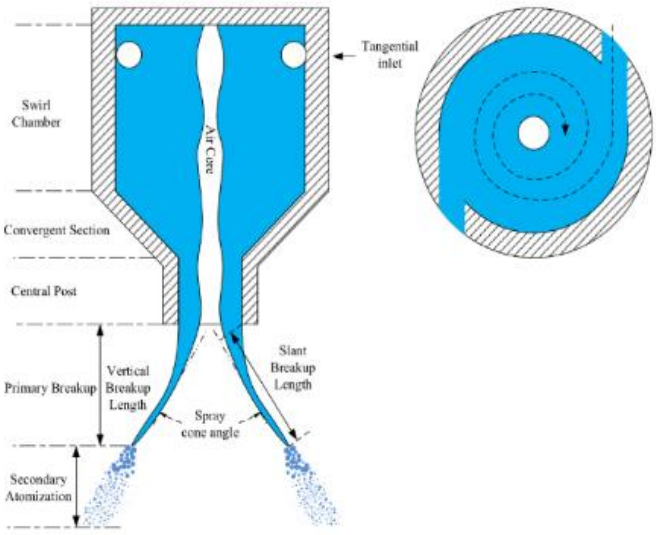

Figure 11: Swirl-type of injector [Kang]

Another development is the pintle injector first explored by TRW [Dressler]. This essentially is a coaxial injector where one propellant flows through the outer annulus and the other flows along the stem of the pintle until it interacts with the specially shaped tip, see Figure 12. The tip causes the core flow to spray outward in a broad cone or flat sheet that intersects the cylindrical stream of the other propellant. Pintle injectors enjoy several advantages first; the design is inherently simpler in the sense that only a single injector element is required which makes a pintle injector simpler to build. Second advantage is the inherent combustion stability afforded by this injector. There has never been an instance of combustion instability associated with pintle engines. Third attractive feature involve its throttle-ability. Throttling ratio of 20:1 has been demonstrated with hypergolic propellants. Fourth advantage is that the pintle arrangement can be set up to get fuel-film cooling of the inside of the combustion chamber essentially automatically.

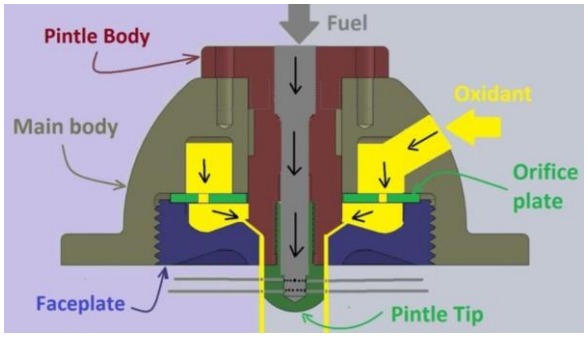

Figure 12: Pintle injector [Rezende]

Selection of the best type of injector configuration is usually based on experience obtained from existing engines. In case of a newly developed injector type, a lot of testing must be performed including real combustion tests in a real engine to show that the type developed is suitable.

Dirt can build up in the orifices restricting the flow of liquid. To prevent orifices from clogging, usually a filter screen is in each propellant feed just upstream of the injector. Of course, the filter screen should be of a size smaller than the size of the orifices in the injector head.

4.2 Combustor tube

The combustor tube is that part of the combustor wherein the flow mixes, vaporizes and combusts. Essentially it is a hollow tube, hence its name. The tube wall has to withstand the high pressure within and must cope with the heat transferred from the hot gases to the “cold” wall and the associated cooling required.

The main distinction is in single wall designs, like radiation-cooled rocket engines and double wall designs. The latter are mostly applied in high performance rocket motors that experience high heat loads.

In a single wall design, the structural material may be capable of carrying the heat and pressure loads or it may be protected by some thermal insulation material or by a coolant film. In case the structural material carries both loads, it usually has a coating which protects the material from oxidation.

Double wall designs allow for efficient removal of excess heat either through regenerative or dump cooling. Early combustor (thrust chamber) designs had low chamber pressure, low heat flux and low coolant pressure requirements, which could be satisfied by a simple "double wall chamber" design with regenerative and film cooling. For higher heat flows, "tubular wall" combustion chambers are used. This is by far the most widely used design approach for most large rocket engine applications. These chamber designs have been

successfully used for amongst others the Ariane 5 HM-60, the Japanese LE5, and the USA H-1, J-2, F-1, and RS-27 rocket engines.

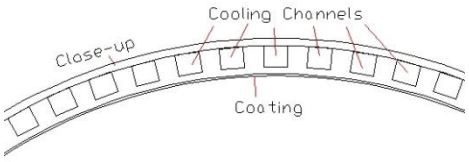

Figure 13: Example of channel wall

To cope with still higher heat flow, "channel wall" combustors are used. These are so named because the coolant flows through rectangular channels, which are machined or formed into a hot gas liner fabricated from a high-conductivity material, see Figure 13. The figure shows that the wall consists of three layers: a coating, the slotted high-conductivity material, and the close-up. These three layers can be different materials or the same.

4.3 Catalyst bed

Monopropellant decomposition chambers contain a catalyst bed with a catalyst to further the decomposition of the propellant. This catalyst bed is contained by retainer gauzes, see Figure 14. The propellant flow is spread evenly over the catalyst bed by the injector. Sometimes the retainer gauzes assist in the spreading of the monopropellant over the bed. They also support the catalyst bed to prevent deformation.

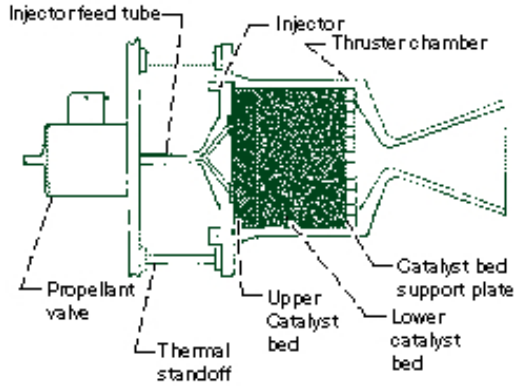

Figure 14: Monopropellant thruster

Most hydrazine thrusters use a catalyst bed made from iridium impregnated alumina pellets 1.5 to 3 mm in diameter (smallest pellets in upper catalyst bed). An alternative is to use finely divided iridium on an aluminium oxide support or platinum-iridium mesh. Generally, iridium is present to the extent of 30% of the total catalyst mass. To allow proper operation of the catalyst, the catalyst bed may be conditioned by one or more heater elements. In case of hydrogen peroxide propellant, silver wire cloth and/or silver plated nickel screens are used as catalyst.

4.4 Chamber throat assembly

The connection of the chamber/combustor tube to the nozzle is mostly through a throat assembly. In most rocket motors this is a convergent-divergent nozzle part, sometimes integrally connected to the tubular section of the chamber that allows for the chamber to be tested at sea level conditions (separate from the nozzle) without flow separation. The design of the convergent is mostly aimed at reducing pressure losses due to the flow contraction; see sections on liquid injection and nozzle design. For small combustion chambers the convergent volume is about $1/10^{th}$ the volume of the combustor tube.

4.5 Chamber materials

Typical materials used for high-thrust liquid rocket engines are stainless steel as structural material and as high-conductivity material some kind of copper or nickel alloy to transfer the heat to a coolant. A typical such copper alloy is NARloy Z with a thermal conductivity of 330 W/m-K.

Bi-propellant RCS thrusters mostly use refractory metals like rhenium, molybdenum, columbium (Niobium) and alloys of these elements as the structural material. Advantage of these materials is that they can withstand very high temperatures. However, they are very susceptible to oxidation. To this end, usually a silicide coating is used to provide protection against the aggressive combustion gases. Recently, one is considering the

use of ceramic-matrix carbon as the structural material as this requires no coating and is equally capable of attaining high temperatures. As the heat loading of the injector is less than for the combustor tube and contraction, titanium can be used as the structural material.

Hydrazine monopropellant thrusters typically experience decomposition temperatures in the range 1000-1500 K at a chamber pressure up to about 20 bars. Typical structural material for hydrazine monopropellant thrusters is either stainless steel or brass (copper alloy C3600). Sometimes also nickel alloys as Haynes 25 or 188 are used.

Thrust chambers for hydrogen peroxide monopropellant thrusters can be fabricated from either stainless steel or brass (e.g. copper alloy C36000). The thermal expansion rate of the latter closely matches that of the silver catalyst, which makes that as the chamber heats up both the chamber and catalyst expand at a similar rate. Brass also has the advantages of being easily machined and of having high strength.

Some characteristic data of thrust chamber materials are given in appendix K.

5 Design and sizing of elements

All processes occurring in the combustion chamber (vaporization, mixing, chemical reactions, etc.) take some time to happen. The minimum size of the combustion chamber while still ensuring satisfactory combustion is determined by the time needed for vaporization, mixing, ignition and chemical reactions to occur: If the chamber is too short, part of the energy will be released outside the chamber and hence does not contribute optimally to the thrust; If the chamber is too long, thermal energy (heat) will leak away to the combustor wall and hence, thrust decreases. In addition, the thrusters will be relatively heavy. So, it follows that there is an optimum size for the combustion chamber.

Important parameters in sizing a thrust chamber include chamber volume, shape, mass, operating pressure, materials used, etc.

The various steps in sizing as considered in this work are:

- Determine chamber pressure
- Select number of injector elements and injector type
- Select chamber shape
- Size injector elements and chamber
- Select chamber material
- Dimension chamber
- Compare results and select best design or if necessary, iterate on the design.

Important design issues related to the design of the various components are discussed in some detail hereafter.

5.1 Distributor

To allow an even distribution over the injector orifices, the velocity of the liquid in the distributor must be as low as possible. Typical flow velocities in the distributor should be well below 10-15 m/s and at the most 20% of the injection velocity, see next section. Once the flow velocity in the distributor has been selected, the flow cross-sectional area can be determined using the law of mass conservation:

$$m = \rho \cdot v \cdot A = \rho \cdot Q \tag{5-1}$$

Where:

- m = mass flow
- ρ = specific mass of fluid
- v = flow velocity
- A = flow cross-sectional area

- Q = flow rate through manifold

For a bipropellant system of course, we must reckon with two fluids each with its own density. In that case, oxidizer and fuel mass flow rate can be determined from total mass flow rate and the O/F mass ratio. Data on propellant density may be obtained from the literature or from measurements. In most liquid cooled rocket motors, the distributor allows for injection of fuel close to the chamber wall. This protects the chamber wall from overheating. The reason for taking the fuel and not the oxidizer is that the latter may react (oxidation reaction) with the metallic chamber wall and hence leads to corrosion.

The pressure at the inlet of the distributor (inlet of thruster) is generally referred to as the inlet pressure. Notice that because of the low flow velocity in the distributor, the static pressure is about equal to the total pressure. This pressure must be more than the chamber pressure, but not too much, as else the feed system needed to feed the propellants into the combustor becomes too heavy. To limit any pressure loss, it is important that the manifolds are nicely shaped with a gradual transition between pipe sections of different size.

5.2 Injector and the injector elements

For attaining a good distribution of the propellants over the chamber, we need to consider the number of the individual injector elements and how these are distributed (the pattern) over the face of the injector. Only once the number of elements is known and their respective design and size, the mass flow rate per element can be determined. Conservation of mass dictates for each:

$$m = \rho \cdot v \cdot A = \rho \cdot v_i \cdot n \cdot A_i = \rho \cdot n \cdot Q_i \tag{5-2}$$

Where:
- v_i = injection velocity
- A_i = flow cross-sectional area of injector element: $A_i = A/n$
- n = number of injector elements)
- Q_i = flow rate through a single element: $Q_i = Q/n$

As the pattern depends on the spray characteristics, the pattern is in general designed in an iterative way, meaning that a first pattern is selected with the individual elements. The spray characteristics are checked. If necessary, the design is adapted and so on.

Important for the design of each element is that they properly atomize and distribute the propellants over the combustor tube. Important design parameters for the injection elements are injection velocity and the size (area) of the hollow injector tubes. In this section, we will show how these parameters are related and how they determine the jet structure. But first we will discuss desirable spray properties.

5.2.1 Droplet formation and spray properties

The way in which a liquid jet is resolved into drops depends on the velocity of the jet. We distinguish:
- Capillary resolution: At flow velocities in the order of m/s, droplet formation will be due to capillary resolution. The jet shows perpendicular constriction lines at some distance from the holes. These constrictions increase as the jet progresses and finally cause the formation of equidistant drops.
- Oscillations in the flow: At about 10 m/s, droplet formation is caused by oscillations in the flow. The jet performs transversal oscillations which accelerate the formation of droplets
- Atomization: At flow velocities in the order of 100 m/s, the static pressure in the jet drops below the vapour pressure of the liquid. The ensuing vaporization causes the jet to break up into a mist/spray immediately on leaving the hole, this is called *atomization*.

Figure 15 shows images of jet breakup by a coaxial gas flow at various ratio of liquid to gas velocity taken from [Lasheras]. Central jet is formed by a liquid being injected at a low flow velocity (< 1 m/s). Gas is injected from an annulus around the liquid flow at velocities in range 19 m/s (figure a) to 50 m/s (figure d).

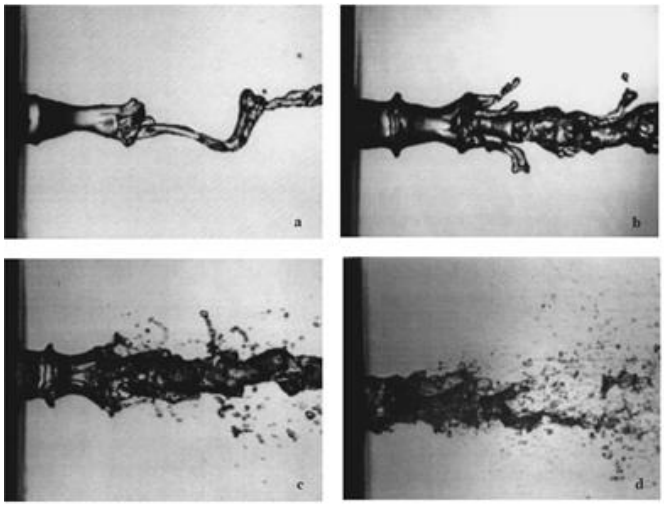

Figure 15: Images of jet breakup by a coaxial gas flow at various ratio of liquid to gas velocity

Onset of spray formation can be seen in figure c, whereas a more developed spray is seen in figure d. The latter situation is more favourable for a rocket engine as it allows for a shorter design of the combustion chamber.

For attaining a good fill of the combustion chamber and a proper combustion efficiency while limiting the size of the combustion chamber, it is important that the jet breaks up into small droplets and fills up the chamber. In general, it follows that the smaller the droplets, the larger the area of the liquid is that is in contact with the surrounding flow. As a result, this leads to improved vaporization and the subsequent combustion. How good a jet fills up the chamber and how small the droplets are is determined by the spray properties of the jet.

A spray is roughly defined by four parameters (Fig. 1): the spray tip penetration S, the spray (cone) angle θ, the break-up length L_b (or liquid length) and the global Sauter mean diameter (SMD) x_{32}.

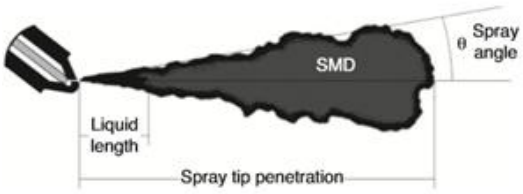

Figure 16: Different spray parameters

Of these, the breakup length (liquid length) in figure gives the length of the continuous liquid jet past the nozzle exit, whereas the spray cone angle and the spray tip penetration define the size of the spray in macroscopic terms. The SMD is defined as the diameter of a drop having the same volume/surface area ratio as the entire spray. It is generally given by:

$$\bar{x}_{32} = \frac{\sum_{i=1}^{N_{drops}} d_i^{\,3}}{\sum_{i=1}^{N_{drops}} d_i^{\,2}} \tag{5-3}$$

Where d_i is diameter of individual droplet i and N_{drops} is total number of droplets in spray. Typically, the size of the droplets shows quite a variety. In that case the SMD allows for a simple means of typifying the droplet size, whereas it also turns out to be of more physical meaning that just the average droplet diameter. The spray characteristics we are looking for are:

- Cone angle: Cone angle should allow for distributing the propellant over some known cross-section within a short distance.
- Droplet velocity: Droplet velocity should be small enough to allow for evaporation and subsequent combustion to take place in the chamber.
- Droplet size: Combustion efficiency tends to increase with decreasing droplet size as smaller droplets have a higher ratio of surface area to volume (hence the importance of SMD) than large droplets. On the other hand, for wall cooling purposes there may be a need for the spray to penetrate the chamber. Often, spray penetration is improved by increasing the droplet size. Controlling droplet size is therefore essential.

5.2.2. Required droplet size

Through injection, droplets are generally given some velocity in the direction of the chamber outlet. It is this velocity together with the length of the chamber that determines the stay time of a droplet in the chamber. If the velocity of the droplet remains constant, it can easily be found that a droplet travelling at 20 m/s only needs 25 ms to travel an 0.5 m chamber length. Given that in this this the droplet not only has to evaporate but also has to mix and give out is reaction energy, even less time is available for evaporation.

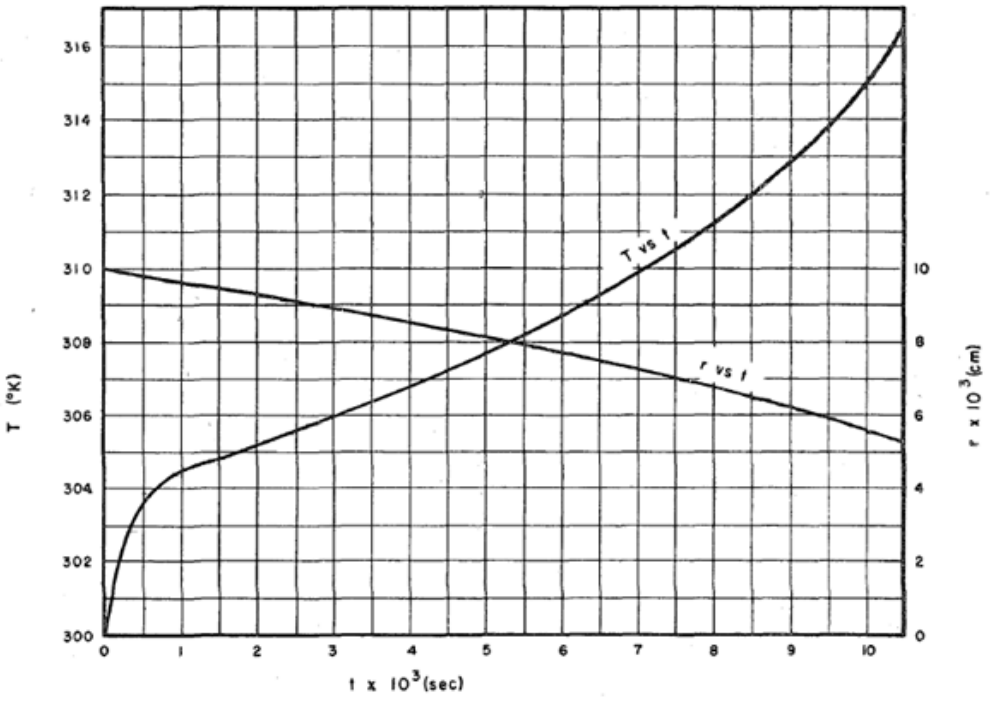

Figure 17: Temperature and size (radius) history for a hydrazine droplet surrounded by hot gases at 3000 K; Initial droplet temperature is 300 K and initial droplet radius is 100 micrometre [Penner]

From the figure we learn that after 10 ms, the droplet size has reduced from an initial value of 100 μm to almost 50 μm and hence almost double the time would be needed to make sure the droplet is fully evaporated before leaving the combustor. As SMD gives an average value, the SMD should be chosen below 100 μm as otherwise too many droplets will leave the engine not fully evaporated.

How quickly a droplet evaporates depends on amongst others the heat of vaporization of the liquid propellant as well as on the amount of heat transferred from the hot gas to the

liquid surface. The latter depends on the temperature difference between the hot gas flow and the droplets and the coefficient of convective heat transfer.

A simple relation for the rate at which the droplet reduces can be determined assuming that, at every time step, the heat flowing to the droplet is balanced by the liquid evaporated. It follows for each time step:

$$q \times S = m_{vap} \times \Delta H_{vap} = dr \times \rho_{liquid} \times S \times \Delta H_{vap} \tag{5-4}$$

Where q is net heat flux to droplet, S is surface area of droplet, $\rho_{liquiid}$ is mass density of liquid, dr is thickness of thin shell being vaporized per unit of time (surface regression rate) and ΔH_{vap} is enthalpy rise needed for liquid vaporization. The latter is not necessarily identical to the heat of vaporization as this assumes that the whole droplet has been heated up to the vaporization temperature.

Simplifying the above relation by dividing out the surface area of the droplet and after some reworking follows:

$$dr = {}^{q}\!/_{\rho_{liquid}} \times \Delta H_{vap} \tag{5-5}$$

Assuming heat flux, mass density and enthalpy change to be constant, it follows that the thickness of the vaporized layer is constant in time and hence, we find that the droplet diameter varies linearly with time:

$$d = d_o - 2dr \cdot t \tag{5-6}$$

Here d is instantaneous droplet diameter, d_o is initial droplet diameter and t is time.

In practice, droplet vaporization is slightly more complex as, for instance, the droplet temperature is not constant, see Figure 17, with a tendency for the temperature rise to increase with decreasing size of the droplet. This will of course affect the heat flux as well as the enthalpy needed for vaporization. More importantly, also the coefficient of heat transfer itself may vary depending on the droplet size. More detailed analysis has led to a variety of different theoretical models of which the d^2 law of droplet vaporization is one [Godsave]:

$$d^2 = d_o^2 - \lambda t \tag{5-7}$$

Here λ is a vaporization constant, which can be determined from experiments or from more detailed modelling.

5.2.3 Important parameters governing the spray parameters

From the foregoing follows that controlling droplet size is essential. For this a good understanding of the atomization behaviour is needed including the recognition of the impact of the injected fluid(s). From experiments, it shows that the main parameters which affect the spray characteristics generally are the geometry of the injector, the velocity with which the jet is injected (injection velocity), the interaction with other jets and of the respective jets with the environment, the diameter (and length) of the injector tube (discharge orifice), and the properties (mass density, surface tension, viscosity) of the fluid(s) being injected. For design purposes, these parameters are generally grouped into 2/3 dimensionless numbers of importance for jet breakup.

The first dimensionless number is the Reynolds number (Re), which can be thought of as a measure for the relative importance of momentum forces to viscous forces. For a jet discharged from an injector element, it is generally written as:

$$Re = \frac{\rho \cdot v \cdot d_j}{\mu} \tag{5-8}$$

Where:

- ρ is density of the liquid injected
- v is injection velocity
- d_j is initial jet diameter
- μ is dynamic viscosity of the liquid.

The second dimensionless number is the Weber number (We), which can be seen as a measure of the relative importance of the fluid's inertia (or drag experienced by the jet) compared to its surface tension. It can be written as:

$$We = \frac{\text{Inertia}}{\text{Surface tension}} = \frac{\rho_{gas} \cdot v^2 \cdot d_j}{\sigma} \tag{5-9}$$

Where:

- ρ_{gas} is density of the surrounding air.
- σ is the surface tension of the liquid.

The latter relation is modified in the case of coaxial injection in that the velocity v is taken to be the relative velocity between the liquid jet and the coaxial gas flow.

Figure 18 [Hulka, 2008] shows typical jet break up regions in relation to Reynolds number and Weber number for coaxial injection. Oxidizer is injected as liquid whereas the fuel is injected as gas. Since oxidizer is the least volatile, it is the determining component for jet breakup. Also shown in figure are various rocket engines employing coaxial injection. The figure clearly shows that injectors for rocket engines are operating in the turbulent regime and atomization regime.

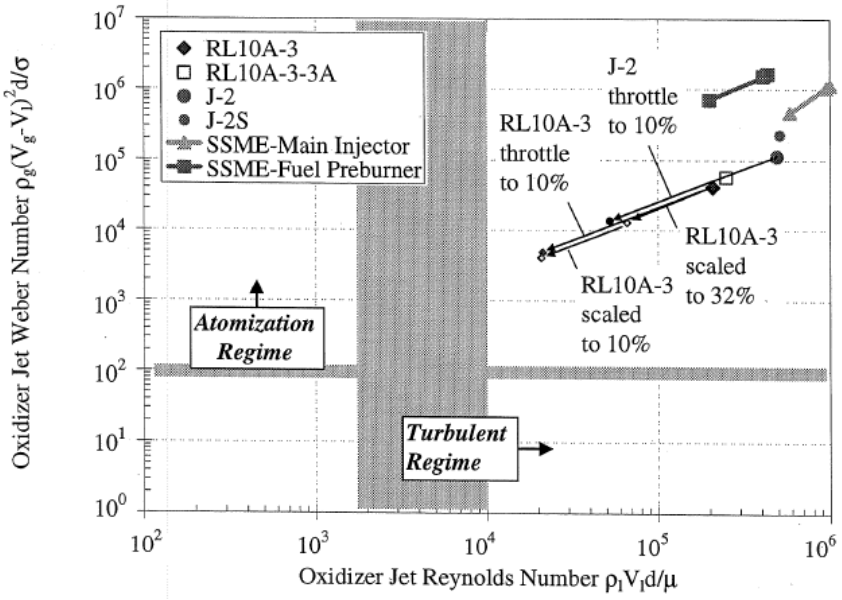

Figure 18: Values of Weber number and Reynolds number for a range of rocket engines with coaxial injection

Typically, we find that for a given injector geometry that Reynolds and Weber number increase with increasing mass flow rate, i.e. increasing jet velocity. Using water as the fluid to be injected via a 1 mm diameter cylindrical injector element, it follows a minimum mass flow rate (m) of about 10 mg/s is needed to attain Re in excess of 10,000 and We more than 100. With increasing mass flow and hence injection velocity both numbers will further rise. Some further values are given in next table.

m [g/s]	v [m/s]	Re [-]	We [-]
1	1.273	1.43E3	17.5
5	6.366	7.15E3	87.4
10	12.73	1.43E4	174.8
50	63.66	7.15E4	874
100	127.3	1.43E5	1747.5
500	636.6	7.15E5	8737.

Table 2: Effect of mass flow rate m on injection velocity v, Re and We for 1 mm diameter cylindrical injector element using water at standard conditions as injected fluid and zero gas velocity, i.e. no gas flow.

It shall be clear that in case of a high gas velocity co-flow, Re and We can be significantly increased compared to the case with no co-flow. However, this effect is significantly influenced by the amount of gas in the co-flow. This can be signified by the gas to liquid momentum ratio (MR) or the momentum flux ratio (MFR), defined as[2]:

$$\mathrm{MR} = \frac{\rho_{\mathrm{gas}} \cdot \left(\mathrm{v}_{\mathrm{gas}}\right)^2 \cdot \mathrm{A}_{\mathrm{gas}}}{\rho_{\mathrm{liquid}} \cdot \left(\mathrm{v}_{\mathrm{liquid}}\right)^2 \cdot \mathrm{A}_{\mathrm{liquid}}} \tag{5-10}$$

$$\mathrm{MFR} = \frac{\rho_{\mathrm{gas}} \cdot \left(\mathrm{v}_{\mathrm{gas}}\right)^2}{\rho_{\mathrm{liquid}} \cdot \left(\mathrm{v}_{\mathrm{liquid}}\right)^2} \tag{5-11}$$

Both ratios are in use, although the latter one seem more favoured for atomization studies. Typical values for gas to liquid momentum flux ratio in hydrogen-oxygen rocket engines with liquid oxidizer injection and gaseous hydrogen injection are in range from 1-15 (see slide in presentation slide deck), but higher ratios are under investigation as a higher momentum ratio leads to more efficient mixing and atomization. Note that this momentum (flux) ratio also plays a key role in the design of impinging injectors.

Various relations exist that describe the droplet size (distribution), cone angle and penetration for different types of injector elements. For instance, typical relations for drop size for various types of injector elements can be obtained from [NASA SP-8089] and information on spray angle and droplet size distribution etc. can be obtained from amongst others [Lefebvre]. A warning is given to not blindly apply correlations obtained from others. For instance, in a study on the RL10 LRE shear coaxial injector, predicted droplet size (SMD) using existing correlations ranged between 0.1 μm to 900 μm for LOX/GH2 and between 7 μm and 100 μm when replacing the propellants by water and air [Rahman]. This in part is attributed to the quite different Re and We range for which the correlations taken from literature were obtained. Additionally, it is given for consideration that also combustion itself may affect the atomization as heat transfer may cause a rise in temperature of the fluid and hence will affect the fluid properties.

Since some time, numerical flow solvers have progressed to a point where it becomes possible to simulate in more detail the atomization occurring for simplified geometries. At TU-Delft [Pal] is the first who investigate the usefulness of such simulations for actual design purposes or rocket injector elements. Results showed to be very promising, but not yet to the point where the results could be applied to an actual design.

5.2.4. Sizing of the injector elements

From the foregoing, it should be taken that it is important to attain high values of Re and We and that (for a given fluid) this leads to high injection velocities. A disadvantage of the high injection velocities is that also the accompanying pressure drop increases and hence more power is needed to pressurize the fluids. In general, one tries to limit the pressure drop to the bare minimum. In case the pressure drop becomes too high, one starts looking for an alternative configuration that allows for better atomization properties

[2] In some works, the investigators use liquid to gas momentum (flux) ratio.

at reduced pressure drop. In this section, we will discuss the role of the injector elements in the pressure drop attained. But first, we will discuss the manufacturability of the injector element.

Although in general the smaller the discharge orifice is, the smaller the droplets, practical values for the diameter of the discharge orifices are limited to orifice diameters in range 0.5-3 mm. The advantages of a large diameter are:

- easier to drill.
- easier to align impinging elements.
- unlikely to encounter combustion instability.
- less contamination sensitive.

The length of an orifice is usually chosen such that the length to diameter ratio of the orifice is more than 4 (L/D > 4) and preferably around 10 to allow for fully developed flow. This minimum length to diameter ratio is necessary to prevent the occurrence of hydraulic flip, i.e. separation[3] of the flow from the orifice wall. It reduces the mass flow rate of propellant and causes the mis-impingement of impinging type injectors. Detached flow can be counteracted by further increasing the pressure which causes the flow to reattach.

Injector pressure drop

For good injection characteristics a high injection velocity is needed. However, with increasing injection velocity the pressure drop occurring over the injector plate increases. This pressure drop comes from the changes in the flow that occur because of the change in flow channel geometry as well as from increased friction losses due to an increased velocity in the injector elements/tubes. In the next few pages some fundamentals will be presented.

An injector element can be considered as a succession of two joints of coaxial pipes of different diameters, see illustration below. In case of an injector flow, the liquid flows from a large manifold into the injector tube from where it is injected into the large combustion chamber.

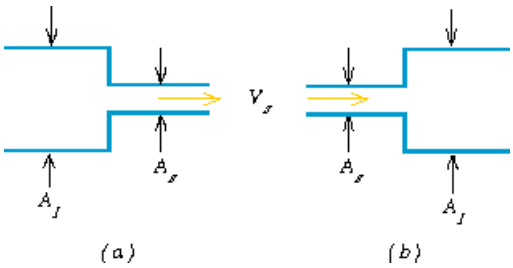

In case of a flow of an incompressible medium from a large vessel into a small duct (compare the flow of water from a bottle through the neck of the bottle), we can use Bernoulli's equation:

$$p_0 + \frac{1}{2} \cdot \rho \cdot v_0^2 = p_1 + \frac{1}{2} \cdot \rho \cdot v_1^2 \tag{5-12}$$

For $v_0 << v_1$:

$$\Delta p = \frac{1}{2} \cdot \rho \cdot v_1^2 \tag{5-13}$$

[3] An abrupt change of flow direction at the orifice entrance reduces the local static pressure up to the saturation pressure, and cavitation bubbles appear at the location. These bubbles make the inner flow highly turbulent, and thus jet characteristics become dependent on the flow time. The development of cavitation bubbles can cause the liquid flow to separate from the orifice wall.

In practice, some losses e.g. due to friction and possibly flow separation occur associated with how well the contraction/convergent and/or divergent/expansion are formed, and we find an additional pressure drop that cannot be recovered when bringing the flow to a complete stand still, i.e. it affects the total pressure in the flow. This pressure loss is generally expressed as:

$$\Delta p = \zeta \cdot \frac{1}{2} \cdot \rho \cdot v^2 \tag{5-14}$$

Here the pressure loss is defined in terms of a (dimensionless) loss coefficient ζ (also referred to as resistance coefficient), and the dynamic pressure in the smaller pipe [Bejan]. Of these the pressure loss coefficient depends mainly on the shape of the contraction and/or expansion. Essentially all changes of the flow cross-section may cause pressure loss due to friction effects. Here we focus on contractions and expansions as experienced in an injector element.

For a sudden contraction (turbulent flow) the loss coefficient depends upon the area ratio as shown in the following table.

Table 3: Loss Coefficient for Sudden Contractions

A_s/A_l	0	0.1	0.2	0.3	0.4	0.6	0.8
ζ_c	0.50	0.46	0.41	0.36	0.30	0.18	0.06

The results in the table can be approximated using[4]:

$$\zeta_c = 0.5 \cdot \left(1 - \frac{A_s}{A_l}\right)^{3/4} \tag{5-15}$$

For a sudden expansion we find:

$$\zeta_e = \left(1 - \frac{A_s}{A_l}\right)^2 \tag{5-16}$$

In case of a compression, followed by an expansion, the total loss factor is given by:

$$\zeta = \zeta_e + \zeta_c \tag{5-17}$$

Note that if more changes in flow cross-sectional area occur, the above sum can be extended to include a term for each of the expansions/contractions.

In the limit case where the area of the combustion chamber and the flow cross-sectional area of the injector manifold are much larger than the cross-sectional area of the injector hole, we find for the compression loss factor a value of 0.5 and for the expansion loss factor a value of 1. This then would indicate a total loss factor of 1.5 for the injector. By making the transition between the two areas more gradual, the loss factor is reduced. What should be clear though is that the pressure loss greatly depends on the injection velocity and hence for a low pressure drop, the injection velocity should be kept low.

[4] In literature, this relation is written in different ways as it has a semi-empirical character. The most convenient way of writing is:

$$\zeta_c = \frac{K_{compression}}{2} \cdot \left(1 - \frac{A_s}{A_l}\right)$$

Here K is a constant, which depends on the geometry (sharp or with rounded features and the Reynolds number). Relation given in text is a 'best' fit to the data given in table shown above the relation. This led to a modified exponent (not 1 but 0.75).

Once the loss factor is known (either from theory or from calibration measurements, see later), the injection velocity can be determined based on the pressure drop measured over the injector. It follows:

$$v_i = \sqrt{\frac{1}{\zeta}} \cdot \sqrt{\frac{2 \cdot \Delta p}{\rho}} \tag{5-18}$$

Multiplying the injection velocity with the injector cross-sectional area gives the volumetric flow rate (Q) and multiplying the latter with the mass density gives the mass flow rate. Using the earlier definition of the discharge coefficient (m_{real}/m_{ideal}), we obtain:

$$C_d = \sqrt{\frac{1}{\zeta}} \tag{5-19}$$

Here C_d is the discharge coefficient, which essentially is a down rating of the area of an orifice or nozzle due to flow separation or friction. Like the total loss factor, it is a dimensionless parameter characteristic for the shape of the injector and strongly related to the flow conditions in the injector. Using the earlier calculated value of 1.5, we find a value for the discharge coefficient of about 0.82 (value of 1 means no loss). In practice, for a well-shaped injector nozzle a value between 0.5-0.7 is feasible. More specific values of the discharge coefficient for a range of injector elements can be taken from [Sutton].

Figure 19 shows typical pressure drop (loss) over an injector with a discharge coefficient of 0.7 in relation to injection velocity of a fluid with a mass density of 1000 kg/m^3.

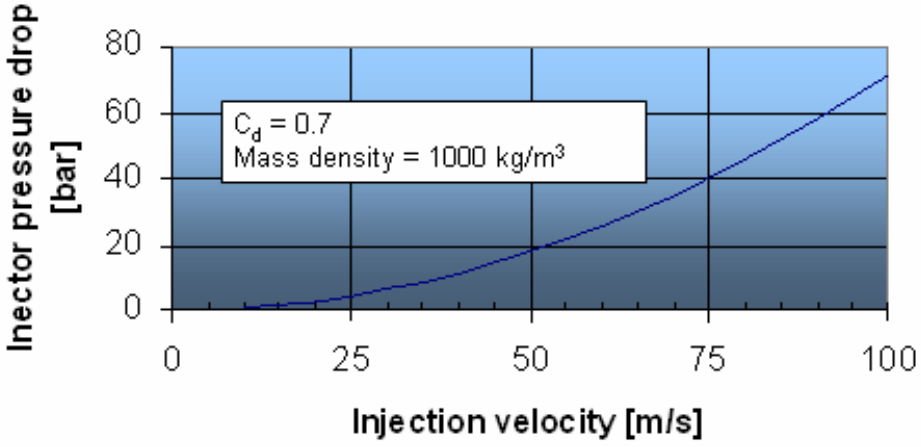

Figure 19: Injector pressure loss

For small thrusters that usually operate at low feed pressure, we find that injection velocity should be below about 40 – 50 m/s (depending on the liquid density) as else the pressure drop becomes too high. For motors operating at higher pressures, higher injection velocities are possible. For motors using hydrogen, even higher velocities are possible, since hydrogen density is about a factor 10-15 lower than for most common propellants. Another solution of course is to adopt other injector elements that allow for a lower value of the discharge coefficient.

Minimum pressure drop required for stability

Given the minimum pressure drop required [Huzel et al], [Humble], we also find that there is a minimum value for the injection velocity regarding stability. Based on a minimum pressure drop of 20% we find for a liquid with a density equal to water a minimum injection velocity of about 25 m/s at a chamber pressure of 20 bar.

Mass flow rate

Total mass flow rate through the injector can be obtained by combining relations (5-2) and (5-18). This gives:

$$m = C_d A\sqrt{2\rho}\sqrt{\Delta p} = c\left(\Delta p\right)^{0.5} \tag{5-20}$$

Here c is some constant that depends on the fluid mass density, the injector cross-sectional area (depends on cross-sectional area of single injector and the number of injector elements) and the injector geometry. From the relation we learn that with increasing mass flow rate the pressure drop increases.

In case of bipropellant motors the two propellants each may experience a different pressure drop even though the chamber pressure is equal for both. Also with varying mass flow rate, the pressure drop may differ slightly and may cause a change in mixture ratio, see also the next section.

Orifice diameter ratio [NASA SP-8089]

According to the orifice diameter ratio for unlike-impinging doublet elements flowing liquid fuel and liquid oxidizer must be close to one to attain optimum mixing. An optimum seems to lie at about 1.22. Beyond this value, the level of mixing suffers dramatically. For like-impinging doublet elements, the orifice sizes of the impinging jet are kept equal. For non-impinging showerhead elements, the ratio of orifice diameters has no effect on mixing. Still the size of the injector element greatly determines the mixing and atomization attained. For coaxial elements a mixing decrease has been reported when the ratio of annulus width to centre-jet diameter increases.

Jet angle [NASA SP-8089]

Impinging types of injectors, disintegrate a jet by impact with one or more other jets. The level of disintegration is governed by amongst others the velocity of the jets, and the angle at which they intersect. The angle between a jet and the chamber axis is referred to as the jet angle, γ. In case of two jets with respective jet angles γ_o and γ_f, we find that the resulting angle γ_r is determined by the respective momentum, see Figure 20.

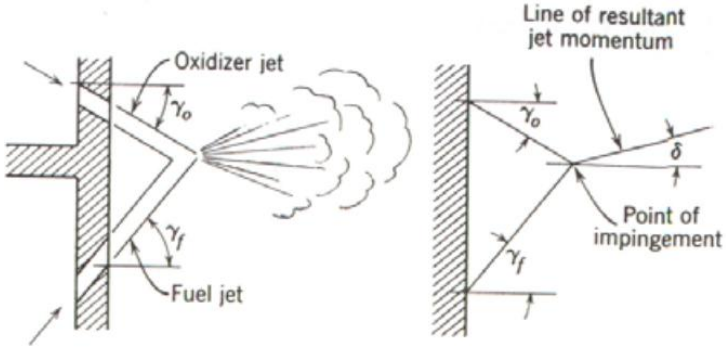

Figure 20: Impinging injector flow geometry [Huzel]

It follows[5]:

$$\tan\gamma_r = \frac{m_o \cdot v_o \cdot \sin\gamma_o - m_f \cdot v_f \cdot \sin\gamma_f}{m_o \cdot v_o \cdot \cos\gamma_o + m_f \cdot v_f \cdot \cos\gamma_f} \tag{5-21}$$

The larger the angle between the two jets, the better the droplet formation (drop size decreases about proportional to impingement angle). However, with increasing angle also backsplash increases as well as heat transfer to the injector face, with the associated danger of injector-face burn-out. Typical angles are in between 40-80 degrees. In case of like-on-like impingement, the jet angle is identical for both jets. In case of unlike impingement, this may differ, depending on the criterion used for the

[5] Notice that the angle δ and γ_r are not identical.

momentum of the combined jet. In most cases we try to have zero momentum in radial direction and the jet travelling in axial direction.

Impingement distance for doublets or triplets should be about 5 to 7 orifice diameters in order to limit the heat loads on the injector face.

Water flow calibration

The injector discharge coefficient is usually determined experimentally. This is sometimes referred to as calibration of the injector. It is usually performed by recording pressure differences versus mass flow rate. The latter is determined using weighing tanks and time recordings. Use can also be made of volumetric flow rate, in case we have a scale on the tank.

$$Q_i = C_d \cdot A_i \cdot \sqrt{\frac{2 \cdot \Delta p}{\rho}} \tag{5-22}$$

Here Q is the volumetric flow rate.

Care should be given to the fact that the discharge coefficient changes with changing Reynolds Number and is correct for only one set of conditions. This is an important point and cannot be stressed enough.

Water flow calibration can also be used to check the flow pattern and orifice alignment, see Figure 21.

Figure 21: Water spray test (courtesy Armadillo Aerospace)

Injector structural design loads

According to [Huzel et al], the main loads to be considered in the structural design of the injectors result from propellant pressures behind the injector face and in the manifolds. During steady state operation, the pressure load on the injector face is equal to the injector pressure drop:

$$p_{inj} = \Delta p_i \tag{5-23}$$

During start transients, however, maximum pressure loads on the injector may be substantially higher than during steady state. When the propellant valves are opened rapidly, severe hydraulic ram can occur. This pressure load can be estimated empirically as:

$$p_{inj} = 4 \cdot \Delta p_i \tag{5-24}$$

Development

The development of a rocket injector is a costly business. For example, in 2003 GenCorp Aerojet was awarded a $485,000 contract to design and test a high performance/high technology rocket injector, using MON-25/Monomethyl hydrazine propellants, for use in a Martian-simulated environment. The development will be a seven-month effort. The initial effort of the program will focus on injector design characteristics required to produce high performance and stable combustion using low temperature propellants which have freezing points below -50 °C, like the Martian environment. Subsequent phases will further develop, and test new-technology lightweight components intended for the final flight version of the engine.

5.3 Combustion

As a first approach, liquid propellant combustion can be modelled using chemical equilibrium chemistry. For this RPA or the NASA CEA tool, which have been described earlier (see chapter on equilibrium chemistry) can be used. Both RPA and NASA CEA output the theoretical properties of the combustion mixture in the chamber. How well this model compares with reality can be determined from the combustion quality. Combustion quality (or c* efficiency) can be determined from experiments or even more detailed modelling considering all intricacies of non-equilibrium chemistry and heat loss to the chamber wall. Figure 22 [Hulka, 2010] shows a typical result of such a more detailed model. The figure clearly shows that the c* efficiency increases with increasing distance to the injector face. However, at about 10 inches (~25 cm) from the injector face, the c* efficiency already is close to the limit value. Making the chamber much longer is not useful and only adds to the mass of the combustor and hence the engine.

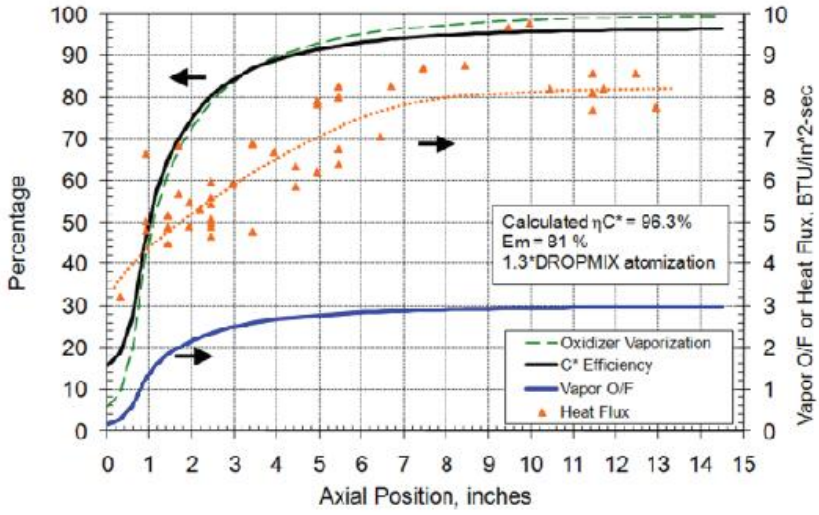

Figure 22: Results of detailed theoretical analysis of combustion in a liquid oxygen – methane combustor [Hulka, 2010]

Results also show the amount of oxidizer vaporization, which increases from about 0% to almost 100% at 10 inches from the injector face. This of course depends on the level of atomization attained by the injector.

The length needed for the combustor to allow for proper combustion depends on the propellants (hypergolic or not) and all the processes of importance for combustion. This is illustrated in Figure 23. Figure 23a shows the processes involved in the combustion of a hypergolic (self-igniting) propellant. Two different flame types can be distinguished. The first type is a diffusion flame, where the fuel and oxidizer are originally separated and the mixing and the reaction take place at the same time. The second type is a premixed flame, wherein the fuel and oxidizer are mixed before reaching the flame.

The combustion process for non-hypergolic propellants is somewhat similar. The possible reaction phenomena are shown in Figure 23b. Combustion takes place either in

a heterogeneous mixture of a liquid or gaseous phase or in a homogeneous mixture of atomised propellants. In the first case droplets of one of the propellants will react with the surrounding gas of the other propellant in a diffusion flame. In the second case, the homogeneous mixture of gases reacts with a premixed flame.

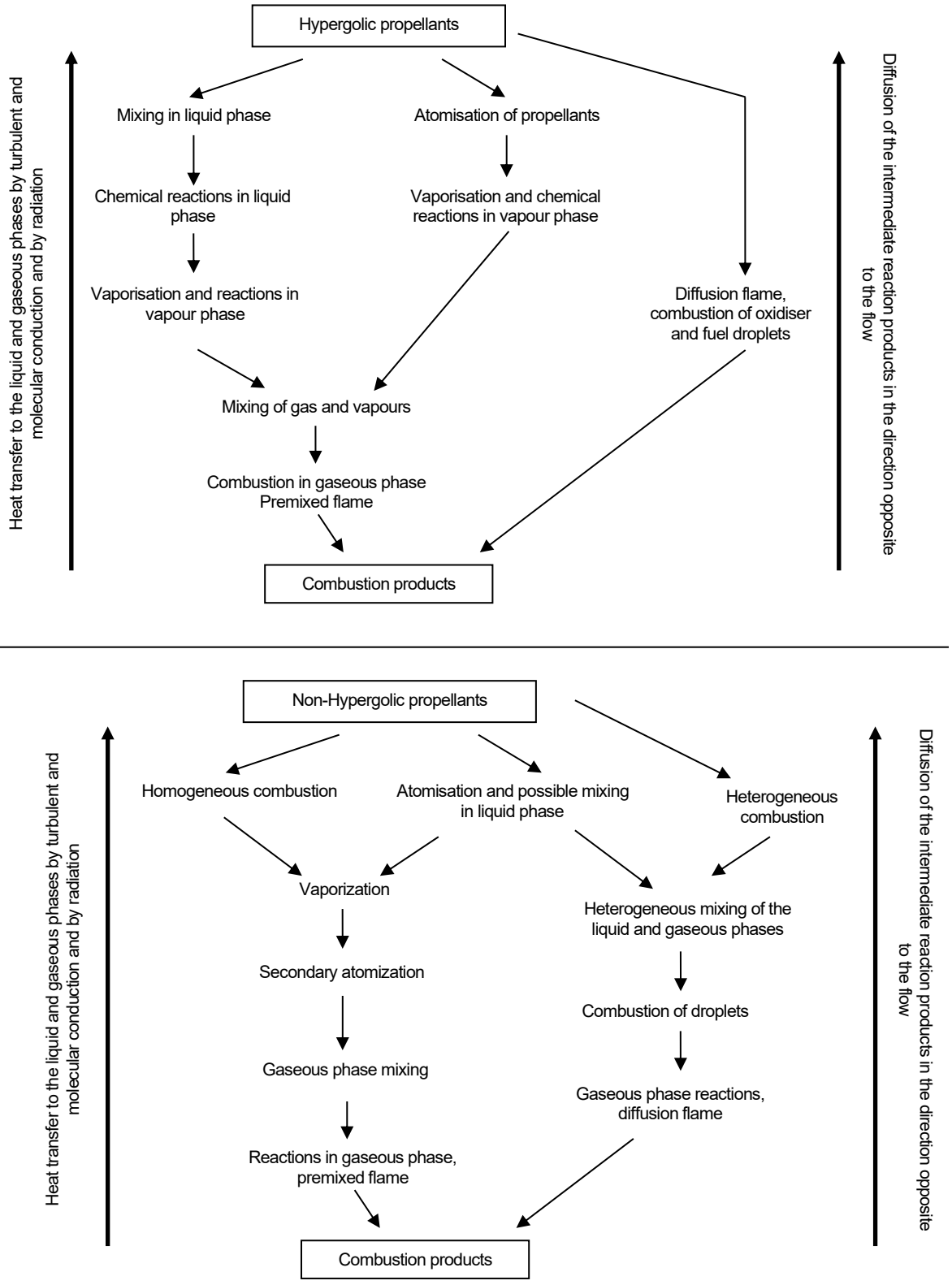

Figure 23: Schematic representation of combustion in a rocket motor; A) hypergolic mixture, B) non-hypergolic mixture

The time available for the flow to vaporize, mix, etcetera is called the *dwell time* or *residence time* and can be expressed as:

$$\tau = L_c/U_c \tag{5-25}$$

L_c is length of combustor and U_c is (average) flow velocity in combustor. Multiplying denominator and numerator with the gas density in the chamber, ρ_c, and the chamber cross-sectional area, A_c, we get:

$$\tau = \rho_c \cdot L_c \cdot A_c/(\rho_c \cdot U_c \cdot A_c) = \rho_c \cdot V_c/m \tag{5-26}$$

Here V_c is chamber volume and m is mass flow rate.

Using an earlier derived expression for the characteristic velocity, we get:

$$\tau = \frac{\rho_c \cdot V_c}{p_c \cdot A_t} \cdot c^* = \frac{1}{R \cdot T_c} \cdot c^* \cdot \frac{V_c}{A_t} = \frac{1}{\Gamma^2} \cdot \frac{1}{c^*} \cdot \frac{V_c}{A_t} = \frac{1}{\Gamma^2} \cdot \frac{L^*}{c^*} \tag{5-27}$$

Here we introduce the *characteristic length*, L*, which is defined as the ratio between the chamber volume and the throat area, A_t:

$$L^* = V_c/A_t \tag{5-28}$$

L* is a constant that depends on the type of propellant. Typical values for L* can be obtained from Table 4.

Table 4: L* values for specific propellants

For gaseous oxygen/hydrocarbon fuels, an L* of 1.25 to 2.5 m is appropriate. For liquid rocket propellants: Huzel and Huang (1992): - oxygen-kerosene: 1.02 < L* < 1.25 m - oxygen-hydrogen: 0.76 < L* < 1.02 m - oxygen-hydrogen (hydrogen is injected as gas): 0.56 < L* < 0.71 m - nitrogen tetroxide/hydrazine-based fuel: 0.60 < L* < 0.89 m - hydrogen-peroxide/RP-1: 1.52 < L* < 1.78 m (including catalyst bed) Barrère et al. (1960): - oxygen- ethyl alcohol: 2.5 < L* < 3 m - nitric acid - UDMH: 1.5 m < L* < 2.5 m - nitric acid - hydrocarbons: 2.0 m < L* < 3.0 m and Dadieu, Damm and Schmidt: - LOX - gasoline: 1.5 m < L* < 2.5 m - nitric acid - UDMH: 1.5 m < L* < 2.0 m - nitromethane (monopropellant): L* = 4.0 m (including catalyst bed)

This shows that the minimum chamber size that still guarantees a satisfactory combustion process, is found from the minimum value of L*. The residence time depends most on the slowest process taking place in the chamber; this is generally the vaporization of the propellants.

As far as large-sized combustion chambers are concerned, it is possible to detect a trend in the evolution of the shape, see Figure 4. When the first chambers were developed, the design of the injection system and nature of the propellants were such that, to obtain a satisfactory combustion quality, it was necessary to employ long combustor lengths. The chamber cross section was large compared to the throat area to ensure low heat transfer to the wall. Progress made in injection and cooling techniques, the development of new

materials made it possible to reduce the length of the chamber and to also reduce chamber diameter (assuming a cylindrical design).

5.4 Combustion stability

Combustion instability, or “dynamic instabilities” refer to damaging oscillations driven by fluctuations in the combustion and are a key risk to any rocket development program. In current testing practice any detectable vibration is generally the signal.

Instability in the combustion is associated with oscillations in pressure which leads to an increase of local heat transfer rates, see Figure 24.

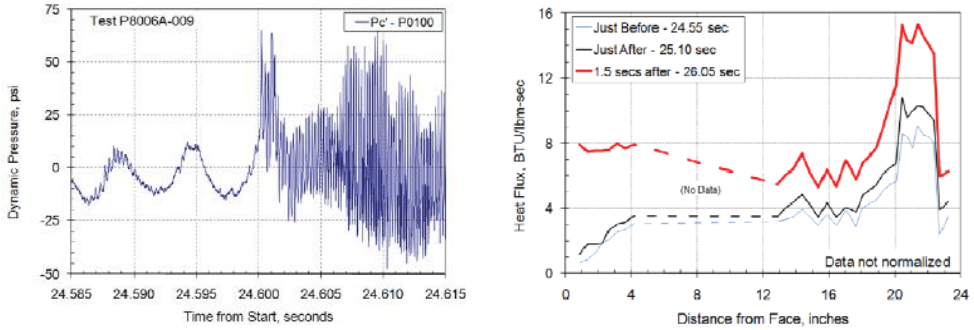

Figure 24: Pressure trace (left) and heat flux (right) data for rocket engine experiencing instabilities [Hulka]

From the figures, we should learn that up to about 24.6 second in the burn, combustion is stable. After that severe pressure oscillations occur, which seem to become more severe in time. The right figure shows three lines for the heat flux distribution throughout the engine. Lower line gives heat flux distribution before onset of instability and top line shows heat flux distribution sometime after onset of instability. The results clearly shows a 2-4 fold increase in heat flux depending on the location. Recently [Govaert] has developed a model that allows for determining the effect of instabilities on flame length (an implicitly also on liquid breakup length] and hence on heat transfer.

This increase in heat flux may lead to burning of the injector plate or other walls as shown in next figure.

Figure 25: Damaged injector plate as a result from combustion instability (courtesy NASA)

At worst, the combined pressure oscillations and increased heat transfer rates may lead to a total engine failure.

Combustion by nature is accompanied by pressure oscillations and not all oscillations lead to excessive heating and or worse failures. Various degrees of unstable combustion are distinguished:

- Stable: Pressure oscillations occur, but they seem to be of a constant nature. We tend to speak about rough combustion; NASA specifications allow up to 5% of the chamber pressure oscillations for stable combustion [Huzel et al 1992].

- Mildly unstable: The growth in amplitude of the pressure disturbance is limited over the time considered and can be dealt with.
- Very (or highly) unstable combustion: This is in case of significant and continuously growing or amplified pressure oscillations in the combustion chamber.

What to do if oscillations are a problem depends on the cause of the instability. Instability may stem from several causes that are typically associated to the frequency of the oscillations. Three frequency ranges are commonly distinguished:

- Low frequency: Chugging mode
  Characteristic frequency range is between 10 and 200 Hz. This instability occurs due to an interaction between the chamber and feed system.

One low frequency phenomenon experienced in liquid propelled rockets is POGO. In a liquid-fuelled vehicle, the engine pumps propellants through feed lines to the engine's thrust chamber. Inevitably, the tanks, feed lines, and engine vibrate during lift-off and ascent. This vibration causes the flow of the propellants in the feed lines and engine to oscillate, leading to thrust oscillation. This oscillation can cause the structure to vibrate even more, which increases the fluid oscillations, which causes greater vibration, and so on in a progressive feedback loop.

- Medium frequency: Buzzing mode
  Characteristic frequency range is (arbitrarily) between 20 and 1000 Hz. This instability is a result from either flow instabilities or resonance with chamber structure

- High frequency: Screaming mode
  Characteristic frequency range is above 1000 Hz. This instability is due to interactions of the combustion process with chamber acoustics

To prevent chugging, the feed system and chamber need to be decoupled. This can be accomplished by designing for a significant pressure drop over the injector well in excess of the 5% of the chamber pressure oscillations that are considered still acceptable. Injector pressure drop requirement differs with the type of injector considered. According to [Humble et al], the pressure drop requirement is 10-15% for unlike-impinging injectors and 20-25% for like impinging injectors. For concentric injectors, the pressure drop requirement may be as low as 5%.

To prevent medium frequency and high frequency instability other measures need to be considered that require more insight in the source of the instability. Over the years, a large amount of experimental work has been carried out, in different configurations, to identify the fundamental mechanisms. Theoretical analysis has also been developed to explain the processes leading to instability. More recently, numerical methods have been devised to test concepts and to develop descriptive models. A discussion of the modelling issues and methods which may be used to analyse combustion instabilities, and their active control can be found in [Candel].

5.5 Pressure drop due to flow acceleration

Fluid entering the chamber via the injector will vaporize and react forming a low-density gas mixture. Because of conservation of mass, this will lead to an increase in flow velocity. When the flow is turbulent, the velocity distribution across the chamber is relatively uniform, so that the longitudinal momentum of the flow is approximately equal to the product of mass flow and flow velocity. The change in longitudinal momentum must be balanced by the pressure difference applied between the two ends of the passage:

$$
\begin{aligned}
&-A \cdot dp = m \cdot dv \Rightarrow \\
&-A \cdot (p_i - p_c) = m \cdot (v_i - v_c) \approx -m \cdot v_c \Rightarrow \\
&p_i - p_c = \rho_c \cdot {v_c}^2 = \gamma \cdot p_c \cdot {M_c}^2
\end{aligned}
\tag{5-29}
$$

Here p_i is the pressure just behind the injector face, and p_c, v_c, and M_c respectively are the pressure, velocity and Mach number at the end of the combustion chamber just in front of the convergent section.

The static pressure drop occurring in the combustion chamber as a function of the Mach number is presented in Figure 26.

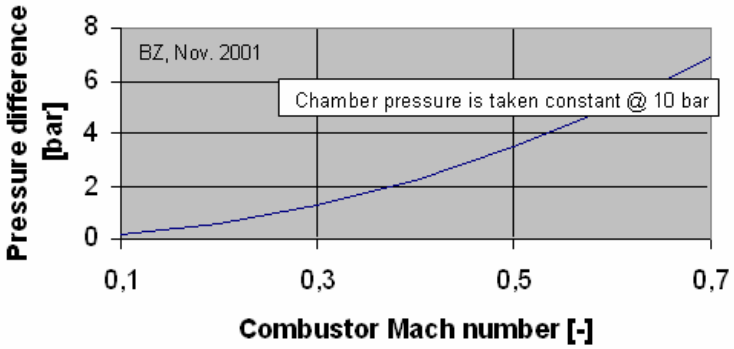

Figure 26: Pressure drop in combustion chamber

A low flow velocity is needed to allow the propellants to fully combust within the chamber. However, a too low a velocity will lead to a long chamber and hence a high combustor mass. Selecting a combustion chamber cross sectional area of about three times the nozzle throat area will result in a combustion chamber Mach number of about 0.3. In practical cases, the contraction ratio mostly is taken larger than 3. For example, for the HM-60 a value of 5 is used. Using the earlier determined HM-60 combustor volume, it follows for the length of the combustor a value of less than about ~ 0.2 m.

5.6 Catalyst bed

Important for the design of a catalyst bed is a large surface area in a small volume. Most hydrazine thrusters use a catalyst bed made from iridium impregnated alumina pellets 1.5 to 3 mm in diameter (smallest pellets in upper catalyst bed). An alternative is to use finely divided iridium on an aluminium oxide support or platinum-iridium mesh. A typical catalyst bed for a 1 N hydrazine thruster is 25 -50 mm long and 6.5 mm in diameter for a hydrazine loading of 0.015-0.060 gram/mm^2-s. Generally, iridium is present to the extent of 30% of the total catalyst mass. To allow proper operation of the catalyst, the catalyst bed may be conditioned by one or more heater elements.

In case of hydrogen peroxide propellant, silver wire cloth and/or silver-plated nickel screens are used as catalyst. Typical reactivity data for hydrogen peroxide with silver catalyst have been determined by [Bengtson] and are **9.4 to 11.4** g of 85% H_2O_2/(minute-cm^2) using silver plated nickel screens of 28 x 28 mesh, with a wire diameter of 0.19 mm. According to [Jonker], attention must be paid to differences in thermal expansion between the catalyst bed and the chamber as this might lead to a wet start. The nickel-based silver-plated screens increase temperature compatibility compared to silver wire cloth. Due to the melting points of both pure silver and brass, the concentration of hydrogen peroxide is kept at a maximum of 85%.

The life of the catalyst bed may be an important factor in thruster life. This is for instance the case for hydrazine thrusters, where life of the catalytic bed mainly depends on the degradation that occurs in the bed [Brown]. This depends on 1) mechanical failure of the catalyst pellets, and 2) reduction of catalytic activity caused by impurities on the surface

of the pellets. To avoid mechanical failure, the catalyst bed is preheated to a temperature of 200 -315 degree Celsius. To avoid reduction of catalytic activity, super-pure hydrazine is used.

The flow through a catalyst bed usually is accompanied by a strong pressure drop. This in part is associated with the reactions taking place, but also because the catalyst bed provides for flow blockage which must be overcome. A possible approach might be to use relations for the pressure drop that occurs for single phase flow through a tube filled with a porous medium, see for instance the work of Ergun [Levenspiel] and then add a correction for two-phase flow. However, further investigation is needed.

5.7 Chamber throat assembly

The design of the convergent is mostly aimed at reducing pressure losses due to the flow contraction; see sections on liquid injection and nozzle design. For small combustion chambers the convergent volume is about $1/10^{th}$ the volume of the combustor tube. Velocity, pressure and temperature of the hot gas in the convergent can be determined using ideal rocket theory. For Reynolds numbers (based on throat conditions) in excess of about 100,000, little or no build-up of a boundary layer occurs and hence there is little effect on the flow. For Reynolds numbers below about 1000, boundary layer effects may be much more pronounced.

5.8 Chamber material selection

Chamber materials used are primarily selected based on their ability to withstand the combined heat and pressure load as well as their compatibility with the coolant fluid. In addition, for multi-shot (pulsed) engines/thrusters, the resistance to fatigue as well as stress corrosion is important.

Choice of chamber material depends on the use of the material (structural material, insulation, and conductor) and considerations concerning strength, density, corrosion resistance[6], fatigue resistance, brittleness, etc. For an explanation of these terms, you are referred to for instance material handbooks. Material properties for a range of materials can be found in annex K.

An important parameter in the comparison of materials is the “specific strength”. This is defined as the ratio between strength and density. The higher the specific strength the stronger or the lighter the structure will be. Sometimes specific strength is expressed in m^2s^2. For example, for titanium, this gives a value of 23×10^4 m^2s^2.

5.9 Chamber wall thickness based on internal pressure

Once chamber shape and volume are determined, we can determine the chamber wall thickness. This thickness mainly depends on internal pressure and can be estimated using thin shell theory [Megson], see also chapter “Design of thin shell structures”. Internal pressure values depend on combustion pressure. This is usually in range from a few bars for small thrusters up to 200 bars for the Space Shuttle Main Engine.

Next to internal pressure, several other loads exist that should be considered when determining the wall thickness. Typical such loads are e.g. handling loads or because of thermal gradients.

[6] Material compatibility with a propellant is classified sequentially from Class 1 materials, which exhibit virtually no reaction with the propellant, to Class 4 materials, which react strongly with the propellant.

The use of thin-shell theory may also lead to very small thicknesses, especially in case of small thrusters and low pressures. In that case one may find that thickness is limited from manufacturing; minimum thickness is about 0.1-0.2 mm for stainless steel, 0.2 mm for aluminium, and 0.5 mm for titanium. In this section, we consider only the effect of internal pressure loading.

5.10 Chamber mass

Chamber mass estimation is discussed in detail in the chapter on thrust chamber mass estimation.

5.11 Chamber service life

A well-known phenomenon in the field of structural engineering is that repeated stressing of a material can cause failure, even when the applied stress is well below the yield stress. This is referred to as low cycle[7] thermal (due to differences in expansion) fatigue. According to [Sutton], low cycle fatigue is one of the most important causes of rocket combustion chamber failing with cracks sometimes appearing already after the first burn.

For more information, see the chapter entitled “Design of thin shell structures”.

5.12 Other chamber characteristics

Besides mass, and size also other parameters, like cost, reliability, and safety, are of importance to consider when designing a rocket thrust chamber. Below some parameters are briefly touched upon. Some further information can be obtained from [Wood].

Chamber production and development costs depend on chamber type, shape, size, and lot acceptance testing. Production costs furthermore depend on quantity. A simple cost model that provides a useful method for quick turnaround, rough-order-of-magnitude cost estimating of liquid rocket engines is the NASA/Air Force Cost model (NAFCOM), but various other sources are also available.

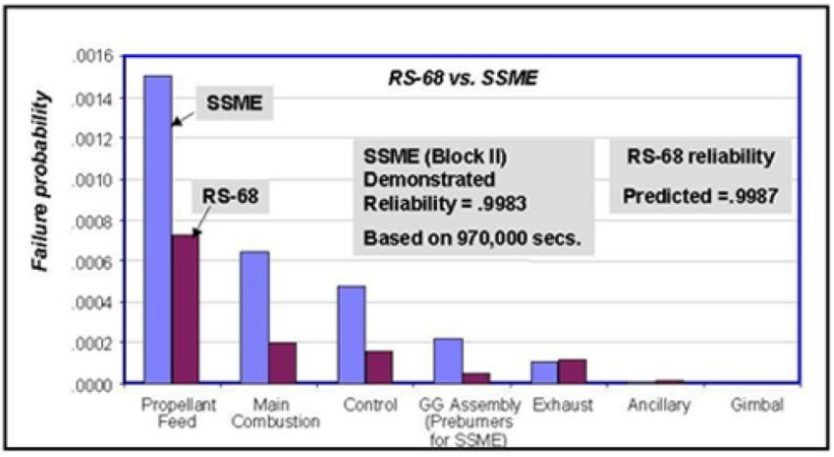

Figure 27: Failure probability of two large liquid rocket engines [Wood]

Above figure shows failure probability data for the main components of the SSME (demonstrated) and RS-68 (predicted) liquid rocket engines. It shows a demonstrated reliability (reliability = 1 - failure probability) for the SSME of 0.9983 and a predicted reliability for the RS-68 of 0.9987. In general, we can say that the simpler the engine is, the higher its reliability. For instance, pressure-fed monopropellant engines that are

[7] Less than 1000 cycles.

radiation cooled are considered of a much simpler design than the bipropellant, pump-fed, re-generatively cooled large rocket engines, like the SSME.

To estimate these characteristics for conceptual design purposes, it is advised to use either estimation by analogy or parametric estimation. For later stages, we can use either parametric, or engineering build up estimation. It is for the reasons of estimation that it is advised to develop a data base with actual (historic) values on the characteristics of interest and to the level of detail considered necessary.

Example

In this example, we consider the design of the combustion chamber of an MMH-NTO bipropellant thruster with vacuum thrust of 400 N and I_{sp} of 320 sec at a mass mixture ratio of 1.65. In this design, we will determine amongst others the length and diameter of the combustor, pressure drop over the chamber, injection velocity, and the number and size of the injector holes. We use as a given pressure at the injector end of the combustor of 10 bar, an L* value of 0.9 m and an injector discharge factor of 0.7.

For this propellant combination at this mass mixture ratio, chemical analysis has provided us with the properties of the gas mixture in the combustion chamber. In this example, we use a characteristic velocity c* = 1685 m/s, hot gas temperature in the chamber T_c = 3210K, molar mass of the combustion products is 22.1 gram/mole and specific heat ratio γ = 1.2

As a first step, we determine the total propellant mass flow rate and the fuel and oxidizer mass flow rate from the given thrust, specific impulse and mass mixture ratio. Total mass flow rate is:

$$m = F/\left(I_{sp}\cdot g_o\right) = 400N/\left(314s\cdot 9.81m/s^2\right) = 0.127kg/s$$

Mass flow rate of oxidizer follows using:

$$m_{ox} = \left(\frac{O/F}{O/F+1}\right)\cdot m = \frac{1.65}{2.65}\cdot 0.127kg/s = 0.079kg/s$$

This gives for the fuel mass flow rate: m_{fuel}=0.048kg/s

Selecting a chamber Mach number of 0.3, we find a pressure drop over the chamber of:

$$p_i - p_c = \rho_c\cdot w_c^{\,2} = \gamma\cdot p_c\cdot M_c^{\,2} = (1.2)(10bar)0.3^2 = 1.08bar$$

This then gives a chamber pressure (at nozzle inlet) of 8.92 bar.

Using the known chamber pressure of 8.92 bar, the total mass flow rate and characteristic velocity, we find for the throat area (A_t) and throat diameter (D_t):

$$A_t = \frac{mc^*}{p_c} = \frac{0.127kg/s\cdot 1685m/s}{8.92E5Pa} = 2.40E-4m^2$$

$$D_t\ (\text{round throat}) = 1.75cm$$

Using the given value of L* = 0.90 m, it follows for the chamber volume:

$$V_c = L^*A_t = 0.90m\cdot 2.40E-4m^2 = 2.16E-4m^3$$

To determine the chamber diameter, we first determine the gas mass density in the chamber and the velocity of sound. Using the ideal gas law, it follows for the mass density

$$\rho_c = p_c / (RT_c) = 8.92E5Pa / (8314.46J/kmol/K / 22.1kg/kmol \cdot 3210K)$$
$$\rho_c = 0.739kg/m^3$$

The speed of sound is:

$$a_c = \sqrt{\gamma RT_c} = \sqrt{1.2 \cdot 8314.46 \cdot 22.1 \cdot 3210} = 1203.8m/s$$

Using the earlier selected chamber Mach number, we obtain a flow velocity in the chamber of 361.2 m.

Chamber diameter is now determined by using:

$$m = \rho_c \cdot w_c \cdot A_c \Rightarrow$$
$$A_c = \frac{(0.127kg/s)}{0.739 \cdot (0.3 \cdot 1204m/s)} = 4.76E-4m^2$$
$$D_c = 2.46cm$$

Using the earlier calculated chamber volume, we find a chamber length of 0.45 m, which shows that the chamber is of a very slender design. Selecting a smaller Mach number in the chamber surely will lead to an increased chamber diameter and a shorter chamber length. This, however, is not explored in this example.

To determine the pressure at the thruster inlet, we need to determine the injector pressure drop. For now, we assume a pressure drop of 2 bars to ensure stable combustion. This leads to a pressure of 12 bars at the thruster inlet.

The injection velocity that results in a pressure drop of 2 bars over the injector and the given discharge coefficient of 0.7 is:

MMH:

$$v_i = C_d \cdot \sqrt{\frac{2 \cdot \Delta p}{\rho}} = 0.7 \sqrt{\frac{2 \cdot 2E5}{874}} = 15.0 m/s$$

NTO:

$$v_i = C_d \cdot \sqrt{\frac{2 \cdot \Delta p}{\rho}} = 0.7 \sqrt{\frac{2 \cdot 2E5}{1450}} = 11.6 m/s$$

Here the MMH and NTO mass density have been taken equal to 874 kg/m^3 and 1450 kg/m^3, respectively. The results show moderate injection velocity for both propellants.

To determine the number and size of injector holes, we use as a starting point the experience that for a 200N MMH/NTO thruster [Pages] we use 4 unlike impinging elements. So selecting 8 unlike impinging elements, we obtain in the case of the MMH fuel a mass flow rate of 0.048kg/s / 8 = 0.006 kg/s per element and for the NTO oxidizer flow a mass flow rate of 0.079kg/s / 8 = ~0.01 kg/s.

Using the calculated mass flow rate per element and injection velocity, the size of the individual elements can be calculated, see Table 5.

Table 5: Injector element characteristics

Injector element characteristics	MMH	NTO
Cross-sectional area [m^2]	4.57E-7	5.87E-7
Diameter [mm]	0.763	0.865
Re	11699	34379
We	24.1	18.3

From the table, it shows that the diameter of the injector elements is slightly different. This difference can be reduced to zero, when using different injector geometries with different discharge coefficient and/or by accepting a slightly higher pressure drop for the NTO. This will allow increasing the NTO flow velocity and hence reduce the diameter of the injector element. Still, one must weigh the consequences of this decision for the design of the feed system.

The table also shows values of the Reynolds number and the Weber number (in air). Values of viscosity and surface tension used for the propellants have been obtained from [Sutton]. These values are considered reasonable design values for unlike impinging elements.

Notice that given our very slender chamber design so far, it might be difficult to manufacture the injector disc for this engine. Selecting a lower number of injector elements might be a solution. This, though, as well as the effect on Re and We is left for the reader to explore for him/herself.

Problems

1. Consider the design of a liquid rocket motor operating in a vacuum environment. You select a propellant combination for which the following data are given:
   - L*: 1 m.
   - c*: 2360 m/s (constant).
   - Molar mass: 12.
   - Hot gas temperature: 3400 K.
   - Motor inlet pressure of 120 bar (constant).
   - Nozzle throat area of 0.01118 m^2.
   - The drop in pressure over the chamber is negligibly small.

   The injector used has been calibrated using the propellants themselves and it is found that the drop in pressure over the injector for both fuel and oxidizer and mass flow rate are related according to:

   $$m = 5\,(\Delta p)^n$$

   Here m is in kg/s and Δp in bar.

   Calculate for this motor equilibrium chamber pressure and mass flow rate for the case n = 0.7.

2. Determine the injector tube internal diameter and angle settings for the injector tubes of a multiple element, doublet impinging stream injector that uses alcohol and liquid oxygen as propellants. The resultant momentum should be axial, and the angle between the oxygen and fuel jets should be 60 degrees given that:
   - Number of jet pairs: 4 (meaning there are 4 elements)
   - Discharge factor oxidizer injection holes: 0.87
   - Discharge factor fuel injection holes: 0.91
   - Oxygen mass density: 1137 kg/m^3
   - Fuel mass density: 817 kg/m^3
   - Mass mixture ratio: 1.20
   - Chamber pressure: 20.68 bar

- Negligible drop in pressure over the chamber
- Fuel pressure: 27.58 bar
- Oxygen pressure: 26.20 bar
- Thrust: 1112 N
- Actual specific impulse 218 s

3. For the European HM-60 liquid hydrogen – liquid oxygen rocket engine the following data are given:
   - Mass flow rate fuel: 34.0 kg/s
   - Mass flow rate oxidizer: 198.0 kg/s
   - Chamber pressure: 100 bar
   - Pressure drop over the chamber itself is negligible
   - Injector pressure drop fuel: 18.4 bar
   - Injector pressure drop oxidizer: 23.0 bar
   - Type of injector elements: coaxial (oxygen is injected through centre); all elements are of an identical design
   - Number of elements: 516
   - All hydrogen fuel is used to cool the engine. After cooling the hydrogen has a temperature of 300 K; this temperature may be considered equal to the hydrogen temperature at injection in the chamber.
   - LOX temperature at engine inlet: 95.5K
   - Injector element discharge coefficient (fuel and oxidizer): 0.8

   Calculate for this engine:
   a. Fuel and oxidizer injection velocity
   b. Oxidizer jet Reynolds number
   c. Oxidizer jet Weber number
   d. Fuel to oxidizer momentum ratio, -momentum flux ratio and -velocity ratio
   e. Draw a single injector element, given that the inner tube has a wall thickness of 0.5 mm. Clearly include in your drawing the (cross-sectional) dimensions of the element

4. Consider a monopropellant thruster with a sea level thrust and specific impulse of 50 N and 192 s, respectively. Given are that this thruster operates at a loading factor of 107.9 kg/(m^2·s) (based on chamber cross-sectional area) and propellant is characterized by c* = 1,344 m/s and L* = 1.3 m. Furthermore, we have for this thruster a nozzle with a throat diameter of 6.7 mm and a geometric expansion ratio, ε = 3.50, see figure.

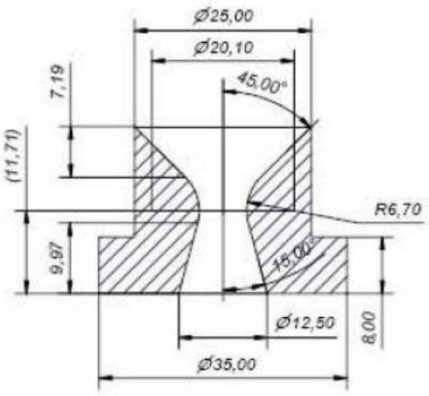

   Calculate for this thruster....
   a) Mass flow rate
   b) Chamber diameter
   c) Throat area
   d) Chamber volume
   e) Chamber length

5. Mixture ratio and c* efficiency
   A liquid propellant rocket engine with a combustor of 0.5 m length uses hydrazine as fuel and nitro-tetroxide (NTO) as oxidizer. The rate of hydrazine injection is 4 kg/s and that of NTO is 6 kg/s. Mass density of the liquid hydrazine is 1140 kg/m^3 and of NTO 1440 kg/m^3. Additionally, are given:

   - The initial diameter of hydrazine and NTO droplets formed in the spray is 0.3 mm and the axial velocity of the droplets is 50 m/s.
   - The evaporation of the droplets is assumed to be given by the law:

$$d^2 = d_0^2 - \lambda t,$$

where the evaporation constant λ is 3 mm^2/s for hydrazine droplets and 5 mm^2/s for NTO droplets.

- The characteristic velocity c* is determined by the expression:

$$c^* = 2000 - 100(|R - 1.4|),$$

wherein c* is in m/s and R is (vapor) mixture ratio.

Determine:

a) Overall mass mixture ratio (of the injected propellants) at injection
b) Number of liquid droplets formed based on given mean diameter
c) Mixture ratio of the vaporized propellant at 6 equidistant points along the combustion chamber axis.
d) c* quality that results for the described motor, thereby considering the effects of incomplete vaporization.

Suppose we double the combustor length to 1.0 m. Furthermore, we divide the injector disk in four different areas with its own propellant flow, thereby ensuring that the overall mass mixture ratio is still 1.5. Consider a core flow (central in the chamber) having 40% of the propellant flow and 3 co-annular (about the core flow) flows having 30%, 20% and 10% of the total propellant flow, respectively. The mixture ratio of the core is 1.6. The mixture ratio of the flows conveying 30% and 20% of the flow is 1.5 and 1.4 respectively. Determine for this case:

e) Mixture ratio of the remaining stream adjacent to the chamber walls.
f) Total c* efficiency (averaged over all four streams) for the motor based on the degree of vaporization accomplished in the individual streams.

References

1. Barrère M., Jaumotte A., Fraeijs de Veubeke F., and Vandenkerckhove J., Rocket Propulsion, Elsevier Publishing Company, 1960.
2. Bejan A, Heat Transfer, John Wiley and Sons Inc., New York, 1993.
3. Bengtson E., website http://www.peroxidepropulsion.com, June 2005.
4. Brown C.D., Spacecraft propulsion, AIAA Education Series, 1995.
5. Candel S., Ducruix S., Durox D., Veynante D., Combustion Dynamics: Analysis and Control Modeling, Laboratoire EM2C, CNRS, Ecole Centrale Paris, 92295 Châtenay-Malabry Cedex, France, published by VKI, 2001.
6. Dresler G.A., Bauer J.M., TRW Pintle Engine Heritage and Performance Characteristics. AIAA 2000-3871, 2000.
7. Godsave G.A.E., Studies of the combustion of drops in a fuel spray - the burning of single drops, 1950.
8. Govaert T, Armbruster W, Hardi J., Suslov D., Oschwald M, Zandbergen B.T.C., Heat loads on the wall of a cryogenic rocket thrust chamber during thermo-acoustic instabilities, submitted to Journal of Propulsion and Power, 2020.
9. Huzel D.K. and Huang D.H., Design of liquid-propellant rocket engines, NASA SP-126, 1971.
10. Hulka J.R., Scaling of Performance in Liquid Propellant Rocket Engine Combustion Devices, 44th AIAA/ASME/SAE/ASEE Joint Propulsion Conference, AIAA 2008-5113, 2008.
11. Hulka J.R., Jones G.W., Performance and Stability Analyses of Rocket Thrust Chambers with Oxygen/Methane Propellants, AIAA., 46th AIAA/ASME/SAE/ASEE Joint Propulsion Conference, Nashville, 25-28 Jul. 2010.

12. Humble R, et al., Space Propulsion Analysis and Design, Space Technology Series, McGraw-Hill Companies Inc. 1995.
13. Jonker W., Mayer A.E.H.J., and Zandbergen, B.T.C., Development of a rocket engine igniter using the catalytic decomposition of hydrogenperoxide, 8th International hydrogen peroxide propulsion conference, Purdue University, West Lafayette, Indiana USA, September 2005.
14. Lasheras J.C., Hopfinger E.J. Liquid Jet Instability and Atomization in Coaxial Gas Stream, in Annu. Rev. Fluid Mech. 2000. 32:275–308.
15. Lefebvre A.H., Properties of Sprays, International Conference on Mechanics of Two-Phase Flows, Taipei, Taiwan, June 12-15, 1989.
16. Levenspiel O., Engineering Flow and heat Exchange, Revised ed., Plenum 1998.
17. Locke J.M., Pal S, Woodward R.D., Santoro R.J., High Speed Visualization of LOX/GH_2 Rocket Injector Flowfield: Hot-Fire and Cold-Flow Experiments, AIAA 2010-7145, 2010.
18. McHugh B., Numerical analysis of Existing Liquid Rocket Engines as a Design Process Starter, AIAA 95-9270, 1995.
19. Megson T.H.G. Aircraft Structures for engineering students, Edward Arnold, 3rd Ed. ISBN 03407-05884.
20. NASA, Liquid Rocket Engine Injectors, NASA SP-8089, March 1976.
21. Pages, X. Design and development status of a 200 N reaction control engine, AIAA 96-3017, 1996.
22. Pal B., Roekaerts D.J.E.M., Zandbergen B.T.C., Numerical Investigation of Atomization Using a Hybrid Eulerian-Lagrangian Solver, accepted for publication in Progress in Computational Fluid Dynamics, An Int. J., 2021.
23. PBNA Polytechnisch Zakboekje, 48th edition, 1998.
24. Penner S.S., On Maximum Evaporation Rates of Liquid Droplets in Rocket Motors, March 1953.
25. Pouliquen M.F. HM60 Cryogenic Rocket Engine for Future European Launchers, J. Spacecraft and Rockets, Vol 21, No 4, 1984.
26. Rahman S.A., Santoro R.J., A review of coaxial gas/liquid spray experiments and corrrelations, AIAA 94-2772, 30th Joint Propulsion Conference, Indianapolis, June 27-29, 1994.
27. Rezende R.N., Pimenta A., de Castro Perez V., Experiments with the pintle injector, conference paper, DOI: 10.2514/6.2015-3810, July 2015.
28. Schöyer H., Caporicci M., Hüfenbach, B., Schnork A.J., The design of the European advanced technology engine, ATE, http://arc.aiaa.org/doi/abs/10.2514/6.1992-3662, 1992.
29. Sutton G.P., Rocket Propulsion Elements, 6th edition, John Wiley & Sons Inc., 1992.
30. Wood B.K., Propulsion for the 21st Century—RS-68, AIAA 2002-4324, 38th Joint Liquid Propulsion Conference, Indianapolis, Indiana, July 2002.

For further reading

1. Thrust chamber life prediction (NASA-CR-134806, 1975)
2. Reliability as an Independent Variable Applied to Liquid Rocket Engine Test Plans, by Strunz and Herrmann, Journal of Propulsion and Power, Vol. 27, No. 5, September–October 2011.

SRM Combustor Design

Contents

SRM Combustor Design 255

Contents 255

List of symbols 256

1 Introduction 257

2 Processes occurring in the combustor 257

3 Rate of generation of gaseous propellant and thrust 258

4 The shape of the grain 259

5 The regression rate 264

6 Internal ballistics 267

7 Pressure drop in chamber 270

8 Sensitivity parameters 272

9 Erosive burning 273

10 Combustion instabilities 274

11 Ignition and extinction 275

12 Solid and liquid particles in the flow 275

13 Combustor casing 279

14 Insulator and liner 280

15 Testing 282

Problems 282

References 285

For further reading 285

List of symbols

Roman

a	Burning rate coefficient
A	Area
C	Circumference
C_F	Thrust coefficient
c*	Characteristic velocity
c_p	Specific heat at constant pressure
D	Diameter
F	Thrust
I	Total impulse
I_{sp}	Specific impulse
K	Klemmung
L	Length
m	Mass flow
M	Mass
M	Mach number
n	Pressure exponent
p	Pressure
r	Regression rate
R	Specific gas constant
S	Surface
t	Time
T	Temperature
u	Velocity
U	Velocity
V	Volume
w	Web thickness
W	Weight
W_f	Web fraction
x	Coordinate

Greek

γ	Specific heat ratio
ρ	Density
Γ	Vandenkerckhove parameter
π	Sensitivity
Λ	Fraction

Subscripts

b	Related to the burning of the motor
c	Chamber or contraction
case	Motor case
e	Exit
g	Gas
i	Port of internal burning grain
i	Conditions at start of burning
o	Total
p	Pressure
p	Propellant
s	Solid
t	Throat
V	Volume

1 Introduction

The combustion chamber of a solid-propellant rocket is essentially a high-pressure vessel, or case as it is called, containing the entire solid mass of propellant in the form of a shaped propellant charge, also commonly referred to as propellant grain. Burning takes place only at the surface of the grain where the temperature is high enough to sustain a chemical reaction. The propellant that does not yet burn acts as insulation for the wall of the case, see Figure 1.

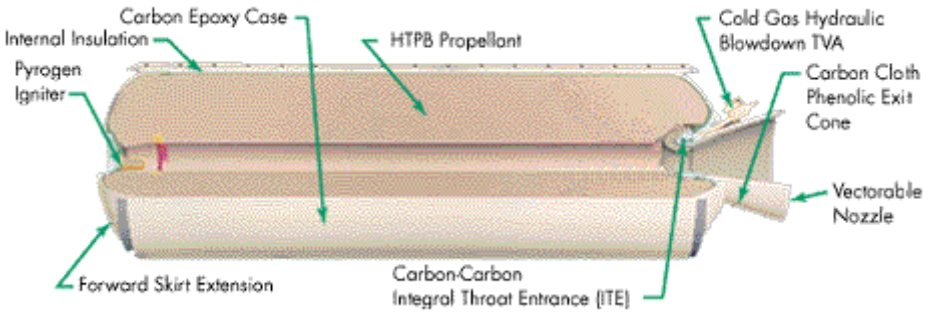

Figure 1: Typical solid rocket motor with case-bonded grain and other components.

To withstand the high temperature environment, the motor case in addition may be protected by thermal insulation. This is especially the case for those surfaces that otherwise would be directly exposed to the hot combustion gases. The figure also shows that the case not only serves to contain the propellant and to achieve a good combustion efficiency but also may house the rocket motor igniter and provides for structural interfacing with the rocket nozzle, and nozzle steering device(s).

Some typical design characteristics of solid propellant combustion chambers include:

- Motor case is usually of a spherical or cylindrical shape.
- Grain can be of a complex geometry with or without a central bore (port).
- Case consists of head end, body and aft end. Connections can be welded, bolted, screwed or 'glued'.
- Case materials include steel, aluminium alloy or (glass or carbon) fibre reinforced composite materials.

Typical operational characteristics are:

- Chamber pressure of high-performance solid rocket motors can be up to 6 - 7 MPa.
- Combustion temperatures can be up to 3500 K.
- Combustion times range from a few tenths of a second up to several minutes.
- Solid motors typically operate with a single start and burn until the propellant is gone.

Important performance characteristics are the mass flow generated and the characteristic velocity. The latter depends on the propellant used and the combustion quality attained in the combustion chamber. Hereafter, we will discuss a few issues relating to the operation and design and development of a solid rocket combustor.

2 Processes occurring in the combustor

Solid propellant burning usually takes place in a very thin layer (about 100 μm) close to the solid propellant surface. Compare the burning of a candle flame. It is essentially the heat transferred from the combustion zone to the initially solid propellant that causes propellant heating with subsequent melting and vaporization. The latter leading to solid propellant regression.

Different types of propellants exist, being homogeneous and heterogeneous propellants, see section on propellants. Depending on the type of propellant the combustion processes differ. For example, for a composite propellant we find that at micro-scale (1 to 10 µm resolution) combustion is complex and layered. Deep in the interior of the propellant, solids are surrounded by binder. A multiphase "melt layer" (order of 10 µm) lies at the boundary of the burning surface. Surface flames with heights of 1 mm or less lie above the melt layer, and beyond that lies a hydrodynamic outflow region that in turn matches with the fluid dynamics that derives from the interior ballistic core region of the motor, see Figure 2.

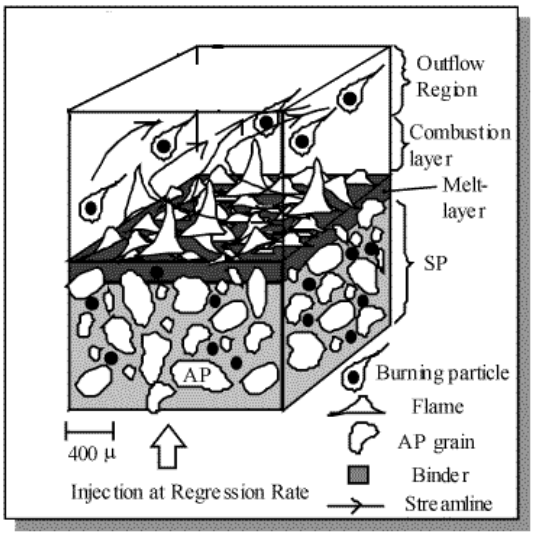

Figure 2: Schematic of combustion of composite solid propellant (SP).

Processes involved in composite propellant regression include:

- Chemical reactions in combustion zone
- Heat transport from combustion zone to the solid
- Melting, liquefaction, and vaporization of solids and binder pyrolysis
- Diffusion of species
- Flow processes

3 Rate of generation of gaseous propellant and thrust

The thrust of a rocket motor can be described using:

$$F = m \cdot C_F \cdot c^* \tag{3-1}$$

Of these, the thrust coefficient C_F depends mainly on the nozzle design, whereas the characteristic velocity c* depends on the propellants selected and the design of the combustion chamber. The mass flow m greatly depends on the rate of generation of gaseous propellant.

For a solid propellant combustion chamber the rate of generation of gaseous propellant is equal to the rate of consumption of solid material. Piobert in 1839 postulated that the burning of a solid grain occurs in parallel layers from the surface to the interior. Piobert's postulate, also known as Piobert's burning law, has been shown to be a pretty good approximation by observation of partially burned grains of powder. The rate with which the solid surface regresses in a direction perpendicular to the burning surface is referred to as the regression rate. The rate of consumption of solid material then depends on the regression rate[1] 'r', the density of the solid propellant 'ρ_p' and the surface of the solid

[1] In some texts, sometimes the term burning rate is used. This term however is associated with the burning of a granule, which burns on all its sides, and is equal to the rate at which the granule reduces in size. Hence, it is equal to twice the regression rate.

propellant grain subjected to burning, i.e. the burn surface 'S'. Assuming constant conditions along the burn surface, it follows:

$$m = \rho_p \cdot r \cdot S \tag{3-2}$$

This equation shows that mass flow increases with increasing regression rate and burn surface of the propellant grain. These two items will be dealt with in some detail in the next two sections.

4 The shape of the grain

From the preceding section we learn that the burn surface greatly determines the consumption of solid material. The size of this surface depends on the shape of the grain and whether the grain adheres to the chamber wall, referred to as "case bonded" or is "free-standing". Nowadays most solid propellant motors use case bonded grains that burn from the inside as this provides for protection of the case against the high temperature of the combustion gases. Only when high thrust and short burning times are desired, like in bazooka-types of missiles, a large burning area is needed, and a free-standing grain may be used.
A complicating factor is that generally during combustion the burn surface changes. We distinguish:

- "Neutral burning" grain: during the period of burning the burn surface remains constant.
- "Progressive burning" grain: the area increases with time.
- "Regressive burning" grain: the area decreases with time.

How the burn surface changes in time greatly depends on the initial geometry.

4.1 Grain geometries

There are two basic types of geometries used in space industry, see Figure 3. The first are end-burning configurations, where the front of the flame travels in layers from the nozzle end of the block (hence end-burning) towards the top of the casing.

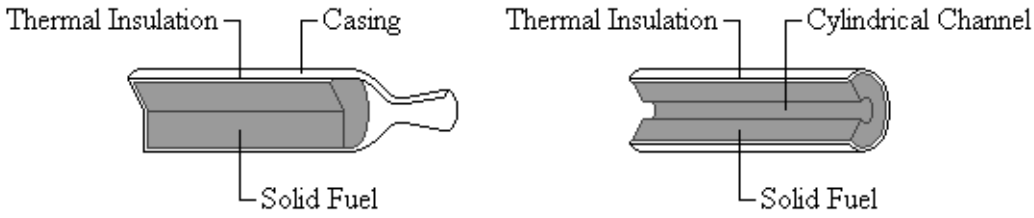

Figure 3: Grain types; end-burning (left) and internal-burning configuration.

The second, which is more usual, are internal burning configurations, wherein the combustion surface develops along the length of a central channel. Sometimes the channel has a star shaped, or other, geometry to moderate the growth of this surface. The cross-sectional area of this channel or port is called the "port area" A_i.

The end-burning grains burn up more slowly than the side-burning grain, as the area of the burn surface is smaller. It is used for military missiles with a large action radius that require a long-sustained flight at low thrust. Side-burning grains are preferred for boosters for large space rockets and for small military rockets that combine high thrust with short burn times.

To be able to determine how the burn surface evolves in time, it is important to consider that a solid propellant grain burns only at the surface and normal to the surface. This implies that a surface which is initially convex towards the gas phase, remains convex (Figure 4a) and a surface concave towards the gas phase, remains concave (Figure 4b).

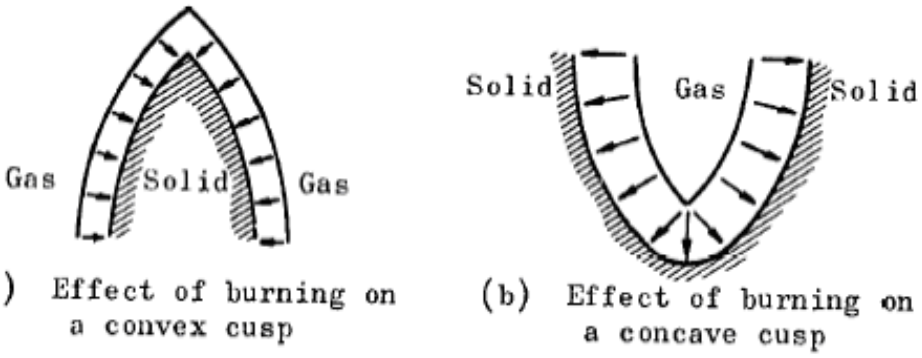

Figure 4: Convex burning surfaces remain convex; concave burning surfaces remain concave.

The burn surface at any point recedes in the direction normal (perpendicular) to the surface at that point, the result being a relationship between burn surface and web distance burned that depends almost entirely on the *grain initial shape* and restricted (inhibited) boundaries. This important concept is illustrated in Figure 5, where the contour lines represent the core shape at successive moments in time during the burn.

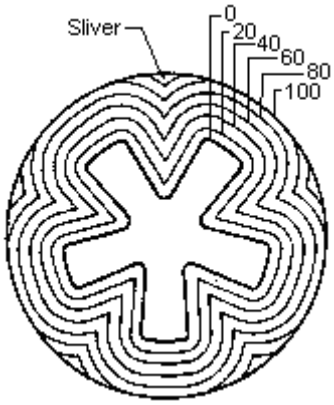

Figure 5: Evolution of burning area in time.

From the figure it follows that the burn time is determined by the thickness of the grain. An important parameter is here the “web thickness” defined by:

$$w = \int_{t=0}^{t=t_b} r \cdot dt \qquad (4\text{-}1)$$

Notice that the regression rate may vary during the burning. This is discussed later in more detail.

Some possible end-burning grain configurations are shown in Figure 6.

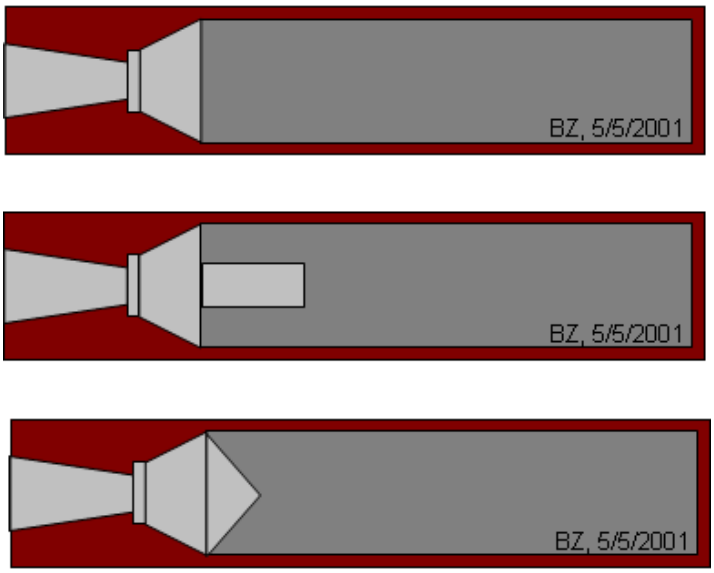

Figure 6: End-burner configurations; true end burner (top), core end-burner (middle), and cone end-burner

The true end-burner burns from one end to the other, like a cigarette. It is the simplest of all grain geometries. The core end-burner allows the user to characterize a small initial pressure spike for extra take off power. The cone end-burner performs basically the same function as the Core End Burner.

In Figure 7 some possible cross-sections for internal-burning grain types and there thrust-time shapes are shown. The latter relation is discussed in more detail in the section on internal ballistics.

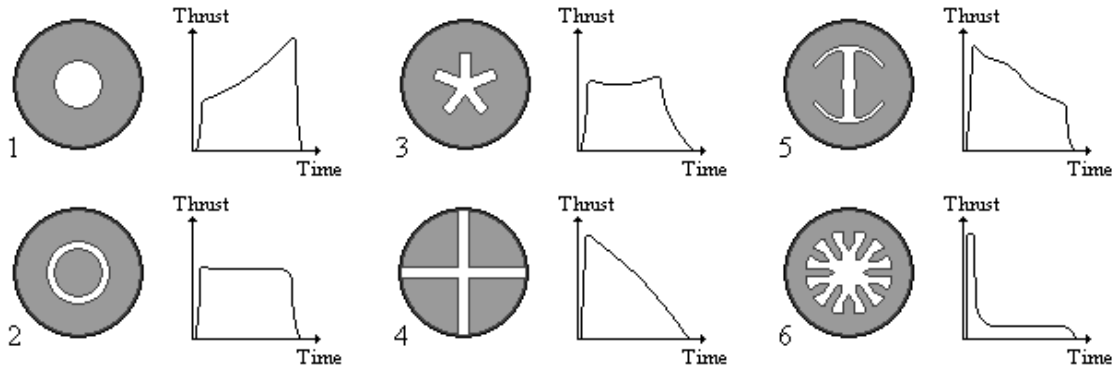

1 = Tubular configuration 2 = Rod & tube configuration
3 = Star configuration 4 = Cross configuration
5 = Double anchor configuration 6 = Multi-fin configuration

Figure 7: Internal-burning charge designs with their thrust-time programs.

In Figure 7 two examples of neutral burning grains are shown. The first one has a star-configuration; the second has a rod and tube configuration. When burning, the total area of the burning surface will remain constant, causing a constant thrust. The rod and tube are not used much, because to fasten the rod, struts are needed that must be able to withstand the high combustion temperature. Another possible configuration for a neutral burning grain is the tubular grain with restricted ends, burning at its inner and outer surface. The disadvantage of this configuration is that the chamber wall is not insulated by the unburned propellant and must be heat resistant.

A tubular grain burning from the inside only, as shown in the first picture of Figure 7 burns progressively as the area of the burning surface increases linearly with time. The double anchor configuration burns regressively. By choosing a suitable shape of the port area and by using a combination of propellants with different burning rates, almost any desired thrust-time diagram can be realized.
Beside internal and end-burning geometries also combinations exist, see Figure 8. The finocyl geometry shown consists of fins/slots that merge into a central cylindrical port.

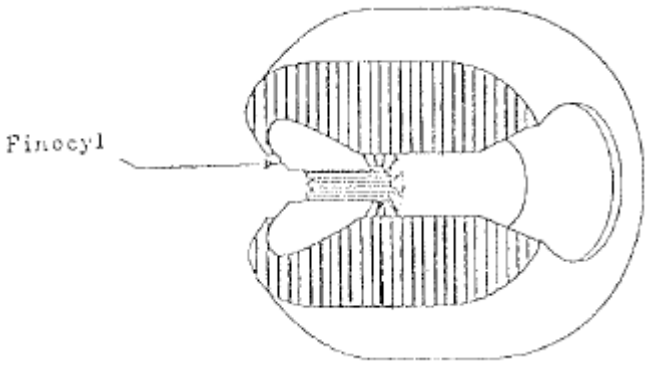

Figure 8: Finocyl grain (from AIAA 97-3340)

Although such grains are of a complex shape, they are becoming increasingly popular, since they can be designed such that, they offer a good to excellent burning area neutrality, a large burning area and web thickness.

After burn-out of a grain, parts of the propellant grain may remain unburned. The remaining propellant is usually present in the form of slivers, see Figure 5.

4.2 Grain characteristic parameters

In this section we will introduce some parameters that allow for characterizing the various grains in a comparative way.

The **Volumetric Loading Fraction** is defined as the fraction of propellant volume to available chamber volume, and relates the volumetric efficiency of the motor or how much propellant we can pack in the motor:

$$\Lambda_V = \frac{V_p}{V_{case}} \tag{4-2}$$

Where V_p is propellant volume and V_{case} is available chamber volume. It is greatly determined by the grain geometry. Highest load factor is usually for end-burning grains with values in the range of 0.9-0.95. For internal burning grains lower load factors apply. For example, for a tubular grain with a core diameter of 400 mm and an outer diameter of 1000 mm follows a load factor of maximum 0.84. Considering that the convergent section is not filled with propellant, an even smaller load factor of 0.75-0.80 is more likely.

The **Web Fraction** is the ratio of propellant web thickness to grain outer radius, and is given by:

$$W_f = \frac{2 \cdot w}{D} \tag{4-3}$$

where w is web thickness and D is grain diameter. Clearly, to maximize burn duration, it is necessary to maximize the web fraction (i.e. thickness). The "price" for maximizing web

thickness is reduction of the grain core diameter. This must be carefully considered, as explained below.

The **Port-to-Throat** area ratio is given by the flow channel cross-sectional area to the nozzle throat cross-sectional area:

$$\frac{A_i}{A_t} = \frac{\pi \cdot D_i^2}{4 \cdot A_t} \tag{4-4}$$

where A_i is the flow (channel) area of the grain, A_t is the throat cross-sectional area, and D_i is port hydraulic diameter. Gas velocity along the length of the flow channel is influenced significantly by the magnitude of the port-to-throat area ratio. Choked flow occurs when the ratio is 1.0, with flow velocity through the port being equal to the flow velocity through the nozzle throat (sonic). Severe erosive burning (core stripping) may occur under such a condition and is generally avoided in design. The criticality of the port-to-throat ratio, however, depends upon the mass flow rate at a given location. In fact, a ratio of 1.0 (or less) may be used at the forward end of the grain where mass flow rate is minimum. The port-to-throat area ratio is often used as an index from which erosive burning tendencies are established. For those propellants where this has not been established, a ratio of 2.0 to 3.0 (dependent upon grain L/D ratio) is suggested.

Length-to-Diameter ratio is the grain overall length in relation to the grain outer diameter. This parameter is very significant in motor design, as larger L/D values tend to result in greater erosive burning effects (including negative erosive burning). High L/D values tend to generate high mass flow rate differentials along the grain length and may be best served with a tapered core or stepped core diameters (largest diameter near to the nozzle).

Characteristics of some common grain types are shown in the table 1.

Table 1: Grain characteristics

Configuration	Volumetric loading fraction	Web thickness	Burning area	Sliver fraction	Web fraction (inverse of)	Comments
STAR	0.75-0.90	intermediate	intermediate	5-10%	3.5-5.5	Case-bonded and free-standing grains
SLOTTED TUBE	0.75-0.85	large	large	0%	~3	Case-bonded grains
WAGON WHEEL	0.5-0.7	small	very large	5-10%	6-12	Free standing and case-bonded grains
STAR (with full head-end web)	0.75-0.85	intermediate	intermediate	5-10%	3	Case-bonded grains
TRUE END-BURNING	0.98-1	very large	small	0%	1	Low thrust

4.3 Inhibiter

The burn surface, and hence the thrust profile, can be modified by covering part of the grain surfaces by an inert material. Such a material is referred to as an inhibiter material. Inhibitor materials should have good adhesion to the propellant and be able to resist high heat loading. Typical inhibitor materials for double-base propellants are ethyl-cellulose or cellulose acetate. For composite propellants, inhibitor materials can be like insulator and/or liner materials, see a later section in this work, be it that their exact composition may differ as of tailoring to the specific needs.

4.4 Grain design

Only the very simple grain geometries like the end-burner and the 2-D tubular grains can be simply calculated by hand. Typical relations that allow for solid rocket motor grain analysis can be obtained from e.g. [Hartfield] and [Stalin]. However, even for the tubular grain, it quickly becomes a time-consuming task in case a variation in regression rate, as of varying conditions in the motor, must be considered. To reduce the work, several computerized design tools have been developed, including:

- Burnsim: Solid Propellant Internal Ballistics Simulation Research Rocket Motor design software. It supports the calculation of many 2-D grain configurations.
- GDP: Commercial grain design program by AED. Capable of calculating all 2-D designs, like star, tubular, etc. Grains which cannot be treated analytically, are treated graphically. Demo available for DOS platforms (works also under Win 95/98/NT)

Most of these tools do not allow a direct design based on given performances but rather allow the designer to quickly evaluate the effect of changes in the design on the motor performances. It is for this reason that the designer must have some basic knowledge about the various grain geometries and their effect on motor thrust performance and more specifically on mass flow rate.

5 The regression rate

The "regression or burning rate" is the velocity with which the burning surface of the grain regresses. An overview of various solid propellants and their burning rate can be obtained from TU Delft: Solid rocket propellants and their properties. In general, solid propellants burn with a burning rate between 0.1 and 80 mm/sec. This burning rate varies with the constituents, their mixture ratio, their fineness, the combustion pressure (p) and the initial temperature (T_i) of the grain.

The influence of these parameters on r can be determined by measurements in a "strand burner" or "Crawford bomb", see Figure 9. The strand of propellant is inhibited on the outside and burning will only take place in longitudinal direction. The melting of two electrical wires, fixed at a known distance from each other, start and stop a chronometer.

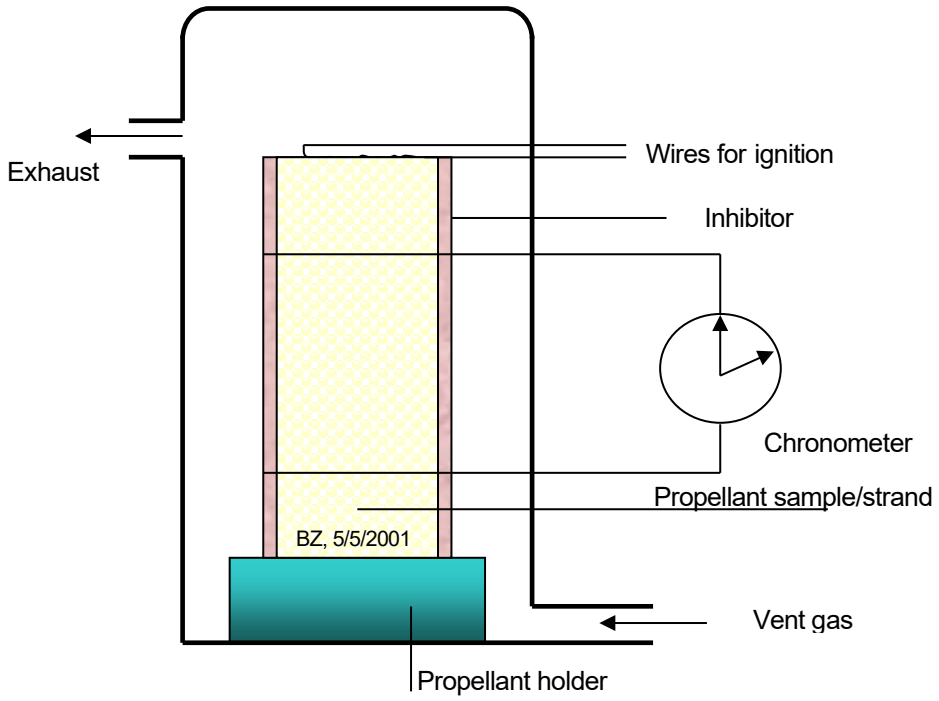

Figure 9: Schematic drawing of a Crawford bomb or strand burner.

The next figure is typical for the dependence of regression rate on pressure.

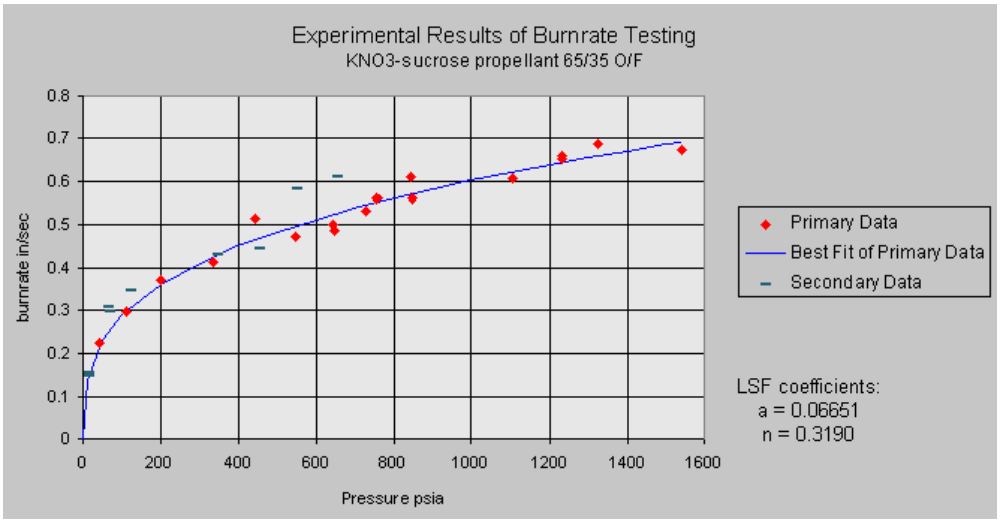

Figure 10: Solid propellant regression rate versus pressure (R. Nakka)

When plotting the results on a double logarithmic scale we find a linear relation according to:

$$\log r = n\{\log (p)\} + \log (a) + \log r_o$$

It turns out that regression rate dependence on pressure can be expressed as:

$$r = a \cdot p^n + b \tag{5-1}$$

This equation is referred to as Saint Robert's equation.

In many cases a good approximation is given by De Vieille's law:

$$r = a \cdot p^n \tag{5-2}$$

n is called the "burning rate exponent" and a is called the "burning rate coefficient". The pressure exponent, n, is dimensionless and independent of the units used for pressure or regression rate. The rate coefficient, a, however, determines the units that the regression rate will have (e.g. cm/sec, mm/sec, etc.). Values of the burning rate coefficient and exponent for a range of composite and double base propellants can be obtained from Schőyer et al.

Due to the nonlinear relationship between the regression rate and the pressure exponent, the regression rate is very sensitive to n. High values of n result in rapid (and potentially catastrophic) changes in regression rate with changing operating pressure. For this reason, the burning rate exponent must be smaller or equal to one. The lower the value of the pressure exponent, the less sensitive and thus "safer" the propellant would be. A propellant with a value of n, say less than 0.5 is considered a reasonably safe propellant. If r is independent of p over a certain pressure interval (n = 0), one speaks of "plateau-burning"; if r decreases with increasing pressure (n < 0), one speaks of "mesa-burning" propellants. In Figure 11 an example of plateau-burning and mesa-burning propellant for a certain pressure interval is given. The figure shows that the parameters a and n only are constant over certain pressure intervals, which in practice is also the case.

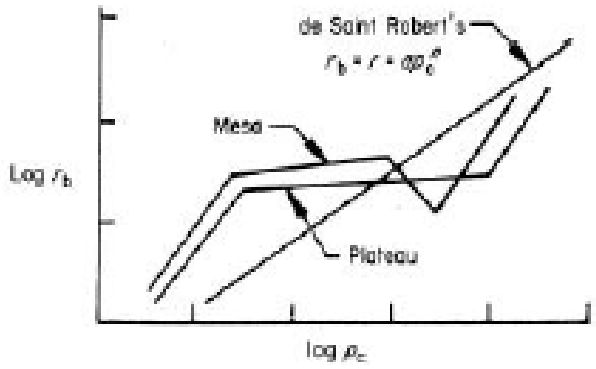

Figure 11: Burning rate versus pressure; (a) plateau-burning, (b) mesa-burning [NASA SP 8039].

One of the drawbacks of solid propellants is their sensitivity to the initial temperature of the grain, which is usually equal to the ambient temperature, whereas for most applications a major requirement is that solid propellant rockets should function uniformly, independent from the environmental conditions.

For a given solid propellant, the regression rate can vary significantly over the range of normal operating temperatures. This sensitivity can be enhanced or decreased by the addition of certain chemicals. It can be determined through burning rate measurements with a strand burner capable of initial temperatures of -75 °C to + 90 °C. A typical result is shown in Figure 12.

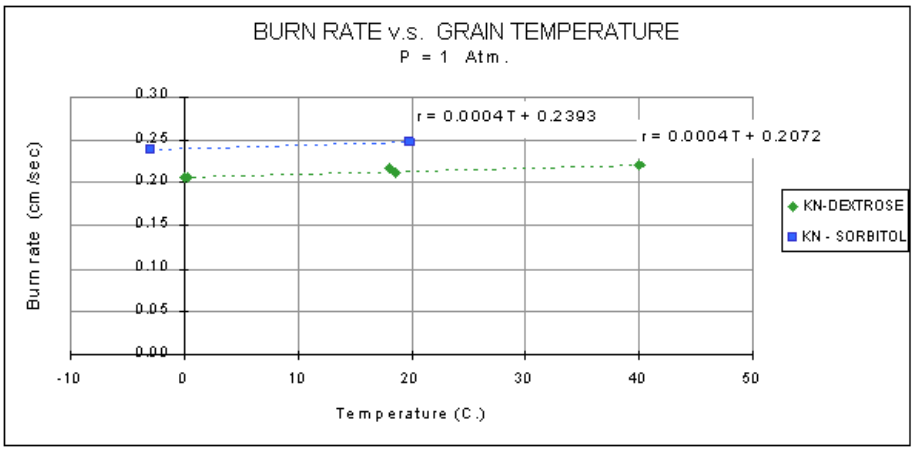

Figure 12: Effect of propellant temperature on regression rate (R. Nakka).

As a general result, we find that the temperature effect mainly changes the constant and not the slope n.

The sensitivity of the regression rate r to variations in the initial temperature T_i at constant pressure p can now be defined as:

$$\sigma = \left(\frac{\delta \ln(r)}{\delta T_i} \right)_p \Rightarrow \sigma = \frac{1}{r} \cdot \left(\frac{\delta r}{\delta T_i} \right)_p \tag{5-3}$$

Applying De Vieille's law, we obtain:

$$\sigma = \left(\frac{\delta \ln(r)}{\delta T_i} \right)_p \Rightarrow \sigma = \frac{1}{r} \cdot \left(\frac{\delta r}{\delta T_i} \right)_p = \frac{1}{a \cdot p^n} \cdot \left[p^n \cdot \left(\frac{\delta a}{\delta T_i} \right)_p + a \cdot \left(\frac{\delta p^n}{\delta T_i} \right)_p \right] \tag{5-4}$$

and since the pressure is kept constant:

$$\sigma = \frac{1}{a} \cdot \left(\frac{\delta a}{\delta T_i} \right)_p \Rightarrow \sigma = \left(\frac{\delta \ln(a)}{\delta T_i} \right)_p \Rightarrow a = a_o \cdot e^{\sigma \cdot (T_i - T_{i,o})} \tag{5-5}$$

Here $T_{i,o}$ is a reference temperature; and a_o is a constant.

Example calculation: For a certain solid propellant is given that the regression rate changes from 2 mm/s to 2.15 mm/s when the propellant temperature increases from -30°C to 60°C. Assuming that the effect is limited to the regression rate coefficient only, we find that the temperature coefficient is about 8 x 10^{-4} 1/K or 0.08 %/K.

Values for the sensitivity of the regression rate to variations in the initial temperature for some propellants can be obtained from Schőyer et al.

Some solid propellants experience an effect of (linear or rotational) acceleration (due to the motion of the vehicle) on the regression rate. This effect is most noticeable for composite propellants that have solid metal particles. According to Schöyer, typical such effects can be neglected for acceleration levels up to about 100 m/s^2. This is well above typical acceleration levels for space vehicles so here acceleration effects on regression rate can be neglected. For most military and sounding rockets, though the acceleration levels can be much higher. In that case one must seriously consider the effect of acceleration loads on fuel regression.

Modelling of solid propellant regression is quite complex and will not be explained here. For further information, one is referred to the work of amongst others K. Kuo.

6 Internal ballistics

In this section the equations that govern the equilibrium of the mass flow through the nozzle and the mass flow generated by the burning propellant are derived.

Assumptions:

- The chamber pressure p_c is constant throughout the chamber.
- The burning rate is constant; $r = a \cdot p_c^{\,n}$.
- The mass flow m through the nozzle is constant; $m = p_c \, A_t / c^*$.
- The combustion products are ideal gases.

The decrease of propellant mass per unit time is equal to the mass flow through the nozzle m and the increase of gas accumulated in the chamber:

$$\frac{dM_p}{dt} = m + \frac{d(\rho_c V_c)}{dt} \tag{6-1}$$

This decrease of propellant mass is caused by the burning process that takes place at constant burning rate r over the burning surface S:

$$\frac{dM_p}{dt} = \rho_p \cdot S \cdot r = \rho_p \cdot S \cdot a \cdot p_c^{\,n} \tag{6-2}$$

Combining (6-1) and (6-2) gives:

$$\rho_p \cdot S \cdot a \cdot p_c^{\,n} = \frac{p_c \cdot A_t}{c^*} + \rho_c \cdot \frac{dV_c}{dt} + V_c \cdot \frac{d\rho_c}{dt} \tag{6-3}$$

The change of chamber volume with time is constant:

$$\frac{dV_c}{dt} = r \cdot S \tag{6-4}$$

The change of the density of the combustion products with time can be expressed as a change of pressure by applying the ideal gas law. The combustion temperature T_c is assumed to remain constant.

$$\frac{d\rho_c}{dt} \cong \frac{1}{R \cdot T_c} \cdot \frac{dp_c}{dt} = \frac{1}{\Gamma^2 \cdot c^{*2}} \cdot \frac{dp_c}{dt} \tag{6-5}$$

Here $c^* = \frac{1}{\Gamma} \cdot \sqrt{R \cdot T_c}$ is used.

Substitution of (6-4) and (6-5) into (6-3) yields:

$$\left(\rho_p - \rho_c\right) \cdot S \cdot a \cdot p_c{}^n = \frac{p_c \cdot A_t}{c^*} + \frac{V_c}{\Gamma^2 \cdot c^{*2}} \cdot \frac{dp_c}{dt} \tag{6-6}$$

After some rearranging, this differential equation for the chamber pressure as function of time can be written as:

$$\frac{V_c}{\Gamma^2} \cdot \frac{dp_c}{dt} = c^{*2} \cdot \left(\rho_p - \rho_c\right) \cdot S \cdot a \cdot p_c{}^n - c^* A_t \cdot p_c \tag{6-7}$$

If constant chamber pressure is assumed ($dp_c/dt = 0$), the process inside the chamber is assumed to be at equilibrium and the chamber pressure can be expressed as a function of the other parameters:

$$p_c = \left(c^* \cdot \left(\rho_p - \rho_c\right) \cdot a \cdot \frac{S}{A_t} \right)^{1/(1-n)} \tag{6-8}$$

The ratio between the area of the burning surface, S and the throat area, A_t, is called the "Klemmung" K. For most solid propellant motors, the value of K lies somewhere between 100 and 1000. If the burning rate is independent of pressure (n = 0), the chamber pressure is proportional to K, as is shown by (6-8).

As the density of the gases amounts to about 2% of the density of the propellant, the former can be neglected and (6-8) reduces to:

$$p_c \approx \left(c^* \cdot \rho_p \cdot a \cdot \frac{S}{A_t} \right)^{1/(1-n)} \tag{6-9}$$

The exponent 1/(1-n) is called the "geometric amplification factor" of the grain. For stability reasons, n must never be larger than 1. This can be reasoned in the following way. The generation of gas is proportional to the burning rate which is a function of the chamber pressure:

$$m_g = \frac{dM_p}{dt} = \rho_p \cdot S \cdot a \cdot p_c{}^n \tag{6-10}$$

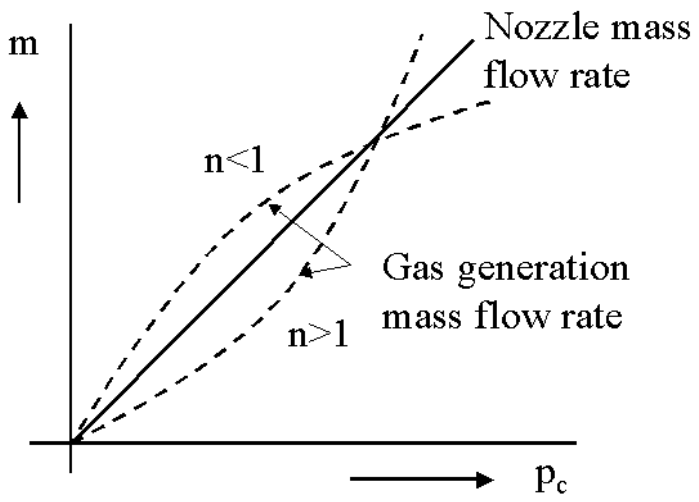

Figure 13: The balance of mass in a solid rocket motor combustion chamber.

If T_c is constant, the mass flow through the nozzle is proportional to p_c, as is expressed by:

$$m = p_c \cdot {A_t}/{c^*} \tag{6-11}$$

This relationship is depicted as a straight line in Figure 13. The two dotted curves through the origin represent the mass produced at the burning surface for the cases n < 1 and n > 1. At point S there is a balance between mass production and outflux of mass through the nozzle.
In the case that n > 1, a small increase in pressure p_c would lead to a higher production of mass than the amount which can leave the nozzle, and the pressure would rise further. For a small decrease in pressure more gas would leave the chamber than is produced and the pressure will drop and finally die out.
If however, 0 < n < 1, a small change in pressure would stimulate or repress the production of mass in such a way that the pressure will adjust itself to its steady state equilibrium value.

From (3-1) and (6-11) it follows that thrust is proportional to chamber pressure:

$$F = C_F \cdot p_c \cdot A_t \tag{6-12}$$

Hence knowing how the chamber pressure evolves in time means we know how thrust evolves in time.

How does the core shape influence the pressure-time and hence the thrust-time curve? The chamber pressure (and thrust) that a rocket motor generates is proportional to the burning area at any instant in time. This is referred to as the *instantaneous burning area*. As stated earlier, the burning surface at any point recedes in the direction normal (perpendicular) to the surface at that point, the result being a relationship between burning surface and web distance burned that depends almost entirely on the *grain initial shape* and restricted (inhibited) boundaries. It is equation (6-9) that allows us to determine the pressure evolution as a function of the burning area, provided that we are dealing with quasi-stationary

The next figure illustrates the pressure-time as calculated for a tubular-shaped grain.

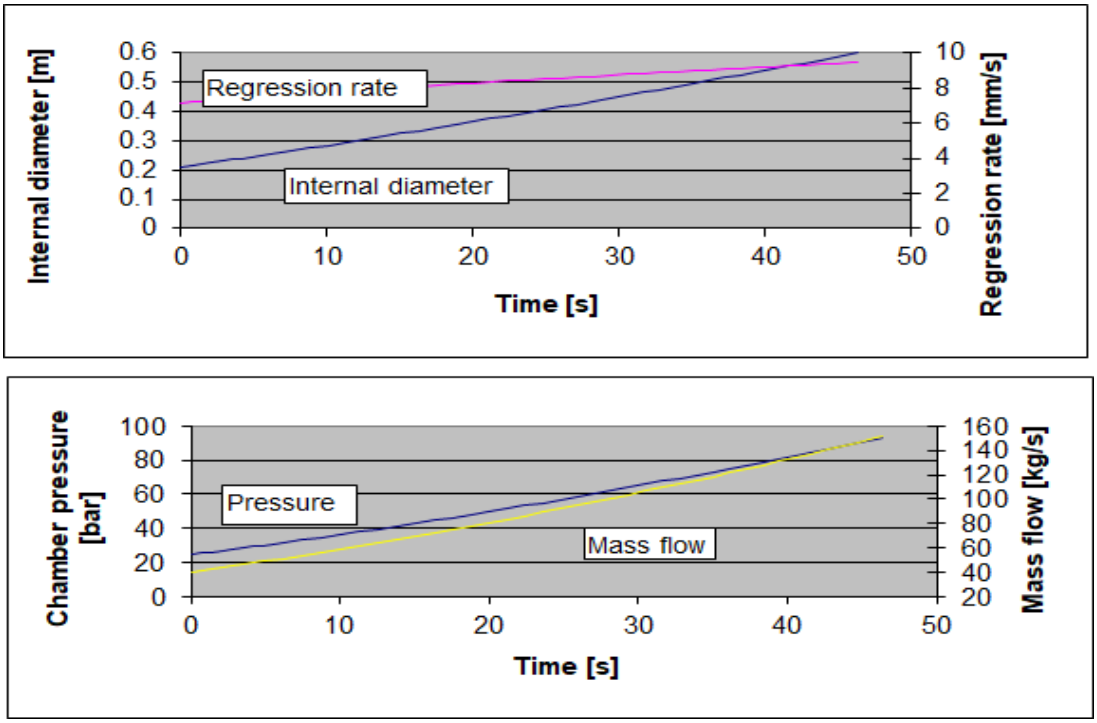

Figure 14: Calculated evolution in time of chamber conditions for a typical tubular grain.

The results in Figure 14 have been calculated for a tubular grain with a length of 5 m, an outer diameter of 0.6 m and an initial core diameter of 0.35 times the outer diameter using the following values:

- Throat diameter: 0.15 m
- Total temperature: 3000 K
- Specific heat ratio: 1.2
- Specific heat of combustion gases: 1000 J/kg/K (value of air)
- Solid propellant density: 1700 kg/m^3
- Regression rate: 8.86 mm/s at 6.9 MPa
- Regression rate exponent: 0.21

The regression rate data apply to the Minuteman solid rocket motor and have been taken from 'Rocket Propulsion Elements', by G.P. Sutton, 5th ed. (page 263)

The figure clearly illustrates the large variation in pressure (factor 4) and mass flow (factor 5) occurring throughout the burn time. The larger increase in mass flow is attributed to the increase in regression rate.

7 Pressure drop in chamber

In the solid propellant combustion chamber a pressure drop occurs along the axis of the combustion chamber. This pressure drop is necessary to accelerate the increasing flow of gas out of the port.

It is possible to make a simple calculation of the pressure drop within a solid-propellant grain. An incremental control volume is considered, see Figure 15.

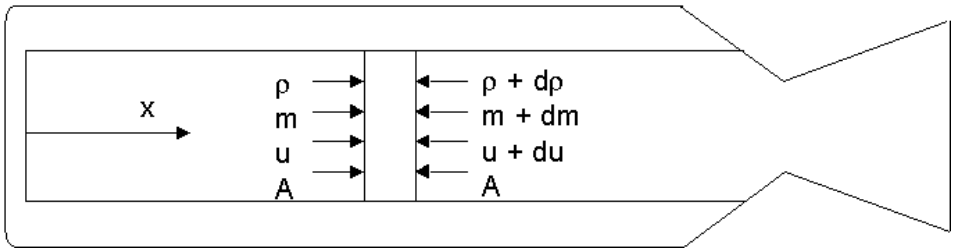

Figure 15: Incremental control volume for the calculation of pressure drop within a solid propellant combustion chamber.

The law of conservation of linear momentum holds:

$$-A \cdot dp = d(m \cdot u) \tag{7-1}$$

At x_o is 0, the pressure is assumed to take the value p_o,. Integration of (7-1) between x_o and a certain value of x gives:

$$p_o - p_x = \int_{x_o}^{x} \frac{d(m \cdot u)}{A} \tag{7-2}$$

Throughout the chamber, A will be almost constant. For production reasons there might be a small increase of the port area towards the throat as this permits the core to be taken out after the curing process of the grain. If the flow velocity at x_o is equal to zero eq. (7-2) can be written as:

$$p_o - p_x = \frac{(m \cdot u)_x}{A} \tag{7-3}$$

With the continuity equation

$$m_x = \rho_x \cdot u_x \cdot A_x \tag{7-4}$$

One gets:

$$p_o - p_x = \rho_x \cdot {u_x}^2 \tag{7-5}$$

For the mass flow one can also write:

$$m_x = \rho \cdot r \cdot C \cdot x \tag{7-6}$$

Here C is the circumference of the port area and x the length of the part of the grain between the front end and the coordinate x.

Now also the energy equation holds:

$$c_p \cdot T_o = c_p \cdot T_x + \frac{1}{2}{u_x}^2 = \frac{\gamma}{\gamma - 1} \cdot \frac{p_x}{\rho_x} + \frac{1}{2}{u_x}^2 \tag{7-7}$$

ρ_x and u_x can be expressed in p_x with eqs. (7-4), (7-5) and (7-6):

$$u_x = \frac{p_o - p_x}{\frac{r \cdot \rho_p \cdot C \cdot x}{A_p}} \text{ and } \rho_x = \left(\frac{r \cdot \rho_p \cdot C \cdot x}{A_p} \right)^2 \cdot \frac{1}{p_o - p_x} \tag{7-8}$$

Substituting these expressions in the energy equation gives after some algebraic manipulations a quadratic equation in p_x/p_o:

$$\frac{\gamma+1}{\gamma-1}\cdot\left(\frac{p_x}{p_o}\right)^2-\frac{2}{\gamma-1}\cdot\frac{p_x}{p_o}-1+2\cdot c_p\cdot T_o\cdot\left(\frac{r\cdot\rho_p\cdot C\cdot x}{A_p\cdot p_o}\right)^2=0 \qquad (7\text{-}9)$$

From this equation follows the solution:

$$\frac{p_x}{p_o}=\frac{1}{\gamma+1}\cdot\left[1+\sqrt{1+\left(\gamma^2-1\right)\cdot\left(1-2c_p\cdot T_o\cdot\left(\frac{r\cdot\rho_p\cdot c\cdot x}{A_p\cdot p_o}\right)^2\right)}\right] \qquad (7\text{-}10)$$

Eq. (7-10) can also be expressed in the Mach number M_x

$$\frac{p_o}{p_x}=1+\gamma\cdot M_x{}^2 \qquad (7\text{-}11)$$

In Figure 16 the pressure ratio p_s/p_o and the Mach number M_x are given as function of x for a solid propellant rocket motor with a cylindrical port of 0.1m diameter. With increasing distance from the front-end the pressure decreases slowly and the Mach number increases. From eq (7-10) we observe that a limiting case exists if the expression under the square root becomes zero, for which $p_x/p_o = 1/(\gamma+1)$. From eq.(7-11) follows for this limiting case: $M_x = 1$. Thus, for a cylindrical grain with uniform mass addition holds the condition: $M_x < 1$ and the flow cannot change from subsonic to supersonic.

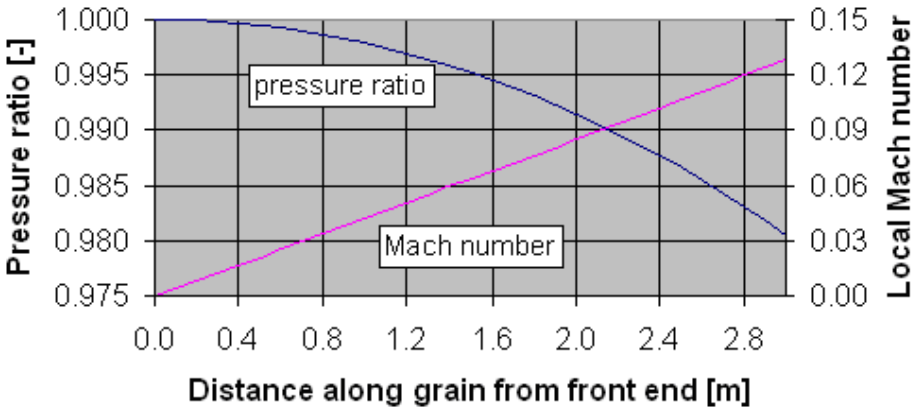

Figure 16: Theoretical predicted variation of pressure for a grain with cylindrical port 0.1 m in diameter and 3 m in length; typical propellant properties.

8 Sensitivity parameters

The sensitivity of the burning rate to the initial temperature of the grain is defined in (5-3).

The sensitivity of the chamber pressure to the initial temperature with constant Klemmung is defined as:

$$\left(\pi_p\right)_K=\frac{1}{p_c}\cdot\left(\frac{\partial p_c}{\partial T_i}\right)_K \qquad (8\text{-}1)$$

Chamber pressure and burning rate sensitivity to initial temperature are related. From (5-3) follows:

$$\sigma = \frac{1}{a \cdot p^n} \cdot p^n \cdot \left(\frac{\delta a}{\delta T_i}\right)_p = \frac{1}{a} \cdot \frac{da}{dT_i} \tag{8-2}$$

Using (8-1) and (6-9) we find:

$$\begin{aligned}
\left(\frac{\partial p_c}{\partial T_i}\right)_K &= \left(c^* \cdot \rho_p \cdot K\right)^{1/(1-n)} \cdot \frac{\partial a^{1/(1-n)}}{\partial T_i} \\
\left(\frac{\partial p_c}{\partial T_i}\right)_K &= \left(c^* \cdot \rho_p \cdot K\right)^{1/(1-n)} \cdot \frac{1}{1-n} \cdot a^{1/(1-n)-1} \cdot \frac{\partial a}{\partial T_i} \\
\left(\frac{\partial p_c}{\partial T_i}\right)_K &= \left(c^* \cdot \rho_p \cdot a \cdot K\right)^{1/(1-n)} \cdot \frac{1}{1-n} \cdot \frac{1}{a} \cdot \frac{\partial a}{\partial T_i} = \frac{1}{1-n} \cdot \sigma \cdot p_c
\end{aligned} \tag{8-3}$$

And:

$$\left(\pi_p\right)_K = \frac{1}{1-n} \cdot \sigma \tag{8-4}$$

9 Erosive burning

A general design challenge for solid propellant rocket motors is that you want to pack as much propellant into the motor as possible (a higher volumetric loading). An immediate way to get a higher volumetric loading is to decrease the core diameter. In fact you can decrease the core diameter until the core diameter is identical to the throat diameter. As you approach that condition, you're getting more propellant in the motor but you're also increasing the core Mach number and therefore erosive burning may occur.

"Erosive burning" is the process where the hot, high temperature gases flowing at a high velocity inside the core of the motor flowing over the burning surface of the core speed up the burn rate of the propellant. This generally occurs when the velocity of the gas flow exceeds the so-called "threshold velocity" u_o. It follows:

$$\begin{aligned}
&u \le u_o : r = r_o \\
&u > u_o : r = r_o \cdot \left[1 + K \cdot \left(u - u_o\right)\right]
\end{aligned} \tag{9-1}$$

Here K is a constant.

One of the fundamental things that is understood about erosive burning is that a propellant that is already exhibiting a low regression rate will have its regression rate increased by a much higher percentage than a propellant that's already burning at a high burn rate. Thus, propellants or motors operating at low chamber pressures or with low burn rates are more susceptible to erosive burning.

Predicting erosive burning gets very empirical because the increase in burn rate is a function of many things; the modulus of elasticity of the propellant (the rate at which the propellant can bend and flex), and the size of the ammonium perchlorate crystals in the propellant (larger crystals tend to be rougher in terms of the propellant surface so as the gas scrubs over the surface the burn rate will increase at a proportionally higher rate).

Failure of motors from erosive burning effects is a very common occurrence. As the erosive burning causes the burn rate to increase and raises the chamber pressure, this increase in the chamber pressure in turn raises the burn rate even further, etc. Finally the erosive burning becomes so severe that as the scrubbing of the hot gas over the propellant continues, chunks of propellant can be ripped from the face of the grain, greatly increasing the surface area. A motor failing from erosive burning will typically explode right at the beginning of the burn as the core Mach number and the erosive

burning itself are highest at the beginning of the burn. In fact a design trade can be made where erosive burning can provide a little bit of a spike at the beginning of the motor thrust; then as the core diameter grows the core Mach number falls, and erosive burning is reduced.

A general rule of thumb to use when designing solid propellant rocket motors is to have the diameter of the throat be approximately 3/4th the diameter of the core. The Mach numbers in the core will not be very high. It's very conservative but it will give good operability of the motor, and you'll have a good, safe, conservative design.

10 Combustion instabilities

Solid propellant combustion chambers are sometimes subject to combustion instabilities in the form of large pressure oscillations (5-30% of average chamber pressure) in the chamber *(*Figure 17*).*

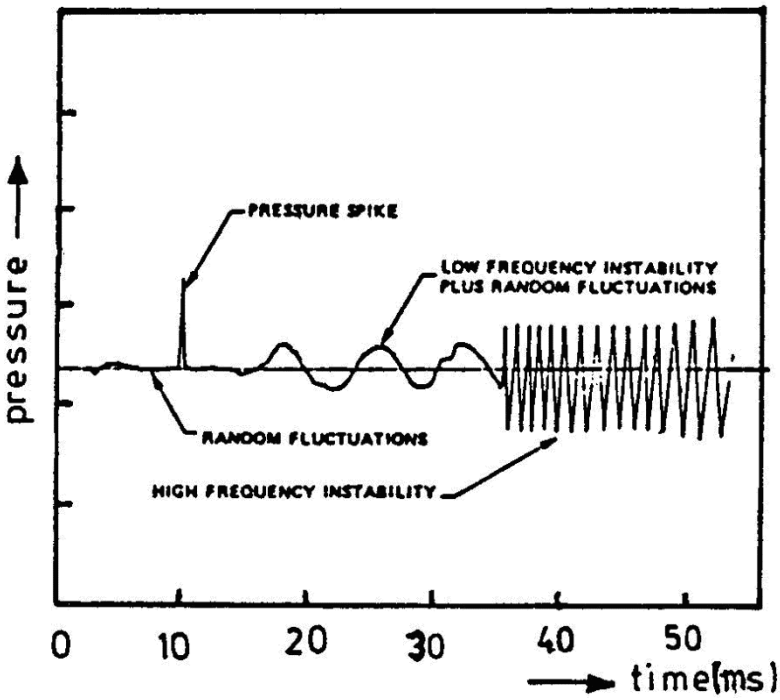

Figure 17: Pressure time diagram showing strong oscillations.

Instabilities can cause engine failure either through excess pressure, increased wall heat transfer, erosive burning or a combination of these. When strong oscillations are encountered, it is usually necessary to take corrective measures on the engine. Sutton indicates three possible remedies:

1. Changing the grain geometry e.g. through simply drilling radial holes at intervals along the grain.
2. Changing the propellant composition.
3. Placing an irregular rod of non-burning material within the free volume, thereby changing again the cavity as with the first remedy listed.

An important instability in solid rocket motors is “chuffing”. This is when the motor spurts and fires, goes out, spurts again and goes out. This is typical of a motor where the chamber pressure has gotten too low. Chuffing is a phenomenon caused by unstable pressure waves inside the motor. It can be the result of not having a convergent section of the nozzle that goes all the way to the wall of the motor or just having a small or no convergent section. Typically chuffing can be avoided by having the motor operate at a higher chamber pressure. In fact, chuffing is extremely rare above 15 bar chamber pressure. In high power rocket motors for years chuffing was a problem, but it has almost been eliminated by just operating the motors at chamber pressures above 15 bar. If the

motor chuffs you must raise the chamber pressure, and the way to do that for the same design (same surface area of the grain) is to reduce the diameter of the throat and therefore raise the Klemmung of the motor.

11 Ignition and extinction

SRB Ignition of a solid rocket motor is normally achieved by some ignition system that includes an igniter device which provides a means of heating the surface of the propellant charge to a high enough temperature to induce combustion. This igniter may be located either at the forward end or the aft end of the chamber (nozzle end). Two categories of igniters are found in SRMs:

1. pyrotechnic igniters, which utilize explosives like black powder or small pellets of propellants that once ignited, results in a large surface burning area. The heat produced by this process then ignites the main grain. This type is commonly used for small to medium sized SRMs.
2. pyrogen igniters, which consist principally of miniature rocket motors with fast burning grains. Once ignited, the resulting flame spreads throughout the gas cavity area. The hot gases of the flame then interact and effectively ignite the main grain. This type of igniter is more common amongst larger SRMs.

All igniters essentially consist of a pressure shell (case) filled with an igniter charge and an initiation system. The igniter charge is a more easily ignitable material, like a metal-oxidizer mixture, than the solid propellant itself. The burning of the igniter charge is initiated by the initiation system, which may be an electric squib or other externally energized means. Most ignition systems include some kind of “arming” feature that prevents ignition by unintended stimuli. For example, for the Space Shuttle SRB ignition can occur only when a manual lock pin from each SRB safe and arm device has been removed. The ground crew removes the pin during pre-launch activities. Next the SRB safe and arm device is rotated to the arm position. Some further details on the dimensioning and sizing of igniters can be found in the chapter on ignition.

Extinction and when necessary, re-ignition of a solid rocket combustion chamber is hard to realize, unlike liquid propellant combustion chambers, where this can simply be done by closing and opening a valve. Usually, operation is stopped by blowing off suitable ports or the nozzle(s) themselves, thus rapidly reducing the chamber pressure and extinguishing the flame. As an alternative, one might consider extinguishing the flame by injection of an inert gas.

12 Solid and liquid particles in the flow

Many solid propellants contain metal additives like Al, B, Mg, which enhance the flame temperature. When burning, they form oxides like Al_2O_3, B_2O_3 and MgO with high melting points. That means that the gas flow which is expanded through the nozzle may contain liquid or solid particles that effect the properties of the flow and consequently effect the performance of the motor. On one hand, the addition of the metals will increase the flame temperature, causing a higher I_{sp}; on the other hand, the presence of heavy particles in the flow will diminish somewhat the I_{sp}.
As the size of the particles is large compared to the size of the gas molecules (a few microns in diameter), they are not subject to Brownian motion. It is realistic to assume no change of state of the solid particles during the expansion process in the nozzle, as the temperature of the gas flow decreases. Therefore, the mathematical treatment of the flow with these solid particles considered, will be like the frozen flow concept discussed earlier. On the other hand, very small particles (diameter less than 0.1 micron) can be considered to behave like a gas of high molecular weight. Using this assumption a two-phase flow will be analysed below.

Consider for the analysis an incremental flow volume as shown in next figure.

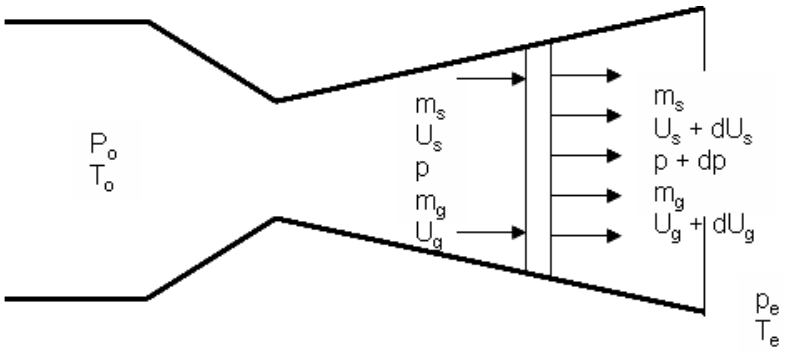

Figure 18: Incremental control volume for the development of two-phase flow equation

It is also assumed that the mass flow of the solid particles, m_s, and the mass flow of the gas, m_g, are constant during expansion. In the direction of the increasing x-coordinate, the pressure decreases and the area of the cross-section of the nozzle increases: $dp/dx < 0$; $dA/dx > 0$.

In case of liquid and solid particles in the flow, the total flow of mass in the motor consists of gas and solid/liquid particles:

$$m = m_g + m_s \tag{12-1}$$

The mass flow of condensed particles can be expressed as a fraction of the total mass flow:

$$\Phi = \frac{m_s}{m_s + m_g} \Rightarrow 1 - \Phi = \frac{m_g}{m_s + m_g} \tag{12-2}$$

The continuity equation for both the gas flow and the solid particles is:

$$\begin{aligned} m_s &= \rho_s \cdot U_s \cdot A \\ m_g &= \rho_g \cdot U_g \cdot A \end{aligned} \tag{12-3}$$

The law of conservation of linear momentum gives:

$$-dp \cdot A = m_g \cdot (U_g + dU_g) + m_s \cdot (U_s + dU_s) - m_g \cdot U_g - m_s \cdot U_s \tag{12-4}$$

Combining (12-3) and (12-4) yields:

$$-dp = \rho_g \cdot U_g \cdot dU_g + \rho_s \cdot U_s \cdot dU_s \tag{12-5}$$

Rewriting this equation in terms of the fraction of the solid gives:

$$-\frac{dp}{\rho_g} = \frac{\Phi}{1-\Phi} \cdot U_s \cdot dU_s + U_g \cdot dU_g \tag{12-6}$$

For a steady state adiabatic flow, the conservation of energy can be written as:

$$m_s \cdot c_s \cdot dT_s + m_g \cdot c_p \cdot dT_g + m_s \cdot U_s \cdot dU_s + m_g \cdot U_g \cdot dU_g = 0 \tag{12-7}$$

Rewriting this equation gives:

$$\Phi \cdot c_s dT_s + (1-\Phi) \cdot c_p dT_g + \Phi \cdot U_s \cdot dU_s + (1-\Phi) \cdot U_g \cdot dU_g = 0 \tag{12-8}$$

Combining the momentum and the energy equation thereby eliminating $U_g\,dU_g$ results to:

$$\frac{\Phi}{1-\Phi} c_s \cdot dT_s + c_p \cdot dT_g + \frac{\Phi}{1-\Phi}\left(U_s - U_g\right)\cdot dU_s = \frac{dp}{\rho_g} \tag{12-9}$$

From this equation, one can finally determine important parameters like the exhaust velocity and the specific impulse. The exact solution of (12-9) can only be approximated by numerical methods. Therefore, some limiting cases will be considered here. The particles and the gas flow may have different temperatures and different flow velocities. The difference in temperature depends on the heat transfer between the gas and the particles; the difference in velocity depends on the drag of the particles.
4 distinct cases can be distinguished:

- High drag ($U_s = U_g$), high heat transfer ($T_s = T_g$).
- High drag, low heat transfer ($T_s = T_c$).
- Low drag ($U_s = 0$), high heat transfer.
- Low drag, low heat transfer.

The cases for fast heat transfer and high drag and slow heat transfer and low drag will be worked out in further detail.

Case a: **Fast heat transfer and high drag**

It follows: $T_s = T_g = T$; $U_s = U_g = U$

Combining the momentum (12-6) and energy equation (12-8) gives:

$$\left(\frac{\Phi}{1-\Phi} c_s + c_p\right)\cdot dT = \frac{dp}{\rho_g} \tag{12-10}$$

With use of the perfect gas law, this changes into:

$$\left(\frac{\Phi}{1-\Phi} c_s + c_p\right)\cdot \frac{1}{R_g \cdot T_g}\cdot dT = \frac{dp}{p} \tag{12-11}$$

Integration of this equation from the state of combustion to the state where the gases are exhausted, gives:

$$\frac{T_e}{T_c} = \left(\frac{p_e}{p_c}\right)^n \text{ with } n = \frac{R}{\frac{\phi}{1-\phi}\cdot c_s + c_p} \tag{12-12}$$

The law of conservation of energy can now be rewritten as:

$$\left[\Phi \cdot c_s + (1-\Phi)\cdot c_p\right]\cdot dT + U \cdot dU = 0 \tag{12-13}$$

Integration gives for the exhaust velocity U_e:

$$U_e = \sqrt{2\left[\phi \cdot c_s + (1-\phi)\cdot c_p\right]\cdot T_c\left(1-\left(\frac{p_e}{p_c}\right)^n\right)} \tag{12-14}$$

This expression for the exhaust velocity is like the general velocity equation for the ideal rocket motor. A correct value of c_p must be introduced and the exponent $(\gamma-1)/\gamma$ is replaced by n. This causes the exhaust velocity to be somewhat lower than in the case without solid particles

Case b: Slow heat transfer and low drag

It follows: T_s = constant; U_s = constant.

From the general equation (12-9) follows now:

$$c_p \cdot dT_g = \frac{dp}{\rho_g} \tag{12-15}$$

With the perfect gas law, this becomes:

$$\frac{c_p}{R_g} \cdot \frac{dT_g}{T_g} = \frac{dp}{p} \tag{12-16}$$

Integration from the state of combustion to the exhaust gives:

$$\frac{T_{g_e}}{T_{g_c}} = \left(\frac{p_e}{p_c} \right)^{\frac{\gamma-1}{\gamma}} \tag{12-17}$$

Integration of the law of conservation of energy (12-8) gives:

$$U_e = \sqrt{2\, c_p \cdot T_c \left(1 - \left(\frac{p_e}{p_c} \right)^{\frac{\gamma-1}{\gamma}} \right)} \tag{12-18}$$

The exhaust velocity is the same as for gases that do not contain solid particles.

Now that we have established the effect of two-phase flow on the exhaust velocity, we can determine its effect on specific impulse thereby considering not only the effects on exhaust velocity, but also on mass flow. The specific impulse can be expressed as:

$$\left(I_{sp} \right)_{eff} = \frac{1}{g_o} \cdot \frac{\sum m_i \cdot U_{e_i}}{\sum m_i} \tag{12-19}$$

As the mass of the solid particles represents about 10% of the total mass flow and as Us will usually be low because of little drag, it is realistic to assume that $m_s\,(U_e)_s << m_g\,(U_e)_g$. In that case, an approximated value of the I_{sp} is found by:

$$\left(I_{sp} \right)_{eff} \cong \frac{m_g \cdot \left(U_e \right)_g}{m_g + m_s} \cdot \frac{1}{g_o} \cong \frac{1}{g_o} \cdot \left(1 - \Phi \right) \cdot \left(U_e \right)_g \tag{12-20}$$

where $(U_e)_g$ is independent of the presence of particles.

The effect of the particles is to reduce the I_{sp} by the factor $1-\Phi$. If drag is high, the solid particles are accelerated, and their velocity will almost become equal to the velocity of the gas flow. The case of fast heat transfer ($T_s \approx T_g$) combined with low drag ($U_s \approx$ constant) and the case of slow heat transfer ($T_s \approx$ constant) combined with high drag ($U_s \approx U_g$) can be treated mathematically in a similar way as cases a and b in this section. In all four cases the I_{sp} will be lower than when no solid particles are present in the flow. The influence of heat transfer and drag can be shown by an example.

The following conditions are assumed:

T_c = 2777.7K	c_s = 2.1 kJ/kg-K
M = 25 kg/kmol	p_c = 54.4 atm
γ = 1.2	p_e = 1 atm
	Φ = 0.10

The effect of the particles on specific impulse under these limiting conditions is indicated in the following table.

Table 2: Effect of particles on the specific impulse under the considered limiting conditions

	No particles present	Accelerated particles		Non-accelerated particles	
		Complete heat transfer	No heat transfer	Complete heat transfer	No heat transfer
		$U_s = U_g$ $T_s = T_g$	$U_s = U_g$ T_s = const.	$U_s \cong 0$ $T_s = T_g$	$U_s \cong 0$ T_s = const.
$I_{sp\,(s)}$	236	228	224	216	213

In those cases where the particles were not accelerated, their momentum flux was neglected in the calculation of the thrust ($m_s U_s << m_g U_g$). As the condensed material does not expand in the nozzle, the presence of the particles brings about a significant loss (compare the case of no particles with the case of accelerated particles and complete heat transfer). The velocity lag of non-accelerated particles accounts for a substantial additional loss of specific impulse. The presence of absence of fluid-particle heat transfer is of less importance.

13 Combustor casing

A solid propellant rocket casing is primarily a pressure vessel, usually consisting of a cylindrical body and a forward and aft dome (front and aft head), which must be provided with suitable ports for nozzles, igniters and other items, and for cylindrical extensions called skirts, see Figure 19. Skirts are integral extensions of the case body which serve as attachment interfaces with other stages or other hardware.

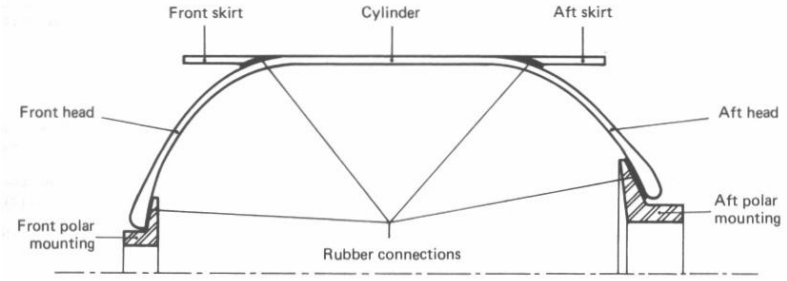

Figure 19: Typical lay-out SRM case [Evans]

To provide for low mass, suitable wall material(s) and wall thickness(es) shall be selected. Typical wall materials include steel, titanium and increasingly common composite (e.g. glass-, Kevlar- and graphite/carbon fibre with epoxy as matrix) materials. Typical properties of these materials have been collected in Annex K. Chamber wall thickness depends greatly on internal pressure. Besides internal pressure several other loads exist that should be considered. Typical such loads are e.g. thrust and bending loads, but also handling loads or loads due to a thermal gradient. It also may be that thickness is limited from manufacturing. More details can be found in chapter entitled “Design of thin shell structures”.

To control failure in case of burst, a solid rocket motor must be fitted with a pressure limiting device, such as shear pins to retain the nozzle or head, or a burst plug; the purpose of such is to provide for a controlled release of pressure before it reaches this critical value.

Very large casings may be built in segments as opposed to single case units, with each segment containing its own cast propellant. For example, the Ariane 5 solid rocket motor casing is made up of 7 ring segments of diameter 3.049 m, 8 mm thick. Six of them, each with a length of 3.351 m, are joined in pairs in the factory (factory joints of Clevis-Tang type) to form the lower and central segments. The seventh, with a length of 2.2258 m, assembled to the forward bulkhead or dome with a height of 1.140 m, constitutes the front segment. A lower bulkhead/dome with a height of 1.005 m, will be connected to the lower segment and carries the nozzle. All parts are pressure tested before joining to form the various segments. After joining the segments, the three segments are fitted with the thermal protection and the forward segment is loaded with propellant. Then the segments are shipped to Guiana. At the Guiana Space Centre, the lower and central segment are charged, and the motor is assembled (field joints) and integrated with the engine (nozzle) and the additional equipment (skirts, actuation unit, etc.) The way the segments are linked is one of the most critical problems posed by this engine (see also Challenger Shuttle Disaster). Notice the O-ring type of seals to ensure that the joint is leak-tight.

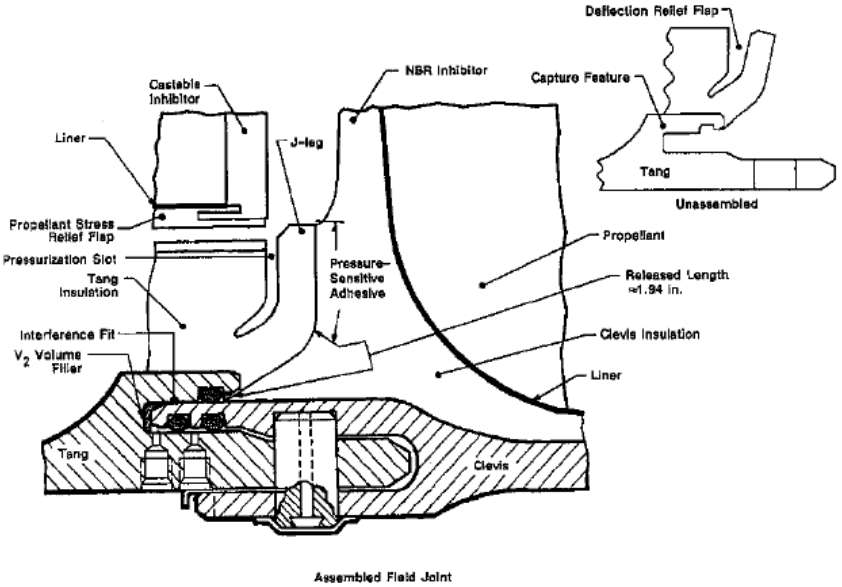

Figure 20: Cross-section of Solid Rocket Booster (Tang and Clevis) field joint (courtesy NASA)

Segmenting a design may be desirable to allow for transportation and for homogeneous casting. However, according to Koelle a segmented design generally is heavier than a single case unit. The following quality measure (denoted by Q) can be used to compare different case designs if they are of equal length:

$$Q = \frac{p_b V_{case}}{M_{case} \cdot g_o} \tag{13-1}$$

Here p_b is burst pressure, V_{case} is internal volume, M_{case} is case mass, and g_o is standard acceleration at sea level. This factor has the dimension of a length. Case volume depends on the volume required to store the propellant and for proper combustion. Case mass depends on materials used, their thickness, etc. A first estimate for case mass can be obtained based on shell mass, where shell mass may be estimated from shell thickness. For more details, see chapter entitled “Mass estimation of thin-walled structures”.

14 Insulator and liner

To protect the motor case against the hot erosive environment inside the combustor, an insulator is required. This insulator is especially needed for those areas that are exposed longest to this environment as at the aft head end/closure of the case and at the igniter

(provided this is installed at the front end). However, as the web thickness varies over the grain, also other parts of the motor case may be exposed for some time to this hot environment. For instance, the Space Shuttle solid rocket motors have various segments that have a tapered grain as to accommodate thrust programming. Protecting the case with an insulator prevents the case to fail. Examples of motor case insulation materials used include Nitrile Butadiene Rubber (NBR), Ethylene-Propylene-Diene-Monomer (EPDM) rubber filled with silica (in old SRMs asbestos has been used), or aramid, graphite or carbon pulp. Most of these insulators are ablative types of insulated that slowly regress through ablation). For more information on ablative cooling, see the earlier chapter on cooling of rocket motors. Care should be given to ensure sufficient thickness of this type of insulator in relation to the time the material is exposed. Typical ablation rates obtained with aramid filled EPDM in the advanced solid rocket motor (a replacement for the reusable Space Shuttle solid rocket motor) as reported by [Bell] are in the range of 0.2 mm/s to 0.6 mm/s at the aft dome. Thickness is determined by exposure time and ablation rate with some manufacturing tolerance of 0.5 to 1 mm and a safety factor of 2. Exposure time typically follows from grain burn back analysis, see earlier in this section on SRM combustors, but at the aft dome, there is a section that is exposed during the full burn time. For the Space Shuttle SRM, with a burn time of about two minutes, the insulator design is shown in the next figure, taken from [McDonald]. In this design, thermal safety factors of 2 on ablation/erosion and 1.25 on char have been applied.

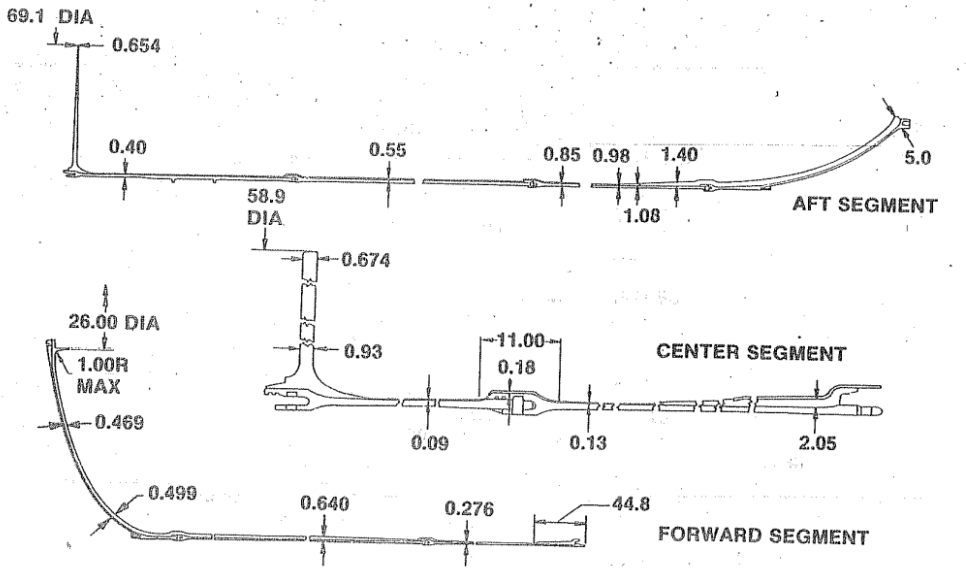

Figure 21: Space Shuttle RSRM motor case insulation thickness variation (all measures in inches).

Typical properties of some insulator materials (mass density, ultimate tensile strength and coefficient of thermal expansion), can be found in annex K. Some information related to their manufacturing can be obtained from [Meiirbekov].

To ensure a proper connection of the grain to the structure, thereby preventing an unfortunate enlarging of the burn surface as well as the movement of the grain in the motor, some liner is needed. This liner is a thin adhesive layer between the insulator and the propellant grain that fixes the propellant in the grain. Solid rocket motor liners are typically made from elastomeric polymers like Hydroxyl-Terminated Polybutadiene (HTPB), reinforced with carbon black particles for improved mechanical and thermal properties. Other common materials include silica-phenolic for its insulation and EPDM-based ablatives reinforced with aramid or phenolic) fibres for heat shielding. From this, it shall be clear that liner and insulator materials can be one and the same material.

For illustration, it is mentioned that for the Space Shuttle solid rocket booster [McDonald], the mass of the insulation is about 8.2 tons (as compared to a case structural mass of ~44 tons). This gives a mass percentage of ~20% = 8.2 tons/44 tons*100%). Liner mass and inhibitor mass are 1.4% and 1.9% of the structural mass of the case, respectively.

15 Testing

Major combustor development tests relate to grain/propellant development and combustor case development.

Tests on casing
All the casing components are to be subjected to a high level of stress to reach the safety margins required. This may include incorporating a burst test (hydro-proof test) of the casing demonstrating the designed-in safety (qualification load is two times nominal flight load of 1.4 -1.5 times worst case flight load). Typically, several cases are hydro-proof tested to establish variability and design margins. Non-destructive testing using X-ray and ultrasonics is used to establish unit to unit “fingerprints”.
In case the casing is of a segmented design, special care must be given to testing the leak-tightness of the joints. In practice, this may be performed by rapid pressurisation of the joints, e.g. by using a gas generator.
In a later stage also compatibility with other motor hardware (skirts, nozzle, etc.) shall be verified. Especially the leak tightness of the case to nozzle joint is critical.

Propellant/grain tests
Typically, when developing a solid rocket motor, you will create a new propellant, and you really don't know much about its ballistic characteristics. Different HTPB/AP/Al based propellants at a Klemmung of say 200, may exhibit chamber pressures anywhere from 5 to 50 bar. It would depend on the propellant, the size of the Ammonium Perchlorate (AP) crystals in the propellant, the aluminium content and the size of the aluminium particles, and the different burn rate additives that were added. It is a very empirical phenomenon determining just what the chamber pressure will be. So, a typical design technique used is to construct the motor and fire it. First, however, you need to validate controllable propellant mixing for example by checking physical, ballistic and mechanical characteristics of the propellant. Also, tests should be performed to test casting or the loading of the propellant in the case. Initially this is with inert material, later this is with the real propellant. Finally, tests shall be performed to determine the combustion quality, the actual pressure, etc.

Problems

1. For a solid rocket motor the following properties have been established:
   - Solid propellant density: 1720 [kg/m^3]
   - Chamber (hot gas) temperature: 2220 [K]
   - Chamber pressure: 13.80 [MPa]
   - Specific heat ratio of hot gases: 1.27
   - Regression rate (or burning rate): r = 3.81 [cm/s]
   - Molar mass of hot gases in combustion chamber: 22.1

   Calculate for this motor:
   a. The "Klemmung" (K)

   Given is that you design the motor for flight at sea level, and that you select a cigarette burning grain, a thrust of 4500 [N] and a burn time of 15 [s].

   Determine:
   b. Area of burning surface and throat diameter
   c. Initial volume and mass of solid propellant
   d. Specific impulse
   e. Regression rate

2. For a solid propellant are given:
   - Burning rate = 8 [mm/s] at 10 [bar] pressure and 20 °[C]
   - Pressure exponent = 0.4

- Temperature sensitivity is 0.5% per °[C].

Calculate for this propellant the burning rate at 0°[C] and 40°[C].

3. A fuel-rich solid propellant gas generator is used to drive a turbine of a liquid propellant turbo-pump. The gas generator is required to produce a steady mass flow rate of 0.257 kg/s. The propellant used for the gas generator has the following characteristics:
   - Burn rate at standard conditions (294 K and 6.895 MPa): 4 mm/sec
   - Burn time: 110 sec
   - Chamber pressure: 5.1 MPa
   - Pressure exponent n: 0.55
   - Propellant mass density: 1470 kg/m^3

   Determine the size (dimensions) of a cylindrical end-burning grain that suits the above requirements.

4. A solid propellant rocket with an end-burning grain is required to have the following characteristics at a normal ambient temperature of T_i^o=15 ^{o}C: sea level thrust F=4.91 kN and a burn time of 15 s. The characteristics of the propellant, a potassium perchlorate-asphalt combination (76.5%$KClO_4$ and 23.5% asphalt and oil) are as follows (all pressures are expressed in bar; sea level pressure may be taken equal to 1 bar):
   - Burning rate (cm/s), $r = \{0.102\ e^{[0.0015(Ti-15)]}\}\ p^{0.745}$
   - Characteristic velocity (cm/s), $c^* = \{105{,}100\ e^{[0.00021(Ti-15)]}\}\ p^{0.015}$
   - Specific heat ratio, $\gamma = 1.27$
   - Molecular weight, W = 30
   - Propellant density, ρ_p = 1770 kg/m^3
   - Chamber pressure, p_c = 135.5 bar

   Determine for this rocket:
   a. Combustor/chamber temperature.
   b. Specific impulse.
   c. Propellant grain dimensions A_b and L;
   d. Influence of a 1% variation in the burn rate of the propellant on the thrust and the chamber pressure.
   e. Motor performance at T_i = 55 ^{o}C and -25 ^{o}C.

5. You are designing a SRM with a propellant mass of 1800 kg. You select an internal burning cylindrical grain with a cylindrical port (not a Bates grain). Given are:
   - Propellant mass density is 1500 kg/m^3
   - Regression rate: 2 cm/s (constant)
   - Web thickness: 20 cm
   - The length of grain is identical to the length of motor case

   Questions:
   a. Determine size (length and outer diameter of grain) and volumetric loading fraction as a function of initial grain port diameter and list the values obtained for a port diameter of 0.4 m and 0.7 m.
   b. Plot port diameter, mass flow rate, and burn surface area versus time for a grain length to outer diameter ratio of 1.75. Generate a table that provides values of mass flow rate and burn surface area at start and just prior to end of burn.
   c. Discuss how the grain dimensions and burn time change in case the regression rate given is increased. Propellant mass is to remain constant.

6. A solid propellant motor operating at sea level is characterized by two operating phases: boost and cruise. The motor is required to operate at a

range of ambient temperatures (T_i) between 0° C and 50° C. Nominal design is for T_i = 20° C.

The propellant grain is divided into one large end-burning cylindrical grain and a number (n) of smaller diameter cylindrical propellant rods which burn at the circumference, but not the ends (see schematic).

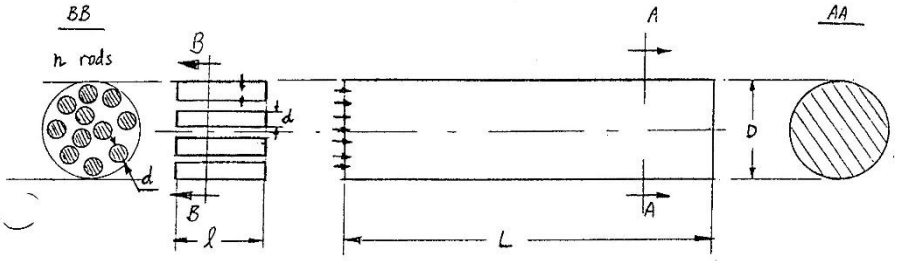

During the boost phase, all the charges burn together, while during the cruise phase, only the end-burning charge remains.

Under nominal operating conditions, the boost phase has to provide a total impulse of I = 490 Ns. The nozzle is adapted to the cruise phase operation (end burning charge only), which provides 300 N thrust for 40 s.

Constraints: The design constraint is that under no conditions (including extreme ambient temperatures) would the chamber pressure exceed 200 atm.

Given are: C*= constant, ρ_p = 1.65 g/cm^3, Mw = 25 g/mol, γ = 1.2, Π_r = 0.15%/°C, D = 10 cm.

Under nominal cruise conditions I_{sp} = 225 s and r [cm/s] = 0.25(P_c[atm])$^{0.4}$

Assumptions: Assume that the overall cross section of the propellant rods is equal to 40% of the cruise grain cross section. Also assume that during the boost phase, the mean values of C_F and F are their average between the initial and final values.

Find (not necessarily in the order indicated):
1. A_t, P_e, C*
2. For nominal initial temperature (T_i = 20°C):
   a. Plot the variation of thrust with time.
   b. For the cruise phase, find r, P_c
   c. For the beginning of the boost phase, find P_c, F and I_{sp}.
   d. For the end of the boost phase, find P_c, F and I_{sp}.
3. Find d, l, L, n = number of rods (may be non-integer)

7. Two-phase flow loss
You are designing a rocket motor with the following properties:
   - Chamber temperature: 2800 [K]
   - Average molar mass of exhaust products: 25 [kg/kmol]
   - Specific heat ratio: 1.2
   - Chamber pressure: 5.5 [MPa]
   - Ideal expansion at sea level

   a. Determine for this motor the specific impulse in absence of any losses.

   Given that we have 10% condensed material in the exhaust with a specific heat of 2100 [J/(kg K)] determine the specific impulse in case we assume:
   b. Fast impulse- (high drag) and heat transfer
   c. Fast impulse- and negligible heat transfer

References

1. Barrère M., Jaumotte A., Fraeijs de Veubeke F., and Vandenkerckhove J., Rocket Propulsion, Elsevier Publishing Company, 1960.
2. Bell, M.S., Tam, W.F.S., ASRM Case Insulation Design and Development, Aerojet-General Corp, NASA-CR-191947, October 1992.
3. Evans P.R., Composite motor case design, chapter in “Design methods in solid rocket motors”, AGARD-LS-150, 1987.
4. Hartfield R., Jenkins R, Burkhalter J., Foster W., A review of analytical methods for solid rocket motor grain analysis, AIAA 2003-4507, July 2003.
5. Humble R.W., Henry G.N. and Larson W.J., Space Propulsion Analysis and Design, 1995.
6. Koelle D.E., Transcost 6.0, TCS Ottobrunn, Liebigweg 10, Germany, 1995.
7. McDonald A.J., Design Evolution of the Space Shuttle Solid Rocket Motors, Morton Thiokol inc., published by AIAA, 1985.
8. Megson T.H.G., Aircraft Structures for engineering students, Edward Arnold, 3rd. Ed. ISBN 03407-05884.
9. Meiirbekov M., Sadykov M., Kuandyk A., Nurzhanov M., Yesbolov N., Baiserikov B., Kulbekov A., Modern thermal protection systems for solid rocket motors: A comparative review of composite manufacturing technologies, published by Elservier B.V., August 2025.
10. Schőyer H.F.R. et al, Rocket Propulsion and Spaceflight Dynamics, 1979.
11. Stalin P., Santosh Kumar Y.N.V., Nazumuddin S.K., Design and geometrical analysis of propellant grain configurations of a solid rocket motor, in Internat. Journal of Engineering Development and Research, vol. 2, Issue 4, 2014.
12. Sutton G.P., Rocket Propulsion Elements, 6th edition, John Wiley & Sons Inc., 1992
13. PBNA Polytechnisch Zakboekje, 48th edition, 1998.

For further reading

- Design Methods in Solid Rocket Motors, AGARD Lecture Series No. 150, 1988
- Solid rocket motor technology, AGARD-CPP-259
- Low pressure combustion characteristics of composite propellant, by H.F.R. Schőyer and P.A.O.G. Korting, LR report LR-367, 1982
- Some typical solid propellant rocket motors, by B.T.C. Zandbergen, TU-Delft/LR, M-712, September 1995.

- This page is intentionally left blank -

HYBRID COMBUSTOR DESIGN

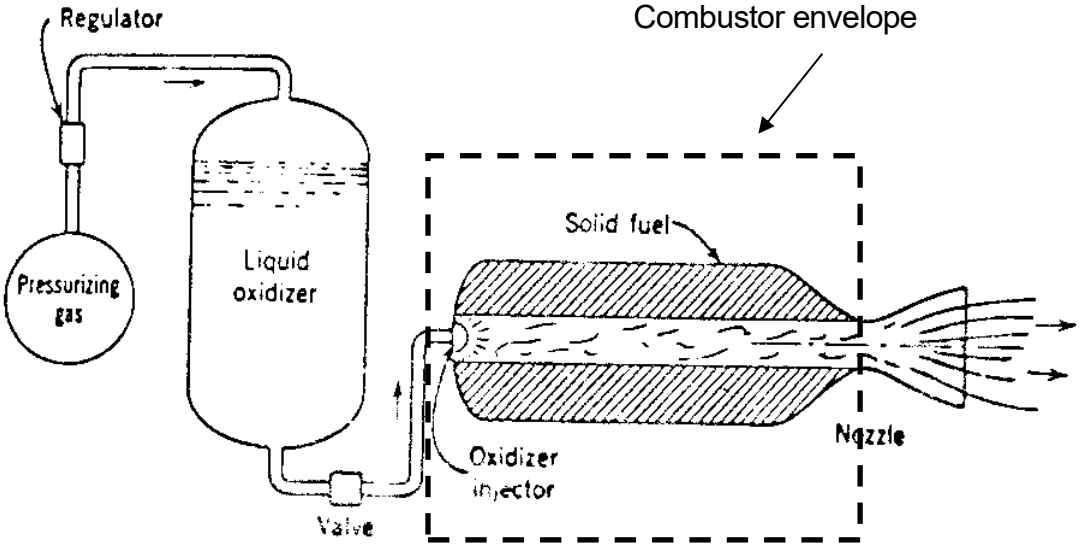

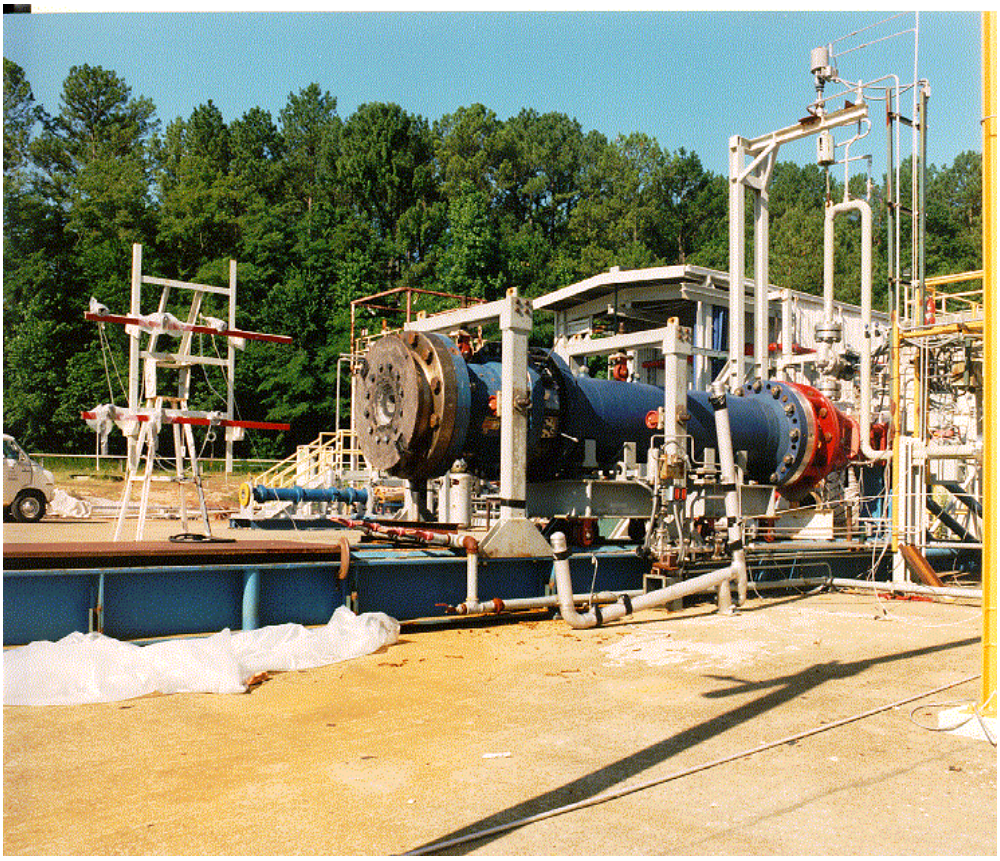

Contents

Contents 288

Revisions table 288

List of symbols 289

1 Introduction 290

2 Hybrid combustor lay-out 291

3 Test combustors 293

4 Liquid injection 294

5 Fuel regression rate 294

6 Internal ballistics modelling 300

7 Casing 302

8 Homework problems 302

References 304

Revisions table

ID	Description
February 2016	Added text on theoretical performances of hybrid rocket motors Added one more homework problem Decimal separator changed from comma to point Added text on pressure drop over combustor Included reference to appendices on regression rate determination
August 2017	Added small section on liquid injection Added two more homework problems

List of symbols

Roman

A	Area
B	Spalding number
c_f	Local skin friction coefficient
c*	Characteristic velocity
G	Mass flux
h	Enthalpy, heat
L	Length of fuel grain
m	Mass flow
M	Mass
p	Pressure
Pr	Prandtl number
q	Heat flux
Q	Heat rate
r	Regression rate
R	Radius
Re	Reynolds number
St	Stanton number
tTime	
T	Temperature
v	Velocity
V	Volume
x	Distance along grain in axial direction

Greek

Φ	Oxidiser-to-fuel mass ratio
μ	Dynamic viscosity
ρ	Density

Subscripts

c	Chamber, convection
f	Fuel
mel	Melting
ox	Oxidiser
p	Port
Pyr	Pyrolysis
s	Solid
t	Throat
v	Fuel gasification
vap	Vaporization

1 Introduction

In a hybrid rocket combustor, the propellant combination used consists of a solid component and a liquid or gaseous component. it is usually the fuel that is stored in the solid state and the oxidiser in the liquid (or gaseous) state[1]. Figure 1 shows a schematic diagram of a typical hybrid rocket system.

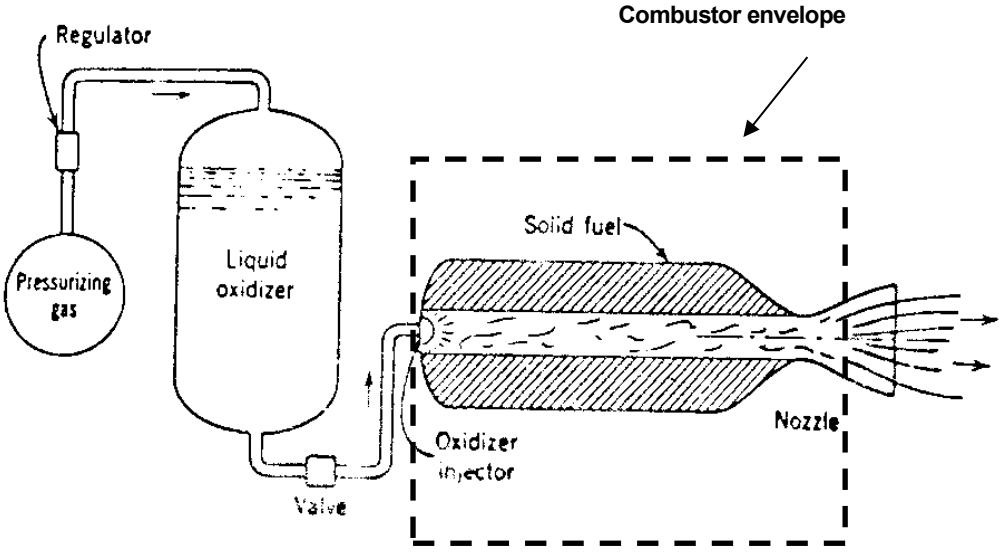

Figure 1: Hybrid rocket system layout

For reasons of simplicity, the solid propellant component, hereafter taken to be the fuel, is stored in the rocket combustion chamber into which the liquid or gaseous oxidiser is injected and burned. The solid is stored in the form of a shaped block (fuel grain), which allows for designing for different fuel mass flow rates.
The solid fuels today[2] are like the organic binders used in solid propellant motors. However, for manufacturing purposes, HTPB (rubber) or PMMA (Plexiglas) are preferred. Nano-sized energetic metal particles like Al and B or metal containing particles like B_4C are added to enhance the I_{sp} and/or the regression rate. Typically, the solid fuel is mixed and then poured into the casing of the motor and allowed to set and turn into a rubbery, semisolid form - like how gelatine is mixed, poured and allowed to set until it becomes almost solid.
The oxidizers used in hybrid rockets are either gaseous or liquid. For operational purposes liquids like liquid oxygen, hydrogen peroxide nitrous oxide, nitric acid and nitrogen tetroxide (LOX, H_2O_2, N_2O, HNO_3, and N_2O_4) are considered. Of these the first three are considered non-toxic. Nitrous oxide furthermore has the advantage that it is benign, storable, and self-pressurizing to about 48 bars at room temperature. For research and educational purposes, O_2 stored in high-pressure bottles is preferred (cheap and reliable). Typical hybrid propellant densities found are in the range 1000-1200 kg/m^3.

Attainable performances using hybrid rocket motors depend on the fuel and oxidizer selected, the mixture ratio at which they are burned, the combustion pressure and the combustion and nozzle quality. Theoretical optimum values for sea level specific impulse for hybrid propellant rocket motors are in the range 210-325 s, depending on the propellant combination selected [Calabro]. Theoretical sea level performances for some nitrous-oxide based hybrid propellant combinations as a function of oxidizer-to-fuel mass ratio at a combustion chamber pressure of about 35 bar and assuming ideal expansion are given in Figure 2.

[1] Rocket motors, which use a liquid fuel and a solid oxidizer, usually are referred to as *inverse* hybrid rocket motors.
[2] In the early days of hybrid rocket motor development fuels also included wood, and wax loaded with carbon black.

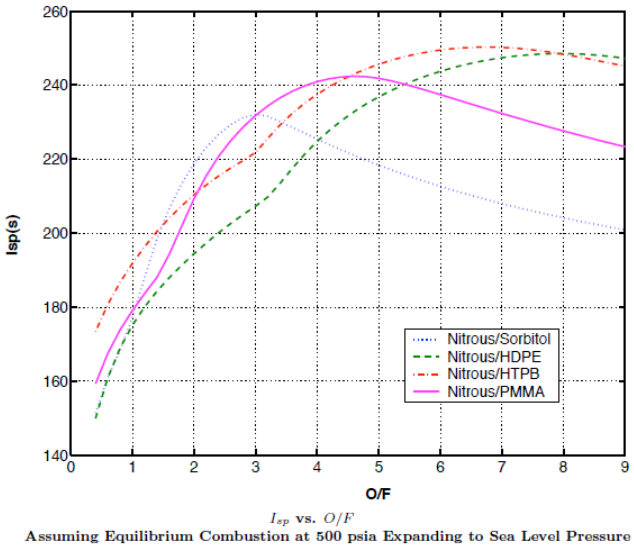

Figure 2: Theoretical performance for various nitrous oxide-based hybrid propellant combinations [Lohner]

An overview of combustion quality and I_{sp} quality of hybrid rocket motors for a range of hybrid propellant compositions can be obtained from [Bozic]

The burning of the inert solid fuel is very similar to the way a household candle burns. In the combustor the oxidizer flows down a port in the solid fuel grain and reacts with the solid fuel. This produces the hot exhaust gases required to produce thrust. This process can be seen in the following figure:

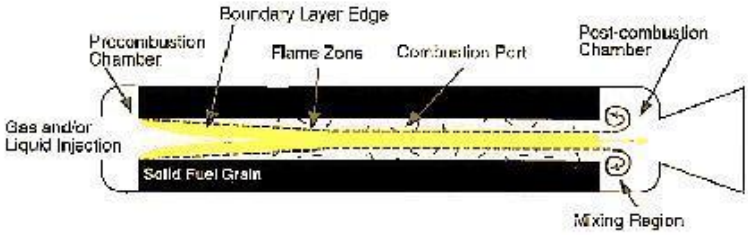

Figure 3: Hybrid combustion

The amount of oxidizer that flows through the port is constant. However, the fuel mass flow is almost zero at the head end, whereas it is maximum at the exit of the grain port. This means that the oxidizer-to-fuel ratio (O/F), varies along the length of the hybrid fuel grain, i.e., it has an axial dependency. In a liquid rocket, the injectors generally inject both the fuel and the oxidiser at one end of the combustion chamber thus there is no axial dependency. In a solid rocket motor, there is no injector head, and every particle is bound of fuel and oxidiser, thus ensuring the O/F remains pretty much constant.
Furthermore, because of a change in burn surface, we should also expect that fuel mass flow rate changes in time and hence also the O/F ratio.

2 Hybrid combustor lay-out

The burning of the inert solid fuel with the gaseous or liquid oxidiser occurs in a hybrid propellant combustor or shortly hybrid combustor. In every hybrid combustor, next to the combustor case itself and the insulation, we can distinguish five main parts:

- One or more fuel grains
- A liquid injector
- An igniter
- A flame stabilizer
- A pre- and post-combustion chamber

These parts will be discussed in more detail hereafter.

2.1 Fuel grain configuration

The configuration of the fuel grain is important, as next to the fuel regression rate, it determines the mass flow rate at which the fuel enters the combustion port. In addition, it largely determines the volumetric efficiency (length and outer diameter) of the motor. The next figure shows some typical configurations used in hybrid rocket motors.

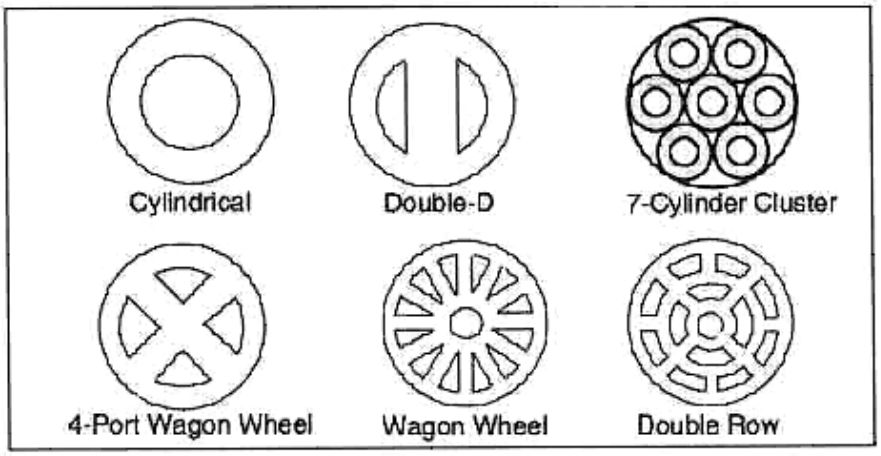

Figure 4: Typical port configurations for hybrid rockets

Comparing the cylindrical single-port configuration with the cylindrical multi-port configuration, we find that they both offer a progressive burning surface. Compared to the multi-port configuration, the single port configuration offers ease of manufacturing and minimum number of slivers. On the other hand, however, it requires longer length to diameter ratios to achieve an appropriate oxidizer-to-fuel mass mixture ratio. In general, the multi-port configuration allows for quite short and compact motors, with length to diameter ratios in between 3-7.

In general, the trick is to choose the best configuration with respect to manufacturing, and volumetric loading efficiency of the solid.

2.2 Liquid injector

There are two methods of injection that can be used for injecting the liquid (or gas) into the combustion chamber of a hybrid rocket motor[3]:

1. Direct injection into the fuel grain port.
2. Injection into a pre-combustion chamber.

For hybrid rocket motors on the high power and amateur rocketry level, where a single circular port geometry is most frequently used, direct injection of the liquid is the best approach, since there is no need to inject multiple liquid streams down multiple ports, and hence less requirement for a homogenised liquid stream from multiple injector nozzles.

Injection into a pre-combustion chamber is more useful for larger motors, or motors where a multi-port geometry is used for the fuel grain, since multiple injectors are more common, and even mixing of the liquid stream needs to be achieved before it is passed over the solid grain.

[3] Feeding of the liquid into the combustor, i.e. the combustion port can be by pressurized gas, gas generator or pump. In case of selecting a blow down pressurized-gas system, one should take into account that the feed pressure drops during operation and hence the liquid mass flow rate varies.

2.3 Igniter

To start the combustion, an ignition device is needed. Sometimes ignition is achieved by a hypergolic mixture. Once combustion is established, operation continues until the flow of the liquid or gaseous component is halted.

2.4 Flame stabilizer

When putting a candle in high-velocity airflow, there is a large change that it is blown out. To allow flame stabilization, a rearward-facing step may be used to generate a region of relatively low flow velocities directly behind the step. This, however, may increase uneven burning along the grain. Typical levels of oxidizer mass flux in the absence of flame stabilization measures reported are in the range 80-200 kg/m^2-s with the lowest value giving the lowest flow velocity in the grain port.

2.5 Pre- and post-combustion chamber

A pre- and post-combustion chamber sometimes are included. A pre-combustion chamber ensures even mixing of the oxidiser stream before it is passed over the fuel grain. This is particularly important in case of a multi-port fuel grain. An aft or post combustion chamber allows the flow to settle and enhances the complete combustion of the fuel (improved combustion quality). Typical values of combustor quality are in the range 80-95%.

3 Test combustors

Before use in light-weight flight motors, all propellants are characterized in a heavy test combustor. At a minimum, fuel regression rate verification tests, and oxidizer injection flow tests are required. Figure 4 shows a laboratory scale test motor for propellant characterization. It basically is of a modular design and includes a solid fuel grain, a settling chamber, an oxidiser injector, an aft combustion chamber, mounting rods, and an electrically fired chemical torch igniter. In principle, it can use any solid fuel in combination with gaseous oxidiser (or even air) as propellant. The shape of the grain is mostly cylindrical with a single central port usually also of a cylindrical shape. The length of the grain can vary between about 0.2 m to 1.0 m. To prevent excessive heating of the nozzle, water is used as coolant. This motor, furthermore, can be equipped with nozzles varying in diameter.

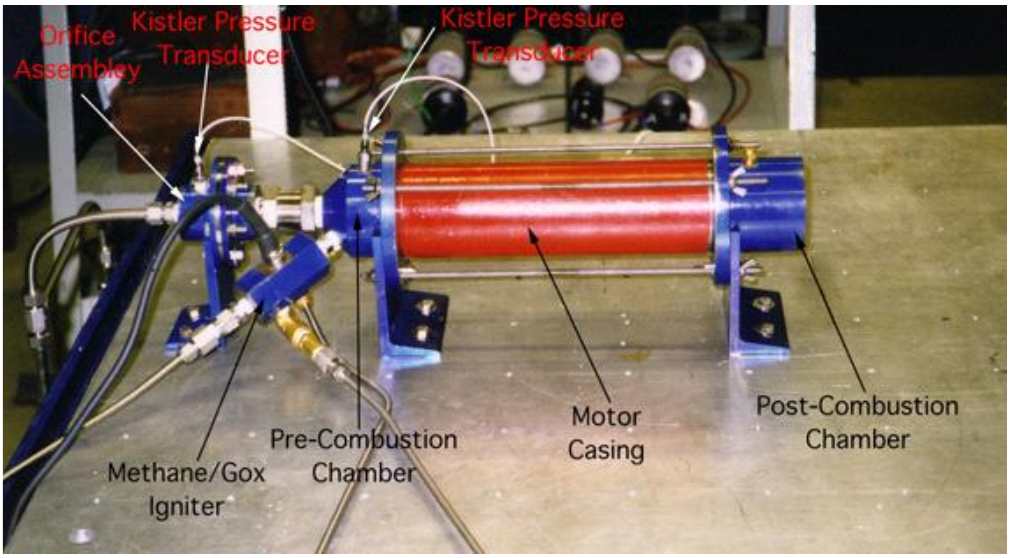

Figure 5: Test combustor (courtesy Stanford University)

A normal operation sequence is as follows. First, a valve in the oxidizer feed line is opened, allowing the oxidizer to flow into the combustor. Prior to entering the settling chamber, some (gaseous) fuel is added to the flow to establish an ignitable mixture. Then ignition is initiated. The hot ignition gases flow into the combustor and cause the (initially solid) fuel to evaporate and mix with the incoming flow. This phase is usually referred to as the ignition phase. When the temperature of the gas flowing through the chamber is sufficiently high, the gaseous fuel reacts with the oxidizer in the flow, hence starting combustion. After some time, the igniter fuel flow is stopped and the combustion must continue by itself, i.e. the combustion phase. The combustion stops by closing the earlier mentioned valve in the oxidizer feed line.

4 Liquid injection

Liquid injection in a hybrid rocket motor is comparable to liquid injection in a liquid rocket engine, be it that usually only a single component is injected. It can also be compared to for instance the injection of diesel or fuel in an internal combustion engine. Like for most injectors, the purpose is to obtain a spray consisting of small droplets nicely distributed over the chamber. A spray can be roughly described by four parameters (Figure 6): the spray tip penetration S, the spray angle θ, the break-up length (or liquid length) and the global Sauter mean diameter[4].

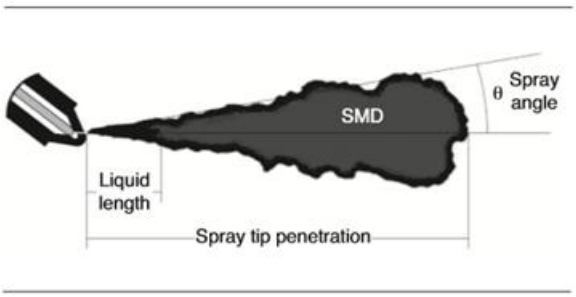

Figure 6: Spray characteristics

Depending on the injector shape selected, the pressure drop over the injector, the liquid injected and whether liquid injection occurs in an evacuated chamber or a chamber filled with some medium, like pressurized combustion gases, the spray characteristics will vary. Relations for the 4 characteristic parameters for various types of injectors are amongst others discussed in [Dos Santos] or [Lefebvre]. Of course, the best spray is the spray that allows for the highest combustion efficiency. This requires the designer to select the best injector that fits the injection conditions best as to allow for optimizing the combustion, while ensuring that stabilities do not progress upstream in the feed system. For this, like for the liquid rocket engine, it is necessary to have a sufficiently high pressure drop over the injector.

5 Fuel regression rate

In a hybrid rocket motor the oxidizer and the solid fuel can react, because the hot gases from the combustion process cause a small layer of the fuel to vaporize. This fuel then reacts with the unused oxidizer to produce more combustion gases.
The rate, at which the fuel burns, is referred to as the **regression rate** and is measured in units of length divided by units of time. Typical regression rates are of the order of mm/s.

5.1 Empirical results

Several methods exist to determine the regression rate of the solid. These methods all determine the regression rate by dividing the distance regressed normal to the fuel surface by the time span over which this regression takes place. Usually, this time span is kept as short as possible, because the operating conditions in the motor tend to change when regression occurs. Differences between the various methods are mainly in the

[4] Sauter Mean Diameter or SMD is defined as the diameter of a drop having the same volume/surface area ratio as the entire spray.

method used to determine the distance regressed and the associated time span. Three methods used and applied to grains with an initially cylindrical port are:

1. An (overall) average distance regressed for the whole fuel grain determined from port geometry and solid density by weighing the fuel grain before and after the test and with the burn time determined from a pressure-history plot. In case a short burn time is chosen, the change in port area may be thus limited that the regression rate can still be seen as an instantaneous value.
2. The distance regressed is determined locally from measurement of the internal shape of the grain before and after the test with the burn time determined in the same way as in the first method. This regression rate usually is referred to as the local average regression rate.
3. Ultrasonic equipment is used to locally determine the thickness of the solid as function of time. This allows determining the difference in fuel thickness over a short time span of not more than some tenths of a second. Since this time span is very short, the regression rate, which results from this method, is usually referred to as the (local) instantaneous regression rate.

Burn time may be determined from a chamber pressure[5] versus time plot, see for instance Figure 7.

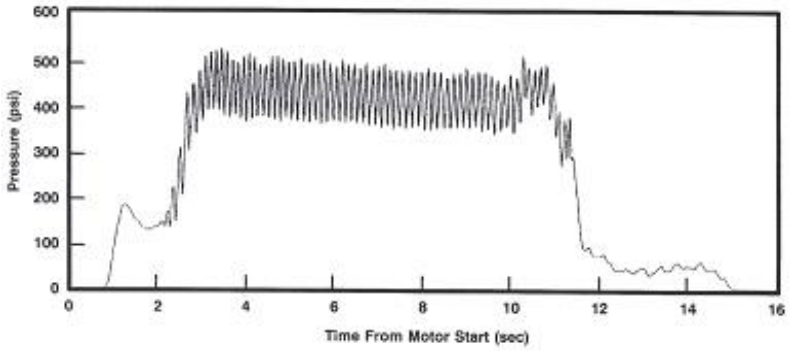

Figure 7: Pressure history plot

Chamber pressure history may be determined by using amongst others a piezo-electric pressure transducer. Even so, the determination of the burn time from a pressure-time plot may present some difficulty, since it is not always clear where the actual burning starts and stops.

Even burning

In regression rate studies, one usually speaks about even burning, when the regression rate is constant along the grain. Even burning is important to ensure high fuel utilization and to allow the use of equation 2 for determining the fuel mass flow. In figure 4, the internal shape of an initially cylindrical fuel grain is given after about 30 s of combustion in a 0,3 m long fuel grain [van der Geld, Korting, and Wijchers (1987)]. From this plot, we learn that for this grain uneven burning is rather limited, except at the head-end of the grain. This finding is very much in agreement with those of amongst others [Grigorian (1994)].

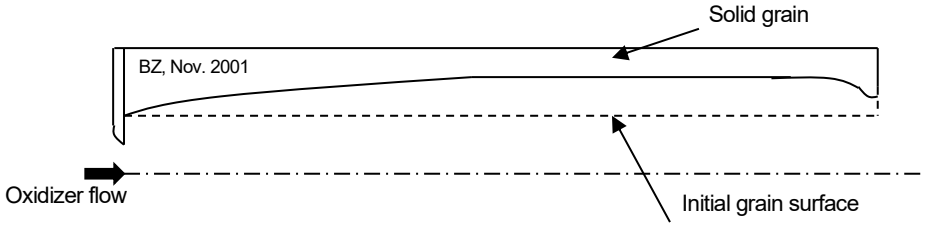

Figure 8: Typical hybrid combustor solid fuel surface profile after combustion.

[5] Static and total (combustion) chamber pressure are almost identical in the combustion chamber. This is mainly because of low flow velocities in the combustion chamber.

Regression rate history

The next figure gives a plot of the regression rate as a function of time at a specific location in the fuel grain as determined by [van der Geld, Korting, and Wijchers (1987)] using air as oxidizer and Plexiglas as fuel. The plot indicates that the regression rate is fairly stable in time, except during the ignition phase. Comparable results have been found by [Grigorian (1994)], who performed tests using different port diameters.

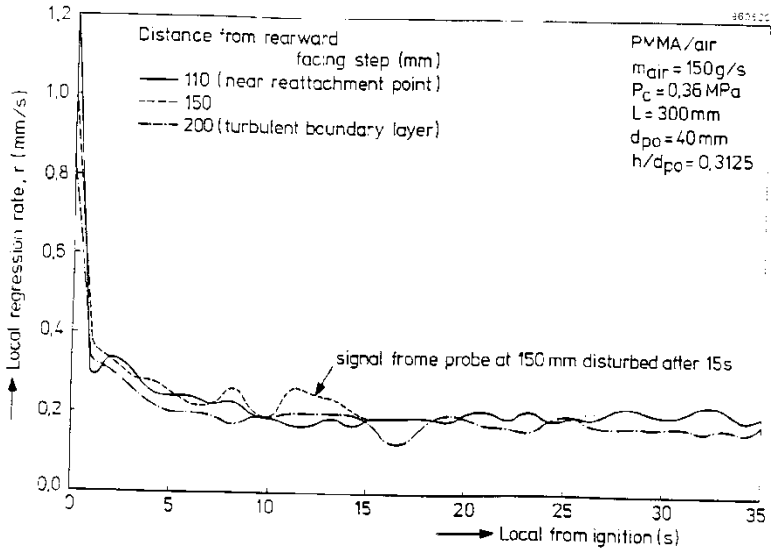

Figure 9: Typical regression rate histories [van der Geld, Korting, Wijchers (1987)].

Time-averaged overall fuel regression rate

The time-averaged regression rate is mostly used for ballistic design calculations. It is determined by weighing the fuel grain before and after the test and measuring the burn time. Typical values found depend on the hybrid propellant combination and are of the order of 0,5-2 mm/s ± 0,01 mm/s, see also table 1. For some hybrid propellants, however, values of up to 10 mm/s have been reported [Schmucker (1972)].

Data analysis suggests that the (time and space averaged) fuel regression rate, r, can be expressed in terms of the oxidizer mass flux, G_{ox}, or the total mass flux, G:

$$r = a \cdot G_{ox}^{\ k} \qquad \text{or} \qquad r = a' \cdot G^{k'} \tag{4.1}$$

With:

$$G_{ox} = \frac{m_{ox}}{A_p} \qquad \text{or} \qquad G = \frac{m}{A_p} \tag{4.2}$$

Here m_{ox} is the oxidizer mass flow and m the total (oxidizer + fuel) mass flow through the (cross-sectional) area A_p of the bore. A value for the fuel mass flow can be determined from the mass loss and the burn time, whereas a value for the oxidizer mass flow follows from flow measurement. The port area can be taken equal to either the initial port area (at the start of the test) or the average port area over the test duration. Other options are also possible, but these are the ones used most frequently.

There is also some experimental evidence of a slight dependence on pressure, p, and fuel grain length, L, expressed by:

$$r = a \cdot G_{ox}^{\ k} \cdot p^{l} \cdot L^{m} \tag{4.3}$$

In this equation k, l, and m are referred to as regression rate exponents and a as regression rate constant. Typical regression rate formulas that illustrate the effect of various design parameters on solid regression are given in the following table.

Table 1: Regression rate formula for specific hybrid propellants

Propellant combination	Regression rate formula (r in cm/s)	Remarks	Source
85% Hydrogen peroxide and polyethylene	$7x10^{-4}\ G^{0.8}\ L^{-0.2}$	G is total propellant mass flux in kg/(m^{2}s); length of fuel grain L in m.	Bettner, M. and Humble, R.W.
Polybutadiene and liquid oxygen	$2x10^{-3}\ G^{0.763}\ L^{-0.148}$	G is total propellant mass flux in kg/(m^{2}s), length of fuel grain L in m.	AMROC
Polybutadiene and gaseous oxygen	$4.27x10^{-3}\ G_{ox}^{0.681}$	G_{ox} is oxidiser mass flux in kg/(m^{2}s).	Sutton G.P.
Paraffin and gaseous oxygen	$6.86x10^{-3}\ G^{0.5047}$	G is mass flux in port in kg/(m^{2}s)	Nakagawa

Recent experimental investigations [Risha, 2001] have shown that adding energetic metallic powders can lead to an increase of up to 50% in regression rate compared to the pure fuel.

5.2 Theoretical modelling

To determine the regression rate experimentally, usually extensive testing is required. However, this can be very expensive. Hence, since about 1946 [Green (1963)], a great many theoretical studies have dealt with the problem of predicting the regression rate of the solid.

Sutton has suggested that the basic mechanism governing the fuel vaporization and hence the regression rate is the transfer of heat from a flame zone close to the vaporizing surface to this surface. This process is shown schematically in the following figure:

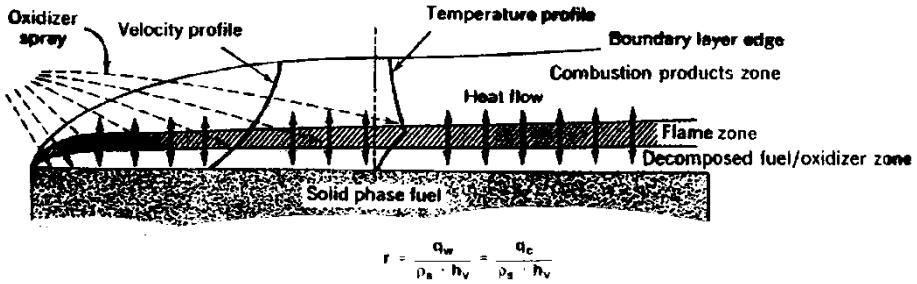

Figure 10: Solid fuel regression (source "Rocket propulsion Elements", by G.P. Sutton)

The heat transfer from the hot flame to the solid fuel basically may be due to both convection and radiation. With use of the heat transfer equation, the burning rate coefficients can be deduced in the following, simplified way.

Consider steady state burning. The heat transfer through the burning surface is equal to:

$$Q_w = m_f \cdot h_v = \rho_f \cdot r \cdot h_v \cdot S \tag{4.4}$$

And per unit surface area:

$$q_w = \rho_f \cdot r \cdot h_v \tag{4.5}$$

Here h_v is the enthalpy due to gasification of the solid fuel at the burning surface. In other words, this is the heat needed to gasify unit mass of solid. [De Wilde] uses the following expression to determine the heat of gasification of a solid:

$$h_v = \int c \, . dT + h_{mel} + h_{vap} + h_{pyr} \tag{4.6}$$

With:

- h_v effective heat of gasification
- h_{mel} heat of solid-to-liquid phase change (melting)
- h_{vap} heat of liquid-to-gas phase change (vaporization)
- h_{pyr} heat of fuel pyrolysis (breaking/unzipping of bonds)
- c specific heat
- T temperature

[de Wilde] determined values for the heat of gasification of polyethylene between 1700-2900 kJ/kg and for Plexiglas from 1750-2500 kJ/kg, depending on the temperature at which the fuel is gasified.

For a first approximation, and since the emissivity of gases generally is low, radiation heat transfer is usually neglected. In that case, all heat transfer is due to convection, and we may write:

$$q_w = q_c = St \cdot \rho \cdot v \cdot \Delta h_T \tag{4.7}$$

The Stanton number, St, is often not known but can be replaced by the local coefficient of friction c_f, as follows from the Reynolds analogy:

$$St \cdot Pr^{0,67} = c_f / 2 \tag{4.8}$$

Taking the Prandtl number equal to 1, one has:

$$St = c_f / 2 \tag{4.9}$$

The friction coefficient is defined as the ratio between the shear stress at the wal, τ_o, and the dynamic pressure of the flow:

$$c_f = \frac{\tau_o}{1/2 \cdot \rho \cdot v^2} \tag{4.10}$$

The fuel regression rate follows from the heat transfer through the burning surface and is equal to:

$$\rho_f \cdot r = \frac{q_w}{h_v} \tag{4.11}$$

Combining the equation for convective heat transfer and using the Reynolds analogy (Pr = 1) yields:

$$\rho_f \cdot r = \frac{c_f}{2} \cdot \rho \cdot v \cdot \frac{\Delta h_T}{h_v} \tag{4.12}$$

The ratio between the enthalpy difference Δh_T between the hot gases and the wal and h_v, the enthalpy needed for the gasification[6] of the solid fuel, is called the Spalding number, B:

$$B = \frac{\Delta h_T}{h_v} \tag{4.13}$$

Typical ratios of $\Delta h_T/h_v$ reported for hybrid fuels are in the range 1 to 10. For example, for polyethylene at 750 K follows that h_v = 1700 kJ/kg. Using oxygen as the oxidizer, leading

[6] Heat of gasification is sometimes erroneously referred to as heat of evaporation.

to a (stoichiometric) flame temperature of 3000 K[7] [Zandbergen (1991)], it follows for the sensible enthalpy a value of about 3136 kJ/kg. This then gives for B a value slightly below 2.

The fuel regression rate can thus be written as:

$$\rho_f \cdot r = \frac{c_f}{2} \cdot \rho \cdot v \cdot B \tag{4.14}$$

For incompressible turbulent flow over a flat plate, without mass addition, the friction coefficient at location x is related to the Reynolds number determined at location x (Blasius):

$$c_{f,o} = 0.06 \cdot Re_x^{-0.2} = 0.06 \cdot \left(\frac{G \cdot x}{\mu} \right)^{-0.2} \tag{4.15}$$

If mass addition is taken into consideration, the value of c_f can be related to $c_{f,o}$ and the Spalding number:

$$c_f = 1.2 \cdot c_{f,o} \cdot (B)^{-0.77} \tag{4.16}$$

This is valid for a range $5 < B < 200$[8]. A further modification may be to take into account the effect of temperature on density and viscosity of the fluid, see section on heat transfer. This is left for the reader to explore for himself.

Using the equation for the local skin friction coefficient, we find for the fuel regression rate:

$$\begin{aligned} \rho_f \cdot r &= 0.036 \cdot G \cdot Re_x^{-0.2} \cdot B^{0.23} \\ r &= \frac{0.036}{\rho_f} \cdot \left(\frac{x}{\mu} \right)^{-0.2} \cdot G^{0.8} \cdot B^{0.23} \end{aligned} \tag{4.17}$$

For a given propellant combination fuel density is constant, and viscosity and the Spalding number depend only weakly on temperature, hence we may also write for the local instantaneous regression rate:

$$r = a \cdot (x)^{-0.2} \cdot G^{0.8} \tag{4.18}$$

In case the fuel mass flow is neglibly small compared to the oxidiser mass flow we find for the average regression rate of the solid fuel after integration over the length L of the grain:

$$\bar{r} = 1.25 \cdot \frac{0.036}{\rho_f} \cdot \left(\frac{L}{\mu} \right)^{-0,2} \cdot G_{ox}^{\ 0.8} \cdot B^{0.23} = a' \cdot (L)^{-0.2} \cdot G_{ox}^{\ 0.8} \tag{4.19}$$

It then shows that for a given propellant combination, the regression rate (whether local or averaged over the grain) depends on the oxidizer mass flux to the power 0.8. Furthermore, we find that there is a slight effect of distance travelled along the grain and hence of the grain length (to the power -0.2).

The simple model derived above clearly confirms the influence of mass flux and length of the fuel grain on regression rate as found in experiments. No relationship is found

[7] According to [Marxman, Wooldridge and Muzzy (1964)] some data exists, that indicate that the flame temperature differs from the theoretical flame temperature at the stoichiometric mixture ratio.

[8] A more accurate relation valid at lower values for B is [*Lees (1958)*]:

$$c_f = c_{f,o} \cdot \frac{\ln(1+B)}{B}$$

between pressure and regression rate. This, however, is attributed to not taking into account radiation heat transfer, which is known to have a pressure dependence. Further questions that may be raised to using this simple model are whether it is correct to use a simple flat plate approximation for the modelling of the convective heat transfer even though it is based on the mass flux as the main parameter. For these aspects, the reader is referred to a.o. [Green (1963)], who gives an excellent overview of several other models used to predict the regression rate.

6 Internal ballistics modelling

Internal ballistics deals with the flow of the combustion gases in a hybrid rocket motor and the gas mass generated per unit time. Internal ballistics modeling is of importance as it allows determining the motor pressure, and whether the motor operates in a stable or unstable way. For instance, the motor pressure may determine the amount of oxidizer that flows into the chamber, or the feeding pressure needed to ensure a given mass flow rate. The oxidizer mass flow rate in turn determines the regression rate and hence the oxidizer to fuel mass mixture ratio.

Fuel mass flow

The fuel mass flow in a hybrid rocket motor depends on fuel regression rate, fuel density and area of burning surface:

$$m_f = \rho_f \cdot r \cdot S \tag{5.1}$$

In this relationship, it is assumed that regression rate and density of the fuel are constant along the grain. Only the dependence of the regression rate in time is considered. Using:

$$\bar{r} = a_o \cdot G_{ox}^{\ k} \tag{5.2}$$

$$G_{ox} = \frac{m_{ox}}{A_p} \tag{5.3}$$

With the constant 'a_o' being a regression rate coefficient incorporating grain length, it follows for the fuel mass flow:

$$m_f = \rho_f \cdot r \cdot S = \rho_f \cdot a_o \cdot G_{ox}^{\ k} \cdot S \tag{5.4}$$

Here both oxidizer mass flux and area of the burning surface vary with time.
Assuming a burning law exponent close to 0.5 (k = 0.5) for G_{ox}, we find for a cylindrical port:

$$m_f = \rho_f \cdot a \cdot \sqrt{\frac{m_{ox}}{\pi \cdot R^2}} \cdot 2\pi \cdot R \cdot L = 2\rho_f \cdot a \cdot \sqrt{m_{ox} \cdot \pi} \cdot L \tag{5.5}$$

From this relationship, we learn that when the oxidizer mass flow is kept constant, the fuel mass flow will also be constant (with time).

In figure 9 results are given for a case with k equal to 0.8, again for a fuel grain with a cylindrical port geometry.

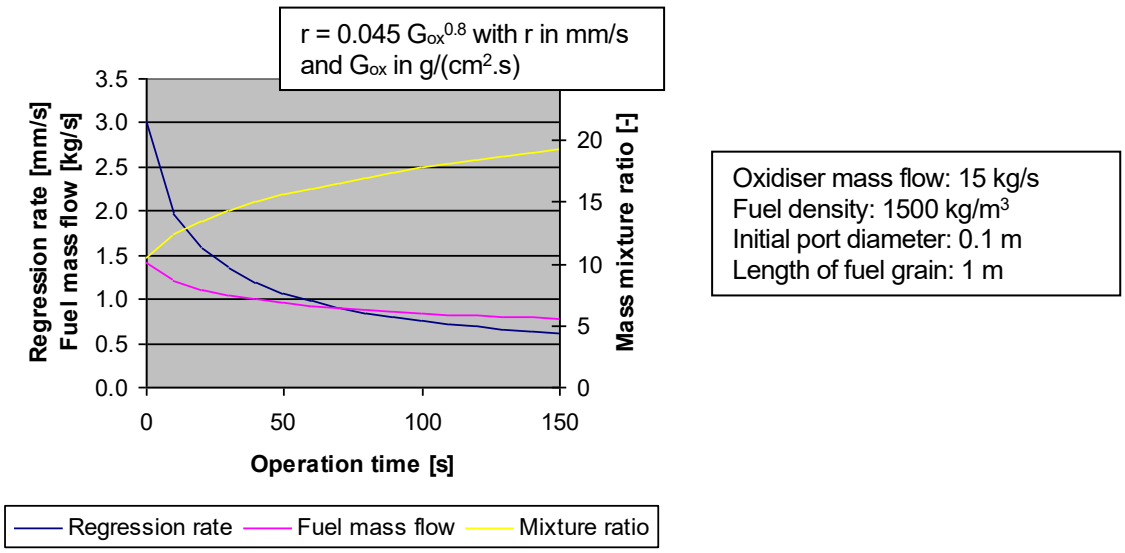

Figure 11: Fuel regression rate and mass flow versus time

Results indicate that regression rate decreases in time (from about 3 mm/s to 0.5 mm/s). This is attributed to the increasing diameter, which leads to a decreasing oxidizer mass flux. Results indicate also a decreasing fuel mass flow even though we know that the burning surface must increase in time. Therefore, we find that the oxidiser-to-fuel mass ratio increases with time from about 10 to 20.

Operating pressure

The law of conservation of mass basically says that the propellant mass flow entering the motor, $m_{ox} + m_f$, should equal the sum of the increase in gas mass M_c per unit time in the combustion chamber and the mass flowing through the nozzle per unit of time m_n.

$$m_{ox} + m_f = m_n + dM_g/dt \tag{5.6}$$

Where:

$$\frac{dM_g}{dt} = \frac{d(\rho_c V_c)}{dt} = \rho_c \cdot \frac{\partial V_c}{\partial t} + V_c \cdot \frac{\partial \rho_c}{\partial t}$$

$$\frac{\partial V_c}{\partial t} = r \cdot S \tag{5.7}$$

$$\frac{\partial \rho_c}{\partial t} = \frac{V_c}{R \cdot T_c} \cdot \frac{\partial p_c}{\partial t} = 0 \quad \text{(quasi - steady conditions)}$$

In general, during steady state burning, the progressivity or regressivity of the grain is slight and the chamber pressure does not vary much (quasi-neutral burning), compare for solid rocket motors. Therefore, the time derivative of the chamber pressure is assumed zero.

It follows from the conservation of mass that under quasi-steady state conditions the propellant mass flow entering the motor, $m_{ox} + mf$, equals the gas mass m_n discharged through the nozzle per unit of time:

$$m_{ox} + (\rho_f - \rho_c) \cdot r \cdot S = \frac{p_c \cdot A_t}{c^*} \tag{5.8}$$

Using ($\rho_c << \rho_f$), we get:

$$m_{ox} + \rho_f \cdot r \cdot S = m_{ox} + m_f = \frac{p_c \cdot A_t}{c^*} \tag{5.9}$$

Substitution of

$$r = a \cdot G_{ox}^{\ n} \tag{5.10}$$

gives for the operating pressure (quasi-steady state):

$$p_c \approx c^* \cdot \rho_f \cdot a \cdot G_{ox}{}^n \cdot \frac{S}{A_t} \cdot (\Phi + 1) \tag{5.11}$$

With Φ representing the O/F ratio. This relationship shows that during operation of a hybrid rocket motor (at constant oxidizer mass flux), chamber pressure tends to change due to changes in fuel mass flow and characteristic velocity (due to a changing oxidizer to fuel mass flow ratio, see also figure 9).

In practice, hybrid rocket motors tend to operate in a fairly rough way (rougher than liquid and solid propellant rocket motors) with large pressure variations about some mean value, see figure 5. If well designed, pressure fluctuations can be kept to about 2-5% about the mean.

7 Casing

The casing of the hybrid combustor is primarily a pressure vessel and like for a solid rocket motor generally consists of a cylindrical body and a forward and aft dome. It is different from a solid rocket motor casing in that it must allow for mounting an injector plate. In that respect it compares well with a liquid propellant combustor. The igniter may be mounted on to the side or like for a liquid rocket engine mounted on the head end dome. In the latter case an igniter tube is used to feed the hot ignition gasses into the engine. For further details, the reader is referred to the sections on combustor structural design in the chapters “LRE combustor design” and “SRM combustor design”.

8 Homework problems

1) Theory shows that regression rate can be written as equation (4.18) , where 'G' is total (oxidizer and fuel) mass flux, 'x' is distance measured from leading edge of grain, and 'a' is regression rate constant. Theory shows that 'a' depends on the solid fuel density ρ_f, the Spalding number or blowing coefficient 'B' and the dynamic viscosity of the reactant mixture μ.

$$r = a \cdot G^{0.8} \cdot x^{-0.2} \tag{7.1}$$

Determine:

a) A value for the regression rate constant ‘a’ using a fuel density of 1200 [kg/m^3], a dynamic viscosity of 10 x 10^{-6} [Pa s], and a Spalding number (B) of 8.
b) An expression for the average regression rate over the length 'L' of the fuel grain at a certain instant in time assuming a tubular fuel grain and that the fuel mass flow rate is much smaller than the oxidizer mass flow rate.
c) An expression for the time-average regression rate for a tubular grain with length L, initial diameter D_o, and instantaneous diameter D.

2) You are investigating the use of a new liquid oxidizer - solid hydrocarbon propellant combination for use in a hybrid rocket motor. The fuel regression rate for this propellant combination is determined by the following relation:

$$r = 0.036 \cdot \left(\frac{G^{0.8}}{\rho_f} \right) \cdot \left(\frac{\mu}{x} \right)^{0.2} \cdot B^{0.23} \tag{7.2}$$

Where G is total (oxidizer and fuel) mass flux, ρ_f is density of fuel (1600 kg/m^3), μ is dynamic viscosity of hot gas (10 x 10^{-6} Pa.s), x is distance measured from leading edge of grain, and B is Spalding number or blowing coefficient, here taken equal to 5.

You have selected a single port cylindrical fuel grain configuration with a cylindrical port (outside diameter of 40 cm, internal diameter of 20 cm and a length of 2 m). Furthermore, you have selected a (constant) oxidizer mass flow of 5 kg/s.

Determine for this configuration:

a) Average regression rate at start of combustion (t = 0 s);
b) Average regression rate at end of combustion given that the average distance regressed equals 75 mm.
c) Total fuel mass flow rate and mixture ratio at start of combustion and at web burnout (based on average regression rate).
d) Sliver mass (mass remaining at end of burn; depends on local regression rate). Consider that, because of uneven burning, locally regression may be up to 3 times higher than when averaged over the full grain surface.

3) For a four-port wagon wheel grain, see figure, you estimate a constant (both in time and place) fuel regression rate of 0.8 cm/s.

4-Port Wagon Wheel

You aim for the grain to burn for 20 seconds. Given are that the grain has a length of 6.5 m and an outer diameter of 160 cm. In addition, it is given that the thickness of the spokes is twice that of the outer rim.

Calculate for this grain the initial (at start of combustion) burn surface.

4) Figure shows a grain with a cruciform shaped port. The angle between the two arms is 90° and the initial length and width of each of the two arms is 0.58 m and 0.2 m, respectively.

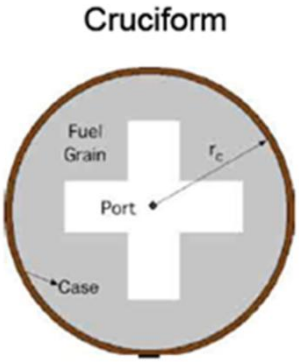

Consider for this grain a constant (independent of time and location along the grain) fuel regression rate of 2 mm/s. Furthermore, are given a grain length of 10 m, a grain outer diameter of 1 m.

a) Calculate for this grain the initial (at start of combustion) burn surface.

b) After some time, the grain has regressed over 10 cm. Determine for this condition the resulting burn surface, assuming that the cruciform shape is maintained (no rounding of corners).

5) Hybrid rocket motor design (adapted from Sutton)

A hybrid rocket engine uses nitric acid as a liquid oxidizer and a plastic (hydrocarbon) as a fuel. Its characteristics are as follows:

- I_s (actual) 205 sec at p = 17 bar
- r (averaged over the burn time): 1,25 mm/sec
- Chamber pressure initial (@ start of combustion): 17 bar
- Average mixture ratio: 4.6
- Mass density of polyethylene: 940 kg/m^3
- Specific heat ratio of combustion gases: 1.14
- Chamber length is 1.1 times the length of the fuel grain

Determine the principal dimensions of a rocket chamber and grain and make an estimate of the total propellant mass of the unit for a total impulse of 225 kNsec, a minimum duration of 50 sec (average thrust of 4500 N), and an optimum operating altitude of 3000 m. When applicable, also determine sliver mass and volumetric loading fraction.

Note: End of combustion is taken here at the time of web burnout.

References

1) Abramowitz M., Stegun I.A, Handbook of mathematical functions, Dover Books, New York, 1965.

2) AMROC, Design and testing of AMROC's 250,000 lbf thrust hybrid rocket motor, AIAA 93-2551, 1993.

3) Bettner and Humble, Polyethylene and Hydrogen Peroxide Hybrid Testing at the United States Air Force Academy, USAFA.

4) Bozic O., Porrman D., Lancelle D., Hartwig A., Program AHRES and its contribution to assess features and current limitations of hybrid rocket propulsion, IAC-120C4.2.8, 63rd IAC, October 2012.

5) Calabro M., Overview on Hybrid Propulsion, Progress in Propulsion Physics 2, 353-374, 2011.

6) Dos Santos F. and Le Moyne L., Spray Atomization Models in Engine Applications, from Correlations to Direct Numerical Simulations, retrieved from http://ogst.ifpenergiesnouvelles.fr/articles/ogst/pdf/2011/05/ogst100079.pdf (November 2016)

7) Geld, C.W.M. van der, Korting, P.A.O.G. and Wijchers, T. Combustion of PMMA, PE and PS in a ramjet, TU-Delft/LR, LR-514, Delft, April 1987.

8) Green L. (jr.), Introductory considerations on hybrid rocket combustion, Progress in Astronautics and Aeronautics, Vol. 15, pp. 451-484, 1963.

9) Grigorian, V. Propellant characterisation and design of a hybrid rocket engine, IAF conference paper, IAF ST-94-W.2.576, October 1994.

10) Lefebvre, A.H., Properties of Sprays, International Conference on Mechanics of Two-Phase Flows, Taipei, Taiwan, June 12-15, 1989.

11) Lohner K., Dyer J., Doran E., Dunn Z, Zilliac Z., Fuel Regression Rate Characterization Using a Laboratory Scale Nitrous Oxide Hybrid Propulsion System, AIAA 2006-4671, 2006

12) Nakagawa I., Hikone S., Suzuki T., A study on the regression rate of paraffin-based hybrid rocket fuels, AIAA-2009-4935, 45th Joint propulsion conference, Denver, Colorado, August 2009.

13) Risha G.A., Ulas A., Boyer E., Kumar S., and Kuo K., Combustion of HTPB-Based Solid Fuels Containing Nano-sized Energetic Powder in a Hybrid Rocket Motor, AIAA 2001-3535, 2001.

14) SPIAG, Solid Rocket Motor briefing, June 1999.

15) Sutton G.P., Rocket propulsion elements, 6th ed., Wiley Interscience, 1992.

16) Wilde J.P. de, Fuel pyrolysis effects on hybrid rocket and solid fuel ramjet combustor performance, DUP, 1991

17) Zandbergen B.T.C., Some typical hybrid propellant rocket motors, TU-Delft/LR, M-680, November 1995.

18) http://www.spacedev.com, August 2003.

Mass estimation/scaling of LRE thrust chambers, SRM and HRM

Contents

Contents 305

List of symbols 306

Acronyms 306

1 Introduction 307

2 Shell mass estimation basics 308

3 Combustion chamber/motor casing 308

4 Injector plate 309

5 Conical nozzle (divergent) 310

6 Combined chamber, injector and nozzle 311

7 SRM and HRM shell mass 312

8 Validation 313

9 Summary of main findings and conclusions 318

References 319

Revisions table

ID	Description
Version 1.1, August 2017	Some small changes made to text
Version 1.2, August 2018	Major rewrite of introduction More detailed contents table Added section on SRM and HRM shell mass estimation Validation section has been extended
Version 1.3, August 2020	Relations 4-1, 6-1, 6-3 and 6-4 have been corrected

List of symbols

Roman

D	Diameter
E	Young's modulus
j	safety factor
K	shell mass correction factor
M	mass
N	number of cycles
p	pressure
r	radius
R	blow-down ratio
R_a	absolute gas constant
S	surface
t	thickness
T	temperature
V	volume

Greek

ε	strain
μ	Poisson ratio
ρ	density
σ	ultimate stress
ψ	thrust-to-weight ratio

Subscripts

b	burst
f	fibre
g	pressure gas
h	hydrostatic
i	initial
p	propellant
t	tank
u	ullage
v	vapour

Acronyms

MEOP	Maximum Expected Operating Pressure

1 Introduction

Various methods exist to estimate liquid rocket engine thrust chamber mass and solid and hybrid rocket motor dry mass[1]. An obvious method is to collect mass data on thrust chambers, and/or solid/liquid rocket motors and use regression analysis to determine a relation between chamber/motor mass on one hand and some design parameter, like thrust or propellant mass carried within, on the other hand, see for instance appendix H for liquid rocket engines and appendix J for solid rocket motors. This method, though, has a few disadvantages, being:

- Mass data is sometimes hard to come by; we typically need a minimum of 10 data points with at least an order difference in the value of the design parameter to allow meaningful regression.
- Rocket thrust chambers or rocket motors sometimes differ greatly in their design including for instance single-wall radiation cooled thrust chambers, single wall ablation and insulation cooled chambers, double wall designs, different materials being used, etc. In case this is not considered in the regression analysis, this generally leads to a high estimation uncertainty of roughly 20-40% (1-sigma). To improve estimation efficiency, different classes of thrust chambers/solid and hybrid rocket motors can be distinguished, but for each class at least 10 additional data points are needed.

Here, we will take a slightly different approach using simple analytical relations that will allow us a more fundamental insight into the parameters determining thrust chamber /rocket motor mass. For this approach, we consider the thrust chamber/rocket motor to consist of 3 major components, being the chamber/motor case, injector plate (LRE and HRM only) and nozzle divergent:

$$M_{chamber} = \sum_{i=1}^{3} M_i \tag{1-1}$$

Of course, the method can be adapted to also include other masses, like the mass of the igniter or of the insulator/ablator protecting the chamber wall, but for now, for simplicity, we stick to these 3 components. In the end, it is the accuracy attained that helps to decide if more detailed modelling is needed or not.

The method that will be presented assumes that each element can be treated as a thin shell[2] with internal pressure being the most important load. Component mass is than estimated from:

$$M_i = K_i \times M_{i,shell} \tag{1-2}$$

Where K_i is a component correction factor that allows considering per component additional mass items like mounting provisions, thermal insulation, and provisions for cooling. Multiplying the K-factors from the elements leads to an overall K-factor. Values of the component K-factors and the overall K-factor shall be determined using actual data for the components and the total thrust chamber obtained from literature. Hereafter, we will first explain how shell mass is determined (section 2). In sections 3 to 5, we will develop estimation rules for chamber/case, injector plate and nozzle based on applying thin shell theory to simple geometries (sphere, cylinder, cone, plate). In sections 6 and 7 we will derive some compound relations that allow for mass estimation of thrust chamber and solid and hybrid rocket motor directly. Here it will be shown that the two main parameters affecting the mass of thrust chamber/motor are thrust level and nozzle area ratio. In section 8, we will apply the relations developed to a few existing thrust chambers/motors to demonstrate its strength, but also its weaknesses. In section 9, we will summarize the main findings.

[1] Mass of solid and hybrid rocket motor without propellant load.

[2] In thin shell theory, it is assumed that the wall thickness of an internally pressurized element is much smaller than its radius ($t << R$). This theory usually gives realistic numbers up to about $t < 0.1\ R$.

2 Shell mass estimation basics

Any element that has a flat or curved plate-like structure with a thickness t and plate area S made of a material with a homogeneous mass density can be considered a shell element. The mass of such a shell can be estimated using:

$$M_{shell} = \rho_i \cdot S_i \cdot t_i \tag{2-1}$$

Where ρ is density of shell material. Note that in case t is not constant, we can use an average value for t.

In case the shell consists of multiple layers, i.e. a compound shell, like when dealing with composite over-wrapped chamber walls or a double wall chamber or a chamber wall covered by an insulation material or ablator, we may write:

$$M_{shell,\,i} = \sum_n \rho_n \cdot S_n \cdot t_n \tag{2-2}$$

Where n refers to the different material layers. Applying a thin shell approach (t << R) to simple geometrical shapes that form part of in internally pressurized vessel, the wall thickness can be determined using simple analytical relations.

A note of caution should be given on the use of thin shell theory in the sense that for small pressure vessels and low operating pressures, unreasonably low thickness values may result. In that case we should consider using minimum wall thickness as follows from manufacturing, see chapter “Design of thin shell structures”.

3 Combustion chamber/motor casing

For the chamber we will consider a spherical chamber (section 3.1) followed by a cylindrical chamber (section 3.2). Here we will primarily use the theory presented in the earlier mentioned chapter “Design of thin shell structures”.

3.1 Spherical chamber/combustor case

Considering internal pressure only, chamber/case wall thickness of a spherical shaped combustor can be calculated using:

$$t = \frac{p_b \cdot D_c}{4\sigma} = \frac{MEOP \cdot D_c}{4\sigma} \cdot j \tag{3-1}$$

Here σ is ultimate strength of material, t is thickness of shell, p_b is burst pressure, i.e. the pressure at which the shell is likely to fail catastrophically, MEOP is (maximum) expected operating pressure, D_c is diameter of chamber and j is overall safety factor given by:

$$j = KP \text{ x } KM \text{ x } FOSY \text{ (or } FOSU) \tag{3-2}$$

Its value varies from 1.1 to 1.8 for yield and from 1.25 to 2.1 for ultimate strength.

Using the relation for shell mass and combining with known information on combustor geometry (surface area and volume), we obtain:

$$\left(M_{case,sphere}\right)_{id} = \frac{3}{2} \cdot \frac{\rho}{\sigma} \cdot j \cdot MEOP \cdot V_c = k_{g,sphere} \cdot \frac{\rho}{\sigma} \cdot j \cdot MEOP \cdot V_c \tag{3-3}$$

This relation show that combustion chamber/case shell mass primarily depends on the specific strength of the material selected, the chamber pressure[3] and the size (volume) of the chamber/case. The factor k_g (k_g = 3/2) is introduced here to signify a geometry (dependent) factor. Note that the above relation is quite simplified (injector plate missing) and hence is not expected to give accurate results.

When estimating mass, we have only considered internal pressure loads. Other loads, like thermal loads and low cycle fatigue (from repeated burn cycles), can be considered by a loads correction factor, k_{loads}, leading to the final relation:

$$M_{case,sphere} = k_{loads,sphere} \cdot k_{g,sphere} \cdot \frac{\rho}{\sigma} \cdot j \cdot MEOP \cdot V_c \tag{3-4}$$

The value of this loads correction factor can be determined following an analysis of the effect of temperature loads and cycling.

3.2 Cylindrical chamber or combustor case with flat end closures

For simplicity, we assume that the cylindrical chamber/case consists of a cylindrical part and 2 flat end closures (front head end and convergent) and that all parts are made of the same material. In addition, we assume that the thickness is constant for all parts and is determined by the thickness of the cylindrical part[4]. The latter is twice the thickness that follows for the spherical case/combustor, see lecture material on "Thin-shell structures". Using the relation for shell mass and combining with known information on thrust chamber geometry (surface area and volume) and introducing again a loads correction factor, we obtain[5]:

$$M_{case,cyl} = k_{loads} \cdot k_{g,cyl} \cdot \frac{\rho}{\sigma} \cdot j \cdot MEOP \cdot V_c \tag{3-5}$$

Where geometry factor $k_{g,cyl}$ is given by:

$$k_{g,cyl} = \frac{1}{L / D_c} + 2 \tag{3-6}$$

4 Injector plate

Two types of injector plates are to be distinguished, being a mono- and a bipropellant injector plate.

Monopropellant injector

It is assumed that the monopropellant injector plate is clamped in the barrel wall without any further support with a uniform pressure loading p, see figure. Its diameter is taken equal to the chamber diameter.

[3] In some motors at start-up a considerable pressure surge occurs that results in an instantaneous combustion chamber pressure several times more than the equilibrium pressure. In that case, the pressure used to obtain wall thickness must be modified by some factor considering this surge.

[4] Alternatively, front and aft head thickness can be estimated using simple stress theory for circular plate with integral flat head or bolted or riveted head or integrally forged head, see section “Design of thin shell structures”.

[5] Comparing relation (3-6) with the relation (13-1) in section on combustor casing (chapter SRM combustor design) allows us to relate the quality factor Q to specific strength of the material used and its geometrical parameters.

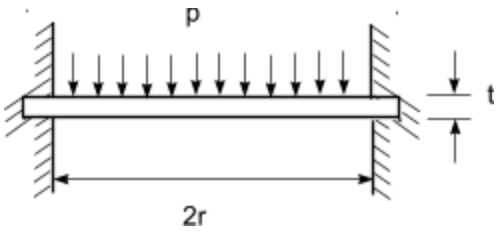

Figure 1: Schematized monopropellant injector plate

Using [Roark], we find the following relation for the dominant stress in the plate:

$$\sigma = C \cdot MEOP \cdot \left(\frac{D_c}{t}\right)^2 \tag{4-1}$$

Where we have replacing p by MEOP (in this case the pressure at the front end of the plate just prior to combustion start up), the plate radius r by the chamber diameter D_c and C is a constant that depends on how the plate is joined (for fixed edge clamping C = 0.0884). Introducing the overall safety factor j and the loads correction factor, we obtain for the mass of the injector plate:

$$M_{inj,\,mono} = k_{loads} \cdot \frac{\rho}{\sigma} \cdot j \cdot \left(0.3\, A_c \cdot D_c \cdot \sqrt{MEOP \cdot \sigma}\right) \tag{4-2}$$

Bipropellant injector

The bipropellant is assumed to consist of two plates that each must be designed for MEOP. If both plates must carry in the most extreme case the chamber MEOP, we find that the mass of the bipropellant injector plate is about twice the value of the monopropellant plate. This leads to the following relation:

$$M_{inj,\,bi} = k_{loads} \cdot \frac{\rho}{\sigma} \cdot j \cdot \left(0.6\, A_c \cdot D_c \cdot \sqrt{MEOP \cdot \sigma}\right) \tag{4-3}$$

5 Conical nozzle (divergent)

According to thin shell theory the thickness of the shell of a conical nozzle can be determined from:

$$t_n = \frac{MEOP \cdot D_{\perp}}{2\sigma} \cdot j \tag{5-1}$$

For an explanation of the symbols used, see Chapter “Nozzle design”.

A complicating factor here is that the pressure in the nozzle is not constant but decreases in the direction of the nozzle exit. On the other hand, the diameter increases in the direction of the nozzle exit to a value well above that for the combustion chamber. For simplicity, we assume that average nozzle wall thickness can be set equal to thickness of the cylindrical chamber wall[6] as advocated by for instance [Humble et al].

[6] Large liquid rocket engines usually employ a nozzle wall of a tapered design. The possibility of such a tapered design can be easily understood when considering that pressure drops significantly (sometimes up to a factor 1000-10000), whereas the change in diameter usually is limited up to about 20.

Using the general relation for the surface area of a truncated cone, we find for the surface area of the divergent part of the conical nozzle (convergent part is already included in the shell of the combustion chamber, since we assumed the chamber to be either spherical or cylindrical with two end surfaces):

$$S = \pi \cdot \left(\frac{D_e + D_i}{2} \right) \cdot s \tag{5-2}$$

Where D_i is nozzle divergent inlet diameter (usually equal to the throat diameter except in case a nozzle extension is used), D_e is nozzle exit diameter, and s is length of (divergent part of) nozzle measured along the wall:

$$s = {L_n}/{\cos\alpha} = \frac{D_e - D_i}{2} \Big/ \sin\alpha \tag{5-3}$$

With α is divergence half angle of nozzle and L_n is length of nozzle measured along nozzle axis.

The relation (5-2) can also be written as:

$$S = A_i \cdot \frac{\varepsilon - 1}{\sin\alpha} \tag{5-4}$$

Where A_i is cross-sectional area of inlet of nozzle divergent, and ε is geometric expansion ratio of divergent.

Substitution of the appropriate relation for the thickness and (5-4) in (2-1) gives after some reworking for the mass of the divergent nozzle shell:

$$M_n = k_{loads} \cdot \frac{\rho}{\sigma} \cdot j \cdot \left(A_i \cdot \frac{\varepsilon - 1}{\sin\alpha} \cdot \frac{MEOP \cdot D_c}{2} \right) \tag{5-5}$$

And for $\varepsilon >> 1$:

$$M_n \approx k_{loads} \cdot \frac{\rho}{\sigma} \cdot j \cdot \left(A_i \cdot \frac{\varepsilon}{\sin\alpha} \cdot \frac{MEOP \cdot D_c}{2} \right) \tag{5-6}$$

6 Combined chamber, injector and nozzle

Combining the results for chamber, injector and nozzle and assuming identical loads correction factor and overall safety factor for the three components (not necessarily the case), we obtain for a bipropellant thrust chamber:

$$M = k_{loads} \cdot \frac{\rho}{\sigma} \cdot j \cdot MEOP \cdot \left(\begin{array}{r} k_g \cdot V_c + 0.6 \cdot A_c \cdot D_c \cdot \sqrt{\sigma / MEOP} \\ + A_t \cdot \frac{\varepsilon}{\sin\alpha} \cdot \frac{D_c}{2} \end{array} \right) \tag{6-1}$$

Notice that we have replaced nozzle divergent inlet area by the nozzle throat area.

Considering that MEOP depends on chamber pressure and using the earlier derived relation between characteristic velocity (c*), chamber pressure (p_c), mass flow (m) and throat area:

$$m \cdot c^* = p_c \cdot A_t \tag{6-2}$$

and between chamber volume, throat area and characteristic length:

$$L^* = \frac{V_c}{A_t} \tag{6-3}$$

we get setting p_c equal to MEOP:

$$M = k_{loads} \cdot \frac{\rho}{\sigma} \cdot j \cdot m \cdot c^* \cdot \left(k_g \cdot L^* + 0.6 \cdot \frac{A_c}{A_t} \cdot D_c \cdot \sqrt{\sigma / MEOP} + \frac{\varepsilon}{\sin\alpha} \cdot \frac{D_c}{2} \right) \tag{6-4}$$

This relation shows that thrust chamber or motor shell mass scales linearly with mass flow rate. Furthermore, realizing that the product of mass flow rate times characteristic velocity makes up a major part of thrust, it also is clear that the larger the thrust, the heavier the thrust chamber or motor gets:

$$M = k_{loads} \cdot \frac{\rho}{\sigma} \cdot j \cdot \frac{F}{C_F} \cdot \left(k_g \cdot L^* + 0.6 \cdot \frac{A_c}{A_t} \cdot D_c \cdot \sqrt{\sigma / MEOP} + \frac{\varepsilon}{\sin\alpha} \cdot \frac{D_c}{2} \right) \tag{6-5}$$

Where C_F is the earlier defined thrust coefficient. This generally varies only to a limited extend.

Of the other parameters in above relations, the nozzle area ratio is also an important parameter in mass estimation as it may vary from engine to engine. The other parameters, like nozzle divergence angle and L*, have a limited influence due to that in practice only small variations are applied. For instance, nozzle divergence angle is in range 12^o - 18^o.

7 SRM and HRM shell mass

Solid and hybrid rocket motors essentially can use the same methods as applied above for liquid rocket thrust chambers. Some differences should be considered. For instance, an SRM has no injector plate. An HRM does have an injector plate, but as only a single propellant is used, a single plate is assumed. Furthermore, HRMs usually do not have a spherical case, whereas some SRMs do.

For instance, combining relation (3-5) and (5-6) leads to the following relation that allows for mass estimation of an SRM:

$$M = k_{loads} \cdot \frac{\rho}{\sigma} \cdot j \cdot MEOP \cdot \left(k_g \cdot V_c + A_t \cdot \frac{\varepsilon}{\sin\alpha} \cdot \frac{D_c}{2} \right) \tag{7-1}$$

Note that for SRMs and HRMs, the volume V_c refers to the total volume enclosed by the motor case and not only the volume of the combustion chamber as in an LRE.

For large SRMs where the nozzle is much smaller than the case (and hence also its mass), we can simplify the above relation to:

$$M = k_{loads} \cdot \frac{\rho}{\sigma} \cdot j \cdot MEOP \cdot k_g \cdot V_c \tag{7-2}$$

This relation clearly shows the importance of the chamber volume. Considering that the latter relates to a large extend to propellant mass (case volume is propellant volume +

port volume), we can immediately understand why in some other works, dry motor mass is given in relation to propellant mass (and or total impulse[7]), see e.g. appendix J. Relations (7-1) and (7-2) also show the importance of the selected construction material. It is for this reason that in appendix J mass estimation relationships are differentiated after the type of construction material.

In appendix J, it is also mentioned a considerable data spread as expressed by an RSE in range 12 to 36%. Using the relations presented above, we can determine possible reasons for the data spread, being:

- different construction materials used
- variations in design chamber pressure
- variations in chamber shape (geometry)
- variations in nozzle area ratio
- other mass elements like liner, igniter, ablation and insulation materials, which may not all scale to the same extent with the internal volume of the motor
- different safety factors used
- differences in design load cases
- etc.

The next table provides an overview of relations useful for dry mass estimation of solid and hybrid rocket motors.

Table 1: Estimation relationships for solid (SRM) and hybrid rocket motor HRM shell mass

Motor type	**Relation**
SRM/HRM motor case - Sphere - Cylinder with flat ends - Cylinder with spherical ends	 Use relation (3-4) Use relation (3-5) Determine thickness for spherical heads using (2-3) and apply twice this thickness to the cylindrical (barrel) wall. Determine sphere surface and cylinder surface. Determine mass using: $M_c = \rho \cdot (S_{sphere} + 2\, S_{cyl}) \cdot t_{sphere}$ Here it is assumed that head ends, and barrel wall are made of one and the same material.
SRM/HRM nozzle divergent	Use relation (5-5) in case of small nozzle area ratio otherwise use relation (5-6); For nozzle thickness, use relation (5-1) based on chamber diameter.
HRM injector	Use relation (4-2)

8 Validation

In the foregoing, analytical relations have been presented that allow for (dry) mass estimation of LRE thrust chambers and solid and hybrid rocket motors. These relations provide insight in how certain parameters affect chamber/motor mass. Still many simplifying assumptions have been made that may cause an inaccurate result. To validate the modelling as presented, we should compare the theoretical results with actual results. This is what will be illustrated in this section.

A first step (step 1) is such a process is to collect relevant data. Table 2 gives relevant data for the thrust chamber of specific large liquid rocket engines. Typical data for high- and low-thrust SRMs are collected in appendix J. Mass data given in Table 2 and appendix J are all inclusive, meaning that the mass of throat inserts, ablative layers,

[7] Total impulse produced by a rocket motor can be determined from the product of thrust times operation time. Rearranging shows that total impulse is equal to propellant mass times (effective) exhaust velocity. Since for SRMs exhaust velocity does not vary greatly, total impulse is linearly proportional to propellant mass.

insulating layers, anti-oxidation layers, etc. are included. Step 2 is to see what materials have been used for the respective motors and to collect relevant material data. For this plenty of material handbooks are available. A somewhat complicating factor is that material properties vary with operating temperature and that they tend to vary with production process. Data on safety factors used may be determined from the difference between burst pressure and chamber pressure. Next, the data collected is used to determine the theoretical shell mass of the various rocket motors (step 3) and the results compared with actual mass data (step 4). In a final step 5, representative values for the shell mass correction factor K are determined. To illustrate the method an example calculation is given in section 8.1. In section 8.2 some further results for LRE thrust chambers are given. Solid rocket motors are covered in section 8.3.

8.1 Example LRE thrust chamber mass calculation

In this section we provide an example calculation of the thrust chamber mass of the Viking 5 engine. For this engine thrust chamber mass data are available from an internal source. For other engines such data was found largely lacking.

8.1.1 Combustion chamber

Combustion chamber mass is estimated using (3-5). First, we determine the specific strength of the material used. We assume that the material is Haynes 188, which has a mass density of 8980 kg/m^3. Next, we assume that the material average temperature is 538 ^{o}C. At this temperature, we find an ultimate tensile strength of 748 MPa. From the data table, we can obtain the chamber length and diameter, and chamber pressure. Chamber volume is calculated using:

$$V_c = \frac{\pi}{4} \cdot D_c^{\,2} \cdot L_c = \frac{\pi}{4} \cdot 0.53^2 \cdot 0.97 = 0.214 \ \ m^3 \tag{8-1}$$

Taking an overall safety factor of 1.5 and a loads correction factor equal to unity, we find for the wall thickness:

$$t = \frac{p_c \cdot D_c}{2\sigma} \cdot j = \frac{58 \times 10^5 \cdot 0.53}{2 \cdot 748 \times 10^6} \cdot 1.5 = 3.1 \,\text{mm} \tag{8-2}$$

It follows for the chamber mass:

$$M_c = \left(\frac{1}{0.97 / 0.53} + 2 \right) \cdot \frac{8980}{748 \times 10^6} \cdot 1.5 \cdot 58 \times 10^5 \cdot 0.214 = 57.1 \,\text{kg} \tag{8-3}$$

8.1.2 Injector

Injector mass is estimated using (4-3). Taking Haynes as the injector material at identical conditions as for the chamber, an overall safety factor of 1.5 and again assuming a loads correction factor equal to unity, we obtain for the injector mass:

$$M_{inj,\,bi} = \frac{8980}{748E6} \cdot 1.5 \cdot \left(0.6 \; 0.2206 \cdot 0.53 \cdot \sqrt{58E5 \cdot 748E6} \right) = 83.2 \text{ kg}$$

Table 2: Characteristic data of some large liquid rocket engines for mass estimation [CAPCOM], [McHugh], [Kirner], [Schöyer]

Part	Parameter	Viking 5	ATE	HM60	LE-5
Combustion chamber					
	Propellant	UH25-NTO	MMH-MON-3	LH_2-LOX	LH_2-LOX
	Mass	N.A.		417 kg	40.8 kg
	Material	Cobalt Ni-alloy	Narloy Z	Ni outer shell with Cu-Ag-zirconium liner	A-286[2] later changed to Ni-200
	Shape	Cylindrical	Cylindrical	Cylindrical	Cylindrical
	Cooling	Film/Radiation	Regenerative	Regenerative	Regenerative
	Characteristic length			0.84	0.84 m
	Length	0.97[1]/1.30 m	0.179 m	0.426	0.351 m
	Chamber diameter	0.53 m	0.119 m	0.415 m	0.240 m
	Throat diameter	0.306 m	0.0376 m	0.262	0.136 m
	Contraction ratio	3.0	10	2.50	3.11
	Area ratio	2.56			8.48
	Average wall temperature		555 K		
	Chamber pressure Burst pressure	58 bar	90 bar	110 bar	36.8 bar
Nozzle or nozzle extension					
	Mass	N.A.		170 kg	70 kg
	Material	Cobalt Ni-alloy	C-103 or Haynes 188[3]	Inconel	A-286
	Shape	Bell	Bell	Bell	Bell
	Cooling	Radiation	Film/radiation	Dump	Dump
	Length	1.207 m	0.85 m	1.80 m	1.843 m
	Inlet diameter	0.49 m	0.254 m	0.59 m	0.418 m
	Throat diameter	NA	NA	NA	NA
	Exit diameter	0.99 m	0.720 m	1.76 m	1.608 m
	Surface area			7.6 m^2	
	Nozzle area ratio				
	Nozzle extension area ratio	10.5	11.2	9.31	14.8
Thrust chamber					
	Mass	319 kg +124 kg for injector head		~625 kg	
	Length	2.173 m			

1) First value gives length of cylindrical part; second value gives length of chamber including nozzle convergent
2) Iron based super alloy
3) Cobalt based super alloy

8.1.3 Nozzle divergent

To calculate the mass of the Viking nozzle extension, we use relation (5-6). We assume again that the material is Haynes 188 and that the material average temperature is 538°C. This gives us a mass density of 8980 kg/m^3 and an ultimate tensile strength of 748 MPa [Haynes]. From the data table, we can obtain the length and diameter of the nozzle, and the chamber pressure. The safety factor is taken equal to 1.5. Nozzle inlet area is determined from the inlet diameter using:

$$A_i = \frac{\pi}{4} \cdot D_i^2 = \frac{\pi}{4} \cdot 0.49^2 = 0.189 \ \ m^2 \tag{8-4}$$

Nozzle divergence angle is estimated using:

$$\tan\alpha = \frac{(D_e - D_i)/2}{L_n} = \frac{(0.99 - .49)/2}{1.207} \Rightarrow \alpha = 11.7^\circ \tag{8-5}$$

It follows:

$$M_n = \frac{8980}{748x10^6} \cdot 1.5 \cdot \left(0.189 \cdot \frac{10.5-1}{\sin(11.7)} \cdot \frac{58x10^5 \cdot 0.53}{2} \right) = 24.4x10^1 \ \text{kg} \qquad (8\text{-}6)$$

8.1.4 Mass comparison

Summing the calculated mass of combustion chamber and nozzle, we find a total thrust chamber mass of 57 + 83 + 244 = 384 kg. Comparing this result with the actual chamber mass of 319 kg, we find the two values reasonably close. Remarkable though is that we find for the thrust chamber a K-factor below 1. This may be attributed to the simple modelling used, like our assumption that the nozzle has an identical thickness as the chamber, but it also may depend on whether the selected material properties, chamber pressure values and safety factors are correct.

8.2 Some more results for LRE thrust chambers

We present here the results as found for the HM60 and LE-5 nozzle extension. These results have been obtained using a safety factor of 2 and the following material properties:

- A-286: Mass density of 7940 kg/m^3 and an ultimate tensile strength of 620 MPa [Ferguson Metals];
- Inconel: Mass density of 8280 kg/m^3 and an ultimate tensile strength of 1250 MPa [SSE].

As the representative material strength, we have taken the ultimate tensile strength at room temperature, because both nozzles are dump cooled. This severely limits the temperature to be attained by the nozzle wall. The results are presented in Table 3.

Table 3: Estimated mass of nozzle extension of some large liquid rocket engines

	HM60	LE-5
Wall thickness [mm]	3.96	1.42
Surface area [m^2]	7.34	6.15
Mass [kg]	241	70.7

Comparing these data with the actual mass data, we find a nozzle extension K-factor for the HM60 of 0.70 and for the LE-5 of 0.99 indicating that the method used leads to an overestimation of nozzle mass. This is possibly due to the assumption of constant wall thickness, whereas large rocket motors are known to use some tapering of the nozzle wall thickness.

8.3 SRM mass estimation

Detailed information on the mass of nozzle and case for some low/medium-thrust SRMs with a spherical motor case given in appendix J have been obtained, see Table 4. These data have been used as starting point to estimate the mass of motor case. Nozzle mass was not estimated as little to no information could be found on the nozzle materials in use.

For the estimation use has been made of relation (3-3) with Titanium selected as the structural material. For the estimation we used a titanium mass density of 4430 kg/m^3 and an ultimate tensile strength of 950 MPa. In addition, we selected an overall safety factor of 1.25 and only considered internal pressure as the dimensioning load. Results are given in Table 5 together with the data as obtained from literature. In this table also the factor describing the ratio between the estimated and the actual mass is given.

Table 4: Characteristics of SRMs with spherical motor case [ATK]

Characteristic	**STAR 17**	**STAR 24**	**STAR 26**	**STAR 26B**
Case material	Titanium	Titanium	D6AC steel	Titanium
Nozzle material	N.A.*	N.A.	N.A.	N.A.
Maximum chamber pressure [bar]	68.95	36.13	44.82	46.88
Motor case diameter [m]	0.442	0.6223	0.664	0.664
Case mass [kg]	3.99	6.35	17.96	10.66
Nozzle assembly mass [kg]	3.18	5.90	10.57	8.75
Miscellaneous** mass [kg]	2.27	6.49	10.25	3.99
Propellant mass [kg]	69.63	199.85	230.65	237.68
Total mass [kg]	79.06	218.58	269.43	261.08
Burn time average thrust [N]	1115.8	1891.5	1891.5	3530.8
Nozzle expansion ratio [-]	60.7	37.8	16.7	17.8
Throat diameter [m]	0.0348	0.0615	0.0615	0.0753

* N.A. stands for "Not Available"

** Miscellaneous mass includes the mass of the ignition system, insulation and further miscellaneous items.

Table 5: Comparison of estimated case shell mass and mass data from literature

Characteristic	**STAR 17**	**STAR 24**	**STAR 26**	**STAR 26B**
Case mass (actual) [kg]	3.99	6.35	17.96	10.66
Case shell mass (estimated) [kg]	2.73	3.99	10.34	6.28
Case total to shell mass factor [-]	1.46	1.59	1.74	1.70

From Table 4, we first of all learn that miscellaneous mass makes up quite a substantial amount of mass (roughly 30% of total dry motor mass) next to motor case and nozzle and hence, it may be questioned whether modelling also the miscellaneous mass items may lead to better predictions. This though is considered out of scope for the present discussion.

Table 5 shows that estimated case mass is in reasonable agreement with actual mass data. Difference is only a factor 1.45 to 1.75. This factor of course depends on the chosen overall safety factor. Selecting a different value leads to different values of the K-factor for the motor case. More importantly though is that the K-factor varies only little, which is a confirmation that the method can predict mass reasonably well.

In Table 6 data is provided on characteristics of SRMs with a cylindro-spherical motor case and carbon-phenolic exit cone. Also, in this case the data have been used to estimate motor case mass and nozzle mass. For the estimation we have used the method as indicated in Table 1 for a cylindrical motor case with two spherical head ends and the relation for the mass of the nozzle divergent. Mass density and strength of the Titanium case material were kept the same as for the motors with spherical case. with Titanium selected as the structural material for both the motor case and the nozzle. For the estimation we used a titanium mass density of 4430 kg/m^3 and an ultimate tensile strength of 950 MPa. Mass density and UTS for carbon phenolic has been taken equal to 1400 kg/m^3 and 137 MPa, respectively, and were taken from [Mraz]. In addition, we selected again an overall safety factor of 1.25 and only considered internal pressure as the dimensioning load. Results are given in Table 5 together with the data as obtained from literature. In this table also the factor describing the ratio between the estimated and the actual mass is given.

Table 6: Characteristics of SRMs with titanium cylindro-spherical motor case and carbon-phenolic nozzle [ATK]

Characteristic	Star 30C	Star 30E	Star 37FM	Star 48A*
Total impulse [kNs]	1673.0	1812.9	3094.3	6798.7
Maximum chamber pressure [bar]	41.64	40.68	44.26	41.85
Motor diameter [m]	0.762	0.762	0.935	1.245
Length of cylindrical section [m]	0.278	0.33	0.321	0.381
Case mass [kg]	16.19	17.19	32.25	69.67
Nozzle assembly mass [kg]	15.65	15.24	34.02	38.28
Miscellaneous* mass [kg]	9.25	10.07	15.42	35.61
Propellant mass [kg]	590.8	631.4	1063.3	2430.0
Total mass [kg]	631.9	673.9	1145.0	2573.6
Burn time average thrust [N]	3311.2	3583.4	4819.4	7869.8
Nozzle expansion ratio [-]	63.2	58.6	48.2	31.2
Throat diameter [m]	0.0734	0.0762	0.0894	0.1140

* Miscellaneous mass includes the mass of the ignition system, insulation and further miscellaneous items.

Table 7: Comparison of estimated mass using simple analytical relations and mass data from literature

Characteristic	Star 30C	Star 30E	Star 37FM	Star 48A*
Case mass (actual) [kg]	16.19	17.19	32.25	69.67
Case shell mass (estimated) [kg]	14.6	15.4	27.9	59.6
Case total to shell mass factor [-]	1.11	1.12	1.15	1.17
Nozzle assembly mass (actual) [kg]	15.65	15.24	34.02	38.28
Nozzle mass (estimated) [kg]	17.26	16.83	25.35	33.22
Nozzle assembly to shell mass factor [-]	0.9	0.9	1.3	1.2

Results shown in Table 7 demonstrate that the method presented here works reasonably well for cylindro-spherical rocket motors with estimated case mass being almost identical (but slightly less) than the actual mass. Same goes for the nozzle although the differences are a bit larger (factor 0.9 to 1.3). The reason for this is not clear but considering that the nozzle on average makes up 25% of total mass, the effect is considered quite limited.

9 Summary of main findings and conclusions

Using simple theory and assuming internal pressure is the only load acting, simple analytical relations have been derived for the mass of thin shell pressurized components like SRMs, HRMs and LREs. A correction factor considering low cycle life and other loads may be added to consider the effect of other loads. In the present work though this factor is set equal to unity.
The relations derived at show that LRE thrust chamber mass and hybrid, and solid rocket motor mass varies with thrust (LRE thrust chamber) or thrust, propellant mass or total impulse delivered (SRMs). Also, the relations show the importance of selecting materials with high specific strength and the effect of selecting a proper overall safety factor. Other factors have much less influence as the range over which they are varied is sometimes rather limited. We mention L* or c*, nozzle divergence angle, chamber contraction ratio, etc. It is concluded that the relations are helpful in a search for realistic Mass Estimation Relationships (MERs).

Another important finding is that the relationships also allow for explaining why simple mass estimation relationships obtained from regression analysis do show considerable spread.

For several cases, we have used the relationships to estimate LRE thrust chamber mass and SRM dry mass and to determine overall and/or component K-factors. Even though the results are quite limited and some further work is needed, the following findings are reported:

1. The validation of the method requires extensive data to be available over a substantial range to allow for a meaningful assessment.
2. The collection of LRE thrust chamber data and HRM and SRM data is full of challenges. Even for the limited amount of rocket motors included in our data table, we have not been able to come up with all data needed. We mention mass data, but also material data and more important even working temperature of the wall of combustion chamber and nozzle. Also, data on safety factors used have not been found. The importance of the latter is that the resulting mass estimate is linearly dependent on it.
3. All results so far have been calculated assuming a safety factor of 1.5 (LRE) or 1.25 (SRMs). It is found that using these safety factors reasonable K-factors have been obtained, which would allow for this method to be used in preliminary design studies. Availability of safety factor data would allow for more solid information on the K-factors to be used.
4. Reasonable K-factors (in range 0.9-1.7) have been obtained for several cases, mostly for SRMs. It is considered that the range can be further narrowed down in case more information on used materials (especially for the nozzle) becomes available.
5. The number of data points for LRE thrust chambers and HRM are too limited to come to any conclusion on useful K-factor values for these engines/motors or their components. Further research is recommended though as the method allows for more detailed modelling that simple one-parameter regression relationships.

References

1) An., Technical data sheet Iron-base Superalloy Type A286, Ferguson Metals, Hamilton, Ohio.

2) An., Haynes International data sheet Haynes 188 alloy, 2000.

3) CAPCOM: Les Moteurs Viking D'Ariane 4, webpage.

4) Humble R.W., Henry G.N., and Larson W.J., Space Propulsion Analysis and Design, Space Technology Series, McGraw-Hill Publishing Company, 1995.

5) Kirner, E., Thelemann, D. Wolf, D., Development status of the Vulcain thrust Chamber, Acta Astronautica, Vol. 29, No. 4, 1993.

6) Manski, AIAA-89-2279. 1989.

7) McHugh B., Numerical analysis of Existing Liquid Rocket Engines as a Design Process Starter, AIAA 95-9270, 1995.

8) Schöyer HFR., Caporicci, M., Hufenbach B., Schnork AJ., The Design of the European Advanced Technology Engine, ATE, ESTEC/ESA, AIAA=92-3662, 1992.

9) Mraz S., Basics of Aerospace Materials: Aluminum and Composites, April 2016. Retrieved 31 July 2018, from https://www.machinedesign.com/materials/basics-aerospace-materials-aluminum-and-composites

- This page is intentionally left blank -

Courtesy Pressure Systems Inc. (PSI)

B.T.C. Zandbergen

Contents

Contents 321

List of symbols 323

Acronyms 323

1 General 324

2 Tank shapes, arrangements, and add-ons 325

3 Design and sizing of fluid storage system 332

4 Fluid storage system mass 339

5 Other system characteristics 346

6 Development and Testing 347

7 Problems 348

For further study 348

References 348

List of symbols

Roman

E	Young's modulus (modulus of elasticity)
F	fill ratio
g	gravitational acceleration
H	height of fluid colon
j	safety factor
K	shell mass correction factor
K_f	fibre strength reduction factor
K_m	tank figure of merit
$K_{t,prop}$	tank mass factor
M	mass
N	number of cycles
p	pressure
r	radius
R	blow-down ratio
R_a	absolute gas constant
S	surface
t	thickness
T	temperature
V	volume
Z	compressibility factor

Greek

β	coefficient of cubical expansion
ε	strain
μ	Poisson ratio
ρ	density
σ	ultimate stress
ψ	thrust-to-weight ratio

Subscripts

b	burst
f	fibre
g	pressure gas
h	hydrostatic
i	initial
id	ideal
p	propellant
t	tank
u	ullage
v	vapour

Acronyms

COPV	Carbon-fibre Over-wrapped pressure Vessel
EPS	Etage Propergol Solide
ID	identifier
MEOP	Maximum Expected Operating Pressure
PMD	Propellant Management Device
PSI	Pressure Systems Inc.
PV	Pressure Vessel
RSE	Relative Standard Error of estimation

1 General

All spacecraft and rocket stages equipped with a liquid or cold gas propulsion system require some storage or tankage system, i.e. a system of storage tanks for the different fluids needed to allow for a proper functioning of the propulsion system. We distinguish between liquid and gas storage systems. The latter specifically allowing for the storage of gaseous propellants and/or pressurants.

The two main functions of the storage system are to store the different fluids needed for propulsion and to keep them fit for use. This latter task is referred to as fluid management and essentially is about ensuring an undisturbed flow of propellant of the proper quality when needed. However, the inclusion of a storage system also brings disadvantages with respect to. system mass, size, cost and reliability. For instance, for the Ariane 5 L9.7 upper stage (EPS) the tankage system makes up roughly 35% of the total stage dry mass (422 kg on a stage dry mass of 1256 kg) [Ley]. For the SNAP spacecraft propulsion system, see table 1, this is 18 kg on a total of 34 kg of propulsion system mass [Asato]. Also clear from the table is that the tanks form a major contribution to the propulsion system mass.

Table 1: SNAP propulsion system [Asato]

Component	Size	Qty	Unit Mass (kg)	Mass (kg)
N2H4 Required		173300 cc		**130**
Tank	48.3 cm ∅	3	6	18
Filter		2	0.15	0.3
Isolation Valve		2	0.5	1
Thrusters	22N	8	0.5	4
Pressure Transducer		1	0.2	0.4
N_2H_4 Fill/Drain Valve		1	0.1	0.1
GN_2 Fill/Drain Valve		1 per tank	0.1	0.3
Tubing & Fittings		lot	2	2
Brackets, excluding tank support		lot	4.6	4.6
Thermal (thermostats, heaters)		lot	1.4	1.4
Electrical (cables, connect)		lot	2.2	2.2
Total HW Mass				**34.1**

Hence, for space applications, much attention is on techniques to reduce tank mass. This is, because every kilogram saved reduces launch cost with about $ 4,400 to $ 53,400, depending on the target orbit, and because the storage system makes up a large portion of propulsion system dry mass. Recent developments to produce light tanks include the introduction of composite propellant and pressurized gas tanks, lightweight aluminium-lithium propellant tanks, and carbon-fibre tanks to store cryogenic propellants. Earlier developments introduced high-pressure storage (especially for gases), and cryogenic storage of normally gaseous propellants, like hydrogen, and oxygen.

Other very important aspects or design challenges for the storage system are to reduce tank cost, to limit tank volume, to ensure that most of the propellants (if not all) are expelled at the proper rate, to prevent tank failure, and to limit boil-off (mainly for cryogenic propellants), propellant sloshing and friction effects. In addition, we need to consider potential interface issues like the need for structurally mounting the tank(s) in

the vehicle, and the placement of the tank(s) in the spacecraft for e.g. Centre of Gravity (CoG) control. To ensure that all such aspects and potential issues are taken care of in the design, these aspects/issues generally end up in a requirements list. As an example, table 2 shows typical requirements for cryogenic propellant tanks for a re-usable launch vehicle as defined by NASA.

Table 2: Cryogenic tank requirements for re-usable launch vehicle [NASA]

Requirement ID.	Requirement
1	400 Mission Cycles, Qualified for 2300 Pressure Cycles
2	Maximum On-Orbit Mission Time 10 Days
3	Low-Cost System
4	High Reliability per Stage (0.999999)
5	Quick Turn-Around
6	Technology Readiness Level 6 or better demonstrated by 2005
7	Integrated Vehicle Health Monitoring System
8	Satisfy NASA, AIAA/ANS and MIL-STD Design Requirements for Pressure Vessels and Pressurized Structures for Metals and Composites

Once a set of requirements has been set, the design can start. Hereafter, we will first list and describe the various items that make up the storage system. Next, we show different storage system arrangements and present and discuss design and sizing details of such systems thereby considering expulsion efficiency, boil-off, propellant management and tank material selection.

2 Tank shapes, arrangements, and add-ons

In this chapter the various elements that make up a tankage system and how they are arranged are discussed.

2.1 Tank shapes and arrangements

A “tank” essentially is a thin-walled container that allows for storage of a liquid or gaseous fluid until its use in some device. Some typical tanks used on spacecraft are shown on the cover of this document. The optimum shape for tanks is spherical, for it gives a tank with the least mass. On the other hand, cylindrical tanks offer better use of available volume in the vehicle. Both spherical and cylindrical tanks are common in most spacecraft propulsion systems. Sometimes, when other requirements than low mass are critical, we find quite irregular shapes like pear, torus[1], and even flat shaped tanks.

For launcher stages flying in the atmosphere spherical tanks are not common; rather we use propellant tanks of a cylindrical shape as it allows for more optimum use of the available space. Cylindrical tanks are equipped with spherical or elliptical end caps and sometimes even flat caps.

Tanks can be arranged in several ways and the tank design can be used to exercise some control over the change in the location of the centre of gravity and the mass moments of inertia, especially when multiple tanks are used to store a propellant. Typical configurations are shown in Figures 1 and 2.

The Aestus stage shown in Figure 1 is equipped with 4 identical propellant tanks (2 for MON and 2 for MMH) and 2 pressurized gas tanks. The latter stores the pressure gas

[1] a doughnut-shaped surface generated by a circle rotated about an axis in its plane that does not intersect the circle.

that forces the liquids to the thrusters. The tanks on the Aestus stage are configured close to the centre line of the stage to allow proper control of the centre of mass of the vehicle.

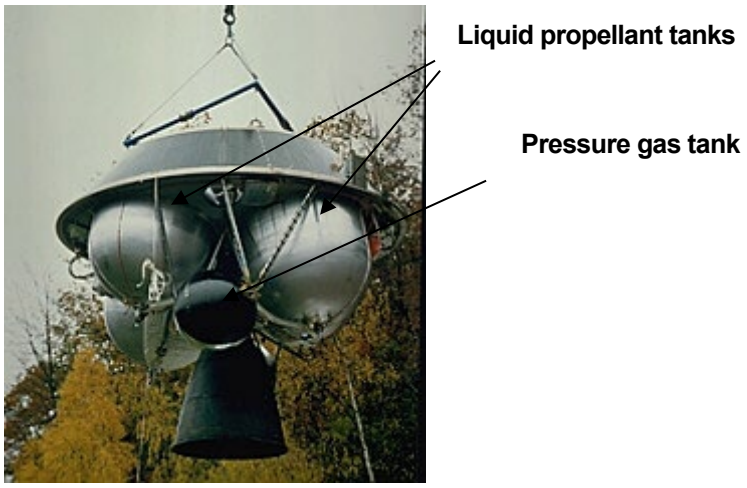

Figure 1: Ariane 5 Aestus stage

Rocket launchers commonly use the tandem configuration; see figure 2, either with a common bulkhead or with external piping. Other important configurations are the concentric tank and the multi-tank. In recent launch vehicle stage designs, the tanks use the skin of the vehicle as a wall of the tank. We refer to this as an “integral tank” design.

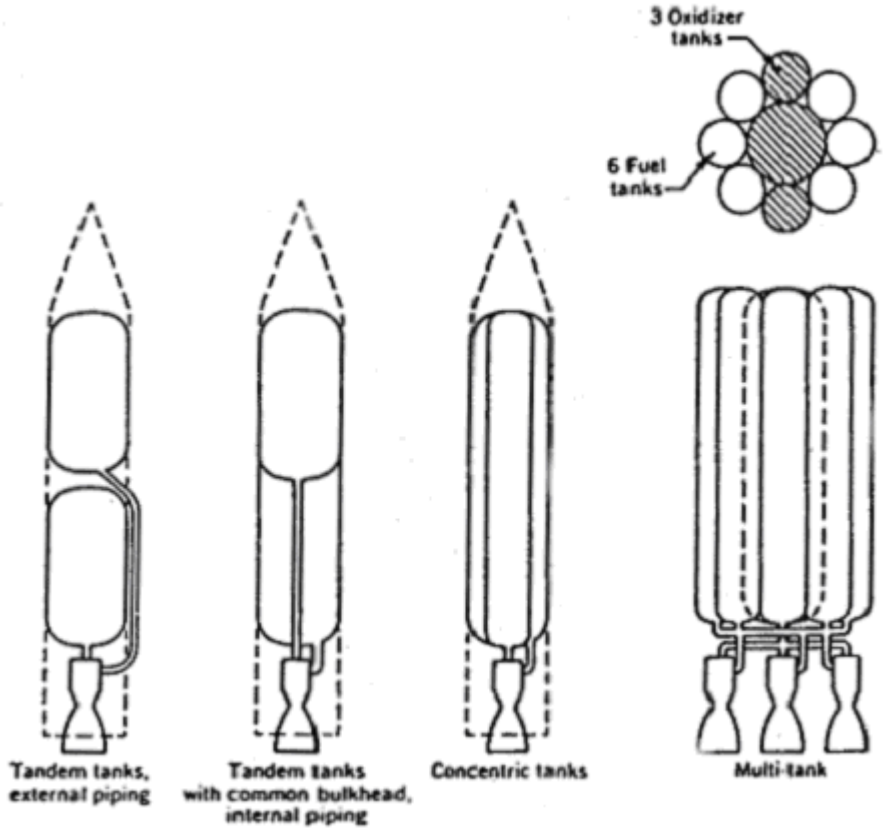

Figure 2: Typical tank arrangements launcher stages [Sutton]

Typical materials used for liquid propellant tanks include:

- Metals recommended for service with liquid hydrogen, liquid oxygen, and kerosene are aluminium alloy 2219, 6061, and 7020, and lithium aluminium alloy.

- Metals recommended for service with nitrogen-tetroxide, hydrazine, unsymmetrical di-methyl-hydrazine, and mono-methyl-hydrazine are titanium (Ti-6Al-4V), aluminium (e.g. 6061) and stainless steel (CRES[2] 301 or 304L).
- Graphite-fibre/epoxy-matrix composites are recently studied for use with cryogenic propellants.

Materials for gas tanks include aluminium, titanium and stainless steel. Over the past few years, however, all-metal tanks have been replaced by so-called 'pre-stressed composite' pressure vessels, which offer a mass reduction of 60% and more. Composite tanks consist of a high-strength metallic liner to ensure leak tightness over-wrapped by the fibre material to provide the high strength to low weight ratio. The fibres are under a tensile pre-stress; hence the term 'pre-stressed composite' and the metal liner is under an initial compression to ensure that both materials reach their ultimate design strength simultaneously at the design pressure. As liner material usually titanium (Ti6Al4V) or steel alloy is used and carbon (like graphite) and Kevlar as the fibre material and epoxy as the matrix material.

2.2 Propellant management devices

The operation of a propulsion system using liquid propellants under space conditions may expose the propulsion system to a dynamical regime not usually encountered in terrestrial applications, namely that of free fall or low residual acceleration. Active measures must be adopted to ensure that liquid propellant, rather than gas or vapour, is available at the tank outlet for rocket motor restart. To manage the liquid propellant, they may use artificial gravity induced by a spinning spacecraft of by a settling burn from another small rocket, positive expulsion, and capillary or surface tension devices.

Positive expulsion systems use a pressure gas in combination with an active element to force the propellants from the tank into the feed lines and to separate the pressure gas from the liquid propellant under all dynamic conditions.

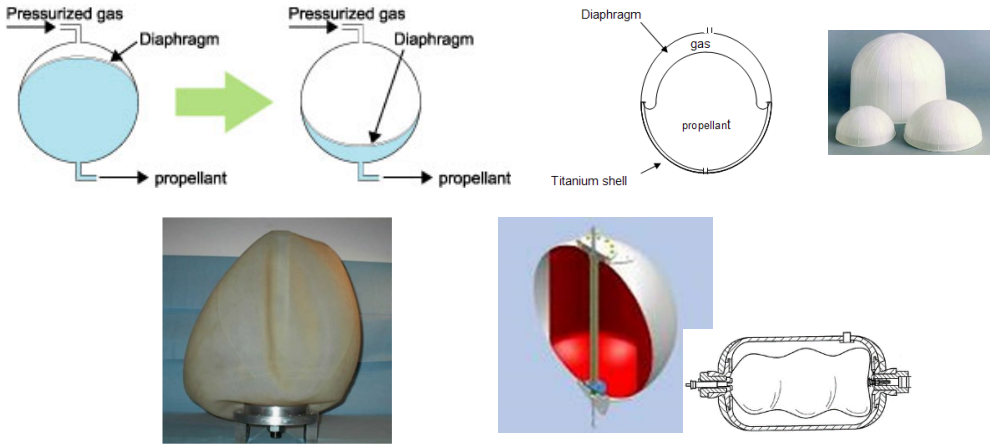

Figure 3: Spherical positive expulsion tank with diaphragm (top row) and bladder (bottom row) [Sutton]

Various basic types of active elements for positive expulsion are distinguished, see above figure:

1. Diaphragm. A diaphragm essentially is a membrane that separates propellant from pressurant. In most cases, the diaphragm is hemispherical or hemispherical with a cylindrical section. Its outermost edge is sealed against the pressure shell. The diaphragm is made either of an elastomer or a metal.
2. Bladder. Bladder essentially is a balloon like in a soccer ball containing the propellant. It has a relatively small opening attached to the tank outlet (and/or

[2] Corrosion resistant steel.

inlet). As such, it provides a relatively small sealing area compared to the use of a diaphragm, and can be easier installed and/or replaced

3. Piston or bellows (not commonly used).

Surface tension systems passively manage propellants in a near zero gravity environment by using vanes, screens or sponges to wick the propellant into the propellant-tank outlets. In this manner, the pressurizing gas is always maintained away from the tank outlet.

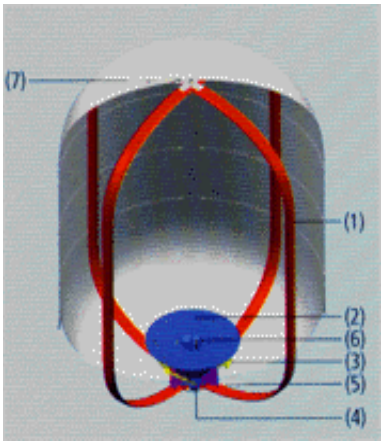

1. Propellant Acquisition Vanes
2. Propellant refillable reservoir
3. Upper screen
4. Lower screen
5. Propellant port
6. Venting tube
7. Gas port

Figure 4: Cylindrical tank with surface tension type of PMD (courtesy EADS)

Three basic types of surface tension type of PMD designs can be distinguished:

1. Partial control. Partial control devices hold a fraction of the propellant in the tank over the outlet and leave the remaining liquid free. Partial control PMDs are generally composed of traps, trough, sponges or a combination of the three.
2. Total control or slosh control is used when slosh control is a concern. These devices consist of a large, compartmented trap which contains almost all the propellant. The trap is separated into compartments by porous barriers.
3. Total communication: To ensure a flow path to the tank outlet from wherever the bulk liquid is in the tank until the tank is depleted. Total communication devices are usually liner, gallery or vane devices.

Typical positive expulsion, and capillary surface tension hardware (left) and diaphragm (right) is shown in fig. 5.

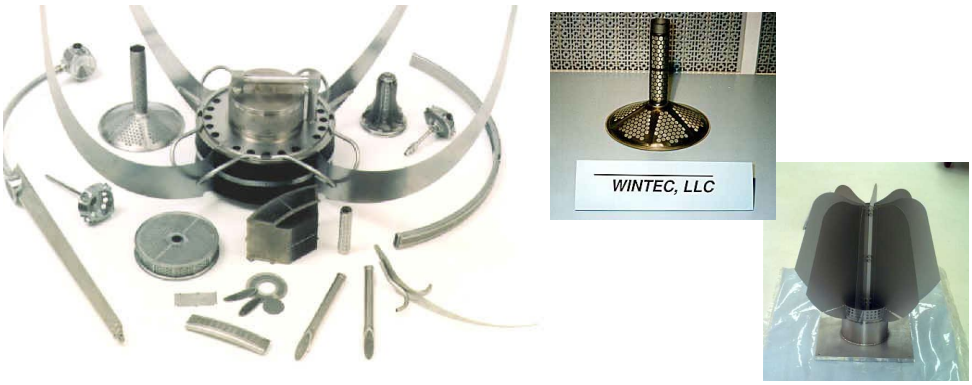

Figure 5: Typical PMD devices (left picture by courtesy of PSI; Other pictures courtesy of Wintec LLC)

In addition to the problem of propellant configuration within the tank, the response to dynamic excitation in flight in the form of propellant sloshing may also be important. Some propellants have a viscosity substantially less than water (about a factor ten).

The damping of free surface oscillation in the fluid, which would otherwise give rise to substantial fluctuating forces and moments on the tank wall, may also require active provisions in the form of turbulence generating baffles.

A third problem is the occurrence of vortexing during tank emptying. This usually occurs just before the tank empties and is associated with a visible whirlpool on the liquid surface that might cause gases to escape in the feed lines, causing flow blockage. To prevent the occurrence of vortexing, anti-vortex baffles can be used, see figure 6.

Figure 6: Anti-vortex device (courtesy Air Liquide)

Sometimes this same function can also be performed using surface tension devices.

Materials used for diaphragms include elastomeric[3] (rubber-like) materials like Ethylene Propylene Terpolymer (EPT), and butyl rubber. Instead of rubber materials, also metals can be used as diaphragm material. A typical such metal is aluminium. Materials used for screens in surface tension devices are e.g. steel (304L) and Titanium (Ti99.4).

2.3 Tank mounting provisions

To allow attaching the propellant tank in a spacecraft or launcher, mounting provisions such as skids, fastenings, brackets, cradles, lifting lugs, etc., intended to carry loadings shall be permanently secured to tanks. All tank mountings shall be designed to prevent the concentration of excessive loads on the tank shell.

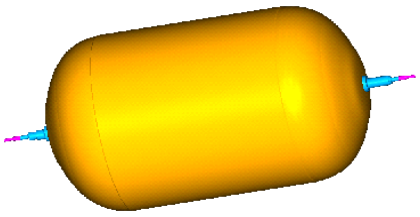

Figure 7: Boss mounting (courtesy PSI)

Typical mountings of spherical tanks include polar (top and bottom) boss[4] mounting, see figure 7, where the tank is mounted on struts or through-bulkhead panels on the spacecraft.

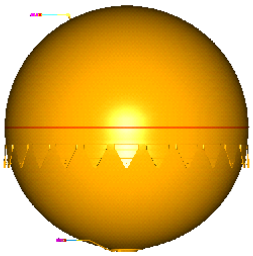

Figure 8: Equatorial mounting using tabs (courtesy PSI)

For cylindrical tanks, also equatorial mounting e.g. through tabs[5] is considered, see figure 8. A third option is to use lugs[6]. Strap mounted tanks are usually simple spheres with no external

[3] An elastomeric material is a material that can be stretched to approximately twice its original length with relatively low stress at room temperature, and which returns forcibly to about its original size and shape when the stretching force is released.

[4] This is the simplest mount method from a tank fabrication approach. Tank is mounted on struts or through bulkhead panels on the spacecraft.

[5] Tabs are machined from a forged cylinder that is welded to the tank (girth tabs shown). This mount method is used when the tank is installed in a spacecraft cylindrical structure. The tabs provide an added benefit of integral tank-to-structure compliance

[6] Several lugs - typically 3 to 4 - are machined around the tank circumference, or welded onto a centre cylinder ring and machined, or adhesively bonded and over-wrapped.

details beyond tube ports or threaded boss ports. The tanks are then retained in a cradle by metal straps in tension. The tank mount approach is driven by cost trade-off between the complexity and cost of tank mount fabrication along with impact on tank weight versus the weight and cost impact of a particular mount method on the spacecraft structure.

2.4 Valves and in-and outlet tubes

Tanks are equipped with a fill and drain valves and the associated in- and outlet tubes to allow filling and draining of the tank. In case also a pressure gas is loaded in the tank, we need a second set of fill and drain valves and in- and outlet tubes for the pressure gas.

In case of storing propellants with a vapour pressure higher than the design pressure, tanks are equipped with vents or other pressure relief provisions to prevent self-over-pressurization with the danger of tank rupturing. The same holds in case propellants are stored that are known to decompose in time, like the monopropellants hydrogen peroxide and hydrazine or in case of boil-off of cryogenic propellants. Materials used for valves, and in- and outlet tubes, are mostly the same metals as used for the tank wall structure. To provide sealing/prevent leakage, Nylon and Teflon are used.

2.5 Liner

A liner is used to cover the tank on the inside in case the structural material used for the tank is not compatible with the propellant or is not leak-tight. Both metallic as well silicone and other elastomeric liners can be used, depending on the pressure level in the tank.

2.6 Pressure gas diffuser

The main function of a pressure gas diffuser is to introduce the pressure gas evenly into the propellant tank thereby minimizing disturbances at the gas-liquid interface. Such devices are used mostly on large tanks, e.g. of rocket stages, as these tanks are too large to allow a diaphragm to be installed. Historically, ullage gas diffusers are large, bulky devices that occupy a significant portion of the tank and thus decrease the amount of room available for propellant.

2.7 Instrumentation

Tanks can be equipped with an instrumentation system, including amongst others pressure and temperature sensors that allow inputs for thermal control and for indication of propellant level.

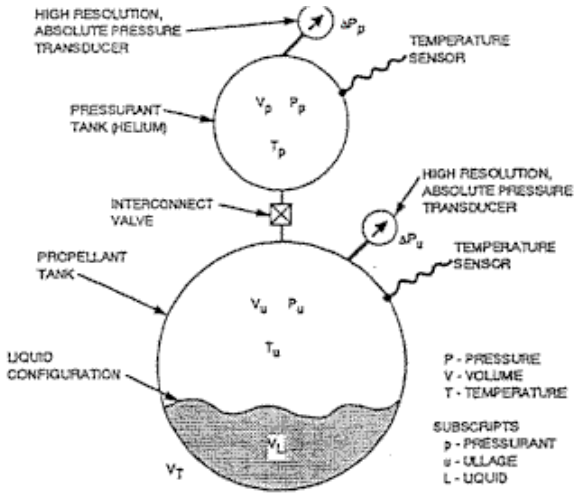

Figure 9: Generic propellant gauging system

Figure shows a generic propellant gauging system for a regulated system, where the propellant tank is pressured by a pressure gas from a separate tank through a latching valve. Separate pressure transducers measure the pressures in each tank. Temperatures of

the helium gas and ullage are also measured. The pressure gas tank volume and propellant tank volume are known quantities from ground test data. From the pressure and temperature measurements performed in space the ullage volume can be determined, which when subtracted from the propellant tank volume yields the desired propellant liquid volume. Considering temperatures, we can determine the propellant load remaining.

2.8 Tank insulation

With long-duration cryogenic storage, propellants will boil off because of the environmental heating of the tank. Next table taken from NASA shows some typical boil-off data as experienced for some existing designs.

Table 3: Boil-off rate for a number of existing (and flown) cryogenic tank systems. [NASA]

System	Boil-off	Size	Time on orbit
Titan-Centaur 5 Hydrogen Tank	4.8%/Day total tank capacity (21%/Day remaining propellant) during extended coast	3.05m Dia 7.39m Long 35 cubic meters	9 hours
Power Reactant Storage Hydrogen Tank	2.03%/Day not operating	1.05 m Dia Sphere 0.606 cubic meters	21 days
Cosmic Background Explorer Helium Dewar	0.26%/day steady state 0.37%/day during first 30 days	1.7m Dia 2.2m Long 0.650 cubic meters	306 days

To accommodate boil-off, extra propellant is required along with larger propellant tanks.

For extended storage periods, like during ground hold or when coasting, cryogenic tanks are insulated using multi-layer insulation (MLI) shields (on spacecraft) or closed cell foams (on launchers), like polystyrene or polyimide, that are bonded or sprayed on the tank surface; porous external insulation layers have to be sealed to prevent moisture from being condensed inside the insulation layer. Note that even with insulation, it is not always possible to prevent the continuous evaporation of the cryogenic fluid. For instance, the USA Centaur upper stage uses a combination of polyimide foam and MLI. Still, data on boil off indicates for this stage a loss rate in the range of 2% of the initial propellant mass per day [Knol]. A study by [Perczynski] indicates though that by proper design a loss rate of less than 0.17% per day or even less is feasible. In a recent study by [Pietrobon] for a Moon mission using a combination of liquid hydrogen and liquid oxygen as propellant, it was reported a total boil-off of ~5% for liquid hydrogen and 0.5-1% for liquid oxygen in 30 days.

Another aspect that we must consider is that the propellants will cool the tank wall temperature far below the ambient air temperature. This causes condensation of moisture on the outside of the tank and usually formation of ice during the period prior to launch. The ice is undesirable, because it increases the vehicle mass and can cause valves to malfunction.

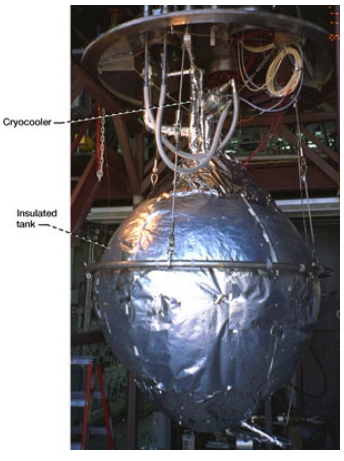

Figure 10: Insulated cryogenic tank equipped with cryo cooler (courtesy NASA-Lewis)

2.9 Refrigeration system

To allow storing cryogenic propellants for a longer time or to limit boil-off losses, some form of a powered refrigeration system or rather a cryo-cooler may be used to minimize evaporation losses. For example, most launchers using cryogenic propellants have a way for the propellant to be re-circulated through an umbilical to an external cooler while waiting for launch. Figure 10 shows a pressurized tank insulated with 34 layers of multilayer insulation, and a cryo-cooler to cool the cryogenic liquid. Not shown is a condenser. The latter is used

to transmit heat entering the tank by condensing hydrogen vapour, which extends into the ullage of the liquid hydrogen tank.

2.10 Heater system

Sometimes tanks are equipped with a heater system including e.g. bonded strip heaters to prevent the propellant from freezing. For example, the freezing point of hydrazine is 274.55 K (1.4 ^{o}C) and of nitrogen tetroxide 263.85K (-9.3 ^{o}C). As heaters require power, this is one of the reasons why engineers appreciate propellants that have a low freezing point.

3 Design and sizing of fluid storage system

Important parameters in sizing the fluid storage system include tank volume, shape, mass, operating pressure, materials used, etc.

The various steps in tank sizing (next to the generation of requirements and selecting potential design solutions for evaluation) are:

1. Determine propellant load (mass)
2. Calculate propellant volume
3. Calculate tank volume
4. Select tank shape(s) and determine tank dimensions
5. Select tank material
6. Dimension tank
7. Compare results and select best design

These steps are discussed in some details below.

3.1 Propellant load (mass)

Propellant load follows from rocket equation or total impulse requirement, and (effective) exhaust velocity. To this we should add some design margin as well as additional propellant to consider propellant remaining behind in the tank(s) and feed line(s), boil-off (in case of cryogenic propellants), and loading uncertainty. This gives:

$$M_p = M_{\Delta v} + M_{margin} + M_{expulsion} + M_{boil-off} + M_{error} \tag{3.1}$$

Design margin[7] for liquid propellant loads depend on the mission but can be as high as 25% [Larson & Wertz] for early conceptual designs.

The amount of propellant remaining behind is indicated by the “expulsion efficiency”, defined by the ratio of propellant mass expelled to initial propellant mass. Typical values of the expulsion efficiency reported are in the range 0.97-0.99 [Sutton], 0.95 [Larson & Wertz], 0.97 for four different cono-spheroid tanks with metallic diaphragm [Woodruff] and 0.9975 for the Messenger propellant tank equipped with vortex suppressor and slosh baffle [Tam]. The actual value depends on the specific tank configuration and the type of propellant management device selected.

The amount of propellant boil-off depends largely on the amount of heat that is transferred to the cold propellant and the thermal properties of this propellant. Both heat transfer and propellant heating have been dealt with earlier to a level sufficient for simple estimations and hence this subject will not be treated here any further.

Loading uncertainty is typically below 0.5%.

[7] It is important that margins are applied only once. Erroneously one sometimes finds a margin on mission characteristic velocity and on propellant load calculated.

3.2 Tank volume

Tank volume depends on propellant volume and ullage volume. Ullage volume is necessary to allow for thermal expansion of the propellant liquids and for the ejection of dissolved gasses or the accumulation of gaseous products of slow reactions within the propellant during storage. For blow down systems[8], tank volume is also determined by the amount of pressure gas stored in the propellant tank. It follows:

$$V_t = V_p + V_u + V_{pmd} \tag{3.2}$$

Here 'V' refers to volume and the subscripts 't', 'p', 'u', and 'pmd' to tank, propellant, ullage, and propellant management devices, respectively.

Propellant volume

Propellant volume is calculated from required propellant mass 'M_p' and known propellant mass density 'ρ_p' according to:

$$V_p = \frac{M_p}{\rho_p} \tag{3.3}$$

High propellant density implies low propellant storage volume, and hence storage system mass. For a first analysis, mass density of liquids is usually taken to be a constant value. Typical mass density for a range of rocket propellants at standard conditions can be found in the chapter "Propellants and propellant properties". Keep in mind that with changing storage temperature, the density varies. Again, some further details can be obtained from above referred to chapter.

Storage of propellants at elevated pressures including supercritical[9] storage further affects required propellant volume. For instance, from NIST chemistry webbook, we learn that mass density of liquid hydrogen at 20.4 K at 3 bar is 71.1 kg/m^3, which is an increase with ~0.3% with respect to the mass density at 1 atm. Next to the NIST chemistry webbook, various handbooks are available that provide more exact data on mass density of liquids.

Gaseous species generally have low mass density, leading to a relatively large storage volume. Density of gases initially can be determined using the ideal gas law:

$$M_p = \rho_p \cdot V_p = \frac{p}{\frac{R_a}{M} \cdot T} \cdot V_p \Rightarrow V_p = \frac{M_p \cdot \frac{R_a}{M} \cdot T}{p} \tag{3.4}$$

[8] Blow down systems use a pressure gas stored in the propellant tank to feed the propellants from the tank to the thrusters(s). Because all pressure gas is stored in the tank right from the start, the feed pressure will drop during tank emptying.

[9] Under certain conditions, particularly elevated pressure or temperature, the physical distinction between the liquid and vapour phases disappears, and the resulting single-phase fluid is referred to as supercritical [Westerdijk]. Supercritical fluid storage has the advantage that it avoids the necessity of separating the gas and liquid phase as is common for below super critical fluid storage. Another advantage is that for supercritical fluids, very significant changes in density can be achieved by comparatively small pressure and/or temperature changes, particularly around the critical point. This allows for a high-density fluid, hence reducing storage space and tank mass. The obvious disadvantage is the high-pressure levels required that translate directly into an increased tank mass. Supercritical conditions exist for hydrogen at pressures above about 12.9 bar; for oxygen, this pressure is 50.4 bar. Supercritical cryogenic fluid storage has been employed in the past, for example during the Gemini and Apollo program and more recently on the Space Shuttle.

With ‘p’ is pressure, ‘R_a’ is universal gas constant, ‘M’ is molar mass, and ‘T’ is temperature.

For this, the molar mass or the specific gas constant of the gas (or the gas mixture) should be known. In Chapter “Propellants and propellant properties” typical molar mass and mass density values are given for a range of gases under standard conditions (1 bar and 273 K).

High pressure storage of gases allows reducing the needed volume. However, at elevated pressures, most gases do no longer act as an ideal gas requiring more or sometimes even less storage volume to store a given mass. The change in mass density is usually accounted for by incorporating a compressibility factor ‘Z’ in the ideal gas law:

$$V_p = \frac{M_p \cdot Z \cdot \frac{R_a}{\mathrm{M}} \cdot T}{p} \tag{3.5}$$

For a given gas mass, we find that for Z < 1 the required volume decreases compared to an ideal gas. Or when filling, we find that because of compressibility the resulting tank pressure is reduced. Or when keeping the pressure constant, we find that we need to fill the tank with more gas (higher gas mass). Typical values of Z for a number of gases are shown in Figure 11.

Figure 11: Compressibility factor for various gases at 293 K as a function of pressure (in psig)[10]

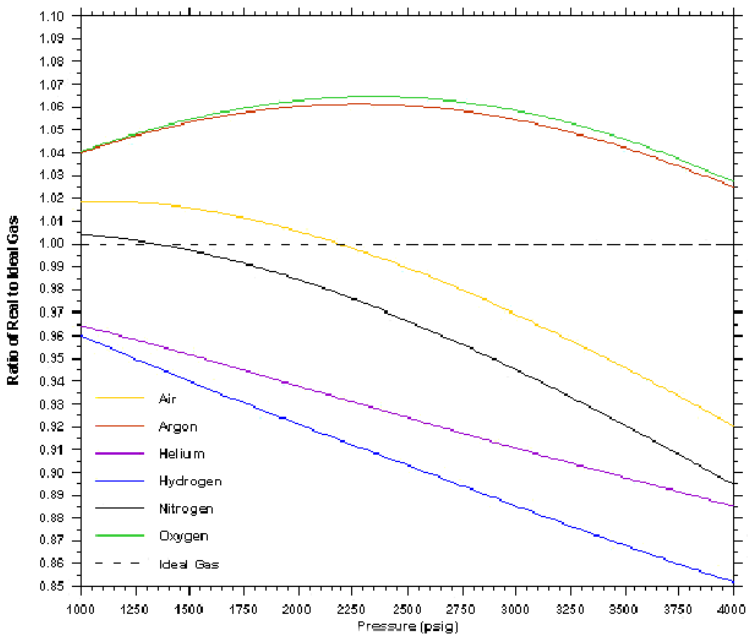

Real values can also be obtained from amongst others the NIST chemistry webbook.

Example problem: Given is a total required propane mass of 1000 kg. Find the propellant volume in case this propane is stored either in the liquid or gaseous state at 1 bar pressure.

Solution: Propellant volume can be calculated using the given mass and tabulated data on density. From [CRC], we learn that liquid density of propane is 582 kg/m^3 at the boiling point of -42.1 °C at 1 bar pressure. Gaseous propane at the same pressure is 2.423 kg/m^3. Hence, liquid density is about 240 times larger than gas density

[10] 1000 psig is about 69 bar relative to 1 atm. Hence 1000 psig equals about 70 bar.

leading to a much lower required volume in case of liquid storage. However, because of the low boiling point, we are required to either store the propane cryogenically. Hence cryogenic storage of propane at 1 bar pressure allows for a liquid propellant volume of about 1.72 m^3, whereas in the gaseous state the propane has a volume of 412.7 m^3.

Ullage volume

Ullage volume of a tank is the amount by which the contents fall short of filling the tank. It is necessary to allow for thermal expansion of the liquid stored, see previous section, the ejection of dissolved gasses (dissolved in the propellant), and/or the accumulation of gaseous products of slow reactions within the propellant during storage. For example, hydrogen peroxide when stored at 293 K will decompose at a rate of 2% per year. At a temperature of 343 K this already increases to 2% per week with still higher rates at higher temperatures.
In case no ullage is available, even small changes in temperature or the formation of gaseous constituents can lead to a substantial increase in pressure with the danger of tank rupture. For example, consider a spherical titanium tank of 1 m diameter and 2 mm wall thickness completely filled with alcohol at 1 bar and 293 K. Let us determine the effect of a 20 K temperature rise on tank pressure. For this, we use the relation between pressure and volume change for a spherical tank [Nash]:

$$\Delta V = \frac{2\pi \cdot p \cdot r^4}{E \cdot t} \cdot (1 - \mu) \tag{3.6}$$

With 'μ' is Poisson's ratio, 'E' is Young's modulus (modulus of elasticity), 't' is tank wall thickness, 'p' is tank pressure, and 'r' is tank radius. We assume a modulus of elasticity for the titanium material of 114 GPa and a Poisson ratio of 0.33, see table 5. Tank volume is found to be equal to 0.5236 m^3. Since alcohol has a mean coefficient of cubic expansion of 1.1×10^{-3} per unit volume, per degree Kelvin (see earlier chapter on propellant properties) we find that a temperature increase of 20 K translates into a volume increase with a factor 1.022 to 0.0115 m^3. To account for this volume increase, it follows that the diameter should increase with 7.3 mm on an initial diameter of 1 m. Substitution of numerical values gives:

$$0.0115 = \frac{2\pi \cdot p \cdot 0.5^4}{114 \times 10^9 \cdot 0.002} \cdot (1 - 0.33) \tag{3.7}$$

Solving for the pressure, we find a pressure of about 99.8 bar. If the tank was designed for a tank pressure of 20 bars, it is not difficult to imagine what the result will be. Fortunately, the problem may be alleviated by that also the tank itself will increase in volume with increasing temperature.

Ullage volume is usually expressed as a percentage of total tank volume. Typical values mentioned in literature are 3-10% [Sutton], and about 5-10% [Larson & Wertz].

PMD volume

No methods have been found to easily incorporate the effect of PMD volume of tank volume. So, any estimation may be quite off. Hence, it is advised to determine the volume the PMD takes up by immersing it in e.g. water and determine the volume displaced.

Growth capability

Tanks are high-cost items, mostly of the associated development cost. Hence, most tanks come in standard sizes. Also, when designing a new tank for a specific mission, the tank is usually designed with some growth potential. This is to cope with a change

(increase) in mission requirements. As a result, tanks usually have a total capability higher than the required capability. For example, Rosetta mission requirements dictate a total Δv requirement of 2200 m/s, which leads to a propellant requirement of 1578 kg. Total propellant capability on board of the Rosetta spacecraft is 1903 kg, which indicates a growth capability or growth margin of 20.6% [Verdant & Schwehm].

Pressure gas volume in propellant tank (blow down system only)

For blow down systems the pressure gas is also stored in the propellant tank. In that case, [Larson and Wertz] relate the propellant volume and (initial) gas volume in the tank through the blow-down ratio as follows:

$$R = \frac{\left(V_g + V_p\right)}{V_g} = \frac{V_t}{V_g} \tag{3.8}$$

To limit the pressure change of the pressure gas, the blow-down ratio is usually selected in the range 1.5-2.5. This indicates that initial gas volume is of the order of 40-67% of total tank volume. The effect of the blow-down ratio on the propellant feeding can be determined from the treatment of blow down feed systems.

Instead of the blow-down ratio sometimes the fill ratio 'F' is used. It is defined as:

$$F = \frac{V_p}{V_t} = 1 - \frac{V_g}{V_t} = 1 - \frac{1}{R} \tag{3.9}$$

3.3 Tank dimensions

Once tank volume is determined, we can determine the tank dimensions. Annex G shows some simple geometries together with the resulting volume and surface area. The latter is for example of importance to determine tank mass and in case of cryogenic propellants for the heat flow.

3.4 Tank pressure

To keep gas tanks as small as possible, the pressure gas must be stored under high pressure, requiring for thick-walled tanks. For liquid propellant tanks two different pressure regimes are distinguished:

- Medium pressure (2-5 MPa) used in pressurized-gas feed systems. The pressure in the tank must exceed the chamber pressure and the pressure loss in ducts and injector.
- Low pressure (0.07-0.6 MPa) used in pump feed systems. The pressure suppresses cavitation in the pumps and provides stiffness to the tanks.

Tank design pressure should be equal to or larger than the sum of vapour pressure and hydrostatic pressure, see hereafter.

Vapour pressure

We all know that for an open container filled with water this water will evaporate over time. The same effect usually occurs with other liquids. In a closed container a slightly different phenomenon occurs. Now molecules from the liquid evaporate as before, but some of these evaporated molecules may also return to the liquid. Over time equilibrium is established so that the rate at which molecules evaporate is equal to the rate at which the gas molecules return to the liquid. We call the gas pressure under these equilibrium conditions the equilibrium vapour pressure, or simply the vapour

pressure. Typical values of vapour pressure can be found in [Martinez] or [NIST]. We find that the values depend on the substance considered. For instance, the vapour pressure of hydrazine and nitrogen tetroxide at 313 K is 4511 Pa and 2.4 bar, respectively. In addition, vapour pressure depends on temperature, see figure 12.

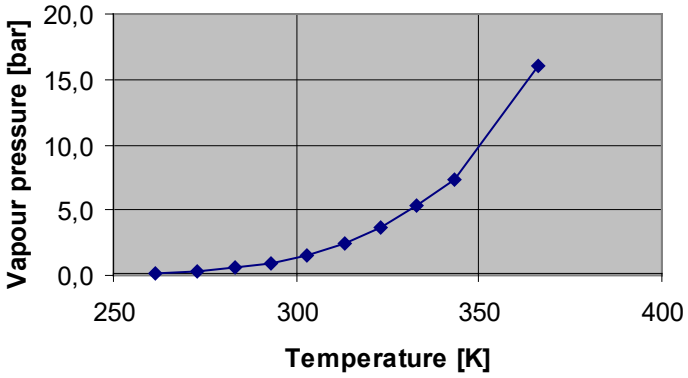

Figure 12: Vapour pressure of Nitrogen tetroxide

Effect of temperature can be approximated using the Shomate equation:

$$\ln(p_v) = \frac{A - B}{T + C} \tag{3.10}$$

Usually, T is taken in Kelvin and p in bar. Typical values of the constants for Oxygen are A = 3.95, B = 340, C = -4.14. Typical values of the constants A, B, and C for some (not all) substances can be found in [NIST] or [Schricke].

In case of the earlier discussed storage of propane, instead of selecting cryogenic storage, we could also have selected to store it at higher pressure. For example, when storing the propane at a pressure of more than 15 bars, it is possible to keep the fluid in the liquid state even when the temperature rises to 313 K. A slight decrease in propellant density though must be accepted (from 582 kg/m^3 to 524 kg/m^3).

An interesting aspect when considering vapour pressure is the temperature range of the tank. At high temperatures, the amount of vapour in the gas mixture in the tank will increase. In case of too high a pressure, a relief valve will be opened to reduce any overpressure. However, in that case also propellant is expelled and hence the propellant load should be corrected for any loss occurring.

Hydrostatic pressure

An important factor determining the pressure loads on the tanks walls of launcher stages is the hydrostatic pressure, which relates to the weight of a fluid colon according to:

$$p_{hyd} = \rho_p \cdot g \cdot H \tag{3.11}$$

With 'H' is the height of the fluid between the upper level of the liquid and the tank wall. Notice that the height H varies in case the rocket makes an angle with the vertical. During the period of propelled flight, it is also necessary to consider the added load due to the acceleration of the vehicle:

$$p_{hyd} = \rho_p \cdot \psi \cdot g \cdot H \tag{3.12}$$

With 'ψ' is thrust-to-weight ratio. Further details on how to estimate the effect on wall stresses and tank wall thickness are given in chapter "Design of thin-shell structures".

Example problem: A vertical axis cylindrical propellant storage tank, fabricated from stainless steel, has a total height of 20 m, a radius of 4 m, and is filled with liquid oxygen to a height of 18 m. The remaining volume is filled with oxygen gas pressurized to 5 bars. Launch loads are about 6g maximum. You are asked to determine for this tank the wall thickness at the base of the tank both with and without considering launch loads. You may assume a density for the liquid oxygen of 1140 kg/m^3 and for the strength of the tank material 600 MPa.

Solution: The fluid colon exerts a pressure at the base at sea level of about 1140 kg/m^3 x 18 m x 9.81 m/s^2 = 2,0 bars at 1 g. Including launch loads, this pressure is about 12 bars. Critical pressure for tank wall thickness according to [Nash] is the circumferential stress where the pressure is given by the sum of the gas pressure and the pressure exerted by the fluid colon. In case of only the 5-bar gas pressure (no fluid present in tank), we find for the tank thickness a value of 3.33 mm. With fluid in the tank, but no launch loads the wall thickness increases to 4.68 mm, and when considering the launch loads, we get about 11.4 mm.

Cycle life (low cycle[11] fatigue)

Usually, a substantial amount of analysis is performed with respect to low cycle fatigue performance. A typical spacecraft fluid storage cycle life requirement is 8-16 proof (pressure) cycles and 50-100 operation (MEOP) cycles. Low cycle fatigue can be predicted using the Wöhler curve or the Coffin-Manson relationship relating strain amplitude and fatigue life. This is explained in some detail in chapter "Design of thin-shell structures".

Other loads

Sometimes, next to internal pressure loads, we should also consider other loads, like launch loads and handling loads. Also, especially when the tank wall also serves as the outer structural wall of the vehicle (integrated tank). it should not only withstand the pressure loads but also provide the necessary strength to withstand bending moments due to wind loadings, and forces operating during the launch trajectory. Sometimes, the walls also must transfer the thrust and must withstand aerodynamic heating. For detailed calculation of the effect of bending and lateral loads on the tank structure, you are referred to handbooks on the design of structures.

3.5 Tank material selection

Choice of tank materials depends on the use of the material (wall structure, liner, seal, PMD, and thermal insulation) and considerations concerning density, corrosiveness[12], fatigue resistance, brittleness, etc. Typical material properties can be taken from handbooks and/or manufacturer information. Data for some specific materials have been collected in Annex K.

An important parameter in the comparison of materials is the "specific strength". This is defined as the ratio between the strength and the density. The higher the specific strength the stronger or the lighter the structure will be. Typical specific strength values for a range of materials can be obtained from Annex K.

[11] Less than 1000 cycles.

[12] Material compatibility with a propellant is classified sequentially from Class 1 materials, which exhibit virtually no reaction with the propellant, to Class 4 materials, which react strongly with the propellant.

3.6 PMD selection

Selecting the right type of PMD is an important matter as it affects not only the mass of the tank, but also the expulsion efficiency. According to [Erichsen], when adding an elastomeric diaphragm, we add about a factor 2 to the mass of the propellant tank. In a later section, we will show this is a reasonable average figure. In Table 4, some characteristics of various types of PMDs are compared.

Table 4: Typical properties of PMDs [Sutton]

Selection criteria	Elastomeric diaphragm	Inflatable elastomeric bladder	Metallic diaphragm	Surface tension screen
Application history	Extensive	Extensive	Limited	Extensive
Mass (normalized)	1.0	1.1	1.2	0.9
Expulsion efficiency	Excellent (0.99 and higher)	Good	Fair (0.96)	Good
Long service life	Excellent	Excellent	Excellent	Excellent
Preflight check	Leak test	Leak test	Leak test	None
Disadvantages	Chemical deterioration	Chemical deterioration	Limited geometries	Limited to low accelerations

Most small tanks today are equipped with a diaphragm. Two types of diaphragms are available including elastomeric (rubber) and metallic diaphragm. The former being the preferred choice offering highest expulsion efficiency and lowest mass. Compared to the bladder type of device, the elastomeric diaphragm is easier to manufacture and offers lower mass. The bladder tank on the other hand has a relatively small sealing area, which is good for preventing leakage, and can be easier installed and/or replaced. Both elastomeric options (bladder and diaphragm) may suffer in case the propellant is incompatible with the elastomer. In that case the use of a metallic diaphragm is the preferred choice.

For larger tanks, the trend today is towards the use of (partial or full) surface tension screens. They have the advantage that there is essentially no limitation to the tank size. This is especially important for long cylindrical tanks as used in launchers. An important disadvantage is that the design and analysis effort for surface tension devices is much higher than for simple diaphragm tanks, especially since we cannot test the proper operation of such devices on Earth.

For details on the physics of surface tension devices, including vanes, sponges, traps, etc., see e.g. http://www.pmdtechnology.com/PMD%20Physics.html or the work of Jaekl as mentioned in the “For further study” section in this chapter.

4 Fluid storage system mass

Fluid storage system mass essentially is made up of the summed masses of the fluid storage tanks. Individual tank masses can be obtained from literature (in case an existing tank is selected) or needs to be determined from analysis. Tank mass of specific tanks has been collected in Table 10 (at the end of this chapter) and Table 5. The mass of a single tank can be written as the summed mass of the tank shell and the mass of other devices, like the mass of the PMD, tank instrumentation, etc. This mass is also referred to as tank mass or tank assembly mass. In next few paragraphs, we will first discuss shell mass estimation based on thin-shell theory as to allow good insight in the main parameters determining the shell mass. In section 4.2, we discuss mass estimation of PMD devices. In section 4.3 some simple mass estimation methods are discussed.

4.1 Shell mass

Tank shell mass can be estimated using [Larson], [Sutton]:

$$M_{tank\ shell} = K_{shell} \cdot \left(M_{shell}\right)_{id} \tag{4.1}$$

Where $M_{shell,id}$ gives ideal shell mass based on thin-shell theory[13] and internal pressure only and K_{shell} is some correction factor that considers local thickening for joints, tank attachments, tank openings, etc. Ideal shell mass can be obtained from:

$$M_{shell,id} = \sum_i \rho_i \cdot S_i \cdot t_i \tag{4.2}$$

Where i refers to the various parts of a tank shell (for a cylindrical tank this may be the cylindrical tube and the two head ends), ρ is density of shell material, S is shell surface area, and t is wall thickness. Note that in the relation above, it is assumed that the layer has a constant thickness and mass density.

In case a shell consists of multiple layers, like when dealing with composite over-wrapped tanks, we may write:

$$M_{shell,id} = \sum_i \sum_j \rho_{ij} \cdot S_{ij} \cdot t_{ij} \tag{4.3}$$

Where j refers to the various material layers.

In case of a fully metallic spherical tank, the wall thickness simply follows from the relation for the circumferential (hoop) stresses existing in the walls due to this loading:

$$t = \frac{p_b \cdot r}{2\sigma} \tag{4.4}$$

Where σ is ultimate strength of material, t is thickness of shell, p_b is burst pressure, i.e. the pressure at which the shell is likely to fail catastrophically, and r is radius of tank. [Larson and Wertz] take the burst pressure identical to the MEOP[14] or design pressure, whereas [Sutton] takes the burst pressure equal to 1,5-2 times MEOP, [Humble et al] and [Erichsen] mention a factor 2, and [Jansen and Kletzkyne] mention a factor 2-4.

The shell thickness of a spherical, composite over-wrapped, tank can be calculated using [Jansen & Kletzkyne]:

$$\sigma_M \cdot t_M + \frac{\sigma_f \cdot t_f}{K_f} = \frac{p_b \cdot r}{2} \tag{4.5}$$

Where subscripts ‘M’ and ‘f’ refer to the metal liner and fibre and K is a strength reduction factor that considers the effect of filler material and fibre direction on fibre strength. Typically, the thickness of a metal liner is 0.5 – 0.8 mm for titanium and 1 mm for stainless steel and the strength reduction factor is about a factor 2.

According to theory [Nash], shell thickness for a cylindrical tank (except for the thickness of the end caps) is twice that of a spherical tank. If the end closure of the

[13] Thin shell theory can be applied in case shell thickness is limited to less than 10% of the radius of curvature of the shell.

[14] MEOP is the pressure not normally expected to be exceeded during the operation of the motor. The design criterion is absence of permanent deformation of the casing under this operating condition, that is, the Yield Strength of the casing material is not exceeded.

cylindrical tank is spherical, its thickness follows from that of a spherical tank with the same diameter (radius). For more details, see e.g. chapter “Design of thin-shell structures”.

Using the relation for shell mass and combining with known information on tank geometry (surface area and volume), we obtain[15]:

$$- \ \text{Spherical}: M_{shell,id} = \frac{3}{2} \cdot \frac{\rho}{\sigma} \cdot V_t \cdot p_b = k_s \cdot V_t \cdot p_b \qquad (4.6)$$

$$- \ \text{Cylindrical}: M_{shell,id} = 2 \cdot \frac{\rho}{\sigma} \cdot V_t \cdot p_b = k_{cl} \cdot V_t \cdot p_b \ \ ; \ \ L/D >> 1 \qquad (4.7)$$

Here the factor ρ/σ is the inverse of the specific strength of the tank material, see our earlier discussion and safety factor is taken equal to 1. Note that the expression given for the cylindrical tank only holds in case for a length to diameter ratio of the tank well more than 1. To obtain a more exact relationship, see chapter “Design of thin-shell structures”.

From these relations we learn that, for a given material, tank shell mass is proportional to tank volume and tank (burst) pressure only.

Table 7 gives calculated shell mass based on (1) given burst pressure, tank volume, and tank geometry, and (2) given wall thickness and tank geometry for some titanium tanks using material properties taken from Annex K.

The difference between the actual mass and the calculated shell mass is attributed to the presence of PMD (propellant tanks only) as well as tank add-ons not accounted for. The effect of PMD is discussed in next section in more detail.

Table 5: Shell mass from specific titanium propellant and pressurant tanks (safety factor set equal to 1)

Spacecraft programme	Volume [l]	Mass [kg]	Shape	Minimum burst pressure [bar]	Minimum wall thickness [mm]	Surface area [m^2]	Shell mass based on burst pressure [kg]	Shell mass based on minimum wall thickness [kg]
				Propellant tanks				
COS-B	20.2	1.3	S	73.98	0.610	0.36	0.96	0.97
Hipparcos	22.8	1.65	CS	59.98	0.483	0.39	0.88	0.83
HS-376	65.42	3.63	CS	50.06	0.660	0.79	2.10	2.29
Brasilsat	209.27	5.44	S	37.24	-	1.70	5.00	-
				Pressurant tanks				
DMSP & Tiros	6.55	3.36	S	620	3.353	0.17	2.61	2.51
Lockheed Missiles	36.05	15.87	S	496	5.004	0.53	11.47	11.69
Atlas Centaur	120.7	35.83	S	391	5.740	1.18	30.29	30.02

S: Spherical
CS: Cono spherical

As a note of warning, it is mentioned that there is a need to check tank wall thickness values determined as the theory does not prevent one from working with unrealistically thin tank walls, that can never be produced or only at very high cost. Some typical tank thicknesses are given in above table and in the Table 10 at the end of this chapter.

4.2 PMD mass

Mass of diaphragm

Diaphragm mass can be calculated from the density of the diaphragm material times the volume needed. To this, we should add some additional mass to account for the

[15] Spherical end caps and long cylindrical section (radius << length of cylinder)

diaphragm mounting feature. For an elastomeric diaphragm [Ballinger et al] mention a nominal thickness of 1.524 mm when fully extended. In that case, its surface approximates one-half the tanks' internal surface. Ballinger et al also mention a typical diaphragm mass for an 0.7 m diameter tank including the retaining ring of around 2.0 kg. Assuming a density of the rubber of 860 g/l, we find that for this tank the diaphragm mass is about 1 kg as is the retaining ring. Unlike the diaphragm, it is expected that the retaining ring scales with tank diameter and not tank surface. This gives:

$$M_{diaphr} = (D / 0.7)^2 + D / 0.7 \tag{4.8}$$

In this equation, D is tank diameter in (m) and M_{diaphr} is diaphragm mass in (kg). To validate the correctness of this relationship, we have compared calculated results using this relationship with the gross diaphragm mass of four other tanks, see the table below.

Table 6: Diaphragm mass (data from PSI)

Tank diameter [m]	Calculated mass [kg]	Actual mass [kg]	Actual/calculated mass ratio [-]
0.327	0.69	0.454	0.66
0.391	0.543	0.539	0.99
0.484	1.17	0.78	0.67
0.711	2.05	2.02	0.99
1.016	3.56	3.44	1.03

Results indicate reasonable agreement.

Mass of surface tension devices

Data from [Lockheed] suggest a mass of surface tension type of PMDs in the range of 5-40% of net (excluding PMD and insulation mass) tank mass. The large range is explained from the use of surface tension devices that span the full tank or only a small part, e.g. at the tank outlet.

4.3 Tank (assembly) mass

In this section, three different tank mass estimation methods will be presented. All methods have been taken from literature [Humble], [Larson], and [Trotsenburg].

1 Tank performance factor or PV method

In this method tank mass is estimated using a tank performance factor or tank figure of merit. This factor than relates tank mass to tank volume and a representative tank pressure. It follows:

$$K_{pv} = \frac{p_{t,ref} \cdot V_t}{M_t} \tag{4.9}$$

Here K is a tank performance factor and is usually expressed in m^2/s^2 and $p_{t,ref}$ is a reference tank pressure. Data from existing tanks have been used to determine representative values of this tank performance factor. This has been done by [Trotsenburg] using MEOP as the representative tank pressure. Trotsenburg obtained values in the range 1×10^4 -16×10^4 m^2/s^2 depending on the tank material, see table 8.

Using the values given in the table, we can now estimate tank mass in a fairly simple way. Advantage of the method is that it allows considering that tank assembly mass scales with tank volume and burst pressure. However, geometry effects are neglected, see our earlier discussion on shell mass estimation. This might explain some of the

range of the values given in table for the tank performance factor. A further disadvantage of the method is that it does not allow for estimating the effect of different materials (at least when considering new materials not included in table) and for changing material properties. Also, the method does not allow for the effect of changing the safety factor used. For this, it is better to use the earlier described ideal shell mass and PMD mass estimation method.

Table 7: Range of typical tank performance factors (given are the 1 and 2 sigma range about the average K-value)

Type of Tank	**Range (+/-1 σ) (m^2/s^2) x 10^4**	**Range (+/-2 σ) (m^2/s^2) x 10^4**	**Remarks**
COPV	8.29 - 16.11	4.38 - 20.02	Compressed Gas
Titanium	5.87 - 6.99	5.31 - 7.55	Compressed Gas
Diaphragm	1.53 - 2.97	0.81 - 3.69	Liquid Propellant
Surface Tension	2.28 - 4.36	1.24 - 5.40	Liquid Propellant
No PMD	3.41 - 4.71	2.76 - 5.36	Liquid Propellant

Note that the values of the K-factor are affected in case we change the reference tank pressure, e.g. burst pressure instead of MEOP.

In the work of [Humble] et al the K-factor is divided by the gravitational acceleration, at sea level 'g'. This way we can express the K-factor in m. For instance, a K-factor of 10000 m^2/s^2 divided by 9.81 m/s^2 would mean a value of $K_{pv,m}$ of 1020 m. Here the subscript m has been added to indicate that this factor differs from the K-factor introduced in the text by a factor 'g'. In the work of Humble also the burst pressure is taken as the tank representative pressure.

2 Shell-mass factor method

According to [Larson & Wertz] tank assembly mass, i.e. the sum of shell mass and tank add-ons including mounting provisions, propellant management devices, and in/outlet provisions, can be estimated from shell mass using:

$$M_t = K_{shell} \cdot M_{shell,id} \tag{4.10}$$

With 'K_{shell}' a shell-mass correction factor that considers tank add-ons. Values reported for K_{shell} range from 1.2-1.3 [Larson & Wertz] to 2-2.5 [Humble et al], indicating quite some difference. Ideal shell mass is estimated using the same method as discussed in section 4.1. Advantage of the shell-mass factor method as compared to the earlier method is that no info is needed on PMD mass. Furthermore, compared to the pV-method it allows for considering the effect of different materials and safety factors.

To verify the above given values for K_{shell}, some typical values have been collected for a range of spherical pressure gas tanks and propellant tanks with no PMD present (used in amongst others spin stabilized spacecraft). Shell mass has been determined using the relationship between shell mass, tank volume and burst pressure. Material properties are taken from handbooks. Next table shows an overview of the results obtained.

Table 8: Shell mass correction factor for some specific spherical storable propellant (excluding PMD) and pressurant tanks

Tank material	Ultimate stress [MPa]	Mass density [kg/m^3]	Volume range [liter]	Shell mass correction factor (mean/SSD)
Fibre overwrapped	1379	1440	1-400	3.41/0.91
Titanium	1080	4428	1-200	1.41 /0.28

Tabulated results show that shell mass correction factor for the two materials considered is different. The difference may be attributed due to inaccuracies in the material properties assumed and or the use of a liner for the overwrapped tanks which is not considered yet. No effects of size could be established although small tanks tend to have slightly higher K_{shell} values.

The same exercise has been performed for a range of spherical and cylindrical titanium propellant tanks equipped with PMD. The results are shown in next figure.

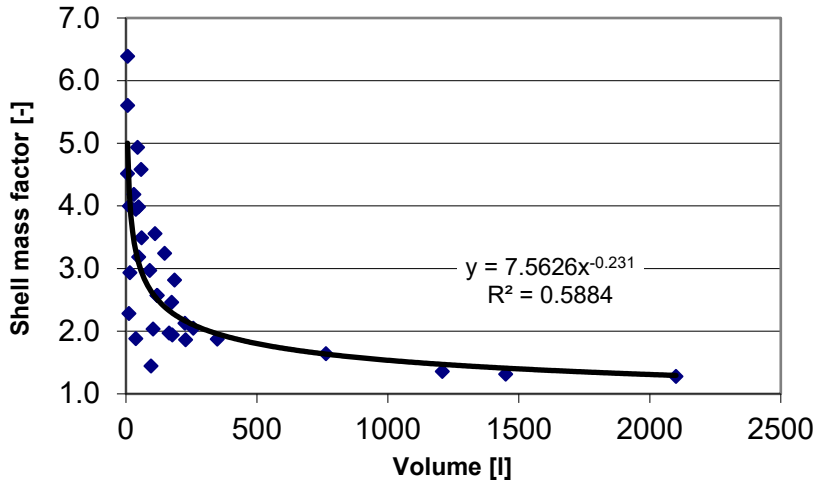

Figure 13: Shell to tank mass factor for a range of titanium storable propellant tanks

Also plotted in figure is a regression relationship. R-squared value for this relationship is 0.63. From the regression relationship a clear size effect can be noted. However, only few data of large tanks were available. Still, for smaller tanks one may expect a larger variation as mass is less critical. The relative standard error of estimate[16] (RSE) in relation to the power curve is determined at 26.2%.

3: Tank mass factor method

A third method given is based on the assumption that tank mass is the dominant mass in the system and that tank mass can be related to the mass of the fluid contained according to:

$$K_{t,prop} = \frac{M_t}{M_{prop}} \tag{4.11}$$

Here $K_{t,prop}$ is referred to as "tank mass factor". This leads to a simple mass estimation relationship, for which little information about the actual system is needed. However, considering the earlier given relationship for shell mass, we find that the above relationship is only correct in case we assume (1) a fixed mass density, fill ratio, tank geometry, tank material, PMD and burst pressure and (2) that tank mass scales with tank volume only. [Larson & Wertz] report values for the tank mass factor in the range 0.05-0.15 indicating that tank mass makes up 5-15% of propellant mass. Some further such relations are given below [Maryland]:

- Cryogenic tanks (excluding insulation material)
  - LOX: 0.0152 M_{LOX} + 318
  - LH_2: 0.0694 M_{LH2} + 363

[16] $RSE = \sqrt{\frac{1}{m-2} \cdot \sum_i \left(\frac{y_i}{f(x_i)} - 1 \right)^2}$

With m is number of data points, Y is real value and f(x) is estimate. We use m-2 because two parameters (the constant and the power) are estimated to estimate the sum of squares

- Large (1000's of kg) storable propellant tanks: 0.316 $(M_p)^{0,6}$
- Monopropellant tanks: 0.1 M_p
- Small gas tanks: 2 times the mass of the contents

Note all mass values are in [kg].

Unfortunately, no indication is given on the accuracy of the above relations. This remains to be investigated. As an illustration of the disadvantage associated with the use of the above relationships, though, it is noted that 1 kg of helium gas and 1 kg of nitrogen gas at identical pressures and temperature clearly require different tank volumes and hence a different tank mass.

Figure 14 presents some actual values for the tank mass factor for the same tanks as used to generate figure 13. Again, a trend line has been added. The R-squared value of this line is 0.69 and the RSE is 50%. The latter value is much worse than the RSE related to the regression relationship given earlier. This is attributed to the fact that the relationship used in figure 13 allows for considering much more detail. Using the relationship from below figure now also the relationship given by [Maryland] for storable propellant tanks can be checked.

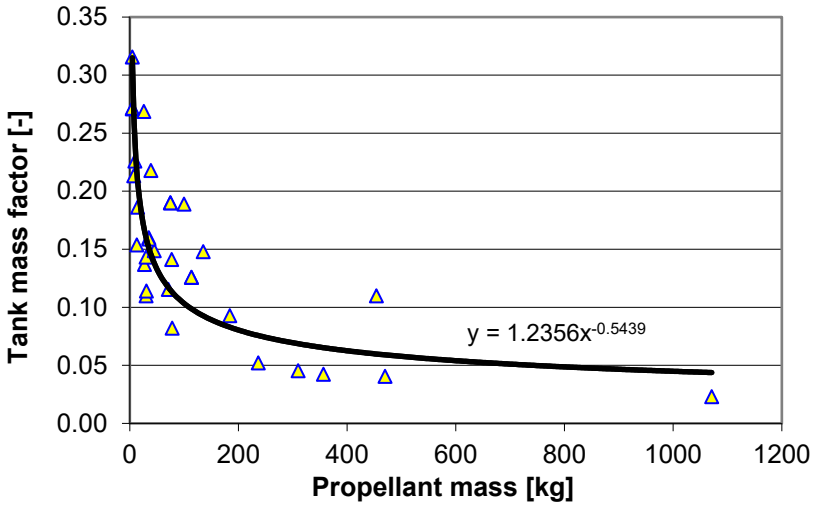

Figure 14: tank mass factor spherical and cylindrical storable propellant tanks

In the foregoing, various models have been presented that allow for an estimation of tank volume and tank assembly mass. However, like with all modelling, we should strive to find out how perfect our model is, like we illustrated when determining the RSE of the power relation shown in figure 14. For this reason, we need actual data to allow comparison with calculated data. A database can help in this matter.

Correction for insulation mass

In case insulation is needed, further correction of tank mass is needed. For instance, to prevent air from liquefying on the tank walls of the External Tank of the Space Shuttle, spray on foams is used. From [NASA] we learn that these foams have a density of on average 38.4 kg/m^3 and a thickness ranging from 2.5 to 5 cm. From the same source, we find that the total foam mass used on ET is about 2.2 metric ton (total tank dry mass is ~26.7 metric ton). Insulation mass per unit area is about 1.123 kg/m^2 for the oxygen tank and more than double that value for the hydrogen tank. These values agree nicely with typical insulation masses for launch vehicle stages equipped with liquid oxygen and liquid hydrogen tanks as given by [Maryland], which are 1.123 kg/m^2 and 2.88 kg/m^2, respectively. Of course, the values depend on the amount of boil-off accepted and the properties of the insulation material. Next to using foam, also paints, Multi-Layer Insulation (MLI), and vapour cooled shield as well as using low conductivity tank attachments/support materials can be used to keep the tank cool and limit boil-off.

4.4 Example mass estimation

Here, we will use the methods presented earlier to calculate the tank assembly mass of the following tank, used on the Eurostar satellite. The following data are given:

- Feed system: Regulated system
- Tank type: Surface tension tank
- Propellant load: 310 kg of Nitrogen tetroxide
- Tank material: Titanium
- Tank size: 58.42 cm ∅ x 101,6 cm
- Tank volume: 225.4 l
- MEOP: 17.6 bar
- Burst pressure: 35.9 bar

First, we estimate tank mass based on shell mass. Using the Titanium material data as given earlier in table 8, we find an approximate shell mass of 9.12 kg. to this, we add a factor 1.40, see table 8 to consider mounting provisions, etc., but excluding PMD. To consider the mass of the surface tension type of PMD, we add a factor 1.225 (average of range 1.05-1.40, see section on PMD mass estimation). This gives a total tank mass of 15.64 kg. Assuming an RSE of 25% (like the RSE for the relationship providing the shell mass correction factor), this gives a 1 sigma tank mass range of 11.7 – 19.6 kg.

Next, using the tank figure of merit method and selecting a value for the tank figure of merit for surface tension tanks of 3.3 x 10^4 m^2/s^2, we find:

$$M_t = \frac{225.5 \cdot 10^{-3} \cdot 17.6 \cdot 10^5}{3.3 \cdot 10^4} = 11.9 \ \text{kg}$$

Taking the extremes for surface tension tanks, we find a tank mass in the range 9.0 – 17.2 kg.

Finally, we estimate tank assembly mass using the tank mass factor relating tank mass and propellant mass. We find a value for the tank mass factor of 0.055 at 310 kg. This gives for the tank mass a value of 16.9 kg. Considering the RSE of 50%, we find that the tank mass is in the range 8.5 – 25.4 kg.

Comparing the results with the actual tank mass of 15.4 kg, we find that the first method is nearest and shows least uncertainty. The other methods are OK, but less accurate.

5 Other system characteristics

Besides system mass, and tank volume, several other parameters are of interest for the design. These parameters include such parameters as cost, reliability, and safety. For example, propellant tanks are high-cost items, see table on next page.

Based on the data presented in table including some data for some more tanks, it was found that tank production and development costs can be related to tank size. Tank development cost per unit of tank volume was found to be in range 300 – 2000 US$/litre (FY 2000 US$) and tank production cost in range 15-500 US$/litre. Of course, prices tend to differ depending on tank type, shape, size, and lot acceptance testing. For instance, larger tanks are at the low end of the indicated ranges whereas small tanks are closer to the high end. Production costs furthermore depend on quantity. The data available did not allow considering all these aspects.

Table 9: Development and production cost data of specific tanks [Jane's]

Tank	Production cost	Development cost
Composite pressurant tank	50 – 77 kEuro (2001)	
Iridium composite pressure gas tank	4 M$ for 75 Iridium hydrazine tanks or 53.3 k$ each (1994)	Not available
Iridium hydrazine tank	Not available	1.5 M$ (1994)
Space Shuttle external tank	30 M$ (1995)	About $ 600 million (1982)
Ariane 5 ME	Not available	62.8 M$ (2014)

Typical tank reliability data for spacecraft show a failure rate of 5.7×10^{-8} failures per hour. This gives a reliability of 0.995 over a 10-year life. For launch vehicles this is roughly 0.0036 failures per launch. The somewhat higher failure rate for launch vehicles may be associated to that most tanks are of the integral type, whereas most spacecraft tanks are more pure pressure vessels.

To estimate these characteristics for conceptual design purposes, it is advised to use either estimation by analogy of parametric estimation. For later stages, we can use either parametric, or engineering build up estimation. It is for the reasons of estimation that it is advised to develop a data base with actual (historic) values on the characteristics of interest and to the level of detail considered necessary.

6 Development and Testing

The design and manufacture of a pressure vessel for space application requires many disciplines to work together, including stress analysts, design engineers, manufacturing engineers, planners, tool engineers, and highly skilled workers such as machinists, and welders. The development of a completely new tank design including the manufacturing and assembly of the parts according to the flight standard and qualification typically takes two years. In case of a derived tank design, with no qualification needed, this can be reduced to about 1 year. A typical development and test sequence includes:

Trade study (approximately 3 months duration)
Design of tank shell and PMD including vortex suppression, structural verification, baffle design (including drop tower tests) and structural load analysis
Manufacturing and machining of forgings
Assembly of engineering and qualification model
Qualification testing (functional and mechanical)

Qualification testing includes volumetric capacity verification, pressure cycle testing[17], loaded sine and random vibration testing. It is to be concluded by destructive burst testing. All flight tanks are proto-flight tested prior to precision clean and delivery. Proof pressure used typically is a factor 1.25-1.5 larger than MEOP. In destructive burst testing the burst pressure can be determined and compared with the calculated burst pressure. The latter typically is taken in range 1.5-2.0 times MEOP. Both burst and proof testing may be conducted by filling the tank by water until the test goal has been reached. Next figure shows a tank prior and after destructive burst test.

[17] Pressure cycle testing is usually conducted hydrostatically. Typical number of cycles is in the range of 15 proof cycles and 100 MEOP cycles.

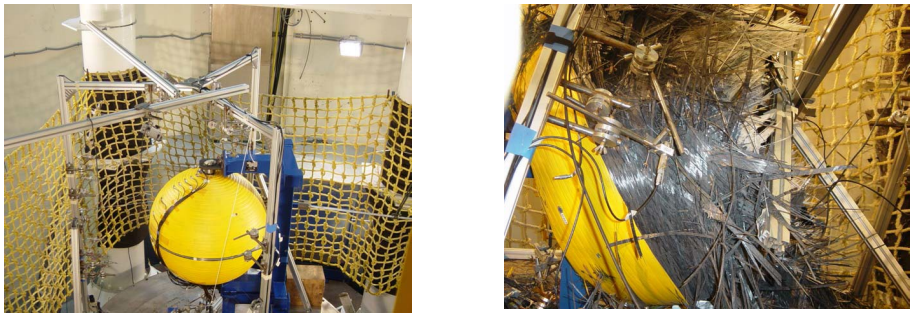

Figure 15: Figure (top) shows tank before burst test and (bottom) after burst test [Benedic].

7 Problems

1) For a rocket using Nitrogen tetroxide (NTO or MON25) as oxidizer and monomethyl-hydrazine (MMH) as fuel is given a (mass) mixture ratio of 1.65. Propellant load (including margin, etc.) is 3000 kg. Propellant temperature range is +5 to +40°C. Determine for this rocket:
   - required oxidizer and fuel volume.
   - tank volume assuming a fill ratio of 50% and 90%, respectively.

2) Using the tank data provided in Table 10, you are asked to:
   - Calculate tank mass factor K_t
   - Calculate tank performance factor (both according to Humble and Erichsen),
   - Calculate shell mass and shell mass correction factor K (according to Larson)
   - Compare the calculated values with the values given in the text. What can you infer?

   For typical material properties, you are referred to annex K. In case a burst safety factor is needed, you are to select a value of 1.5.

3) Derive a relation for tank shell mass for toroidal tanks relating shell mass with volume and tank pressure.

4) We consider using Inconel 600 to design a tank of 0.5 m diameter with a MEOP of 30 bar and a burst safety factor of 1.5. For this Inconel material are given a Young's modulus of 170 GPa, a yield strength of 263 MPa, and a Poisson ratio of 0.33. Using the Inconel 600 data on low cycle fatigue, given in chapter "Design of thin shell structures" and assuming elastic strain only, determine for this tank:
   a) the fatigue strength coefficient and exponent.
   b) the thickness needed to withstand 1000 pressure cycles.

For further study

- *Tam, W.H., Ballinger, I.A., Kuo, J., Lay, W.D., McCleskey, S.F., Morales, P., Taylor, Z.R., and Epstein, S.J.,* Design and Manufacture of a Composite Overwrapped Xenon Conical Pressure Vessel, AIAA 96-2752, 1996.
- *Jaekle, D.E. (jr.),* Propellant Management Device Conceptual Design and Analysis: Traps and Throughs, AIAA-95-2531, 1995
- *Thomas, D.A.,* Long-life Assessment of Graphite/Epoxy Materials for Space Station Freedom Pressure Vessels, J. Propulsion, Vol.8, No. 1, Jan-Feb. 1992.

References

1) *An.,* Mass estimation relationships, Maryland University.
2) *Asato D.,* XSuperNova / Acceleration Probe (SNAP) propulsion system (presentation), NASA Goddard space Flight centre, 2001.

3) *Ballinger I.A., Lay W.D., and Tam W.H.,* Review and History of PSI Elastomeric Diaphragm Tanks, AIAA 95-2534, 1995.
4) *Benedic F., Leard J.-P., Lefloch C.,* Helium High Pressure Tanks at EADS Space Transportation; New Technology with Thermoplastic Liner, *EADS ST, France.*
5) CAPCOM Espace Ariane 4 webpages
6) *CRC,* Handbook of Chemistry and Physics, 60th edition, CRC Press, Boca Raton, 1980.
7) *Erichsen P.,* Performance Evaluation of Spacecraft Propulsion Systems in Relation to Mission Impulse Requirements, Swedish Space Corporation.
8) ESA Ariane 5 webpage.
9) *Humble R.W., Henry G.N., and Larson W.J.,* Space Propulsion Analysis and Design, Space Technology Series, McGraw-Hill Publishing Company, 1995.
10) *Jane's,* Jane's Space Directory 1995-96.
11) *Jansen D.P.L.F., Kletzkine Ph.,* Preliminary design for a 3 kN Hybrid Propellant Engine, ESA Journal, Vol.12, No.4, 1988.
12) *Knol R.H., et al.,* Design, Development, and Testing of Shuttle/Centaur G-Prime Cryogenic Tankage Thermal Protection System, Cleveland OH, USA, NASA Lewis Research Centre, 1987.
13) Ley W., Wittmann K., Hallmann W., Handbook of Space Technology.
14) *Lawrie A., Godwin R.,* Saturn V: The complete manufacturing and test records, Apogee Books, ISBN1-894959-19-4, 2005. See also: Saturn first stage fact sheet, 1996.
15) *Lockheed,* Surface tension tank data, July 1990.
16) *Martinez I,:* http://imartinez.etsin.upm.es/dat1/ePv.htm
17) Nagai N., Noda R., Development status of H-II rocket first stage propulsion system, NASDA, AIAA, 1998.
18) *NASA Facts*, Marshall Space Flight Center, Huntsville, Alabama 35812, External Tank Thermal Protection System, September 2003.
19) *NASA Facts,* Marshall Space Flight Center, Huntsville, Alabama 35812, Super lightweight tank, April 2005.
20) *Nash W.,* Strength of Materials, 4th edition, Schaum's Outline Series, 1998.
21) *NIST*, NIST thermochemical database: http://webbook.nist.gov/chemistry/
22) *Perczynski, P, Zandbergen B. and Starke J.*, Thermal Protection System for Long term in-orbit Cryogenic Propellant Storage, IAC-09.D2.3.6, International Astronautical Conference, Korea, 2009.
23) *Pietrobon Steven, S.,* Lunar Orbit Propellant Transfer.
24) *Schricke R.,* Calculation of propellant Tankage Ullage Volume and Related Parameters, EWP,1525, 1988.
25) *Sutton G.P.,* Rocket Propulsion Elements, 6th edition, John Wiley & Sons, 1992.
26) *Tam W.H, Wiley, S., Dommer, K, Mosher, L, and Persons, D.,* Design and Manufacture of the Messenger Propellant Tank Assembly, AIAA 2002-4139, 2002.
27) *Verdant M., Schwehm, G.M.,* The International Rosetta mission, ESA bulletin, 93, 1998.
28) *Westerdijk J.B., Baljet H.P.G., Stammers E., and Buize W.,* Thermo-dynamics (in Dutch), TU-Delft, February 1988.
29) *Woodruff W.L.,* An experimental evaluation of metallic diaphragms for positive fuel expulsion in the Atmospheric Explorer, hydrazine propulsion system.
30) *Zoun R.,* Health monitoring of space systems, MSc.Thesis, TU-Delft, Faculty of Aerospace Engineering, Delft, March 24, 2003.

Table 10: Characteristics of some large propellant tanks [NASA], [ESA], [Capcom],[Nagai], [Lawrie]

Launcher stage tank	Manufacturer	Propellant	Propellant load	Tank volume	Tank mass[18]	Tank pressure	Tank material (and thickness[19])	Tank shape (dimensions)
			[kg]	[m^3]	[kg]	[Bar]		
Space Shuttle External Tank (ET)	Lockheed Martin	LH2	104308	1514	29930[20]	3	Al2219 alloy (2.5 mm thick)	Cylindrical (46.88m length, 8.4m Ø)
		LOX	625850	559		1.43		
Ariane 5 EPC	Cryospace	LH2	25600	390	4400[21]	2.5	Al 2219 (1.3mm thick)	Cylindrical (23.8m overall length, 5.4m Ø hemi-spherical domes)
		LOX	130600	130		3.6	Al 2219 (4.7mm thick)	
Ariane 4 PAL	Aeritalia	NTO	24609		830	4.45	SS (2.1mm thick)	Cylindrical (cylindrical section 4.92m long, 2.15m Ø)
H-II stage 1	MHI	LH2	12600			3.39	Al 2219	Cylindrical with hemi-spherical end caps (4.0m Ø)
		LOX	73600			4.26	Al 2219	Cylindrical with hemi-spherical end caps (4.0m Ø)
Ariane 4 stage 3 (H10+)	Air Liquide	LH2	2021		670	2.9	Al 7020 (1.5 mm thick)	Cylindrical with hemispherical end caps (cylindrical section 6.624m long & 2.6m Ø)
		LOX	9847			2.1		
Ariane 4 stage 1	Alenia	UH25	84200	100	[22]	5	15CDV6 steel	2 identical cylindrical tanks, each with an overall length 10.09m (cylindrical section 7.4m long with ellipsoidal domes of height 1.35 m) and 3.8m Ø.
		NTO	142900	100		5		
Saturn V stage 1	Boeing	RP-1	6.30E+05	817	~11000	3	Al 2219 T87 (4.90-4.32mm thick decreased in 4 steps to minimize mass)	Cylindrical with hemispherical end caps (10.06m Ø)[23]
		LOX	1.43E+06	1305	~19000	1.8 (26 psia)	Al 2219 T87 (6.45-4.83mm thickness decreased in 8 steps)	

[18] All tank masses are approximate values only. Values are very hard to come by and it cannot be excluded that values quoted are including mass elements that are not normally part of a tank. As examples of such items, we mention inter-tank sections (like for the Shuttle ET) and the Saturn V S1C stage, front and aft skirt, but most likely also insulation. The latter only for tanks carrying cryogenic propellants.

[19] All thickness values are nominal values and refer to skin thickness only. Thickness of stiffeners and stringers not considered.

[20] Multiple versions exist. Version in table is lightweight tank which uses Al2219 as tank material. The 3rd generation (super lightweight tank) uses Al-Li and has a mass of 26,500 kg.

[21] See https://forum.kerbalspaceprogram.com/topic/168384-arianespace-launch-thread/page/23/. Not clear is if value is with or without thermal insulation. [Castellini], see page 122, reports 4898 kg for the summed mass of oxidizer and fuel tank of Ariane 5 EPC H173 stage, which is slightly higher than for the H158 stage.

[22] Stage dry mass is 17.5 tons.

[23] Not included yet is the intertank structure 6.3 m heigh and with also a diameter of 10.06 m. Mass of this structure is 6.5 t not included in tank mass figures.

Contents

List of symbols 352

1 Introduction 354

2 General 355

3 Pressurized-tank feed systems 356

3.1 Types of pressurized systems 357

3.2 Pressurant gases 359

3.3 Pressurization system mass estimation 359

4 Pump-fed systems 364

4.1 Pumps 366

4.2 Pump drive mechanism 373

4.3 Turbines 374

4.4 Turbo-pump assembly and mass 379

4.5 Gas generators 380

4.6 Cycle options 382

4.7 Tank pressurization 384

5 Fluid distribution system 384

5.1 Components 385

5.2 Arrangement 387

5.3 Materials 387

5.4 Preliminary design method 388

5.5 Testing 391

6 Working point and calibration 391

7 Example calculation: blow down system 393

Problems 396

References 398

List of symbols

Roman

A	area
b	width of impeller
B	blow-down ratio
C	absolute velocity
D	diameter
e	surface roughness
E	Young's modulus
f	friction factor
F	fill ratio
g	gravitational acceleration
H	height of fluid colon
j	safety factor
L	Length
m	mass flow rate
M	mass
n	polytropic coefficient
N	number of cycles
p	pressure
P	power
Q	volume flow rate
R	radius, specific gas constant
R_a	absolute gas constant
Re	Reynolds number
t	thickness
T	temperature, torque
U	impeller/rotor velocity
v	velocity
V	volume
w	relative velocity
W	work

Greek

Δ	difference
γ	angle, specific heat ratio
Φ	dimensionless flow variable
η	efficiency
υ	dynamic viscosity
ρ	density
σ	ultimate stress
ψ	dimensionless pressure variable
ω	rotational velocity

Subscripts

c	chamber
eq	equivalent
f	final
g	gas lines
i	initial
in	propellant inlet of thruster
lam	laminar
loss	losses
p	pump

t	turbine
th	theoretical
tp	turbo-pump
turb	turbulent

Acronyms

ID	Internal Diameter
MEOP	Maximum Expected Operating Pressure
OD	Outer Diameter
RCS	Reaction Control System
SEE	Standard Error of Estimation
TET	Turbine Entry Temperature
LOX	Liquid Oxygen

1 Introduction

The feed system of a liquid propellant rocket engine ensures the transport of the liquid or gaseous propellant(s) from the tanks to the thrust chamber at the proper rate thereby considering aspects as mass, size, power usage, reliability, cost, etc. It essentially consists of a pressurization system forcing the propellant(s) to flow from the storage system to the thrust generation system and a distribution system directing the flow.

Two principal types of feed systems are distinguished: those that use high pressure gas for expelling or displacing the propellants from the tanks (pressurized-tank) and those that use pumps for moving the propellants from the tanks to the thrust chamber (pump-fed system). Other ways of propellant feeding (not treated here) are:

- Capillary feeding
- Gravity feeding
- Spin motion feeding

Early feed systems were of the pressurized-tank design as it is inherently simpler than a pump-fed system. In the past pressurized-tank systems have been applied on some early rocket stages like the French Diamant A and B launchers and the second stage of the European Europe I and II launchers [Villain]. One disadvantage found is that for high-total impulse missions and for increasing chamber pressures (to limit thrust chamber size and mass), pressurized-tank systems tend to be very heavy, because they require heavy tanks capable of withstanding the internal pressure. It is to reduce system mass through reducing tank mass and at the same time increasing chamber pressure that pump-fed systems have been introduced. Today, pressurized-tank systems are used almost exclusively for low-total impulse missions where long life, short development time, low cost and reliability are more valued than high-performance. Typical applications today include Ariane 5 second stage, Space Shuttle Orbital Manoeuvring System (OMS), and on almost all satellites, and deep space probes.

Research on pump-fed feed systems commenced in the 1930's. A first major application of a pump-fed feed system occurred sometime in the 1940's s on the German V2 rocket. Since that time many strides forward have been made. The advantage of pump-fed systems being that the pressure in the propellant tank(s) can be kept low and the walls of the tanks thin and light. In some cases, the walls can be made so thin that an internal pressure is necessary to provide stiffness and makes them keep their shape.

Table 1: Characteristics of some chemically propelled spacecraft/launchers

Vehicle name	Engine	Into service/launch data	Propellant mass [kg]	Burn time [s]	Specific impulse [s]	Chamber pressure [bar]	Feed system
Diamant A (1st stage)	Vexin	1965	13.5 tons	95	203 (SL)	17.6	Pressurized tank
Diamant B (1st stage)	Valois	1970	17.9 tons	112	219 (SL)	19.6	Pressurized tank
Coralie stage	--	1966	10.1 tons	104	281 (vac)	13.2	Pressurized tank
Ariane 5 2nd stage	Aestus	1999	9.7 tons	800	324 (vac)	10	Pressurized tank
Ariane 5 core stage	HM60	1999	170 tons	590	430 (vac)	110	Pump-fed
Ariane 4 3rd stage	HM7B	1984	10.8 tons	720	444.6 (vac)	35.5	Pump-fed
Ariane 4 2nd stage	Viking 4B	1988	34.5 tons	130	295.5 (vac)	58.5	Pump-fed
Ariane 4 1st stage	4 x Viking 5C	1988	233 tons	206	278.4 (vac)	58.5	Pump-fed
Large GEO telecommunications satellite (Hotbird-7)	--	2002	1.8 tons	--	320 (vac)	< 20	Pressurized tank
Cassini-Huygens deep space probe	--	1997	3.1 tons	--	300 (vac)	< 20	Pressurized tank

Table 1 shows some typical characteristics of some pressurized-tank and pump-fed feed systems. The data confirms that pressurized-tank systems are favoured for motors operating at low chamber pressures and having relatively short operation times (low total impulse), whereas pump-fed systems are favoured for high-total impulse missions requiring high performance (specific impulse). Pump-fed systems are usually aided by some tank pressurization to prevent cavitation and/or to add resistance to buckling due to launch loads.

In the following, we will discuss these systems in some more detail following in part the text of [Timnat], but first we discuss the overall equation governing the operation of a feed system.

2 General

Key performances in the operation of any feed system are:

Head H. This parameter can be regarded as the height of a column to which a liquid can be raised:

$$H = \frac{\Delta p_t}{g \cdot \rho} \tag{2-1}$$

Where Δp_t is (total) pressure difference acting on the column, g is gravitational acceleration, and ρ is mass density of the liquid. It is another expression for the pressure increase/difference that can be accomplished using a pump or pressurized tank. The reason for using head instead of pressure increase, is that it does not change when changing the liquid in the column. Hence, if some device produces a head of 100 meters, it will produce 100 meters of head regardless of the fluid to be transported. Head is referred to as *pressure head* for pressurized-tank systems and *dynamic or pump head* for pump-fed systems.

Capacity Q; volume flow rate of propellant fed to the thrust generation system:

$$Q = m / \rho \tag{2-2}$$

Here m is fluid mass flow rate. It generally follows from the selected/required thrust level, the selected specific impulse and (in case of a multi-propellant) the selected oxidizer-to-fuel mass mixture ratio.

The basic approach to all feed systems is to write the Bernoulli equation between two points, connected by a streamline, where the conditions are known. For example, between the surface of a reservoir (index 0) and a pipe outlet (index 1):

$$H_0 + \frac{p_0}{\rho \cdot g} + \frac{v_0^2}{2g} + H_p = H_1 + \frac{p_1}{\rho \cdot g} + \frac{v_1^2}{2g} + \Delta H_{loss} \tag{2-3}$$

The total head at point 0 must match with the total head at point 1, adjusted for any increase in head due to pumps and any losses due to pipe friction, entries, exits, fittings, etc. We distinguish:

- *Elevation head difference* - This is the difference in vertical distance to which the feed system raises the liquid.
- *Pressure head difference* - The difference in pressure head between outlet and inlet of the system.
- *Velocity head difference* - The difference in velocity head between the outlet and inlet of the system.
- *Friction head*, ΔH_{loss} - These are losses due to the flow of liquid in the lines.
- *Pump static (discharge) head*, H_p - The difference in elevation between the liquid level of the discharge and the centerline of the pump. This head also includes any additional pressure head that may be present at the fluid surface in the discharge section.

3 Pressurized-tank feed systems

In Figure 1 a schematic flow diagram of a pressurized tank feed system is shown.

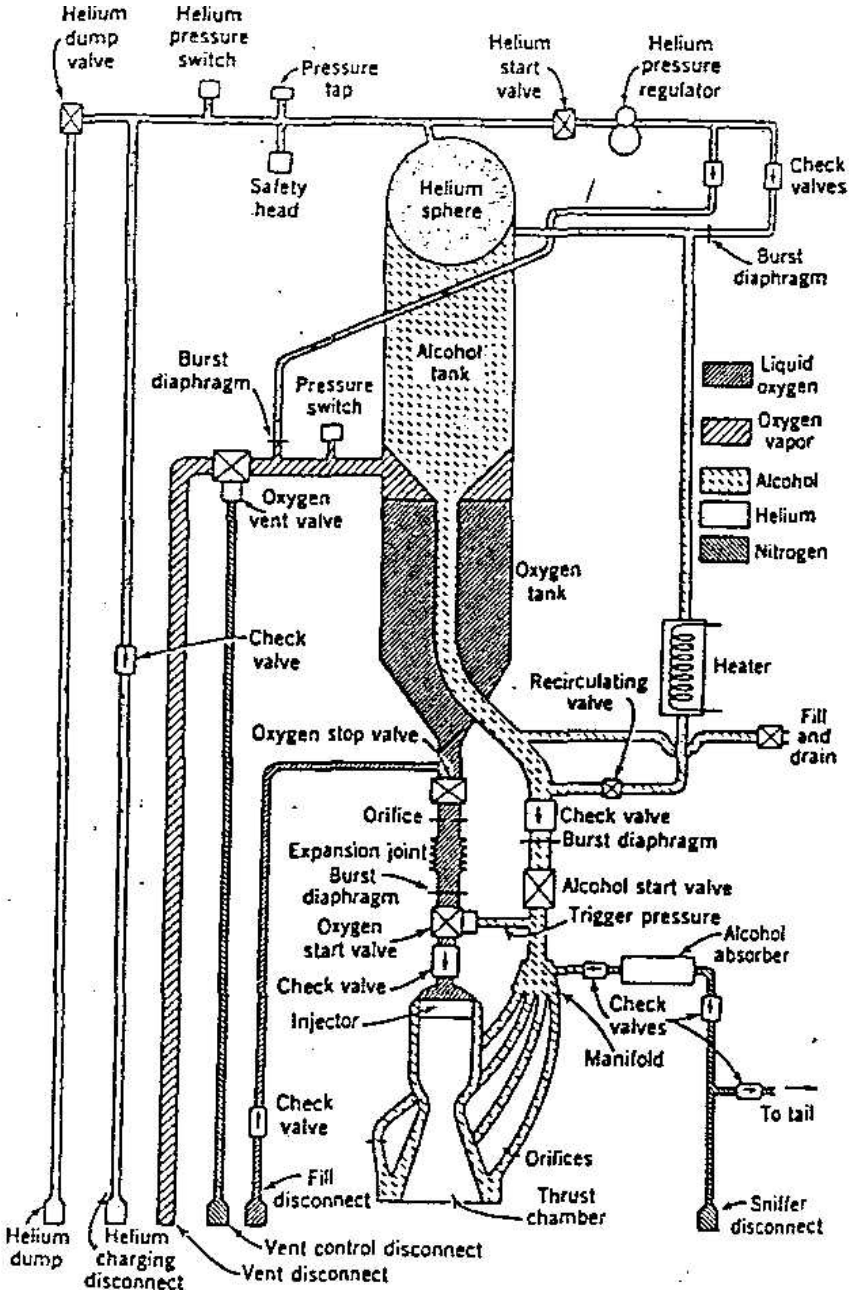

Figure 1: Schematic diagram of pressurized tank feed system.

From this figure one can identify essential components that make up the gas-pressure feed system. We have the Helium pressurant gas stored in the Helium storage tank. Connected to the storage tanks are various fluid lines including a charge (fill) and discharge (dump) line, and delivery lines that go to the two tanks. Located on these lines are various components like control valves that allow for starting/stopping the flow, check (or one-way) valves, a pressure regulator that regulates the tank pressure, a safety or relief valve set to open at a certain pressure. The components identified and their respective task/function are summarized in the Table 2. Typical characteristics of some specific feed systems are given in table 3.

Table 2: Pressurization system components

Component	Task
Pressurant tank(s)	Store the pressurant gas.
Pressurant	Pressurize the propellant, thereby ensuring that the propellant flows from the propellant tank to the thrust generation system.
Pressurant distribution system	Lead the pressurant gas from the storage tank to the propellant tank.
Pressure regulator(s)	Regulate the pressure from the gas down to a set pressure appropriate for the propellant tank.

Table 3: Specific characteristics of some pressurized-tank feed systems.

vehicle (tank)	Type of system	(Initial) tank pressure [bar]	Tank volume [l]	Pressurant	Pressurant mass [kg]
Ariane 5 (LOX tank)	regulated	3.5	120000	Helium	145
Space Shuttle OMS	regulated	17.2	5091	Helium	
DFS	regulated	17	750	Helium	2
OTS	blow-down	22	160	Nitrogen	0.49
SYMPHONIE	regulated	16.5	>150	Helium	0.58

Typically, we find that pressurized feed systems are mostly applied for low thrust, low total impulse (less than 10-15 MNs) spacecraft missions. Typical chamber pressures are in the range 3-20 bar.

3.1 Types of pressurized systems

Two types of pressure-gas feed systems are distinguished, being blow-down and regulated, see also Table 3. Below, we will discuss the basic lay-out of these systems as well as their respective advantages and disadvantages.

3.1.1 Lay-out

The Figure 2 present a schematic of a blow-down (left) and a regulated system.

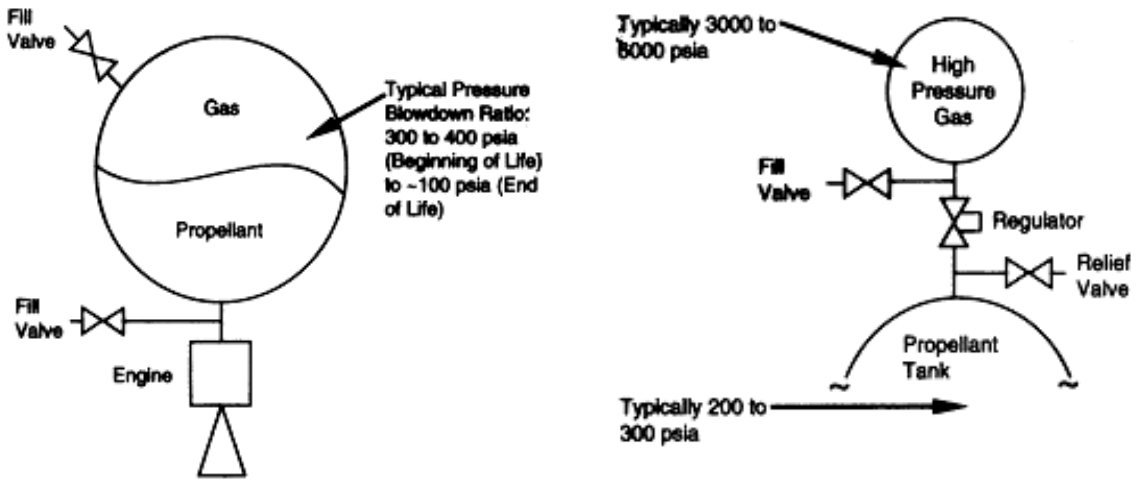

Figure 2: Pressurized feed system options [SMAD]; 100 psia ~ 6.9 bar

In a blow-down system the pressurant is stored in the propellant tank. Typical storage pressures are in the range up to about 30 bar due to limitations in propellant tank mass. To prevent the pressurant gas from dissolving in the propellant, usually a physical separation (for instance a metallic or rubber membrane) between pressurant and propellant is needed. Because of this membrane each propellant tank requires a separate fill and relieve valve for the pressurant. The latter is needed to prevent catastrophic failure in case the pressure of the tank becomes too high.

In a regulated system, the pressurant is stored in a separate tank. Typical pressurant tank storage pressures are in the range of several hundred bars. A regulator (hence the term regulated system) regulates the pressure down to a constant value of about 20-30 bar.

To reduce the pressurant storage volume needed, some alternatives to storing a cold gas under high pressure can be considered. We mention:

- Cold gas heated by:
    - small solid propellant charge. This method allows for short operation times only since in time the gas will cool.
    - heater.
    - heat exchanger. This method is used in practice on many pump-fed systems to ensure a sufficient high pressure in the propellant tank to prevent cavitation to occur in the pump(s).
- Hot gas generator that generates a hot gas at high pressure. For further information, see later entry on hot gas generators.
- Self-pressurization. This requires a propellant with a high vapour pressure, like e.g. butane or propane.

For large pump-fed systems, the tanks themselves might be pressurized to a relatively moderate pressure of up to about 5 bar. This supports the tank walls in carrying buckling loads and helps to prevent cavitation in the pumps.

3.1.2 Advantages and disadvantages

Comparing the schematic of the blow-down system with that of the regulated system, we find that the latter is less simple as it requires more components including a separate pressurant tank as well as a regulator and a gas distribution system with associated valves and filters. This makes the regulated system more costly and less reliable than a blow-down system.

Comparing the operation of the two systems, we find that for a blow-down system the gas pressure decreases due to tank emptying. This will also cause a decrease in propellant mass flow and chamber pressure. The degree in which depends on the initial volume available for the pressurant gas and the type of expansion the pressurant goes through.

Characteristic for the operation of a regulated system is that the propellant tank pressure remains constant even though the pressure in the pressurant tank drops. This constant pressure allows for constant thrust and specific impulse, which simplifies the task of precise orbit acquisition and saves propellant. However, to allow good operation of the pressure regulator, the pressure in the pressurant tank should be at least a factor 1.5-2 higher than in the propellant tank.

Because of the relatively low storage pressure in case of a blow down system, blow-down systems require a larger storage volume for an identical amount of pressurant gas than regulated systems. Increasing the propellant tank pressure will lower the required storage volume but leads to an increase in propellant tank mass.

The various advantages and disadvantages discussed in the foregoing are summarized in the next table.

Table 4: Summary overview of advantages and disadvantages of different types of gas-pressure feed systems

Parameter	Blow down	Regulated
Performance	Mass flow and mixture ratio (bipropellants only) varies during operation	Stable mass flow and mixture ratio
Mass	High tank mass; limited component mass	Limited tank mass; high component mass
Volume	Large	Limited due to high pressure storage of pressurant
Reliability	High	Low
Cost	Low	High

3.2 Pressurant gases

Typical cold gases used as pressurant are Helium and Nitrogen. The main reason for their use is that they are chemically inert gases. For typical properties see [NIST].

3.3 Pressurization system mass estimation

To estimate the mass of the pressurization system we need to consider the mass of the main components of the system. For the determination of the mass of the pressurant tank(s), pressure regulator(s) and pressurant distribution system you are referred to the sections dealing with tank mass and distribution system mass. Here we will focus on pressurant mass only.

The total pressurant mass mainly depends on the type of feed system used, the size of the propellant storage tanks and the type of expansion the pressurant gas undergoes during propellant expulsion from the tanks. Other issues that need to be considered when determining the amount of pressurant, include the amount of pressurant remaining behind in the pressurant storage tank (when present), the amount dissolving in the fuel and oxidizer and the amount remaining behind in the propellant (and pressurant) feed lines. It follows:

$$M_{total} = M_{Pressurant\ Tank} + M_{Lines} + M_{Fuel\ Tank} + + M_{Oxidizer\ Tank} + M_{Dissolved\ in\ Fuel} + M_{Dissolved\ in\ Oxidizer} + M_{margin} \quad (3\text{-}1)$$

Pressurant mass in the lines is usually very small as the line volume is kept small. For instance, for Venus Express, line volume is 0.0007 m^3 as compared to a propellant volume of 0.2703 m^3.

Essential for any pressurized-tank system to operate is that the gas pressure in the propellant tank, p_{tank}, whether regulated or not, must be higher than the thruster inlet pressure p_{in} and the pressure losses occurring in the feed system (piping, valves, bends, filters, etc.):

$$p_{tank} = p_{in} + \Delta p_{loss} \quad (3\text{-}2)$$

p_{in} is known once we have determined the thruster to be used. The pressure losses occurring in the feed system will be determined in the section on the distribution system.

We will now use the feed pressure as a starting point to determine the amount of pressurant gas need. We start by considering a blow down system as this system is the easiest to analyse. Next, we consider a regulated system.

Pressurant mass estimation in this work assumes that vapour pressure of the propellant is zero (blow down system and regulated system) and that all pressurant initially is stored in the pressurant tank (regulated system) or in the propellant tank (blow down). Additionally, it is assumed that the pressurant gas is not heated.

3.3.1 Blow-down system

In a blow-down system the pressurant gas is stored in the propellant tank. The tank fill is indicated by the fill ratio (F):

$$F = V_p / V_{tank} \tag{3-3}$$

Where V is volume, and the subscript p refers to the propellant. We find $0 < F < 1$. Notice that the fill ratio changes during operation.

During operation the pressure drops due to tank emptying until it reaches its lowest value close before tank emptying. How much pressure drops during operation follows from the blow-down ratio (B), which is defined as:

$$B = (V_g)_f / (V_g)_i \approx V_{tank} / (V_g)_i = 1 / (1 - F_i) \tag{3-4}$$

Where V_g is gas volume, and the subscripts i and f refer to the initial and final conditions.

Since we know the minimum required feed pressure, we can compute the mass of pressurant in the tank using the ideal gas[1] law:

$$M_{gas} = \rho_{gas} \cdot V_{gas} = \frac{p_{gas} \cdot V_{gas}}{R \cdot T_{gas}} \tag{3-5}$$

Where ρ is density, V is volume, p is pressure, R is specific gas constant, T is temperature and subscript gas indicates that all parameters are for the pressurant gas.

The gas temperature depends on the type of expansion:

- Isothermal expansion: During expansion of the pressurant gas in the pressurant tank the gas temperature remains constant. This is e.g. the case for low duty cycle propulsion applications, where the expansion process is slow and heat exchange occurs with the environment or can be accomplished by heating of the pressurant tank(s).
- Isentropic expansion is when during expansion no heat exchange takes place from the gas to the environment or vice versa. This is e.g. the case when expansion is fast and heat exchange with the environment is negligibly small. It follows:

  $$\frac{T_f}{T_i} = \left(\frac{p_f}{p_i}\right)^{\frac{\gamma-1}{\gamma}} \tag{3-6}$$

  A fast expansion can of course also be isotherm, but in that case, it is likely that some heating must take place.
- Polytropic expansion is in between isothermal and isentropic expansion.

In case of isothermal expansion ($T_i = T_f = T$), we find for the mass of pressurant gas:

$$M_{gas} = \rho_{gas} \cdot V_{gas} = \frac{p_f \cdot V_{tank}}{R \cdot T} \tag{3-7}$$

Where gas volume is taken equal to tank volume (V_{tank}) and gas pressure is taken equal to the final pressure (p_f) in the tank, which should equal the minimum required feed pressure.

[1] An ideal gas has the following properties (see also earlier lectures):
- The volume occupied by the molecules is insignificant compared to the volume occupied by the gas.
- There are no attractive or repulsive forces between the molecules or molecules and walls.
- All collisions of molecules are perfectly elastic, i.e., there is no loss of internal energy upon collisions.

The initial pressure, then follows directly from the final pressure and the blow-down ratio:

$$p_i = \frac{p_f}{1 - F_i} = B \cdot p_f \tag{3-8}$$

In case of isentropic expansion, we find:

$$M_{gas} = \frac{p_f \cdot V_{tank}}{R \cdot T_i} \cdot \left(\frac{p_i}{p_f} \right)^{\left(\frac{\gamma - 1}{\gamma} \right)} \tag{3-9}$$

Where the subscript i refers to the initial conditions, i.e., the conditions at the start of the expansion. For the initial pressure we find:

$$p_i = B \cdot p_f \cdot \frac{T_i}{T_f} \tag{3-10}$$

3.3.2 Regulated system

In case of a regulated system, the situation is not much different from the blow-down situation, except that we must consider the mass of pressurant gas remaining unused in the pressurant tank and pressurant tubing. The pressure at end of operation in the pressurant tank typically is about a factor 1.5-2 higher than the pressure in the propellant tank. This is because for a pressure regulator to work accurately[2] some minimum pressure is needed before the regulator (high-pressure end). Initial filling of the propellant tank with pressurant is referred to as priming, i.e. the system is made ready for operation. This may happen already on ground so that less pressurant needs to be carried in flight or just prior to start of operation.

Here the case of isentropic expansion with final pressurant tank pressure being equal to propellant tank pressure is worked out in detail. Other cases (isothermal or poly-tropic expansion with unequal pressure in pressurant tank and propellant tank) are left for the reader to explore for him/herself.

For the gas mass we can write:

$$M_{gas,\,total} = M_{gas\ pressurant\ tank,\ final} + M_{gas\ propellant\ tank,\ final} \tag{3-11}$$

Or in short form:

$$M_{gas,\,total} = M_{gas\ press,f} + M_{gas\ prop,f} \tag{3-12}$$

Introducing that gas mass can be determined from gas density and volume, it follows:

$$\rho_{gas,i} \cdot V_{press} = \rho_{gas\ press,f} \cdot V_{press} + \rho_{gas\ prop,f} \cdot V_{prop} \tag{3-13}$$

Reworking gives:

$$V_{press} = \frac{\rho_{gas\ prop,f} \cdot V_{prop}}{\left(\rho_{gas,i} - \rho_{gas\ press,f} \right)} \tag{3-14}$$

We can now write for the gas mass:

$$M_{gas,total} = \rho_{gas,i} \cdot V_{press} = \rho_{gas,i} \cdot \frac{\rho_{gas\ prop,f} \cdot V_{prop}}{\left(\rho_{gas,i} - \rho_{gas\ press,f} \right)} \tag{3-15}$$

[2] Above a pressure ratio of 1.5 to 2, the flow in the regulator reaches sonic conditions and the gas flow rate depends on the size of the vena contracta (throat) only. For smaller pressure differences, the gas flow rate reduces with reducing pressure difference.

Or:

$$M_{gas,total} = \frac{\rho_{gas\ prop,f} \cdot V_{prop}}{\left(1 - \frac{\rho_{gas\ press,f}}{\rho_{gas,i}}\right)} \tag{3-16}$$

As in most cases densities are not known, but instead pressures and temperatures are, we will rework the above relation to include pressures and temperatures and not mass density.

The denominator can be expressed in pressures using Poisson relations. This is because we assume isentropic expansion of the pressurant in the pressurant tank from the initial situation (subscript "i" to the final situation, subscript "f". It follows:

$$M_{gas,total} = \frac{\rho_{gas\ prop,f} \cdot V_{prop}}{\left(1 - \left(\frac{p_{gas\ press,f}}{p_{gas,i}}\right)^{1/\gamma}\right)} \tag{3-17}$$

Turning our attention to the mass density of the pressurant gas in the propellant tank in the final condition, we must consider that the flow through the regulator is not an isentropic process. In a pressure regulator significant changes in pressure and temperature can occur to the fluid. If there is no transfer of heat to or from the surroundings, no work done on or by the surroundings, and no change in kinetic and potential energy of the fluid, the process can be considered isenthalpic. This means that the enthalpy over the regulator does not change. In case of an ideal gas this would mean that when flowing through the regulator, the temperature of the gas does not change from inlet to outlet, provided that the kinetic energy at in- and outlet is negligible. In that case we can use the ideal gas relation to express density in relation to the gas pressure and temperature in the propellant tank:

$$\rho_{gas\ prop,fl} = \frac{p_{gas\ prop,f}}{R \cdot T_{gas\ prop,f}} \tag{3-18}$$

The temperature of the pressurant flowing in the propellant tank will drop in temperature as the temperature of the pressurant in the pressurant tank drops (because of isentropic expansion). As an assumption, we will consider the final temperature of the pressurant tank to be the arithmetic mean of the initial and final pressurant temperature in the pressurant tank [Huzel]. It follows:

$$M_{gas,total} = \frac{\frac{p_{gas\ prop,f}}{R \cdot T_{gas\ prop,f}} \cdot V_{prop}}{\left(1 - \left(\frac{p_{gas\ press,f}}{p_{gas,i}}\right)^{1/\gamma}\right)} = \frac{\frac{p_{gas\ prop,f}}{R \cdot \left(\frac{T_{gas\ press,i} + T_{gas\ press,f}}{2}\right)} \cdot V_{prop}}{\left(1 - \left(\frac{p_{gas\ press,f}}{p_{gas,i}}\right)^{1/\gamma}\right)} \tag{3-19}$$

Further reworking, thereby omitting final temperature of pressurant gas flowing into propellant tank, gives:

$$M_{gas,total} = \frac{\frac{p_{gas\ prop,f}}{\frac{R \cdot T_{gas\ press,i}}{2}\left(1 + \left(\frac{p_{gas\ press,f}}{p_{gas\ press,i}}\right)^{\frac{\gamma-1}{\gamma}}\right)} \cdot V_{prop}}{\left(1 - \left(\frac{p_{gas\ press,f}}{p_{gas,i}}\right)^{1/\gamma}\right)} \tag{3-20}$$

Above relation allows for calculating pressurant gas mass given the initial and final conditions in the pressurant tank and the propellant tank pressure. Note that using the Poisson relation, also the final temperature of the pressurant gas can be determined. As this temperature may drop dramatically, this introduces the question whether the assumption of no heat transfer with the environment is still valid.

Other researchers have used slightly different methods to predict pressurant gas mass. [Sutton, 1992], for instance presents a simplified analysis also based on the assumption of adiabatic conditions. As a result, the following approximation to calculate the required pressurant mass for an adiabatic process follows:

$$M_{gas} = \frac{p_{tank} \cdot V_{tank}}{R \cdot T_i} \cdot \left[\frac{\gamma}{1-(p_f / p_i)} \right] \tag{3-21}$$

Here M_g is the required pressurant mass, p_{tank} is required tank pressure (constant) and V_{tank} is propellant tank volume, p_f and p_i are final and initial gas pressure in the gas tank, T_i is initial pressurant temperature, and γ is specific heat ratio for the pressurant gas.

Example
What Nitrogen tank volume is required to pressurize the propellant tanks of a 400 N thrust rocket thrust chamber using liquid Hydrogen (density is 75 kg/m^3) as a propellant for 5000 s at a specific impulse of 800 s. The Nitrogen tank pressure is 200 bars and for the Hydrogen tank 20 bars. Initial temperature of the Nitrogen gas is 298 K, specific gas constant is 297 J/kg/K and specific heat ratio is 1.4.

Solution:
The required propellant flow is 400N / (800 x 10) = 0.05 kg/s. This gives a total propellant mass M_p = 0.05 kg/sec x 5000 sec = 250 kg. The propellant volume is 250/75 = 3.33 m^3. With 10% allowed for ullage and excess propellants this gives about 3.66 m^3. With the propellant tank volume known, we can now determine the required pressurant mass.

Applying the relation (3-20), we find a pressurant gas mass of 135 kg. In addition, we can determine, as we assumed isentropic expansion in the pressurant tank and given a pressure ratio between initial and final pressure in the pressurant tank of 10, a temperature ratio of 1.93 between initial and final temperature in the pressurant tank. Hence, the final temperature of the pressurant gas in the pressurant tank is 154 K. The average temperature of the pressurant gas in the propellant tank is (298 K + 154 K)/2 = 226 K.

With an additional 5% to provide some margin, the high-pressure tank volume is:

$$V_g = 1.05 \cdot V_g = 1.05 \cdot \frac{M_g \cdot R \cdot T}{p} = 1.05 \cdot \frac{135 \cdot 297 \cdot 298}{200 \times 10^5} = 0.62 \ \text{m}^3$$

Using the relation of Sutton, it follows for the required Nitrogen pressurant mass:

$$M_g = \frac{p_t \cdot V_t}{R \cdot T_i} \cdot \left[\frac{\gamma}{1-(p_e / p_i)} \right] = \frac{20 \times 10^5 \cdot 3.66}{8314.32/28 \cdot 298} \cdot \left[\frac{1.4}{1-(20/200)} \right] = 128 \ \text{kg}$$

Where p_f is taken equal to p_t. This is slightly below the value that follows from the relation (3-20). This is attributed to the assumption of an average temperature for the pressurant gas in the propellant tank, which is not necessarily true as the temperature does not vary in a linear fashion.

3.3.3 Non-ideal gas effects

Non ideal gas effects include compressibility effects (see elsewhere in this work) and leads to the temperature not being constant in an isenthalpic process.

Most gases at normal temperatures are slightly cooled at throttling (due to expansion), except for hydrogen and helium. The internal cooling happens because heat is converted to work that is exerted to overcome intermolecular forces. Ideal gas relations disregard any intermolecular forces and thus miss out on this effect. However, in practice this is not always true. For instance, in case we have Helium gas at 200 bar and 298 K before the regulator. It follows an enthalpy of the Helium of 1617 kJ/kg-K (from NIST database). After the regulator, the pressure has decreased to 20 bar. From NIST, we find that to conserve enthalpy, the temperature of the Helium at this pressure increases to about 309 K. So, we find that the helium gas slightly increases in temperature upon throttling. This rise in temperature due to throttling is usually referred to as the Joule-Thomson effect. Nitrogen does not have this increase in temperature and hence experiences a small temperature drop.

3.3.4 Effect of pressurant heating

For pressure-fed systems requiring a lot of pressurant mass, it may be beneficial to consider heating of the pressurant gas to reduce the amount of pressurant mass to be carried on board. This heating may be accomplished by either of the pressurant tank itself or by heating of the pressurant gas on its route to the propellant tank using e.g. excess heat from the thrust chamber in some heat exchanger.

3.3.5 Effect of cryogenic propellants

The amount of pressurant gas needed differs in case the pressurant gas is used to pressurize storable propellant or a cryogenic propellant. In the latter case, the pressurant gas is cooled by the propellant and hence more pressurant gas is needed to pressurize the tank. From literature, it follows actual pressurant gas mass can be a factor (collapse factor) 1.3-1.5 times higher than estimated [Quay]. Recently, some research into this issue has been carried out at TU-Delft [Hermsen].

3.3.6 Effect of pressurant dissolving in propellant

The mass of pressurant dissolved can be estimated using Henry's law and depends on its solubility S. It follows:

$$M_{Dissolved} = S \times p_{pressurant} \times M_{propellant} \tag{3-22}$$

Where $p_{pressurant}$ is partial pressure of pressurant gas in gas volume considered. Typical values for solubility of gases in liquids can be obtained from literature. For instance, the solubility of Helium in water is 3.7×10^{-4} mol per liter of water and per atmosphere of gas (partial) pressure.

4 Pump-fed systems

Some systems use a pump to pressurize the liquid propellant. To drive the pump usually a turbine is used. Together pump and turbine are referred to as "turbopump". Pump feeding has been introduced in the past to reduce the mass of the propellant storage tanks as compared to using a pressurized feed system. When using a pump, tank pressure can be limited to below about 5 bars down to even 0.5 bars for some applications. However, the addition of pumps leads to increased complexity with as result increased development and production cost and reduced reliability. For instance, according to [Jue], the turbopumps of the Space Shuttle Main Engine, are the components most prone to failure.
The high cost and increased complexity associated with pump feed systems is one reason that pump-feed systems are mostly used for high total impulse (> 20 MNs) launcher missions. Typical combustion chamber pressures are in the range 50-200 bar.

A pump-fed system typically consists of one or more pumps that transfer the propellant(s) from their storage tank(s) to the thrust generation system, see Figure 3. Next to a pump, several other items are necessary to make the system work including some power source and a system that converts this power to rotational motion of the pump axis. In most pump-fed rocket motors, the pump is driven by a turbine through shaft action. In many cases pumps and

turbines are built together to compact turbo-pump units. The pumps can be driven directly or by means of a gearbox. The power needed to drive the turbines stems from a gas generator of which various types are possible, depending on the type of propellant used. This can be the main rocket propellant, a special propellant, or a neutral gas at high pressure. s a schematic diagram of a pump-fed system.

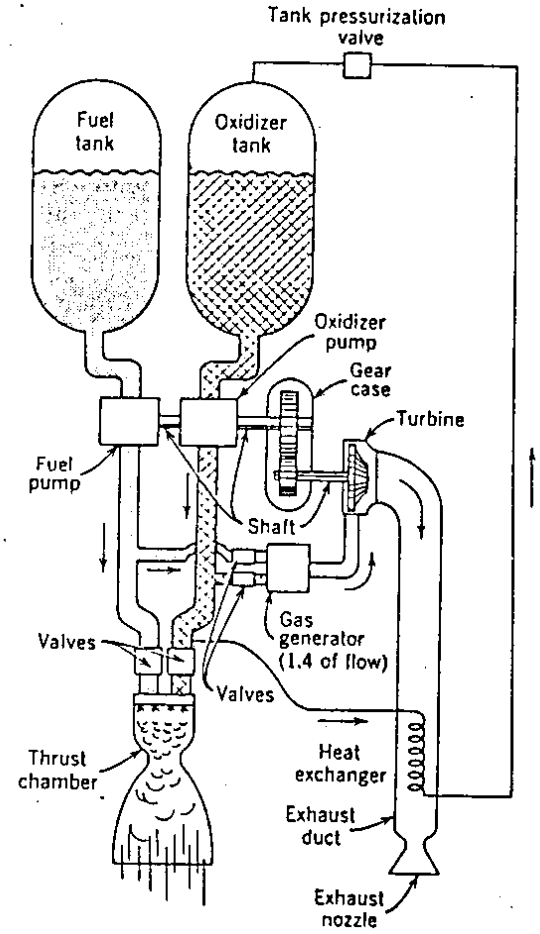

Figure 3: Schematic diagram of pump fed system

A summary of the components making up a pump-fed feed system and their task is given in the next table.

Table 5: Pump feed system components

Component	Task
Pump(s)	Raise, transfer or compress liquids
Pump drive(s)	Drives the pump (ensures pump rotation)
Pump suction and discharge piping	Provide direction to the fluid flow
Pump controls	Controls the power delivered to the flow
Gas turbine(s)	Provides for the power needed by the pump
Gas generator(s)	Provides for the gas needed to drive the turbine
Turbine drive gas distribution system	Ensures the transport of the turbine drive gas from the gas generator to the turbine
Turbine exhaust system	Provide direction to the gases exhausted by the turbine
Gearbox	Reduces the rotational rate of the turbine to an acceptable rate for the pump

Figure 4 [SEP] shows a schematic of the Ariane 4 3rd stage HM7B rocket engine propellant feed system clearly showing the main components in the system. It consists of a high-speed liquid hydrogen pump (60000 rpm), driven directly by the turbine, that boosts hydrogen

pressure from 3 to 55 bar, a low-speed oxygen pump (13000 rpm) driven through a reduction gearbox, to boost LOX pressure from 2 to 50 bar. The turbine itself is driven by combustion gases produced in a gas generator which burns liquid oxygen and hydrogen tapped of at the pump outlets.

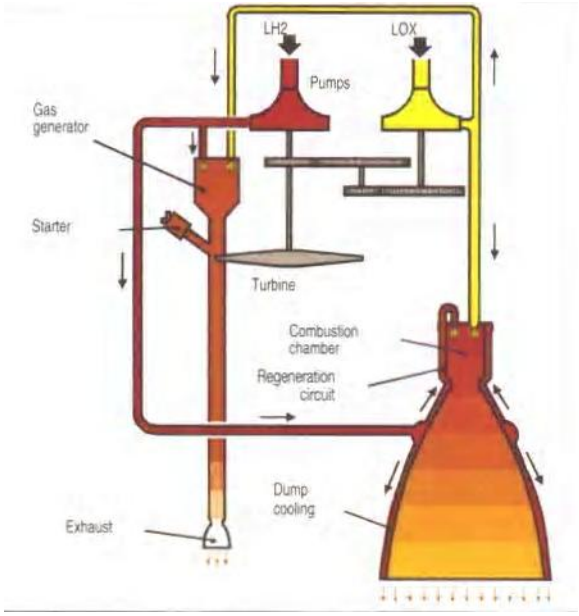

Figure 4: HM7B propellant feed system

In the next few sections, we will first discuss the individual components, after which we will discuss their arrangement in some detail.

4.1 Pumps

A pump is a device used to raise, transfer or compress liquids and gases. Preferably such a pump must be lightweight, high performance and have a small volume (small size). It is for these reasons that for rocket engines almost exclusively rotary pumps are used. In addition, the flow through rotary pumps, unlike for piston type of pumps, is more or less steady.

A typical rotary pump is shown in the next figure. It consists of a rotating impeller, that is immersed in the liquid. The rotation induces an increase in pressure of the liquid by developing a centrifugal force. The impeller also gives the liquid a relatively high velocity that can be converted into pressure in a stationary part of the pump, known as the diffuser (sometimes also referred to as collector).

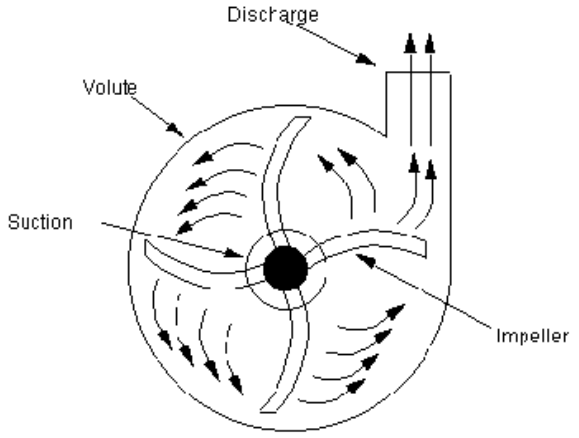

Figure 5: Schematic of pump rotor.

Pump performance

The three key quantities in pump selection (and design) are capacity (volume or mass flow rate), discharge head or increase in pressure and required power (input power). For illustration, the feed system of the HM-60 or Vulcain provides some 200 litres per second of liquid oxygen and 600 litres per second of liquid hydrogen thereby increasing the pressure of the liquid oxygen (LOX) with 130 bar and the liquid hydrogen with 155 bar. Pump efficiency is 74.7% for the LOX pump and 75.2% for the LH_2 pump. Below, we will discuss some of these performances in some detail. Some further performance data are given in the Table 6.

Volume flow rate Q and dynamic or pump head H_p were introduced earlier. Here we discuss three more performance parameters of interest for pump-fed systems.

Pump hydraulic power P_h is the amount of power it takes to raise the liquid to a height equal to the pump head:

$$P_h = m \cdot g \cdot H_p = \frac{m \cdot \Delta p_t}{\rho} = Q \cdot \Delta p_t \tag{4-1}$$

Pump total or brake horsepower is the power needed from the motor accounting for the efficiency of the pump:

$$P_b = \frac{m \cdot \Delta p_t}{\eta_p \cdot \rho} = \frac{Q \cdot \Delta p_t}{\eta_p} \tag{4-2}$$

Typical values of pump efficiency are given in the Table 6.

Net Positive Suction Head requirement ($NPSH_r$)

The performance of a pump is limited by a phenomenon known as “cavitation” which appears as soon as the static pressure at some point in the pump circuit falls below the vapour pressure of the liquid. Bubbles and vapour pockets will form locally and collapse abruptly as soon as they reach a point which pressure is higher than the local vapour pressure. In these regions of condensation violent shocks are produced, leading to rapid erosion of the surfaces. The formation and collapse of the bubbles give rise to pressure fluctuations, which in a rocket are transmitted to the combustion chamber and cause dangerous instability. Cavitation can be avoided if the minimum pressure in the pump is greater than or at least equal to the saturation vapour pressure of the liquid. The pressure necessary at the suction side of the pump to prevent cavitation is referred to as the net positive suction head requirement. It is a characteristic of the pump design and operation and should be provided by the manufacturer.

Table 6: Major specifications/performance data of specific pumps [Schmidt], [Yanagawa], [Jane’s], [Johnsson].

	Rotational speed [rpm]	Mass flow [kg/s]	Pressure rise [MPa]	Efficiency	Required NPSH [m]
SSME LH_2 pump	36.595	73.6	45.8	76.0	15.2 bar
HM60 LOX pump	13830	223.2	13.0	74.7	3.5 bar
HM60 LH_2 pump	32900	42.1	15.5	75.2	2.0 bar
Vulcain 2 LOX pump	12600	273	16.5		
LE-7 LOX pump	20000	229.1	20.9	75.0	30
LE-5 LOX pump	16500	19.4	5.25	65.8	7.5
LE-5 LH_2 pump	50000	3.52	5.6	58.9	56
HM7 LOX pump	13000	11.72	4.8	72.0	1.7 bar
HM7 LH_2 pump	60000	2.56	5.2	61.0	1.5 bar
Vinci LOX pump	19500	33.7			
Vinci LH_2 pump	90000	5.8	22.5		
Small NTO pump	23000	0.641	1.35	67.7	
Small MMH pump	24200	0.313	1.53	55.8	2.07

Types of rotary pumps

Various types of rotary pumps can be distinguished:

- In *centrifugal* pumps, the direction of the flow is largely radial. The volute forces the liquid to discharge from the pump by converting velocity to pressure.
- In *axial* pumps the direction of the flow within the pump is more nearly parallel to the axis of the shaft. The impeller in this case acts as a propeller.
- In a *mixed-flow* pump, the direction of the flow is in between centrifugal and axial.

The main difference between the various types of pumps is in the shape of the rotor and hence the flow direction through the pump. In the next figure some typical propeller shapes are shown together with some of their characteristics.

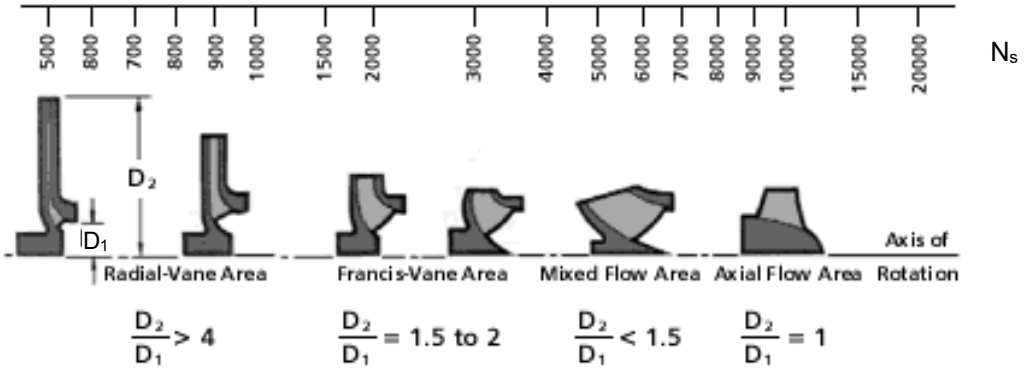

Figure 6: Characteristics of different propeller shapes

The figure clearly shows that for identical volume flow rate centrifugal pumps have the largest and axial pumps the smallest rotor (pump) diameter. In the figure we have also indicated the operating regimes for the various pumps in terms of the so-called pump specific speed N_s, defined as:

$$N_s = \frac{N \cdot \sqrt{Q}}{H^{0,75}} \tag{4-3}$$

With:

- N = Pump shaft speed in rpm
- Q = Capacity in (US) GPM
- H = Total head in feet

All parameter values are typically taken at the point of maximum efficiency, also referred to as the design point.

Notice that the specific speed according to this formula has some dimension. However, it is customary to represent it as a dimensionless number[3]. From the specific speed, we learn that centrifugal pumps allow for higher discharge pressures (head) than axial pumps. On the other hand, axial pumps function better at higher volume flow and/or allow for higher rotational rates. The latter is of importance for the design/selection of the pump turbine and/or the gearbox. Today, the centrifugal pump is the most widely used pump for rocket motors. This is because its operation is well understood, and it is low in price and available in a wide selection of sizes and configurations. Because of the low density of hydrogen, axial flow pumps are mostly used for hydrogen pressurization. To reach sufficiently high pressures, a boost pump may be incorporated.

How the pump performances depend on the rotor shape and the rotational rate is discussed in some detail hereafter.

[3] In European literature, it is common to use a truly non-dimensional form for the specific speed:

$$(N_s)_{SI} = N\, Q^{0.5} / (g\, H)^{0.75}$$

where N is in rad/sec. Q in m^3/s, g = 9.806 m/s^2 and H in m (notice that any set of consistent units will do).

Effect of rotor shape and rotational rate (for further study)

The right side of Figure 7 gives a top view of the impeller of a centrifugal pump. At radius R_x, the impeller-velocity $\underline{U}_x$ and the velocity of the fluid relative to the impeller w_x are shown. The absolute velocity vector is the sum of the vector $\underline{w}_x$ and the local velocity vector of the impeller $\underline{U}_x$

$$\underline{C}_x = \underline{U}_x + \underline{w}_x \tag{4-4}$$

The velocity of the impeller U_x at radius R_x is given by:

$$U_x = \omega \cdot R_x = 2\pi \cdot N \cdot R_x \tag{4-5}$$

where N is the number of revolutions per second.

Due to the change of angular momentum of the flow between R_2 and R_x, the contribution to the torque applied by the flow on the impeller is equal to

$$\underline{T}_{x,2} = \int_{A_2} \underline{R}_2 \times \underline{C}_2 \cdot dm - \int_{A_x} \underline{R}_x \times \underline{C}_x \cdot dm \tag{4-6}$$

Here dm is an infinitesimal small mass flow rate. Evaluating the outer product of vector $\underline{R}$ and $\underline{C}$ gives (see Figure 7)

$$\underline{R} \times \underline{X} = R \cdot C \cdot \sin(\gamma) = R \cdot C \cdot \cos(\alpha) \tag{4-7}$$

As $\gamma = 90^o + \alpha$.

Now the torque applied on the impeller by the flow between the entrance surface A_1 and the exit surface A_2 can be expressed as

$$T = \int_{A_2} R_2 \cdot C_2 \cdot \cos(\alpha_2) \cdot dm - \int_{A_x} R_1 \cdot C_1 \cdot \cos(\alpha_1) \cdot dm \tag{4-8}$$

The theoretical power P applied to the impeller is equal to:

$$P = T \cdot \omega = \int_{A_2} U_2 \cdot C_2 \cdot \cos(\alpha_2) \cdot dm - \int_{A_x} U_1 \cdot C_1 \cdot \cos(\alpha_1) \cdot dm \tag{4-9}$$

For flow velocities uniform at the inlet section A_1 and outlet section A_2 the expressions for the torque and power can be simplified:

$$T = m \cdot R_2 \cdot C_2 \cdot \cos(\alpha_2) - m \cdot R_1 \cdot C_1 \cdot \cos(\alpha_1) \tag{4-10}$$

$$P = m \cdot U_2 \cdot C_2 \cdot \cos(\alpha_2) - m \cdot U_1 \cdot C_1 \cdot \cos(\alpha_1) \tag{4-11}$$

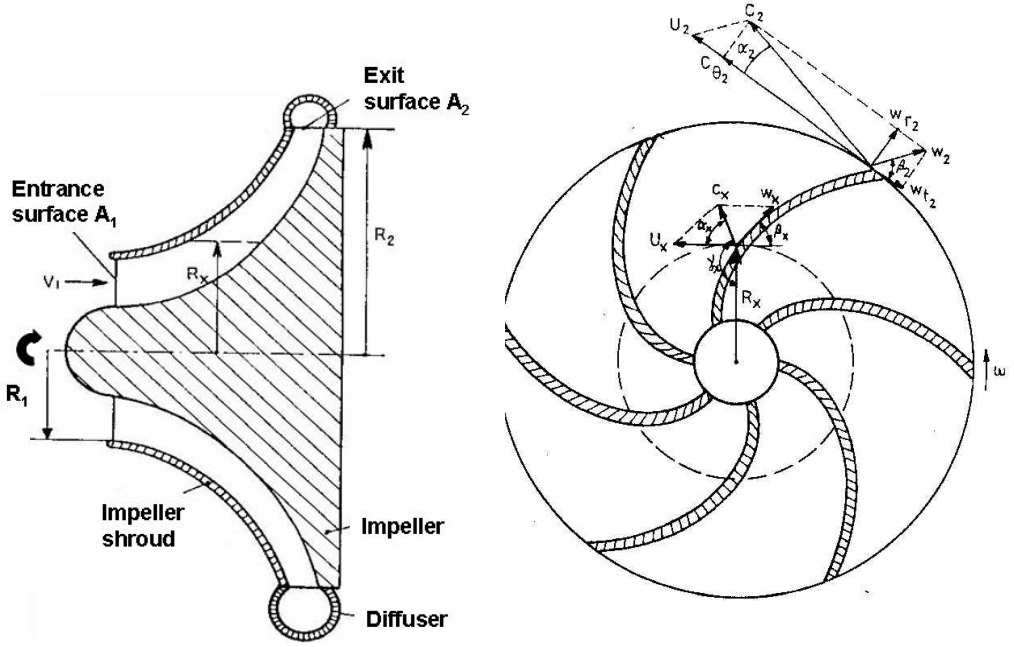

Figure 7: Cross-sectional view of centrifugal pump and top view

For pumps without guide vanes at the inlet, it is assumed that the absolute velocity C_1 is radial (a_1= p/2) The second term of (4-10) and (4-11) becomes zero:

$$T = m \cdot R_2 \cdot C_2 \cdot \cos(\alpha_2) \tag{4-12}$$

$$P = m \cdot U_2 \cdot C_2 \cdot \cos(\alpha_2) \tag{4-13}$$

Now the influence of the shape of the vanes will be discussed. In Figure 8 three possible configurations are shown: backward-leaning blades, radial-blades, and forward-leaning blades. The absolute velocity C is the vector sum of the peripheral velocity off the blade U and the relative velocity w of the fluid with respect to the blade.

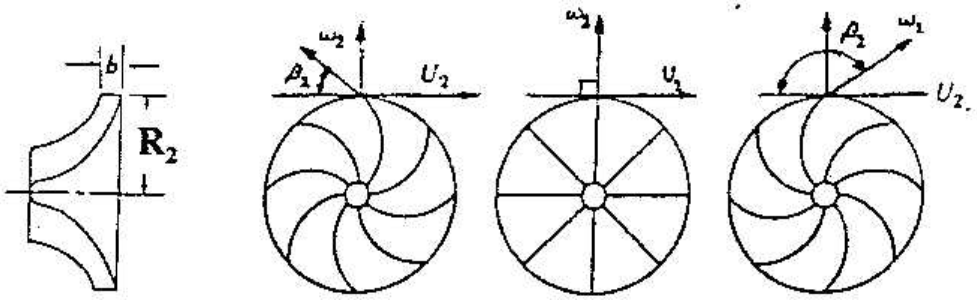

Figure 8: Centrifugal impellers.

The relative velocity vector w can be decomposed into a radial component w_r and a tangential component w_t, see Figure 9.

From continuity, we see that:

$$w_{r_2} = \frac{m}{2\pi \cdot R_2 \cdot b \cdot \rho_p} \tag{4-14}$$

Here, b is the width of the impeller at the exit.

The tangential component $(C_\theta)_2$ of the fluid exit velocity C_2 is rather easily related to the exit fluid angle and the impeller geometry:

$$C_{\theta_2} = U_2 + w_{t_2} \tag{4-15}$$

or

$$C_{\theta_2} = U_2 - w_{r_2} \cdot \cot g(\beta_2)$$

or with (4-14):

$$C_{\theta_2} = U_2 - \frac{m}{2\pi \cdot R_2 \cdot b \cdot \rho_p} \cdot \cot g(\beta_2) \tag{4-16}$$

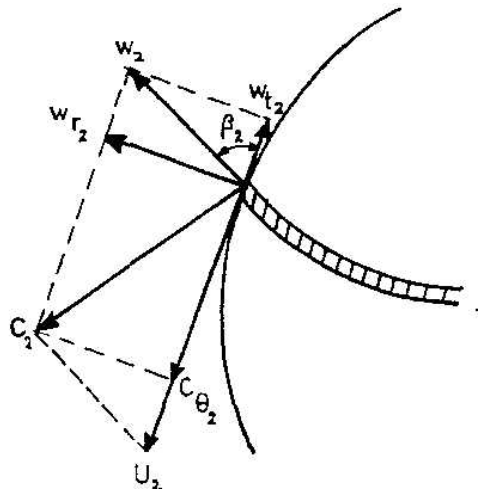

Figure 9: Typical velocity diagram at the end of an impeller.

The power input can be written with (4-13) as

$$P = m \cdot U_2^{\,2} \cdot \left(1 - \frac{m \cdot \cot g(\beta_2)}{2\pi \cdot R_2 \cdot b \cdot \rho_p \cdot U_2}\right) \tag{4-17}$$

Here the power is expressed as a function of the tip velocity of the impeller U_2, its width b, its radius R_2, the fluid density ρ_p and impeller exit angle β_2.

The theoretical rise in total pressure $(\Delta p_t)_{th}$ can be calculated using (4-1):

$$\frac{(\Delta p_t)_{th}}{\rho_p} = U_2^{\,2} \cdot \left(1 - \frac{m \cdot \cot g(\beta_2)}{2\pi \cdot R_2 \cdot b \cdot \rho_p \cdot U_2}\right) \tag{4-18}$$

Due to losses in the compressor flow the actual pressure rise Δp_t will be lower than the theoretical rise $(\Delta p_t)_{th}$. Using (4-2) follows:

$$\frac{\Delta p_t}{\rho_p} = \eta_p \cdot U_2^{\,2} \cdot \left(1 - \frac{m \cdot \cot g(\beta_2)}{2\pi \cdot R_2 \cdot b \cdot \rho_p \cdot U_2}\right) = g_o \cdot H \tag{4-19}$$

Defining the dimensionless pressure and flow variables

$$\Psi = \frac{\Delta p_t}{\rho_p \cdot U_2^{\,2}} \tag{4-20}$$

And

$$\Phi = \frac{m}{2\pi \cdot R_2 \cdot b \cdot \rho_p \cdot U_2} \tag{4-21}$$

The ideal pressure rise through the impellers can be written as ($\eta_p = 1$):

$$\Psi = 1 - \Phi \cdot \cot g(\beta_2) \tag{4-22}$$

The ideal performance of the centrifugal impeller is shown in Figure 10. For a given impeller a single curve determines the pressure rise as a function of tip speed, flow rate, fluid density and mass flow.

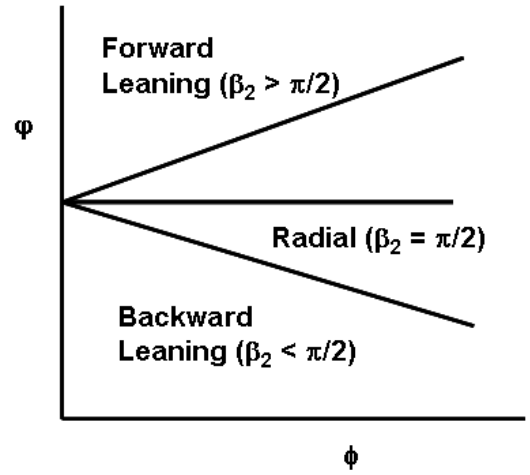

Figure 10: Ideal performance of centrifugal impeller, showing work input per unit mass at constant speed.

Propellant pumps are usually of the backward-leaning type ($\beta_2 < 0$), for several reasons. If the pressure rises with the flow rate, as is the case with forward-leaning blades, the flow can become unstable. Even though the work input of a radial-blade impeller is higher (at a given speed) backward-leaning blades can produce the required pressure rise at higher speeds while stresses in the impeller are still tolerable. Generally, the backward-leaning impellers have somewhat higher efficiency than the other types as the absolute velocity of the flow is lower and losses are proportional to the second power of this velocity.

Affinity laws

Pump performances vary with flow rate. From the preceding section, we can determine how flow rate, pump head, and power vary with varying rotational speed and or density. It follows ($\beta_2 \sim 0$):

$$\frac{Q_2}{Q_1} = \frac{N_2}{N_1}$$

$$\frac{H_2}{H_1} = \left(\frac{N_2}{N_1}\right)^2 \tag{4-23}$$

$$\frac{P_2}{P_1} = \frac{\rho_2}{\rho_1} \cdot \left(\frac{N_2}{N_1}\right)^3$$

The above relations, also referred to as the affinity laws, allow for the calculation of pump performances in case pump performances are given for a fluid, e.g. water, that is different from the fluid to be pumped and/or to determine the effect of a slight change in rotational speed, e.g. in case of a different flow rate. For changes less or equal to 10% or the design rotational rate, efficiency can be assumed to be invariant.

Pump characteristic curve

Pump manufacturers provide information on the performance of their pumps in the form of characteristic curves, commonly called pump curves. In most pump curves, the total dynamic head (H_p), the efficiency (η), the brake horsepower (P_p), and the net positive head (NPSH, not shown here)) required by the pump are plotted as ordinates against the capacity (flow rate) Q in cubic meters per second as the abscissa. These curves (usually for water as the liquid) are available from the manufacturer and are used as a basis for pump acceptance tests.
A pump is typically rated at its point of maximum efficiency, i.e. the design point. The corresponding performances are referred to as rated performances. We have rated discharge, Q_r, rated head, H_r , etc.

Figure 11 shows a typical characteristic curve for a centrifugal and parallel pump. Comparison shows that the head curve for a radial flow pump is relatively flat and that the head decreases gradually as the flow increases. Note that the brake horsepower increases gradually over the flow range with the maximum normally at the point of maximum flow. Mixed flow centrifugal pumps and axial flow or propeller pumps have considerably different characteristics. The head curve for a mixed flow pump is steeper than for a radial flow pump. The shut-off head is usually 150% to 200% of the design head, the brake horsepower remains fairly constant over the flow range. For a typical axial flow pump, the head and brake horsepower both increase drastically near shutoff.

Pump flow control

Various methods exist to allow for pump flow control. We distinguish:

- Discharge throttling. A valve placed in the discharge line allows to vary the pressure drop across the valve.
- Suction throttling. Instead of in the discharge line, the valve is placed in the pump suction line. Disadvantage in this case is that cavitation is more apt to occur.
- Speed control (variable speed pump) allows to reduce the energy input to the system instead of dumping the excess as with placing a control valve in the system.

Series/parallel placement of pumps

- Identical pumps in series will double the head while the capacity remains the same. If they are different sizes we will be limited to the capacity of the smaller pump, and the heads will add together.
- Identical pumps hooked up in parallel will double the capacity of one pump, but the head will remain the same.

4.2 Pump drive mechanism

A pump drive is a rotating device that drives a rocket pump through shaft action, e.g. a gas turbine or an electric motor. Sometimes a gear box is included to allow greater variation in pump speed, see e.g. Figure 4. Because of the inclusion of a drive mechanism, we have additional losses. These losses are generally given by the mechanical efficiency (due to rotational motion of axis): η_m.

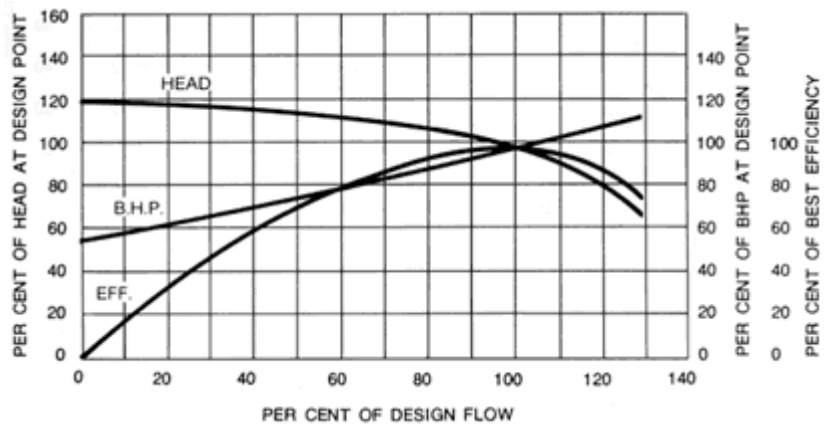

a) Centrifugal pump

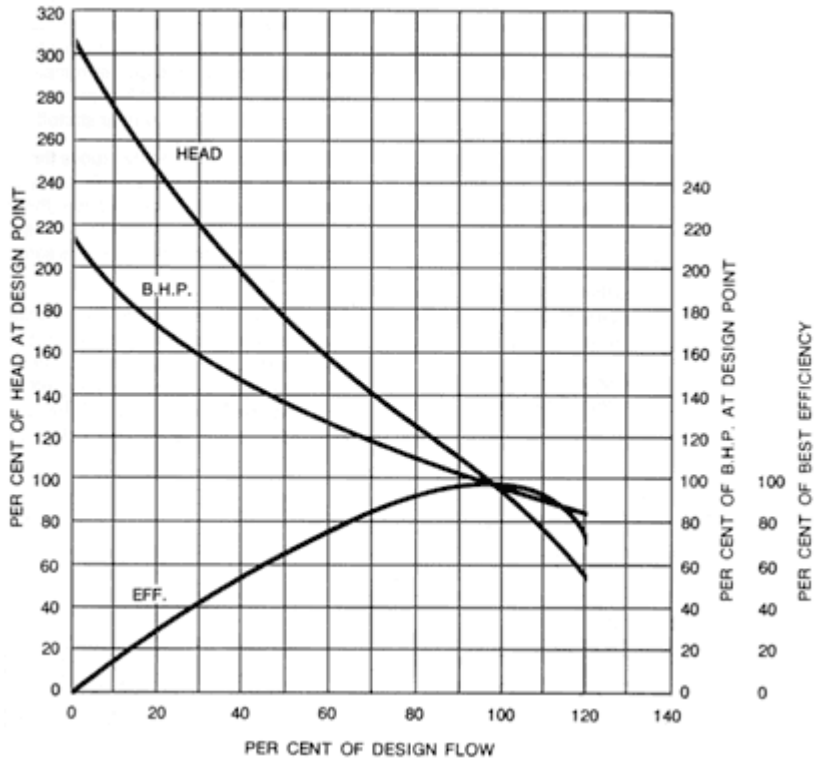

b) Axial pump

Figure 11: Typical pump characteristic curves

4.3 Turbines

One or more turbines provide for the power needed to drive the pump(s) and to make up for the power loss in the distribution system.

The power required from the turbine follows from the oxidizer and fuel pumps with the mechanical efficiency η_m. To this, we will need to add the power loss in the tubing.

$$P_T = \frac{1}{\eta_m} \cdot \sum_i \cdot \left(\frac{m \cdot \frac{\Delta p}{\rho}}{\eta_p} \right)_i + \Delta P_{tubing} \tag{4-24}$$

The calculation of the power loss in the tubing will be discussed in more detail in the section dealing with the distribution system.

A turbine takes advantage of the principle that when a given mass of fluid suddenly changes its velocity, a force is then exerted by the mass in direct proportion to the rate of change of velocity. In a simple turbine, see Figure 12, the rotor consists of a single disk (or wheel) mounted on an axle. The disk has curved blades around the edges. Guide vanes (or nozzles) aim the fluid at the blades and adjust its speed. In many turbines, a casing encloses the rotor. The casing holds the fluid against the rotor so that none of the fluid's energy is lost. In a turbine with more than one disk, the disks are mounted on a common axle, one behind the other. A stationary ring of curved guide vanes (stationary blades or stator) is attached to the inside of the casing in front of each wheel. These stationary blades direct the flow of fluid toward the wheels. A disk and a set of stationary blades is called a stage.

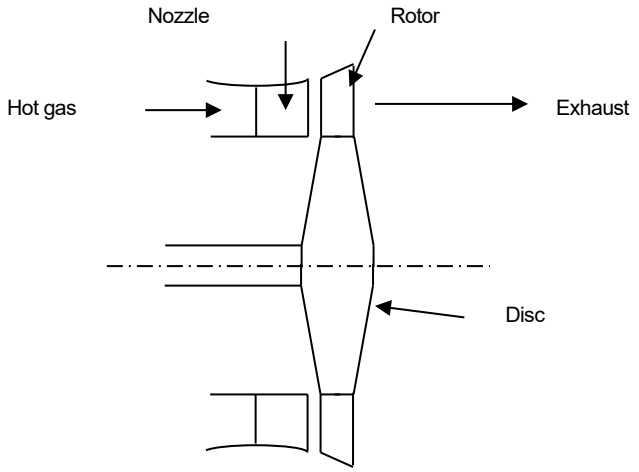

Figure 12: Layout of axial turbine stage

Like for pumps, we distinguish axial and radial turbines depending on the direction of the fluid flow through the rotor. The turbines used in rocket motors are usually of the axial type. This is because axial turbines compared to radial turbines of the same overall diameter, are capable of handling considerably greater mass flow and multi-staging is much easier to arrange. For small mass flows, however, the radial turbine is more efficient and is capable of a higher-pressure ratio per stage than the axial one. Some characteristics of specific turbines used in rocket motors are given in the Table 7.

Table 7: Turbine characteristics [Schmidt], [Helmers], [Kamijo].

Turbine	Turbine speed [rpm]	Shaft power delivered [MW]	Turbine efficiency [%]	Turbine mass flow [kg/s]	Inlet stagnation temperature [K]	Inlet stagnation pressure [bar]	Pressure ratio [-]
Vinci LOX	19500	0.35					
Vinci LH_2	91000	2.45		4.9	245	190	
HM7B	60000	0.38	42.8	0.25	800-900	22.9	16
Vulcain 1 LOX	13400	3.7	29.3	3.67	900	71.4	13
Vulcain 1 LH_2	34500	11.9	61.5	5.12	873	78.6	17.4
Vulcain 2 LOX	12660	5.13			873	72	12
Vulcain 2 LH_2	34070-35680	11.41-14.29			873	78-91	17.4-15.5
LE-7 LOX	20900	6.4	48.5		970	23.5	1.43
LE-5 LOX	16500		39.2	0.39	693	4.87	1.87
LE-5 LH_2	50000		47.6	0.423	842	24.0	4.82

Values of pressure ratio depend on the feed cycle, see later section.

In the following sections we will first consider the power output of a turbine in more detail. Second, we will discuss the relation between power output, rotational rate and blade shape.

Power output

A (gas)turbine can be considered thermodynamically as an open system. From thermodynamics, it then follows for the technical work (per unit mass):

$$W = h_1 - h_3 + g \cdot (z_1 - z_3) - \frac{1}{2} \cdot \left({v_3}^2 - {v_1}^2 \right) \tag{4-25}$$

where h is enthalpy, z is elevation and v is (absolute) velocity, 1 and 3 refer to the in- and outlet, respectively, and the process is assumed to be adiabatic. Next, assuming elevation to be equal to zero, the energy extracted (work performed) from the fluid can be expressed in terms of total enthalpy change or, when assuming a constant specific heat of the drive gas, total temperature change. Customary is to use the conditions at the entrée of the pump to determine the value of the specific heat. Effect of changes in specific heat will end up in the turbine efficiency. Multiplying the technical work with the mass of turbine drive gases flowing through the turbine per second then gives the power produced:

$$P_T = m_T \cdot c_p \cdot \left(T_{t_1} - \left(T_{t_3} \right)_{is} \right) = m_T \cdot c_p \cdot T_{t_1} \cdot \left(1 - \frac{\left(T_{t_3} \right)_{is}}{T_{t_1}} \right) \tag{4-26}$$

An actual turbine does less work because of friction losses, leakage losses along the blades, heat transfer to the surroundings, and mechanical friction. These effects are considered by the turbine efficiency η_T. It is defined as actual power output divided by ideal power output:

$$\eta_T = \frac{\left(P_T \right)_{act}}{\left(P_T \right)_{is}} = \frac{h_{t_1} - h_{t_3}}{h_{t_1} - \left(h_{t_3} \right)_{is}} = \frac{T_{t_1} - T_{t_3}}{T_{t_1} - \left(T_{t_3} \right)_{is}} \tag{4-27}$$

If the kinetic energy of the exhaust is wasted, the static exit conditions at station 3 are most times used and the efficiency is called the “total- to-static turbine efficiency”, since the ideal work is based on stagnation (total) inlet conditions and static exit conditions. This efficiency is then defined by:

$$\eta_T = \frac{\Delta h_{act}}{\Delta h_{is}} = \frac{T_{t1} - T_{t3}}{T_{t1} - \left(T_3 \right)_{is}} = \frac{1 - T_{t3} / T_{t1}}{1 - \left(\frac{p_3}{p_{t_1}} \right)^{\frac{\gamma - 1}{\gamma}}} \tag{4-28}$$

Here T_3 is the static temperature reached after an isentropic expansion from $(p_t)_1$ to p_3. The latter being the real outlet static pressure of the turbine. Typical values of turbine efficiency are given in the Table 7.

The actual power output from the turbine now follows from:

$$P_T = m_T \cdot \left(h_{t1} - h_{t3} \right) = \eta_T \cdot m_T \cdot c_p \cdot T_{t1} \cdot \left(1 - \left(\frac{p_3}{p_{t_1}} \right)^{\frac{\gamma - 1}{\gamma}} \right) \tag{4-29}$$

The power output of a gas turbine can be regulated by the addition of a governor. This is a mechanical, hydraulic, or electro valve which controls admission of hot gas into the turbine.

Relation between blade shape, rotational rate and power output (for further study)

In Figure 13 a cross-sectional view of an axial turbine stage is given, showing a detail of the nozzle and rotor blades and the velocity triangles of the hot gas flow.

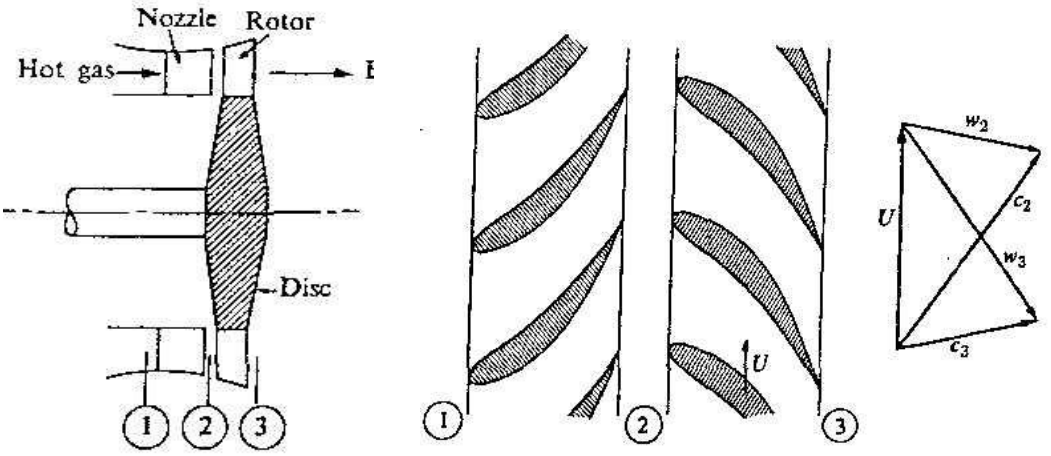

Figure 13: Axial turbine stage blading and velocity triangles.

Here C is the absolute velocity of the flow, U is the velocity of the rotor also referred to as the blade velocity and w is the relative velocity of the flow with respect to the rotor. Subscript 2 refers to the conditions when entering the rotor and 3 when leaving the rotor. Subscript 1 refers to the conditions at entering the row of stationary blades (or the stator). The absolute velocity of the flow is the vector sum of the relative velocity with respect to the rotor and the velocity of the rotor:

$$\underline{C} = \underline{U} + \underline{w} \tag{4-30}$$

The velocity triangle shows that the absolute velocity has changed in direction and in magnitude. The difference between these absolute velocities, $\underline{C}_3$-$\underline{C}_2$ is called ΔC_θ. It is a measure for the decrease in kinetic energy of the flow when moving through the rotor. The change in tangential velocity ΔC_θ is in the direction opposite to the blade speed U. The change of the absolute velocity of the flow from C_2 to C_3 requires a deceleration of the flow. This is accompanied by a reaction force in opposite direction, acting on the rotor. Hence the fluid does work on the rotor.
The torque applied to the rotor is found from the difference of angular momentum of the flow at the inlet and the outlet, like (4-6). This angular momentum is the product of the radius vector and the absolute velocity vector. In evaluating this product, the sine of the enclosed angle appears. The product of the absolute velocity and this sine is the tangential velocity component, $(C_\theta)_2$ at location 2 and $(C_\theta)_3$ at location 3. Now the torque applied on the rotor blades is:

$$T = m \cdot \left(C_{\theta_2} - C_{\theta_3}\right) \cdot R \tag{4-31}$$

The power output is:

$$P_T = m_T \cdot U \cdot \left(C_{\theta_2} - C_{\theta_3}\right) = m_T \cdot C_p \cdot \Delta T_t \tag{4-32}$$

The work per unit mass done by the fluid on the rotor is:

$$W_T = U \cdot \left(C_{\theta_2} - C_{\theta_3}\right) = C_p \cdot \Delta T_t \tag{4-33}$$

thus:

$$\frac{\Delta T_t}{T_{t_1}} = \frac{U \cdot \left(C_{\theta_2} - C_{\theta_3}\right)}{C_p \cdot T_{t_1}} = \frac{U \cdot \Delta C_\theta}{C_p \cdot T_{t_1}} \tag{4-34}$$

This equation shows that the work output (or ΔT_t) per turbine stage is increased by high blade speed U and large turning of the direction of the fluid. Because the turbine must operate with a limited pressure ratio, it is obvious that a high inlet temperature is desirable. Inlet temperature and blade speed are limited by stress considerations.

The velocity of the rotor U can be related to the rotational rate using:

$$U = \omega \cdot R = 2\pi \cdot N \cdot R \tag{4-35}$$

Where N is the number of revolutions per second.

Based on where in the turbine the flow expansion takes place, one distinguishes two types of axial turbines: impulse and reaction turbines. In the impulse turbine, the pressure drop occurs in the row of stationary blades, called the nozzles. The accelerated gas is fed into the blades of the rotor. While the gas is passing through the rotor, the static pressure remains constant while the kinetic energy of the gas is imparted to the rotor. In the reaction turbine the expansion of the gas takes place in the rotor. It is the reaction force due to the gas expansion, like the gas expansion in the rocket nozzle, that drives the rotor. The impulse turbine requires less stages for an equal power output than the reaction turbine and is therefore preferred for applications in rocket engines. In most cases the turbines are directly coupled to the pumps and owing to the possibility of cavitation the turbo-pump shaft usually runs at speeds for which the turbine is relatively inefficient.

Now one stage of an impulse turbine will be considered, see Figure 14. Since there is no static enthalpy change within the rotor, the energy equation within the rotor requires that $w_2 = w_3$.

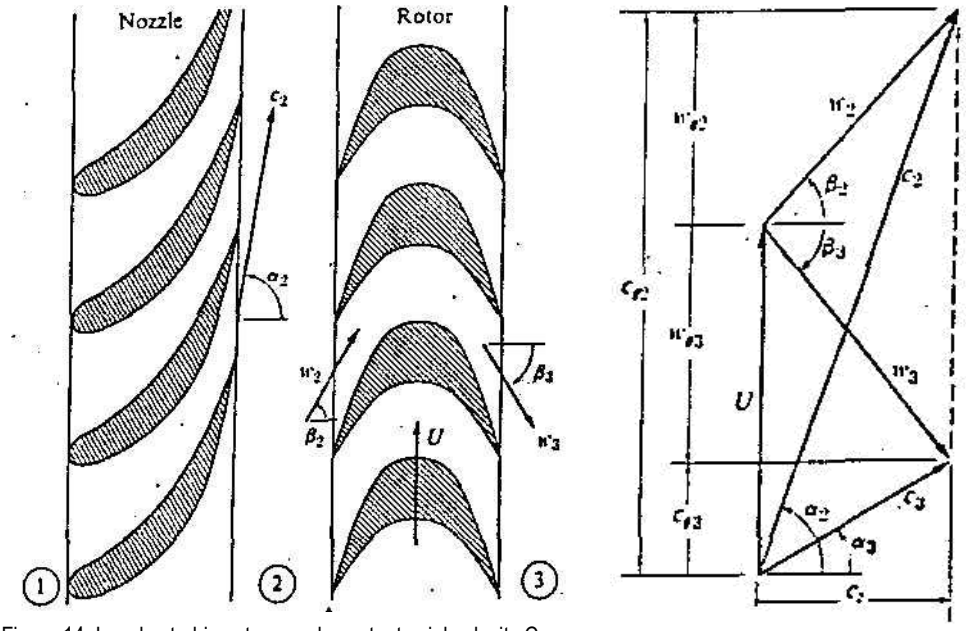

Figure 14: Impulse turbine stage and constant axial velocity C_z.

If the axial velocity component C_z is held constant, then this requirement can be satisfied by $\beta_2 = -\beta_3$. The velocity diagram shows that

$$w_{\theta_2} = w_{\theta_3} \tag{4-36}$$

$$C_{\theta_2} - C_{\theta_3} = 2 \cdot (C_{\theta_2} - U) = 2 \cdot (C_z \cdot \tan(\alpha_2) - U) \tag{4-37}$$

Now (4-34) can be written as

$$\frac{\Delta T_o}{T_{o_1}} = \frac{2U^2}{C_p \cdot T_{o_1}} \cdot \left(\frac{C_z}{U} \cdot \tan(\alpha_2) - 1 \right) \tag{4-38}$$

This equation shows that for large power output the nozzle angle α_2 should be as large as possible. Large values of α_2, however, create large absolute and relative velocities throughout

the stage, causing high losses. Losses seem to be minimized for values of α_2 around 70 degrees.

For the special case of constant C_z and axial exhaust velocity (tangential component $(C_\theta)_3 = 0$ and $(C_\theta)_2 = 2U$), (4-34) becomes

$$\frac{\Delta T_o}{T_{o_1}} = \frac{2U^2}{C_p \cdot T_{o_1}} \tag{4-39}$$

The ideal turbine work per unit mass becomes in this case

$$W_T = 2U^2 \tag{4-40}$$

For a given power and rotor speed and for a given peak temperature, (4-40) is sufficient to determine approximately the mean blade speed (and hence radius) of a single stage impulse turbine having axial outlet velocity. If the blade speed is too high (because of stress limitations) or if the mean diameter is too large relative to the other engine components, it is necessary to use a multi-stage turbine. For Titanium as rotor material, a standard state of the art mean blade speed is about 570 m/s.

4.4 Turbo-pump assembly and mass

Pumps, turbines and gearbox generally are built together to compact turbo-pump units, see for instance Figure 15.

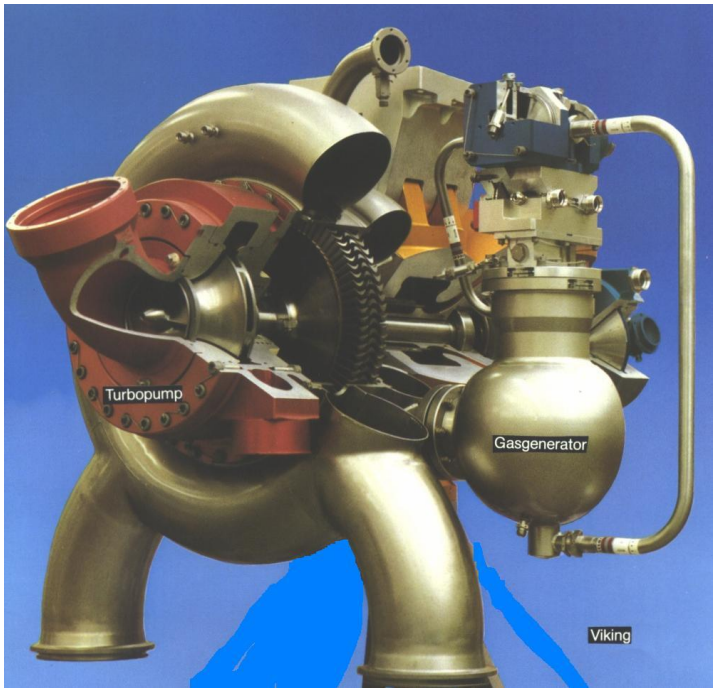

Figure 15: Viking turbo-pump (adapted from SEP folder [SEP])

Turbo-pump mass depends on size, inlet pressure, discharge pressure, mass flow, rotational rate, etc. For initial design, [Manski] relates turbo-pump mass directly to turbo-pump power. [Humble et al] show an identical relationship but also include the pump rotational speed as a variable. Figure 16 shows typical data for specific turbo-pumps. The figure also shows the relationship according to Manski.

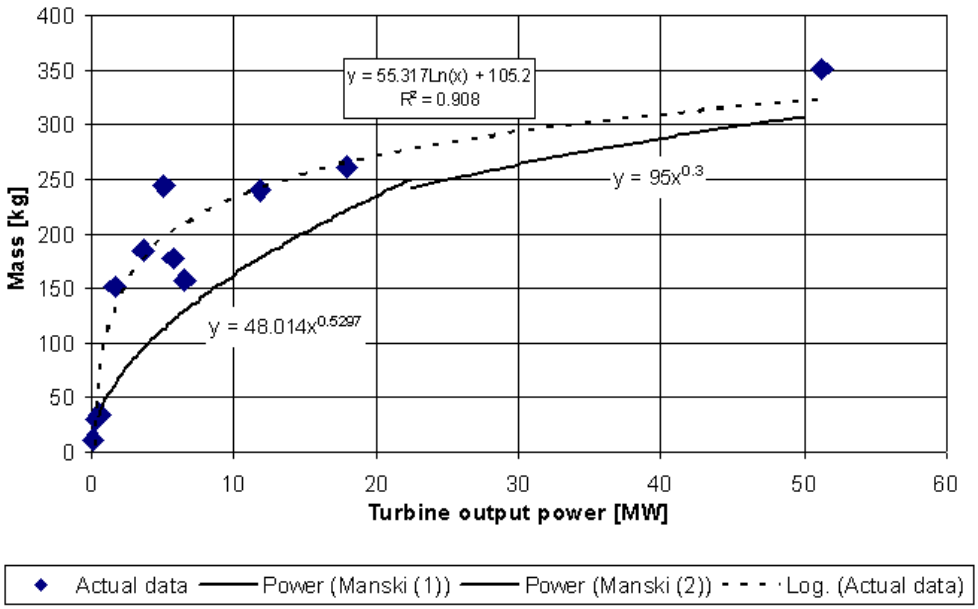

Figure 16: Turbo-pump mass versus power delivered (dotted line has a relative standard error of estimation of ~40%)

Comparison with actual data shows that the Manski relationship slightly underestimates pump mass. A better fit is obtained using the following regression line (also shown in the figure):

$$M_{tp} = 55.31 \times \ln\left(P_{tp}\right) + 105.2 \qquad (4\text{-}41)$$

With:
- M_{tp} = turbo-pump mass (in kg)
- P_{tp} = turbine output power (in MW)

This relation has an R-squared value of 0.908 indicating the quality of the fit.

For other relationships for estimating pump mass see appendix H.

4.5 Gas generators

Various ways exist to generate the hot gases need to drive the turbine. For instance, the turbine of the HM7B is driven by hot gas from a common gas generator, see Figure 4. This gas generator burns a mixture of oxygen and hydrogen (mixture ratio of 0.87) at a combustion pressure of ~35 bar, giving a combustion temperature in the range 800-900 K. The propellants needed for the gas generator are tapped off from the main propellant supply lines. Engine start-up is achieved by a solid gas generator (turbo-pump starter), which generates a high-pressure hot gas stream during a few seconds. This hot gas drives the turbine and through the turbine the oxidiser and fuel pump. Once the propellants start flowing, part of the propellants is tapped of and fed to the gas generator, where they are mixed. Four different types of gas generators are used:
a. solid propellant generators
b. monopropellant generators
c. liquid propellant generators
d. neutral gas generators.

Ad a. Solid propellant generators are small solid propellant rockets producing a gas stream with specified temperature, pressure and mass flow. Because of the high power need and the long operation time of today's large liquid rocket engines, this option is used mainly to start the turbine after which another system takes over. Typical operation times for the solid gas generator in that case are a few seconds.

Ad b. Monopropellant gas generator: use is made of the decomposition of for instance hydrogen peroxide which decomposes into water (steam) and oxygen.) The generator chamber may be fed by pressurization. Figure 17 shows a hydrogen-peroxide gas generator [Hill]. Its working principle is based on catalytic decomposition of hydrogen peroxide across a pellet bed (silicon carbide permanganate impregnated "pebbles"

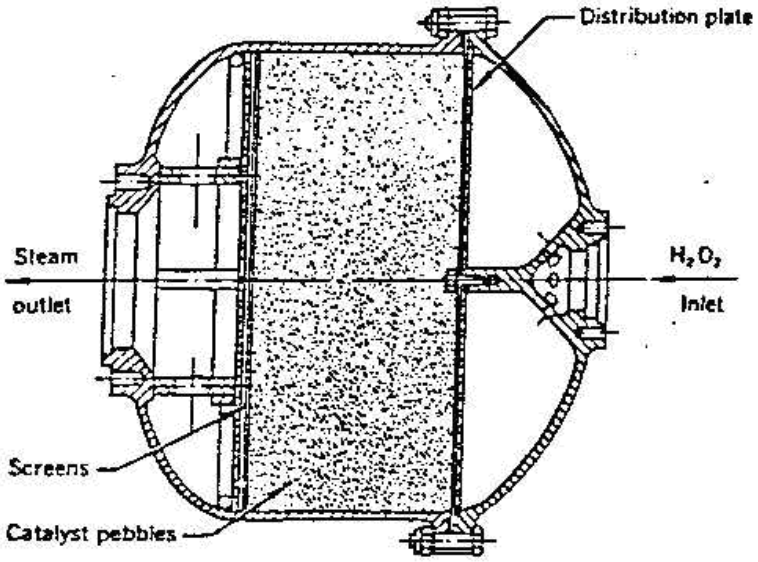

A7 Redstone Production Gas Generator

Figure 17: Hydrogen peroxide monopropellant gas generator.

A hydrogen-peroxide gas generator has for instance been used on the V2–rocket using liquid permanganate as a catalyst. It was used in a similar role on the US Redstone, Jupiter and Viking missiles and on the British Black Knight rockets.

Ad c. Liquid propellant gas generator: This gas generator is essentially a small combustion chamber usually fed with the same propellant as the main combustion chamber. To reduce the combustion temperature, water may be injected, or a fuel rich mixture ratio is used. A typical example is shown in Figure 18 [Hill]. Some characteristics of specific gas generators are given in the Table 8.

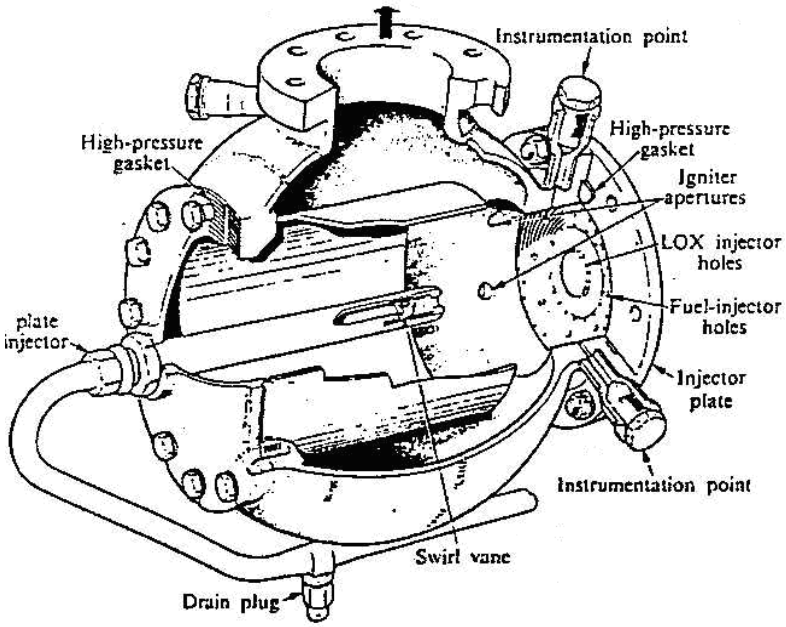

H-1 Liquid Propellant Gas Generator

Figure 18: LOX-kerosene liquid propellant gas generator. About 90 % of the kerosene is injected near the LOX injector, the remaining 10 % being injected from the opposite end to provide cooling.

A special option is that we use the main combustion chamber as the gas generator and tap-of the required amount of turbine drive gases from the main combustion chamber (tap-off cycle). Some cooling of this gas mass flow though is necessary.

Ad d. Neutral gas generators use a neutral gas which is stored under high pressure in a separate tank. This compares reasonably well with pressurized-tank feed systems.
Another option is to heat one of the main propellants using a heat exchanger (expander cycle). The latter does away with a high-pressure storage tank.

Table 8: Characteristics of some gas generators

Gas generator	Propellant/neutral gas	Mass flow delivered [kg/s]	Stagnation temperature of drive gases [K]	Pressure delivered [bar]	Operation time [s]
RD-180	LOX/RP1 (O/F = 54)	887	820	556	
RD-0120	LOX/LH_2 (O/F = 0.81)	78.6	846	424	
SSME	LOX/LH_2 (O/F = 0.90)	91.5	735-868	350-360	480
Vulcain	LOX/LH_2 (O/F = 0.90)	8.9	910	80	590
Vulcain 2	LOX/LH_2 (O/F = 0.90)	9.7	875	101	
LE-7	LOX/LH_2 (O/F = 0.55)	53	810	210	
LE-5A	LOX/LH_2 (O/F = 0.85	0.39	693	26.4	550
Vinci	Hydrogen gas	4.9	245	190	800

Gas generator design compares reasonably well with the design of the rocket combustion chamber except that generally the gas temperature is much lower (in the range up to about 1100 K) to prevent too high TET. Another important requirement is that the combustion gases should contain very few solid particles which could erode the turbine blades and plug the gas channels between them.

4.6 Cycle options

Various feed cycles or ways of arranging the feed system exist. The most important distinction is whether we are dealing with an open cycle or closed cycle:

- Open cycle: Turbine exhaust gases are dumped overboard separately from the main engine mass flow. The gas generator feeding the turbine burns either a propellant different from the main engine or identical but at a different mixture ratio.
- Closed cycle: Turbine exhaust gases are led back to the combustion chamber, where they are further combusted and then expanded through the full expansion ratio. The gas generator combusts the same propellants as the main chamber, but again at an adapted mixture ratio.

As a rule, open cycles are slightly lower performance (2%-5% lower I_{sp}) than closed cycles.

Another distinction is based on how the turbine drive gases are generated, see previous section.

The following feed cycles are commonly distinguished, see also Figure 19:

- Gas generator cycle: Some of the propellant is burned in a gas-generator and the resulting hot gas is used to power the engine's pumps. The gas is then vented to the atmosphere or are fed to the thrust chamber at some point between the throat and the nozzle exit after which they expand in the nozzle. Examples of the gas generator cycle are the European HM60, and HM7A/B engines, the Japanese LE-7 engine and the US F1 and H2 engines.
- Staged combustion cycle: Some of the propellant is burned in a pre-burner and the resulting hot gas is used to power the engine's pumps. The gas is then injected into the main combustion chamber, along with the rest of the propellant and combustion is completed. It essentially is a closed gas generator cycle. Example of the staged combustion cycle is the US SSME.

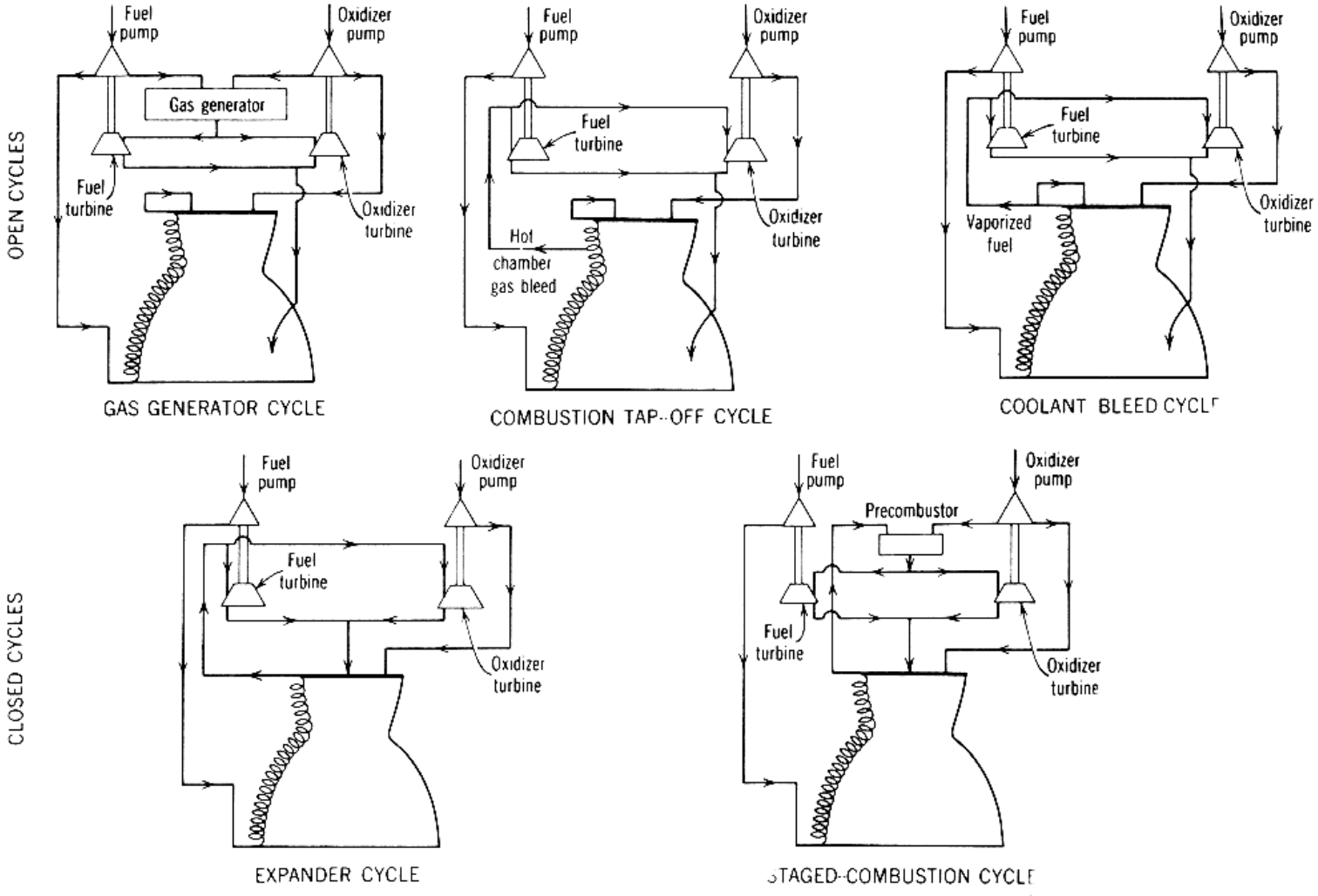

Figure 19: Liquid Rocket Engine feed cycles

- Closed expander cycle: Some of the fuel is heated to drive the turbines after which the turbine exhaust is injected into the main combustion chamber. Example of this cycle is the European Vinci rocket engine.
- Open bleed expander cycle: Some of the fuel is heated to drive the turbines, which is then vented to atmosphere to increase turbine efficiency. While this increases power output, the dumped fuel leads to decreased efficiency. Example of this cycle is the Japanese LE5 (only during start-up).
- Combustion tap-off cycle: Turbine drive gases are taped of from the main combustion chamber. After driving the turbines, the gas is vented to the atmosphere. Example of this cycle is the US J2S engine.

4.7 Tank pressurization

For a pump-fed system it is required that available NPSH ($NPSH_a$) exceeds the required NPSH. This is one of the reasons why, for pump-fed systems, tank pressurization is incorporated. $NPSH_a$ is a measure of the fluid's proximity to its vapor pressure at the operating temperature. It is given by:

$$NPSH_a = \frac{p_t - p_v}{\rho \cdot g} + H_t - \Delta H_{loss} \tag{4-42}$$

Where p_v is vapor pressure, H_t is tank head and ΔH_{loss} the suction line losses and suction equipment pressure drop.

5 Fluid distribution system

The fluid distribution system leads the propellant(s) to its (their) destination. One way of communicating the build-up/lay-out of a distribution system is by way of a piping or flow schematic. A typical flow schematic for a spacecraft RCS system is shown in the Figure 20 and a liquid rocket launcher stage in the Figure 21.

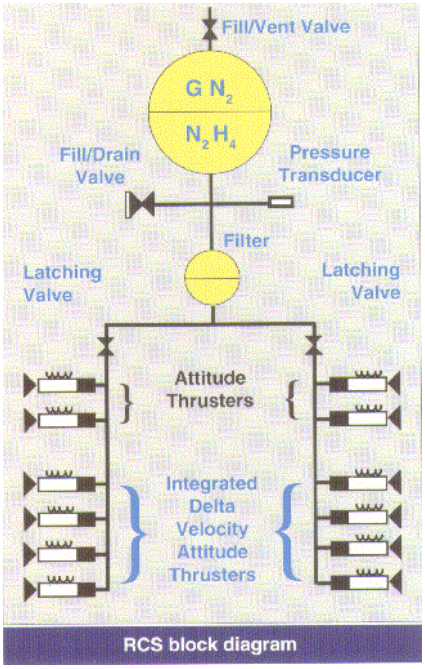

From these two figures, various types of fluid lines can be distinguished. The main types being:

- Propellant supply lines that connect the propellant tank(s) to the various thrusters in the system. For pump-fed systems, we distinguish:
  - Pump suction lines that feed the propellant from the propellant tank(s) to the pump(s).
  - Pump discharge lines which connect the pump to the engine (s). Typically, these lines connect to the engine just before the main propellant valves.
- Pressurant supply lines that connect the propellant tank(s) to the pressurant source(s)
- Turbine drive-hot gas lines that connect a (hot) gas generator with a turbine
- Turbine exhaust lines that duct the exhaust gases overboard. Sometimes a heat exchanger is incorporated to vaporise one or more propellants for tank pressurisation.

Figure 20: SAX RCS flow schematic

In case of pump-fed systems, some of the lines contain flexible lines to permit some degree of movement. This is especially necessary in case of a gimballed engine. Other lines may include hydraulic and/or pneumatic supply lines for valve actuation, purge lines for purging the propellant lines, etc.

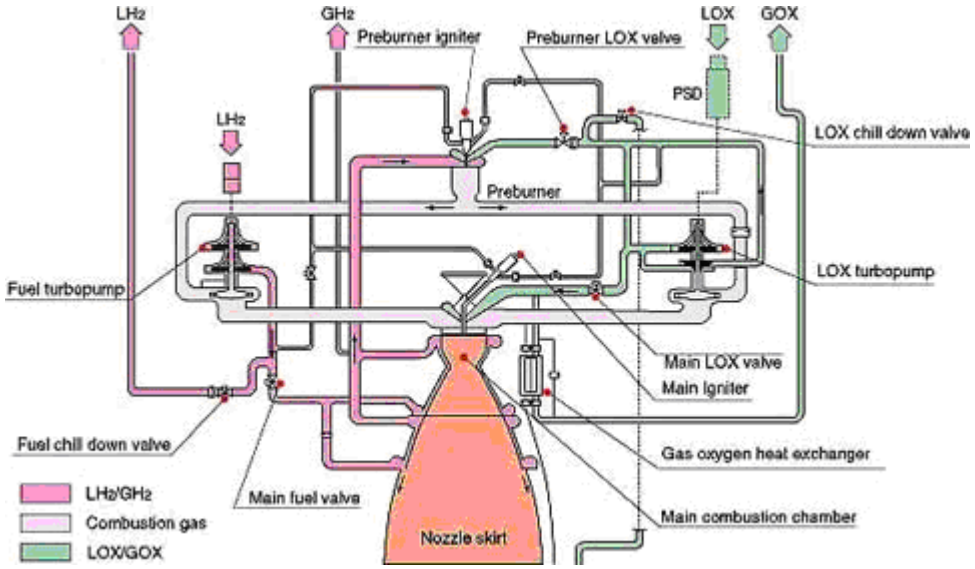

Figure 21: LE-7A piping schematic

Typical tube line sizes used on most spacecraft are 6.35 mm (1/4") and 9.545 mm (3/8") outer diameter (OD). On launcher stages line sizes are much larger being 50 mm (2") for the Aestus engine used on the European Ariane 5 second stage and 43 cm and 30 cm for the SSME used on the US Space Shuttle. In general, one can state that the smaller the pipe sizes the smaller the propellant mass remaining behind in the system, but the larger the pressure drop in the system.

In the following, we will discuss components, system arrangement, materials used and the preliminary design and sizing of the fluid distribution system.

5.1 Components

An overview of the various components that make up the fluid distribution system is given in Table 9. A more detailed overview of some of these components can be found following the table.

Table 9: Overview of fluid distribution system components and their task(s).

Component/device	Task(s)
Piping	Transport the fluid or gas from the tanks to the final destination.
Fittings/joints	To run pipes and their branches in various directions to their destination.
Valves	Regulate/control (stop/start) the fluid flow
Flow measurement devices	Measure mass or volume flow rate
Filters	Filter liquids or gases from impurities
Pressure transducers	Determine the pressure in a pipe section

Piping and fittings

Piping and fittings ensure the proper transfer of the fluid(s) from the storage tanks to other components of the propulsion system.

Valve types

It was the need to start and stop fluid flows, that lead to the invention of valves. All the valves are designed to control flow. However, some throttle the flow, while others perform on-off duties. Valves can be distinguished in several ways:

– According to their use/application:

- Stop/start valves:. Applications: - Opening and closing of gas or propellant circuit.
- Regulation of flow: Many applications require the flow of the fluid be regulated (throttled) at some fixed or variable level between fully zero and maximum flow limits. This is achieved by adapting the valve opening. An important feature for control valves is that the output variable (flow) is related to the input variable (valve position).
- Pressure Relief Valves- Safety valves: Safety valves or pressure relief valves are required to protect the system against excessive pressure. The valve is normally closed and set to open at a pressure slightly higher than the system requires. When open, it relieves the high pressure.
- Fill and drain valves: Fill and drain valves that enable filling and draining of tanks.
- Back flow prevention: In some circumstances it is important to prevent reversed fluid flow. The type of valve for this duty is a non-return-valve (NRV) or check valve also referred to as 1-way valve. Check valves are usually self-acting. The important criteria when selecting these valves are, tight shut off against reverse flow, low resistance to flow for forward flow, fast response.
- Pressure Regulation: Pressure-regulators or pressure-reducing valves regulate the normal operating pressure of a main circuit to a lower setting required in a branch circuit. As soon as the desired pressure is reached in the branch circuit, the valve partially closes and allows just enough fluid through to maintain the desired pressure. The valve is adjustable and can provide any pressure in its range.
- Isolation valves: Isolation valves stop the propellant flow to a given location, usually for maintenance or safety purposes.

– According to how they are actuated:
  - Manually operated
  - Solenoid actuated: The valve is actuated by a specially designed electromagnet. A solenoid valve which utilises the flux of a permanent magnet to stay in its energised position without consuming any electrical power is referred to as a latch valve.
  - Hydraulically activated (used in case of high mass flow rates).
  - Pressure operated (like relief/safety valve, pressure regulator, etc.)
  - Pyrotechnically operated: Single use Normally Open (NO) and Normally Closed (NC) pyrotechnic valves are used to respectively shut off and open the flow path of a fluid or gas (MMH, N_2O_4, He ...)
– According to lay-out:
  - Needle valve: A multi-turn valve which derives its name from the needle-shaped closing element. Typically available in smaller sizes, they are often used on secondary systems for on/off applications, sampling, etc.

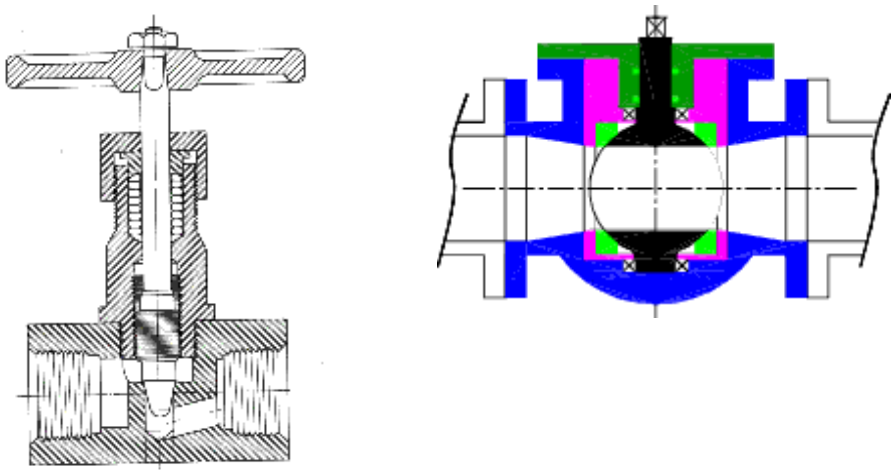

Figure 22: Needle valve (left) and ball valve (right)

- Plug Valve: A quarter-turn on-off valve with a plug with a rectangular hole through which the fluid flows. The plug is either tapered or cylindrical and is in the valve body and can be rotated through a quarter turn to line the hole up with the pipe when open or across the pipe when closed.
- Ball valve: A quarter-turn valve with a spherical closing element held between two seats. Characteristics include quick opening and good shut-off.
- Globe valve: A multi-turn valve with a closing element that moves perpendicularly to the valve body seat and generally seals in a plane parallel to the direction of flow. This type of valves is suited both to throttling and general flow control.
- Gate valve: A multi-turn valve which has a gate-like disk and two seats to close the valve. The gate moves linearly, perpendicular to the direction of flow. This type of valve is normally used in the fully opened or fully closed position; it is not suited to throttling applications. Gate valves provide robust sealing.

Measurement devices:
Typical measurement devices include flow rate measurement devices (orifices, venturies, etc) and pressure and temperature transducers. These are discussed in some detail in a separate paper on measurement devices.

Filters
Filters aboard satellites and spacecraft are mostly unique etched disc filters. Each filter consists of thousands of stacked, chemically etched discs with precise flow paths.

5.2 Arrangement

Some guidelines for arrangement of the distribution system are:

- Consider arrangement of comparable systems as a starting point;
  - Do not stray away from standard (well-proven) components unless necessary.
  - Keep line length(s) as short as possible, but keep in mind that it must be possible to attach the lines to the satellite structure.
  - In case of multiple identical thrusters, strive for identical flow paths (same pipe length, valves, filters, etc.)
  - Number of different parts shall be limited as much as possible (leakage);
  - Make sure that all sections can be filled and drained separately (no air pockets in piping).
  - Use redundancy only when necessary; Passive components are highly reliable.
  - In case of reacting systems use non-return valve in propellant line(s);
  - Instrumentation should only be applied in case it is useful (e.g. to act).
  - Series/parallel placement of latching valves
    - Latching valves get stuck in open position
    - Idem, but now in closed position
  - Series/parallel placement of pressure regulator
    - Regulator opens inadvertently
    - Regulator fails to open
  - In case of pumps
    - Pump suction line: Ideally there should be at least ten (10) pipe diameters of straight pipe between the pump and the first elbow or other equipment.
- From a cost standpoint, a non-optimum (heavier) design using standard available components is usually more favorable compared to an optimum design using specially developed optimized components.
- The inclusion of instrumentation creates an additional burden for the on-board data handling system. In addition, it adds mass and requires (some) power.

5.3 Materials

Typical materials used include structural materials that provide strength as well as sealant materials that prevent leakage:

- Structural materials:

- Mostly titanium & stainless steel (e.g. CRES 304L or 316L).
- Some aluminium
- Use of some composite materials is presently being evaluated

– Seal materials:
- Teflon
- Vespel (a poly-imide plastic)
- Nylon
- EPR

5.4 Preliminary design method

Capacity Q or volume flow rate relates to flow velocity and area (A) of pipe/tube cross-section, according to:

$$Q = v \cdot A \tag{5-1}$$

For a circular cross-section, A follows from the known inner diameter.

Two options exist to realize the needed capacity:
– High flow velocity and small cross-sectional area of tubing, or
– Low flow velocity and large cross-sectional area.

A high flow velocity will allow for a small tube diameter and hence a low tubing mass and cost. In addition, it allows for a fast reaction to changes in pump setting and/or tank pressure. A low flow velocity on the other hand will allow for limited pressure drop in the system and hence a reduction in pump power or pressurant gas mass.

In practice, for liquids, flow velocities range up to 7-15 m/s. For instance, liquid flow velocities in the pump discharge lines for the Space Shuttle Main engine are of the order of 12.5 m/s. For gas lines, flow velocity shall not exceed:

$$v = 175 \cdot (1/\rho)^{0.43} \quad ; \; M < 0.2 \text{ (Incompressible flow)} \tag{5-2}$$

Where ρ is density of gas (kg/m^3).

We will discuss a method that allows analysing the effect of tube size (diameter and length) of the tubing on the pressure drop that occurs in the tubing system as well as its effect on mass. In more detail, we discuss:
– Pressure & power loss due to friction and/or a sudden area change
– Increase in pressure due to valve closing (water-hammer)
– Mass estimation

5.4.1 Pressure loss due to friction

To calculate the pressure loss, we use the Darcy-Weisbach relation:

$$\Delta p = f \frac{L}{D} \frac{1}{2} \rho v^2 \tag{5-3}$$

With f is pipe friction factor, L is characteristic length, D is the inner (pipe) diameter of the component, ρ is flow density, and v is flow velocity.

For straight pipes, the friction factor has a value in the range 0.005 to 0.05, depending on the flow regime (laminar, turbulent or transition flow). The latter largely depends on the Reynolds number (Re). This is a dimensionless number that gives a measure of the ratio of inertial forces to viscous forces.

For straight pipe flows the critical Reynolds numbers are:

- Laminar flow: Re < 2320
- Turbulent flow: Re > 12.000[4]
- Transition flow: Intermediate Re numbers

A relationship for the Reynolds number as well as some simple empirical estimation rules for the pipe friction factor can be obtained from the annex C.

A word of caution: when determining pressure drop around the critical Reynolds number of 2320, the flow may shift from laminar to turbulent depending on the piping system. For this reason, a piping system must never be designed close to the critical Reynolds number.

For valves, filters, etc. it is best to use factory provided information, see for instance Figure 23.

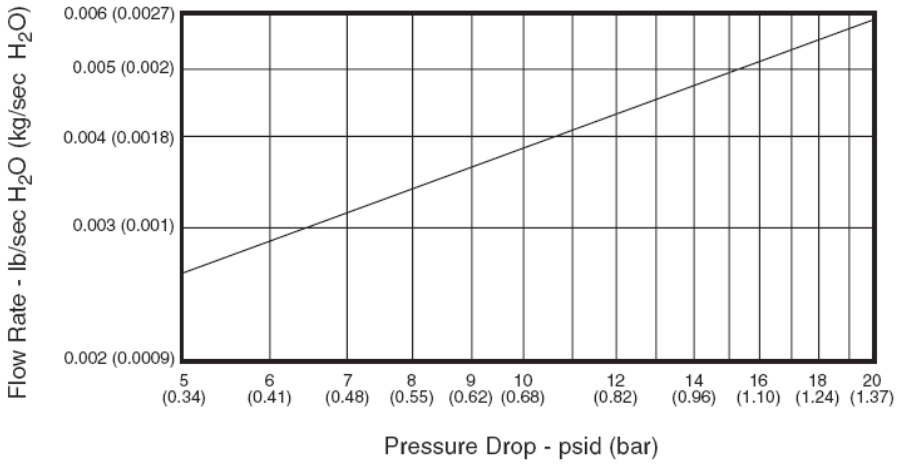

Figure 23: Pressure drop for Moog thruster control valve [Moog]

In case such information is absent we may estimate the pressure drop by considering the flow to be fully turbulent, see annex C.

The length L for pipes is equal to the pipe length. For valves, filters, pipe bends, etc the length L used in (5-3) should be taken equal to the characteristic length (usually expressed in pipe diameters). Typical values can be obtained from the example given later in this chapter.

Density of various liquid propellants can be obtained from earlier chapter on propellant selection, [NIST] or from fluid handbooks. For gases the ideal gas law may be used to find the density under the conditions at hand.

5.4.2 Pressure loss due to a sudden area change

When coaxial pipes of different diameters are joined together, like at the inlet or outlet of a tank, or when we have a junction of different tubes, a pressure loss occurs. This pressure loss may be defined in terms of a loss coefficient ζ as discussed earlier in the section on liquid injection (see design of liquid rocket combustion chamber). You are referred to this section for details on the basic parameters determining the loss coefficient.

5.4.3 Power loss in tubing

Because of friction effects, some power is lost. The power loss can be calculated using:

$$\Delta P_{tubing} = \frac{m \cdot \Delta p}{\rho} = \Delta p \cdot Q \tag{5-4}$$

[4] By careful design of pipe entrances and by minimising ambient disturbances laminar pipe flow can be maintained up to a Reynolds number of 40,000-100,000.

Where Δp is total pressure loss in the system and Q is the volume flow.

5.4.4 Water-hammer

Water- hammer is created by stopping and/or starting a liquid flow suddenly. A common example of a water-hammer occurs in most homes every day. Simply turning off a shower quickly sends a loud thud through the house; this is a perfect example of a water-hammer. It is an impact load or shock pressure that is often more than enough to cause severe damage to piping systems, valves and pressure transducers. A shock pressure can be created in a piping system when a valve in the system is opened or closed quickly, a pump is started or stopped, or when a pump is started in an empty system or section of a system.

The increase in pressure for a given liquid in a rigid pipe is proportional to the change in velocity and the wave velocity in the rigid pipe:

$$\Delta p = \rho \cdot v_w \cdot v \tag{5-5}$$

where ρ is fluid density, v_w is wave velocity (or celerity) or velocity of sound in the fluid, and v is fluid flow velocity. v_w is about 1000 m/sec, so even a low flow velocity can cause a significant pressure surge.

Even at low flow velocities water-hammer can be unacceptably high. For example, for a liquid with a density of 1000 kg/m^3 and a wave velocity of 1000 m/s which flows at a velocity of 7 m/s, we already find a pressure surge of 70 bar.

To circumvent water-hammer we can use slow acting valves. Typically, we use valves with a closing time more than the period of the pipeline = $2L/v_w$ where L is the length of the pipeline.

5.4.5 Mass estimation

Plumbing mass in general depends on number of lines, line sizes, line lengths, number and type of valves used, materials used, wall thickness of the lines, etc. A detailed mass estimate can only be given once all of the above parameters have been determined. Until then, we have to resort to approximate methods. For instance, tubing mass may be determined from thin shell theory for a given burst pressure. However, this method requires much effort when requiring high accuracy and especially when we need to develop such a method also for valves, filters and regulators.

Another method, as earlier introduced, is to collect historical data and use this data to predict the plumbing mass of the system under consideration. Next figure shows plumbing mass versus system dry mass for the reaction control system of 14 different spacecraft, where plumbing mass has been taken equal to RCS dry mass minus thruster mass and tank mass. The data suggest that plumbing mass increases about linearly with system dry mass.

On average, we find that for RCS systems plumbing mass makes up 12.3% of the total propulsion subsystem dry mass with a standard deviation of about 5.3%. So, we have a 65% probability that plumbing mass is in between 7.0% and 17.6% of total propulsion system dry mass.

In case no historical data is available we must resort to other methods which may include the identification of the (number of) components and summing the component masses. Here we usually should add some percentage to consider miscellaneous items like nuts, bolts, etc.

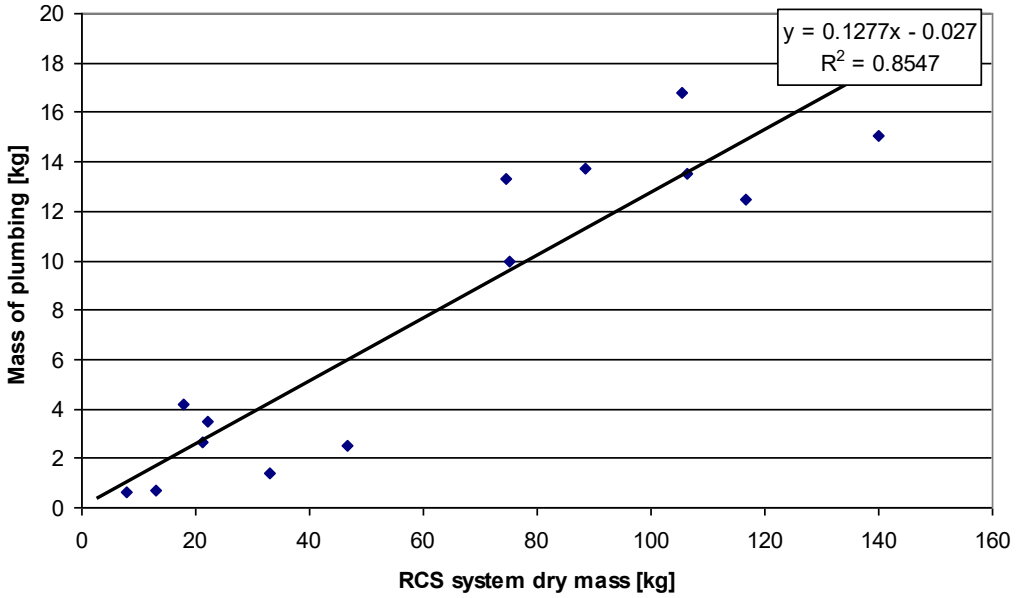

Figure 24: RCS system plumbing mass

5.4.6 Other parameters

Next to mass, pressure drop and power required other parameters are important for system design, including such parameters as reliability, and cost. For now, we leave these parameters for the reader to explore for himself.

5.5 Testing

All feed system components, such as pressure and flow regulators, valves, flow meters, ducts, lines, and tanks shall be calibrated for instance using flow benches.

6 Working point and calibration

To determine the working point for the engine system, we first determine the characteristic system flow (or head) curve. This curve is obtained by summing the pressure or pressure drop versus flow curves of the various flow components. Next we plot the pump developed head versus flow rate for pump-fed systems or tank-head in case of pressurized-tank systems, see Figure 25 and Figure 26. The working point is the point where the two curves meet as in that case the pump developed head or tank head equals the sum of the pressure drop across the feed system, the engine/thruster inlet pressure[5] (pressure just upstream of the main propellant valve(s)) and some pressure margin needed for system calibration. The latter is because generally practical performances will deviate somewhat from their nominal design values. To this end a certain amount of calibration is always required for the engine/propulsion system. Calibration may be by insertion of orifices that are designed to give a certain pressure drop.

[5] Required engine/thruster inlet pressure for the liquid under consideration is dictated by chamber pressure, as well as the pressure drop over chamber, injector, cooling jacket, and thrust chamber manifold.

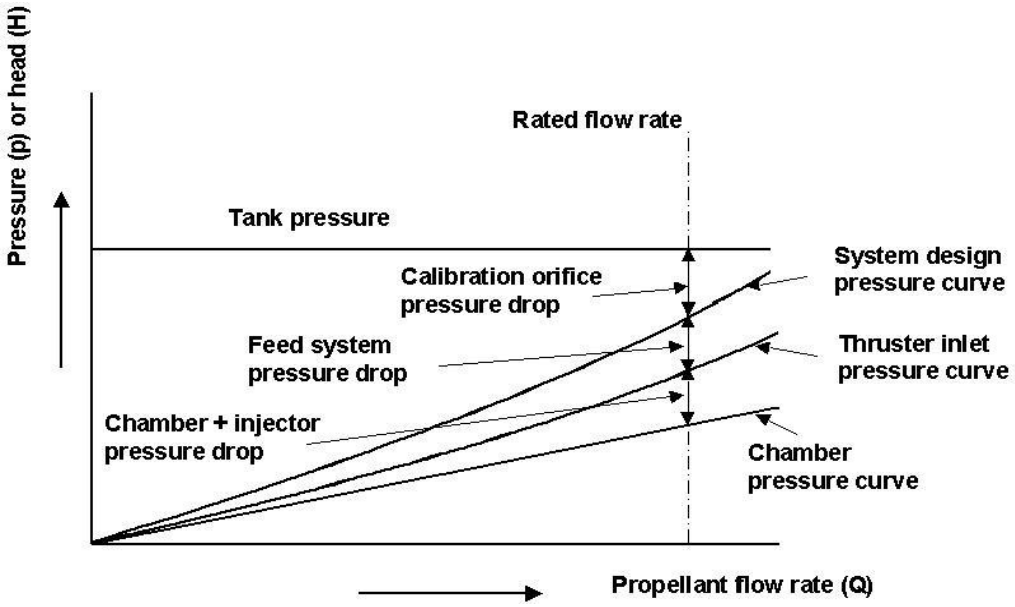

Figure 25: Balancing a pressurized tank system

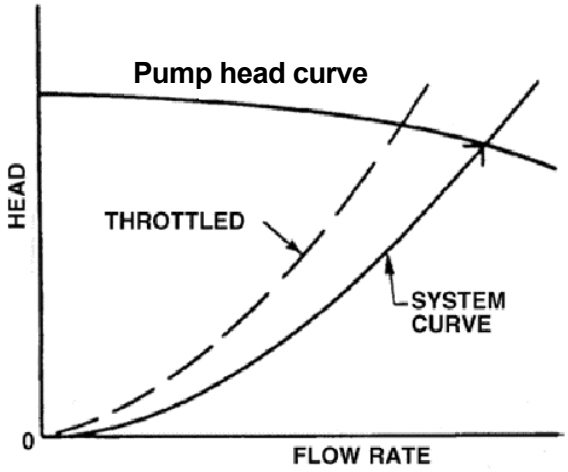

Figure 26: Balancing a pump-fed system

By plotting the system head curve and tank pressure (head) or pump curve together, it can be determined:

1. The working point of the system.
2. What changes will occur if the system head curve or the pump performance or tank pressure curve or tank pressure (or head) changes.

The system head curve may change by opening or closing a valve. Tank pressure may change by changing the setting of a regulator or in case of a blow down system, a change in tank pressure is the nature of the system. Pump curve may change by changing the rotational rate of the pump.

7 Example calculation: blow down system

We are designing the gas supply system for a single nitrogen cold-gas thruster. This supply system consists of a nitrogen gas storage tank and a single branch connecting to the nitrogen cold-gas thruster, see figure.

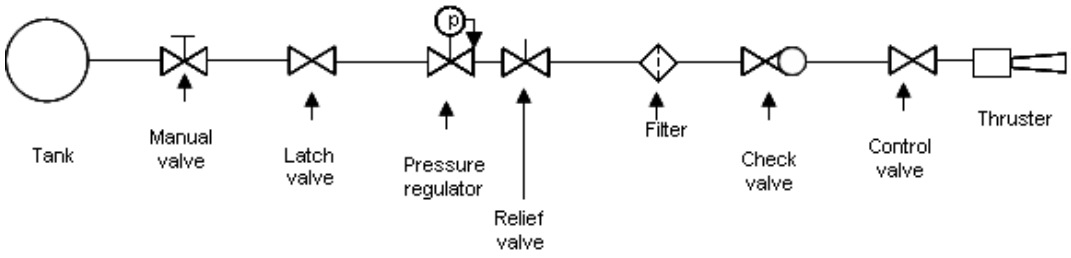

The gas storage tank has a volume of 10 litres and a maximum pressure of 200 bar. The branch connecting the tank to the thruster consists of a high-pressure and a low-pressure section separated by a pressure regulator. The high-pressure section includes rigid high pressure tubing, a manual valve, a latch valve and the pressure regulator. The length of the high-pressure (HP) tubing till the regulator is 1.3 m and the internal diameter is 13 mm. The low-pressure (LP) section has a filter, a check valve and a control valve. Length of the low-pressure tubing is 2 m and the internal diameter is 6.5 mm. In the low-pressure tubing three 90° bends and two T-junctions (flow straight through, not shown in schematic, but situated between relief valve and filter) all with internal diameter 12.7 mm have been incorporated. Regulated pressure in the system is between 5-15 bar.

For this system, we determine the maximum pressure loss that occurs in the gas supply system down from the pressure regulator to the thruster inlet. For this, we use the data from Table 10.

Table 10: Characteristics of gas feed system components for pressure loss calculations

Component	L or L_{eq} [m]	ID [mm]	e/ID [-]	Comments
Rigid LP tubing	1.3	13	0.00012	
Relief valve	18 D	15	0.00010	L_{eq}: [Zandbergen]
Check valve	150 D	12.7 (½")	0.00012	L_{eq}: [Zandbergen]
T-junction I	20 D	12.7 (½")	0.00012	L_{eq}: [Zandbergen]
T-junction II	20 D	12.7 (½")	0.00012	L_{eq}: [Zandbergen]
Filter	250 D	12.7 (½")	0.00012	L_{eq}: [Zandbergen]
Control valve	300 D	12.7 (½")	0.00012	From (1)
Flexible LP tubing	2	6.35 (¼")	0.0	E/ID: [Lmnoeng]
1st 90° bend	20 D	12.7	0.0035	L_{eq}: [Zandbergen]
2nd 90° bend	20 D	12.7	0.0035	L_{eq}: [Zandbergen]
Flexible LP tubing	0.35	6.35	0.0	E/ID: [Lmnoeng]
3rd 90° bend	20 D	12.7	0.0035	L_{eq}: [Zandbergen]

1) http://www.xs4all.nl/~kostermw/dP/science_info/References.htm

To calculate the pressure loss, we use the method outlined in the foregoing section and use the Darcy-Weisbach relation to calculate the pressure drop:

For the tubing, the characteristic length is taken equal to the actual length of the tube, while for the valves, filters, etc. an equivalent length (L_{eq}) is substituted, see table 3. The inner diameter for the various pipe sections can also be obtained from table 3.

Density is calculated using the ideal gas law. For a pressure of 10 bar and a temperature of 293 K, we find for the nitrogen gas:

$$\rho = \frac{10 \times 10^5}{8314.32 / 28.0134 \cdot 293} = 11.50 \text{ kg/m}^3 \qquad (7.1)$$

Notice that we neglect the effect of pressure loss on mass density.

Flow velocity follows from mass flow (m), density and area (A) of pipe cross-section. For a circular cross-section, this area follows from the known inner diameter. At the pressure of 10 bar and temperature of 293 k, and taking a pipe inner diameter of 12.7 mm and a mass flow of 10 g/s, we find:

$$v = \frac{10 \times 10^{-3}}{11.50 \cdot \pi/4 \cdot \left(12.7 \times 10^{-3}\right)^2} = 6.875 \text{ m/s} \tag{7.2}$$

To determine the friction factor, we first determine the Reynolds number and the type of flow. It follows using a value for the dynamic viscosity of nitrogen of 1.7×10^{-5} Pa:

$$\text{Re} = \frac{11.50 \cdot 6.875 \cdot 12.7 \times 10^{-3}}{1.70 \times 10^{-5}} = 59100 \tag{7.3}$$

From this parameter, we find that we are dealing with a turbulent flow. Notice that for lower mass flow at identical pressure, temperature, etc. the Reynolds number decreases down to ~8000 at 2 g/s and hence the flow may change from turbulent to laminar.

In the turbulent flow regime, we use the Blasius equation to determine the friction factor. For a pressure of 10 bar, a gas temperature of 293 K, and a mass flow of 10 g/s, we get:

Turbulent flow:

$$f = 0.316 \cdot \left(\frac{1}{59100}\right)^{0.25} = 0.0202 \tag{7.4}$$

When considering turbulent flow, in case of non-smooth piping, the roughness may lead to an increase in friction factor. From the Moody diagram, we conclude that in the region considered and given the roughness values in table 3, this effect is negligible.

For valves, filters, etc. we should consider the flow to be fully turbulent. An appropriate relation is given in appendix C. Using this relation and taking p = 10 bar, T= 293 K, m = 10 g/s and the values of e/d from Table 10, we find for the pressure drop over the rigid 1.3 m tubing:

$$\Delta p = f \frac{L}{D} \frac{1}{2} \rho v^2 = 0.0202 \cdot \frac{1300}{12.7} \cdot 0.5 \cdot 11.5 \cdot 6.875^2 = 551 \text{ Pa} \tag{7.5}$$

Notice that the actual pressure drop should be slightly lower because of a slightly lower value of the internal diameter.

The pressure drop for all the other components at the above conditions are given in Table 11 and at 5 bar pressure in Table 12.

Table 11: Pressure loss values; p = 10 bar, T = 293 K and m = 10 g/s

Component	L or L_{eq}	ID	e/ID	f_T	f_{turb}	Δp
	[m] or [diam]	[mm]	[-]	[-]	[-]	[Pa]
Rigid LP tubing	1.3	13	0.00012		2.04E-02	5.05E+02
Manual shut-off valve	18	15	0.0001	0.011973		5.86E+01
Check valve	150	12.7 (½")	0.00012	0.012399		5.05E+02
T-junction I	20	12.7 (½")	0.00012	0.012399		6.74E+01
T-junction II	20	12.7 (½")	0.00012	0.012399		6.74E+01
Filter	250	12.7 (½")	0.00012	0.012399		8.42E+02
Control valve	300	12.7 (½")	0.00012	0.012399		1.01E+03
Pressure loss exp.						2.45E+03
Flexible LP tubing	2	6.35	0		1.70E-02	2.33E+04
Pressure loss comp.						1.30E+03
1st 90° bend	20	12.7	0.0035	0.027316		1.48E+02
2nd 90° bend	20	12.7	0.0035	0.027316		1.48E+02
Pressure loss exp.						2.45E+03
Flexible LP tubing	0.35	6.35	0		1.70E-02	4.09E+03
Pressure loss comp.						1.30E+03
3rd 90° bend	20	12.7	0.0035	0.027316		1.48E+02
					Sum	3.84E+04

Table 12: Pressure loss values; p = 5 bar, T = 293 K and m = 10 g/s

Component	L or L_{eq}	ID	e/ID	f_T	f_{turb}	Δp
	[m] or [diam]	[mm]	[-]	[-]	[-]	[Pa]
Rigid LP tubing	1.3	13	0.00012		2.04E-02	1.01E+03
Manual shut-off valve	18	15	0.0001	0.011973		1.17E+02
Check valve	150	12.7 (½")	0.00012	0.012399		1.01E+03
T-junction I	20	12.7 (½")	0.00012	0.012399		1.34E+02
T-junction II	20	12.7 (½")	0.00012	0.012399		1.34E+02
Filter	250	12.7 (½")	0.00012	0.012399		1.68E+03
Control valve	300	12.7 (½")	0.00012	0.012399		2.01E+03
Pressure loss exp.						4.87E+03
Flexible LP tubing	2	6.35	0		1.71E-02	4.65E+04
Pressure loss comp.						2.60E+03
1st 90° bend	20	12.7	0.0035	0.027316		2.96E+02
2nd 90° bend	20	12.7	0.0035	0.027316		2.96E+02
Pressure loss exp.						4.87E+03
Flexible LP tubing	0.35	6.35	0		1.71E-02	8.14E+03
Pressure loss comp.						2.60E+03
3rd 90° bend	20	12.7	0.0035	0.027316		2.96E+02
					Sum	7.66E+04

From the results, we learn that the total pressure drop over the system increases with decreasing pressure (~0.5 bar drop at 10 bar versus ~1 bar drop at 5 bar pressure). We also learn that the largest pressure drop occurs in the flexible LP tubing of 2 m length. This is explained because of the small internal diameter and hence the high flow velocity in that section.

All calculations so far have been performed for a mass flow of 10 g/s. The results for different mass flows at two different regulated pressures are shown in Figure 27.

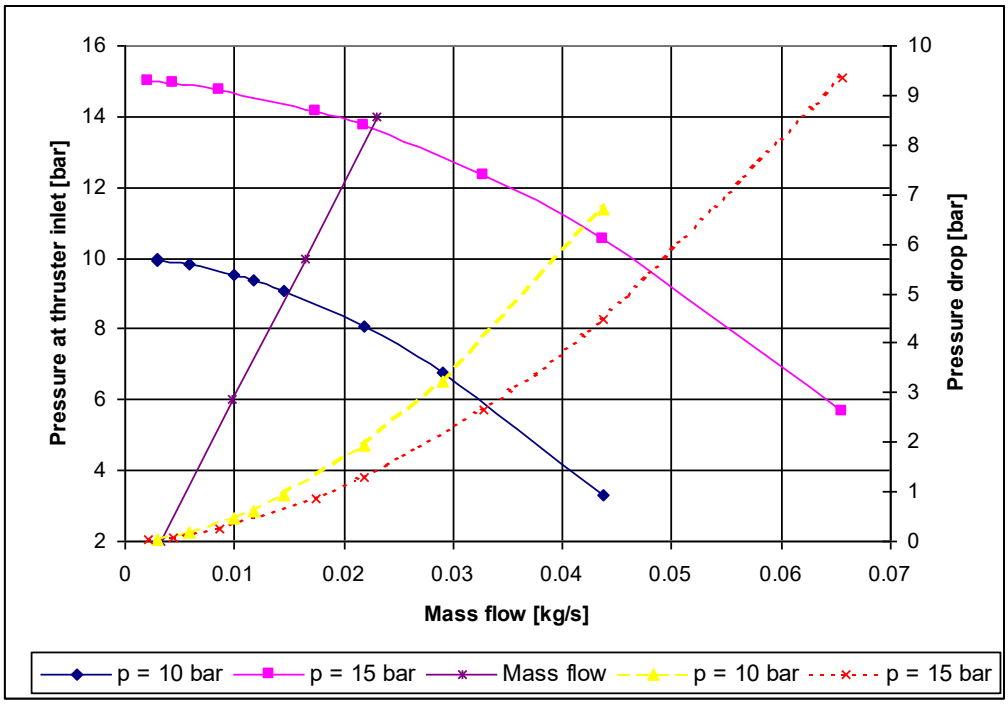

Figure 27: Pressure drop (non-solid line) and pressure at thruster inlet (solid line) versus mass flow for two different regulated pressures (10 and 15 bar); cold gas temperature is 293 K

The results show that with increasing mass flow the pressure drop increases and hence the pressure at the thruster inlet decreases.

For illustrative purposes, we have included in the above figure the critical mass flow for a thruster with a throat diameter of 3 mm as a function of pressure, assuming that the thruster is free from pressure loss (thruster inlet pressure is identical to chamber pressure[6]). The results show that the working point of this thruster differs with a higher mass flow and thruster inlet (chamber) pressure at the higher regulated pressure of 15 bar. Consequently, the thrust produced by this thruster is higher at the higher regulated pressure.

Problems

1. Feed system selection.
   You are designing the propulsion system for the second stage of a new launch vehicle. The total delta V to be delivered by this stage in vacuum is 4 km/s. Total empty stage mass is 1000 kg. For this system you have selected two identical bipropellant engines that work in unison to raise the velocity of the stage. Each engine delivers a vacuum specific impulse of 305 s. The engine uses the bipropellant combination hydrazine (fuel) and NTO in the mixture ratio 1.65 at a chamber pressure of 20 bar. Engine burn time is set at 500 s. You are asked to select for this stage the feed system. Substantiate/motivate your answer.

2. Pressurant mass
   Estimate the mass and volume of nitrogen required to pressurize an NTO-MMH feed system feeding a single-burn 400 N (vacuum thrust) thruster for a duration of 3000 sec. The thruster has a vacuum specific impulse of 300 sec at a propellant mass mixture ratio of 1.65. Propellant tank pressure is 30 bar, propellant fill ratio is 0.9, and the pressurant gas tank pressure is 200 bar (regulated system). Allow for 4% excess propellant, and a nitrogen compressibility factor at 200 bars of 0.95. The nitrogen pressure regulator requires that the gas tank pressure does not fall below 30 bars. Clearly indicate whether you assume isentropic or isothermal expansion and why.

[6] In practice, some pressure loss occurs in the thruster.

3. A LOX tank has a LOX level 20 m above the pump inlet. Tank pressure is 3 bar.
   a) Calculate the static head and static pressure at the pump inlet when the fluid is not moving.

   For a fluid velocity of 10 m/s in the suction piping (pump inlet), and neglecting any friction occurring, calculate the following quantities at the pump inlet:
   b) total head
   c) stagnation pressure
   d) dynamic head
   e) dynamic pressure
   f) static head
   g) static pressure
   h) Compare the above calculated values for static head and pressure to the values calculated under a) and discuss the differences.

4. Hydraulic power
   Water is pumped through a pipe at 10 m^3/s flow rate. The pump head is 300 m. Density of water is 1000 kg/m^3.
   a) Calculate the pump hydraulic power.
   b) If the pump works with an efficiency of 80%, calculate the brake horsepower
   c) Given a mechanical efficiency of 90% and a turbine efficiency of 55%, calculate the turbine output power as well as the power input from the gas generator that provides the turbine drive gases.
   d) Calculate the torque on the turbine shaft, if the turbine rotates at 300rpm.

5. Turbine output power (from Sutton, G.P.)
   Compute the turbine output power for a gas consisting of 64% by weight of water and 36% by weight of oxygen, if the turbine is at 30 bar and 700 K with the outlet at 1.4 bar with 1.23 kg of gas flowing through the turbine each second. The turbine efficiency is 37%.

6. Turbo-pump characteristics
   For the Vulcain 1 (HM60) LOX turbo-pump, the following data are given:
   - Oxygen mass flow: 207 kg/s
   - Pump inlet temperature: 91 K
   - Pump total pressure rise: 130 bar
   - Pump brake horsepower: 3.2 MW
   - Pump rotor speed: 12700 rpm
   - Mechanical efficiency of LOX pump drive axis: 0.85
   - Gas generator gas temperature: 910 K
   - Gas generator mass mixture ratio: 0.91
   - Gas generator pressure: 80 bar
   - TET: 873 K
   - LOX turbine pressure ratio: 12
   - Turbine efficiency: 55%

   Calculate:
   1. pump hydraulic power
   2. pump efficiency
   3. pump head
   4. pump specific speed (in SI units)
   5. turbine output power
   6. total turbine mass flow
   7. pressure at turbine outlet.
   8. turbo-pump mass

References

1) Helmers L., Steen J., Ljungkrona I., Brodin S., and Johnsson R., Turbine design and performance at large tip clearance of unshrouded rotor cascades, AIAA-2003-4766, 2003.
2) Hermsen R., Zandbergen B.T.C., Pressurization system for a cryogenic propellant tank in a pressure-fed high-altitude rocket, 7th European Conference for Aeronautics and Aerospace Sciences (EUCASS), Milan, 2017.
3) Hill P.G., Peterson C.R., Mechanics and thermodynamics of propulsion, Addison-Wesley Publ. Comp., 1965.
4) Humble R.W., Henry G.N. and Larson W.J., Space Propulsion Analysis and Design, McGraw-Hill, 1995.
5) Johnsson G. and Bigert M., Development of small centrifugal pumps for an electrically driven pump system, Acta Astronautica, vol. 21, no. 6/7, pp. 429-438, 1990.
6) Jue, F. Kuck, F., Space Shuttle Main Engine (SSME) options for the future Shutlle, AIAA 2002-3758, 2002.
7) Kamijo K., Yamada H., Sakazume N., and Warashina S., Developmental history of liquid oxygen turbopumps for the LE-7 engine, Trans. Japan Soc. Aero. Space Sci., Vol. 44., No. 145, pp155-163, 2001.
8) Kamijo K., Sogame E., Okayasu A., Development of liquid oxygen and hydrogen turbopumps for the LE-5 engine, J. Spacecraft, Vol. 19, No. 3, pp226-231, 1982.
9) Manski D., AIAA-89-2279, 1988.
10) Moog, Space products Division catalog 1324.
11) NIST chemistry webbook.
12) Quay, L. de, Keith Hodge, B., A history of collapse factor modelling and empirical data for cryogenic propellant tanks, AIAA, 2010.
13) Schmidt G., Technik der Flussigkeits-raketentriebwerke, DaimlerChrysler Aerospace, 1999.
14) SEP, Société Européenne de Propulsion Newsletter, No. 29
15) Sutton G.P., Rocket Propulsion Elements, 6th edition, John Wiley & Sons Inc., 1992.
16) Timnat and van der Laan, Thermo-chemical Rocket Propulsion, LR, TU-Delft, 1985.
17) For further valve info, see e.g.: http://www.ces.clemson.edu/~dbruce/valve3.htm
18) Villain, J., The evolution of liquid propulsion in France in the last 50 years, Acta Astronautica, vol. 22, pp. 213-218, 1990.
19) Wertz J.R. and Larson W.J., Space Mission Analysis and Design, McGraw-Hill, 1999.

Contents

Symbols 394

1 Introduction 395

2 The ignition system 395

3 Typical requirements 396

4 Pyrotechnic igniters 397

5 Pyrogen igniters 399

6 Hypergolic (or pyrophoric) igniters 402

7 Catalytic igniters 402

8 Spark plugs 402

9 Augmented spark or torch igniter 403

10 Ignition sizing 404

10.1 Ignitability 405

10.2 Flame spreading 406

10.3 Igniter flame temperature, power and energy 407

10.4 Ignition pressure 410

10.5 Ignition delay 411

10.6 Igniter location and orientation 412

11 Igniter mass 414

12 Igniter sizing method 415

13 Testing 416

14 Problems 418

Literature 418

Symbols

Roman

G	fraction of igniter charge burned at any time t
H	enthalpy
m	mass flow rate
M	mass
p	pressure
P	power
R	specific gas constant
t	time
T	temperature
V	volume

Greek

Δ	loading density (M_{ign}/V)
λ	impetus
M	molecular mass of gaseous combustion products
ρ	density of igniter charge
σ	fraction condensed particles in igniter combustion products
τ	Ignition delay time

Subscripts

a	ambient
c	blowdown
F	free motor volume
ign	igniter

Acronyms

ASI	Augmented Spark Igniter
HRM	Hybrid Rocket Motor
LOX	Liquid Oxygen
LRE	Liquid Rocket Engine
MON	Mixture of Nitrous oxides
NTO	Nitrogen Tetroxide
PTFE	Poly-Tetrafluoroethene
S&A	Safe and Arm
SRB	Solid Rocket Booster
SRM	Solid Rocket Motor
TBI	Through Bulkhead Initiator

1 Introduction

Most propellants require some external stimulus to set the engine on fire, i.e. to start the combustion reaction. This process of starting the combustion is usually referred to as "pilot-ignition". Pilot ignition together with the ensuing phase of flame spreading up to the point that the full grain is burning is referred to as the ignition phase. The hard- and software involved in ensuring a proper pilot ignition is commonly referred to as the ignition system. The actual device initiating the combustion reaction is referred to as the igniter. For pilot-ignition to occur, the igniter should raise the propellant temperature to a temperature sufficient to allow for self-sustained combustion, thereby considering any heat dissipation occurring in the system. To this end, the igniter produces heat which shall be transferred to the initially cool propellant. This makes heat transfer the dominant process governing the success of motor ignition. The required energetic content of an igniter depends on amongst others the size of the motor and /or the ignitability of the propellant used. For instance, small amateur rockets with an easily ignitable propellant are started using just a pair of electrical wires providing electrical power to a heating element that is in contact with the propellant. Larger rocket motors or rocket motors using a composite propellant require a heavier stimulus. One way is to cast a small ball of easily ignitable propellant, like black powder, onto the heater. This easily ignitable propellant then provides the energy to ignite the main propellant. For example, Goddard's first liquid rockets were ignited using an igniter system containing match heads and black gunpowder to provide the starting fire for ignition of the liquid oxygen (LOX) and gasoline in the combustion chamber. Since the early days of rocketry various types of igniters have been developed including:

- Pyrotechnic
- Pyrogen
- Spark plug
- Catalytic
- Hypergolic
- Spark-Torch (augmented spark ignition)

Once the combustion reaction is initiated, we no longer need the ignition system (unlike in a car) because the energy liberated during combustion keeps the reaction going or until a restart is necessary.

Hereafter, we will first provide for an overall description of the ignition system followed by an introduction of the main design requirements thereby focussing on the igniter itself. Next, we discuss the main types of igniters used today in some detail. This discussion is taken in part from the work of [Timnat] and [Huzel]. Third and finally, we discuss the design and testing of igniters.

2 The ignition system

In this section we will discuss the ignition system in some detail outlining the major components in the system and their main function(s).

The ignition system essentially consists of three main elements being the igniter itself, an initiation system or electronics block and a safe and arm system. A block diagram showing the main elements of the ignition system is shown in Figure 1. The main working element of a rocket ignition system is the igniter. It is essentially the igniter that provides for the actual stimulus needed to start the combustion. Think of it as the match needed to light a cigarette.

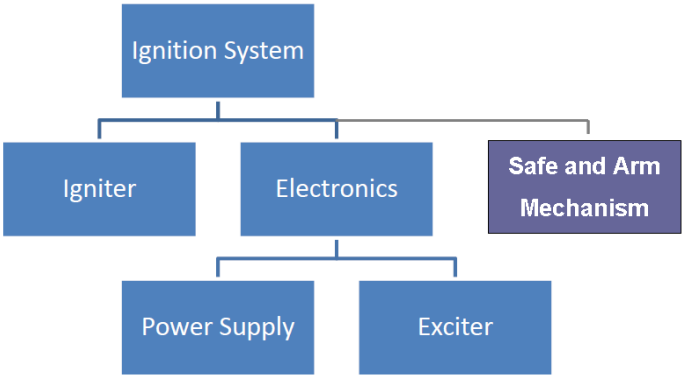

Figure 1: Ignition system block diagram

The initiation system triggers the igniter to release its energy at the right time. It sometimes is further subdivided into a device that generates a trigger pulse to start the energy release of the igniter and a power supply that provides for the required power. For instance, the trigger pulse may be given off by a primer charge, i.e. squib, which is activated by running an electrical current[1] through it. However, the trigger pulse can also be generated using a spark plug or a laser and/or by mechanical means (hammer; compare pistol).

The Safe & Arm (S&A) system ensures physically separating (safe position) the initiation system from the actual igniter to prevent inadvertent ignition. For instance, in the safe position, the electrical wires that power the initiation system are physically disconnected. This is important to prevent stray currents for instance induced by radio or radar equipment or from lightning causing premature ignition. The S&A system remains in the Safe position until commanded into the Arm position. Only then the rocket motor can be ignited. To further safety, the igniter is often removed from the motor for additional safety during storage.

3 Typical requirements

Typical ignition system requirements generally can be subdivided into performance requirements and other requirements. The former are most important for the proper functioning of the igniter and typically include requirements related to:

- Total energy released or impetus[2]. The heat released should be adequate to start the combustion reaction. Most propellants except for hypergolic or self-igniting propellants require an ignition system to start the combustion of the propellants. Generally solid propellants require more energy to ignite than hybrid propellants, which in turn require more energy than liquid propellants as part of the igniter energy is used to bring the propellant from the initial state to the vapour state. The latter being of importance to realize combustion.
- Temperature of the igniter gases. It is important that the energy released heats up the propellant to a temperature high enough to start combustion. An igniter can generate a high power through a high mass flow rate, however, for the grain to start combustion a sufficiently high temperature should be realized. Once a combustible mixture is generated with a temperature above the auto/self-ignition temperature[3], actual combustion commences.

[1] In rocketry, for safety reasons, a minimum current of 1 A is generally required.
[2] Impetus of a propellant or pyrotechnic mixture represents available energy per unit mass.
[3] Self/auto-ignition temperature of a combustible mixture is the lowest temperature of the mixture at which it spontaneously ignites without an external source of ignition, such as a flame or spark.

- Ignition time (or action time): The time that the igniter shall be actively generating the ignition stimulus. Together with the energy released, it determines the igniter power. Typical ignition times are of the order of seconds.
- Ignition delay or ignition time lag: The time lapse occurring between the instance of an igniting action of a propellant and the onset of a specified burning reaction. Motor ignition must usually be accomplished within a fraction of a second. For instance, for the European HM60 rocket motor, ignition delay was specified to be less than 0.2s.
- Pressure overshoot allowed: At some time during ignition combustion starts. During the simultaneous action of the igniter and the combustion the total energy released per unit of time and/or mass flow rate may be higher than when only combustion takes place. This may cause over-pressurisation of the rocket motor, possibly leading to motor failure.
- Number of ignitions: This is especially important in case the engine must make several restarts. As an example, it is mentioned that the European Vinci engine is designed for a minimum of 5 starts. Hence also the ignition system should be suited for at least 5 uses.

Some typical performance requirement values are given in the next table.

Table 1: Requirements for the ignition system of the Vinci liquid rocket engine [Frenken], [Jonker].

Parameter	Value
Output power	> 440 kW
Duration of ignition	2 seconds minimum
Number of ignitions	5 minimum
Starting transient	$p_c \geq 0.95 * p_{nominal}$ in < 100 ms.
Envelope	Must fit existing interface equipment

Other requirements than performance requirements may include physical limitations on size, mass and configuration (location/position of igniter), as well as requirements relating to reliability[4], temperature operating limits, vibration levels, storage life and storage conditions (humidity), handling (drop, vibration), safety, composition of igniter exhaust, etc.

4 Pyrotechnic igniters

Pyrotechnic igniters are flame producing devices (like fireworks) which are often electrically initiated[5]. In a pyrotechnic device the flame is produced by burning a deflagrating[6] pyrotechnic mixture, which creates a flow of hot particles that are injected into the engine/motor. The fuels used in pyrotechnics are metals, such as Zn, Al and Mg, carbon, phosphorus and sulphur, and various organic materials. The oxidisers are mainly the high-energy nitrates, chlorates, perchlorates, and the low-energy metal oxides. The preferred potassium nitrate, chlorate, and perchlorate are often replaced by the cheaper sodium and ammonium salts where the hygroscopic nature of these salts is not detrimental. Antimony sulphide, Sb_2S_3, calcium silicide, $CaSi_2$, and other easily oxidized substances are often seen. These are very sensitive substances, and their mixing is not something that should be done in the home or general laboratory. Those who manufacture the devices are aware of the dangers and know how to meet them.

[4] Most designers prefer to eliminate the ignition system as it is often a cause for failure.
[5] Other means of initiating are for instance through laser or mechanical (e.g. hammer) action.
[6] Pyrotechnic materials are usually classified into two major categories being deflagrating materials that undergo combustion and detonable materials that undergo detonation. The latter are also referred to as high explosives.

Depending on lay-out, we distinguish:

- Basket or can-type igniters, see e.g. Figure 2 and 3, in which the active material is contained in the form of pellets or as a cored grain.
- Jellyroll igniters consist of a pyrotechnic coating reinforced by a flexible sheet of plastic or cloth and rolled into a tube of several layers. A jellyroll igniter can be mounted onto the propellant surface.

Figure 2: Pyrotechnic igniter [SPL]

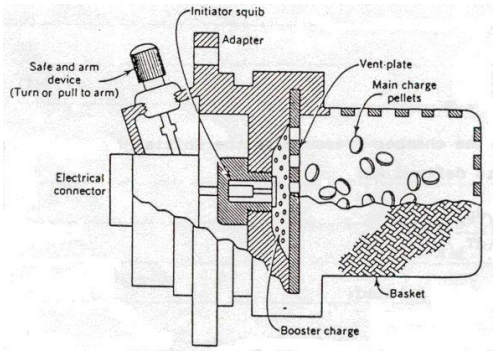

Figure 3: Simplified basket type of pyrotechnic igniter [Sutton].

The schematic of the basket type of pyrotechnic igniter shown above nicely outlines the main elements and their naming. Ignition is initiated by the energy from an electrical impulse. The current running through the resistance wire heats up the wire and sets off the primer charge or squib. The squib in turn ignites a booster charge. This is a more energetic compound with a high burning rate which finally ignites the main igniter charge. The main charge consists of a flame- and gas-producing charge material in pellets which are contained in a cylindrical basket. This basket is either made of plastic that burns or of metal with perforations that allow the hot gases to enter the grain of the rocket and or the engine chamber.

A typical pyrotechnic igniter powder used in small amateur rockets is black powder, which consists of Potassium Nitrate, Charcoal, and Sulphur. The latter allows the powder to ignite more readily with a spark. Some other pyrotechnic compositions are given in Table 2.

Table 2: Formulations of typical igniter compositions for pyrotechnic igniters [NASA], [Valk]; Composition 5 is a black powder composition.

Type	Fuel	Fuel mass percentage	Oxidiser	Oxidiser mass percentage	Binder
1	Aluminium	35	Potassium perchlorate	64	Vegatable oil (1%)
2	Boron	24	Potassium perchlorate	70	6%
3	Boron	19	Potassium nitrate	80	Wax (1%)
4	Magnesium	65	Teflon (PTFE)	30	Viton -A (5%)
5	Charcoal/sulphur	15/10	Potassium nitrate	75	Not Applicable

Binder content usually varies from 1-5%. Binders typically include wax, epoxy resins, Nitrocellulose and Poly-isobutylene. Important for the design of an igniter are the ignitor propellant regression rate and the flame spread rate. The former describes the burning of the solid particles in parallel layers (like for solid propellant grains), whereas the latter describes the rate at which a flame spreads over the surface (increasing the surface area that is burning). For black powder used in many amateur rockets, flame spreading (in the black powder itself) occurs at a rate of 0.1-1.0 m/s depending on

particle size. If, for instance, we use 1 cm^3 of black powder to ignite a rocket motor, it takes about 5-50 ms for the black powder to fully burn assuming the black powder charge is ignited in its centre. Also, for using jellyroll igniters, the flame spreading speed is an important design variable to consider.

Pyrotechnic igniters will cause a flow of hot gas and/or hot particles that will travel with the flow (liquid rocket engines) or impacts on the surface of a solid propellant (solid propellant rocket motors). For hybrid motors both may occur. In a liquid rocket engine, the hot gas and particles will cause evaporation of the main propellants after which combustion can start (if the temperature is right). In SRMs, it are the hot gases that cause the initially solid propellant to heat up and to vaporize and/or the hot particles that set the main charge aflame on certain locations after which the flame spreads along the surface until full-fledged combustion is reached. Similar processes occur in a HRM, where the solid component of the propellant is to be vaporized so that it can react with the vaporized part of the initially liquid component.

Pyrotechnic igniters are mostly used in small solid propellant rockets as the Ariane 4 stage separation rocket motors, and the Black Brant sounding rocket 26 KS 20000 and Nihka 17 KS 12000 solid propellant motors. They have also been used for a range of liquid rocket engines to ignite the main combustion chamber and/or gas generator, like for the European HM7B and HM60. Some performance characteristics of the HM60 pyrotechnic igniters are shown in the Table 3.

Table 3: Performance characteristics of HM60 pyrotechnic components [Stork].

	Thrust chamber igniter	Gas generator igniter
Main charge	Chlorine free ammonium-nitrate propellant in a rubber binder	Chlorine free ammonium-nitrate propellant in a rubber binder
Gas temperature [K]	$2250 < T_t < 2500$	$T_t < 2500$
Static gas temperature		> 1100 K
Mass flow [g/s]	> 300 g/s	> 60 g/s
Operating time	> 1.8 s	> 1.8 s
Ignition delay	$\leq$ 0.2 s	$\leq$ 0.2 s

A pyrotechnic igniter is unsuitable for repeated starts. When restart capability is required in a liquid propellant rocket motor and pyrotechnic ignition is to be used, several pyrotechnic igniters may be provided in such a manner that only one, or when redundancy is required, two igniters are initiated for one start. Furthermore, checkout of the integrity and readiness of a pyrotechnic igniter is difficult. Assurance of their reliability is by statistical and sampling methods (reliability testing).

5 Pyrogen igniters

A pyrogen igniter is an ignition device resembling a small solid propellant rocket motor, see Figure 4, with the combustion products being exhausted into the actual rocket motor thereby initiating combustion. Essentially it is also a pyrotechnic device, but differs from "real" pyrotechnic igniters, see previous section, in that it uses a rocket propellant as main charge and because combustion of the igniter material takes place within a closed chamber, thereby allowing for the igniter material to burn at a pressure different from the main combustion chamber.

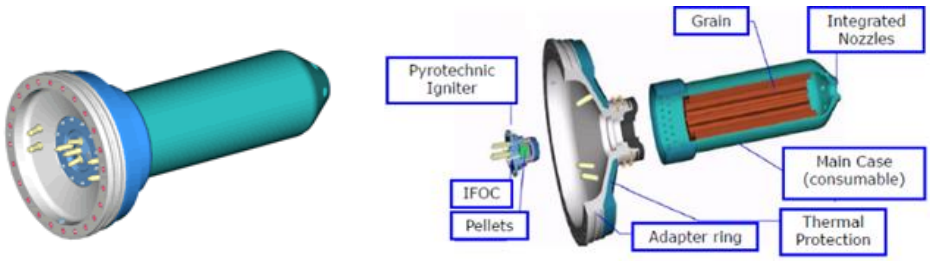

Figure 4: Artist impression of Vega Z23 SRM pyrogen igniter (left) and exploded view (right) [Stork (a)]

Figure 5 shows a schematic of a typical pyrogen igniter containing an internal and external burning propellant grain as the main charge. Igniter start up is by electrical signal, which is transferred to the initiator by an electrical connector. This initiator sets of a booster charge (e.g. B-KNO_3 pellets) which subsequently sets of the main charge. The case ensures the structural integrity of the igniter during operation. To prevent against overheating, it may be insulated inside and out. A nozzle directs the flame into the motor.

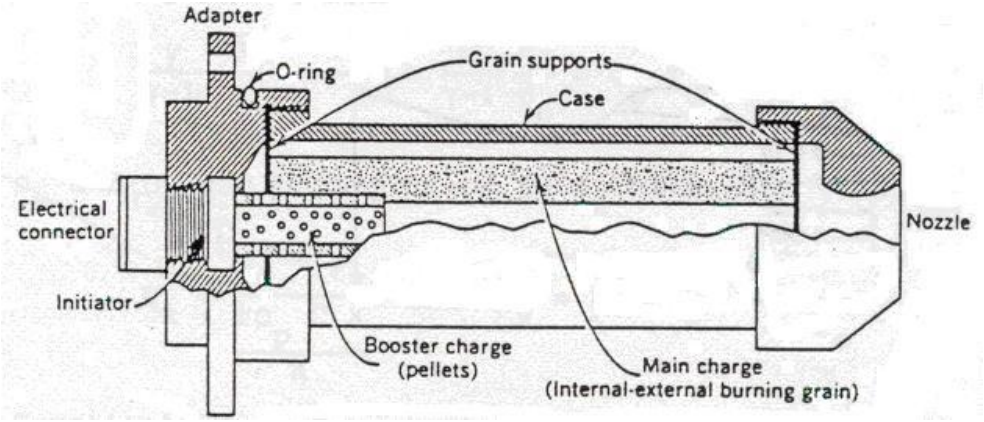

Figure 5: Typical pyrogen (rocket-type) igniter

A recent development is that casings are made of a consumable composite structure, intended to be (partially) consumed during motor functioning, thereby saving mass.

Like pyrotechnic igniters, pyrogen igniters are unsuitable for repeated starts and assurance of their reliability is by statistical and sampling methods (reliability testing). Also, checkout of the integrity and readiness of the igniter is difficult.

Pyrogen igniters are primarily used for applications that require high ignition energy like Solid Rocket Motors (SRMs). Specific characteristics of some pyrogen igniters are summarised in Table 4.

Table 4: Characteristics of some solid rocket motors pyrogen igniters [McDonald], [Gonzalez], [Calabro], [Sutton], [ATK], [BPD], [Castellini], [Boeing], [Encyclopedia Astronautica]

	Space Shuttle SRB	Ariane 5 SRB	Ariane 6 / Vega P120C	Vega P80	Vega Z23	Minuteman 1st stage SRM
Propellant mass [kg]	501746	237100	141600	88383	32947	20789
Motor initial free volume[7] [m^3]	***~70***[8]	40.93	***~14-15***	10.23	3.38	1.314
Igniter location	Head-end	Head-end	Head-end	Head-end	Head-end	Head-end
Igniter propellant	PBAN-type	HTPB-type	HTPB-type	HTPB-type	HTPB-type	PBAN-type
Igniter charge mass [kg]	62	65	36			
Igniter total mass [kg]	272	315	130	<175	34.3	11.79
Igniter burn time [s]	0.34			0.4	0.3	
Length [m]	1.22	1.25	1.0	1.2	0.7	
Max. diameter [m]	0.432	0.47	1.0	0.8	0.4	

Table 4: Continued

	Castor 4AXL	Orbus 21	Vega Z9	Vega Z9A	Orbus 7S	Orbus 6
Propellant mass [kg]	13128	9709	8996	10570	3316	2545
Motor initial free volume [m^3]	***~1.5-2.0***	***~0.45***	0.98			***~0.15***
Igniter location	Head-end	Head-end	Head-end	Head-end	Head-end	Head-end
Igniter propellant			HTPB-type	HTPB-type		
Igniter charge mass [kg]	2.45			3.5		
Igniter total mass [kg]		16.3	<15	15.7	4.54	9.5
Igniter burn time [s]			0.25			
Length [m]			0.6			
Max. diameter [m]			0.3			

[7] Estimated from either case volume minus propellant volume or from motor schematics from which the size of the grain port can be estimated. Propellant volume is obtained from propellant mass divided by mass density (for HTPB propellant typically around 1700-1800 kg/m^3). SRM case volume estimated from case envelope with correction applied for ellipsoidal heads.
[8] Data in bold italics are estimated.

6 Hypergolic (or pyrophoric) igniters

In some early rocket motors, like the famous F-1 rocket engine driving the even more famous Saturn V rocket, a separate hypergolic bipropellant combination has been used to produce a hot flame in the rocket motor, thereby causing the main propellants to start combustion. This method requires the use of an independent igniter feed system in which the two propellants are stored under high pressure. A more elegant way is through use of a hypergolic slug, which injects a very active liquid chemical which is self-igniting with one of the main propellant components but neutral to the other. Some examples are triethyl-aluminium ($(C_2H_5)_3Al$) with LOX and chlorine trifluoride (ClF_3), difluoro-oxide (F_2O), and (di)nitrogen tetroxide (N_2O_4) with various fuels, see also Table 1. The fluid is stored in a separate tank. If a fluid is chosen that is hypergolic with the oxidiser but neutral to the fuel, it is installed in the fuel line. Upon pressurisation of the propellant lines, the fluid flows into (part of) the fuel injector elements prior to the fuel. When the fluid meets with the oxidiser in the chamber, ignition follows. Because the fuel follows the igniter fluid the combustion is sustained. Problematic is that most of the chemicals used in hypergolic igniters are highly toxic and may ignite spontaneously on contact with air, making them difficult to produce, store and handle. Hypergolic ignition has been used in the past on amongst others the Saturn F1 and H1 liquid oxygen-kerosene rocket engines and is currently used on the Atlas RD-180 and EADS 300 N cryogenic engine. Hypergolic ignition is also applied in a range of hybrid rocket motors using LOX as oxidiser and polybutadiene as fuel. Ignition is achieved by injecting LOX with triethyl-aluminium.

Table 5: Hypergolic propellant combinations [Schmidt], and [Huzel].

Oxidiser	Hypergolic with
Oxygen	Triethylaluminium, Analine
Hydrogen-peroxide	Hydrazine-hydrate
Nitrogen-tetroxide (NTO), Nitric acid, Mixed Oxides of Nitrogen (MON)	Hydrazine, mono-methylhydrazine (MMH), Unsymmetrical dimethylhydrazine (UDMH)
Fluorine, chlorine trifluoride, and difluoro-oxide	Almost all fuels

7 Catalytic igniters

Catalytic igniters use a catalyst to decompose a monopropellant thereby producing a hot igniter flame. This flame in turn than is used to ignite the main propellant. This method has for instance been used on the De Havilland Spectre Rocket aircraft power-plant which employs hydrogen peroxide as oxidiser and kerosene as fuel. Ignition is initiated and sustained by passing the oxidiser through a solid silver catalyst bed. The high temperature produced in the combustion chamber by this reaction spontaneously ignites the kerosene fuel. The catalyst may also be liquid. However, the use of a liquid catalyst is considered more problematic and complex due to the need of elaborate timing, valving and interlocking devices. [Jonker] describes the design of a solid catalyst hydrogen-peroxide igniter for use on the European LOX-LH_2 Vinci engine. Installation of this igniter is like an augmented spark igniter. Catalytic ignition has also been proposed for ignition of some hybrid rocket motors using hydrogen peroxide as the main oxidiser [Heslouin], [Sellers].

8 Spark plugs

If the oxidiser and fuel are easily vaporised, proper ignition is obtainable by means of a spark plug as in the case of a motor fed with liquid oxygen and liquid hydrogen or a

hydrocarbon. A spark plug, see Figure 6, essentially consists of two wires separated by a small gap and connected to a power source or electrical exciter. When an electrical voltage is applied to the wires, a current jumps, or arcs, between the wires, producing a spark. A typical spark plug may fire at the rate of 50 sparks per second, releasing approximately 1/10 joule per spark. This corresponds to 5 Joules/sec per plug.

The spark plug in early liquid-propellant rockets was placed in the path of the injection streams or built into the propellant injector. They are eminently suitable for repeated starts. For direct ignition, however, they are confined to relatively small combustion devices. For larger devices augmented spark or torch igniters are to be used, see next section.

Figure 6: Typical spark plug

9 Augmented spark or torch igniter

The limitation of direct spark ignition to small units has led to the design and development of augmented spark or torch igniters (ASI). A typical augmented spark igniter is shown in next figure.

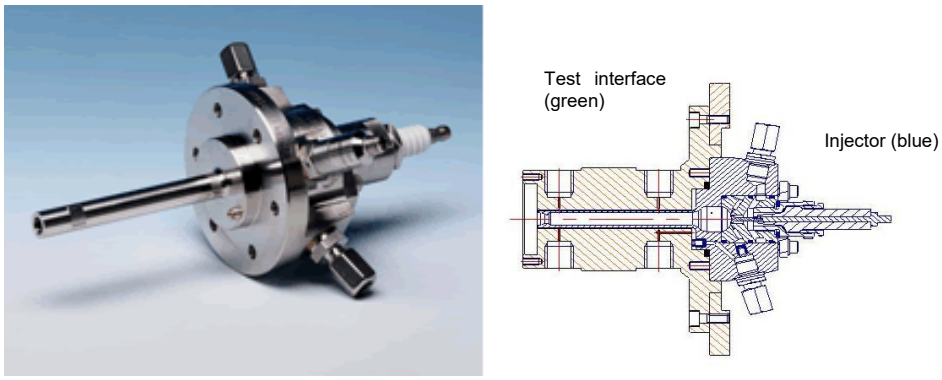

Figure 7: Vinci torch igniter [Stork (b)] hard ware (left) and schematically depicted installed on test interface (right)

A spark plug or electrical exciter fires into a small chamber, see Figure 8, wherein a small amount of oxidiser and fuel is fed and ignited. The resulting hot igniter flame is directed into the main chamber via an igniter tube/nozzle. The latter ensures for sonic separation between the igniter chamber and the actual combustion chamber. The oxidiser and fuel feeding the igniter may be tapped off from the main propellant feed lines or stored separately from the main propellants. In the latter case the igniter propellant may be different from the main propellant. This may be advantageous in case the main chamber uses hydrocarbon (HC) propellant, as such propellants form deposits on the spark plug that can easily cause ignition failures. To improve ignition, sometimes a heat exchanger is used to gasify the propellants prior to entering the ignition chamber. Cooling of the igniter may be provided by one of the propellants.

Sometimes an ignition monitor is mounted in the ASI which indicates if proper ignition has been achieved.

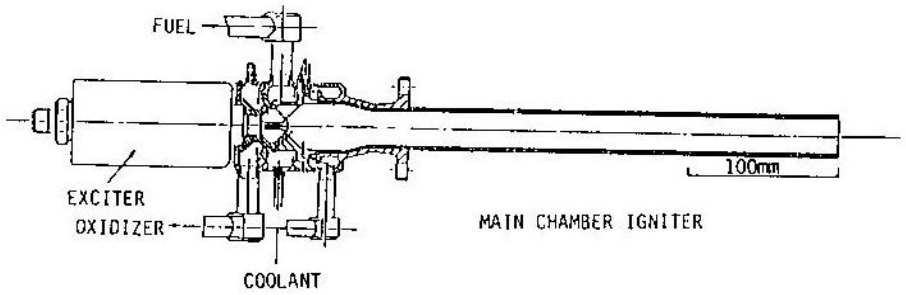

Figure 8: LE-7 spark torch igniter schematic [Torii]

Besides on the LE-7, ASI is applied on amongst others the Japanese LE-7/7A and LE-5 liquid hydrogen - liquid oxygen rocket engine, the Space Shuttle Main Engine, RL10, and Vinci liquid rocket engines, but also on some hybrid rocket motors, like the TU-Delft/TNO 0.1 kN motor [Timnat]. Specific characteristics and their values of some rocket motor ASI are given in the next table.

Table 6: Some specific ASI characteristics [Torii], [Yanagawa], [IFR]

	LE-7 main chamber	LE-7 pre-burner chamber	LE-5 Main chamber	LE-5 pre-burner chamber	SSME main chamber
Main propellants	LOX-LH_2	LOX-LH_2	LOX-LH_2	LOX-LH_2	LOX-LH_2
Chamber mass flow rate	261.9 kg/s	57.2 kg/s	26.9 kg/s		467 kg/s
Chamber pressure	14.7 MPa	24.0 MPa	3.5 MPa	2.6 MPa	20 MPa
Chamber mass mixture ratio	6.9	0.81	5.5	0.85	6.0
Igniter propellant	GOX-GH_2	GOX-GH_2	GOX-GH_2	GOX-GH_2	LOX-GH_2
Igniter propellant mass flow rate	1.34 kg/s	0.57 kg/s	22 g/s	2 g/s	0.73 kg/s
Overall igniter mass mixture ratio	6.0	0.8	1.0	1.0	0.7
Igniter mass mixture ratio in initiator region	40	40	24	24	
Operation time	315 s	315 s			3.5 s
Spark pulse energy	10 mJ	10 mJ			
Cooling	Dump-cooling	Dump-cooling	Film-cooling	Film-cooling	

Lately, instead of a spark plug also a glow plug is used to initiate a torch igniter.

10 Ignition sizing

Two important objectives for the design of an ignition system are to obtain sustained combustion quickly and to avoid pressure overshoot. Both items will be discussed in this section in some detail.

10.1 Ignitability

Practice shows that some propellants can be more readily ignited than others. This depends on the auto-ignition temperature of the propellant combination considered or the minimum ignition energy required for a localised ignition source.

Flammability and auto-ignition temperature

In case we put a combustible mixture in a vessel and start heating the mixture, we will find there is a critical temperature above which a rapid rise in vessel pressure occurs faster than the normal pressure rise due to external heating. This critical temperature is referred to as the auto-ignition or explosion limit temperature. It depends on the components in the mixture, their mixture ratio and the amount available as is illustrated in Figure 9.

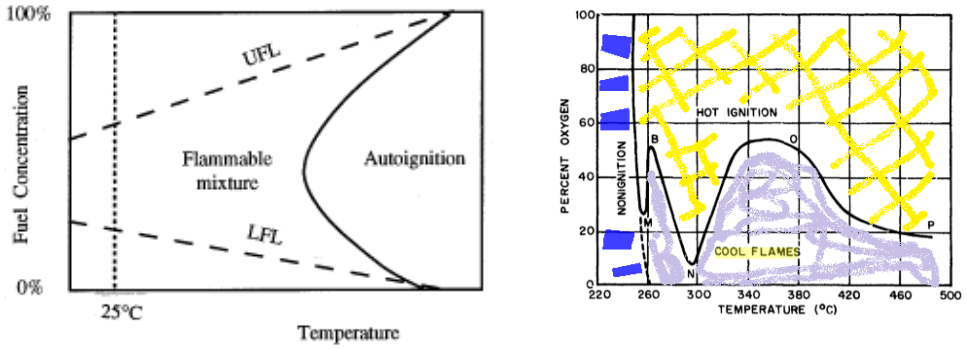

Figure 9: Flammability limits in relation to temperature and concentration [Gexcon] (left) and details of auto-ignition zone (right)

Essentially any mixture heated above the auto/self-ignition temperature will auto-ignite provided that the oxidizer concentration (note that the vertical axis of the two figures is different) is sufficient to attain a hot ignition. Typical auto-ignition temperatures of several species with air at standard pressure (1 atm) are given in Table 7. It is stressed that values will slightly vary depending on the fuel concentration.

Table 7: Auto-ignition temperature of specific substances with air [http://www.engineeringtoolbox.com]

Substance	Auto-ignition temperature (deg C)
Methane	595
Hydrogen	585
Ethyl Alcohol	365
Ethylene	490
Nitrous oxide	575
Wood	300
Bituminous coal	527
Petroleum	400
Peat	227

Auto-ignition temperature also depends on the pressure. For instance, for a stoichiometric hydrogen-oxygen mixture this limit is about 830-835 K at 1 bar pressure and about 775 K at 0.1 bar [Univ. of Cambridge].

From Figure 9 we also learn that reaching the auto-ignition temperature is not a necessary requirement for ignition as even below this temperature a mixture can be ignited, but in that case an external stimulus is needed. Also, it can be noticed that at this lower temperature a mixture will only burn if the fuel-oxidiser mixture ratio is

between the upper (fuel-rich) and lower (oxidiser-rich) flammability limits. Flammability limits, also called flammable limits, give the proportion of combustible gases in a mixture, between which limits this mixture is flammable. The lower flammable limit (LFL) describes the leanest mixture that still sustains a flame, i.e. the mixture with the smallest fraction of combustible gas, while the upper flammable limit (UFL) gives the richest flammable mixture. The figure also shows that with increasing temperature; the flammability limits widen. Next to that also an effect of pressure is to be expected as well as the presence of inert species in the mixture.

Minimum ignition energy

The minimum ignition energy is a measure of how much energy is required for a localised ignition source (like a spark) to successfully ignite a (stagnant) fuel-oxidiser mixture. The process of ignition is envisaged as follows. The localised ignition source creates a small volume of a mixture of liquid and gas drops. The temperature in this drop is considered high enough (< auto-ignition temperature) to instantly cause combustion. If the rate of heat release exceeds the rate of heat loss by e.g. thermal conduction, then the volume quickly grows to fill the entire combustion volume. For gaseous hydrogen-oxygen mixtures this is in the range of a few mJ up to several tens of mJ, depending on the mixture ratio and the absolute pressure [Schmidt]. For kerosene-oxygen mixtures in the range 35 - 40 ^{o}C the minimum ignition energy is found to be about 100 Joule. When the temperature is increased to ^{o}C, the ignition energy decreases to less than 1 mJ. For solid propellants, these values may be much higher as part of the energy is used to heat up the propellant to form a combustible gas mixture.

The minimum spark ignition energy in air and oxygen at 25C and 1 atm for some common chemicals and their flammability limits are given in the table below.

Table 8: Minimum ignition energy and flammability limits of some common fuels [Kuchta], [Coward]

	Minimum ignition energy [mJ]		**Flammability limits LL-UL**		
Fuel	*Air*	*Oxygen*	*air*	*oxygen*	*Nitrous oxide*
Methane	0.30	0.003	5-15%	5-60%	
Methanol	0.14		6.7-36%	6.7-93%	
Propane	0.26	0.002			
Ethylene	0.07	0.001		3-80%	
Ammonia	>1000			15-79%	2.2-70%
Hydrogen	0.017	0.0012		4.1-94%	5.5–80%

LLO = lower Limit, UL = Upper Limit

10.2 Flame spreading

Practice shows that even though only limited amount of energy is needed to ignite a propellant, some motors do not readily obtain full-fledged combustion. This is because of differences in flame spreading. For instance, consider a gasoline spill over a large surface area. To ignite the gasoline only a very small amount of energy (minimum 0.3 mJ) is needed. However, for the flame to spread (hence the term flame-spreading) over the whole spill takes some time, depending on the flammable vapour concentration above the spill. Gasoline with a higher vapour pressure generally experiences slower flame spreading as part of the energy is needed to vaporise the gasoline. Also, external conditions, like wind or flow turbulence, play an important role. From this example, we can easily understand that solid propellants require more energy to ignite than hybrid propellants, which in turn require more energy than liquid or gaseous propellants and how the internal flow conditions in the engine may affect the ignition and flame-spreading process.

10.3 Igniter flame temperature, power and energy

From the foregoing, we learn that to obtain ignition, the igniter flame temperature must be sufficient to increase (part of) the main propellant into the vapour state. If we can increase the temperature further to above the auto ignition temperature this would be even more sure to attain ignition. So, a safe requirement for any igniter would be to require it is able to heat up part of the combustible mixture to a temperature more than its auto-ignition temperature:

$$T_{ign} > T_{auto} \tag{10-1}$$

However, even though the igniter flame is of a sufficiently high temperature, the igniter mass flow might still not be sufficient to ignite the engine/motor in its entirety in a sufficiently short time. As a remedy, one should increase the igniter power either through further increasing the flame temperature and or by increasing the igniter mass flow. Igniter power, P_{ign}, follows using:

$$P_{ign} = m_{ign} (H_{ign} - H_{ref}) \tag{10-2}$$

Where m_{ign} is igniter mass flow, H_{ign} is enthalpy of igniter gases when leaving the igniter and H_{ref} is enthalpy of igniter gases at some reference temperature usually taken equal to the auto-ignition temperature of the propellant to be ignited or 298 K. In the Table 9 values of the heat of reaction and flame temperature of specific igniter mixtures are given. Heats of reaction are all taken relative to 298 K. In case two values are given, the first value is a gross value with all products in the most stable state at 298 K and the second value is a net value with all products in the gaseous state also at 298 K. This mostly relates to water being either in the condensed or vaporized state.

Table 9: Heat of reaction of some igniter propellants (O/F is oxidizer to fuel mass ratio; percentages are weight percentages)

Igniter propellant	Heat of reaction [MJ/kg]	Flame temperature[9] @ 1 bar [K]	Remark
Hydrogen-Oxygen (O/F = 8; stoichiometric)	15.9/13.4	3073	Temp. from CEA
Hydrogen-Oxygen (O/F = 5)	14.9/12.6	2970	Temp. from CEA
Methane-Oxygen (O/F = 4; Stoichiometric)	11.1[10]/-	2829	Temp. from CEA
Methane-Oxygen (O/F = 3.15)	10.5/9.5	2614	Temp. from CEA
Magnesium-Teflon-Viton (54% magnesium-30%Teflon-16% Viton)	6.3	2100	[De Yong]
Boron-Potassium nitrate-wax (80% KNO_3-19% Boron-1% wax)	6.5	4941	Temp. from CEA
Black powder (75% KNO_3-10% sulphur-15% wood coal)	3.2	1600	[Salleh]
Black powder with 10% thermite	3.7	1668	[Salleh]
Black powder with 30% thermite	7.9	2525	[Salleh]
Hydrogen-peroxide (87.5% pure)	5.1/2.8	1275	Temp. from CEA

[9] Calculated using CEA or RPA-Lite.

[10] CEA shows (consider assigned temperature and pressure problem) that the heat of reaction is ~12.0 MJ/kg. This is higher than the 11.1 MJ/kg reported here and taken from calculations in an earlier chapter in this work, see chapter on thermochemistry and look for example calculation on heat of reaction of a stoichiometric mixture of methane and oxygen. For the hydrogen/oxygen mixture, the values as determined in this work were found to match with the outcomes of CEA.

The igniter power required depends on the type of propellants (state of aggregation, their mixture ratio, initial temperature, and whether ignition occurs in vacuum or on ground. Generally, solid propellants require more power to ignite than hybrid propellants, which in turn require more energy than liquid propellants. In addition, larger motors/engines require more power than small motors/engines.

Ignition usually takes some time as the heating and subsequent reaction of the main propellants takes some time. Together with the igniter power this than determines the igniter energy needed. Igniter energy can be determined by multiplying igniter power with the time that the igniter is active. The action time of the igniter depends on the time needed to heat sufficient propellant to the required temperature for self-sustained combustion. Critical is that the time is sufficient to ensure that the rate at which heat is drawn away from the propellant surface by conduction does not prevents the propellant surface from attaining the right temperature. In general, the higher the pressure, the better the heat transfer and hence the shorter the time that the igniter must be active, see also section on ignition delay time.

Form the igniter energy and the heat of reaction of the igniter propellant used, we then can determine a first estimate of igniter propellant mass needed.

10.3.1 LREs

The most effective method to ignite a liquid rocket engine is through spark ignition. Relevant for dimension is knowledge about the minimum ignition energy for spark ignition. For hydrogen-oxygen mixtures this is in the range of a few mJ up to several tens of mJ, depending on the mixture ratio and the absolute pressure [Schmidt]. Other parameters of importance are the mean diameter of the droplets in the mist that results from injection and the flow velocity of the gaseous surroundings.

As stated earlier, spark ignition is mostly limited to small rocket motors. For larger motors it is envisaged that the flame spreading is not fast enough to achieve full combustion before the flame leaves the motor via the nozzle. In that case, we need to resort to another ignition means including ASI, pyrotechnic ignition or hypergolic ignition. One very crude method to size the igniter in that case is to determine the energy required to heat all the propellant flow to the auto-ignition temperature. For instance, for a LOX-LH_2 rocket engine with a mass flow of 240 kg/s and a mass mixture ratio of 5 this means to heat 40 kg of hydrogen and 200 kg of oxygen to the auto-ignition temperature every second. This requires approximately 550-600 MJ/s, depending on the initial temperature of the propellants. If we now use a hydrogen-oxygen torch igniter and take into account the net heating value of hydrogen of 119 MJ/kg (calculation of heating value has been earlier discussed in section "Thermo-chemistry"), we find this requires an igniter hydrogen mass flow of about 5 kg/s. Assuming an oxygen-hydrogen mass mixture ratio of 5 for the igniter, we find an oxidiser mass flow of 25 kg/s and an overall igniter propellant mass flow rate of 30 kg/s. Comparing this value with the results given in the Table 6, we find that this model overestimates the igniter mass flow rate considerably. The reason for this over-estimation is that we do not consider the energy that comes from main propellant combustion. If we take this energy into account, it can be argued that it is sufficient to heat up only $1/8^{th}$ of the total mass flow to the ignition temperature. This than would reduce the required igniter propellant mass flow rate to 3.5-4 kg/s, which is still an overestimation. [Jonker] uses an identical approach but assumes that it is sufficient if the igniter raises the temperature of the bipropellant mixture injected by only the inner ring of injector elements to the auto-ignition temperature. For example, for the LE-7 pre-burner, this means that only about 5% (or $1/20^{th}$) of the total mass flow should be heated to the auto-ignition temperature. The latter assumption seems to give more reasonable results, but further verification is necessary to get more certainty.

10.3.2 SRMs

Ignition of a SRM is a complex phenomenon, involving amongst others transfer of heat due to conduction, radiation and convection, phase transfer, fuel pyrolysis, chemical reactions (both gas-phase and heterogeneous reactions), diffusion, laminar or turbulent flow, 2-phase flow. It is this complexity that makes that most models to size the igniter charge mass are of a highly experimental method. Several methods are described in [Barret] of which we will shortly deal with two methods that are quite commonly used in the early design stages. The first method is the "*free volume*" method. It is based on the correlation that exists between the mass of a given igniter charge ($M_{ign\ charge}$) required to ignite a motor and the free volume (V_F) of that motor: A relation valid for SRM's using an Al-$KClO_3$ (Alclo[11]) igniter pelleted charge is given below estimated from [Barret] and adapted to metric units:

$$M_{ign\ charge} = 0.018\ (V_F)^{0.7} \tag{10-3}$$

where V_F is in cm^3 and M_{ign} is in gram. This relation is valid for SRMs with an initial free volume in the range 0.015 to 150 m^3. Note that the exponent and the constant in the relation may vary in case of using other pyrotechnic compositions, like Boron-Potassium nitrate-wax, and Magnesium-Teflon-Viton with their many variations. One reason for this change is at least the different heats of reaction, but also the way the heat is transferred (convection and/or radiation heat transfer) to the to be ignited propellant.

A second method is the "*critical pressure*" method. It is based on the experience that at low to moderate pressures ignition energy requirements are strongly dependent on the pressure to be attained for stable combustion. For example, double-base propellants are easily ignited but their high-pressure limits require an ignition pressure often above 30 bar. In contrast, composite propellants are more difficult to ignite but exhibit lower combustion limits. [Barrère] uses the following relation to determine the charge size based on attaining a given pressure in the motor port.

$$M_{ign\,charge} = \frac{1}{1-\sigma} \cdot \frac{p_{ign} \cdot V_F}{\frac{R_A}{M_{ign}} \cdot T_{ign}} \tag{10-4}$$

With p_{ign} is ignition pressure, M_{ign} is molecular mass of the gaseous combustion products of the igniter, T_{ign} is combustion temperature of the igniter propellant, and σ is fraction condensed particles in igniter combustion products. Typical propellant properties for black powder are σ = 60%, M = 34.75 kg/kmol, and T_{ign} = 2590 K

For other methods you are referred to [Barret]. For an improved understanding of ignition of solid propellants, the governing equations and boundary conditions, you are referred to amongst others the work of [Kuo].

The two above methods have been validated for the determination of pyrotechnic igniter charge mass by [Salama] using data of 7 pyrotechnically ignited SRMs. They found that the relation as obtained from Sutton underpredicted charge mass (sometimes about a factor 50), whereas the relation taken from Barrère was found to provide values that are of the same order as the actual charge mass.

[11] Aluminium content of ~35% by mass.

10.3.3 HRMs

For an HRM to ignite, the igniter flame should allow for heating up the oxidiser stream to a temperature that causes the initially solid fuel to gasify and to initiate self-sustained combustion. For polyethylene and Plexiglas, being typical hybrid rocket fuels, [Wilde] determined experimentally that fuel gasification (due to fuel pyrolysis) is initiated at about 600-750 K depending on amongst others chamber pressure, oxidiser-fuel mixture ratio and the specific heating conditions, like the flow velocity in the chamber. The criterion for sustained combustion follows from the auto-ignition temperature of LOX-hydrocarbon mixtures which is more than about 800 K. This indicates that the temperature of the oxidiser stream must be more than at least 800 K. In practice, it should be higher than 800 K to make up for the heat that is dissipated in the pyrolysis process, see section on solid fuel regression in chapter on hybrid combustor design, and/or other heat loss.

Another requirement that must be fulfilled to obtain sustained combustion is that the time required for the mixing and subsequent reaction of fuel and oxidiser is shorter than their residence time in the combustor. For further information on this aspect, the reader is referred to the work of amongst others [Kuo] and [Calzone].

10.4 Ignition pressure

Use of an igniter containing an oversized charge may result in an initial pressure "spike" (Figure 10). This over-pressurisation of the rocket motor during start up *may* result for a liquid rocket engine in an engine failure due to a “ZOT”. In that case the chamber pressure spike forces fuel into the LOX injector, leading to a detonation in the LOX manifold. For an SRM, the over-pressurization may lead to a failure due to the shearing of the safety bolts retaining the rocket motor head or nozzle of a SRM. For operational rockets, this should be avoided.

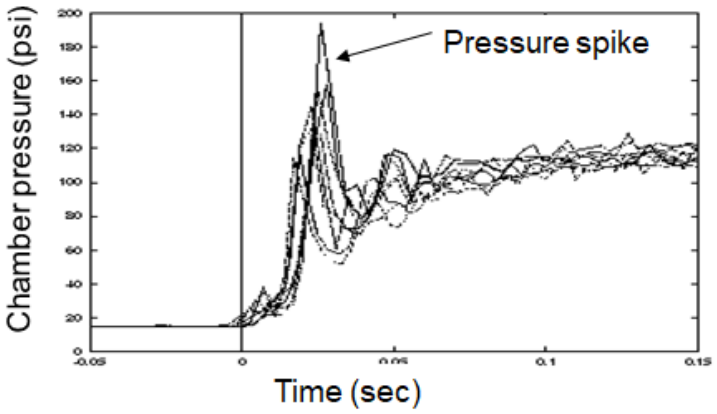

Figure 10: Pressure-time plot demonstrating effect of an over-sized igniter. Plot shows output from multiple pressure transducers.

Ignition pressure for pyrotechnic and pyrogen igniters can be determined in case the fraction of igniter charge G burned at any time t is known:

$$p_{ign} = (R \cdot T \cdot \rho)_{ign} + p_a = R \cdot T_{ign} \cdot \frac{M_{ign} \cdot G}{V_F} + p_a$$

$$p_{ign} = \lambda \cdot \frac{M_{ign}}{V - V_i} \cdot G + p_a \approx \lambda \cdot \Delta \cdot G \cdot \frac{\rho}{\rho - \Delta} + p_a \qquad (10\text{-}5)$$

With Δ is loading density (M_{ign}/V), M_{ign} is mass of igniter charge, p_a is ambient (atmospheric) pressure, V is chamber volume, ρ is density of igniter charge, V_i is igniter volume, and V_F is free volume.

From the ideal gas law follows for the pressure:

$$p = R \cdot T \cdot \rho \tag{10-6}$$

If combustion of the igniter charge occurs rapidly with no pressure loss due to gas seepage through the nozzle opening and considering that the initial chamber pressure is ambient, we find for the ignition pressure:

$$p_{ign} = (R \cdot T \cdot \rho)_{ign} + p_a \tag{10-7}$$

The density of the igniter gas relates to the free volume in the motor and the burned igniter propellant mass at any time t. Introducing the fraction G, I.e. the fraction of igniter charge burned at any time t, we find:

$$p_{ign} = R \cdot T_{ign} \cdot \frac{M_{ign}}{V_f} \cdot G + p_a \tag{10-8}$$

The fraction G can be determined once the shape of the igniter charge and its regression rate are known. The ignition pressure thus calculated is a maximum value. More accurate value can be obtained when considering the residence time of the igniter gases in the combustion chamber.

Ignition pressure for ASI, hypergolic and catalytic igniters can be calculated likewise, except that in that case we should consider igniter propellant mass flow to determine the igniter propellant mass burned.

In practice, at some time during ignition combustion starts. Worst case, the pressure in the chamber becomes equal to the sum of chamber pressure during normal combustion (in absence of ignition) and ignition pressure. It is for this reason that the energy of the igniter is limited so that the ignition pressure is limited to a maximum value. For SRMs this value is set at maximum 30-40% of chamber pressure. For LREs no such data are available.

10.5 Ignition delay

To obtain sustained combustion quickly, ignition delay must be short (typically in the range of ms up to tenths of a second). To determine ignition delay times for liquid rocket engines is very important for the correct operation of the engine. For example, delayed ignition may lead to explosions at start-up commonly referred to as "hard starts".

Next figure shows the pressure development in the chamber for 4 different ignition delay times τ. Along the vertical pressure the ratio is given of the instantaneous chamber pressure p to the final (after ignition) chamber pressure. The horizontal axis represents the time $t + \tau$ passed after the propellants start flowing into the engine also given as a dimensionless ratio. This time is given in a non-dimensional form by dividing by the blow down time t_c., which is the time required for the pressure in the rocket chamber to fall to 1/e of its initial value in absence of mass entering the engine/motor.

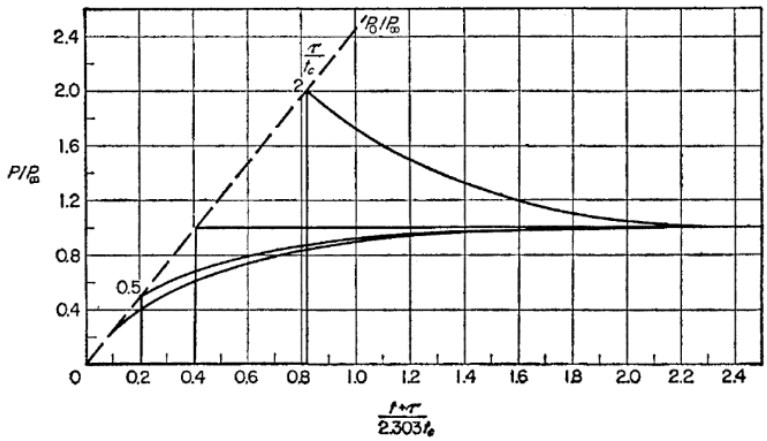

Figure 11: Effect of ignition delay on chamber pressure for a liquid rocket engine [Fletcher]

The 4 different delay times for which the pressure curves are plotted are for a non-dimensional delay time of zero, 0.2, 0.4 and slightly more than 0.8. Clearly can be seen that in the first three cases the pressure ratio always remains below 1. However, in the 4th case, when igniting after the delay time of slightly over 0.8, there is a sudden pressure rise to twice the nominal chamber pressure after which (if the engine is able to sustain this pressure, it reduces to the normal chamber pressure as more gas exits the engine than is entering. The huge pressure rise is associated with the engine being filled with excess propellants because of the delay time in the ignition. For larger delay times, the over-pressure will further increase and hence at some point the over-pressure becomes too high for the engine to bear and a failure will result. Note that since blow down time is of the order of ms, see for determination of the blow down time the earlier chapter on LRE combustor design, ignition delay times of order ms can already be disastrous.

Because of the complexity of modelling ignition, ignition delay times are usually measured in an experimental apparatus that closely resembles the actual test motor. [Barrère] gives an overview describing typical ways of measuring ignition delay using laboratory apparatus and micro-rockets and presents results obtained for some hypergolic propellant combinations. [Kuo] describes a test apparatus used for hybrid propellant ignition studies. Because of the many parameters involved and the complexity of the test apparatus, such tests are usually quite expensive.

10.6 Igniter location and orientation

In most solid, liquid and hybrid rocket motors igniters are placed at the head-end of the chamber, see for instance

Figure 12 and Figure 13. The reason is that if the igniter is placed at the head of the motor the igniter flame will travel down the chamber. If the igniter is placed by the nozzle end, it is more difficult for the hot gas to travel UP the chamber to ignite the propellant at the head end, and in fact a large amount of the hot igniter gas will travel out of the nozzle without lighting any propellant in the motor. This can have the effect of igniting some of the propellant but not having it reach a high enough pressure to choke the nozzle and therefore achieve significant thrust, or (for solid and hybrid motors) enough propellant can ignite to choke the nozzle and produce thrust, but at a very low chamber pressure.

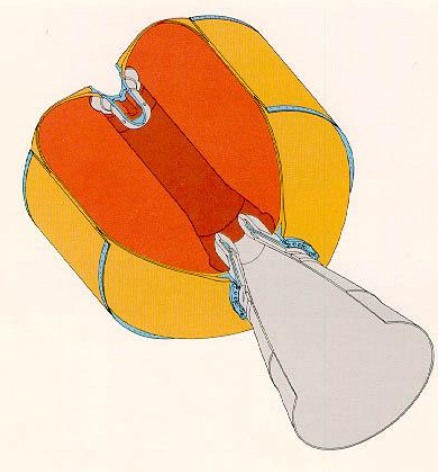

Figure 12: Orbus 21 SRM schematic showing head-end igniter [Purdue]

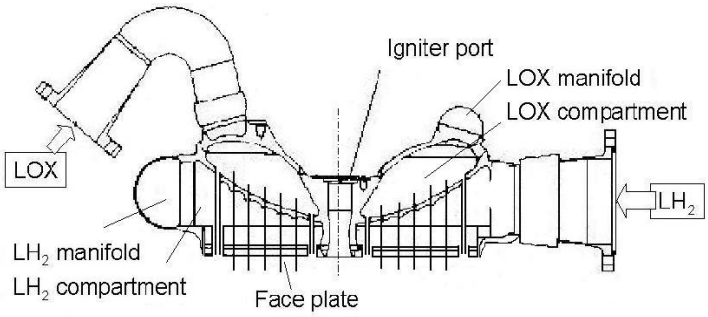

Figure 13: Schematic of injector head with ignitor port of LE-5 engine [Yanagawa]

For some solid rocket space motors placement at the nozzle is favored as this allows for a higher fill ratio of the motor due to the incorporation of a head-end web. For instance, the Thiokol STAR-series motors use a toroidal ignition system, which is integral to the titanium nozzle aft closure, see Figure 14. The ignition system is initiated from a remotely located safe and arm (S&A) device and is initiated by "through bulkhead initiators" (TBI). The TBIs ignite a small transfer propellant grain, which in turn ignites the main igniter propellant in the toroidal igniter chamber. The hot gases generated in this chamber exhaust on to the actual propellant grain from 12 ports in the face of the housing. The earlier mentioned problem of gases remaining at the nozzle end of the chamber is less important for those types of motors because of a greatly reduced length to diameter ratio and because of the zero-gravity environment.

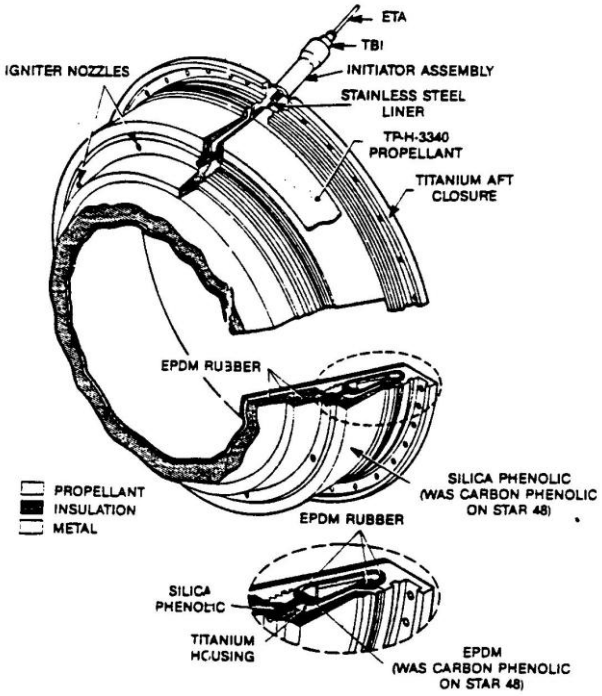

Figure 14: STAR 30 and 37 series toroidal igniter

Also, in the case of a cigarette burning grain, the igniter is located at the nozzle end of the motor.

For SRMs, when using a pyrogenic igniter, the exhaust nozzles may be adapted so that they direct the hot flow more directly onto the propellant surface, see figure hereafter, thereby ensuring improved heat transfer to at least part of the solid surface.

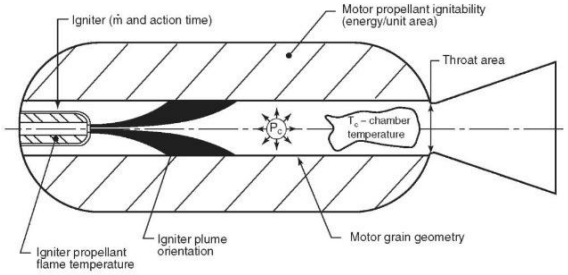

Figure 15: Schematic showing hot plume from igniter directed at propellant surface (from: http://what-when-how.com/space-science-and-technology/solid-fuel-rockets/)

11 Igniter mass

[Humble et al] present a method for the estimation of pyrogen igniter (not charge only) mass, wherein igniter mass is related to the initial free volume within the main chamber:

$$M_{ign} = 0.0138\ (V_F)^{0.571} \qquad (11\text{-}1)$$

where V_F is in cm^3 and M_{ign} is in kilogram. Unfortunately, no information is available on the accuracy of the estimate produced and the range to which it applies. Also, it is not indicated if this mass estimate includes S&A device, possible TBI, electrical power source, etc.

[Castellini] in his research also estimated igniter mass, but using a different relation:

$$M_{ign} = 20.62\ (V_F)^{0.73} \tag{11-2}$$

where V_F is in m^3 and M_{ign} is in kilogram. Above relation is based on 4 data points and has a relative standard error of 31.5%. 3 of the data points used by Castellini are based on Vega SRM igniters that have a combustible case. The fourth data point is made up by the Ariane 5 P230 solid rocket motor igniter.

To validate the above relations, use could be made of data of existing igniters. To this end, Table 10 provides characteristics for a few igniters in comparison to the mass that results from the two estimation relations presented above. It shows that the relation taken from Humble scores worse for small SRMs. So, caution is necessary. Additionally, the table also presents specific thermal energy (igniter thermal energy divided by the grain (or charge) mass), and igniter power flow (igniter thermal energy divided by the igniter burn time).

Table 10: Characteristics of Vega rocket pyrogen igniters [Brauers], [Castellini] in comparison with mass estimation using the Heister / Castellini relation.

	P230 SRM	P80 SRM	Z23 SRM	Z9 SRM
Igniter total mass [kg]	315	130	34.3	14.7
Igniter grain mass [kg]	65	22	9.4	3.3
Igniter thermal energy [MJ]		93.4	42	15.1
Specific thermal energy [MJ/kg]		4.2	4.5	4.6
Igniter burn time [ms]	250	400	300	250
Igniter power [MJ/s] or [MW]		325	114	59
SRM free volume [m^3]	40.93	10.23	3.38	0.98
Igniter total mass (Humble et al) [kg]	306.4	138.8	73.8	36.4
Igniter total mass (Castellini) [kg]	318	114.4	50.6	20.3

Both relations allow for scaling of igniter mass with motor free volume. However, many other variables that may also affect igniter mass, like the structural materials used, and the igniter pressure, are not considered yet. More accurate mass estimation methods as well as mass estimation methods for other types (like pyrotechnic igniters) of igniters are left for future investigations.

12 Igniter sizing method

Any sizing method starts with a proper understanding of the functions of the device to be designed. Hence also for an ignitor or an ignition system we need to understand what the igniter needs to do and how the igniter can fail. Next step is than to derive the requirements that hold for the system to be designed. This may include requirements related to the functional performance (say criteria that tell you how good the device functions), but also requirements related to say mass, cost, reliability, etc. Next, one or more options are selected and analysed/sized to see what makes a feasible design, i.e. a design that fulfils the requirements. Of course, then a choice of the best system can be made considering all requirements. If no feasible design results, requirements may be adapted, and the cycle repeats itself.

The main steps in the actual sizing of an igniter as advised in this work is detailed in below list.

1. Establish main propellant (SRM) or fuel and oxidizer (LRE) flow rate(s);

2. Establish auto-ignition temperature of propellant mixture in combustion chamber; A lower temperature may also do, but for a first estimate auto-ignition temperature provides for a safe limit. For a lower limit, one should at least consider that the propellants need to be in a gaseous form and have a proper oxidizer-to-fuel ratio (see flammability limits) otherwise combustion is not feasible.
3. Determine enthalpy of propellant at initial conditions.
4. Determine rise in enthalpy needed for the virgin material to reach its auto-ignition temperature.
5. Determine needed heating power using information on motor or engine flow rates (see step 1).
6. Determine hot gas temperature of igniter gases/select igniter propellant O/F ratio.
7. Determine igniter propellant flow rate using earlier determined heating power and information on igniter hot gas temperature.
8. Select margin on igniter propellant flow rate; Need to make sure ignition is attained reliably under all foreseen conditions. Conditions usually are covered/defined in the ignition system operating conditions.
9. Factor in the burn time of the igniter and size igniter.
10. Test the igniter and validate its design.

13 Testing

Igniter design and development is still of a very empirical nature as adequate theoretical methods are lacking. This generally implies that considerable amount of test work is necessary leading to high cost and long development times. For example, [Boeing] performed a series of 41 tests to optimise the operational envelope of a H_2O_2/Kerosene torch igniter. Over 350-seconds of hot-fire duration over a wide range of mixture ratios and flow rates demonstrated reliable ignition and hardware tolerance of extreme thermal conditions. This igniter was then integrated into a main injector and main combustion chamber. Seven ignition tests successfully demonstrated the ability of the torch igniter to initiate sustained stable combustion of a H_2O_2-Kerosene injection main chamber under widely varying conditions.

Tests are usually conducted at three levels, being component tests, tests on the complete igniter, and tests with the igniter integrated into the motor. In addition, two types of tests should be distinguished, being development tests and tests aiming to characterise the design. Typically, development precedes characterisation.

Typically, initiators are tested to determine amongst others their sensitivity to an initiating impulse as well as to Electro-Magnetic Interference (EMI), Electro-Static Discharge (ESD). Igniter propellants are tested to determine flame temperature, regression rate (solids only), ignitability, ignition delay, heating value, gas content (absence of solids in combustion products), composition (toxicity) as well as their physical properties (including mass and size). For liquid propellants the parameters of interest are comparable. The igniter chamber is usually pressure tested to ensure that it will survive the igniter chamber pressure.

Typical igniter tests may include ignition test in free atmosphere, see Figure 16. Such tests may allow evaluating amongst other plume shape and/or the ignition behaviour, like ignition transient, of the igniter under various conditions, such as propellant temperature. To ensure safety, initial tests will be performed using so-called battleship igniter chamber casings. These have the same internal volume as the actual igniter but have much thicker walls to ensure structural integrity of the igniter. Once pressure levels have been verified the battleship casing is replaced by the actual casing. Other igniter tests may include tests to determine the igniters sensitivity to undesired external stimuli like EMI, (ESD), shock, etc., to determine sensitivity to ageing, etc.

Figure 16: Torch igniter firing test [SPL]

Tests with the igniter integrated into the motor aim amongst others on verifying ignition delay time and igniter pressure. This may include:

- Ignition tests in ambient, see e.g. Figure 16.
- ignition tests in a simulated volume without main propellant injection to verify amongst others leak tightness and motor pressure transient.
- ignition tests in a simulated volume with main propellant injection (LREs) and or with a reduced web of propellant/fuel simulating the initial burning surface of the grain and chamber free volume for instance to verify the ability of the igniter to ignite the propellant, see e.g. Figure 17 showing a nominal pressure evolution and Figure 10 showing a pressure evolution with a clear over-pressure spike.
- idem, but at (simulated) altitude (only in case the engine is to be ignited at altitude).
- Ignition tests in the actual configuration with the engine or motor operating over the full burn duration. This is to find out if any damage occurs to the igniter that could pose a problem for the proper working of the engine/motor.

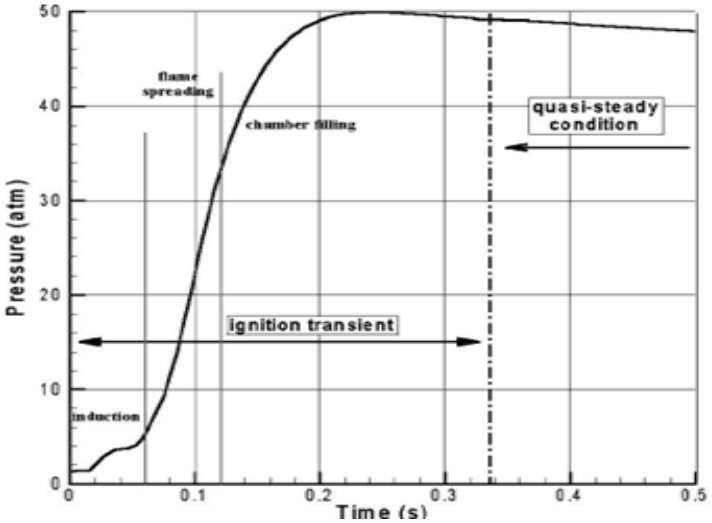

Figure 17: Pressure evolution during ignition [Univ. of Rome]

As mentioned earlier, pressure evolution/history plots are important outputs of any igniter test, next to for instance flame temperature, as it allows to check the proper sizing of the igniter. Figure 17, furthermore, shows the main phases distinguished in the ignition transient of an engine/motor including: 1) induction phase, wherein we see the action of the igniter until first ignition of the propellant grain, 2) flame spreading phase, wherein the flame spreads in the engine/motor up to the point full combustion is reached and 3) chamber filling interval wherein the chamber is filled with combustion gases and the equilibrium pressure is attained. To be able to distinguish these phases, it is important that prior to testing in a simulated volume first the igniter itself is characterized in the volume without the presence of the main propellants.

14 Problems

1. You are designing an igniter for a small SRM containing 3.25 kg of solid propellant in the form of a cigarette burning charge. The motor has an initial free volume of 126 cm^3, burn area at motor start is 48.2 cm^2 and maximum expected operating pressure is 1 MPa. You have selected a mixture of Boron and Potassium Nitrate as the main igniter charge. This mixture provides a combustion temperature of 2666 K. The fraction of condensed particles in the igniter exhaust is 0.2 and the molar mass of the gaseous exhaust is 56 g/mol. Critical pressure for ignition is 5 bar. Determine for this igniter the mass of the main charge using the free volume (FVM) and the critical pressure method (CPM).
2. You are designing a hydrogen-oxygen torch igniter capable of igniting a polyethylene-LOX HRM. Main chamber oxidiser mass flow rate is 150 g/s. Calculate the igniter propellant mass flow rate (O/F = 8) needed to heat up the oxidizer mass flow rate to a temperature of 1200 K in case the net heating value of hydrogen at 298 K is 119 MJ/kg. You may neglect the occurrence of heat loss.

Literature

1) Brauers, B., Goorden, B., Angelone, M., Gautronneau, E, di Vita, G., Qualification and Production of the VEGA Solid Rocket Motor Igniters, AIAA 2009-5322, 2009.

2) ATK, The Space Shuttle Reusable Solid Rocket Motor, ATK folder.

3) Barrère M, Jaumotte A., Fraeijs de Veubeke B., Vandenkerckhove J., Rocket propulsion, Elsevier Publ. Comp., 1960.

4) Barret D.H., Solid Rocket Motor Igniters, NASA SP-8051, 1971.

5) Boeing website, Boeing Successfully Tests Non-Toxic Rocket Propellants, April 25, 2002.

6) Boeing Aerospace Company, Inertial Upper Stage User's guide.

7) BPD, ESTEC-BPD technology program for solid motor, final presentation, ESTEC, September 1989.

8) Calzone R.F., Flammability limits of a solid fuel ramjet combustor, paper presented at ICAS, Beijing, 1992.

9) Castellini, F., Multidisciplinary design optimization for expandable launch vehicles, doctoral dissertation, Politechnico di Milano, 2012.

10) Coward H.F., Jones G.W., Limits of Flammability of Gases and Vapors, Part V: Summary of limits of flammability, Bulletin 503, Bureau of Mines, 1952.

11) De Yong, L.V., Smit, K.J., A Theoretical Study of the Combustion of Magnesium / Teflon / Viton Pyrotechnic Compositions, Materials Research Laboratory, MRL Technical Report MRL-TR-91-25, Springfield, Virginia, December 1991.

12) Encyclopedia Astronautica available via Encyclopedia Astronautica.

13) Fletcher E.A. and Morrell G., "Ignition in liquid rocket engines", in Progress in Combustion Science and Technology, volume 1, Pergamon Press, 1960.

14) Frenken, G., Vermeulen, E., Bouquet, F., Sanders, B., Development status of the ignition system for Vinci, AIAA-2002-4330, 38th AIAA/ASME/SAE/ASEE Joint Propulsion Conference, Indianapolis, Indiana, 2002.

15) GexCon, Gas Explosion Handbook, GexCon web site, 29 August 2005.

16) González-Blázquez A., Constanza A., First Test Tiring of an Ariane-5 Production Booster, ESA bulletin 104, November 2005.

17) Heslouin A., Simon P., Lengell E., Acute G., Foucaud R., Gibek I., Pillet N., Propulsion of Microsatellites by Hybrid Rocket Engines, Onera, France, 2002.

18) Humble R.W., Henry G.N., Larson W.J., Space Propulsion Analysis and Design, McGraw-Hill, 1995.

19) Huzel K.K., et al, Design of liquid propellant rocket engines, 2nd edition, NASA N71-29405-416, Washington, 1971.

20) Jonker W.A., Mayer A.E.H.J., Zandbergen, B.T.C., Development of a rocket engine igniter using the catalytic decomposition of hydrogen peroxide, 2006.

21) Jahannian H., Reusable Ignition System for Future European Launchers, M.Sc. thesis, November 2000.

22) Kuchta J.M., Investigation of Fire and explosion Accidents in the Chemical, Mining, and Fuel-related Industries - A Manual, US Dept of the Interior Bureau of Mines Bulletin 680.

23) Kuo K.K., Principles of Combustion, John Wiley & Sons, New York, 1986.

24) Laan F.H. van der, and Timnat Y.M., Chemical Rocket Propulsion, TU-Delft, Department of Aerospace Engineering, April 1985.

25) Salama A., Belal H., Abdalla H.M., Validation of relations for the determination of pyrotechnic igniter mass, 2020, IOP Conf. Ser.: Mater. Sci. Eng. 973 01200.

26) Salleh, Z., Hamid, A. H. A., Mohamed, W. M. W., Tamimi, A., Sujana, M. J., and Ahmad, K. A. (2021). Chemical Composition of Igniter for Ignition System in Solid Rocket Motor. International Transaction Journal of Engineering, Management, & Applied Sciences & Technologies, 12(9), 12A9P, 1-11. http://TUENGR.COM/V12/12A9P.pdf DOI: 10.14456/ITJEMAST.2021.184

27) Schmidt G., Technik der Flussigkeits-raketentriebwerke, DaimlerChryler Aerospace, 1999.

28) Sellers J.J., Meerman M., Paul M., Sweeting M., A Low-Cost Propulsion Option for Small Satellites, J. of the British Interplanetary Soc., Vol.48, pp.129-138, 1995.

29) SPL, Web site Swish Propulsion Laboratories, 29 August 2005.

30) Stork (a), Ignition Systems: VEGA Consumable Igniters, Stork Product Engineering BV, Amsterdam, The Netherlands.

31) Stork (b), Ignition Systems: Ariane 5 Vinci Ignition System, Stork Product Engineering BV, Amsterdam, The Netherlands.

32) Sutton G.P., Rocket Propulsion Elements, 6th edition, John Wiley & Sons Inc.

33) Timnat Y.M., Korting P.A.O.G., Hybrid rocket motor experiments, Report L-452, TU-Delft, Faculty of Aerospace Engineering, February 1985.

34) Torii Y., Sogame E., Kamijo K., Ito T, Suzuki K., Development status of LE-7, Acta Astronautica, Vol. 17, No.3, 1988.

35) University of Cambridge website, Chemistry, Auto-ignition Chemistry, http://www2.eng.cam.ac.uk/~cnm24/chemistry.htm, 29 August 2005.

36) Univ. of Rome, Mat. integrative corso “Endoreattori a Propellente Solido”, 2007.

37) Purdue, website:
http://roger.ecn.purdue.edu/~propulsi/propulsion/rockets/solids/orbus.html

38) Valk G.C. de, Zee F.W.M., Gadiot, G.M.H.J.L., HM-60 pyrotechnic igniters ignition improvement, AIAA 90-2084, July 16-18, Orlando, Florida, 1990.

39) Wilde J.P. de, Fuel pyrolysis effects on hybrid rocket and solid fuel ramjet combustor performance, DUP, 1991.

40) Yanagawa K., Fujita T. Katsuta H., Miyajima H., Development of LOX/LH2 engine LE-5, AIAA-1984-1223 (9 p.), SAE, and ASME, Joint Propulsion Conference, 20th, Cincinnati, OH, June 11-13, 1984.

Contents

1 Introduction 428

2 Types of thrust control and thrust control requirements 428

2.1 Thrust Magnitude Control requirements 429

2.2 Thrust Vector Control requirements 430

3 Thrust magnitude control options 431

4 Thrust vector control options 432

4.1 Deflection of jet exhaust 432

4.2 Deflection of engine or nozzle 435

4.3 Comparison of TVC techniques 438

5 TVC actuation systems 438

5.1 Dimensioning of TVC actuation system 441

6 Other controls 445

6.1 Start up and shut down control system 445

6.2 Mixture ratio control 446

6.3 Nozzle deployment control 446

7 About control loops 447

8 Problems 448

Literature 451

1 Introduction

The design of a rocket propulsion system is sometimes affected by considerations concerning the control of the system. Parameters that are controlled include engine/vehicle thrust, propellant tank pressure, and mass mixture ratio and nozzle extension deployment.

Thrust control is amongst others necessary to:

- Alter flight direction; Thrusting in the wrong direction or at the wrong time will cause a satellite to be placed in the wrong orbit.
- Reduce acceleration/launch loads. This is especially important towards the end of the flight, when the propellant tanks are almost empty.
- Control the attitude of the vehicle by rotating it about its vehicle axes.
- Compensate for thrust misalignment[1]. In case the thrust vector is not perfectly aligned with the nozzle axis it may cause the vehicle to be diverted from the planned direction. Most solid rocket motors are designed for a thrust misalignment less than 0.25 deg and a thrust offset of less than 0.5% of motor diameter [Knauber], [JPL].
- Compensate for engine out conditions.
- Counteract aerodynamic disturbance torques; For instance, wind gusts may cause the launcher to fly under an angle of attack different from zero, which may lead the vehicle steering off course if not counteracted upon.
- Provide mission flexibility: Freedom of starting and stopping the engine at any time including in emergency cases.

Next to thrust control, there may be a range of other control systems needed to control the operation of a rocket engine. Such systems may include a propellant tank pressurization control for controlling the tank pressure, a start-up and shut down control system to ensure a proper start up (valve sequencing) and shut down of the engine, a propellant utilization control system to ensure that all propellants are utilized in a proper way and a mixture ratio control system to ensure proper combustion chamber temperature and hence the performance (specific impulse) and the maximum material temperature. It is also important in terms of propellant utilization. More recently some engines are equipped with a nozzle extension control system to allow increasing specific impulse at high flight altitude and hence to reduce propellant mass.

In the following, we will discuss various methods for thrust control of rocket motors thereby focussing on system layout, system performance, and design considerations. Additionally, we will also pay attention to some of the other controls.

2 Types of thrust control and thrust control requirements

Two types of thrust control generally are distinguished:

- Thrust Magnitude Control or short TMC: A means of controlling the magnitude of the thrust force produced.
- Thrust Vector Control (TVC): A means to control the direction of the thrust force.

Reasons for thrust control whether TMC or TVC have been listed in the introduction. Thrust control functional requirements are usually generated based

[1] Thrust misalignment can be caused by that the centre of mass is offset or that the nozzle is tilted with respect to the rockets centre line or by asymmetrical flow. Asymmetrical flow can be due to oblique shocks inside the combustion chamber or to manufacturing inaccuracies. It is also possible that the flow is already asymmetrical inside the combustion chamber as may happen in a solid propellant rocket motor if the grain is not symmetrical. When designing a rocket motor, tolerances are set on the physical misalignment of the nozzle assembly. However, engine testing and/or computational modelling is needed to determine the magnitude of the misalignment.

on an analysis of the vehicle flight. Other requirements follow from a top-down analysis. In the next two sections, we will focus on the requirements relating to TMC and TVC.

2.1 Thrust Magnitude Control requirements

The degree of TMC required is usually expressed as a % of the nominal thrust. For instance, the Space Shuttle Main Engine (SSME) thrust can be throttled between 67 to 109% of rated/nominal thrust and the Lunar Module Descent Engine (LMDE) thrust can be throttled between 10-100% of rated/nominal thrust.

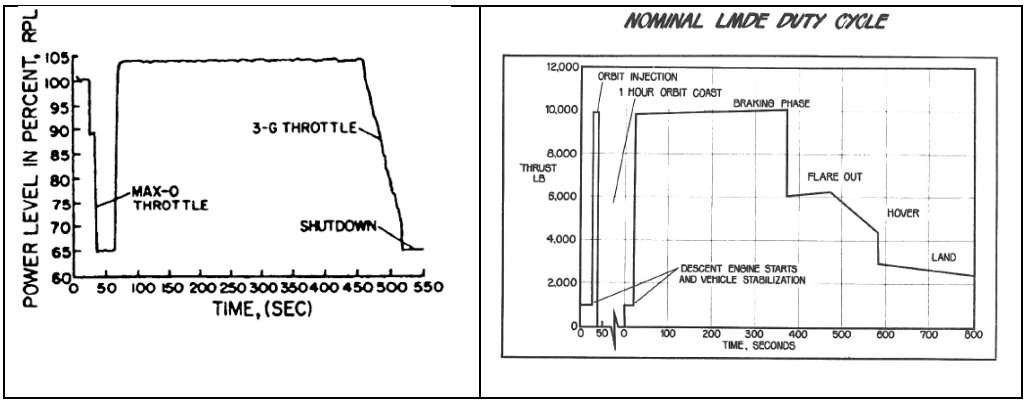

Figure 1: Thrust profile for SSME mission [Rockwell] and Lunar Module Descent Engine [Cherne]

Another important requirement related to TMC is the rate of change that should be realized. This determines the duration that it may take for an engine/motor to change the thrust level from one level to another. For instance, for the SSME, thrust level must be within steady-state limits within 1 second (see Figure 1, left figure) after a commanded change without rate of change exceeding 3.1 MN/s [Mitchell]

For fine attitude control, sometimes the thrust levels are too large to allow for continuous operation. In that case thrusters may be used in a pulsed mode for which the required duty cycle, see Figure 2, of the thruster should be known.

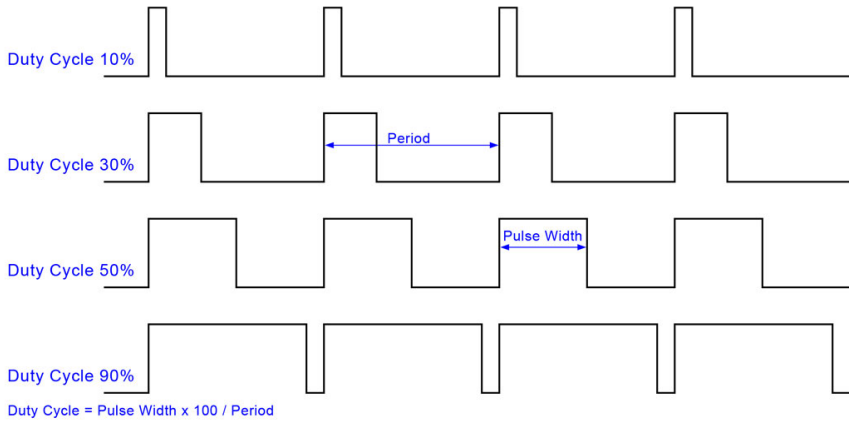

Figure 2: Definition of duty cycle

Duty cycle is typically characterized by stating the fraction of time it is active per cycle, i.e. the duty cycle percentage, see figure. Additionally, it may lead to requirements concerning the thrust rise and decay time of thrusters.

As indicated earlier, typical TMC requirements are derived from extensive flight analysis for which the propulsion engineer must rely on other experts, but once the requirements have been determined, he/she can start the design.

2.2 Thrust Vector Control requirements

The degree of TVC is usually expressed in degrees pitch, yaw, and roll and is derived from the necessary torques to rotate the vehicle about its vehicle axes. Once the torque and lever arm are known, the required side force can be determined and hence also the TVC angle.

Example: Consider a rocket experiencing an aerodynamic torque of 931 kNm that is to be counteracted upon by TVC. Given is that the lever arm of the horizontal force (perpendicular to the rocket axis) provided by the TVC system is 14.5 m. It follows that the TVC system should provide for a horizontal force F = 931 kNm / 14.5 m = 64.2 kN. Given that the nominal axial force is 1 MN, it follows a TVC angle of 3.67 deg.

Table 1 presents TVC angle requirements for various disturbances working on the vehicle including wind, thrust misalignment, etc. and to carry out the pitch program needed to steer the vehicle along its trajectory.

Table 1: Thrust vector deflection angle requirements for gimballed nozzle TVC system [Daniele]

Parameter	Variation	Vehicle
		260 (3.4)/ MS-IVB
1. Steady-state winds	90 percent	1.32
2. Steady-state winds with biased pitch programs[a]	90 percent	.79
3. Wind gusts[b]	3σ	.20
4. Thrust misalinement	3σ	.40
5. Thrusts and weights	3σ	.08
6. Pitch program	Maximum	.73
7. Winds at pitchover without biased pitch programs		.18
Total[c] 1		1.78
Total[d] 2		1.25
Total[e] 3		1.31

[a] 60 percent of steady-state winds.
[b] 15 percent of steady-state winds.
[c] Total consists of item 1 plus root sum square of items 3, 4, and 5.
[d] Total consists of item 2 plus root sum square of items 3, 4, and 5.
[e] Total consists of sum of items 4, 6, and 7.

Next to thrust vector deflection angle also requirements are set for rotational acceleration rate and angular velocity. The former determines how quickly a pre-set angular velocity is reached, which in turn determines the time needed to rotate over some angle. Most of the time the acceleration levels are selected thus high that acceleration/deceleration time is negligible compared to total manoeuvre time. As an example, and to allow to get a feel for order of magnitude, a set of requirements specific to the Space Shuttle main engine can be found in the next table.

Parameter	SSME	Large 260 in SRM	Space Shuttle SRB
Angular capability	+/- 12.5 deg	+/- 1.5 deg	+/- 5 deg
Angular velocity (min/max)	10/20 deg/s	3 deg/s	3 deg/s
Angular acceleration (max)	30 rad/s^2	0.139 rad/s^2	≥ 2 rad/s^2

Table 2: TVC requirements for Space Shuttle Main Engine [Sutton], large 260-inch Solid Rocket Motor [Pelouch], and Space Shuttle Solid Rocket Booster [Verble].

3 Thrust magnitude control options

Thrust magnitude control (TMC) allows for intentionally varying the thrust level. The simplest solution is most probably having multiple chambers/engines and switching them on/off. Figure 3 shows Stentor motor as used in Blue Steel air to ground missiles. Blue Steel used a small and large chamber; both for climb, but the small chamber also for cruise.

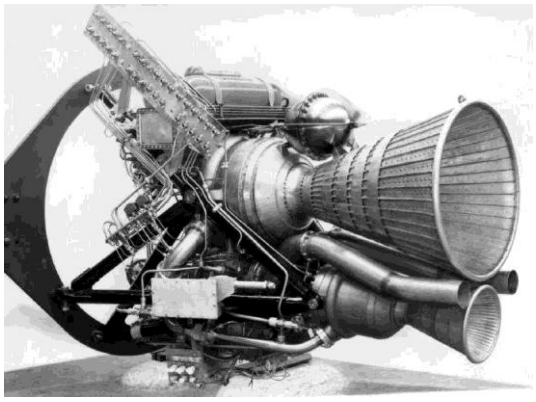

Figure 3: Stentor motor (from www.spaceUK.org)

A similar arrangement has been used on the Atlas rockets. The first stage is equipped with two booster engines and a sustainer engine. During ascent, the two booster engines are shut off and separated, whereas the sustainer engine continues its burn. A similar approach is also used on the reusable Falcon 9 rocket which has 9 engines on its first stage, but during the final stages of the landing of the reusable first stage only 3 engines are firing.

Another option is to vary the thrust produced by a single engine. For liquid rocket engines, thrust can for instance be adapted by throttling the flow rate of the propellants. This can be accomplished using flow control valves or a governor valve that controls the amount of turbine drive gas that flows to the turbo-pumps (see also section on feed system design). A drawback is that as mass flow changes, care must be given to that chamber pressure does not drop below a critical value as it may cause irregular combustion and even extinction [Casiano]. Fixed-geometry injectors allow for a throttling ratio of 2:1 or even 3:1, but for deep throttling other measures are considered like the use of a variable-area-injector. This allows for varying the injection area so that near-optimum injector pressure drops and propellant velocities are maintained at each thrust level. The addition of moving parts though leads to a more complicated design.

For solid propellant rocket engines, to vary the thrust produced by a single rocket motor a different approach is required. Thrust control is realized by for instance varying the throat area by means of a pintle. This is a conical rod with which the area of the throat can be regulated, Figure 4.

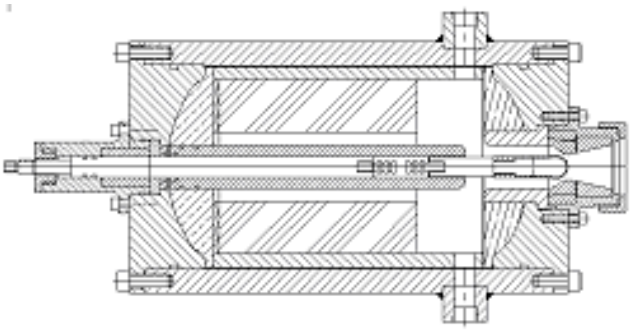

Figure 4: Solid rocket motor with pintle nozzle TMC

When the nozzle throat area and the propellant flow can be controlled independently, the chamber pressure can be maintained fairly constant, and the thrust is almost proportional to the throat area. This probably implies the use of an elaborate system of pumps. In the absence of such an elaborate system, the variation in throat area has a feedback effect on the propellant flow rate. Disadvantage of using a pintle is that it may be subject to severe erosion. Typical candidate material is graphite, as it is very erosion resistant, but also very sensitive to cracking.

Key pintle design issues include:
- Performance/Analysis - Shocks and separation zones mandate a Computer Fluid Dynamics (CFD)-based analysis approach.
- Controls - Fast pintle response requires complex control strategy to avoid thrust "spikes".
- Actuation - The mechanism should be lightweight and powerful enough to move pintle against aerodynamic forces.
- Materials - Materials should be light weight and able to withstand the severe environments without excessive erosion.

4 Thrust vector control options

Moving the thrust vector through small angles for vehicle stability and maneuvering is called Thrust Vector Control (TVC).
There are two ways by which TVC can be achieved:
1. Deflection of (part of) the jet exhaust.
2. Deflection of complete motor, nozzle or part of the nozzle.

These methods will be discussed in more detail below.

4.1 Deflection of jet exhaust

The two primary methods of producing lateral thrust with a fixed nozzle include mechanical interference (MITVC) and secondary injection (SITVC).

Mechanical Interference
Various methods of deflecting the jet exhaust by mechanical means can be distinguished (Figure 6):

a. Jet vanes, i.e. airfoils (rudders), placed in the exhaust flow. Jet vanes have amongst others been used in the V2, Redstone and Scout rocket. Most applications have only limited to short duration (well below 100 s, depending on temperature in jet exhaust) burn motors.

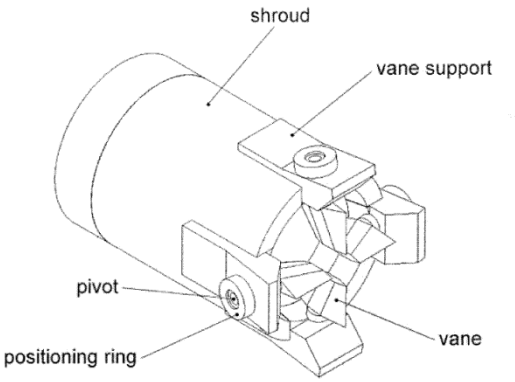

Figure 5: Schematic of jet vanes used for TVC

b. Jetavator, i.e. an aerodynamically contoured ring around the nozzle. Amongst others applied on Polaris rocket and Bomarc booster. Two jetavator rings that are pivoted allow control in pitch, yaw and roll direction.
c. Jet tabs that produce a strong shock, which in turn induce an oblique shock in the nozzle. It simply is a plate located at the nozzle exit that blocks part of the nozzle exit. Jet tab TVC is primarily used on solid rockets that have a short burn time.
d. Probes disturbing the flow inside the nozzle (like the jet tabs), but located more upstream, whereas jet tabs are located at the nozzle exit. Probes have been primarily used on small rocket motors in relation to high TVC angles.

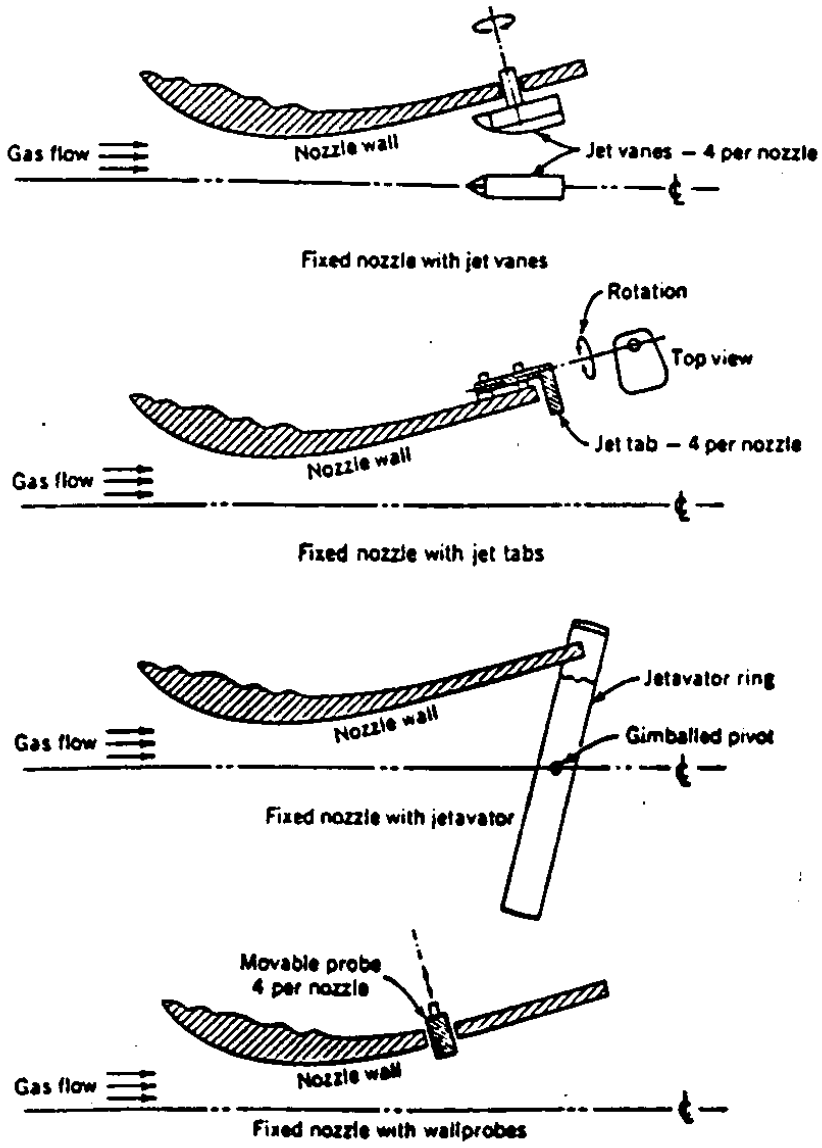

Figure 6: Fixed nozzle TVC devices that mechanically deflect the flow (Mechanical Interference TVC)

Figure 7 shows typical TVC deflection angle and side force ratio versus blockage area ratio for jet tab TVC [Pelouch]. The figure clearly shows a linear relation between deflection angle and blockage ratio.

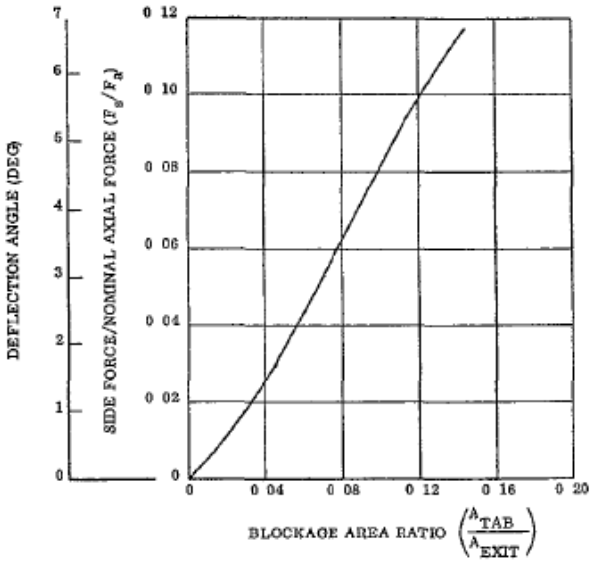

Figure 7: Typical TVC Angle and Side Force Ratio vs Jet Tab Blockage Area Ratio:

Mechanical interference devices all work along the same line: a) they deflect the flow, thereby producing a side force and b) they block the flow thereby decreasing axial thrust. When improving the aerodynamic shape of the mechanical interference, like for jet vanes, the smaller the decrease in axial thrust.

Secondary Injection

Secondary injection of fluid into the nozzle causes local shock waves, resulting in an asymmetrical flow (Figure 8). The fluid used is either hot gas from the combustion chamber or a liquid or gas stored in a separate tank.

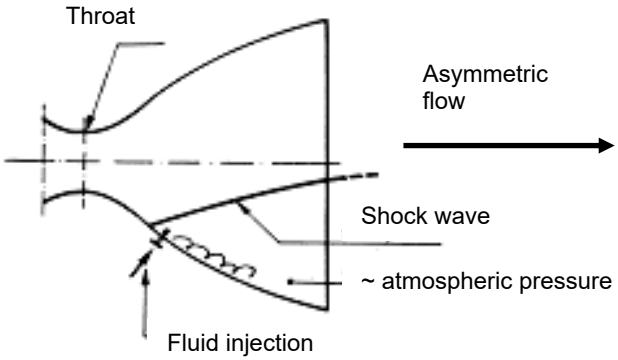

Figure 8: Secondary injection TVC (SITVC)

[Sutton] provides data on the TVC performance that is typical of inert and reactive liquids and hot gas (solid propellant combustion products).

SITVC is used on amongst other US Titan 3 and early Titan 4 solid strap-on boosters. For both Titan 3 and early Titan 4 solid strap-on boosters, liquid nitrogen-tetroxide is injected into the jet exhaust via selected nozzles (out of 24 available around the circumference of the motor nozzle's exit cone), which provides for a thrust vector control, (TVC) of about three degrees (.0524 rad). The total system mass is about 7.1 tons of which the injectants make up about 3.8 tons (stored in a tank about 8.5 m long and 1.1 m diameter). Dry system mass of the TVC injection system is around 3.3 tons [Backlund]. Injection ads about 17.8 kN thrust to each Titan 3 strap-on [Jane's]. More recently [Glen Case] reported a design study of SITVC for a hybrid rocket motor.

An advantage of SITVC is that there is no time limitation. The method works if an injectant is available. Another advantage is that unlike for MITVC axial thrust does not decrease but instead may increase because of the increased mass flow in the jet exhaust. A drawback of SITVC is that a considerable flow of injectant is needed to realize the required side force. Typical values for inert liquids, reactive liquids and propellant hot gas are given in Figure 9.

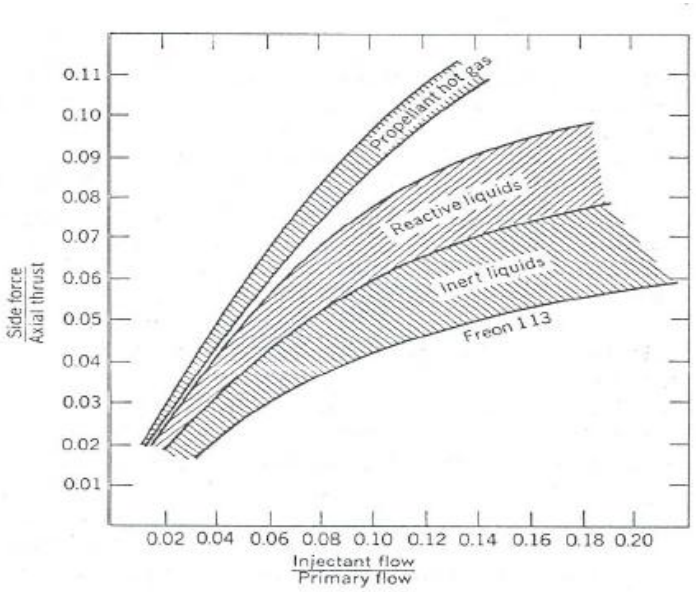

Figure 9: Performance characteristics of different injectants [Sutton]

4.2 Deflection of engine or nozzle

By means of a hinge or gimbal[2], the whole engine (assembly of thrust chamber and turbo-pumps) is pivoted on a bearing and, thus, the thrust vector is rotated, Figure 10. It requires flexible propellant lines (bellows) to allow the propellant to flow from the tanks of the vehicle to the thrust chamber. It also requires robust gimbal-mounted bearings to share the full thrust load.

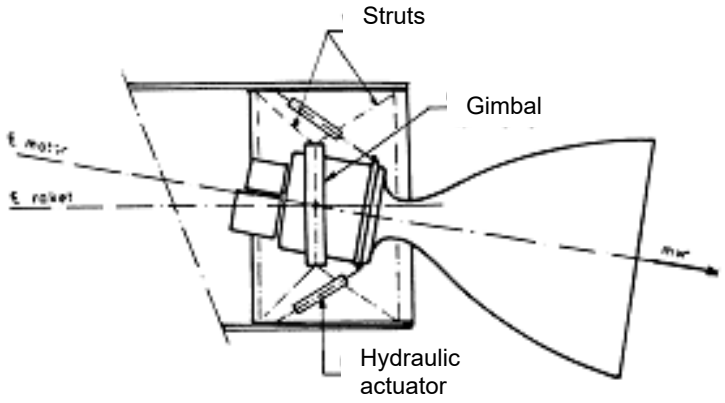

Figure 10: TVC by gimballing of the whole thrust chamber

The gimbals used in rockets most often use hydraulic actuator systems to adjust the direction of the engine. They must be able to adjust a heavy rocket engine (hundreds to thousands of kilograms) that is producing hundreds to hundreds of thousands of Newtons of thrust. Specific performance data of some gimballed engines are given in Table 3. Figure 11 shows Gamma 201 Black Knight engine bay, with its 4 chambers. Each chamber could swing in a radial direction - i.e., inwards and outwards - and used in combination, could control the vehicle in any plane.

[2] A hinge permits rotation about one axis only, while a gimbal is essentially a universal joint.

Table 3: TVC properties of specific gimballed rocket engines [Jane's] and [Sutton]

Engine	Space Shuttle Main Engine	Ariane 5 HM-60 (or Vucain)	H2 LE-7
Vacuum thrust	2091 kN	1145 kN	1078 kN
Engine (dry) mass	3177 kg	1475 kg	1714 kg
Maximum diameter	2.39 m	1.76 m	1.80 m
Gimbal angle	±10.5° for pitch/yaw	±6° for pitch/yaw	±7.5° for pitch/yaw
Angular acceleration	30 rad/s^2	Not available	Not available
Angular velocity (max)	20 deg/s	Not available	Not available
Actuation	Hydraulic	Hydraulic	Hydraulic

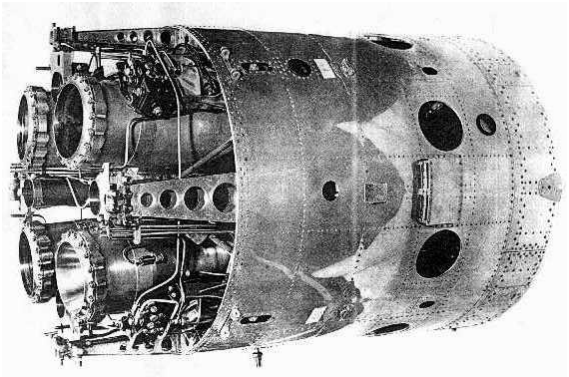

Figure 11: Black Knight Gamma 201 engine (from www.spaceUK.org)

Figure 12 shows Soyuz rocket with “Vernier” rockets, i.e. small rockets mounted on the outside of a larger engine that use their thrust to help direct a larger rocket in flight. Usually, they are fed by the gases that result from a gas generator feeding the turbo-pump or that are bled off from the main thrust chamber.

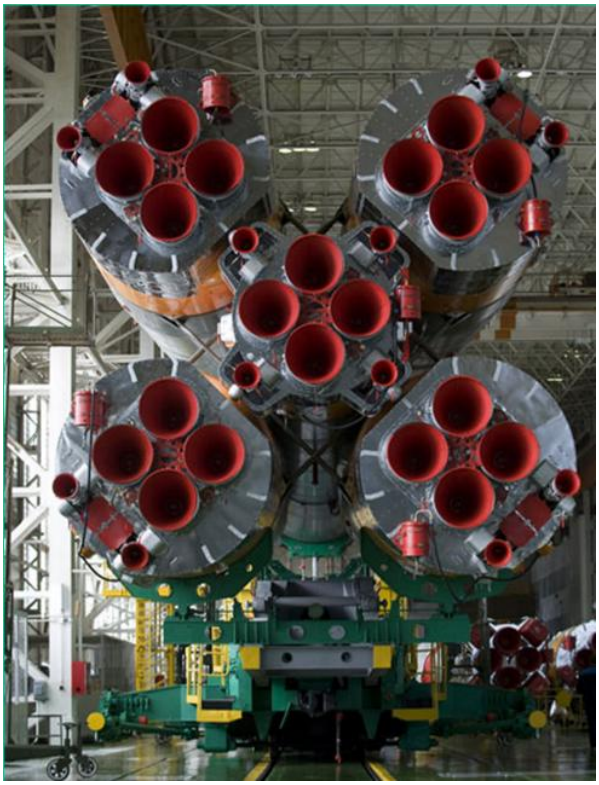

Figure 12: Soyuz rocket with Vernier rockets for TVC

Rotating the complete thrust chamber is not suitable for solid-propellant rocket motors. For such motors mostly only the nozzle or part of the nozzle is rotated, as is shown in Figure 13.

Specific performance data of specific rocket engines equipped with a flexible nozzle are given in Table 4.

Table 4: TVC properties of specific rocket engines equipped with a flexible nozzle [Jane's], [Sutton], [ATK]

Engine	Ariane 5 P230 solid rocket booster	Orbus 21/6/6E	STAR 48 V
Thrust	5.3 MN (S.L.)	195.7/81/81 kN (vacuum)	66 kN (vacuum)
Nozzle mass	6.1 ton	Not available	52.6 kg
Nozzle exit diameter	2.83 m	1.32/0.75/1.44 m	0.75 m
Nozzle deflection	±6° for pitch/yaw	±4°/7°/7° for pitch/yaw	±4° for pitch/yaw
Nozzle rotational rate	Not available	20°/s	30°/s
Actuation	Hydraulic (1100 litre @ 300 bar pressure)	Electro-mechanic (>900 W peak)	Electro-mechanic
System mass	Actuator system: 180 kg Hydraulic system: Not Available	22.4 kg (5.9 kg controller, 7.0 kg actuator, 1.2 kg potentiometer)	~10 kg

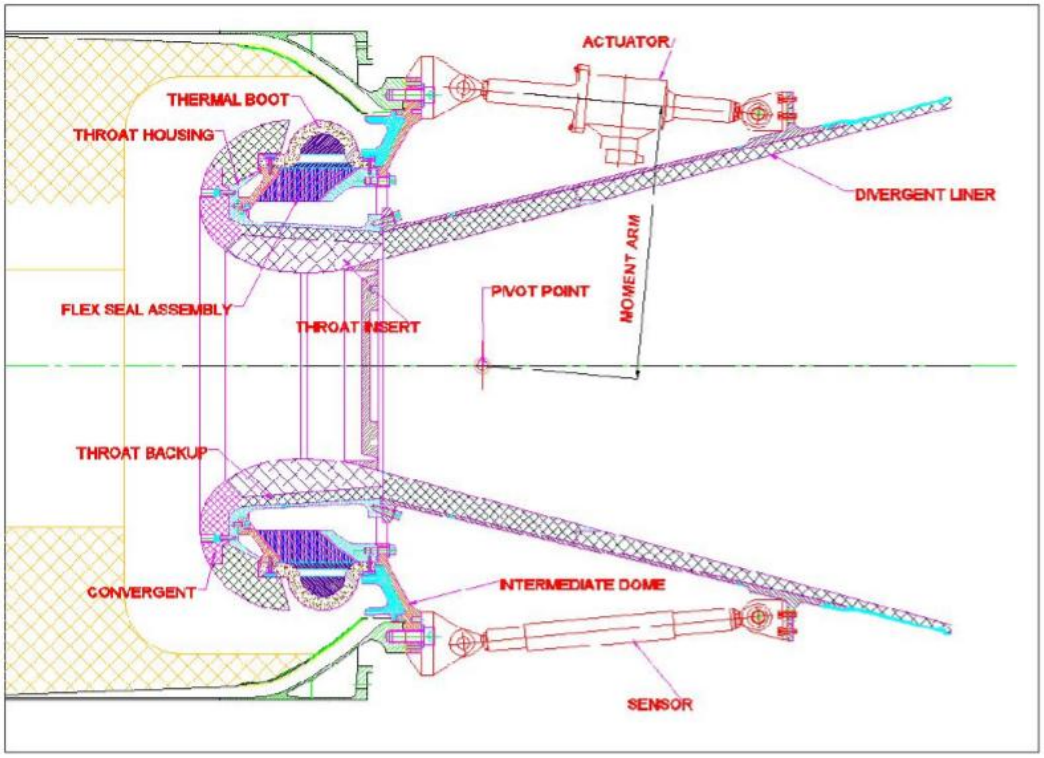

Figure 13: Typical movable nozzle with flex seal and thermal boot protecting the flex seal [Shodhganga]

Key gimbal or hinge design issues include:

a. Required pivotal movement of thrust chamber/ engine assembly or nozzle for TVC. - Typical range is 4-10 degree.
b. Required rotational rate.
c. Required adjustment to allow for compensating thrust misalignment.
d. Thrust level. - This determines the structural and bearing designs of the gimbal or hinge mounts.
e. Propellant ducts installation.
f. Actuation - Mechanism should be lightweight and powerful enough to move engine/nozzle against aerodynamic forces and to overcome inertia and friction forces.

g. Materials - Materials should be light weight and in case the hinge or gimbal is exposed to the hot exhaust gases able to withstand the severe environments without excessive erosion.
h. Lubrication

4.3 Comparison of TVC techniques

Literature can help to get an impression of the advantages and disadvantages of the various TVC techniques so that a comparison can be made and the most promising concepts can be worked out in further detail. As an example, Table 5 provides a comparison of various techniques/methods discussed in the foregoing with respect to the extent in which the jet can be deflected, and the effect on (axial) thrust generated.

Table 5: Performance comparison of TVC techniques (adapted from [Ambrosius])

Technique	**Method**	**Jet deflection angle (up to)**	**Axial thrust (effect on)**
Moving engine	Gimballed engine	10.5	Cosine effect
Moving nozzle	Flexible nozzle	15	Cosine effect
	Ball and socket nozzle	25	Cosine effect
Secondary fluid injection	Liquid injection (inert)	7	Augmentation
	Hot gas injection	12	Depends on duty cycle
Mechanical obstructions	Jetavators / jet tabs	30	10% without actuation, 20-25% with actuation
	Domed deflector	18	0.5% per degree deflection

Mechanical obstruction devices, like vanes, tabs, jetavators or probes need to be heat resistant and suffer from constant erosion, which may lead to reduced effectiveness in time. Furthermore, drag losses will cause the magnitude of the thrust to decrease. Nowadays, mechanical obstructions are mostly used on small solid rocket motors.

A more detailed comparison of various TVC options applied to a 260 in (6.6 m) large solid rocket booster providing an average vacuum thrust of 33 MN and an action time of 143 s is reported in [Pelouch]. The study showed that Mechanical Interference TVC is inferior to SITVC and movable nozzle. The total preliminary weight estimate of a jet tab TVC system, including the baseline nozzle, was 39,200 kg compared to 37,200 kg for LITVC and 25,700 kg (including about 400 kg for the actuation system) for the movable nozzle of which 16,847 kg insulation and 7681 kg structure. The baseline fixed nozzle had a mass of 21,747 kg (17,305 kg insulation and 4.442 kg structure). From these numbers, it follows that adding TVC increases motor mass with about 20% for a movable nozzle, 70% for LITVC and 80% for MITVC systems. [Kesteren] found that for small rocket motors (vacuum thrust ≤ 200 kN) adding TVC almost doubles the motor mass.

5 TVC actuation systems

Once the requirements are known and a feasible option has been selected a more detailed design can be made. This may include the selection of the pivot point, see later, and the determination and design of the actuation system. This will be discussed in more detail hereafter.

Most actuation systems used nowadays for moving the engine or nozzle use linear[3] actuators. These actuators are usually of a hydraulic mechanical or electromechanical nature with electronic components especially designed for the application providing the required signals for precise positioning of components.

The most conventional TVC actuation system is a warm gas generator powering a turbine gear box hydraulic pump arrangement. Figure 14 shows one unit (of two) of the hydro-mechanical system used for actuating the Space Shuttle SRB TVC system [Redmon]. “Each SRB has two self-contained hydraulic power units. The purpose of the SRB hydraulic system is to supply the required hydraulic flow and pressure to extend and retract the actuator piston. The end of the piston is attached to the nozzle of the solid rocket motor to provide thrust vectoring during the mission”. Each HPU consists of an Auxiliary Power Unit (APU), Fuel Supply Module (FSM), hydraulic pump, hydraulic reservoir and hydraulic fluid manifold assembly.

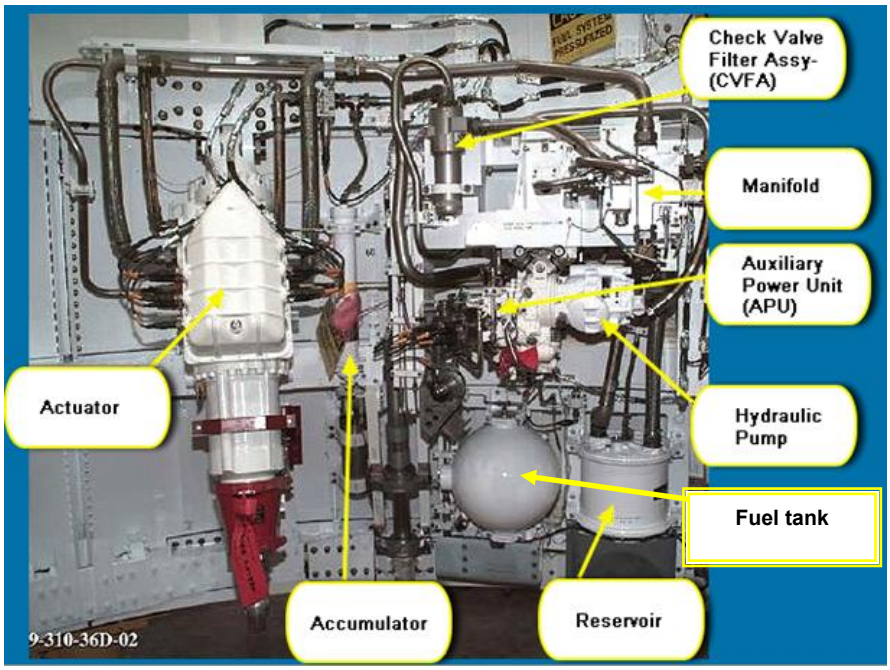

Figure 14: Space Shuttle SRB TVC hydro-mechanical actuation system layout (1 of 2)

The APUs and their fuel systems are isolated from each other, with each FSM (tank) containing 10 kg (22 pounds) of hydrazine. The fuel tank is pressurized with gaseous nitrogen at 27.5 bar (400 psi), which provides the force to expel (positive expulsion) the fuel from the tank to the fuel distribution line, maintaining a positive fuel supply to the APU throughout its operation. The APU turbine assembly provides mechanical power to the APU gearbox, which drives the APU fuel pump, hydraulic pump and lube oil pump. The turbine exhaust of each APU flows over the exterior of the gas generator, cooling it, and is then directed overboard through an exhaust duct. Each HPU on an SRB is connected to both servo-actuators on that SRB via the manifold. One HPU serves as the primary hydraulic source for the servo-actuator, and the other HPU serves as the secondary hydraulics for the servo-actuator. The APU 100-percent speed corresponds to 72,000 rpm, 110-percent to 79,200 rpm, and 112-percent to 80,640 rpm. The purpose of the accumulator is to provide reserve hydraulic power at times when the hydraulic pump cannot meet system demand (load spikes) and to provide damping when transients are encountered.

[3] Linear actuators move an object or piece of equipment in a straight line. They can be designed to move an object extremely accurately and repeatably if required. Most linear actuators work by converting rotary motion from an electric motor into linear motion via a ball screw or a belt.

More recently, EMAs (Electromechanical actuators) have become attractive candidates to replace hydraulic actuators for TVC, thanks to easier implementation and lower maintenance requirements, but also because of a substantial reduction in system mass. Figure 15 shows VEGA rocket TVC electromechanical actuation system. The system consists of Li-ion batteries providing the necessary power, a controller and power distribution unit (see photo on far right), a cable harness for power distribution and telemetry, and two electromechanical actuators (see actuator shown on photo in middle). Figure also shows some data for characteristic actuator parameters. These parameters will be discussed in more detail in the next section.

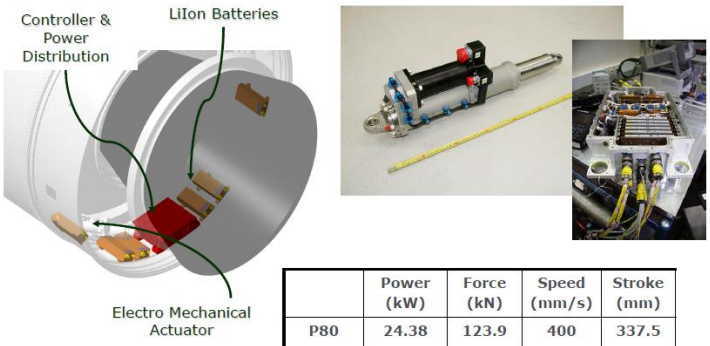

	Power (kW)	Force (kN)	Speed (mm/s)	Stroke (mm)
P80	24.38	123.9	400	337.5
Z23	14	34.9	300	221
Z9	2.576	21.5	126	124

Figure 15: Vega TVC electromechanical actuation system [Vanthuyne]

Figure 16 shows schematic of electro-mechanical actuator and controller.

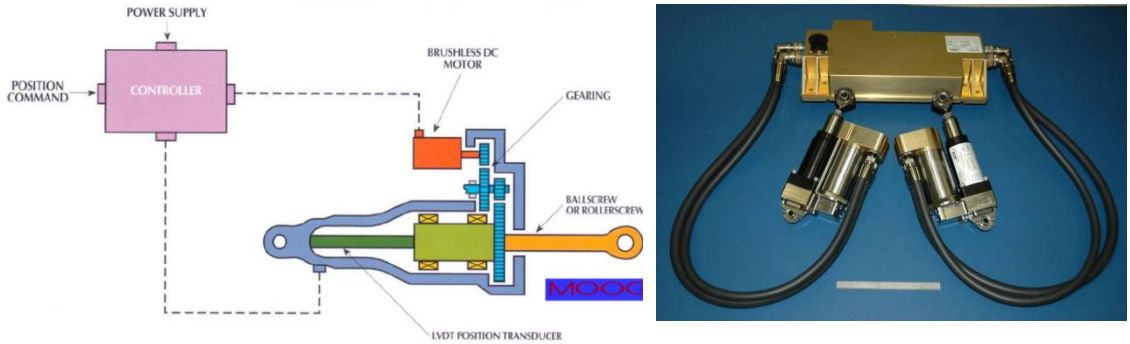

Figure 16: Schematic of electromechanical actuation system (left; courtesy Moog) and two channel linear output electromechanical actuation system (right, courtesy ATK) as used on modern TVC controlled Solid Rocket Motors

Important is to note the DC motor that is part of the actuator and provides for the necessary torque to actuate the ball or roller screw via a gear box. Also indicated in the schematic is the gear box as well as instrumentation needed to provide feedback on the position of the actuator. Figure 17 provides for a typical electromechanical actuator. Clearly visible is the roller screw, the electric motor on top and the two end the two end mounts with ball and socket to ensure proper alignment. A good review article is available from [Qiao et al].

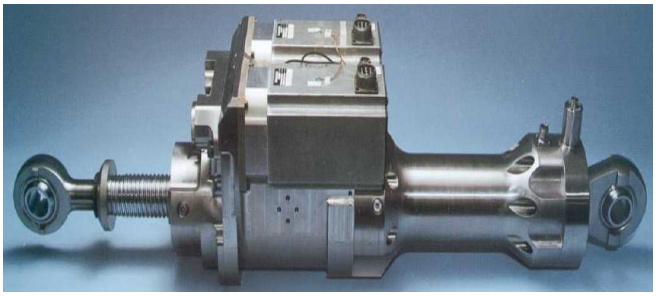

Figure 17: Electromechanical actuator with DC motor on top (courtesy Moog)

5.1 Dimensioning of TVC actuation system

The dimensioning of a TVC system depends on the type of system considered. Here we will focus on systems equipped with a movable nozzle or engine. The schematic of such a system with a rotary actuator is shown in Figure 18. A system equipped with linear actuators is shown in Figure 10.

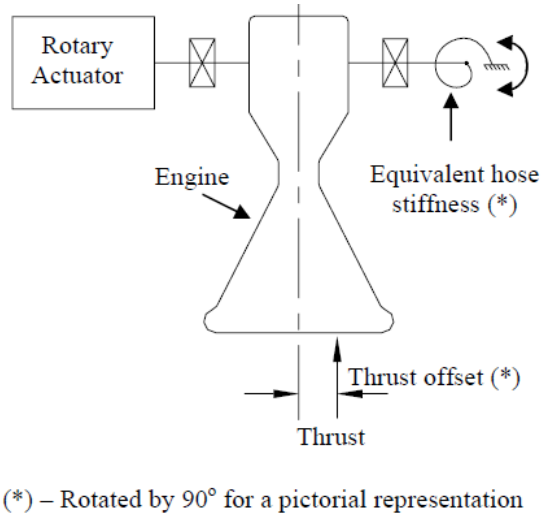

Figure 18: Sketch of TVC system for gimballed engine (depicted is rotation about single axis)

The system essentially consists of a (rotary or linear) actuator that allows for rotating the engine in two directions perpendicular to each other by providing the necessary torque.

Typical requirements related to TVC deal with:

- Angular capability or maximum TVC deflection angle: Sets maximum angular range for the TVC system both in “+” and “-“direction.
- Angular velocity: Determines the time needed for attaining a certain rotation angle.
- Angular acceleration: Sets the time it takes to reach a certain angular velocity. High value of angular acceleration ensures that engine rotation can be approximated as a constant velocity rotation

For instance, for the SSME the following requirements have been considered [Sutton]:

- Angular capability: +/- 12.5 deg
- Angular velocity (max.): 20 deg/s
- Angular velocity (min.): 10 deg/s
- Angular acceleration (max.): 30 rad/s^2

Example: Based on a constant angular acceleration of 30 rad/s², it follows that the SSME attains an angular velocity of 20 deg/s within 12 ms. In the same timeframe the SSME travels over an angle of 0.23 deg. It also follows that it takes about 0.64 s for the SSME to travel from a 0 deg deflection to its maximum deflection of 12.5 deg (including the time needed to bring the SSME to standstill at maximum range).

The angular acceleration together with the engine/nozzle mass moment of inertia about gimbal/hinge axis determines the inertia torque that needs to be provided by the actuation system. For a constant acceleration motion about a fixed axis, it follows for the inertia torque:

$$T_{Inertia} = I \times \alpha \tag{5-1}$$

Here I is mass moment of inertia of movable engine/nozzle and α is angular acceleration applied.

Besides the inertia torque, the torque needed for actuation (per direction) also depends on:

- Friction torque
- Thrust offset
- Spring torque (in case of an elastomeric joint or flexible feed pipes)
- External aerodynamic torque (due to the external air flow about the engine/nozzle)
- Gravitational torque
- Torques due to disturbances from launcher acceleration loads
- Torques due to internal flow aerodynamics

Figure 19 shows torque values estimated for various components relevant to the design of the TVC system of a large SRM. The figure also shows that the torque requirement varies in time with the changing flight conditions and the change in TVC angle (see change in spring torque, both seal and boot spring torque).

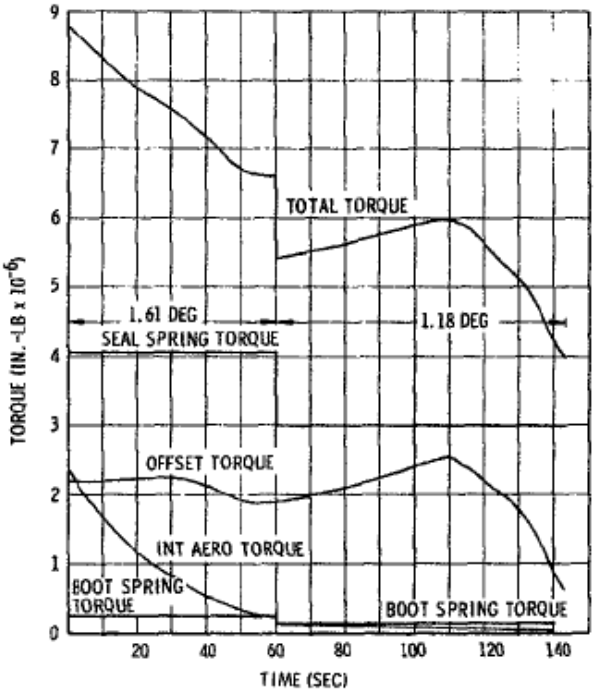

Figure 19: Torques for SRM TVC [Nickels]

An important issue in the design of a TVC system for a movable engine/nozzle is the position of the pivot point.

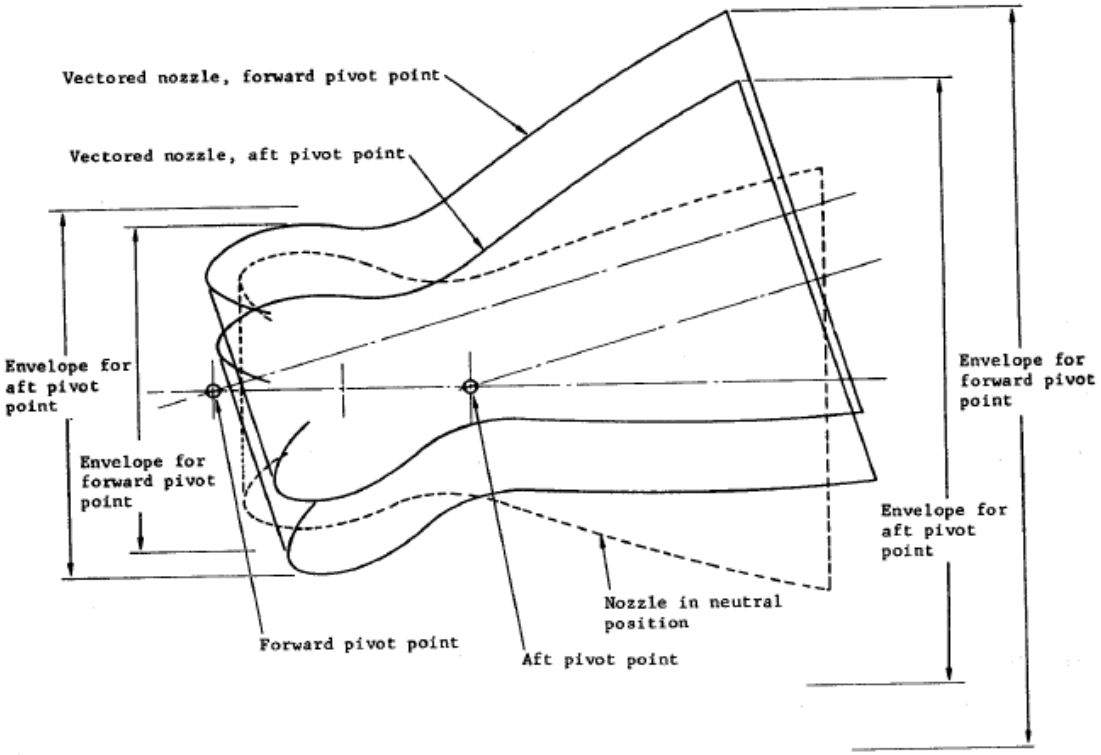

Figure 20: Alternative pivot points [NASA SP-8114]

Figure 20 shows the effect of a change in pivot point on the motor envelope needed for TVC. Clearly a forward pivot point requires a larger envelope at engine aft than an aft pivot point. Next to envelope, the position of the pivot point also affects the inertia torque as a forward pivot point undeniably leads to a much larger mass moment of inertia about the pivot point as compared to the aft pivot point. For instance, for a thrust chamber of mass 217 kg, it is estimated a mass moment of inertia about its Centre of Mass (axis perpendicular to thruster axis) of 250 kg-m^2, whereas when taking the MMOI about a forward pivot point (0.1 m in front of chamber), it follows an MMOI of 610 kg-m^2. The forward pivot point also leads to much higher gravitational torques to be overcome, whereas selecting an aft pivot point allows for a much more balanced design. One can also reason that a forward pivot point leads to larger aerodynamic torques on the engine, depending on whether an engine skirt is available or not.

Once we know the torques that work on the system, we can start the design of the actuation system. Here we will focus on the design of a linear actuator system.

The design of a linear actuator depends upon three parameters: force, stroke, and linear rate. The force ($F_{actuator}$) is derived from the nozzle torque and actuator geometry.

$$\text{Nozzle (total) torque} = F_{actuator} \times a \tag{5-2}$$

Important parameters for sizing the force are the lever arm (a) and the angle the actuator makes with the lever arm, see Figure 10. The stroke of the linear actuator can be readily determined from the required nozzle vector angle and the lever arm. Here we should consider the two extreme positions of the nozzle/engine.

Velocity at which the linear actuator moves determines on one hand the rotational velocity of the engine/nozzle, on the other hand it also determines to a large extend the power to be exerted on the actuator. Mechanical power P essentially follows from:

$$P_{actuator} = F_{actuator} \times v_{actuator} \tag{5-3}$$

Here F refers to the actuator force and v to actuator linear velocity. Actual input power generally is larger due to e.g. friction losses, etc. Example performance data are given in Table 6.

Table 6: Actuator performance characteristics (courtesy Moog)

Output Travel…….+/- 5.5 in	Impulse Load ….. 100,000 lb
Stall Force ……55,000 lb	Acceleration……..60 in/sec^2
Rated Power……..38 HP	Duty Cycle……10 min
Output Force……..48,000 lb	Average Load…15,000 lb
Output Velocity…..5.2 in/sec	Supply Voltage….270 VDC
Full Performance with one motor	MOOG

From the above table we learn that the stroke is +/- 0.14 m. Stroke should be added to null length of actuator to determine length of actuator when fully extended. Nominal (average) load is about 1/3rd of output force. Output force (short duration only) is 213.5 kN (48,000 lb) and output velocity is 0.132 m/s (5.2 in/s). This gives an ideal actuator power of 28.2 kW (~38 HP). Data also shows a linear acceleration of 1.5 m/s^2 which indicates that an actuator reaches rated output velocity in less than 0.1s. Stall force (force in case output velocity is zero m/s) is about a factor 1.2 higher than the output force. A typical DC motor characteristic is shown in Figure 21.

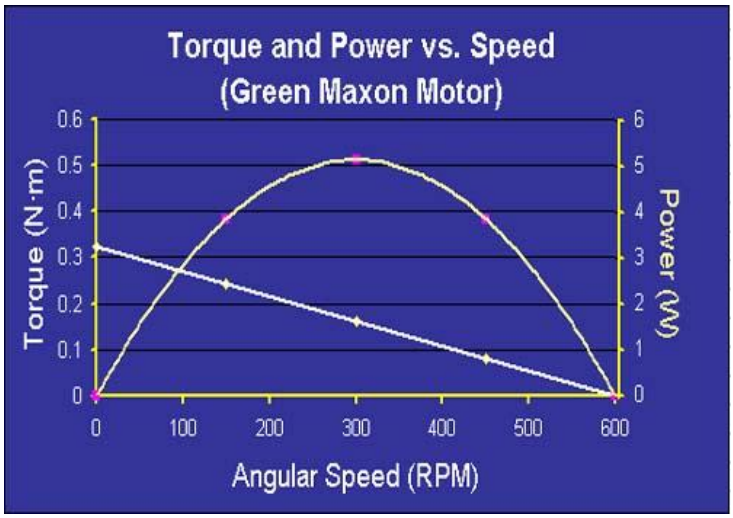

Figure 21: DC motor output characteristic

From this motor characteristic, we learn that torque is linearly dependent on angular speed and that power usage has a maximum at about half maximum speed. One can also see that power increases about linearly with angular speed up to about 1/3rd of zero load speed. Torque at zero speed is referred to as stall torque, whereas speed at zero torque is referred to as zero load speed.

Adding a TVC system of course adds to the total mass of a rocket engine/motor. Figure 22 shows ATK Star 48 B motor with and without TVC system. Clearly the

additional items ensuring proper TVC can be seen in the figure on the right. According to ATK data [ATK], motor inert mass has grown from 131.4 kg to 154.1 kg; an increase of 22.7 kg. Of this total inert mass increase, part is because of the addition of the controller and actuators (power supply not included as this is supplied by the vehicle), and part (8.8 kg; Fixed nozzle mass is 43.8 kg and flexible nozzle mass is 52.5 kg because of a redesigned nozzle suspension system. This increase of about 20% in nozzle mass agrees nicely with the value obtained for the 160-inch SRM flexible nozzle mass increase.

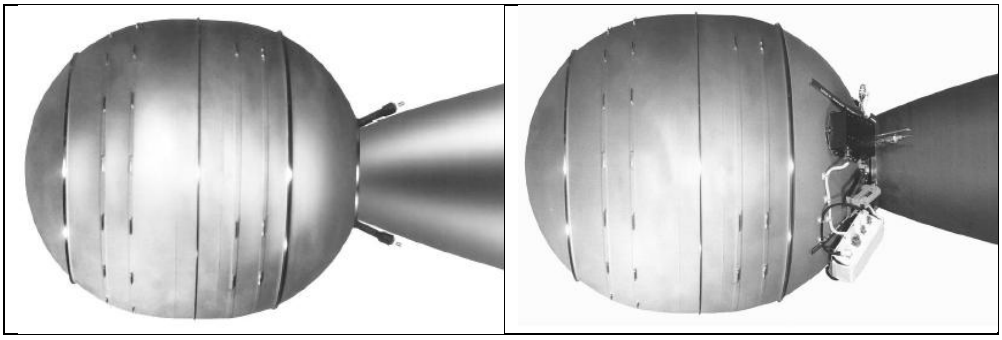

Figure 22: Star 48B SRM (l) and Star 48BV [ATK]

Next to the increased mass of the nozzle also some additional mass needs to be considered for the actuators, the drive mechanisms, the controller and the cable harness. Some typical data for the Vega C Z40 and P120C stage as given by [Gael] are reproduced in the next table.

Table 7: Mass characteristics of current TVC system components

Component	**P120 C**	**Z40**
Electromechanical actuators or EMA (2)	120 kg x 2	60 kg x 2
Integrated Power and Drive Unit or IPDU (1)	51 kg	51 kg
High Power Supply (HPS)	Two battery modules of 12.3 kg each (specific power up to 5.5 kW/kg)	Single battery module of 12.3 kg (specific power up to 5.5 kW/kg)
Cable Harness	Not Available	Not Available

6 Other controls

6.1 Start up and shut down control system

Start up and shut down control is needed to ensure a proper start up (valve sequencing) and shut down of the engine. This is especially important for liquid and hybrid rocket engines during start up as a proper filling of the chamber has to be achieved when the ignition system is fired. A too early firing might lead to an ignition failure and a too late firing might lead to the engine exploding, because of a too high a pressure rise in the main chamber.

Shut down can be easily accomplished by closing the valves in the main feed lines. Still, this must be done in a timely manner as to prevent overshoot in reaching the desired location and/or rotation. Shut down of solid rocket motors (before they run out of propellant) can be accomplished by using a fire extinguisher (i.e. by solid powder or liquid injection) or a blow-out port. The latter causes a sudden pressure drop in the chamber, which leads to flame out.

6.2 Mixture ratio control

The mixture ratio is important since for any propellant combination and pressure level, it sets the combustion temperature and hence the performance and the maximum material temperature. It is also important in terms of propellant utilization especially when considering that during flight boil-off may occur. For liquid bipropellant rocket engines mixture ratio can for instance be controlled by a regulating valve in either the oxidizer or fuel feed line. The same is possible for hybrid rocket engines. For solid rocket motors no such control is possible. Of course, information on propellant remaining should be available. More extensive information can be obtained from [Sutton].

Several studies have been conducted [Colasurdo], to determine the feasibility of rocket engines with variable mass mixture ratio. The underlying idea is that during the initial phase of launch, where propellant density or vehicle size is the more dominant performance parameter, we use a O/F ratio leading to a high-density propellant. At the later phases, we can than switch to another motor setting, giving a lower density, but also a higher specific impulse.

6.3 Nozzle deployment control

A way of improving engine performance is to extend the nozzle during the flight thereby increasing the expansion ratio of the engines and therefore the effective exhaust velocity of the engine. Current solutions, like for the European Vinci, Russian NK33 and US RL10A-4 all have 1 or more nozzle extension rings, which are deployed during flight. When the rocket is launched, the several parts of the nozzle are folded inside each other in quite a compact way, see for instance Figure 23.

When reaching higher altitudes, the nozzle is deployed and expansion of the flow to ambient becomes possible once more. The deployable nozzle extension on the Vinci engine provides a 5% increase in engine specific impulse (and hence also thrust) with a corresponding payload increase [Strøm]. Pratt & Whitney's RL 10A-4 Centaur rocket engine is equipped with a single 508 mm long nozzle extension ring that is electro-mechanically deployed following Centaur separation before engine ignition. It contributes a gain in specific impulse of 6.5 s bringing the vacuum specific impulse to 448.9 s [Jane's]. The 2nd and 3rd stage of the US missile MX Peacekeeper also have an extendible exit cone, but in contrast to the RL10, it is deployed while the engine is operative. By adding more deployable nozzle segments, such a nozzle can be adapted for several altitudes.

Figure 23: Russian NK33 engine with extendible nozzle

To allow for nozzle deployment, an elaborate mechanism is needed, see Figure 24.

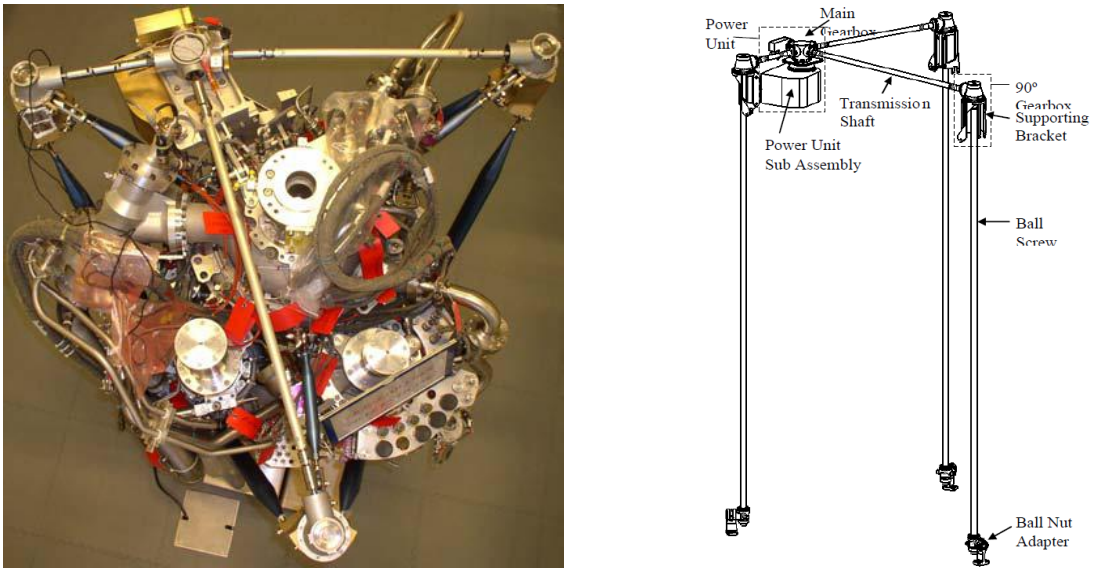

Figure 24: Vinci nozzle extension deployment mechanism [adapted from Strøm]

The Vinci nozzle extension deployment mechanism includes a power unit mounted on top of the Vinci engine, two electric motors, a gearbox, transmission shafts, 90-degree gear box with supporting brackets, ball screws with adapters that attach to the nozzle extension. This system adds considerable mass to the engine, but the gain in specific impulse and hence the reduction in propellant mass more than off-sets the increase in engine mass.

7 About control loops

Two types of control loop are distinguished, being open- and closed-loop control. Hereafter, these two types of control loop are discussed in some more detail. For illustrative reasons, we will consider a simple system comprising an electrical heater heating a gas mass flow, like in a resistojet.

Open-loop control is where the control action does not use feedback information from the system being controlled (Figure 25). It is a simple type of control typically adopted for simple devices. In the above case of heating a gas mass flow we can use it to switch the heater power on/off at a pre-determined time. It is even possible, like in the case of two heaters, to have a setting with one heater on and with two. The disadvantage is that the setting is determined beforehand and if somehow the power is too high or too low to reach the desired temperature, e.g. because of a (non-intentional) change in mass flow, there is no action taken by the control system to correct this situation.

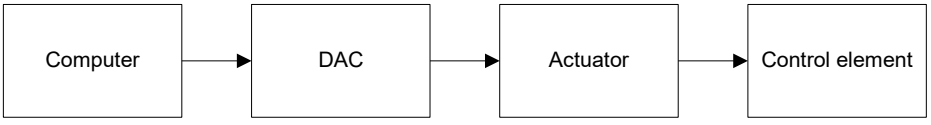

Figure 25: Open-loop control

Closed-loop control is where control action utilizes feedback information from the system (Figure 26). In a closed loop control the commanded input (r) is continuously compared with the controlled output (b) to continuously influence the commanded input. In this way the desired accuracy can be achieved by minimizing the measured error (e).

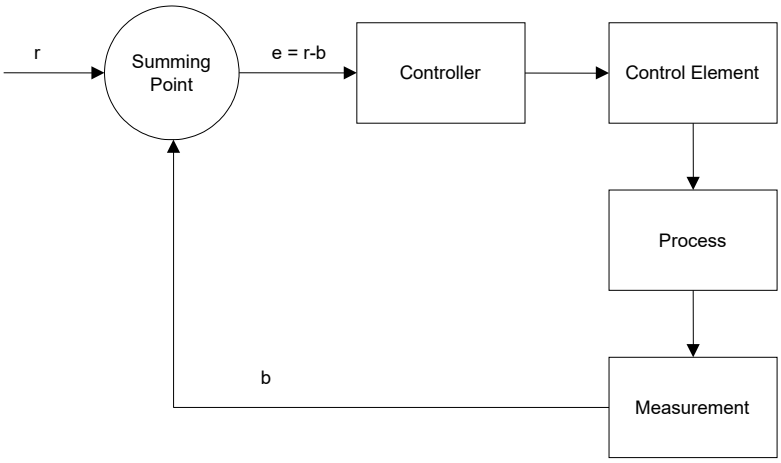

Figure 26: Closed-loop control

For our simple system, the control system might use information on the temperature of the gas mass flow to switch the heater on/off or to change the power setting of the heater, depending on the set-point for this temperature. Closed-loop control allows for more precise control and is especially advantageous when the set-points are varied during motor operation or when the operating conditions vary, for example the change in mass flow occurring because of a decrease in pressure in a blow-down feed system.
Various types of feedback control exist including:

- On-Off Control: The temperature of the mass flow of gas is controlled by switching the heater on when the temperature is below the set-point and off when above.
- Proportional control: Power is applied to the heater in proportion to the difference in temperature between the gas temperature and the set-point.

Other types of control exist, allowing for tighter control closer to the set-point. These, however, are left for the reader to explore for himself.

8 Problems

1. Consider vertical ascent flight of a rocket launch vehicle with the aerodynamic properties as shown in next figure. Rocket is of a cylindrical cross-section with a diameter of 3.8 m.

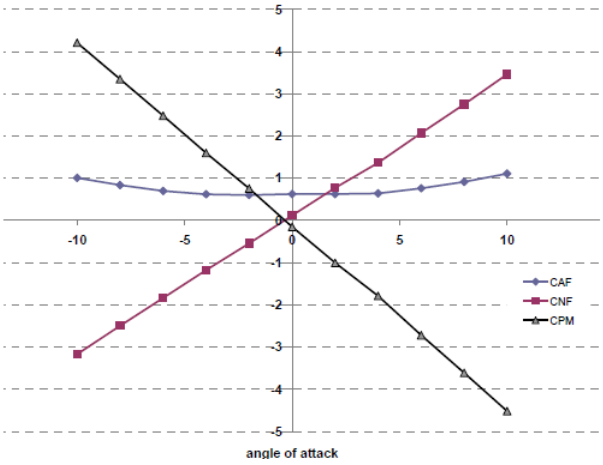

Figure 27: Values of aerodynamic axial and normal force coefficient (CAF and CNF) and aerodynamic pitching moment coefficient (CPM) versus angle of attack (reference area is launcher cross-sectional area and rocket diameter is reference arm for moment calculations.

At 15 km altitude (air density is 0.15 kg/m^3) it reaches a flight velocity of 600 m/s and rocket centre of gravity is 14.7 m up from bottom of vehicle. At that instant, it experiences a horizontal wing gust of 20 m/s. Calculate for this vehicle the aerodynamic pitching moment that it experiences.

2. Consider an axis-symmetric rocket of diameter 5 m propelled by a single rocket engine. This rocket engine is of a single chamber design and provides a nominal thrust of 1 MN along its longitudinal axis. The work point of the thrust is located on the symmetry axis of the rocket 14.7 m below launcher centre of gravity. Calculate for this launcher:
    a) Torque due to thrust misalignment in case thrust misalignment angle is 0.5º.
    b) Misalignment torque that needs to be compensated for in case work line of thrust force has shifted 0.5 cm parallel to vehicle axis.
    c) Describe the effect of tank emptying on rocket centre of gravity and how this affects the torques as determined under 2a and 2b.

3. The rocket described in problem 2 requires a maximum torque of 800 kNm about the pitch/yaw axis to ensure mission success. Calculate for this rocket:
    a) Side force to be generated in case work line of side force intersects the vehicle axis at a location 2 m up from bottom of vehicle.
    b) Same question as under a, but now considering that as of tank emptying, the vehicle's centre of gravity has shifted in a downwards direction with 1 m.
    c) TVC angular range as follows from the above.

4. A gimballed rocket engine producing a thrust of 2 MN has a TVC capability of ±5 degree for yaw/pitch control, see figure.

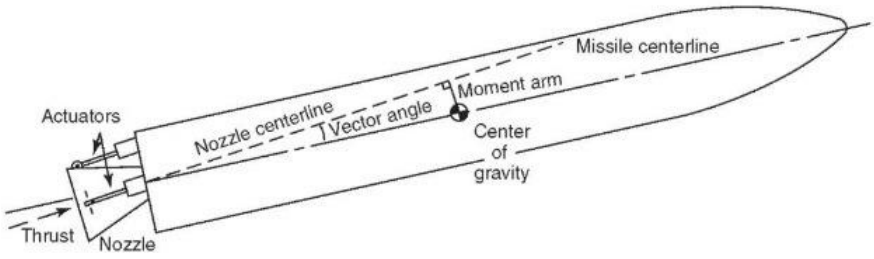

    Determine for this engine:
    a) Maximum thrust in a direction perpendicular to the vehicle axis (vehicle axis coinciding with engine axis in case if no TVC.
    b) Axial thrust in case of maximum TVC.
    c) Maximum torque exerted on vehicle in case centre of gravity is 4 m up from work point of thrust on vehicle axis.

5. The 746-ton heavy Ariane 5 is equipped with two solid rocket boosters each producing a (sea level) thrust of 5 MN and with a mass of 237 ton. For pitch/yaw control, the booster is equipped with a flexible nozzle with maximum 6-degree deflection. Booster centre line is parallel to centre line of the core vehicle at 4.4 m. Vehicle centre of gravity is situated on the centre line of the total vehicle at 19 m distance (at take-off) above ground level. An orthogonal x, y, z co-ordinate system is located at the vehicle centre of gravity with z-axis along the centre line of the core vehicle and x-axis perpendicular to the plane formed by the core stage and the two parallel booster stages. Calculate for this vehicle:
    a) Resulting torque in case one booster does not ignite (no TVC active).
    b) Maximum torque on the vehicle that can be produced by each booster in case the nozzle pivot point is located 1 m above ground level. Discuss whether you consider steering the rocket in a one-engine out case a viable option.
    c) Maximum vehicle angular acceleration (in rad/s^2) about the x-axis at maximum torque (both boosters active) in case the mass moment of

inertia of Ariane 5 about this axis is taken equal to 98 x 10^6 kg-m^2 (other torques acting on the vehicle are considered negligibly small).

d) Time it takes for the vehicle to rotate over an angle of 20° about the x-axis using the above calculated angular acceleration and given that the rotational rate is limited to 0.5 deg/s. Include also the time needed to bring the vehicle to standstill again.

6. In case you have a gimballed rotational symmetric engine with a mass of 1000 kg and a mass moment of inertia about the engine pivot point of 500 kg-m^2. Calculate for this engine:
   a) Inertia torque in case the engine attains an angular acceleration of 20 rad/s^2.
   b) Time it takes for the engine to reach an angular velocity of 20 deg/s.
   c) Time it takes for the engine to swivel over an angle of 10 degree. Include in your time estimate the time needed to accelerate and decelerate.
   d) Required actuator force in case moment arm is 0.4 m (other torques acting on engine are maximum 15000 Nm).

7. Consider a single engine rocket stage with an engine centre line coinciding with the vehicle centre line. This engine is of a gimballed design with gimbal situated on top of engine. Consider that TVC is provided for by a single actuator attached to the engine at a distance 0.3 m below engine pivot point and 0.2 m from engine centre line. The other end of the actuator is fixed to the rocket frame at a point 0.2 m above the chamber pivot point and 0.5 m away from the centre line, see figure.

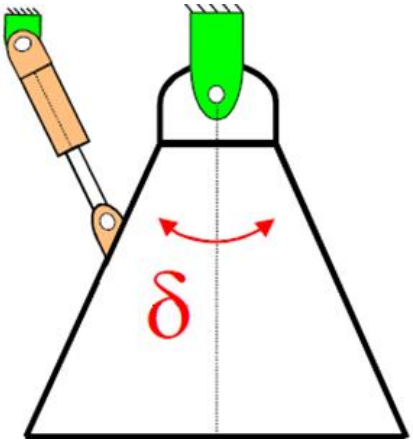

   Calculate for this engine:
   a) Length of actuator in zero position.
   b) Required actuator stroke **g**iven a maximum TVC gimbal angle of 20°.
   c) Angle that centre line of actuator makes with engine centre line (zero deflection); Notice that this angle varies when the engine is deflected from its neutral position.

   Consider a control torque (to overcome engine inertia, spring loads, thrust offset, friction, gravitational torque, and aerodynamic torque) exerted on the engine of 50,000 Nm.
   d) Determine actuator force in case actuator (centre line) makes an angle of 35° with motor axis.

   Given an actuator stroke of 0.2 m, an actuator force of 200 kN and an actuation time of 1 s (from neutral position to maximum deflection), determine:
   e) Actuator output velocity in case we have a constant speed actuation
   f) Mechanical power needed to power the actuator under the above-described conditions
   g) TVC input power given that the mechanical power is provided by an electrical motor with an efficiency of 60%.

Literature

1) Ambrosius, Schöyer, et al., Beginselen van de Ruimtevaart, college Technische Hogeschool Delft, 1980.

2) ATK space propulsion products catalog, September 2012.

3) Backlund S.J. and Rossen J.N., A study of performance and cost improvement potential of the 120-in. (3.05 m) diameter solid rocket motor, NASA CR114390, December 1971.

4) Casiano M.J., Hulka J.R., Yang, V., Liquid-Propellant Rocket Engine Throttling: A Comprehensive Review, JOURNAL OF PROPULSION AND POWER, Vol. 26, No. 5, September–October 2010.

5) Cherne J.M., Mechanical Design of the Lunar Module Descent Engine, TRW.

6) Colasurdo G., Pastrone D., Casalino L., Mixture ratio control to improve hydrogen-fuel rocket performance, J. of Spacecraft and Rockets, Vol. 34, No. 2, 1997.

7) Daniele, Carl J., Scalzott, Leslie L., and Borsody, Janos: Thrust Vector Control Requirements for Launch Vehicles Using a 260-Inch Solid Rocket First Stage. NASA TM X-1906, 1969.

8) Gael, D., Vanthuyne T., Potini A., Pardos I, De Crombrugghe, G., Electromechanical thrust vector control systems for the Vega-C launcher, 8th European Conference for Aeronautics and Space Sciences (EUCASS), DOI: 10.13009/EUCASS2019-186, 2019.

9) Glen Case E., Preliminary Design of a Hybrid Rocket Liquid Injection Thrust Vector Control System. AIAA 2008 – 1420, 2008

10) Humble R.W., Henry G.N., Larson W.J., Space Propulsion Analysis and Design, McGraw-Hill, 1995.

11) Jane's Space Directory 11th edition, A Wilson (ed.), Jane's Information Group, London.

12) JPL, Study of Selected Thrust Vector Control Systems for Solid Propellant Motors, 1965.

13) Van Kesteren M.W., Air Launch versus Ground Launch: A Multidisciplinary Design Optimization Study of Expendable Launch Vehicles on Cost and Performance, TU-Delft MSc thesis report, November 18, 2013.

14) Knauber R.N., Thrust misalignments of fixed-nozzle solid rocket motors, Journal of Spacecraft and Rockets, Vol. 33, No. 6 (1996), pp. 794-799.

15) Laan F.H. van der, and Timnat Y.M., Chemical Rocket Propulsion, TU-Delft, Department of Aerospace Engineering, April 1985.

16) Mitchell W.T. and Searle R.F., SSME Digital Control Design Characteristics, NASA/Rocketdyne, N85-16893, 1985.

17) NASA/SP-8114, Solid rocket thrust vector control.

18) Nickens T.L., Sutton J.L., Erickson L.H., Sottosanti P.J., Thrust Vector Control Study for large (260 IN.) ROCKET MOTOR APPLICATIONS, April 1970 as presented before the JANNAF Interagency Propulsion Committee 26th Solid Propulsion Meeting, 14-16 July 1970 at Washington, D. C.

19) Redmon J., Solid Rocket Booster Thrust Vector Control Subsystem Description, NASA TM-82546, September 1983.

20) Rockwell International Corporation, SSME Engine Redline and Control Overview, Report BD 99-62, 1988.

21) Shodhganga, Design of a flexible seal of a large solid rocket motor, retrieved from http://shodhganga.inflibnet.ac.in/bitstream/10603/8545/12/12_chapter%203.pdf, Date of retrieval 12-2-2016.

22) Strøm S. et al., Design and development of the Nozzle Deployment Mechanism for the Vinci Cryogenic Engine, Kongsberg, Sweden, May 2011.

23) Sutton G.P., Rocket Propulsion Elements, 6th edition, John Wiley & Sons Inc.

24) Pelouch J., Thrust Vector Control (TVC) System Study Program, NASA CR 72727, 1970.

25) Qiao G., Liu G., Shi Z., Wang Y, Ma S., Lima, T.C., A review of electromechanical actuators for More/All Electric aircraft systems, J. Mechanical Engineering Science, 2017.

26) Vanthuyne T., An Electrical Thrust Vector Control System for the VEGA Launcher Proc. '13th European Space Mechanisms and Tribology Symposium – ESMATS 2009', Vienna, Austria, 23–25 September 2009 (ESA SP-670, July 2009).

27) Verble A.J., McCool A.A., Potter, J.H., SPACE TRANSPORTATION SYSTEM SOLID ROCKET BOOSTER THRUST VECTOR CONTROL SYSTEM, NASA TM-78309, October 1980.

Glossary

Ablative cooling: Use of a material on the wall that evaporates or chars during thruster firing and thereby keeps the wall cool

Ablator: A material that wears away under stresses of heat, oxidation, and high velocity gas erosion.

Aerodynamic throat area: Effective flow area of the throat, which is less than the geometric flow area

Annular nozzle: Nozzle with an annular throat formed by an outer wall and a center-body wall

Bates grain: Uninhibited tubular grain which provides a nearly neutral burning characteristic (BAtch TESt motor).

Bell nozzle: Bell-shaped nozzle

Binder: Rubbery or plastic organic fuel used in some solid and hybrid propellants.

Bi-propellant: A rocket propellant consisting of two unmixed or uncombined chemicals (fuel and oxidizer) fed separately into the combustion chamber.

Black powder: A mixture of potassium nitrate, charcoal and sulphur.

Blow down propellant feed system: Pressurizing gas flowing through a fixed orifice with no other regulation to expel liquid propellants.

Booster system: A high thrust propulsion system that quickly brings the vehicle up to speed.

Chemical rocket propulsion: A type of rocket propulsion wherein the propellants are heated by the heat liberated in a chemical reaction and then expand through a nozzle to create thrust.

Cold-gas rocket propulsion: Type of rocket propulsion, wherein the thrust is generated by expansion of a high-pressure gas through a nozzle.

Combustion chamber: Generally a tubular section of a rocket motor (solid, liquid, or hybrid) in which combustion takes place.

Composite propellant: A propellant consisting of a mixture of separate oxidizer(s) and fuel(s).

Coolant: A medium, usually a fluid, which transfers heat from an object.

Cryogenic propellants: Propellants that are liquefied by cooling to extremely low temperatures.

Discharge coefficient: ratio of the actual flow rate to the ideal flow rate calculated on the basis of one-dimensional inviscid flow.

Double Base Propellant: A solid propellant consisting of two solid monopropellants (usually nitroglycerin and nitrocellulose) and various additives.

End-burner: A solid rocket motor which has a cylindrical propellant grain and burns from one end.

Expellant: Working fluid of a non-chemical rocket propulsion system

Fuel: Reducing agent. Component(s) of the propellant which are oxidized or burned.

Gas generator: A chamber in which propellant is burned to produce high pressure gas that is then used to drive a turbine, e.g. turbopump.

Gimbal: A mechanical frame that usually allows rotation over two perpendicular axes of rotation.

Grain: A block of solid propellant or fuel that is stored in the combustion chamber.

Heat exchanger: A device that transfers heat from one fluid (gas or liquid) to another or to the environment.

Heterogeneous propellant: A solid propellant consisting of wherein the individual molecules consist of fuel and oxidizer.

Homogeneous propellant: A solid propellant wherein the individual molecules consist of fuel and oxidizer.

Hypergolic propellant: An oxidizer and a fuel combination which ignites spontaneously when mixed.

Igniter: An expendable device used to ignite a rocket motor.

Inhibitor: Bonding non-propellant material to restrict the burning surface of a propellant grain.

Injector: A system of orifices used to inject liquid propellant into the combustion chamber.

Insulation: Thermal protection used in motors to prevent heat transfer to temperature sensitive materials.

Liner: An insulated sleeve made from phenolic, EPDM, fiberglass, impregnated cardboard, or any number of materials which protects the combustion chamber while the motor is burning.

Mono-propellant: A rocket propellant consisting of a single substance, especially a liquid containing both fuel and oxidizer properties.

Motor case: A thin-walled structure used in solid and hybrid rocket motors to store the solid propellant/fuel and as a vented pressure vessel in which the propellant burns.

Nozzle: The portion of the rocket motor which accelerates the gases to sonic velocity at the narrowest part of the nozzle (the throat) then expands them to greater velocity in the exit cone.

Nozzle exit cone: Applies to the exit or expansion section of a rocket nozzle.

Nozzle extension: Nozzle structure that is attached to the main nozzle in order to increase expansion ratio or to provide change in nozzle construction.

Nozzle throat (assembly): That part of a nozzle between the combustion chamber and nozzle exit cone.

Nuclear-thermal rocket propulsion: Type of rocket propulsion wherein the working fluid is heated in a high temperature nuclear reactor, and then expands through a

nozzle to create thrust. The nuclear reactor's energy replaces the chemical energy of the reactive chemicals in a traditional rocket engine.

Oxidizer: Oxidizing agent. Component(s) of a propellant which provides the combustion supporting element (generally Oxygen, but can be Fluorine, Chlorine, Sulfur, etc.)

Plug nozzle: A doughnut-shaped combustion chamber which discharges engine gases against the surface of a short central cone (the plug).

Pressure regulator: A device that ensures a constant pressure at the outlet of the regulator

Propellant: An energetic material usually consisting of a fuel and an oxidizer that propels a rocket.

Propellant Utilisation System: System consisting of valves, valve actuators, flow meters, tank level sensors and fill/drain facilities. This system controls the flow of propellant during start-up, burn and shutdown and also has provision for interfacing to the launcher fuelling equipment.

Propellant release boot: System that permits shrinkage of the cured propellant grain as it cools and thus prevent strain (deformation) with consequent cracking.

Propulsion: (1) The action or process of propelling. (2) Something that propels.

Prototype design: An initial, development design used to test out principles and concepts but never intended to be a finished or production design.

Pump: A mechanical device used to move liquids or gases.

Raceway: A duct in which control and electrical system wiring or hydraulic leads are placed.

Reaction Control System (RCS): Provides the thrust for attitude (rotational) manoeuvres (pitch, yaw and roll) and for small velocity changes along the vehicle axis (translation manoeuvres).

Regenerative cooling: Cooling of the wall with one of the propellants before it is burned in the combustion chamber.

Resistojet: A thruster wherein the propellant is heated through resistance heating.

Retrorocket: A rocket fired to reduce the speed of a spacecraft.

Rocket motor: This term has two meanings, depending on whether solid-propellant or liquid-propellant rockets are under discussion. The “rocket motor” of a solid-propellant rocket consists of the tube holding the propellant charge and the exhaust nozzle. In liquid-propellant rockets the term originally applied to the combustion chamber and the exhaust nozzle. But for rockets of recent design, in which propellant pumps, etc., are all part of the assembly, the term rocket engine is now commonly used.

Rocket engine: See rocket motor.

Rocket stage: A self-propelled separable element of a rocket vehicle. In a multistage rocket, each rocket unit fires after the one behind it has used up its propellant and (normally) been discarded. It generally includes a main propulsion system, a reaction control system, a thermal protection system, a separation system, an electrical power

system, a range safety system, etc. Sometimes a stage may also be equipped with an avionics system, communications system and an aerodynamic control system.

Single Base Propellant: A solid propellant based on a single monopropellant. In practice usually nitrocellulose in a mixture with stabilizers and plasticizers.

Solar-thermal propulsion: A form of spacecraft propulsion that uses solar power to heat a working fluid after which it expands in a nozzle to generate thrust.

Slush propellant: A mixture of liquid and frozen propellant that is denser than the pure liquid propellant.

Sustainer system: Propulsion system that takes over and maintains flight (flight sustenance) after a booster system has brought the vehicle up to speed.

Squib: A small explosive device used to detonate larger explosive charges. While the term is sometimes used to describe igniters used in hobby rocketry, especially HPR igniters such as electric matches (q.v.), true squibs are almost *never* used as igniters since their purpose is to set up a detonation pressure wave to set off pressure sensitive explosives (e.g. plastic explosive), while an igniter must start a (relatively) low speed flame front so that the motor burns, rather than explodes.

Tank: A vessel or container for holding liquids or gases.

Test Cell: A test stand for a rocket engine surrounded on three sides by a shelter providing protection from weather and limited protection from an accidental explosion.

Thrust chamber: The combination of combustion chamber and exhaust nozzle.

Thrust termination port: A port in the case of a solid rocket motor to vent combustion gases so that rocket operation can be terminated.

Thruster: A small rocket engine. Typically not pump-fed.

Triple Base Propellant: A solid propellant based on three monopropellants and additives. In practice, the monopropellants are usually nitro-glycerine, nitrocellulose, and nitro-guanidine.

Tube-wall construction: Wall that consists of a series of parallel tubes that carry coolant.

Turbine: A shaft with a fan of blades mounted on it, known as the rotor.

Turbo-pump: Type of pump in which the fluid is moved by the blades of a high-speed turbine.

Valve: A device that controls the flow of a fluid.

Answers to problems

In this section, numerical answers to problems are provided. Most answers were already available via ANS[1] with additional feedback on the approach to be taken. As this feature is now no longer available it has been decided to give at least the numerical answers here. This action is not yet fully completed, hence not all problems have answers yet.

Chapter 1: Rocket Propulsion Fundamentals

1) *Variable thrust: M_p = 840.4 kg, F_{max} = 18.06 kN, t_{min} = 186.5 s, and I_{tot} = 2.52 MNs. Constant thrust: M_p = 840.4 kg, F_{max} = 9.81 kN, t_{min} = 257 s, and I_{tot} = 2.52 MNs.*

2) *Constant thrust: M_p = 257.0 kg, F_{max} = 9.81 kN, t_{min} = 209.6 s, and I_{tot} = 2.06 MNs.*

3) *(Effective) exhaust velocity w = 3924 m/s, P_j = 1.96 GW. I = 600 MNs, m = 254.8 kg/s, M_p = 152.9 (metric) ton, V_p = 459 m^3, T/W = 0.62, α = 0.073, and I_{ssp} = 371s.*

4) *P_{jet} = 1.35 GW, I_{tot} = 401 MNs, m = 41.3 kg/s, η_T = 86%, and T/W = 3.36.*

5) *M_p = 105.4 (metric) ton, V_p = 1506 m^3. Hint 1: From the data given in problem 4, we can determine the velocity increment delivered by the original Ariane 5 first stage. Hint 2: Look up engine mass of HM60 engine (it should be ~1300 kg) to determine dry mass of rocket minus engine mass. Next factor in the replacement engines.*

Chapter 2: Sizing Fundamentals

2) *i) 2990 kg, ii) 3679 kg, and iii) 3177 kg.*

3) *Optimum exhaust velocity is 22.45 km/s)*

4) *The linear relation fitting the data points best is Y = 0.0312 X + 67.048, where Y is propulsion system dry mass (in kg) and X = total propellant mass (in kg).*

5) Answer: ~128 ton. This value is found in case the velocity increment to be realized is distributed evenly over the two sub-rockets. Any other distribution gives a higher total mass. Note that using a different effective exhaust velocity or mass fraction for the two sub-rockets will affect the optimal distribution of the velocity increment over the two sub-rockets.

Chapter 3: Thrust and Specific Impulse

1) *a) 2494 m/s, b) 224 N, and c) 2188 m/s at sea level and 2801 m/s in vacuum.*

2) *Sea level: Engine thrust is 832 kN and specific impulse is 333 s.*

Chapter 4: Ideal Thermal Rocket Motor

2) *a) 2,037, b) 0.0491 m^2, c) …, d) 105.2, e) 1253.1, f) …*

3) *a) 1.945, b) 605.2 m/s, c) 806.0 K, d) 5.3 kW*

4) *In the vacuum of Space: a) 1780 m/s, b) 1.0355, c) 188 s, d) 1727 m/s, e) 1.0179, f) 179 s*

5) a) 0.9285, b) 0.9880, c) 0.9174

Chapter 5: Nozzle Design

2) *a) We first use IRT to determine the basic nozzle dimensions. We obtain a mass flow rate of 227 kg/s, a characteristic velocity of 2423.6 m/s, a nozzle throat diameter of 0.2521 m, a nozzle area ratio*

[1] Ans is the standard assessment tool for the entire TU Delft.

of 19.396 and a nozzle exit diameter of 1.0983 m. Length of nozzle exit cone (divergent) = 1.30 m. Here we have assumed the effect of the rounding of the nozzle throat to be negligible.
b) Nozzle thickness is determined using theory presented in annex L. D6AC steel material properties are (taken from annex K). It follows an ultimate strength of 1483 MPa. Pressure in nozzle throat is 63.2 bar and in nozzle exit 0.685 bar. Furthermore, we have assumed a safety factor on ultimate load of 1.5. Yield is not considered a dimensioning load as yield and ultimate strength of D6AC steel are close. It follows for the thickness of the nozzle structural wall:

Parameter	**Nozzle throat**	**Nozzle exit**
Pressure [bar]	*63.2*	*0.685*
Diameter [m]	*0.2521*	*1.0983*
Corrected diameter [m]	*0.2651*	*1.1548*
Nozzle wall thickness (j = 1) [mm]	*0.565*	*0.027*
Nozzle wall thickness (j = 1.5) [mm]	*0.847*	*0.040*

Results have been calculated using a factor of safety of 1.5. For space systems, these usually follows from standards like the ECSS. Clearly the thickness at the nozzle exit is quite small and may be difficult to produce. The same holds for the nozzle throat region. Furthermore, we have assumed that material is at room temperature, which is not always the case. So, this should be verified and if necessary corrected. As a final remark, we state that in practice also other loads may be dimensioning. Here we like to mention specifically handling loads.

3) *Length of the divergent part of the conical nozzle is 2.065 m. So, it means that the contoured part of the bell nozzle should have a length of 85% of this value or 1.755 m.*

Next, we determine nozzle area ratio (46) and use figure on the side (from [Sutton] to estimate the initial and final parabola angle for a 15-degree conical nozzle. This gives a conical nozzle length of 2.497 m. The nozzle to be designed has a length of 1.775 m, which leads to a 70% length of this 15-degree conical nozzle. From the figure below, we find an initial parabola angle of 35 degrees and a final parabola angle of 12-14 degrees.

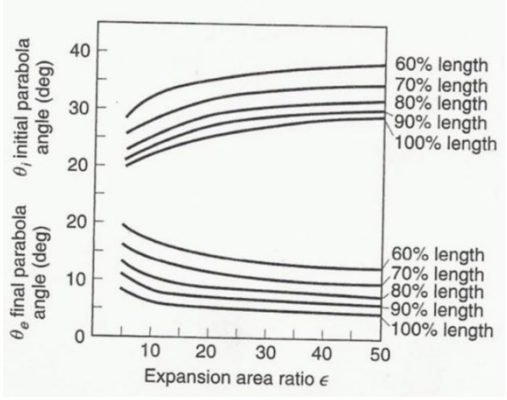

Next figure shows the resulting contour.

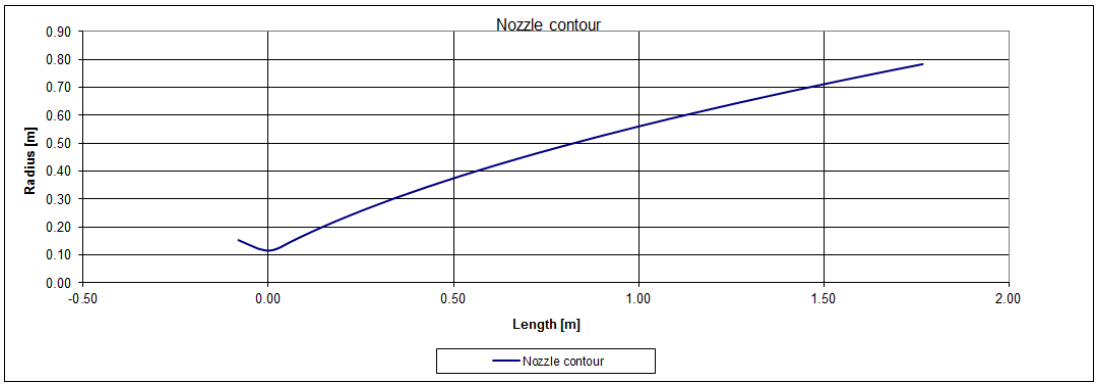

This contour is produced using:

- θ_p *= Nozzle throat divergence half angle = 35 degrees.*
- θ_e *= Nozzle exit divergence half angle = 14.6 degrees.*

Chapter 6: Propellants and Propellant Properties

No problems on offer.

Chapter 7: Thermo-chemistry

1) 1.5E3 kW

3) a) $H_2O_2 \rightarrow 0.5\ O_2 + 1\ H_2O$
b) $2N_2H_4 \rightarrow 2\ NH_3 + 2\ N_2$
c) $H_2 + 0.5\ O_2 \rightarrow 1 H_2O$
d) $H_2 + 2O_2 \rightarrow 1\ H_2O + 1.5\ O_2$
e) $CH_4 + 2\ O_2 \rightarrow 1\ CO_2 + 2\ H_2O$
f) $N_2H_4 + N_2O_4 \rightarrow 4/3\ NH_3 + 2\ NO_2 + 1/3\ N_2$
g) $C_{12} + H_{26} + 12.5\ O_2 \rightarrow 12\,CO + 13\ H_2O$

4) a) O/F = 1.40, b) -, c) 100 grams

6) -97.9 kJ/mol (exothermic)

7) 3.5E3 K

8) 253.8 J/mol/K

Chapter 8: Heat Transfer and Cooling

1) a) 704 K; b) 348.15 K

2) 698.5 K

3) a) Case i: 17428 W/m^2, case ii: 13118 W/m^2, case iii: 8188 W/m^2
Answers are calculated using a hot gas emissivity of 0.2 and a wall emissivity of 0.15 (wall has a temperature of around 773 K).

b) For the case i, there is no difference. For case ii, we find an almost 5 times increase of the heat flux and for the case iii, we find a heat flux of slightly more than double the earlier value.

Chapter 9: Cold Gas Thruster Design

1) a) Mass flow rate is 7.84 mg/s, and nozzle throat (cross-sectional) area is 6.74E-9 m^2. When we assume a nozzle with a circular cross-section, we obtain a nozzle throat diameter of 0.093 mm or 93 μm. Nitrogen gas properties at 5 bar pressure have been obtained from NIST and include a molar mass of 28.0134 gram and a specific heat ratio of 1.409.

b) For a first iteration, we estimate a nozzle area ratio of 20. This area ratio gives a nozzle exit diameter of 0.41 mm and a nozzle pressure ratio of 2.54E-3. Subsequently, we find a true exhaust velocity of 702.4 m/s, a nozzle exit pressure of 1272 Pa, an effective exhaust velocity of 724.3 m/s (slightly higher than 93% of the limit velocity) or a vacuum I_{sp} of 73.9 s.

Varying the area ratio, we find that a vacuum thrust and specific impulse of 5 mN and 65 s, respectively can be realized for a nozzle area ratio of 2.319. Results for both area ratios are summarized in the next table.

Parameter	A_e/A_t = 20	A_e/A_t = 2.319
A_t [m^2]	6.74E-9	6.74E-9
D_e [µm]	410	141
p_e [Pa]	1272	3590
m [g/s]	7.84	7.84
$U_{e,eq\ (vac)}$ [m/s]	724.3	637.4
I_{sp} (vac) [s]	73.9	65.0
F (vac) [mN]	5.68	5.0

From the table, we learn that, for a very modest nozzle area ratio, the minimum required I_{sp} can already be realized, at least that is when using IRT and assuming quality factors including nozzle discharge coefficient are equal to unity.

2) *In real (not ideal) rocket motors, performances tend to reduce. When considering the given nozzle quality factors of 0.90 and nozzle discharge coefficient of 0.8 and keeping the chamber pressure and mass flow rate equal to the values determined above (problem 1), we obtain a new (enlarged) nozzle throat area of 8.43E-9 m^2 or a new (enlarged) nozzle throat diameter of 0.104 mm or 104 μm. To realize a similar I_{sp} as in problem 1, the nozzle area ratio must be increased. The results are shown in next table in comparison to the solution from problem 1 for an area ratio of 2.319. Results clearly show that for identical mass flow rate, the nozzle throat as well as the nozzle area ratio must be increased.*

Parameter	*IRT*	*Non-ideal (nozzle quality = 0.90)*	*Non-ideal (nozzle quality = 0.85)*
Area ratio [-]	*2.319*	*10.678*	*107.9*
A_t [m^2]	*6.74E-9*	*8.43E-9*	*8.43E-9*
D_t [µm]	*93*	*104*	*104*
D_e [µm]	*141*	*338*	*1076*
p_e [Pa]	*3589*	*3232*	*110*
m [g/s]	*7.84*	*7.84*	*7.84*
$C_{F,ideal}$ [-]	*1.483*	*1.648*	*1.745*
$C_{F,real}$ [-]	*Not Applicable*	*1.483*	*1.483*
$U_{e,eq\ (vac)}$ [m/s]	*637.4*	*637.4*	*637.4*
I_{sp} (vac) [s]	*65*	*65*	*65*
F (vac) [mN]	*5.0*	*5.0*	*5.0*

Interesting is to consider what happens in case the nozzle quality factor is lower than the here given 0.9. So, we also calculated a solution in case of a nozzle quality of 0.85. We see that in the nozzle area ratio further is enlarged to allow for sill making the required Isp. For a nozzle quality of 0.80, no satisfactory solution could be found (consider why this is?).

4) *For the thruster designed in problem 2, the resulting nozzle throat pressure and nozzle throat temperature that follow from IRT are 2.63 bar and 243 K. At this temperature and pressure, we find for the dynamic viscosity a value of 15.8 microPascal*s and a gas mass density of 3.6553 kg/m^3. The resulting Reynolds number for the ideal nozzle is 6793, which gives $(1/Re)^{0.5}$ = 0.0121. Using the results of Johnson for nitrogen, we find an actual discharge coefficient (extrapolated from figure) of around 0.925, which is higher than the assumed value of 0.8. Using the results of Wahlen, we find a nozzle efficiency in range 0.90 – 0.85, which compares well with the nozzle quality range for which solutions were provided in the problem 2 answers. As an outcome, we can reduce the nozzle throat a bit, so that we get closer to the throat diameter following from IRT. For the nozzle area ratio it is considered that an area ratio in range 11-100 may work fine for a firs design. Tests must confirm which area ratio gives an appropriate result. Of course, we can also pick a value and if necessary, adapt the design I_{sp} value.*

5) *For the determination of the Knudsen number, we use the relations as given in this chapter, see section on free molecular flow. Nitrogen gas properties at 5 bar pressure and 550 K are obtained from NIST and include a molar mass of 28.0134 gram and a specific heat ratio of 1.388. We calculate a mass flow rate of 3.19 mg/s and a nozzle throat diameter of 0.069 mm (verify). The effective diameter of a nitrogen molecule in the gaseous state is 0.3 to 0.364 nm (see Kinetic diameter - Wikipedia). The number density of nitrogen has been determined using the ideal gas law for the nozzle throat pressure of 2.65 bar and a nozzle throat temperature of 461 K. It follows a value of approximately 4.17E25 molecules/m^3. Using these values, we find a molecular mean free path of ~0.04 micrometre and a Knudsen number of 5E-4. Which shows that in the nozzle throat we can still apply continuum flow. However, as the flow expands in the nozzle, it may be questionable if the nozzle flow can be fully dealt with using continuum flow techniques.*

6) *A similar problem is offered in the next chapter. For this similar problem an answer is provided.*

Chapter 10: LRE Combustor Design

1) *Equilibrium chamber pressure is 95 bar and mass flow rate 47.6 kg/s.*

2) *Fuel injection velocity is 27. 11 m/s, oxidizer injection velocity is 37.4 m/s, fuel injector internal diameter is 1.711 mm and oxidizer fuel injector internal diameter 1.569 mm. The fuel jet makes an angle of 27.7 degrees, and the oxidizer jet an angle of 32.2 degrees with the normal on the distributor plate.*

3) *a) Fuel injection velocity is 555.7 m/s (velocity of sound is m/s), and oxidizer injection velocity is 50.9 m/s.*
b) Oxidizer jet Reynolds number is 8.98E5.
c) Oxidizer jet Weber number is 4.28E3
d) Fuel-to-oxidizer (or gas-to-liquid) momentum ratio, momentum flux ratio and velocity ratio are 1.8757, 0.8, and 10.92 respectively

e) Not Available

4) *a) Mass flow rate is 26.6 g/s (from given thrust and specific impulse)*
b) Chamber diameter is 17.7 mm
c) Throat area is 35.3 mm^2
d) Chamber volume is 45.8 mm^3 (from L)*
e) Chamber length follows from chamber diameter and volume.

5) *a) Overall (design) mass mixture ratio based on the injector inflow is 1.5*
b) Number of liquid droplets formed based on the given droplet diameter is 248,195 droplets of hydrazine and 294,731 droplets of nitrogen-tetroxide (NTO)
c) Mixture ratio of the vaporized propellant at 6 equidistant points along the combustion chamber axis. Overall residence time of the propellants is 0.01 s or 10 ms (length of combustor is 0.5 m and droplet velocity is 50 m/s). It follows:

t [ms]	Droplet diameter N_2H_4 [mm]	Droplet volume [mm^3]	Vapor mass flow rate [kg/s]	Droplet diameter NTO [mm]	Droplet Volume [mm^3]	Vapor mass flow rate [kg/s]	O/F [-]	Total Evaporated [kg/s]
0	0.3	0.01414	0.000	0.3	0.01414	0		0
2	0.290	0.01275	0.393	0.283	0.01185	0.972	2.471	1.365
4	0.279	0.01141	0.773	0.265	0.00970	1.884	2.439	2.657
6	0.268	0.01012	1.138	0.245	0.00770	2.734	2.403	3.872
8	0.257	0.00888	1.488	0.224	0.00585	3.515	2.362	5.004
10	0.245	0.00770	1.823	0.200	0.00419	4.222	2.316	6.045

Results clearly demonstrate that O/F ratio differs along the chamber. This of course leads to different flame temperatures.

d) Results clearly show that not all propellant is vaporized in the combustor, which leads to a low c quality. Based on the design O/F mass mixture ratio, we would expect c* = 1990 m/s. Based on the gaseous O/F ratio at end of combustor (O/F = 2.316), we obtain c* = 1908 m/s, but this is neglecting that a large part (~40%) of the propellant has not been burned in the combustor. When considering the unburned propellant, the "actual" c* reduces to 1153 m/s (= 6.045 kg/s x 1908 m/s/10 kg/s), which leads to a combustion quality of ~58%. Increasing the length of the combustor to 1 m would allow for an increase in c* quality to ~88%.*
e) Mixture ratio of the stream along the wall is 1.335. Notice that this would create a relatively cool zone at the chamber wall. This would help in reducing heat transfer to the wall.
f) Total C efficiency (averaged over all four streams) is 90.9%. Most of this increase is because of the increase in combustor length.*

Chapter 11: Solid Rocket Combustor Design

1) *a) Klemmung K = 152.5, b) Burn surface S = 0.0304 m^2 and throat diameter D_t = 1.593 cm, c) Volume is 17.4 dm^3, propellant mass is ~30 kg (excluding margins), d) I_{sp} = 230 s, e) Regression rate r = 3.81 cm/s.*

2) *Regression rate at initial temperature of 0 °C = 7.2 mm/s.*
Regression rate at initial temperature of 40 °C = 8.8 mm/s.

3) *Burn surface of cylindrical end-burning grain is 5.159E-2 m^2, grain length = 0.3728 m, grain diameter is 0.2563 m.*

4) *a) Chamber temperature = 2.02 E3 K (characteristic velocity = 1131.3 m/s)*
b) Isp = 188.5 s (ideal expansion, nozzle area ratio = 12.792, true exhaust velocity is 1848.3 m/s)
c) Burn surface = 3.797E-2 m^2 (from mass flow rate, regression rate, and mass density, where mass flow rate = 2.6566 kg/s, regression rate = 3.9527 cm/s) and grain length = 0.593 m (from regression rate and given burn time)
d, e) Consider using an iterative approach by estimating a new pressure because of the given change. Determine the resulting regression rate, mass flow rate and c. Use these outcomes to verify if pressure that follows from the relation between mass flow rate, c-star, combustion chamber pressure, and throat area has converged. If not, adapt your estimate.*

1) *a) Regression rate constant* $a = 4.84 \cdot 10^{-6} \left[\frac{m^{2.8}}{s^{0.2} kg^{0.8}}\right]$

b) $r_{av}(t) = a'\left(G_{ox}(t)\right)^{0.8} \frac{1}{L} \int_0^L x^{-0.2}\, dx$

$r_{av}(t)\ 1.25 a G_{ox}(t)^{0.8} L^{-0.2}$

c) $r_{t,av} = r_{av,0} \cdot \frac{2.6\frac{D-D_0}{D_0}}{\left(\frac{D}{D_0}\right)^{2.6} - 1}$

2) *a)* $r_{av,o} = 1.25 \cdot 3{,}258E\text{-}06 \cdot 2^{-0.2} \cdot \left(\frac{5}{\pi/4 \cdot (0.2)^2}\right)^{0.8} = 0.2047\ mm/s$

b) $r_{av,t_b} = 1.25 \cdot 3{,}258E\text{-}06 \cdot 2^{-0.2} \cdot \left(\frac{5}{\pi/4 \cdot (0.35)^2}\right)^{0.8} = 0.0837\ \text{mm/s}$

c) At start of combustion: $m_f = 1600 \cdot 0.2047E - 3 \cdot \pi \cdot 0.2 \cdot 2.0 = 0.417\ kg/s$. *At end of combustion:* $m_f = 1600 \cdot 0.0837E - 3 \cdot \pi \cdot 0.35 \cdot 2.0 = 0.295\ kg/s$; *Notice that the here calculated fuel mass flow rate confirms that fuel mass flow rate is more than a factor of 10 smaller than the oxidizer mass flow rate.*

The variation in port diameter along the grain will influence the fuel mass flow rate at end of combustion. Here we choose to neglect this influence for simplicity. To estimate this effect, it is necessary to compute the progression of the fuel surface in time, thereby allowing for a revised estimate of the mass flux at each instant in time and at each location.

d) Sliver mass
Sliver mass is estimated based on the volume remaining at burnout. The latter depends on the average diameter at burnout: $V_f = \frac{\pi}{4} \cdot [0.4^2 - 0.35^2] \cdot 2 = 0.0589\ m^3$
If follows for the sliver mass: $M_f = \rho_f \cdot V_f = 1600 \cdot 0.0589 = 94.25\ kg$.

This can be compared with a total fuel mass at start of combustion of about 302 kg.

Notice that because we use the average diameter to estimate sliver mass, this may lead to a different result when using the real port geometry (square of average value is not necessarily identical to average of squared values).

3) *Initial burn surface is 41.65 m². (web thickness w, see figure on the side, of outer rim is 16 cm and thickness of the spokes is 32 cm, R_{in} is 64 cm, beta is 14.47 deg, h is 45.97 cm).*

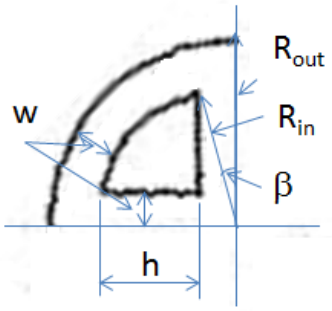

4) *a) Initial grain surface of the cylindrical grain with crucifix port is 23.2 m². It is based on the perimeter of the 2 arms; each has a perimeter of 2*0.38 m + 2*0.2 m = 1.16 m. This gives a total perimeter (2 arms) of 2 x 1.16 = 2.32 m. This should be multiplied by the length of the grain to get the burn surface.*

b) At the moment that the fuel surface has regressed over 10 cm, each arm has a length of 0.78 m. The width of each arm is 0.4 m. This gives a perimeter for the burn surface of each arm of 1.56 m. Total perimeter of the burn surface is 3.12 m and the burn surface is 31.2 m² or about 1.5 times the value at start.

5) *To obtain a first solution, we assume that the specific impulse remains constant over the burn time (later we can verify if this is the case). Furthermore, we assume a cylindrical grain with a cylindrical port that burns from the inside out. It follows:*

a. *Propellant mass is 112 kg.*
b. *Fuel mass is 20 kg (from the given O/F ratio).*
c. *Fuel volume is 21.3 litre.*
d. *Web thickness is 0.0625 m (6.25 cm).*

Next, we assume an initial grain port diameter of 0.2 m (20 cm), it follows:
e. *Initial grain port radius is 10 cm.*
f. *Outer radius of the grain is 16.75 cm (diameter is 33.5 cm).*
g. *Length of the grain is 0.413 m (41.3 cm).*
h. *Initial burn surface is 0.2594 m2*

i. *Initial fuel mass flow rate is 0.324 kg/s.*
j. *Length of the chamber is 1.25 x 41.3 cm is 51.6 cm.*

If for this assignment, also the combustion gas properties are known, we can dimension the nozzle using IRT. In that case, we can also check if the nozzle throat is sufficiently smaller than the grain port thereby ensuring a chamber Mach number < 0.3.

Chapter 14: Liquid Propellant Storage

1) *Answers are provided in the next table for three different propellant temperatures*[2].

O/F	*1.65*	*1.65*	*1.65*
Temperature [deg C]	***5***	***20***	***40***
NTO mass density [kg/m^3]	*1420*	*1390*	*1330*
MMH mass density [kg/m^3]	*890*	*875*	*860*
Propellant load [kg]	*3000*	*3000*	*3000*
Oxidizer mass [kg]	*1868*	*1868*	*1868*
Fuel mass [kg]	*1132*	*1132*	*1132*
Oxidizer volume [m^3]	*1.32*	*1.34*	*1.40*
Fuel volume [m^3]	*1.27*	*1.29*	*1.32*
Total volume [m^3]	*2.59*	*2.64*	*2.72*
Total tank volume (fill ratio = 90%) [m^3]	*2.87*	*2.93*	*3.02*
Total tank volume (fill ratio = 55%) [m^3]	*4.70*	*4.80*	*4.95*

Clearly highest tank volume is associated with highest storage temperature. Furthermore, we see that fuel and oxidizer volume are quite comparable. Hence, one may decide to use the same tank design for fuel and oxidizer.

2) *Next table gives results obtained.*

Tank	***M_{prop} [kg]***	***$K_{t,prop}$ [-]***	***K_{PV} [m^2/s^2]***	***Shell mass [kg]***	***Shell-to-tank mass factor [-]***
Space Shuttle ET	*730,158*	*0.041*[3]	*1.78 E4*	*1506/4791*	*4.75*
Ariane 5 EPC	*156,200*	*0.028*[4]	*3.17 E4*	*875/1473*	*1.87*
Ariane 4 PAL	*37,209*	*0.034*	*NA*	*NA*	*NA*
Ariane 4 stage 3	*11,868*	*0.056*	*NA*	*NA*	*NA*
Saturn V stage 1, fuel tank	*630,000*	*0.017*	*2.23 E4*	*6106*	*1.80*
Saturn V stage 1, oxidizer tank	*1,430,000*	*0.013*	*1.24 E4*	*4151*	*4.58*

Results for tank mass factor are given in column 3. When comparing these values with values as obtained from Larson and Wertz (0.05 – 0.15), we find that current values are lower. This is explainable as Larson and Wertz focus on much smaller vehicles (satellites), whereas here the focus is on launch vehicles. Clearly, the tank mass factor reduces with increasing propellant mass. It is noted that for some tanks only the combined oxidizer and fuel tank mass was available. It is considered that this factor depends on the type of liquid contained in the tank as suggested by the relations from Maryland university as reported in the TRP reader. It may be useful to investigate in more detail and to obtain information on Mean Absolute Percentage Error (MAPE) and the standard deviation on the absolute percentage error.

Tank performance factor is given in column 4. Sufficient data was found to be available for 4 tanks only. It is noted that tank pressures indicated in Table 10 (chapter on storage systems) were considered to equal Maximum Expected Operating Pressure (MEOP) for the tanks. When comparing the values with the values reported in Table 8 (chapter on storage systems), compare with values obtained for tanks with no PMD, the current results show somewhat lower values compared to the mean value of 4.0 E4 m^2/s^2 as found in the table. This again is due to that the values reported earlier were obtained mainly based on satellites and not launch vehicles. Not clear is also if in the data tabulated in the reader insulation mass is considered or not. This may further affect the picture in favour of lower factors for the here calculated tank performance factors. Here some further research may shed some more light.

[2] *Mass density values of fuel and oxidizer have been obtained from a paper by Colozza: (PDF) Comparison of Mars Aircraft Propulsion Systems*
[3] Value is 0.036 for the super lightweight tank.
[4] Value is 0,0289 for Ariane 5 EPC H173 stage.

Shell to tank mass factor is given in the last column. Values for this factor have been calculated using the values as given in the table referred to in the problem as inputs. We have included a Factor of Safety of 1.5 on MEOP in accordance with ECSS-E-ST-32-02C Rev.2 DIR1 11 December 2024. This factor applies to both manned and unmanned spacecraft. All tanks have been assumed to have a cylindrical shape with at bottom and top a 2:1 semi-ellipsoidal endcap. No consideration is given to shared tank walls. All tanks included in table have been calculated using Al 2219 as the structural material. From Annex K we selected an ultimate design strength of 455 MPa (at room temperature), 580 MPa at 90 K and 680 at 20 K and a material mass density of 2810 kg. Estimated tank mass is given in column 5. First value is for the oxidizer tank; second value is for the fuel tank (where applicable). Column 6 gives the estimated thickness of the cylindrical tank wall, which is identical to the thickness of the semi-ellipsoidal endcaps. Wall thickness has been calculated assuming a monocoque wall[5]. The first value reported is for the oxidizer tank and the second for the fuel tank. These values are included for comparison with reported tank skin thickness values, see the data table (Table 10) given in chapter on storage systems.

Results show shell-to-tank tank mass (correction) factors in range 2 – 5. This is quite high and contrary to data earlier shown in chapter on storage systems. It is hypothesized that, for launch vehicles, next to internal pressure loads also other loads should be accounted for, like first and foremost the weight of the propellant leading to hydrostatic loads in the tank, but also attachment loads (from boosters and/or external tank, like for the Space shuttle), launch loads (the weight of upper stages weighs down on the lower stages and especially the cylindrical parts), etc. This should be studied in more detail. A further factor of influence may be the ultimate strength of the material. Strength values have been assumed but may be different from actual strength values.

All in all, this final method has the potential to be most exact, but requires additional modelling, which may make this method unsuitable for quick estimates. The other two methods are simpler to apply, allowing for easy scaling with propellant mass. However, the results may still be quite inaccurate and hence again some further investigations in validating the methods over a large range of propellant mass is advised.

Chapter 15: Liquid Propellant Feeding

1) *From the given data, and using the rocket equation, we calculate a propellant mass of 2809 kg. From this mass and the given specific impulse, we than calculate a total impulse of 8.4 MNs. This is well within the range (< 10-15 MNs) indicated in the reader for selecting a pressure-fed feed system. A final argument for a pressure-fed system is that the chamber pressure is just 20 bar, which is a quite common value for pressure-fed systems.*

2) *The required pressurant mass is 22.8 kg, which is stored in a 106 l pressurant tank at 200 bars. This is based on a total propellant mass to be stored (including excess propellant) of 424.2 kg, a total tank volume of 407 l (fill ratio of 0.9). We have assumed isentropic expansion to occur in the pressurant tank as the system works in a single burst, meaning there is little time for heat to flow from the environment to the tank. This is considered a worst-case situation. In case of isothermal or polytropic expansion, less pressurant gas is needed. In case one wants to be sure, some more detailed modelling or testing is needed. Additionally, we note that the end pressure in the pressurant tank of 30 bar may be too low for the proper operation of the regulator, also, one would like to include some margin. This will require some additional pressurant gas to be loaded and hence a somewhat larger pressurant tank volume. For a more exact estimate, you are advised to follow the modelling guidelines as given in chapter 15.*

3) *a) Static pressure is 5.24 bars, and static head is 46.8 m.*
   b) Total head in the suction piping is 46.8 m.
   c) Stagnation pressure is 5.24 bar.
   d) Dynamic head is 5.1 m.
   e) Dynamic pressure is 0.57 bar.
   f) Static head is 41.7 m.
   g) Static pressure is 4.67 bar.

4) *a) 29.4 MW, b) 36.8 MW, c) 40.9 MW, d) 74.3 MW.*

5) *0.273 MW.*

6) *a) LOX pump hydraulic power is 2.36 MW (oxidizer mass flow rate is 207 kg/s, pump pressure rise is 130 bars and LOX mass density is 1140 kg/m^3).*
   b) Pump head is 1163.6 m (~1.2 km).
   c) Pump efficiency is 73.8% (= 2.36 MW/3.2 MW).

[5] In practice, most tank walls have stiffeners and stringers that help to carry the loads. This also can lead to lower tank wall thickness as follows from the here used thin shell theory.

d) Pump specific speed based on SI units is 0.51. Note that pump rotational speed is based on 12700 RPM and equals 1330 rad/s.
e) Output power required from the turbine to drive the oxygen pump is 3.76 MW. This considers the mechanical efficiency of 0.85.
f) Total turbine mass flow rate is 1.08 kg/s for the given turbine pressure ratio of 12, TET of 873 K, and the gas generator O/F ratio of 0.91. The latter two have been used to calculate the gas properties of the gas leaving the gas generator. Consider that you can use either RPA-lite or CEA or calculate the gas properties of you can compute them yourself assuming complete combustion. We should find a molar mass of 3.85 gram/mole, a specific heat ratio of 1.369 and a specific heat at constant pressure of 8013 J/(kg -K, where the temperature of the oxygen and hydrogen entering the gas generator were set at 91 K and 20 K respectively.
g) The pump mass has been calculated using the relation as provided in the section on turbopump assembly mass estimation. It should give an oxidizer pump mass of ~178 kg.

Chapter 16: Ignition

1) *Using FVM, we should obtain an igniter charge mass of 0.5 g (here we neglected that the relation given in this work has been obtained for Alclo propellants only); Using CPM, we get 0.2 g.*
2) *Igniter propellant mass flow rate is 22.5 g/s.*

Chapter 17: Motor Controls

1) *Aerodynamic pitching moment is 8.9E5 Nm.*

2) *a) 8.727E4 Nm, b) 2.500E4 Nm.*

5) *a) 2.2E7 Nm; b) 9.4E6 Nm; c) 0.192 rad/s^2; d) 40.05 s.*

6) *a) 10 kNm; b) 17.5 ms; c) 517 ms; d) 62.5 kN.*

Appendices

Contents

Annex A: International Chemical Safety Card (ICSC) 468

Annex B: Background on specific thermodynamic properties 471

Annex C: Specific friction factor relations for single phase flow 475

Annex D: Specific Nusselt number relations for single-phase flow 479

Annex E: Gas Injection (draft) 485

Annex F: Hybrid fuel regression rate 487

Annex G: Typical geometries 491

Annex H: Liquid Rocket Engine Mass and Size Estimation Relationships 493

Annex I: Engine mass based on component masses 498

Annex J: Solid rocket motor mass and size estimation relationships 501

Annex K: Properties of specific materials used in rocketry 510

Annex L: Design of thin shell pressurized space structures 519

Annex M: Ariane 5 EAP238 solid rocket motor thickness estimation/verification 533

Annex A: International Chemical Safety Card (ICSC)

The International Occupational Safety and Health Information Centre (SIC) of the International Labour Organization (ILO) offers a database of International Chemical Safety Cards (ISCS). These cards summarize essential health and safety information on chemicals for their use at the "shop floor" level by workers and employers in factories, agriculture, construction and other workplaces. An ICSC is not a legally binding document but consist of a series of standard phrases; mainly summarizing health and safety information collected, verified and peers reviewed by internationally recognized experts. The following pages give an example of such an ICSC.

CARBON DIOXIDE

0021
October 1994

CAS No: 124-38-9
RTECS No: FF6400000
UN No: 1013
EC No:

Carbonic acid gas
Carbonic anhydride
CO_2
Molecular mass: 44.0

TYPES OF HAZARD/ EXPOSURE	ACUTE HAZARDS/SYMPTOMS	PREVENTION	FIRST AID/FIRE FIGHTING
FIRE	Not combustible.		In case of fire in the surroundings: all extinguishing agents allowed.
EXPLOSION	Containers may burst in the heat of a fire!		In case of fire: keep cylinder cool by spraying with water. Combat fire from a sheltered position.
EXPOSURE			
Inhalation	Dizziness. Headache. Elevated blood pressure. Tachycardia.	Ventilation.	Fresh air, rest. Artificial respiration if indicated. Refer for medical attention.
Skin	ON CONTACT WITH LIQUID: FROSTBITE.	Cold-insulating gloves. Protective clothing.	ON FROSTBITE: rinse with plenty of water, do NOT remove clothes. Refer for medical attention.
Eyes	On contact with liquid: frostbite.	Safety goggles, or face shield.	First rinse with plenty of water for several minutes (remove contact lenses if easily possible), then take to a doctor.
Ingestion			

SPILLAGE DISPOSAL	PACKAGING & LABELLING
Ventilation. NEVER direct water jet on liquid (extra personal protection: self-contained breathing apparatus).	Symbol R: S: UN Hazard Class: 2.2

EMERGENCY RESPONSE	STORAGE
Transport Emergency Card: TEC (R)-11-1 (in cylinders); 11-2 (refrigerated gas)	Fireproof if in building. Cool.

IPCS
International Programme on Chemical Safety

Prepared in the context of cooperation between the International Programme on Chemical Safety and the European Commission
© IPCS 1999
SEE IMPORTANT INFORMATION ON THE BACK.

0021	CARBON DIOXIDE

IMPORTANT DATA

Physical State; Appearance
ODOURLESS, COLOURLESS, COMPRESSED LIQUEFIED GAS.

Physical Dangers
The gas is heavier than air and may accumulate in low ceiling spaces causing deficiency of oxygen. Build up of static electricity can occur at fast flow rates and may ignite any explosive mixtures present. Free-flowing liquid condenses to form extremely cold dry ice.

Chemical Dangers
The substance decomposes on heating above 2000°C producing toxic carbon monoxide. Reacts violently with strong bases and alkali metals. Various metal dusts such as magnesium, zirconium, titanium, aluminium, chromium and manganese are ignitable and explosive when suspended and heated in carbon dioxide.

Occupational Exposure Limits
TLV: 5000 ppm; 9000 mg/m^3 (as TWA);
30,000 ppm; 54,000 mg/m^3 (as STEL) (ACGIH 1994-1995).
MAK: 5000 ppm; 9000 mg/m^3 (1993).

Routes of Exposure
The substance can be absorbed into the body by inhalation.

Inhalation Risk
On loss of containment this liquid evaporates very quickly causing supersaturation of the air with serious risk of suffocation when in confined areas.

Effects of Short-term Exposure
Inhalation of high concentrations of this gas may cause hyperventilation and unconciousness. Rapid evaporation of the liquid may cause frostbite.

Effects of Long-term or Repeated Exposure
The substance may have effects on the metabolism.

PHYSICAL PROPERTIES

Sublimation point: -79°C
Solubility in water, ml/100 ml at 20°C: 88
Vapour pressure, kPa at 20°C: 5720
Relative vapour density (air = 1): 1.5

ENVIRONMENTAL DATA

NOTES

Carbon dioxide is given off by many fermentation processes (wine, beer, etc.) and is a major component of flue gas. High concentrations in the air cause a deficiency of oxygen with the risk of unconsciousness or death. Check oxygen content before entering area. No odour warning if toxic concentrations are present. Turn leaking cylinder with the leak up to prevent escape of gas in liquid state. Other UN classification numbers for transport are: UN 1845 carbon dioxide, dry ice; UN 2187 carbon dioxide refrigerated liquid.

ADDITIONAL INFORMATION

LEGAL NOTICE	Neither the EC nor the IPCS nor any person acting on behalf of the EC or the IPCS is responsible for the use which might be made of this information

© IPCS 1999

Annex B: Background on specific thermodynamic properties

In this section we present some background information on:

- Dalton's law of partial pressures for a gas mixture
- Relation between free energy and equilibrium constant
- Entropy of a gas mixture

Relation between partial pressure and molar quantity
According to Dalton's law, the total pressure in the gas mixture equals the sum of the partial pressures of the various components:

$$p = \sum_i p_i \tag{B.1}$$

If a mixture of ideal gases is considered, the ideal gas law gives a relation between partial pressure and molar quantity for each substance i.

$$p_i \cdot V = n_i \cdot R_A \cdot T \tag{B.2}$$

This also holds for the whole mixture:

$$p \cdot V = \sum_i n_i \cdot R_A \cdot T = N \cdot R_A \cdot T \tag{B.3}$$

Comparing the above two relations and after some reworking yields:

$$p_i = n_i \cdot \frac{p}{N} \tag{B.4}$$

This equation shows that the partial pressures are proportional to the molar quantities.

From Wikepedia, we learn that Dalton's law is not exactly followed by real gases. Those deviations are considerably large at high pressures. In such conditions, the volume occupied by the molecules can become significant compared to the free space between them. Moreover, the short average distance between molecules raises the intensity of intermolecular forces between gas molecules enough to substantially change the pressure exerted by them. Neither of those effects is considered by the ideal gas model.

Relation between free energy and equilibrium constant
Gibbs' free energy (G) – the maximum energy available to do non-pressure work. It depends on enthalpy(H), temperature (T) and entropy (S):

$$G = H - TS \tag{B.5}$$

In the above equation H is enthalpy, S is entropy, and T is absolute temperature. Free energy is a state function because it is formally defined only in terms of state functions, the state functions enthalpy and entropy, and the state variable temperature.

An infinitely small change in free energy dG would then be given by dG = dH - d(TS). For any constant-temperature (isothermal) change, this leads to the Gibbs-Helmholtz equation for larger changes:

$$\Delta H = \Delta G + T\Delta S \tag{B.6}$$

This equation has the physical meaning (for constant pressure processes):

$$\begin{aligned}&\text{Total energy available as heat}\\&= \Delta G + \text{energy not available for doing work}\end{aligned} \tag{B.7}$$

It therefore follows that ΔG must be the free energy (available for doing work).

Any process, and in particular any chemical reaction taking place under any conditions, must fall into one of three categories:

- If the free energy change is negative, the process can take place spontaneously doing work on the surroundings as it does so.
- If the free energy change is positive, the process is not spontaneous; it will not occur of itself under these conditions but can be driven by application of sufficient energy from the surroundings.
- If the free energy change of the process is zero, then the system is at equilibrium since the work being done on the process and by the process is equal.

The information contained in free energy values and in equilibrium constant values is the same information, which is the position of chemical equilibrium for the chemical system to which the values refer. There must be, therefore, a relationship between the numerical value for a free energy change and the numerical value for the equilibrium constant whose process corresponds to that change. This relationship is given below:

$$K_p = e^{\left(\frac{-\Delta G}{RT}\right)} \tag{B.8}$$

Where R is the absolute gas constant and T is temperature.

The advantage of the Gibbs free energy is that it can be calculated for a certain temperature based on known values of entropy and enthalpy.

As an example, we will calculate the equilibrium constant for the formation of water from its elements @ 3500 K below. The equilibrium reaction is:

$$H_2 + 1/2O_2 \Leftrightarrow H_2O$$

For the calculation of the Gibbs free energy, we should consider the enthalpy change resulting from the formation of 1 mol of water from its elements at 3500 K. To calculate this heat of formation using Hess's law. According to this law, the heat of formation of water at 3500 K from its elements at 3500 K should equal the enthalpy change from the formation of 1 mol of water at 298 K and the subsequent heating of this one mol to 3500 K. Using NIST database, we find for the heat of formation of 1 mol of gaseous water at 298 K a value of -241.826 kJ. To heat up 1 mol of water from 298 K to 3500 requires 154.8 kJ. The heat needed to heat up the reactants (1 mol of hydrogen and 0.5 mol of oxygen) to 3500 K is 107.6 kJ/mol (H_2) and 118.2 kJ/mol (O_2), respectively. It follows:

$$1 \text{ x } -241.826 + 1 \text{ x } 154.8 = 1 \text{ x } 107.6 + 0.5 \text{ x } 118.2 + Y.$$

Here the heat of formation of water from its elements at 3500 K is indicated as Y. Solving for the unknown Y, we obtain:

$$Y = \Delta H_f^{3500\ K} = -253.696 \text{ kJ}.$$

For the change in entropy follows:

$$\Delta S_{3500\ K} = 295.201 - \left(208.690 + 1/2 \cdot 290.677\right) = -58.8275 \text{ J/(mol K)}$$

This then gives for the change in free energy:

$$\Delta G_{3500\ K} = \Delta H - T \cdot \Delta S = (-253696) - (3500 \cdot -58.8275) = -47.8\ kJ$$

Using the above relationship between the equilibrium constant and the Gibbs free energy, we find for the equilibrium constant:

$$\left(K_p\right)_{H_2O,3500K} = e^{\left(\frac{47800}{8.314 \cdot 3500}\right)} = 5.169$$

The latter value can also be found from the JANAF data tables.

Entropy of a gas mixture

"Entropy" (S) – measure of the disorder in a system. It is defined as $\partial Q/T$ and typically expressed in J/(K-mol). Entropy must be multiplied by the temperature to get energy. Using the first law of thermodynamics, we find:

$$\partial Q = dH - vdp \tag{B.9}$$

$$dS = \frac{dH}{T} - R_A \cdot \frac{dp}{p} \tag{B.10}$$

$$dS = \frac{C_p \cdot dT}{T} - R_A \cdot \frac{dp}{p} \tag{B.11}$$

Integration gives:

$$\Delta S = S_T{}^p - S_{T_o}{}^{p_o} = \int_{T_o}^{T} C_p \cdot \frac{dT}{T} - R_A \cdot \ln\left(\frac{p}{p_o}\right) = 0 \tag{B.12}$$

It is possible by measurement and calculation to determine the amount of entropy that a substance possesses. If the entropy of one mole of a substance is determined at a pressure of 1 atmosphere, we call it the standard entropy, S^o. Several data-books, like the NIST-JANAF thermo-chemical tables, are available that include a listing of standard entropies of a variety of substances at standard conditions (standard pressure of 0,1 MPa and relative to 0 K). The entropy of 1 mole of a substance at a pressure different from the standard pressure then follows from:

$$S_T{}^p = S_T{}^o - R_A \cdot \ln(p) \tag{B.13}$$

Note that in above relation pressure p is p/p_o, but as p_o is taken equal as 1, it is no longer included here.

For a gas mixture of i substances with partial pressure $p_i = n_i(p/N)$, entropy follows using:

$$S_T{}^p = \frac{1}{N}\sum_i n_i \cdot \left[S_T{}^p\right]_i \tag{B.14}$$

$$S_T{}^p = \frac{1}{N}\sum_i n_i \cdot \left[S_T{}^o\right]_i - \frac{R_A}{N} \cdot \left(N \cdot \ln(p) + \sum_i n_i \cdot \ln\left(\frac{n_i}{N}\right)\right) \tag{B.15}$$

Notice that the value of entropy depends on the units used for pressure. Typically we express pressure in bar or atmosphere.

- This page is intentionally left blank -

Annex C: Specific friction factor relations for single phase flow

In this section friction factors are given for specific flow configurations common in thermal rocket motors. Friction factors given apply to single-phase flow only over smooth surfaces or in smooth pipes. Friction factors for flat plate and straight circular pipe flow have been taken from [Bejan], and for helical tubes from [Guo] .

Reynolds number
The Reynolds number Re is a dimensionless number that gives a measure of the ratio of inertial forces to viscous forces. It can be determined using:

$$Re = \frac{\rho \cdot v \cdot L}{\mu} \tag{C.1}$$

Here:
v is the mean fluid velocity
L is a characteristic linear dimension, (travelled length of fluid, or hydraulic radius)
μ is the dynamic viscosity of the fluid
ρ is the mass density of the fluid

Flow over a flat plate
Skin friction coefficient c_f is a dimensionless quantity that follows from shear stress (τ) and dynamic pressure (q) in the flow:

$$c_f = \frac{\tau}{q} = \frac{D}{q \cdot S} \tag{C.2}$$

Here D is the drag force on the plate and S a reference area usually taken to be equal to the plan form area, i.e. the area that can be seen from the plane when looking straight down on the plate. Typical values for the skin friction coefficient for a flat plate are in the range 0.001 to 0.01. Values vary with the Reynolds number and greatly depend on whether the flow is laminar or turbulent. Some detailed relations are given below.

- Incompressible laminar flow ($Re_L < 5 \times 10^5$):

$$c_f = \frac{0,644}{(Re_x)^{0,5}} \text{ (Blasius)} \tag{C.3}$$

- Incompressible turbulent flow ($10^5 < Re_L < 10^7$):

$$c_f = \frac{0,0592}{(Re_x)^{0,2}} \text{ (Blasius)} \tag{C.4}$$

The above two relations both provide a value dependent on the distance x travelled along a plate of length L in flow direction.

Pipe flows
For pipe flows the relation can be written in a similar form.

$$f = \frac{\tau}{q} \tag{C.5}$$

Here f is used to distinguish from the earlier given relations for outer surfaces. The friction factor in the above relation is referred to as the Fanning friction factor. Another form, however, relating the pressure drop due to friction in a pipe with the dynamic pressure has attained higher popularity. It is referred to as the Moody or Blasius friction factor and follows from:

$$\Delta p = f \frac{L}{D} \frac{1}{2} \rho v^2 \qquad \text{(C.6)}$$

With Δp is pressure drop due to friction (i.e. pressure drop in channel of constant cross-section), L is characteristic length, D is the inner diameter of the component, ρ is flow density, and v is flow velocity.

The friction factor f is not a constant and depends on the parameters of the pipe and the velocity of the fluid flow, but it is known to high accuracy within certain flow regimes. It may be evaluated for given conditions using various empirical or theoretical relations, or it may be obtained from published charts. These charts are often referred to as Moody diagrams, after L. F. Moody.

The Darcy–Weisbach friction factor is 4 times larger than the Fanning friction factor, so attention must be paid to note which one of these is meant in any "friction factor" chart or equation being used.

Hereafter, we will introduce specific relations for single phase flow in straight and helically coiled tubes.

Straight circular pipe flow
The friction factor f is given in the next figure.

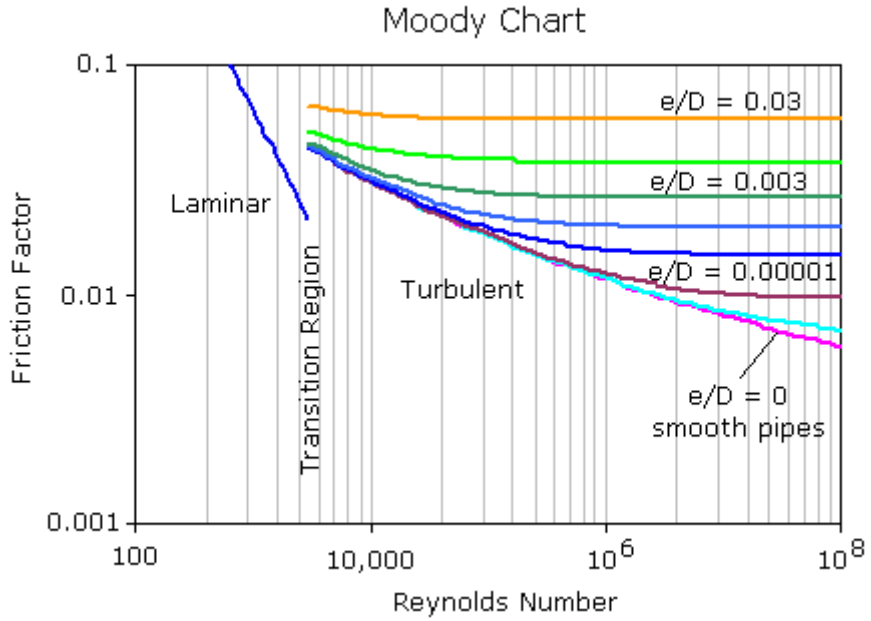

Figure: Friction factor for fluid pipe flow (Moody chart)

From the figure it follows that the friction factor f is in between 0.005 and 0.05 and that its value depends on the Reynolds number of the flow and the pipe smoothness. With respect to Reynolds number we distinguish three different flow regimes:

- Laminar flow: Re < 2320
- Turbulent flow: Re > 10.000
- Transition flow: Intermediate Re numbers

Some empirical relations that allow for calculation of the Darcy-Weisbach friction factor are listed below for the various flow regimes indicated in the figure above.

- Fully developed incompressible laminar flow (Re_D < 2320):

$$f = \frac{64}{Re_D} \text{ (Poisseuille)} \qquad \text{(C.7)}$$

- Fully developed incompressible turbulent flow:
  - $2320 < Re_D < 2 \times 10^4$:

$$f = 0{,}316 \cdot \left(\frac{1}{(Re)_D} \right)^{0{,}25} \quad \text{(Blasius)} \tag{C.8}$$

  - $2 \times 10^4 < Re_D < 10^6$:

$$f = 0{,}184 \cdot \left(\frac{1}{(Re)_D} \right)^{0{,}2} \tag{C.9}$$

  - $3 \times 10^3 < Re_D < 10^7$:

$$f = 0{,}0032 + 0{,}221 \cdot \left(\frac{1}{(Re)_D} \right)^{0{,}237} \quad \text{(Nikuradse)} \tag{C.10}$$

In the above relations, the Reynolds number is based on the pipe diameter D.

For non-smooth pipes, at high Reynolds number values, the friction coefficient is independent of the Reynolds number, see the Moody diagram. In that case, the friction factor can be determined using the following equation from Nikuradse:

$$f_T = 8 \cdot \left(2.457 \cdot \ln\left(3.707 \cdot \frac{1}{e/D} \right) \right)^{-2} \tag{C.11}$$

With e/D is a measure for the pipe roughness and e is the height of the wall roughness[1]. At lower values of Reynolds, you can directly read from the Moody diagram or derive an approximate analytical relation. This will be left to the reader to explore for himself.

Flow inside helically coiled tube.

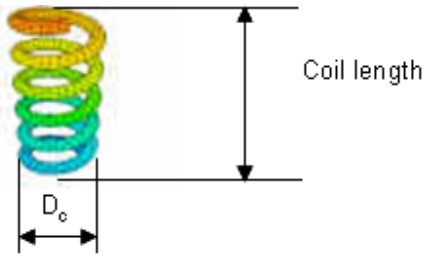

For a helical tube, see figure, with coil diameter D_c and internal tube diameter D the following relations apply:

- Laminar flow, smooth duct:

  [Guo] recommends the following expression suggested by White:

[1] Typical values of wall roughness height (e) for different tubes:
- Aluminum (new): 0.001-0.002 mm
- Stainless Steel (SS): 0.015 mm
- Steel commercial pipe: 0.045-0.09 mm
- Riveted steel: 0.9-9 mm
- Titanium: 0.05 mm
- Glass-fiber Reinforced Pipe (GRP): 0.02 mm

$$f_c/f_s = \frac{1}{1-\left[1-\left\{\frac{11.6}{Re\cdot\left(\frac{D}{D_c}\right)^{0.5}}\right\}^{0.45}\right]^{1/0.45}} \quad \text{(White)} \qquad \text{(C.12)}$$

- Turbulent flow, smooth duct

  [Guo] recommends the following expression suggested by Ito:

$$f_c = 0.304\cdot\left(Re_D\right)^{-0.25} + 0.029\cdot\left(\frac{D}{D_c}\right)^{0.5} \quad \text{(Ito)} \qquad \text{(C.13)}$$

In these relations f_c is friction factor coiled tube and f_s is friction factor straight tube. $(Re_D)_{cr}$ is determined according to Ito:

$$\left(Re_D\right)_{cr} = 20000\cdot\left(\frac{D}{D_c}\right)^{0.32} \quad \text{(Ito)} \qquad \text{(C.14)}$$

Average friction factor for wire mesh screen matrices

For wire mesh screens the following relation may apply [Thakur]:

$$f_p = 2.484\left[\left(\frac{1}{nP}\right)\left(\frac{P_t}{d_w}\right)\right]^{0.699} Re_p^{-0.44} \qquad \text{(C.15)}$$

With:

d_w	Wire diameter of wire screen matrices (m)
f_p	Average friction coefficient
n	Number of layers
P	Porosity of bed, i.e.the fraction of void space in the material
P_t	Pitch of wire mesh screen (m)
Re_P	Reynolds number of packed bed (based on hydraulic diameter)

References

1. *Bejan A.,* Heat Transfer, John Wiley & Sons, Inc., ISBN 0-471-50290-1, 1993.

2. Guo L., Feng Z, Chen X, An experimental investigation of the frictional pressure drop of steam-water two-phase flows in helical coils, Intern. Journal of Heat and Mass Transfer 44, 2001.

3. Thakur N.S., Saini J.S., Solanki S.C., Heat transfer and friction factor correlations for packed bed solar air heater for a low porosity system, Solar Energy 74 (2003) 319–329.

Annex D: Specific Nusselt number relations for single-phase flow

An important parameter in the calculation and/or analysis of problems dealing with convective heat transfer is the Nusselt number (Nu). It gives is the ratio of convective to conductive heat transfer across (normal to) the boundary layer.

In this section some specific Nusselt number relations are given for single-phase flow with forced convection. Relations for free convection and boiling and/or two-phase flow can be found in the work of [Ferreira].

Relations presented are of the form:

$$Nu = f(Re, Pr) \tag{D-1}$$

With:

- Re = Reynolds number [-]
- Pr = Prandtl number [-]

Relations are given for:

- Flat plate flow
- Straight smooth pipe
- Flow in helical tube
- Flow in packed beds of spheres
- Flow between two annular walls

All relations allow for determining an average or overall heat transfer coefficient. This allows for the determination of an average convective heat flux coefficient as well as the total heat load in a fairly straight forward way. Local heat transfer here is neglected but may sometimes show that locally much higher heat transfer rates may be expected.

Two boundary conditions are considered:

- Uniform heat flux thermal boundary condition where the calculation of the heat flux is based on the arithmetic mean temperature difference.
- Uniform wall temperature, where the calculation of the heat flux is based on the logarithmic mean temperature difference.

The resulting Nusselt number relation may depend on the boundary condition considered.

All relations given are valid in case we have moderate temperature differences in the flow and between wall and flow. In case large temperature variations occur, we need to take into account the effect of temperature on fluid properties. This is discussed in some detail in the final section of this work.

A) Flat plate

Laminar flow

In case of laminar flow over a plane wall the following expression can be used to determine an average or overall heat transfer coefficient [Bejan]:

$$Nu_L = 0.664 \cdot Re_L^{0.5} \cdot Pr^{1/3} \tag{D-2}$$

Here the flat plate length L in flow direction is used as the characteristic dimension. The above relationship was first presented by Pohlhausen and is valid for $Re_L < 5 \times 10^5$ and $Pr > 0.5$. All fluid properties are to be evaluated at the conditions that hold outside the boundary layer.

Turbulent flow
In case of turbulent flow along a flat plate of length L, an expression for the average or overall Nusselt number is given by [Bejan]:

$$Nu_L = 0.037 \cdot \left(Re_L^{0.8} - 23550\right) \cdot Pr^{1/3} \quad \text{(D-3)}$$

The formula is valid for Reynolds numbers in between 5 x 10^5 and 10^8 and for Pr > 0.5

Remarks
For expressions that allow determining the Nusselt number as a function of location along the flat plate, see for instance [Bejan].

B) Straight smooth pipe (or tube)

When considering heat transfer in a tube, we should not only consider laminar or turbulent flow, but also whether the boundary layer is fully developed or whether we are dealing with the entrance region of the tube. In the latter case, we should take into account that the Nusselt number varies with the distance travelled in the tube. In real life tube/pipe flows generally are a combination of the two, but for most practical cases, we find that the Nusselt number can be considered constant along the tube.

Thermally fully developed laminar flow
From [Bejan] we learn that for the thermally fully developed flow (long pipe with length to inner diameter ratio equal or in excess of 60) Nu can be considered constant. When using the tube diameter D as the characteristic dimension, it follows:

$$Nu_D = 3.66 \text{ (uniform wall temperature)} \quad \text{(D-4)}$$

$$Nu_D = 4.364 \text{ (uniform wall heat flux)} \quad \text{(D-5)}$$

Entrance region, laminar flow
The thermal entrance length X_T wherein the Nusselt number varies with the axial location in the tube is given by:

$$\frac{X_T}{D} = 0.05 \cdot \left(Re\right)_D \cdot Pr \quad \text{(D-6)}$$

For Pr more than 1, this is always larger than the hydrodynamic entry length.

Developing laminar flow
For applications wherein we must reckon with a simultaneously developing thermal and laminar flow, [Chemsource] recommends calculating the average Nusselt number for a tube of length L using the relationship as proposed by Stephan:

$$Nu_D = 3.657 + \frac{0.0677\left(Re \cdot Pr \cdot \frac{D}{L}\right)^{1.33}}{1 + 0.1 \cdot Pr \cdot \left(Re \cdot \frac{D}{L}\right)^{0.3}} \text{ (uniform wall temperature)} \quad \text{(D-7)}$$

In this relation:
D = (hydraulic) diameter [m] = 4·A/s
A = cross-sectional area [m^2]
s = wetted perimeter [m]
L = tube length [m]

The equation also considers the effect of the entrance region and is valid for Re < 2300 and in case we have a constant wall temperature. Notice that for very long tubes Nu_d reaches the limit value [Bejan] for thermally fully developed flow.

For relatively short tubes a simpler relation is available developed by Sieder and Tate in 1936 who determined an average Nusselt number over the entire length of the tube (including the entrance region)[2] [Chapman]:

$$Nu_D = 1.86 \cdot (Re_D \cdot Pr)^{1/3} \ (L/D)^{-0.333} \qquad \text{(D-8)}$$

This equation is applicable for Re_D Pr D/L > 10 and with all fluid properties evaluated at bulk temperature. Note that this equation can only be used if the outcome is higher than the value that follows in case of a thermally fully developed boundary layer. This is 3.66 in case of uniform wall temperature and 4.36 in case of uniform heat flux.

Turbulent flow

A traditional expression for turbulent pipe flow in a smooth tube of diameter D is due to Colburn:

$$Nu_D = 0.023 \cdot Re_D^{0.8} \cdot Pr^{1/3} \qquad \text{(D-9)}$$

This relation holds in the range 10000 < Re < 1000000, 0.7 < Pr < 700, and L/D > 60. All the physical properties except the viscosity in the Reynolds number are to be evaluated at the mean bulk temperature of the fluid $T_{bulk} = (T_i + T_o)/2$, where T_i and T_o are the inlet and outlet temperatures.

Another correlation (due to Dittus and Boelter, 1930) is:

$$Nu_D = 0.023 \cdot Re_D^{0.8} \cdot Pr^{n} \qquad \text{(D-10)}$$

Here n has a value of 0.4 for heating and 0.3 for cooling. This equation is valid for 2500 < Re < 120000, 0.7 < Pr < 120, and L/D > 60. All the physical properties are to be evaluated at the mean bulk temperature of the fluid $(T_i + T_o)/2$. The maximum deviation between experimental data and values predicted using this equation is of the order of 40% [Bejan].

For short tubes wherein the effect of the entrance region is not negligible, it is proposed to use a relation proposed by Nusselt (1931), who again used the tube diameter D as the characteristic parameter:

$$Nu_D = 0.036 \cdot Re_D^{0.8} \cdot Pr^{1/3} \ (L/D)^{-0.054} \qquad \text{(D-11)}$$

This equation is applicable for 10 < L/D < 400 and properties evaluated at bulk temperature.

C) Heat transfer for flow in a helical tube

For flows through a helical tube, see figure, with coil diameter D_c and internal tube diameter D, the following relations apply:

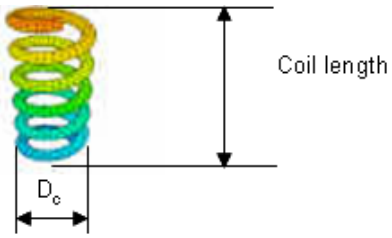

- Laminar flow [Naphon]:

$$Nu_D = \left(0.76 + 0.65 \cdot Re_D^{0.5} \cdot \left(\frac{D}{D_c}\right)^{0.25}\right) \cdot Pr^{0.175} \ \text{(valid for 5 < Pr < 175)} \qquad \text{(D-12)}$$

[2] Note temperature effect as included in the original Sieder-Tate relation has not been included here. For this, see the final section of this annex.

And:

$$Nu_D = 0.913\left(Re_D \cdot \left(\frac{D}{D_c}\right)^{0.5}\right)^{0.476} \cdot Pr^{0.2} \text{ (valid for } 0.7 < Pr < 5) \quad \text{(D-13)}$$

The first relation is accredited to Dravid at al (1971) and the second to Kalb and Seader (1972).

- Turbulent flow [Rohsenow]:

$$Nu_D = 0.023 \cdot Re_D^{0.85} \cdot Pr^{0.4} \cdot \left(\frac{D}{D_c}\right)^{0.1} a \quad \text{(D-14)}$$

The above relation has been derived by Rohsenow based on the work of [Seban and Mclaughlin]. The relation is valid in the range $10.000 < Re_D < 100.000$

D) Heat transfer for flow in packed beds of spheres [Balmer]

For flow through packed beds of spheres, diameter d, by experiment:

$$Nu_d = 1.82 \cdot Re_d^{0.49} \cdot Pr^{0.33} \quad \text{for } Re_d < 350 \quad \text{(D-15)}$$

$$Nu_d = 0.989 \cdot Re_d^{0.59} \cdot Pr^{0.33} \quad \text{for } Re_d > 350 \quad \text{(D-16)}$$

E) Heat transfer for flow between two annular walls [Chemical resources].

- Heat transfer at both walls, same wall temperatures (Stephan):

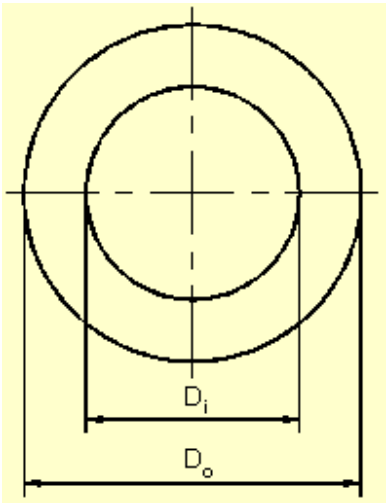

All properties at fluid bulk mean temperature (arithmetic mean of inlet and outlet temperature:

$$\frac{Nu}{Nu_{tube}} = \frac{0.86 \cdot \left(\frac{D_i}{D_o}\right)^{0.84} + \left[1 - 0.14 \cdot \left(\frac{D_i}{D_o}\right)^{0.6}\right]}{1 + \frac{D_i}{D_o}} \quad \text{(D-17)}$$

Where Nu_{tube} is heat transfer in tube with diameter $D = D_o - D_i$.

- Heat transfer at the inner wall, outer wall insulated (Petukhov and Roizen):

$$\frac{Nu}{Nu_{tube}} = 0.86 \cdot \left(\frac{D_o}{D_i}\right)^{0.16} \tag{D-18}$$

- Heat transfer at the outer wall, inner wall insulated (Petukhov and Roizen):

$$\frac{Nu}{Nu_{tube}} = 1 - 0.14 \cdot \left(\frac{D_i}{D_o}\right)^{0.6} \tag{D-19}$$

F) Temperature effects [Chemical resources].

In case there is a large temperature difference between wall and flow, we must take into account the temperature dependency of the fluid properties. For instance, viscosity and mass density are temperature dependent. To correct for temperature effects, the following corrections are recommended:

For liquids [Chemsource]:

$$\frac{Nu}{Nu_o} = \left(\frac{\mu}{\mu_w}\right)^{0.14} \tag{D-20}$$

For gases (turbulent flow only) [Chemsource]:

$$\frac{Nu}{Nu_o} = \left(\frac{T}{T_w}\right)^{0.36} \tag{D-21}$$

Here μ and T denote dynamic viscosity and temperature of the bulk fluid, respectively and Nu_o denotes the uncorrected Nusselt number.

References

1) Balmer D, Generalised Analysis of Heat and Mass Transfer through Boundary Layers, http://www.see.ed.ac.uk/~johnc/teaching/fluidmechanics4/2003-04/fluids17/generalised.html

2) Chapman A.J., Heat transfer, (3rd edition), Macmillan Publ. Co., New York, 1974.

3) Chemical resources website. http://www.cheresources.com/convection.shtml

4) Guyer - Handbook of Applied Thermal Design, Ed. Taylor & Francis

5) Ferreira, R., Heat Transfer and Pressure Drop in Single-Phase and Boiling flow (literature study), TU-Delft, Faculty of Aerospace engineering, 2008.

6) Naphon P., Wongwises, S.,. A review of flow and heat transfer characteristics in curved tubes, University of Technology Thonburi, Bangkok, Thailand.

7) Rohsenow, Hartnett, Ganic - Handbook of Heat Transfer Fundamentals, McGraw Hill. 2nd edition, McGraw-Hill book company, 1985.

8) Seban, Mclaughlin, Heat Transfer in Tube coils with Laminar and Turbulent Flow, Int. J. Heat Mass Transfer, 6, 387, 1963.

- This page is intentionally left blank -

Annex E: Gas Injection (draft)

When gas stored under pressure in a closed vessel is discharged to the atmosphere or vacuum through a hole or other opening, the gas velocity through that opening may be choked (i.e., has attained a maximum) or non-choked. Choked flow occurs in case the absolute source vessel pressure is at least 1.7 to 1.9 times as high as the absolute ambient atmospheric pressure. When the gas velocity is choked, the equation for the mass flow rate is:

$$m = C_d \cdot A \cdot \sqrt{\gamma \cdot \rho \cdot p \cdot \left(\frac{2}{\gamma+1}\right)^{\left(\frac{\gamma+1}{(\gamma-1)}\right)}} \qquad \text{(E-1)}$$

Or in equivalent form:

$$m = C_d \cdot p \cdot A \cdot \sqrt{\frac{\gamma \cdot M}{Z \cdot R_A \cdot T} \cdot \left(\frac{2}{\gamma+1}\right)^{\left(\frac{\gamma+1}{(\gamma-1)}\right)}} \qquad \text{(E-2)}$$

The equation for non-choked flow is:

$$m = C_d \cdot A \cdot \sqrt{2 \cdot \rho \cdot p \cdot \left(\frac{\gamma}{\gamma-1}\right) \cdot \left[\left(\frac{p_a}{p}\right)^{2/\gamma} - \left(\frac{p_a}{p}\right)^{\gamma+1/\gamma}\right]} \qquad \text{(E-3)}$$

Here:

m	= mass flow rate, kg / s
C_d	= discharge coefficient (dimensionless, usually about 0.72)
A	= discharge hole area, m^2
γ	= c_p / c_v of the gas = the isentropic expansion coefficient = (specific heat at constant pressure) / (specific heat at constant volume)
ρ	= real gas density, kg / m^3 at p and T
p	= absolute source or upstream pressure, Pa
p_a	= absolute ambient or downstream pressure, Pa
M	= gas molecular weight
R_A	= Universal Gas Law Constant = 8314.5 (Pa) (m^3) / (kgmol) (°K)
T	= gas temperature, °K
Z	= gas compressibility factor at p and T (dimensionless)

Typical values for the discharge factor range from close to 1 for a nicely rounded or streamlined hole to less than about 0.5 in case of a sharp outlet.

Reference:

(1) Online chemical engineering information, http://www.cheresources.com/discharge.shtml#Pressurized Liquid, 2006.

- This page is intentionally left blank -

Annex F: Hybrid fuel regression rate

Average regression rate; small fuel mass flow

In this Section, an equation for the average fuel regression rate at each instant will be derived under the assumption of a cylindrical grain and that the fuel mass flow is much smaller than the oxidizer mass flow.

A general equation for the regression rate of a solid fuel is:

$$r = a \cdot x^{-0,2} \cdot G^{0,8} \qquad \textbf{(F-1)}$$

with the parameter a depending on the chosen oxidizer-fuel combination, G the mass flux through the combustor, and x the position along the fuel grain

When the fuel mass flow is much smaller than the oxidizer mass flow, but not negligibly small, we can write[3]:

$$r \approx a \cdot G_{ox}^{0.8} \cdot x^{-0.2} \cdot [\,1 + 0.8 \cdot \frac{G_f}{G_{ox}}\,] \qquad \textbf{(F-2)}$$

For an homogeneous grain with a cylindrical port with diameter D, it follows for the fuel mass flux:

$$G_f = 4\,\frac{\rho_s}{D} \int r \cdot dx \qquad \textbf{(F-3)}$$

Taking as a first approximation:

$$r = a \cdot G_{ox}^{0.8} \cdot x^{-0.2} \qquad \textbf{(F-4)}$$

gives for (A-2):

$$G_f = \frac{4 \cdot a \cdot \rho_s}{0.8 \cdot D} \cdot G_{ox}^{0.8} \cdot x^{0.8} \qquad \textbf{(F-5)}$$

Substitution of (F-5) in (F-2) gives:

$$r \approx a \cdot G_{ox}^{0.8} \cdot x^{-0.2} \cdot [\,1 + \frac{4 \cdot a \cdot \rho_s}{G_{ox}^{0.2} \cdot D} \cdot x^{0.8}\,] \qquad \textbf{(F-6)}$$

[3] Use has been made of the following mathematical approximation [*Abramowitz & Stegun (1965)*]:

$$(1+x)^n \approx 1 + n\,x \quad (x << 1)$$

For n = 0.8, this approximation gives good results even when x approaches 0.3.

Integration over the burn area and after division by the length of the grain gives for the average regression rate:

$$r \approx a \cdot G_{ox}^{0.8} \cdot L^{-0.2} \cdot \left[1.25 + \frac{2.5 \cdot a \cdot \rho_s}{G_{ox}^{0.2} \cdot D} \cdot L^{0.8} \right] \qquad \textbf{(F-7)}$$

Here the second term on the Right Hand Site (RHS) gives the contribution due to a small, but non-negligible, fuel mass flow.

Time-average regression rate

In this section a time-average regression rate is determined for a hybrid rocket motor in case that the fuel mass flow is negligibly small.

In that case the regression rate at any instant can be determined using:

$$r_{av} = 1.25 \cdot \left[a \cdot G_{ox}^{0.8} \cdot L^{-0.2} \right] \qquad \textbf{(F-8)}$$

To determine a time-average regression rate, it is convenient to write the above equation as follows:

$$r_{av} = 1.25 \cdot \left[a \cdot L^{-0.2} \cdot G_{ox,o}^{0.8} \right] \cdot \left(\frac{D_o}{D} \right)^{1.6} \qquad \textbf{(F-9)}$$

Where $G_{ox,o}$ is the initial oxidizer mass flux, D_o is the initial port diameter and D the instantaneous port diameter. Furthermore, if we introduce the average regression rate at time is zero:

$$r_{av,o} = 1.25 \cdot \left[a \cdot L^{-0.2} \cdot G_{ox,o}^{0.8} \right] \qquad \textbf{(F-10)}$$

We find:

$$r_{av} = r_{av,o} \cdot \left(\frac{D_o}{D} \right)^{1.6} \qquad \textbf{(F-11)}$$

Since $r_{av} = (dD/2)/dt$, (B-2) can now be integrated to give:

$$\left(\frac{D}{D_o} \right)^{2.6} - \left(\frac{D_o}{D_o} \right)^{2.6} = 2.6 \cdot \left[\frac{r_{av,o} \cdot t_b}{D_o / 2} \right] \qquad \textbf{(F-12)}$$

Substitution of:

$$\overline{r_{av}} \cdot t_b = \frac{D - D_o}{2} \qquad \textbf{(F-13)}$$

gives for the overall (time-)average regression rate:

$$\overline{r_{av}} = r_{av,o} \cdot \left[2.6 \cdot \frac{D - D_o}{D_o} \cdot \left[\left(\frac{D}{D_o} \right)^{2.6} - 1 \right]^{-1} \right] \qquad \textbf{(F-14)}$$

Note that (F-14) is not defined for $D = D_o$[4].

[Marxman, Wooldridge and Muzzy, 1963] use a slightly different approach. They simply combine (F-10) and (F-11) and use the average port diameter durng burning D_{av} to determine the time-average regression rate:

$$r \cdot \rho \approx 1.25 \cdot \left[a \cdot L^{0.2} \cdot G_{ox,o}^{0.8} \right] \cdot \left(\frac{D_o}{D_{av}} \right)^{1.6} \qquad \textbf{(F-15)}$$

where:

$$D_{av} \approx D_o + r_{av,o} \cdot t_b \qquad \textbf{(F-16)}$$

An important criterion for applying F-15 is that D_{av} is ot the same order as D_o.

References

1. Abramowitz, M and Stegun, I.A., Handbook of mathematical functions, Dover Books, New York, 1965.
2. Marxman G.A., Wooldridge, C.E., and Muzzy, R.J., Fundamentals of Hybrid Boundary Layer Combustion, AIAA 64-505, AIAA Heterogeneous Combustion Conference, Palm Beach, Fla., December 11-13, 1963.

[4] A solution for $D = D_o$ can be found using l'Hospital's rule for indeterminate forms.

- This page is intentionally left blank -

Annex G: Typical geometries

Formulas for Surface area (S) and Volume (V)

Right circular cylinder

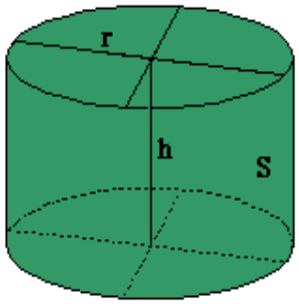

$$S' = 2 \cdot \pi \cdot r \cdot h \text{ (cylindrical surface only)} \quad \text{(G.1)}$$

$$S = 2 \cdot \pi \cdot r \cdot (r + h) \quad \text{(G.2)}$$

$$V = \pi \cdot r^2 \cdot h \quad \text{(G.3)}$$

Sphere

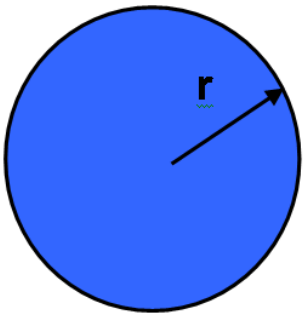

$$S = 4 \cdot \pi \cdot r^2 = \pi \cdot D^2 \quad \text{(G.4)}$$

$$V = \left(\frac{4 \cdot \pi}{3}\right) \cdot r^3 = \left(\frac{\pi}{6}\right) \cdot D^3 \quad \text{(G.5)}$$

Spherical cap

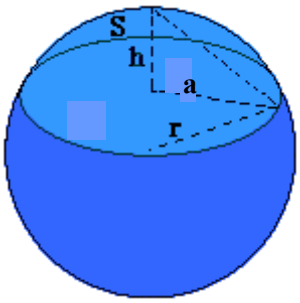

$$S = 2 \cdot \pi \cdot r \cdot h \quad \text{(G.6)}$$

$$V = \left(\frac{\pi}{3}\right) \cdot h^2 \cdot (3r - h) \quad \text{(G.7)}$$

Ellipsoid

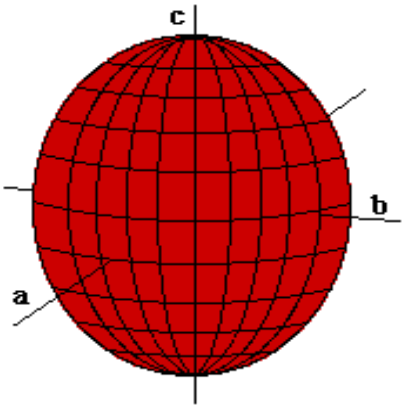

$$S \approx 2 \cdot \pi \cdot a \cdot b \quad \text{(in case c << a and b)} \tag{G.8}$$

$$V = \left(\frac{4 \cdot \pi}{3} \right) \cdot a \cdot b \cdot c \tag{G.9}$$

Torus

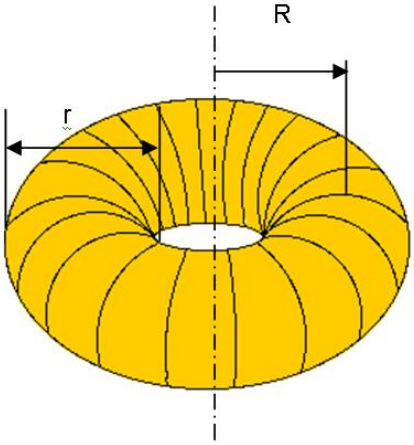

$$S = 4 \cdot \pi^2 \cdot R \cdot r \tag{G.10}$$

$$V = 2 \cdot \pi^2 \cdot R \cdot r^2 \tag{G.11}$$

Annex H: Liquid Rocket Engine Mass and Size Estimation Relationships

In this section various simple expressions are introduced that allow for engine mass and size estimation for pressure-fed storable bipropellant thrusters and hydrazine monopropellant thrusters. Expressions for large pump-fed liquid rocket engines can be found in [Zandbergen, 2015]. Expressions for large solid booster motors and solid rocket upper stage motors can be taken from [Zandbergen, 2005]. Data used for determining the relations are taken from [Zandbergen, 2016] and [Zandbergen 2000].

Total engine mass

From theory, it can be shown that liquid rocket engine or thruster mass is closely related to thrust level, next to various other parameters, see e.g. [Zandbergen, 2015]. Below we will present relations using vacuum thrust as the only determining parameter.

Large Liquid Rocket Engine Assemblies

Typical relations for large LRE are given in [Zandbergen, 2015]. In this publication simple regression rate relationships have been derived to estimate physical liquid rocket engine mass and envelope. These relations have been derived by using multiple regression techniques to fit equations to data obtained from more than 45 historical and current pump-fed liquid rocket engine designs in the thrust range 15 kN to 8 MN including such engines as shown in Figure H-1. The resulting equations allow for a simple approximation of the mass and dimensions of the envelope of a new engine design with only one, see table at the end of this section, or up to maximum 4 inputs. The relationships allow for taking into account as inputs the effect of thrust level, propellant type, single or multi-chamber design, and chamber pressure and expansion ratio. Based on the regression rate relationship used, the resulting approximation contains a relative standard error (RSE[5]) of ±10-25%. A discussion of the data fitting techniques is included as well as an example application of the relationships developed. Also the limitations of the method are outlined followed by the main conclusions of the study.

This publication is available via both the TU-Delft repository and “ResearchGate.net” (web-based).

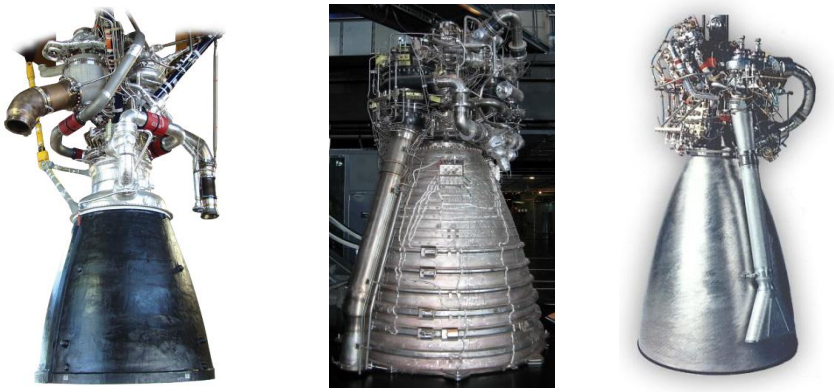

RS-68 (3.3 MN) Vulcain (1.075 MN) HM-7B (62 kN)

Figure H-1: Specific large liquid rocket engines

An overview of some of the more simpler relationships (one variable only) are given in table on next page.

[5] Relative standard error (RSE) is defined as:

$$RSE = \sqrt{\frac{\sum_{j=1}^{N}\left(\frac{y_j}{f(x_j)}-1\right)^2}{N-K}} \times 100\%$$

Here N is total number of data points, K is the number of independent variables estimated in the regression curve, y is the actual value, f(x) is the estimated value, x is the independent variable, and j refers to the various data points.

Table 1: Large rocket engine estimation relationships for mass (M, in kg), length (L in m), and diameter (D in m) as a function of vacuum thrust (Thrust in N) [Zandbergen]

ID	Estimation relationship	Range	RSE
M-C1	$M = 0.00514*Thrust^{0.92068}$	0.6 kN – 3.4 MN	13.1%
L-C1	$L = 0.1667*Thrust^{0.2238}$	1.7 – 5.2 m	10.6%
D-C1	$D=0.1503*Thrust^{0.1915}$	0.9 – 3.1 m	19.1%
M-S1	M = 1.104E-3*Thrust+27.02	0.5 kN - 8 MN	25.8%
L-S1	$L = 0.1362*Thrust^{0.2279}$	1.4 – 5.8 m	17.6%
D-S1	$D = 0.0455*Thrust^{0.2745}$	0.6 – 4.0 m	14.7%

Pressure-fed, Storable Bipropellant thrusters

Mass data of 38 storable bipropellant (NTO - hydrazine, NTO - MMH, NTO - A-50, UDMH – IRFNA) thrusters in thrust range 4 N to 45,000 N are plotted in Figure H-2. Mass data given include the mass of the thrust chamber (combustion chamber, injector and nozzle) and the thruster valve(s). For small thrusters, the latter can make up a considerable part of the total mass reported. The data have been taken from [Zandbergen, 2016]. Regression analysis shows that the data is best represented by the following power curve:

$$M = 0.1103\ F^{0.6319};\ RSE = 53.8\% \qquad (B.1)$$

Here M is thruster mass given in kilogram and F is vacuum thrust in Newton.

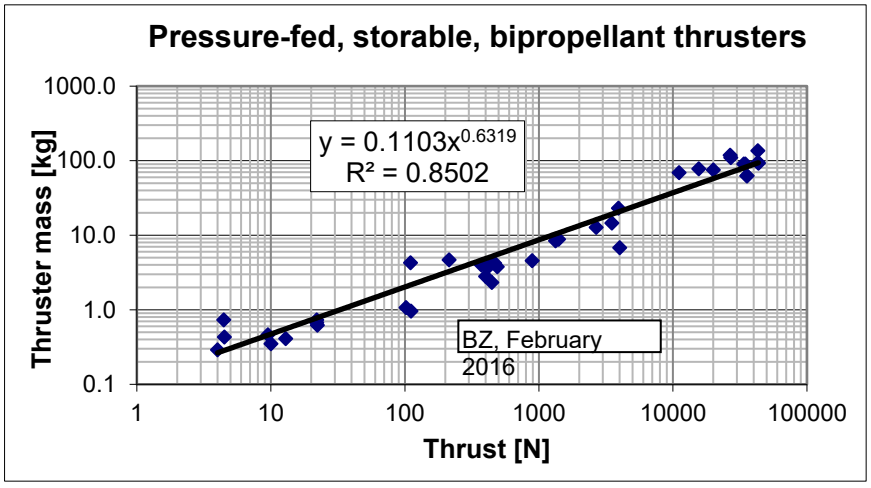

Figure H-2: Mass of pressure-fed, storable, bipropellant thrusters

The fairly large value of the RSE shows that proper margins must be taken into account when using the above relation for thruster mass estimation. A better estimate may be possible in case we also take into account that modern small storable bipropellant thruster are no longer cooled by ablation, but by radiation cooling and/or film cooling with some even using a form of regenerative cooling and/or when considering the effect of having a single or a dual seat valve; the latter is more leak tight than the former. Some thrusters are offered both with single seat or dual seat valves and especially for small thrusters, dual seat valves do lead to a significant increase in total thruster mass. This may also explain why especially at low thrust values (very small engines), there is a considerable spread.

Hydrazine monopropellant thrusters

Mass data of 28 hydrazine monopropellant thrusters (including thruster valve) in thrust range 0.5N – 445 N are plotted in the next figure versus (vacuum) thrust. All data have been taken from [Zandbergen, 2016]. Regression analysis shows that the data is best represented by the following linear relation:

$$M = 0.0046\ F + 0.293\ ;\ RSE = 27.1\% \qquad (B.2)$$

The relative standard error is given as 27.1% of the estimated value.

The data presented shows that engine/thruster mass can be reasonably well predicted given some thrust level. Still some error (or uncertainty) exists in our estimate, most likely depending on the design solutions considered. Also the relations do not provide insight in the effect of chamber material used, chamber pressure, nozzle expansion ratio, etc., which are also expected to be of influence. For this more detailed modelling is needed.

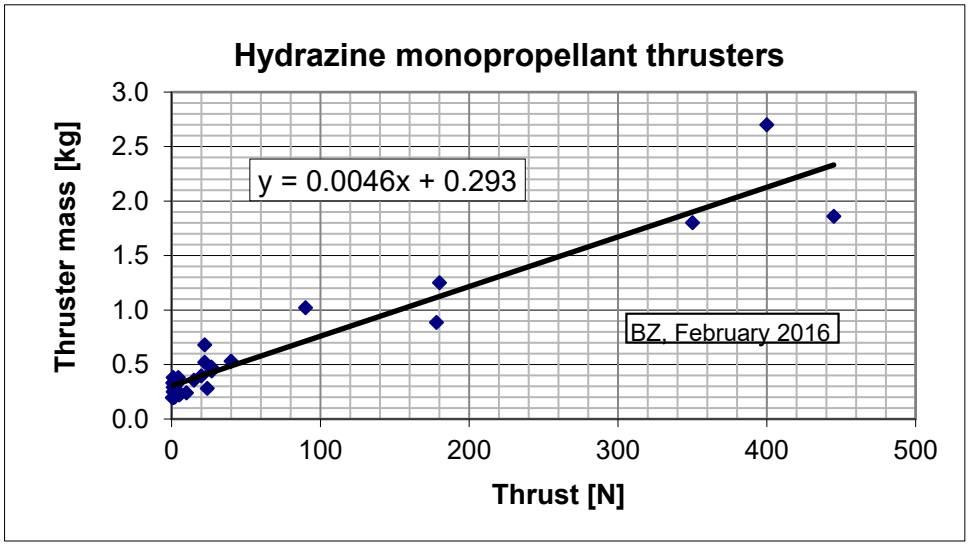

Figure H-3: Mass of hydrazine monopropellant thrusters

Size of engine/thruster envelope

Humble et al in "Space Propulsion Analysis and Design" (1995) have shown that as a first approximation engine thrust correlates well with engine length respectively (maximum) diameter, i.e. the engine envelope. Using this result as a starting point, we have plotted engine length and maximum diameter versus vacuum thrust for existing liquid propellant rocket engines in various classes. Next regression relationships have been determined. Results for large liquid rocket engines can be found in [Zandbergen, 2015]. Hereafter the results are given for small pressure-fed, storable bipropellant and monopropellant thrusters. For modelling applications the results also include a curve fit. First however, we define the envelope of a rocket engine as the smallest enclosure that encloses the rocket engine completely. Rocket engine is here taken to be the whole of thrust chamber (nozzle + combustion chamber) and flow control valve(s), see Figure H-4, and is referred here to as the thruster assembly.

400 N R1E thruster (Marquardt) 22N thruster (EADS) 4 N S4 thruster (EADS)

Figure H-4: Specific pressure-fed storable bipropellant liquid rocket thrusters

From Figure H-4 we also learn that the largest diameter of the thruster assembly does not necessarily equal the nozzle exit diameter as is commonly considered. Also engine length may be substantially different from the length of the thrust chamber.

Pressure-fed, storable bipropellant thrusters

Size data of 23 (length) and 25 (diameter) storable bipropellant (NTO - hydrazine, NTO - MMH, NTO - A-50, UDMH – IRFNA) thrusters in thrust range 4 N to 45,000 N are plotted in Figure H-5. Also a curve fit has been included.

a) Length

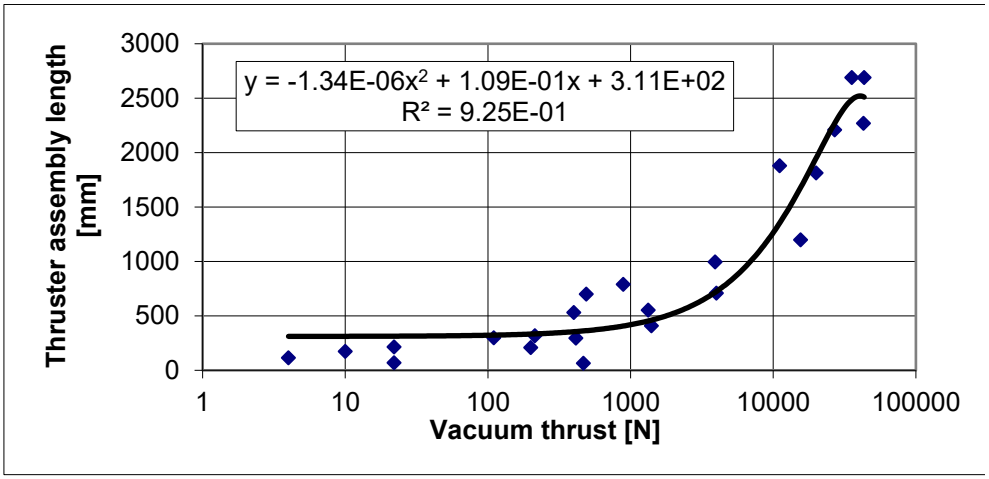

b) Diameter

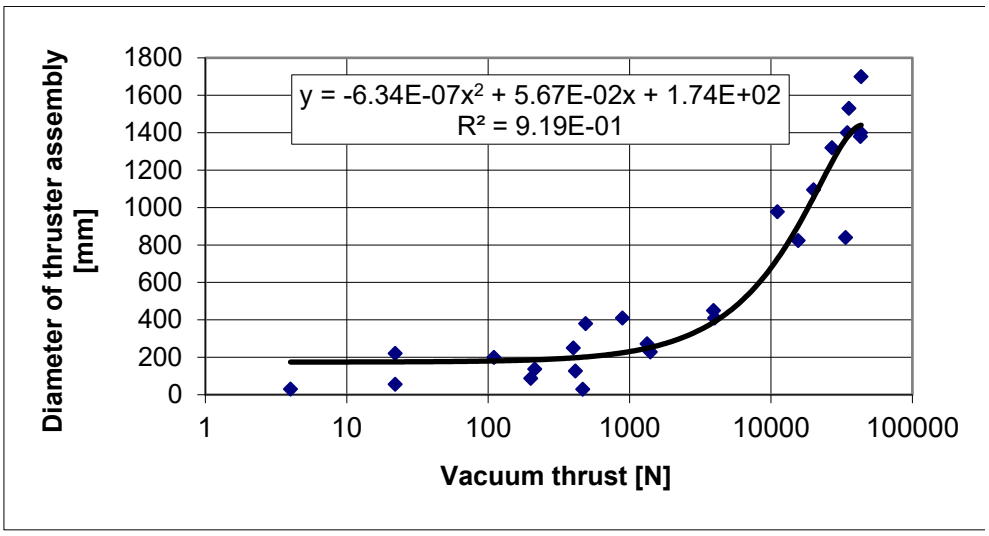

Figure H-5: Length and diameter of envelope of pressure-fed, storable bipropellant, thruster assemblies (including thruster control valves)

The results confirm that length and diameter to some extent is correlated with thrust. However, the results also indicate that there is considerable spread about the curve fit. This is attributed to differences in amongst others expansion ratio (larger expansion ratio leads to a longer nozzle), chamber pressure (higher chamber pressure reduces throat area and for a constant expansion ratio also the nozzle exit area), and the propellant combination used for the different engines. When using the curve fit to estimate an envelope this spread should be considered by taking adequate margins for the envelope in the design. As a measure for the spread the relative standard error (RSE; for a definition, see [Zandbergen, 2015]) has been determined, which gives an RSE of 47.9% on length and 44.5% on diameter of pressure-fed, storable bipropellant, thruster assemblies.

Pressure-fed, monopropellant thrusters

Size data of 26 (length) and 17 (diameter) monopropellant thrusters in thrust range 0.5 N to 445 N are plotted in Figure H-5. Also, a curve fit has been included.

a) Length

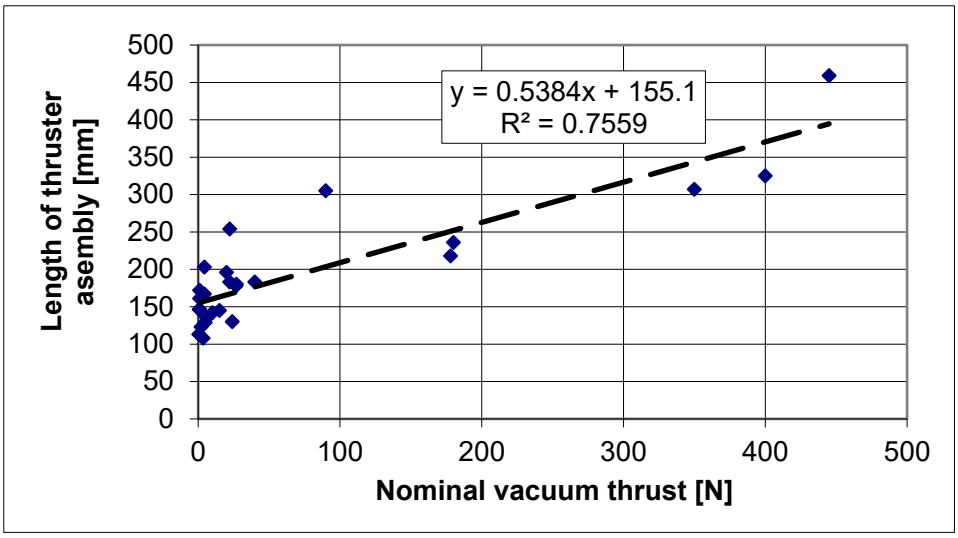

b) Diameter

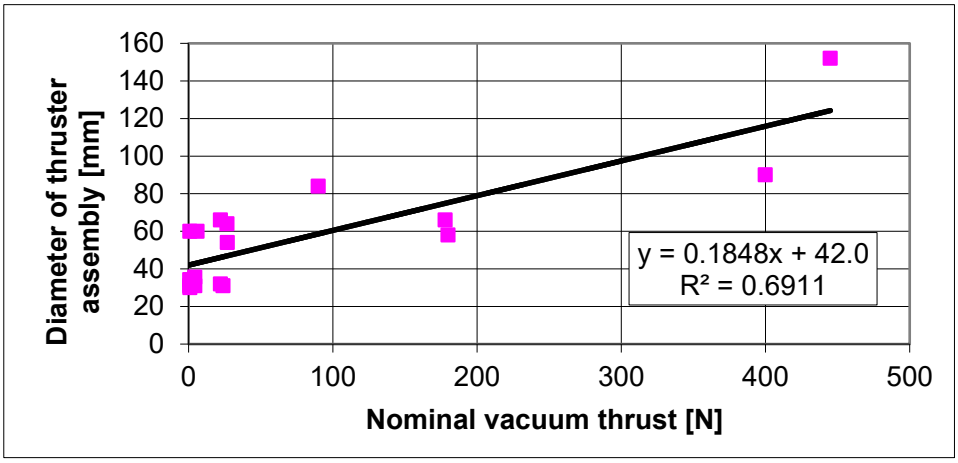

Figure H-6: Length and diameter of envelope of hydrazine monopropellant thrusters (including thruster control valve)

The results confirm again that length and diameter are correlated with thrust. Results also indicate that there is considerable spread about the curve fit. Like for the bipropellant thrusters discussed earlier, this is attributed to differences in amongst others expansion ratio (larger expansion ratio leads to a longer nozzle), chamber pressure (higher chamber pressure reduces throat area and for a constant expansion ratio also the nozzle exit area) for the different engines. When using the curve fit to estimate an envelope this spread should be considered by taking adequate margins for the envelope in the design. Relative standard error of estimate has been determined, which gives an RSE of 20.7% on length and 31.9% on diameter.

References

1) Zandbergen B.T.C., Rocket Engine database, February 2016.
2) Zandbergen B.T.C., Simple mass and size estimation relationships of pump fed rocket engines for launch vehicle conceptual design, 6th European Conference for Aeronautics and Space Sciences (EUCASS), Krakow, Poland; 06/2015.
3) Zandbergen B.T.C., Modern liquid propellant rocket engines; 2000 Outlook, Internal Publication, Delft University of Technology, Faculty of Aerospace Engineering, Delft, The Netherlands, March 2000.

Annex I: Engine mass based on component masses

Total engine mass is made up of the summed mass of its components.

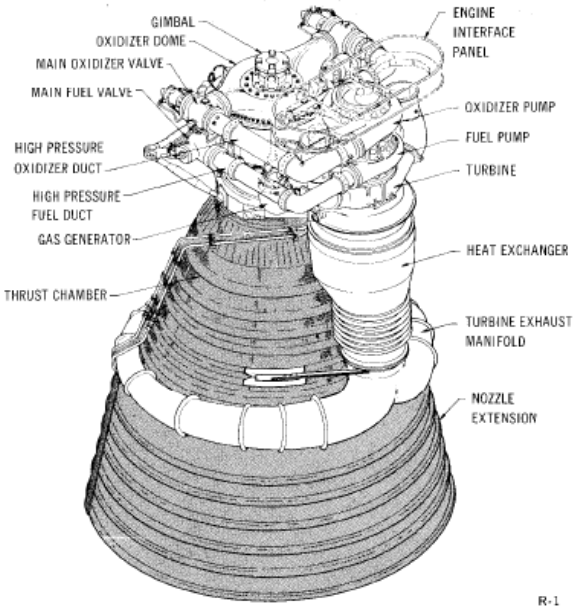

Figure I-1: Typical rocket engine and its constituents (courtesy NASA)

Main engine systems include 1) combustor and nozzle assembly, 2) pumps groups, 3) propellant feed system and 4) miscellaneous items (like pre-burner and thrust control items). A typical mass distribution for the Space Shuttle Main Engine is given in figure I-2.

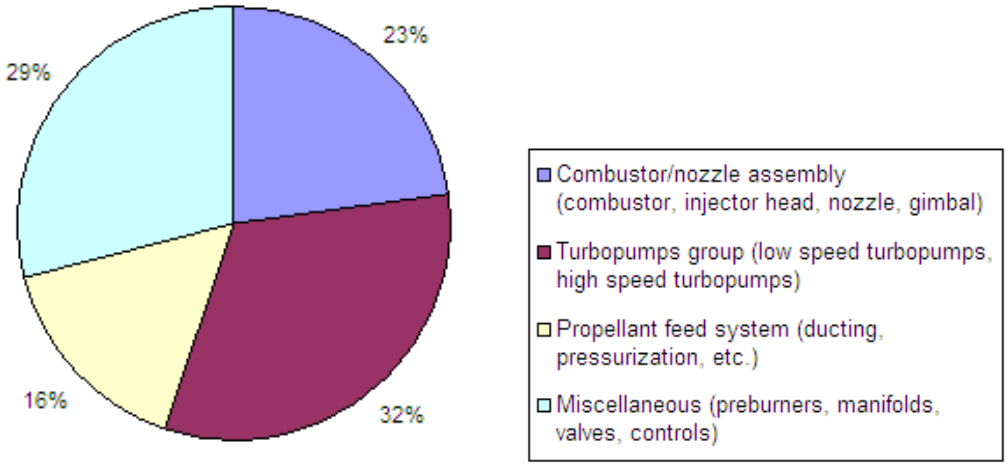

Figure I-2: SSME mass distribution

Schingloff model

For estimating engine mass from component masses, [Schlingloff] developed the following model:

$$M = 1.34 \cdot \left(M_{pumps} + M_{valves} + M_{chamber} + M_{injector} + M_{nozzle} \right) \qquad \text{Eq. (I-1)}$$

It essentially says that engine mass is the sum of the mass of combustor, injector and nozzle (i.e. the three together make up the combustor/nozzle assembly) and pumps and valves. The factor 1.34 is added to allow considering miscellaneous items, like gas generator, gimbal and piping) that also form part of the engine. Mass estimation relationships as given by Schlingloff for the various items are:

Combustor tube mass

Combustor tube mass is modelled dependent on the vacuum thrust generated:

$$M_{chamber} = 0.75\ (F)^{0.85} \qquad \text{Eq. (I-2)}$$

Here M is in kg with vacuum thrust F specified in kN.

Injector mass

Injector mass is simply modeled as being 33.3% (1/3rd) of combustor tube mass.

$$M_{injector} = 1/3\ M_{chamber} \qquad \text{Eq. (I-3)}$$

Nozzle mass

Nozzle mass has been determined as a function of vacuum thrust level F, expansion ratio ε and chamber pressure p_c.

$$M_{nozzle} = \varepsilon \times F\ (0.00225\ C_{nozzle} + (0.225\text{-}0.075\ C_{nozzle})/p_c) \qquad \text{Eq. (I-4)}$$

Here C_{nozzle} = 1.0 for regenerative cooled nozzles and 0.0 for dump-cooled nozzles. The mass M has dimensions of kilograms, and the chamber pressure p_c is given in bars.

Valves

Valve mass is again related to vacuum thrust F and chamber pressure p_c.

$$M_{valves} = 0.02\ (F.p_c)^{0.71} \qquad \text{Eq. (I-5)}$$

M is in kg and vacuum thrust F is specified in kN.

Turbo pump mass

Total turbo-pump mass, i.e. summed mass of fuel and oxidizer pumps including pre-pumps when present, is given by [Schlingloff] as:

$$M_{pumps} = C_{propellant} \times C_{pumps} \times (F\ p_c)^{0.71} \qquad \text{Eq. (I-6)}$$

$C_{propellant}$ = 0.19 for high energetic propellants and 0.11 for low energetic propellants. C_{pumps} is 0.5 for engines with pre-pumps and 1.0 for engines without pre-pumps. The mass M has the dimensions of kilograms, vacuum thrust F is specified in kN and the chamber pressure p_c in bar. Unfortunately, no definition is available on what are high or low energetic propellants.

Validating the Schlingloff model

As a check we have used the above relationship to predict the mass of the pump systems of some existing engines (6 in total). Results show a relative standard error of about 40%. In one case estimated engine mass was even 80% more than actual engine mass. So, this indicates that there is some room for improvement. This could be by developing improved estimation relationships or by adding more details in the estimation.

Next table provides an overview of mass estimation methods and where they can be found in this work.

Table I-1: Overview of sections in lecture notes “Thermal rocket propulsion” that deal with mass estimation

Component/system	Detailed in
Thrust chamber system	Chapter 13
Turbo-pump system	Chapter 15, section 4.4
Pressurization system	Chapter 15, section 3.3
Fluid storage system	Chapter 14, section 4
Plumbing system	Chapter 15, section 5.4
Ignition system	Chapter 16, section 10

Checking the turbo-pump mass estimation models

As an example, we will check the turbo-pump mass model as given by Schlingloff by comparison with the turbo-pump mass estimation model introduced in chapter 15. In this chapter it was shown that the following logarithmic regression line relating turbo-pump mass to turbine power output allows for a reasonable fit (relative standard error of 40%) over a power output range of 0.3 MW to 50 MW:

$$M_{tp} = 55.31 \times \ln\left(P_{tp}\right) + 105.2 \qquad \text{Eq. (I-7)}$$

With:
M_{tp} = turbo-pump mass (in kg)
P_{tp} = turbine output power (in MW)

This relation has an R-squared value of 0.908 indicating the quality of the fit. Still, from the figure, we learn that for specific cases our estimate can be off more than 100%. Possible reasons are erroneous data and/or still other factors that determine the mass of the turbo-pump.

To check the turbo-pump mass estimation the results obtained using (I-6) and (I-7) have been compared to actual results. Results are summarized in Table I-2.

Table I-2: Pump mass estimation results from different methods compared to actual data.

Engine	Thrust [kN]	Chamber pressure [bar]	Pump power (fuel/oxidizer or total) [MW]	Total Pump mass [kg]	Pump mass (Schlingloff) [kg]	Pump mass (this work) [kg]
HM60	1015	100	11.9/3.7	425	681	419
HM-7B	62.2	36.5	0.38	30	46	52
J-2	1023	51.7	5.94/1.76	305	429	340

The few results as presented in the table seem to confirm that the method as obtained in the chapter 15 provides results closest to reality. However, at low power levels the comparison remains poor.

References

1) Schlingloff H., Astronautical Engineering, Ingenieurburo Dr. Schlingloff Publications, Bad Abbach, Germany 2005.

Annex J: Solid rocket motor mass and size estimation relationships

To allow for early solid rocket motor (SRM) design studies and/or trade studies, it is important to be able to estimate SRM mass and size in relation to important design parameters, like propellant mass or total impulse to be produced or case material to be selected, etc. In this section various simple mass and size estimation relationships will be developed using regression analysis. This is a statistical process for developing estimating relationships from historical data and allows for estimating an unknown parameter (the dependent variable) in relation to one or more design parameters (the independent variables), whose values are selected by the designer.

To set up the database, first the most important parameters affecting the mass and size of an SRM had to be identified. An overview of these parameters is provided in the table below. Notice that the parameters are not necessarily independent from each other.

Table 1: Parameters affecting SRM mass and size

Parameter	ID	Effect
Thrust	THRUST	High thrust tends to lead to high mass flow rates and hence influences mass and size of the rocket nozzle
Burn time	t_b	Burn time together with thrust and specific impulse determines total propellant mass. It also has an effect on motor diameter and on thickness of (parts of) the insulation used to shield the case/nozzle structural material from the high temperature combustion products/gases.
Specific impulse	ISP	Specific impulse determines propellant mass needed for a mission (determined by total impulse) and as such also effects propellant volume.
Propellant volume	VOL	Propellant volume affects case volume and as such also case mass.
Propellant composition	PROP	Determines propellant mass density and as such also propellant volume (given propellant mass). Composition also influences motor specific impulse. More energetic propellants (high characteristic velocity) tend to lead to higher specific impulse levels.
Grain geometry	GG	Determines propellant volumetric loading fraction and hence influences total motor volume and diameter and hence on case size and mass.
Slenderness	L/D	Slenderness together with motor diameter determines motor length. Booster stages and lower stages of launch vehicles usually have the highest slenderness. Upper stages generally are more of a bulkier design to ensure effective usage of available space.
Expansion ration	AE	Expansion ratio determines the pressure drop over the nozzle and hence influences motor specific impulse (via the thrust coefficient). Expansion ratio is also expected to affect the mass of the rocket nozzle.
Chamber pressure	PRES	Affects regression rate, size of the rocket nozzle (given mass flow rate and propellant) and thickness of SRM case and nozzle.
Case/nozzle material	M	Different materials have different specific strengths (strength/mass density). A material with a high specific strength will lead to a reduced mass of the structural element (nozzle or case). Specific strength ratio difference between different materials used for SRM construction can be up to a factor 5.
Structural Safety Margin	SSM	Determine thickness of case and nozzle structure and hence case and nozzle mass. Variation in this parameter is limited, but some difference may exist between structures built up from metallic materials and composite materials. SSM values depend on the burst pressure, which for space SRMs typically is up to 1.5 times the Maximum Expected Operating Pressure (MEOP),

Next, literature was consulted to identify data values and the data found was tabulated. As a result, a database has been developed consisting of 68 high-end solid rocket motors[6] ranging from the 7.6kN STAR 13B to the 12.9MN Reusable Solid Rocket Motor V (RSRM V). All motors selected have been applied on one or more spacecraft (satellite or space launch vehicle). The data for the individual rocket stages is obtained from publicly available literature sources including the propulsion products catalog from ATK [1] with some updated data of Northrop Grumman (NG) [2], which since then has acquired ATK, the work of Sutton [3], Backlund et al [4], NASDA [5], ISRO [6] and data collected by Zandbergen [7]. Data for the European motors comes from [8], [9], [10] and [11]. Some specific impulse values have been obtained from [12]. For the identification of the constituents for the different propellants also [13] has been consulted. An overview of the motor data collected is given in Table 2 and Table 3.

Table 2 provides general motor data for 36 high thrust SRMs (thrust level range 225kN-12.9 MN). Table 3 is identical, but for low thrust motors (thrust level range 5kN-225kN. Both ranges have been selected such that there is a factor of 50 between highest and lowest thrust value covered. The distinction in thrust level is somewhat arbitrary but is done to allow detecting scale effects and to allow for an almost equal number of data points in the two sets of tables. As a rule, in case no data could be found, the table cell is marked by “NA” (Not Available).

Data tabulated in Table 2 and Table 3 include average vacuum thrust, case material, propellant constituents, effective vacuum specific impulse, average chamber pressure, propellant mass, motor inert mass and motor length and diameter. Of these, vacuum thrust, effective vacuum specific impulse and chamber pressure are taken as average value over the burn time. This is mostly because detailed information on how the values vary over the burn time was not available in the open literature used for this study. A special note is needed regarding the specific impulse. Here an effective value is taken. Meaning that the values are actual values as found in practice considering real operating conditions with changing nozzle diameters. In general, this leads to somewhat lower specific values than follows from just the propellant. For instance, for the STAR 27 motor [Sutton] gives a propellant vacuum specific impulse of 290.8 sec, whereas for the effective specific impulse ATK gives a value of 287.9 sec. This indicates a difference of 3 seconds or 1%. Care has been given to provide comparable values for all motors, but in open literature, the values are not always unambiguously defined. Length and diameter in the table are based on the overall envelope of the SRM. Values have not been corrected for additional equipment needed for e.g. TVC mounted on the outside of the motor. When reporting mass and length data, care is given to report only data related to SRM mass and length and not to report data that are valid for a complete booster or stage (including additional equipment, like a nose section, a stage separation system with separation motors, TVC fluids, a parachute, etc.). In [14], it is shown that especially for solid rocket boosters, the additional mass is considerable. For instance, for the Japanese SRB-A booster (used on HIIA launcher) a stage inert mass is given of 11.5 ton, whereas the actual motor SRM mass is reported as 6 ton. Burn time values have been taken directly from literature, or they have been determined from available data on total impulse and specific impulse. No distinction is made between burn time and action time of the motor. Also, no data has been included on grain geometry and structural safety margin. This is mostly because little or no data on these parameters could be found.

It is important for any estimation relationship to be determined that sufficient data points are available for analysis. For simple linear regression with one independent variable, we need at least 10 data points to allow for a reasonably accurate relationship to be established. Adding more independent variables requires the addition of further data points to maintain accuracy. The current database of 68 motors hence would allow for maximum 6-7 independent variables. Additionally, it is considered that best relationships can be determined if each of the independent variables at least spans one order of magnitude in range.

[6] Care has been taken that only data related to SRMs and not solid (booster) stages are included. The difference is that we only consider the basic SRM itself and not such elements such as booster nose section, booster attachment structures for parallel staging, nor stage separation motors as well as actuators needed for gimballed nozzles, or the liquid injection system needed for liquid (or gas) injection TVC systems. The latter were common on booster stages of the Japanese H2 rocket (SRB) and the USA Titan IV and Titan III, whereas the former are common for modern mechanically actuated TVC systems.

Table 2: High and moderate thrust SRM general data

#	Engine name	Vacuum thrust	Case material	Propellant constituents	Effective vacuum specific impulse	Chamber pressure	Propellant mass	Total inert mass	Motor length	Motor diameter	Burn time	TVC	Area ratio
		[kN]	[-]	[-]	[s]	[bar]	[kg]	[kg]	[m]	[m]	[s]	[-]	[-]
1	Titan 4 SRB (UA1207)	5915	D6AC steel	PBAN/Al/AP70	272	NA	268920	34006	34.43	3.11	119.5	Yes	10
2	SRMU (Titan 4B)	6408	Graphite epoxy	88% solids HTPB	281.1	NA	313284	36565	34.26	3.2	135.7	Yes	15.7
3	RSRM	10811	D6AC steel	PBAN14/Al16/AP	268.5	45	502789	66621	38.44	3.71	122.2	Yes	7.72
4	RSRM V	12859	D6AC steel	PBAN14/Al16/AP	267.1	43.14	647642	85419	47.36	3.71	131.9	Yes	6.55
5	Ariane 5-P230	4984	D6AC steel	HTPB14/Al18/AP	273	NA	237100	31000	26.77	3.049	132.6	Yes	9.6
6	Titan 3 SRB (UA1205)	4793	D6AC steel	PBAN/Al/AP70	265.2	NA	192466	25135	25.65	3.11	113.7	Yes	10
7	H2 SRB	1685	NT-150 steel	HTPB14/Al18/AP	273	46	59150	10000	19.26	1.81	94	Yes	10
8	S-139 (PSLV)	3463	M-250 Steel	HTPB, 18% Al	269	NA	138200	18475	20.35	2.8	107	Yes	8
9	Thiokol M55	1015	D6AC steel	HTBP14/ Al16/AP70	262	53.8	20789	2141	7.49	1.67	52.6	Yes	10
10	Castor 4A (TX780)	488.9	AISI 4130 steel	HTPB/Al20/AP	267.8	46.6	10101	1477	9.199	1.016	53.1	No	8.3
11	CASTOR IVA-XL	609.9	AISI 4130 steel	HTPB, 20% Al	281.9	42.2	13112	1948	11.608	1.019	59.4	No	15.6
12	CASTOR IVB	423.3	AISI 4130 steel	HTPB, 20% Al	267.2	31.65	10155	1385	8.984	1.019	65	No	8.0
13	ASLV stage 1	502.6	M-250 Steel	HTPB, 18% Al	259	NA	8900	1534	9.9899	1.000	46	No	6.7
14	H1 SRB (Castor 2)	258.9	D6AC steel	CTPB, 20% Al	266.1	44.0	3730	750	6.039	0.787	37	No	7.45
15	Ariane 4 strap-ons	720	AISI 4130 steel	CTPB13/Al16/AP71	263	NA	9640	1930	11.32	1.07	33	No	8.3
16	CASTOR 1	306	AISI 4130 steel	PBAA, 14% AL	258.1	34.6	3317	535	5.92	0.787	27.4	No	6.05
17	Castor 120	1650	Carbon-epoxy	HTPB/Al19/AP69	280.1	85.9	48596	4072	8.81	2.363	81	Yes	18.9
18	H2 SRB-A	1800	Carbon-epoxy	HTPB-based	280	NA	65000	6000	12	2.5	100	Yes	16.3
19	P-80	2261	Carbon-epoxy	HTBP12/Al 19/AP69	280.1	88.6	88000	7300	10.50	3.00	117	Yes	16
20	Z-23	949.3	Carbon-epoxy	HTBP12/Al 19/AP69	287.5	71	23906	1845	7.58	1.93	71	Yes	27
21	CASTOR 30	259	Carbon-epoxy	HTPB, 20% Al	293.1	52.54	12836	1224	3.51	2.334	143.0	Yes	50
22	CASTOR 30B	230	Carbon-epoxy	HTPB, 20% Al	300.6	NA	12887	1083	4.17	2.334	126.7	Yes	NA
23	Z-9	263	Carbon-epoxy	HTBP12/Al19/AP69	294.4	52.6	10115	833	4.12	1.93	107	Yes	72.45
24	GEM-40 (fixed)	499	Graphite epoxy	88% solids HTPB	274	56.4	11766	1237	11.41	1.026	63.3	No	9.0
25	GEM-40 VN	479	Graphite epoxy	88% solids HTPB	267.7	54.8	11792	1327	10.80	1.026	64.6	Yes	9.0
26	Star 92	256.1	Graphite epoxy	HTPB, 20% Al	290.1	54.54	15821	1016	3.63	2.36	175.6	No	39.0
27	Orion 50S XL	626.3	Graphite epoxy	HTPB, 19% Al	292.8	74	15023	1157	10.26	1.27	69.1	No	34.3
28	Orion 50S	465.1	Graphite epoxy	HTPB, 19% Al	292.3	56.1	12163	1016	8.86	1.27	75.3	No	35.3
29	Orion 50S XLT	614.9	Graphite epoxy	HTPB, 19% Al	284.6	74.7	15023	1157	9.88	1.27	68.4	Yes	24.8
30	Orion 50S XLG	588	Graphite epoxy	HTPB, 19% Al	272.3	74.7	15023	1179	9.45	1.27	68.4	Yes	14.2
31	Orion 50ST	454.4	Graphite epoxy	HTPB, 19% Al	285	58.6	12157	1016	8.46	1.27	75	Yes	26.7
32	GEM-46 (fixed, GI)	611	Graphite epoxy	87% solids HTPB	279	65.8	16790	2000	12.59	1.146	76	No	13.8
33	GEM-46 (VN, GI)	611	Graphite epoxy	87% solids HTPB	279	63.1	16843	2275	12.48	1.146	77	Yes	13.8
34	GEM-46 (fixed, AI)	601	Graphite epoxy	87% solids HTPB	290.6	65.8	16780	2288	12.92	1.146	NA	No	24.6
35	GEM-60 (fixed)	830	Graphite epoxy	87% solids HTPB	275	NA	29533	3485	13.16	1.524	91	No	11
36	GEM-60 (VN)	879	Graphite epoxy	87% solids HTPB	274.1	56.4	29612	3940	13.16	1.524	91	Yes	11.0

Table 3: Low thrust SRMs general data

#	Engine name	Vacuum Thrust [kN]	Case material [-]	Propellant constituents [-]	Effective vacuum specific impulse [s]	Chamber pressure [bar]	Propellant mass [kg]	Total inert mass [kg]	Motor length [m]	Motor diameter [m]	Burn time [s]	TVC [-]	Expansion ratio [-]
1	Orbus 6	80.95	Kevlar-epoxy	HTBP14/Al18/AP68	289.1	42.1	2722	233	1.98	1.60	101	Yes	47.3
2	Orbus 21	195.7	Kevlar-epoxy	HTPB, 86% solids	295.1	45.2	9709	689	3.15	2.34	145	Yes	63.9
3	Orion 32	102.2	Graphite -epoxy	HTPB, 20% Al	278.1	52.1	2009	217.3	3.038	0.8255	53.6	Yes	21.8
4	Orion 38	32.2	Graphite-epoxy	HTPB, 19% Al	287	39.4	771	122	1.35	0.965	67.7	Yes	49.3
5	Orion 50 XL	160.6	Graphite-epoxy	HTPB, 19% Al	290.7	68.3	3924	395	3.10	1.27	69.7	Yes	43.5
6	Orion 50	114.6	Graphite-epoxy	HTPB, 19% Al	290.2	55.8	3025	345	2.67	1.27	75.6	Yes	52.1
7	Mage 1	19.4	Kevlar-epoxy	CTPB 16-12	295	35	335	33.3	1.12	0.762	50	No	45
8	Mage 2	32.3	Kevlar-epoxy	HTBP11/Al18/AP71	294	35	450	40	1.52	0.762	44	No	65
9	STAR 31	82.3	Kevlar-epoxy	HTBP11/Al18/AP71	293.5	49.1	1286	108	2.87	0.764	45	No	58
10	IRIS	57	Kevlar-epoxy	HTPB 13%, Al 18%	291	42.5	1574	147	1.94	1.3	79	No	60
11	STAR 75	200.17	Graphite-epoxy	HTBP11/Al18/AP71	288	42.47	7503	562.9	2.59	1.905	105	No	17.7
12	STAR 13B	7.6	Titanium	CTBP14/Al16/AP70	285	56.7	41	5.81	0.638	0.3454	14.8	No	49.8
13	STAR 26C	35.1	Titanium	NA	272.1	44.13	334	27.49	0.841	0.663	16.8	No	17.8
14	STAR 30E	35.2	Titanium	HTBP11/Al18/AP71	292.8	37.0	232	30.6	1.69	0.762	51,1	No	58.6
15	STAR 37 FMV	48.84	Titanium	HTBP11/Al18/AP71	293.7	37.2	1064	105.9	1.918	0.9347	62.7	Yes	70
16	STAR 37 FM	47.85	Titanium	HTBP11/Al18/AP71	291.8	37.23	1057	81.96	1.68	0.9347	63.7	No	48.2
17	AUS 51	59.33	Titanium	HTPB…	295.5	NA	1897	110	2.13	1.3	92.5	No	60
18	STAR 17	10.9	Titanium	CTBP14/Al16/AP70	286.2	55.4	70	9.43	0.687	0.442	17.6	No	60.7
19	STAR 24	18.5	Titanium	CTBP14/Al16/AP70	282.9	33.5	200	18.3	1.03	0.622	29.6	No	37.8
20	STAR 17A	16	Titanium	CTBP14/Al16/AP70%	286.7	46.2	112	13.4	0.981	0.442	19.4	No	53.2
21	STAR 27H	20.68	Titanium	HTBP11/Al18/AP71	291.4	41.09	337.8	29.98	1.219	0.6934	46.3	No	81.7
22	STAR 30E	35.1	Titanium	HTBP11/Al18/AP71	290.4	37	631	42.5	1.69	0.762	51.1	No	58.6
23	STAR 26	33.4	Steel	NA	271	39.6	231	38.8	0.838	0.66	17.8	No	16.7
24	STAR 30C/BP	32.5	Titanium	HTBP11/Al18/AP71	291.8	39.6	591	41.1	1.633	0.762	51	No	63.2
25	STAR 30BP	26.6	Titanium	HTBP11/Al18/AP71	293	35.4	515	37.7	1.829	0.762	54	No	73.7
26	STAR 27	25.4	Titanium	HTBP12/Al16/ AP72	287.9	38.8	334	27.5	1.24	0.6934	37.3	No	48.8
27	Star 26B	34.62	Titanium	NA	272.4	42.95	238	23.4	0.841	0.663	17.8	No	17.8
28	STAR 24C	20.3	Titanium	CTBP14/Al16/AP70	282.3	37.5	220	19.7	0.64	0.622	29.6	No	37.1
29	STAR 30C	32.47	Titanium	HTBP11/Al18/AP71	288.8	38.06	590.8	38.46	1.49	0.762	51	No	46.4
30	STAR 48A short nozzle	77.18	Titanium	HTBP11/Al18/AP71	285.3	37.44	2430	134.6	2.032	1.2426	87.2	No	32.2
31	STAR 48A long nozzle	78.96	Titanium	HTBP11/Al18/AP71	291.9	37.44	2430	151.5	2.235	1.2426	87.2	No	43.1
32	STAR 48B	67.2	Titanium	HTBP11/Al18/AP71	286	39.9	2010	124	2.032	1.24	84.1	No	39.6
33	STAR 48V	68.6	Titanium	HTBP11/Al18/AP71	292.1	39.9	2010	154	2.075	1.24	84.1	Yes	54.8

The data collected in the foregoing two tables have been collected with great care. Still errors cannot be fully excluded. For seemingly identical motors different documents may give different data. Also, some documents showed errors in the data. Finally, although great care has been given to filling in the right data, typos cannot fully be excluded.

Based on the data given in the tables, some first observations are given:

1. Thrust varies from 6.7 kN to more than 12.9 MN. This shows a difference of about a factor 2000.
2. Typical motor (case) materials include metals, like various types of steel and titanium, and composite materials such as graphite epoxy filament and carbon epoxy filament and Kevlar epoxy filament. In general, a graphite or carbon epoxy filament is lighter than Kevlar epoxy, a little stiffer (maybe), but when it takes a hit, it tends to shatter and break. Kevlar epoxy is more resilient. Graphite and carbon epoxy are both carbon-based. The difference is that there is a different degree of graphitization.
3. Propellant constituents include HTPB/CTPB/PBAN/PBAA polymer as binder, Aluminum (Al) as fuel and Ammonium-Perchlorate (AP) as oxidizer. Numbers indicate mass percentage of species in total propellant. HTPB refers to hydroxyl-terminated polybutadiene, CTPB to Carboxyl-terminated polybutadiene, PBAN to Polybutadiene acrylonitrile and PBAA to PolyButadiene Acrilic Acid. The majority of SRMs in the database use either HTPB or CTPB type of propellants with only modest variations in aluminum and AP content.
4. Vacuum effective specific impulse values are quite similar with a minimum of 258s and a maximum of ~300s. This is attributed to the small difference in propellant composition and the limited effect of the area ratio. Area ratio variation is from 6 (lowest) to 82 (highest). Effect of PBAN versus HTPB on specific impulse has been investigated by Moore [9] and is reported to be of the order of 2s.
5. Average chamber pressure varies between 2-3 from about 30 bar to almost 80 bar.
6. Propellant mass ranges from 85% to 95% of total motor mass, with inert mass making up the remainder.
7. Some SRMs (GEM-40, GEM-46 and GEM-60) are available in a version with fixed and gimballed nozzle. Data shows that for these motors in general motor inert mass increases when a fixed nozzle is replaced by a movable nozzle.
8. L/D ratio is in range 1 to 13. Space motors usually are short and bulky, whereas motors for launch vehicle stages tend to be long and slender (to limit aerodynamic drag).
9. Motor burn time is between 15s to 175s with an average burn time of 74s.

Generating relationships

Regression analysis has been performed using IBM SPSS. This is a statistical software package that allows for amongst others multivariate regression analysis based on user-defined data. In this case, the data as tabulated in the foregoing tables has been used. The package also allows for determining the goodness of fit, i.e. the R-square value also referred to as the coefficient of determination. As the accuracy of the relationships is important to know, in a separate step also the RMS value of the percentage error relative to the estimate (and not the true value) is determined, hereafter referred to as the relative standard (percentage) error (RSE)

RSE is calculated using:

$$\mathrm{RSE} = \sqrt{\frac{\sum_{j=1}^{n}\left(\frac{y_j}{f(x_j)} - 1\right)^2}{N - K}} \times 100\% \qquad (1)$$

RSE is here expressed as a percentage of the estimated (not the true) value. For example, if the estimate of engine mass is 100 kg and the standard error of the estimate is 8 kg, the RSE of the estimate = (8/100) * 100%, or 8 percent. Estimates that have a large SPE are considered less reliable than estimates with small RSEs. Of course, there is no absolute cutoff point, but in general, estimates with RSE above 30% are considered carefully.

Estimation relationships

In this section estimation relationships are provided for specific impulse, total mass and length and diameter of motor envelope.

Vacuum effective specific impulse

Motor vacuum effective specific impulse is plotted versus area ratio in next figure.

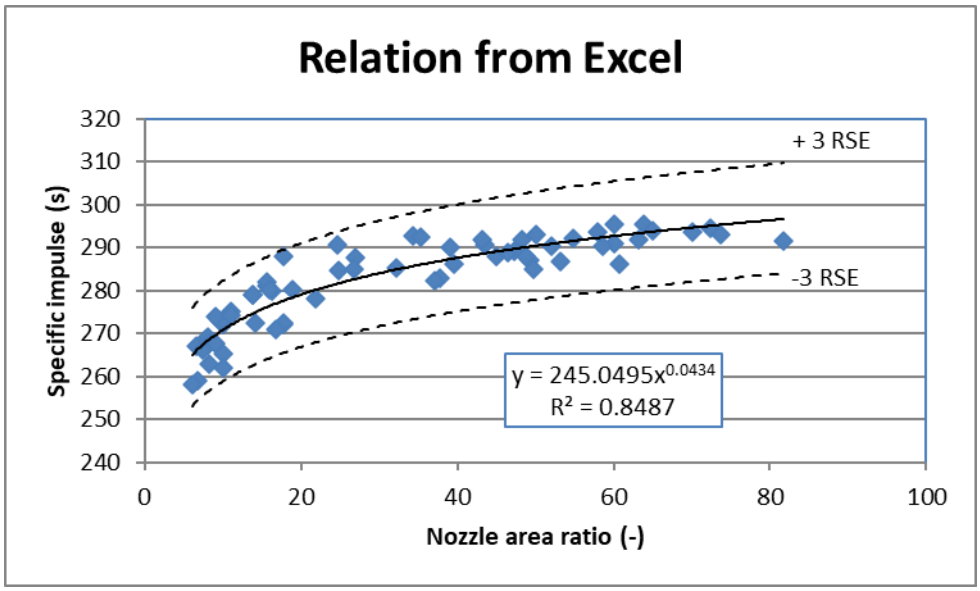

Figure 1: Vacuum effective specific impulse of specific SRMs with associated regression curve.

Results indicate a vacuum effective specific impulse in the range of 260 to 300 s with the higher values at larger area ratio. In figure also a power-law relation is provided relating specific impulse to area ratio. This relation is also given in the table below including the R-square value and the RSE. No distinction is made after the type of propellant used.

Table 4: Specific impulse estimation relationships in relation to nozzle area ratio and propellant type

ID	Estimation relationship	R^2	RSE	N
I.1	$I_{sp} = 245.05\ AE^{0.0434}$	0.849	1.44%	67
I.2	$I_{sp} = 246.56\ AE^{0.0419} \times 0.9945^{Type}$ (Type is 0 for HTPB and CTPB and type is 1 for PBAN/PBAA)	0.857	1.53%	64

Relation I.2 allows determining the specific impulse while making a distinction for the type of propellant. Two groups of propellants are HTPB/CTPB and PBAN/PBAA. The difference in specific impulse for these two groups is about 0.4%, which is almost negligible. In the work of Moore, the effect was reported as in the range of up to 2% [14].

Mass estimation relationships

Next table shows various inert mass estimation relationships developed.

Table 5: Inert mass estimation relationships in relation to propellant mass and SRM case material (C/G epoxy refers to carbon epoxy and graphite epoxy

ID	Case material	Estimation relationship	Propellant mass range	R^2	RSE	N
MI.1	All	$M_{inert} = 0.1294\ M_{prop}$	0.2-647 t	0.996	31.9%	68
MI.2	Steel	$M_{inert} = 0.1316\ M_{prop}$	0.2-647 t	0.990	23.9%	16
MI.3	Titanium	$M_{inert} = 0.2991\ M_{prop}^{0.7939}$	41-2430 kg	0.954	16.3%	20
MI.4	C/G epoxy	$M_{inert} = 0.1124\ M_{prop}$	0.335-315 t	0.987	23.9%	26
MI.5	Kevlar epoxy	$M_{inert} = 0.2227\ M_{prop}^{0.8756}$	335-9709 kg	0.999	11.1%	6
M_{inert} = motor inert mass in kg M_{prop} = propellant mass in kg						

Relation MI.1 shows data for all SRMs in the database, without making a distinction between the case material used. Relation indicates an almost linear dependence of motor inert mass on propellant mass, see also next figure showing SRM inert mass versus propellant mass.

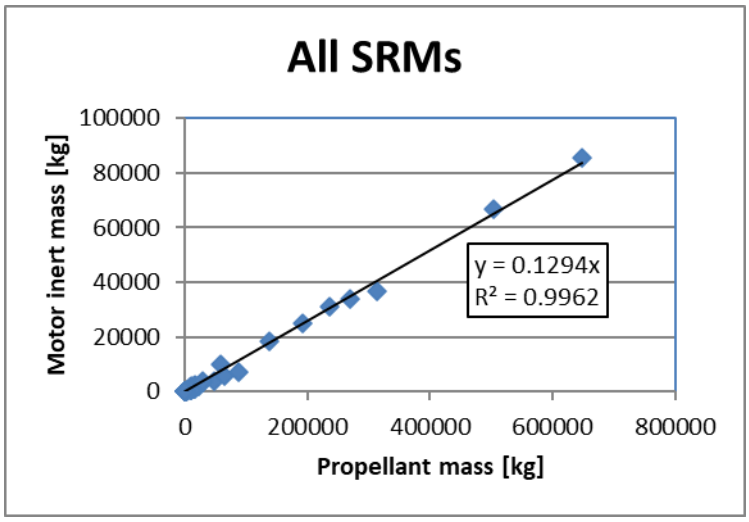

Figure 2: Inert mass of specific SRMs with associated regression curve

The goodness of fit can also be judged from the R-squared value. Here the high R-squared value confirms that propellant mass is a key parameter determining motor inert mass. From the figure, we can see that actual data are spread about the curve representing the relationship. The magnitude of the spread is given by the RSE, which is about 32 %.

Next relations in the table aim to separate the effects of the different case materials. Results show that the exponent in all cases is close to 1, which adds confidence to the results found. Only for Titanium and Kevlar epoxy, the exponent is somewhat below 1. This is because for both only small motors have been produced so far, and these tend to differ from the trend line shown in Figure 2. This is attributed to the trendline shape being greatly affected by the datapoints furthest away from the origin. Independent from the value of the exponent, these relations allow for determining the inert mass difference resulting from the different case materials, at least within the range of applicability of the various relations. SRMs with a steel case typically show to be the heaviest.

RSE in all cases is close to one. Still, we find that that the attained RSE is considerable and hence all relations are up for further detailing, thereby considering more independent variables, like the safety margin selected, the design chamber pressure, whether the nozzle is fixed or articulated, etc.

Envelope length and diameter estimation relationships

Table 6 shows relationships for determining SRM envelope length and diameter.

Table 6: SRM envelope length and diameter relationships in relation to propellant mass (M_{prop}) and motor burn time (t_b)

	Relation	Range	R^2	RSE	N
L.1	$L = 0.0696\ M_{prop}^{0.4865}$	M_{prop}: 40 kg – 670 t	0.931	36.9%	68
D.1	$D = 0.1876\ M_{prop}^{0.2201}$		0.831	24.3%	
L.2	$L = 0.6185\ M_{prop}^{0.5474} * t_b^{-0.6175}$	M_{prop}: 40 kg – 670 t	0.949	27.6%	68
D.2	$D = 0.0266\ M_{prop}^{0.1437} * t_b^{0.6182}$	t_b: 15 s – 150 s	0.930	24.4%	

L and D in m, M in kg and t in seconds.

Relations L.1 and D.1 are plotted in next figures together with the data points and two dotted lines representing ± 1 RSE. From the figures, motor length and diameter increase with increasing propellant mass.

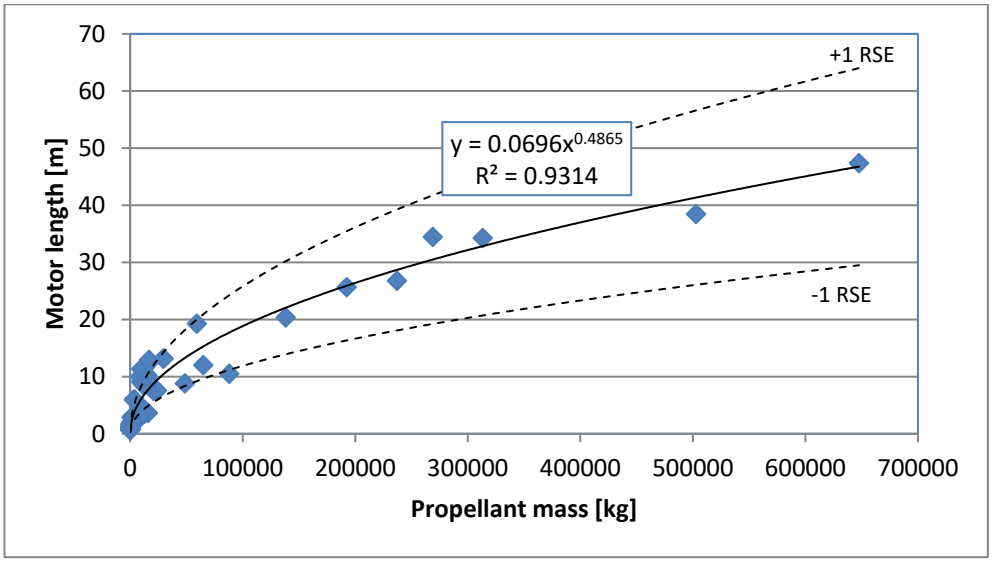

Figure 4: SRM envelope length versus propellant mass with associated regression curve

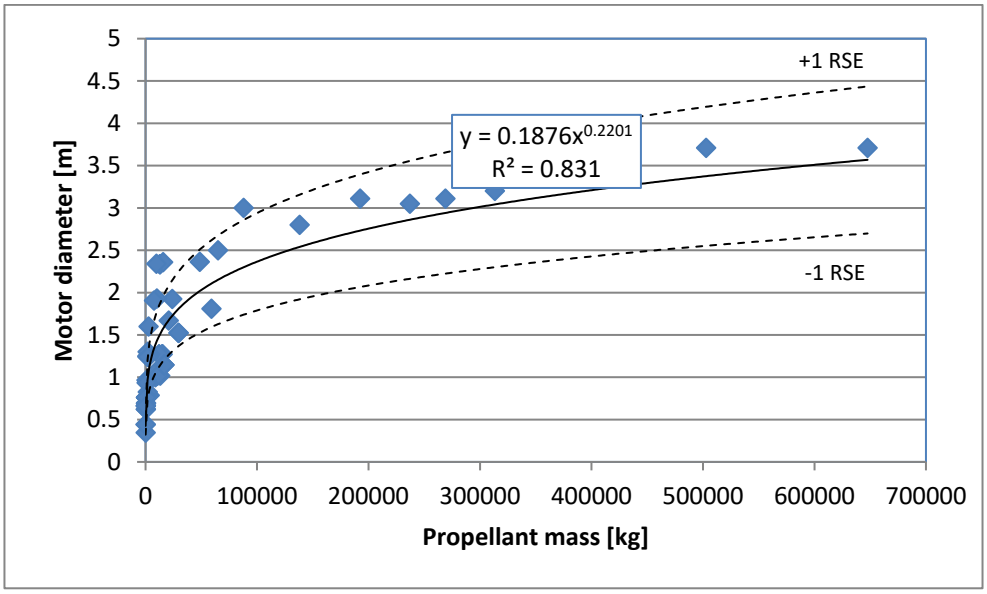

Figure 5: SRM envelope diameter versus propellant mass with associated regression curve

Also clear from the figures is that actual data is spread about the curve. The magnitude of this spread is again given by the RSE. To reduce the RSE, also a second set of relationships has been generated (L.2 and D.2) that also consider the effect of burn time. It is considered that with increasing burn time the web thickness will increase. For cylindrical burning grain this will then influence the case diameter. Results show that the RSE decreases, which is positive. The effect is limited for envelope diameter, but significant for envelope length. For length, it may be considered for future work to also consider the effect of nozzle submergence and the nozzle contour. Both have an effect on motor length.

References

1) ATK Space Propulsion Products Catalog, ATK, 2008.

2) Northrop Grumman Propulsion Products Catalog, Northrop Grumman, 2016. Retrieved June 2025 from: https://cdn.northropgrumman.com/-/media/wp-content/uploads/NG-Propulsion-Products-Catalog.pdf?v=1.0.0

3) Space Propulsion Elements, G.P. Sutton and O. Biblarz, 7th edition, John Wiley & Sons, 2001.

4) A study of performance and cost improvement potential of the 120-in. (3.05 m) diameter solid rocket motor by Backlund, S.J. and Rossen J.N., NASA CR114390, December 1971.

5) Development status of Japan's new launch vehicle: H-II rocket, M. Miyazawa and Y. Fukushima, NASDA, Tokyo, Japan, Acta Astronautica Vol. 25, No. 5/6, pp. 251-264, 1991.

6) ISRO'S solid rocket motors, R. Nagappa, M. R. Kurup and A. E. Muthunayagam, Indian Space Research Organization, Vikram Sarabhai Space Centre, Trivandrum 695022, India, Acta Astronautica Vol. 19, No. 8, pp. 681-697, 1989.

7) Some typical solid propellant rocket motors, Zandbergen B.T.C., TU-Delft/LR, M-712, September 1995.

8) Launcher analysis and cost benefits, Max Calabro (TIA) and Emmanuella Gizzi (AVIO), published by EU, Ref. Ares (2018) 1042920 - 23/02/2018, February 2018.

9) Vega Solid Rocket Motors Development and Qualification, by S. Bianchi and F. Serraglia, F. Giliberti and F. Betti, C. Milana AIAA 2010-7084, 2010.

10) Fiat Avio Vega webpages retrieved June 2025 from: https://www.avio.com/vega, https://www.avio.com/p-80

11) Large Space Solid Rocket Motors in Europe, by Uhrig. G, and Boury, D., AIAA-98-3980, July 1998.

12) Diaminoglyoxime and diamino-furazan in propellants based on ammonium perchlorate, Willer R.L., Chi M.S., Gleeson R., and Hill J.C., US Patent 5071495 A, 1990.

13) Assessment of HTPB and PBAN propellant usage in the United States, Moore, T.L., AIAA 33rd Joint Propulsion Conference, AIAA, 1997.

14) Space Launcher Large Solid Propulsion Overview Market Analysis and General Trends, Boury D. and Thinat F.-X., 45th AIAA/ASME/SAE/ASEE Joint Propulsion Conference & Exhibit, AIAA 2009-5519, June 2009.

Annex K: Properties of specific materials used in rocketry

When developing rocket propulsion systems, a large variety of materials is used for many different purposes. To allow for a quick assessment early in the design, it is important that a suitable database is available that provides for realistic data for these materials. This section intends to provide for such a database thereby focussing mainly on structural materials and not on energetic materials (like propellants) or other materials. In addition, we will also include a range of materials that is used as liner material in liquid rocket engines and/or insulator and ablator materials in solid and hybrid rocket motors. Important material data that will be provided includes mass density, ultimate and yield stress, Young's modulus, Poison ratio, maximum use temperature, thermal conductivity, specific heat, etc.

In this work we will first provide an overview of specific materials and typical uses (section 1). In section 2, we present for specific materials the important material data at room temperature. In section 3, we will present some data of materials specifically designed to operate at high temperature and in section 4, we present some further material on metals working at elevated temperatures.

1. Overview of materials and their uses

A list of typical structural materials used in liquid, solid and hybrid rocket propulsion systems is given in Table 1Table . Also indicated in the table are their main uses thereby focussing on materials related to thrust production and/or propellant storage. As a warning, it is noted that some materials given in the table may still be used for some of the other uses in the table.

Table 1: Rocket propulsion materials and their primary uses in rocket propulsion systems

Material	LRE chamber wall	SRM/HRM motor case	SRM/HRM nozzle	Fluid storage tank	Remarks
Aluminium 7075 T6	X	X		X	
Aluminium 2019				X	Excellent low temperature properties
Al-Li				X	Excellent low temperature properties
D6AC steel		X			SRM/HRM motor case
AISI 302 steel				X	Good low temperature properties
AISI 4130 steel		X	X		
347 CRES	X	X			
Ti6Al4V (grade 5), STA	X	X	X	X	
Ni-200	X				LRE structural jacket
Haynes 25 or 188 (Ni-alloy)	X				Structural jacket and nozzle extension. Has good high temperature properties
Inconel X-750	X				
Inconel 600 (sheet or plate)	X				LRE nozzle extension
Inconel 718	X				
A-286 (Inconel)	X				LRE thrust chamber wall and nozzle extension
Columbium c103[2)], cold worked	X				Radiation cooled chambers
Copper	X				Heat sink material
Narloy Z (copper 96.5% alloy)	X				LRE chamber liner material only
GRCop 84 (copper alloy)	X				LRE chamber liner material only
Glass-epoxy		X	X	X	
Graphite-epoxy[1)]		X		X	
Kevlar 49- or Aramid-epoxy		X		X	
Silica-phenolic			X		Ablator
Graphite-phenolic[1)]			X		Ablator
Carbon/Carbon (C/C)			X		Insulation material
Carbon/Silicon Carbide (SiC)			X		Insulation material
Alumina or Silica	X				High temperature resistant coatings
Silica filled EPDM rubber		X	X		Insulation material

1) Epoxy and phenolic resins can be used. The difference is that phenolic resins are easier to handle and are less high temperature resistant. This makes phenolic resins the resin of use in ablating systems.
2) Columbium C103 is a Niobium alloy.
3) NI 200 is a pure Nickel. It is readily welded and will retain its properties at both sub-zero and elevated temperatures.
4) Inconel is a Nickel alloy

2. Material data at room temperature

In this section we present for specific materials the important material data at room temperature. We first start with several common materials as already indicated in Table . In later tables we will address some materials in more detail.

Table 2 presents data of common materials at room temperature. Note that data may depend on how the material is produced. For composite materials, the data depends on amount of resin and fibre direction. Hence data should be considered as indicative only. In the table also the specific strength is included. The higher this value is, the lighter the construction can be. Here we can see the great advantage of the epoxy and phenolic materials, which provide high strength at low mass density.

The table also provides melting temperature and maximum operating temperature. From the results presented, it should be clear that the melting temperature is not to be seen as the maximum operating temperature. It should also be realized that the maximum operating temperature is not a fixed value but depends on what the designer considers an acceptable degradation in terms of strength. Notice that for Inconel 718 also a minimum temperature is indicated. It follows that Inconel is also good at low temperatures, which is ideal when considering engines operating at cryogenic temperatures (this is especially important for engine start-up conditions).

Table 2: Data of specific materials used in rocket propulsion systems (all data taken at room temperature) [Specialmetals],[Kuhn],[UP],[Hightemp],[Aircraft materials],[Sulaiman], [Humble], [Fountainhead], [NASA SP 8115]

Material	Mass density	Ultimate Tensile Strength (UTS)	Yield Strength	Specific strength	Poisson ratio	Young's Modulus	Melting point	Max service temperature	Coefficient of thermal expansion	Heat capacity	Thermal conductivity
	[kg/m^3]	[N/mm^2]	[N/mm^2]	[MN-m/kg]	[-]	[GPa]	[K]	[K]	[mm/(m.K)]	[kJ/(kg.K)]	[W/(m.K)]
Aluminium 7075 T6	2810	570	505	0.20	0.33	72	750		25.2	0.9600	130.0
Aluminium 2019 T6	2840	420	295	0.15							
Aluminium 2019 T851	2840	455	350	0.16							
Aluminium 2019 T87	2840	475	395	0.17							
Al-Li 2195 T6/T83	2685	598/630	522/600	0.19	0.33	107a		<450			
D6AC steel	7780	1483	1379	0.19	0.32	200		<1180			
15CDV6 steel	7830	980	835	0.13							
15CDV6 steel (improved)	7830	1080	930	0.14							
AISI 302 steel, annealed strip	7860	620	275	0.08		193	1683	925	18.4	0.5000	16.2
AISI 302 steel, cold rolled	7860	1550		0.20		193	1683	925	18.4	0.5000	16.2
AISI 4130 steel, normalized @ 870 K	7850	670	435	0.09	0.30	205		<1140		0.4770	42.7
AISI 4130 steel, Heat treated	7850	1241	1243	0.16	0.30	205					
301 CRES stainless steel	8000	1207	931	0.15							
347 CRES stainless steel	7910	515	205	0.07		193			18.9	0.5000	21.4
Maraging C350 steel	8008	1140	827	0.14	0.3	200					
Ti6Al4V (grade 5), STA	4428	1225	1100	0.28	0.33	114	1933		9.7	0.5263	6.7
Haynes 188 (@ room temperature)	8980	946	464	0.11				<1000	11.5		10.8
Haynes 188 (@ 538 °C)	*8980*	*748*	*290*	*0.08*				*<1000*	*14.8*		*19.9*
Inconel X-750 (Ni-alloy)	8280	1250	850	0.15			1680		12.6	0.4310	12.0
Inconel 600 (sheet or plate)	8470	676	290	0.08		206		613	13.3		
Inconel 718	8190	1240	1036	0.15		211	>1533	73 to 825[1)]	13.0	0.4350	11.4
Ni-200	8890	462	148	0.05			1708				70.2
A-286 (Ni alloy)	7920	620	275	0.08	0.3	201	>1643	<700		0.42	15.1-23.9
Niobium (Columbium), cold worked	8600	550		0.06	0.38	130	2750	<1255	7.1	0.2600	0.54
Copper	8940	220	70	0.02		117	1356			0.39	390
Narloy Z (copper 96.5% alloy)	9130	117	90	0.01				<740	22.0		290
GRCop 84 (copper alloy)	8756	155	120	0.02				<1000	20.0		351
Glass epoxy or E-glass (fabric)	1900	1250	N.A.	0.60	0.20						
Graphite epoxy (fabric)	1530	965	N.A.	0.63	0.10						
Kevlar 49 (or Aramid) epoxy (p)[2,3)]	1350	1410	N.A.	1.04	0.20						
Kevlar 49 (or Aramid) epoxy (v)[2,3)]	1350	30	N.A.	0.02							
Carbon/Carbon	1600-1950	700	N.A.					2300-2400		2.093	1.5-37.4
Carbon-phenolic	1400-1500	110-140	N.A.	0.05	0.34			2850		1.507	1.0
Silica-phenolic	1700-1800	80-190	N.A.	0.24						1.256	0.55
Pyrolytic graphite	1600-2200						3900			0.712	1700 (p), 3.5 (v)

1) Operating range
2) p indicates properties are in plane, whereas v refers to properties perpendicular to the plane of the composite material
3) Aramid and Kevlar are often used interchangeably, but Kevlar is a specific brand name for a type of aramid fibre.

3. High temperature materials

In Table 3 specific properties are given of some refractory metals. This is a special class of metals that are extraordinarily resistant to heat and wear and are used for the design of amongst other radiative cooled rocket motors. The data has been taken from [Rembar], [Rowe] and [Fagan]. Non-metallic materials to resist high temperature include a range of ceramic matrix composites and Carbon/Carbon. Physical and mechanical properties of ceramic matrix composites (Alumina/Alumina, Carbon/Silicon Carbide and Silicon- SiliconCarbide) next to alumina are shown in Table 4 in part taken from Wikipedia.

Table 3: Typical properties of refractory metals [Rembar], [Rowe] and [Fagan]

		Molybdenum	Tungsten	Tantalum	Niobium
Mass	Density at 20° C gm/cc	10.2	19.3	16.6	8.58
Thermal Properties	Melting Point, °C	2610	3410	2996	2477
	Boiling Point, °C	5560	5900	6100	4744
	Linear Coefficient of Expansion per °C	4.9×10^{-6}	4.3×10^{-6}	6.5×10^{-6}	9.5×10^{-6}
	Thermal Conductivity at 20°C, W/(mK)	146	167	54	52
	Specific Heat at 20°C, J/(kg*K)	255	133	150	270
Electrical Properties	Conductivity, % IACS	30%	31%	13%	13%
	Resistivity, microohms-cm; 20°C	5.7	5.5	13.5	14.1
	Temperature Coefficient of Resistivity per °C	0.0046	0.0046	0.0038	
Mechanical Properties	Tensile Strength at room temperature, MPa	689-1378	689-3447	241-482	330-400
	Tensile Strength-500°C, MPa	241-448	517-1378	172-310	206-512
	Tensile Strength-1000°C, MPa	137-206	344-517	89-117	75-130
	Tensile Strength-1500°C, MPa	20-50	120-180	35-60	30-50
	Young's Modulus of Elasticity; GPa				
	Room Temperature	317	406	186	
	500°C	282	379	172	89
	1000°C	268	344	151	79
Spectral Emissivity		0.37 (1000°C)	0.45 (900°C)	0.46 (900°C)	
Working Temperature		1600°C	1700°C	Room	

Table 4: Properties of specific ceramic matrix composite (CMC) materials [Wikipedia]

Type of material	Al_2O_3/Al_2O_3	Al_2O_3	CVI-C/SiC	LPI-C/SiC	LSI-C/SiC	SiSiC
Density [g/cm^3]	2.1	3.9	2.1	1.9	1.9	3.1
Tensile strength [MPa]	65	250	310	250	190	200
Elongation (%)	0.12	0.1	0.75	0.5	0.35	0.05
Young's modulus [GPa]	50	400	95	65	60	395
Thermal conductivity (p) [W/(m*K)			15	11	21	>100
Thermal conductivity (v) [W/(m*K)			7	5	15	>100
Linear expansion (p) [10^{-6} 1/K]			1.3	1.2	0	4
Linear expansion (v) [10^{-6} 1/K]			3	4	3	4
Maximum use temperature [K]	1700	2000	1700		2300-2400	1400-1900

In the table, CVI, LPI, and LSI denote the manufacturing process of the C/SiC-material.

It is clear from the above two tables that suitable materials exist that allow for high temperature applications, where the CMC materials do allow for temperatures in range up to 1700 K. Note that Alumina itself is not considered a CMC material. Even though it allows for a higher temperature, its use is limited as it is quite brittle.

Typical materials in use for SRMs and HRMs, but sometimes also considered for LRE, include graphite, carbon-carbon and carbon-ceramic for areas that experience high heat flux (nozzle throat), and silica/graphite/carbon embedded in a phenolic resin for areas that experience moderate to low heat flux. All these materials can be used in case of extremely high temperatures, but one should consider the rate of ablation as it will change the nozzle shape and expansion ratio.

In the below figure some typical ablation rates are given for some early ablators, including glass-phenolic material (Phenol/Glas). From this figure, one can quickly figure out the required thickness of the material in relation to its location in the nozzle and the motor burn time.

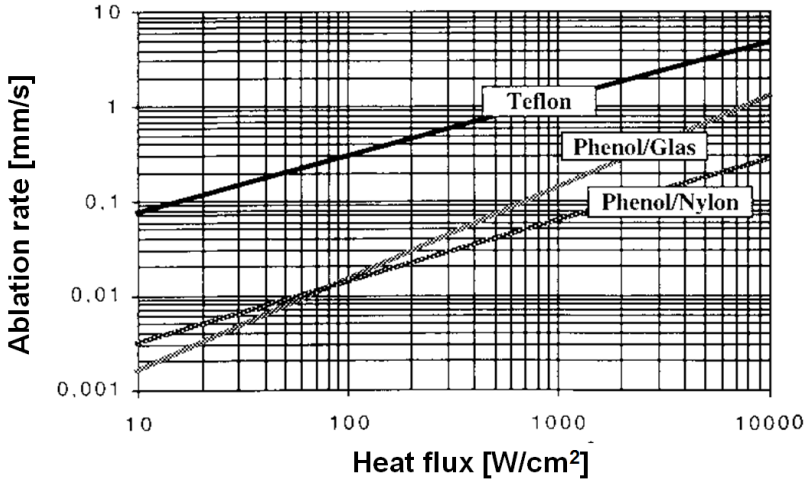

Figure 1: Ablation rate of some early ablators [Schmidt]

In a US study on nozzle ablation rates of silica-phenolic materials [Ross] test results are given for silica-phenolic SRM nozzle that shows, like in above figure, a (time-average) ablation rate that varies linearly with heat flux. It is mentioned an ablation rate of 0.0254 mm/s at a heat flux of ~1MW/m^2 increasing to 0.30 mm/s at a heat flux of ~2.5 MW/m^2. In a second study [Asaro] the ablative properties of different carbon fibre reinforced resins were tested at a heat flux of 5.5 MW/m^2. Results showed a linear erosion rate in range of 0.058 to 0.065 mm/s. A third study by Jiang et al. [Jiang] investigating ablation rates of T705 graphite, whole felt C/C composite, axial rod braided C/C composite, and carbon/ceramic composite in the nozzle throat region of a small HRM nozzle showed ablation rates of 0.045 mm/s, 0.022 mm/s, 0.03 mm/s, and 0.01 mm/s, respectively.

Table 5, and Table 6 provide some important properties of insulator and ablator materials used in solid and hybrid rocket motors.

Table 5: Properties of some ablator materials (properties depend on fibre content and orientation) [Humble]

Material	Density [kg/m^3]	Heat capacity [kJ/kg-K]	Thermal conductivity [W/m-K]	Maximum Temperature of use [K]	Ultimate tensile Strength [MPa]
Carbon phenolic	1400-1500	1.1	0.3-5.4	2500 ºC	110-140
Graphite phenolic	1350-1540	0.6 @ 300 ºC		2500 ºC	40-150
Silica phenolic	1700-1800	1.0	0.6-0.9	1700 ºC	80-190

Table 6: Properties of some insulator materials used in HRM and SRM [Sutton], [Humble]

		ATJ molded graphite	Pyrolytic graphite	Carbon-carbon
Density	kg/m^3	1539-1729	2187-2220	1716-1993
Thermal conductivity at room temperature	W/m/K	89.65-112.2	3.1-3.7	1.5-37.4
Specific heat	kJ/(kg.K)	-	-	2.1
Erosion rate (typical)	mm/s	0.1524-0.1016	0.0508-0.0254	0.0127-0.0254

All the values provided depend to some extent on the exact composition of the composite material and are to be verified when performing actual engineering.

4. Temperature dependency of material properties.

Most rocket motor or propulsion system structural materials typically function in a normal operating range around room temperature. However, some materials do have to operate at temperatures away from normal room temperature either because they serve at a higher operating temperature or serve as heat transfer material or must hold propellants at cryogenic temperatures. This change in temperature may affect the properties of the materials. Here we will mostly focus on the effect on the mechanical properties.

Most materials tend to weaken noticeable with increasing temperature. On the other hand, some materials show increasing strength at lower temperatures without becoming too brittle.

Figure 13 shows temperature dependence of Inconel 600. A maximum use temperature of about 900 K can be deduced from this table. At higher temperatures, the drop in both tensile and yield strength becomes dramatic.

Table 7: Inconel 600 Typical Elevated Temperature Tensile Properties (from: High Temperature Metals)

Temperature	Tensile Strength	0.2% Yield Strength	% Elongation
°C	MPa	MPa	
316	624	214	46
427	610	203	49
538	579	196	47
649	448	183	39
760	190	117	46
871	103	62	80
982	52	28	118

Next figure show temperature dependent properties of two Inconel alloys (A286 and INCONEL 718). A286 has amongst others been used as structural material for the Japanese LE-5 engine and INCONEL 718 has been used on the European Vulcain 2 engine (mainly for the manifolds and the injector elements) as well as the HM60 nozzle extension and the US SSME thrust chamber jacket.

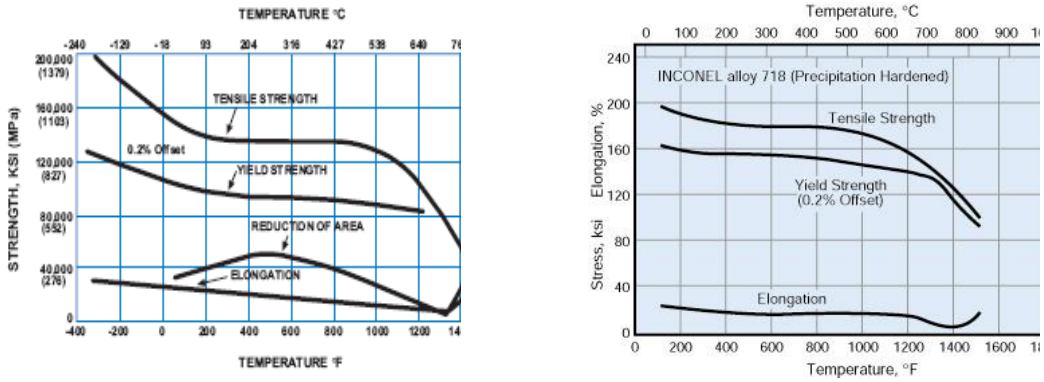

Figure 2: Temperature dependency of structural properties of two metals [Special metals]

Both materials show a maximum operation temperature in the range of 800 - 900 K, be it that Inconel 718 may allow for slightly higher temperature than A286.

Figure 3 shows the temperature dependent yield strength of three typical liner materials used in liquid cooled rocket motors. Narloy-Z is used as liner material in the space shuttle main engine and GRCop is considered for replacing this material. Yield strength is important as no deformation of the liner is allowed during operation. Figure shows that maximum operating temperature for the liner materials is about 740 K for Narloy Z and about 1000 K for GRCop.

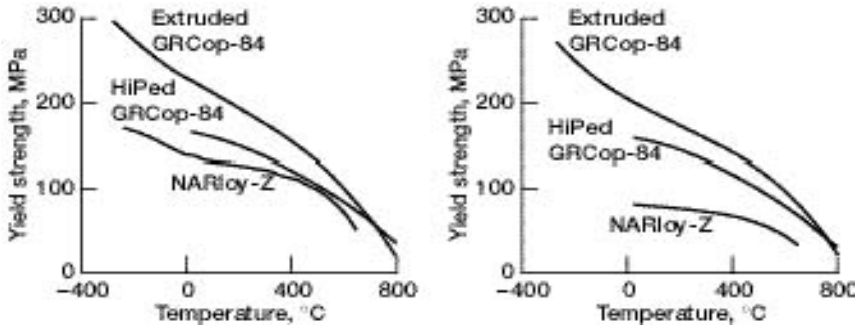

Before brazing

After brazing

Figure 3: Temperature dependency of typical LRE liner materials [NASA]

Figure not only shows dependency of properties on material but also show that brazing (a method of joining) also affects the properties.

It is noted that if a material is rapidly heated as in rocket motors, the strength may be less pronounced as is indicated in the above figures. This is e.g. illustrated in the figure below, taken from [NACA].

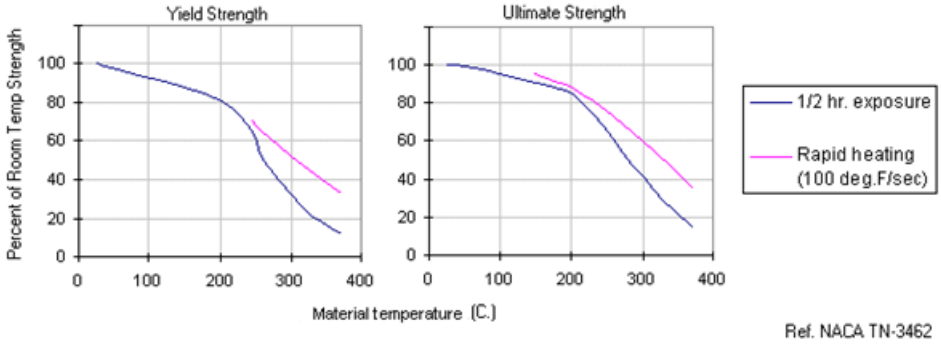

Figure 4: Effect of heating rate on material properties reduction.

With increasing temperature, most metallic materials reduce in strength. On the other hand, when lowering the temperature they increase in strength. This is shown for two materials used for the construction of cryogenic tanks in next table.

Table 8: Mechanical properties of Aluminium 2219 alloy and Aluminium-lithium alloy at low temperatures [Pietrobon]. Values depend on the specific temper applied.

Aluminium properties.

Alloy	Al 2219	AlLi 2195
Density (kg/m^3)	2840	2685
Specific Yield Strength at 20 K (m^2/s^2)	170240	226680
Specific Yield Strength at 80 K (m^2/s^2)	163000	219690
Specific Yield Strength at 25 C (m^2/s^2)	136700	194270
Yield Strength at 20 K (MPa)	483.5	608.6
Yield Strength at 80 K (MPa)	462.9	589.9
Yield Strength at 25 C (MPa)	388.2	521.6

Above materials not only increase in strength but also remain ductile and workable (weldable). Ultimate strength values can be obtained from [Simon]. Also, some alloy steels are suitable for use at low temperatures (down to about 77 K) including 300 series steel, and A201 and T-1 steel [David]. Nowadays also some composite materials are considered for use at low temperatures. Some fundamental information can be obtained from [Schutz].

References:

1) Aircraft materials, http://www.aircraftmaterials.com/data/alstst/15cdv6.html, retrieved 2 August 2018.
2) Asaro L., Manfredi L.B., and Rodriguez, E.S., Study of the ablative properties of phenolic/carbon composites modified with mesoporous silica particles, Journal of Composite Materials, 2018
3) David, E., Materials for cryogenic applications, in conference proceeding, 12th International Scientific Conference; Achievements in mechanical and materials engineering,
4) Schmidt G., Technik der flussigkeits-raketentriebwerke, DaimlerChrysler Aerospace, 1999.
5) Fagan, Ed Fagan Inc., Special purpose alloys, https://www.edfagan.com/refractory-metals-alloys-physical-mechanical-properties.php, retrieved August 2, 2018.
6) Fountainhead Alloys, http://fountainheadalloys.com/maraging-c-350/, retrieved December 19, 2019.
7) Ghosn L.J., and Raj S.V., Residual Stresses in Thermal Barrier Coatings for a Cu-8Cr-4Nb Substrate System, NASA TM-2002-211561, 2002.
8) Heimerl G., Tensile properties of 7075-T6 and 2024-T3 aluminum alloy sheet, NACA TN-3462, 1955.
9) Hightemp, High Temp Metals Technical Data, retrieved from http://www.hightempmetals.com/, retrieved August 2, 2018.
10) Humble R.W., Henry G.N., Larson W.J., Space propulsion analysis fundamentals, Space Technology Series, McGraw-Hill Publ. Comp., 1995.
11) Jiang X, Tian H., Tan G., Zhao S., Guobiao. C, Experiments of ablation characteristics for different nozzle materials and transient simulations on thermochemical erosion in hybrid rocket motors, Acta Astronautica Volume 212, November 2023, Pages 455-466.
12) Kuhl, Riccius and Haidn: Thermomechanical Analysis and Optimization of Cryogenic Liquid Rocket Engines
13) Simon N.J., Drexler E.S., Reed R.P. Review of cryogenic mechanical and thermal properties of Al-Li alloys and Alloy 2219, NIST, NISTIR 3971, 1991.
14) Solid rocket motor nozzles, NASA SP 8115, June 1975.
15) Pietrobon, S.S., Analysis of propellant tank masses, Small World Communications, Australia, July 2009.
16) REMBAR, Refractory metal technical data, https://www.rembar.com/resources/technical-data/, retrieved August 2, 2018.
17) Ross L.G. and Le Febvre C.A., Determination of the effects of liquid injectants on nozzle ablative performance, by United Technology Center 1050 E. NASA CR-72792/UTC-2359. December 31, 1970.
18) Rowe, D., Refractory metals, in Heat Treating Progress, November/December 2003.
19) Schutz, J.B., Properties of composite materials for cryogenic applications, January 1998, https://doi.org/10.1016/S0011-2275(97)00102-1
20) Special metals, retrieved from http://www.specialmetals.com/products/index.html
21) Sulaiman S., Yunus R., Ibrahim, N.A., Rezaiei, Effect of hardener on mechanical properties of carbon fibre reinforced phenolic resign composites, in Journal of Engineering Science and Technology, Vol. 3, No. 1 (2008) 79 – 86, 2008.
22) UP, United Performance Metals, https://www.upmet.com/, retrieved August 2,2018.
23) Wertz J.R. and Larson W.J., Space Mission Analysis and Design, 3rd ed., 1999.
24) Wikipedia, Ceramic matrix composite, https://en.wikipedia.org/wiki/Ceramic_matrix_composite, retrieved August 2, 2018.

This page is intentionally left blanc.

Annex L: Design of thin shell pressurized space structures

Contents

Contents 519

List of symbols 520

Acronyms 520

1 Introduction 521

2 Design philosophy 521

3 Internal pressure load 522

4 Stresses under uniform internal pressure loading 523

5 Hydrostatic pressure load 527

6 Temperature load 527

7 Cycle life (low cycle fatigue) 529

8 Stresses due to compressive loading 530

9 Combining loads 531

10 Other loads 531

11 Effect of safety factors 531

12 Wall thickness with respect to manufacturing 531

References 531

List of symbols

Roman

a	semi major axis length
b	semi-minor axis length
C	factor expressing the quality of a joint
E	Young's modulus
g	gravitational acceleration
H	height of fluid colon
j	safety factor
K	factor expressing effect of ratio of major to minor axis on stress in ellipsoid
M	bending moment
N	number of cycles
p	pressure
P	load
R	radius
t	thickness
T	temperature

Greek

ε	strain
γ	reduction factor used to correlate buckling theory to test results
ϕ	parametric parameter used in calculation of allowable buckling stress level
λ	coefficient of thermal expansion
ν	Poisson ratio
ρ	density
σ	ultimate stress

Subscripts

b	burst
h	hoop
i	initial
m	meridional
M	metal liner
p	propellant
t	tank
v	vapour

Acronyms

AL	Acceptance Load
COPV	Carbon fibre Over-wrapped Pressure Vessel
DL	Design Load
ID	IDentifier
FoS	Factor of Safety
LL	Limit Load
MEOP	Maximum Expected Operating Pressure
MoS	Margin of Safety
PV	Pressure Vessel
QL	Qualification Load
UL	Ultimate Load
YL	Yield Load

1 Introduction

The structural design of any rocket-based propulsion system must allow for sufficient load bearing capacity to prevent structural failure.

In this section we describe how to develop a preliminary structural design of various propulsion system components, like tanks, combustion chamber, motor case, nozzle, piping, and pumps, with space application in mind. We use as basic assumption that structurally these items can be considered as thin-walled pressure vessels for which the internal pressure (whether from gas pressure or liquid pressure) is the most important load. For this, we will treat each structural element as a thin shell[1] structure, i.e. a structure in which the stresses do not vary through the thickness. As typical structural elements we will only deal with geometrically simple elements for which analytical solutions are readily available from literature. Elements considered include spherical and cylindrical elements, but also flat, conical, toroidal and tori-spherical and ellipsoidal elements will be considered as these will provide for the means to also assess the head end of chambers, tanks, etc. Focus in this work is on developing understanding from simple relationships and not achieving highest accuracy. The latter requires a more in-depth treatment for which the reader is referred to the work of for instance [Sarafin et al] and [Wijker et al].

2 Design philosophy

A structure should be designed strong enough to withstand the loads exerted on it. The design philosophy as followed for spacecraft in [ECSS-E-30][2] is represented in Figure 5.

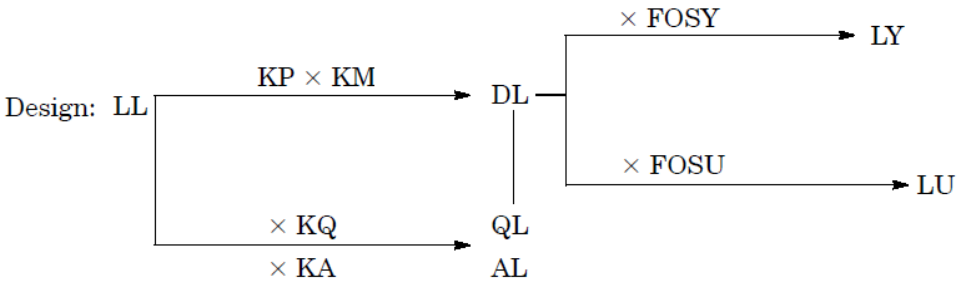

Figure 5: Design philosophy

Here:

- LL is Limit Load or worst-case flight load.
- DL is Design Load (currently also referred to as DLL): Load at which the structure must be testable. This load is key for obtaining a sufficiently reliable structure.
- KP and KM are factors that consider uncertainty in predictions and mass (of elements to be supported) during design. KP depends on development philosophy adopted like proto-flight or prototype approach.
- LY is Yield Load.
- LU is Ultimate Load.
- FOSY and FOSU are Factors of Safety selected such that acceptable risks result during testing of yielding or ultimate failure during test at DL;
- QL is Qualification Load.
- AL is Acceptance Load.
- KQ and KA are minimum load factors requested by the launch authorities to ensure the design can withstand launch loads safely (without failure).

[1] Thin shell theory can be applied in case shell thickness is limited to less than 10% of the radius of curvature of the shell. Also, there must be no discontinuities in the structure.

[2] This document has been superseded by ECSS-E-ST-32-10C Rev.2 Corrigendum 1, 1 August 2019. Changes are limited but nevertheless important. This is left for the reader to explore for him/herself.

For unmanned spacecraft and launch vehicles, the following values are commonly used for the various load factors here given assuming a uniform geometry[3]:

- KM 1.1 to 1.0
- KP 1.3 to 1.0
- FOSY 1.1 to 1.25
- FOSU 1.25 to 1.5
- KQ 1.25 for ARIANE family
- KA 1.1 for ARIANE family

Both KM and KP are generally defined at system level and can be reduced during the development. For man-rated spacecraft higher values may apply for FOSU.

Other documents containing information on safety factors used for aerospace applications are [FAA] and [NASA, 2008]. Notice that both FAA and NASA may use a different philosophy and or different values for the various load factors.

A part will have a proper margin of safety (MoS) if its actual design strength exceeds the strength required to withstand the ultimate load (UL). Here MoS is defined as:

$$\mathrm{MoS} = \frac{\text{Failure load}}{\text{Design load}} - 1 \tag{0-1}$$

A MoS more than 0 means a positive margin of safety.

3 Internal pressure load

When designing a pressure vessel subjected to a uniform internal pressure load, the following important definitions apply:

- *Design pressure*: Maximum Expected Operating Pressure (MEOP) considering "hot day firing", and manufacturing variability. MEOP is the pressure not normally expected to be exceeded (with a probability of 99.9% or better) during the operation of the pressure vessel. The design criterion is absence of permanent deformation of the casing under this operating condition, that is, the Yield Strength (YS) of the casing material is not exceeded.[4]
- A *Design Safety Factor* is specified with the value typically dependent on how conservative the design is chosen to be.
- *Design burst pressure* is the pressure at which the shell is likely to fail catastrophically.
- *Burst Safety Factor* is given as the ratio of the Burst pressure to the Design Pressure. Its value, like for the design safety factor, depends on the test option selected and on how conservative the design is chosen to be.
- *Number of pressure cycles* is the number of full pressure cycles the pressure vessel undergoes. This is important with respect to low cycle fatigue of the vessel. For instance, the Messenger spacecraft propellant tanks are qualification tested with a total of 16 proof (acceptance load) and 100 MEOP pressure cycles [Tam]. Also, small spacecraft thrusters undergo many cycles during their life. Typical number of pressure cycles in that case may easily be in the range 10,000 – 100,000 cycles. For the Space Shuttle reusable solid rocket motors, the initial number of pressure cycles was 3 including proof testing and motor pressurizations, which was later increased to include three proof cycles to all case hardware prior to use to prevent dimensional changes from subsequent pressure cycles [Moore].

[3] For discontinuities, joints, etc. higher safety factors may be required then here given.

[4] Note that for composite materials, there is no distinction between Ultimate Tensile Strength (UTS) and Yield Strength (YS) and hence this criterion will always be met as of the higher factor of safety on tensile strength. For metallic materials, this criterion shall be critically assessed.

4 Stresses under uniform internal pressure loading

In this section, we will discuss stresses occurring in various pressure vessel components based on internal uniform pressure loading only. This means that stresses due to bending, torsion loads etc. are not considered. Main purpose is to improve the understanding of how stresses and thickness of thin shell elements are related.

In case of a single wall structure the stress resulting from the internal pressure load can be assumed constant over the wall thickness. In that case wall thickness, t, can be determined using:

$$\sigma = \frac{P_{max}}{t} \tag{0-2}$$

With P_{max} is maximum load (in N/m) and σ is allowable material design stress.

If the shell is a pressure vessel with internal pressure, p, the hoop (circumferential) load, P_h, is [Sarafin]:

$$P_h = p \cdot R_h \cdot \left(2 - \frac{R_h}{R_m}\right) \tag{0-3}$$

Where R_h is hoop radius and R_m is meridional radius of curvature of vessel.

The longitudinal or meridional load (also referred to as axial load for cylindrical structures) follows from [Sarafin]:

$$P_m = \left(\frac{p \cdot R_h}{2}\right) \tag{0-4}$$

The stress resulting from the hoop load and the meridional load are referred to as hoop stress and meridional stress respectively.

The above relations form the basis for determining the thickness of the various pressure vessel components, see hereafter.

4.1 Maximum stress in various single wall pressure shell components

Typical pressure vessel components in propulsion systems include cylindrical, spherical, conical (nozzles), and ellipsoidal components as well as flat components (flat head ends of motors, tanks, etc.). For determining the thickness of these components, we will focus on highest stress only.

Sphere

For a sphere of radius R, it follows that hoop stress and meridional stress are identical and equal to:

$$\sigma = \frac{p \cdot R}{2t} \tag{0-5}$$

Cylinder

For a cylinder of cylindrical radius R ($R_m \rightarrow \infty$), it follows that hoop stress is twice the meridional stress.

$$\sigma = \frac{p \cdot R}{t} \tag{0-6}$$

Conical shell

In case of a conical shell, like e.g. the nozzle of a rocket motor:

$$\sigma = \frac{p \cdot R_{\perp}}{t} \tag{0-7}$$

With $R_{\perp}$ is radius of curvature in a direction perpendicular to the conical shell. This result compares well with that of the cylinder except that for the conical shell the stress varies with location along the cone. Highest stress occurs at the largest diameter.

Ellipsoid

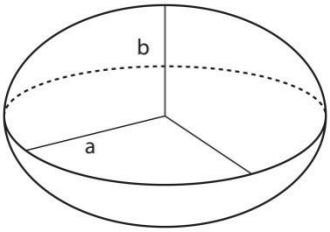

$$\sigma = \frac{p \cdot a \cdot K}{t} \tag{0-8}$$

$$K = \frac{1}{6}\left(2 + \left(\frac{a}{b}\right)^2\right) \tag{0-9}$$

Here 'a' is length of semi major axis and 'b' is length of semi minor axis. K is a factor that considers different ratio of a to b; In case a = b (representing a spheroid), it follows K = 0.5 and in case a = 2b, K = 1. It follows that in that case the stress is equal to the hoop stress in a cylinder of same radius.

Flat shell

For a flat plate of outer diameter D we obtain:

$$\sigma = C \cdot p \cdot \left(\frac{D}{t}\right)^2 \tag{0-10}$$

Here D is diameter, p is pressure, t is thickness and C is a coefficient that depends on how the flat plate is joined with the pressure vessel. For instance, C is 0.162 for an integral flat head or a flat head rigidly bolted (or riveted) on a shell flange or 0.35 for an integral forged head.

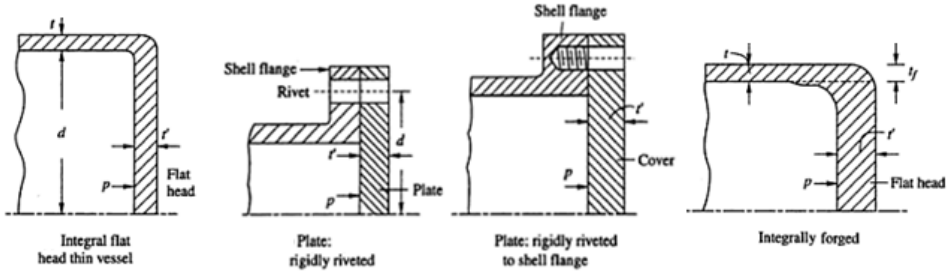

Figure 6: Different flat head designs

For fixed edge clamping C = 0.0884 [Roarke]. For flanged heads, one is referred to the literature, like ASME Boiler and Pressure Vessel Code.

Example 1:

Consider a carbon epoxy open cylinder of diameter 1 m. Internal pressure (MEOP) is 20 bar (absolute). Given is an ultimate strength of Carbon-epoxy of 1720 MPa. Neglecting load and

design factors, this gives a thickness of minimum 0.3 mm. Of course, when adding proper load and design factors, this thickness increases.

Example 2:
Consider the injection head of a Vulcain-like liquid hydrogen-oxygen cryogenic rocket engine of chamber diameter 0.415 m. Given is that the injection head is schematized to consist of three circular flat plates, see schematic.

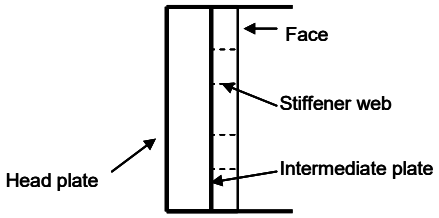

Figure: Injector schematic

Consider that critical pressure loading occurs at start-up, before combustion is established. For an engine inlet pressure of 150 bar (no difference considered between fuel and oxidizer) the pressure drop that should be withstood by each of the three plates is roughly 150 bar maximum. Taking Inconel 718 as the structural material with an ultimate tensile strength of 1300 MPa and considering that the upper most plate (head plate) is forged and the other two are clamped (no further supporting structures applied and neglecting effect of injector holes in the clamped plates). We obtain:

- Thickness forged plate: 26.3 mm
- Thickness clamped plates (each): 13.3 mm

4.2 Deformation from internal pressure load

A pressure vessel will grow both in longitudinal as well as in circumferential direction as of the Internal pressure loading. These deformations must be considered in designing the vessel shell as well as for the design of the support of the pressure vessel and the mounting of additional items, like insulation, etc. Below we will introduce relations for estimating the growth in size due to internal pressure loading based on [Nash].
Stress and strain of the cylindrical vessel are related by the general statement of Hooke's law:

$$\varepsilon_x = \frac{1}{E} \cdot \left(\sigma_x - \upsilon\left(\sigma_y + \sigma_z\right)\right) \tag{0-11}$$

Analogues for y and z direction

Nash shows that for a sphere the increase in radius is:

$$\Delta R = \frac{p \cdot R^2}{2E \cdot t} \cdot \left(1 - \upsilon\right) \tag{0-12}$$

For a cylinder closed at both ends by cover plates and subject to a uniform internal pressure p Nash shows that the increase in radius is governed by:

$$\Delta R = \frac{p \cdot R^2}{E \cdot t} \cdot \left(1 - \frac{\upsilon}{2}\right) \tag{0-13}$$

The increase in cylinder length is given by:

$$\Delta L = \frac{p \cdot R \cdot L}{2 \cdot E \cdot t} \cdot \left(1 - 2\upsilon\right) \tag{0-14}$$

In case of absence of endcaps, like in an open-ended stream tube or the divergent nozzle section, we have:

$$\Delta R = \frac{p \cdot R^2}{E \cdot t} \tag{0-15}$$

Example:
Consider a carbon epoxy open cylinder of diameter 1 m and thickness 1 mm. Internal pressure is 20 bar (absolute). Given a Young's modulus of the carbon epoxy of 142 GPa, it follows a growth in radius of about 3.5 mm.

4.3 Maximum stress in compound wall shell components

For some vessel components, nowadays use is made of a compound shell, i.e. a shell consisting of two or more layers of different materials. This is the case for e.g. carbon overwrapped tanks and nozzles, but also for the two-walled shell of regenerative or dump cooled liquid rocket engines.

Considering all layers independently under the same loading, it is to be expected that the layers will expand differently to the internal pressure. However, the two cylinders are obviously going to remain in contact. For instance, if the inner layer would grow more than the outer layer, the outer layer will induce an interfacial pressure on the inner layer limiting its growth. On the other hand, when the inner layer grows less, the outer layer starts pulling on the inner layer which compares with an increase in pressure over the inner layer which causes it to increase its radius.

For the inner layer we obtain:

$$\Delta R_i = \frac{(p - p_c) \cdot R_i^2}{E_i \cdot t_i} \tag{0-16}$$

And for the outer layer:

$$\Delta R_o = \frac{p_c \cdot R_o^2}{E_o \cdot t_o} \tag{0-17}$$

Here p_c is interfacial pressure or contact pressure and subscripts 'I' and 'o' refer to inner and outer layer, respectively.

Example:
Consider a carbon epoxy overwrapped open cylinder of internal diameter 1 m without any pressure load applied. We assume the following material properties:

- Carbon epoxy: E = 142 GPa
- Titanium liner: E = 114 GPa

Next, we consider the case with an applied internal pressure of 200 bars (absolute). This leads to a minimum thickness of the Carbon epoxy layer of about 3.0 mm. For reasons of safety, we select a safety factor of 2, which leads to a Carbon epoxy thickness of 6.0 mm. Liner thickness is selected as 1 mm (minimum thickness that can be manufactured).

Here the Carbon epoxy shell is assumed to carry the main pressure loading, whereas the titanium liner is to ensure leak tightness of the shell.

Growth of the Carbon epoxy shell independently is 7.0 mm. Growth of the liner independently is 43.9 mm. So, the carbon epoxy shell reduces the pressure load on the inner shell (the liner). We obtain for the liner using (0-16) and (0-17):

$$43.9\times10^{-3}\ \text{mm} - \frac{p_c \cdot 0.500^2}{114\times10^9 \cdot 1\times10^{-3}} = \frac{p_c \cdot 0.506^2}{142\times10^9 \cdot 6\times10^{-3}}$$

It follows an interfacial or contact pressure of 164 bar. So, the liner effectively reduces the internal pressure load of the outer wall with 32 bar.

The calculation of wall thickness in case of a composite wall is treated in more detail in [AGARD LS-150].

5 Hydrostatic pressure load

For the design of a propellant tank, the hydrostatic pressure exerted on the wall by the fluid may be an important load to consider, especially when the vehicle undergoes large accelerations. Consider a vertical positioned tank with spherical endcaps of radius R, filled with a propellant with density ρ to a height H. The weight of the system is supported by a ring-like support at the top and the bottom is unsupported; we find for the circumferential or hoop stress in the cylindrical part:

$$\sigma_c = \frac{\rho \cdot R}{t} \cdot (H - R) \tag{0-18}$$

The longitudinal stress is given by:

$$\sigma_l = \frac{\rho \cdot R}{2t} \cdot \left(H - \frac{R}{3}\right) \tag{0-19}$$

The maximum stress in the spherical endcap occurs in the apex (tip) of the bottom shell and is given by:

$$\sigma = \frac{\rho \cdot R \cdot H}{2t} \tag{0-20}$$

6 Temperature load

When dealing with rocket thrust chambers and/or cryogenic feed system components (tanks, pumps, feed pipes, and valves), one must consider that the working temperature can be very different from those during manufacture and that large temperature differences may exist between different parts or even over a single part. For illustration consider a cryogenic tank where internal insulation is applied on to the tank wall to prevent boil-off or external insulation to prevent aero-heating. Another example we can find in the design of a film-cooled rocket engine, where temperature differences of order 100 K may occur over the wall thickness. In case of a temperature difference differences in expansion may occur, which in turn may lead to significant stresses in the wall material. In case we are dealing with a wall consisting of a single layer, these stresses can be modelled using [Sarafin]:

$$\sigma = \frac{\lambda \cdot E \cdot \Delta T}{2 \cdot (1 - \upsilon)} \tag{0-21}$$

With:

- E = modulus of elasticity (Young's modulus)
- λ = coefficient of thermal expansion
- ΔT = temperature difference
- υ = Poisson ratio

For example, for an aluminium wall of a cryogenic tank with a temperature difference of 273 K, we obtain:

$$\sigma = \frac{22\times10^{-6} \cdot 72\times10^9 \cdot 273}{2 \cdot (1 - 0.3)} = 309\ \text{MPa}$$

Here we have taken the properties of aluminium 2219 as given in [SMAD, table 11-52].

In case of a large temperature difference, we may apply a separate layer to protect the structural material from the detrimental effects of a high or a low temperature. Consider e.g. the application of an insulating material on a cryogenic tank, or a thermal liner on the wall of an actively cooled rocket motor to conduct the heat to the coolant. This can severely limit the heat flow and hence also the temperature difference over the tank wall. This in turn reduces the stress in the tank wall.

However, when applying insulation materials, one must consider stresses resulting from differences in thermal expansion of dissimilar materials; see the earlier section on compound walls.

Example:
A thin steel cylindrical shaped combustion wall is equipped with an inner thermal insulating liner as shown in Figure 7. Initial temperature is 300K.

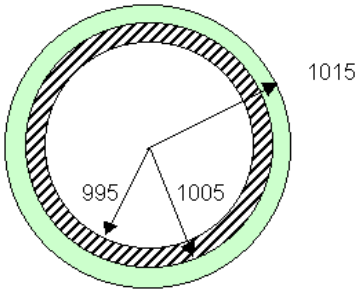

Due to combustion, the inner liner rises to a temperature of 800 K, whereas the steel is kept at an average (average over the wall) temperature of 300K. In case we take:

- Steel: E = 200 GPa
  $\lambda = 11.2 \times 10^{-6}$/K
- Liner: E = 90 GPa
  $\lambda = 15.5 \times 10^{-6}$/K

Both materials determine the stresses in the two shells due to the difference in thermal expansion of the two materials.

Figure 7: Cross-section of cylindrical tube with insulating liner on the inside

The simplest approach is to first consider the two shells independently from each other. Due to the temperature rise of the liner its circumference increases by an amount 2π x 1000 mm x 500 K x 15.5 x 10^{-6}/K = 49 mm. This compares with an increase in radius of 7.8 mm. Note that this is equivalent to the growth in liner radius that results from an internal pressure loading of 69.8 bar. The steel wall essentially does not expand as its temperature remains essentially equal to room temperature. Now combining the two layers, it follows that the inner wall exerts an internal pressure on the steel wall thereby increasing its radius, whereas the outer wall pressurizes the inner wall thereby limiting the growth in radius of the internal layer. It follows using (0-16) and (0-17):

$$7.8\times10^{-3}\ \text{mm} - \frac{p_c \cdot 1.000^2}{90\times10^9 \cdot 10\times10^{-3}} = \frac{p_c \cdot 1.010^2}{200\times10^9 \cdot 10\times10^{-3}}$$

This gives for the contact pressure a value of 48.1 bar. Applying now equation (0-6), we obtain:

Steel shell:

$$\sigma_m = \left(\frac{p\cdot R}{t}\right) = \left(\frac{48.1\times10^5 \cdot 1.010}{10\times10^{-3}}\right) = 485.9\ \text{MPa}$$

Liner:

$$\sigma_m = -\left(\frac{p\cdot R}{t}\right) = \left(\frac{48.1\times10^5 \cdot 1.000}{10\times10^{-3}}\right) = -481.0\ \text{MPa}$$

If, for example, the shell is subject to a uniform internal pressure the stresses from differential expansion would merely be added algebraically to the stresses found from the internal pressure loading, see also section on combined loads.

7 Cycle life (low cycle[5] fatigue)

A well-known phenomenon in the field of structural engineering is that repeated stressing of a material can cause failure, even when the applied stress is well below the yield stress. This is referred to as fatigue. Low cycle (thermal) fatigue is one of the most important causes of chamber/nozzle and fluid tank failing [NASA, 1975].

To be able to predict low cycle fatigue, we should have knowledge about the occurring stress levels or strain. Stress and strain are related by the general statement of Hooke's law. For the x direction:

$$\varepsilon_x = \frac{1}{E} \cdot \left(\sigma_x - \upsilon\left(\sigma_y + \sigma_z\right)\right) \tag{0-22}$$

Analogues relations apply for y and z direction.

[Nash] gives the following relation for the circumferential strain of a thin-walled spherical shell subject:

$$\varepsilon_c = \frac{1}{E} \cdot \left[\sigma_c - \mu \cdot \sigma_c\right] \tag{0-23}$$

The effect of cycling on strength can be determined from the Wőhler curve relating allowable stress (σ) levels to the number of cycles (N) or the Coffin-Manson relationship relating the range of strains that occur in a material and the number of cycles to failure:

$$\frac{\Delta\varepsilon}{2} = \frac{\sigma_f}{E} \cdot \left(2N_f\right)^b + \varepsilon_f \cdot \left(2N_f\right)^c \tag{0-24}$$

Where:

- $\Delta\varepsilon$ is strain range[6],
- N_f is the number of cycles to failure,
- E is Young's modulus,
- σ_f is fatigue strength coefficient,
- b is fatigue strength exponent,
- ε_f is fatigue ductility coefficient,
- c is fatigue ductility exponent (-0,5 – -0,7 for metals).

The first term in the coffin-Manson relationship represents elastic deformation effects and the second plastic deformation effects on cycle life. The various coefficient and exponents in the relation given must be obtained from material tests, see for instance the Figure 8 taken from [Hennessy].

To determine the cycle life, the strain range shall be calculated for the loads that are typical for the shell using the relation between strain and stress. Next, solving the Coffin-Manson relationship will provide the number of cycles. Typical strain-life data [Special Metals] for Inconel 600 indicate low-cycle fatigue strength of 1000 cycles at 1.25% strain (fully reversed[7]) and 10.000 cycles at 0.5% strain

[5] Low cycle fatigue generally is limited to less than 1000-10,000 cycles, although this boundary is not absolute.

[6] Strain range = algebraic difference between maximum and minimum strain over one cycle where tensile strains are considered positive and compressive strains negative. Strain amplitude is strain range divided by 2.

[7] Fully reversed cyclic loading means giving identical maximum tensile and compressive strain

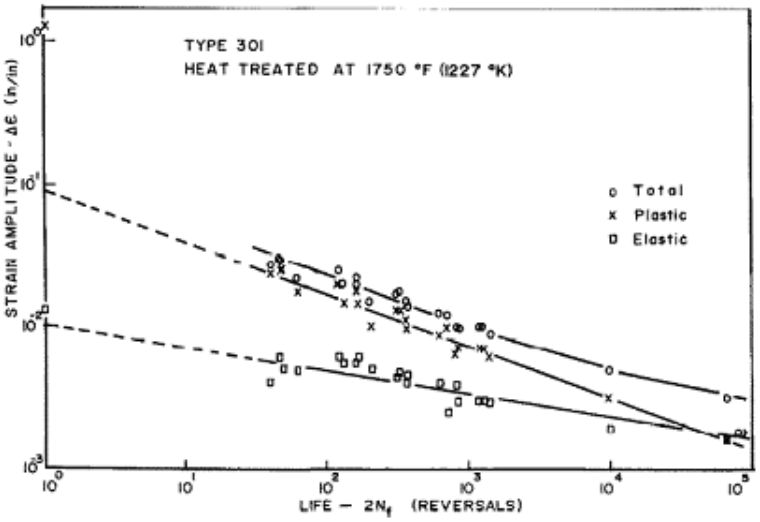

Figure 8: Strain life relations for type 301 stainless steel tested at 295 K.

In the early design stages simple structural analysis is used with appropriate safety factors to ensure sufficient strength under all conditions. In the later stages of the design Finite Element Analysis (FEA) and structural testing shall be used to verify the design.

At very low stress levels, below the endurance limit of a material, generally no fatigue will occur. This, however, may have considerable consequence for the mass of the structure, since the endurance limit typically can be as low as between 20-60% of the ultimate strength, depending on the material used and even then, an appreciable safety factor is needed to allow for stress concentrations.

Recently, one was considering the approach of measuring the occurring stress or strain, to allow for monitoring the remaining life of a structure [Zoun].

8 Stresses due to compressive loading

In case the shell is part of the structure of a launcher, it may also have to withstand large compressive loads e.g. during the acceleration of the launcher (i.e. inertia loads) or when the internal pressure is lower than the external pressure. Shells may buckle under such loading.

The equation for the theoretical cylinder buckling stress, σ_{cr}, is [Larson]:

$$\sigma_{cr} = \frac{\gamma \cdot E}{\sqrt{3 \cdot (1-\upsilon^2)}} \cdot \frac{t}{R} \tag{0-25}$$

Where R is cylinder radius, t is wall thickness and γ is a reduction factor used to correlate theory to test results and depends on a parametric parameter, ϕ, for cylinders:

$$\phi = \frac{1}{16} \cdot \sqrt{\frac{R}{t}} \quad \text{(for R/t < 1500 and L/R < 5)} \tag{0-26}$$

$$\gamma = 1 - 0.910 \cdot \left(1 - e^{-\phi}\right) \tag{0-27}$$

With L is length of shell. For conical shell structures, the reader is referred to [Wijker].

This theory allows for a quick assessment of the effects on buckling load but is quite idealized. In practice imperfections will exist in the structure that will reduce the load carrying capability.

9 Combining loads

We can quickly evaluate combined axial and bending loads on a thin wall cylinder using the equivalent axial load P_{eq} [Sarafin]:

$$P_{eq} = P \pm \frac{2M}{R} \tag{0-28}$$

Where M is bending moment and R is radius of cylinder.

Another option is by summing the stresses from the various individual loads. This is possible in case all stresses lead to loads normal to the surface. However, we should give care to whether we are dealing with tension or compression.

Inclusion of shear loads, and torsion loads in the present discussion is considered out of scope. For this, you are referred to general textbooks on the mechanics of structures.

10 Other loads

Important loads for the design of thin-walled pressure vessels are internal pressure loads and loads induced by differences in thermal expansion as well as loads induced by vehicle/launcher acceleration. For a truly proper design, also attention should be given to the effect of a number of other loads that might be acting on the structure. This is for example the case for an (integrated) propellant tank or a SRM motor casing, which also serves as the outer structural wall of the vehicle. In that case, it should not only withstand the pressure loads, but also loads induced by wind loading, thrust vector control forces, etc.

A more extensive overview on such other loads can be obtained from [ECSS-E-30].

11 Effect of safety factors

The thickness determined using the relations in the foregoing should be treated as a minimum required thickness. For instance, the relations given do not consider allowances needed for joining different elements through welding, riveting or bolting. Also, the relations do not allow for considering stress concentration near inlet and outlet ports or holes in the walls and for mounting attachments. For this we need to include an appropriate value for KP, see earlier. Next, we need to consider whether the structure is safeguarded against burst and or yield failure. Again, we refer to the earlier introduced design philosophy.

12 Wall thickness with respect to manufacturing

Minimum wall thickness depends on considerations regarding machinability, i.e. how well it can be forged, casted, welded, etc. For example, general material thickness guidelines for welding are: MIG with short-circuiting metal transfer is recommended for steels from about 6.35 mm thick down to about 0.51 mm. The pulsed arc method is appropriate for sheet down to 1.22 mm. In contrast, TIG can be used to weld sheet as thin as 0.13 mm.

In general, the following minimum wall thickness is used: 0.1-0.2 mm for stainless steel, 0.2 mm for aluminium and 0.5 mm for titanium. However, these values may reduce as from technology progress.

References

1. *AGARD LS-150,* Design methods in Solid Rocket Motors, AGARD, 1987.

2. *ECSS-E-30*, Space Engineering, Mechanical, Structure, Part 2A, April 2000.

3. *FAA*, "Guide to Verifying Safety-Critical Structures for Reusable Launch and Reentry Vehicles", Version 1.0, FAA, November 2005.

4. *Hennessy D., Steckel G. and Altstetter, C.,* Phase transformation of stainless-steel during fatigue, Metallurgical transactions, Volume 7A, March 1976, pp. 415-424.

5. Larson W.J., Wertz J.R., Space Mission Analysis and Design, 3rd edition, Kluwer Academic Publishers, 1999.

6. *Moore D.R., and Phelps, W.J.*, Reusable Solid Rocket Motor—Accomplishments, Lessons, and a Culture of Success, NASA NAS8-97238.

7. *NASA*, Structural Design and Test Factors of Safety for Spaceflight Hardware, NASA-STD-5001A, 2008.

8. *NASA*, Thrust chamber life prediction (NASA-CR-134806, 1975)

9. *Nash W.;* Strength of materials, Schaum's Outline series, McGraw-Hill, 1998.

10. Roark R.J., Formulas for stress and strain, New York, McGraw-Hill, 1989.

11. *Sarafin T.P., Doukas P.G., McCandless J.R. and Britton W.R.,* Structures and Mechanisms, Chapter in Space Mission Analysis and Design, 3rd ed., 1999.

12. *Patki A.V.,* Structural Reliability in Aerospace Design, ESA Journal 1988, Vol. 12, 1988.

13. *Tam W.H., Wiley S., Dommer K., Mosher L. and Persons D.,* Design and Manufacture of the MESSENGER Propellant Tank Assembly, AIAA 2002-4139, 2002.

14. *Wijker, J.J.,* Structures and mechanisms, chapter in Space Engineering and Technology II, Delft University of Technology, 2003.

15. Zoun R., Health monitoring of space systems, MSc. Thesis, TU-Delft, Faculty of Aerospace Engineering, Delft, March 24, 2003.

Annex M: Ariane 5 EAP238 solid rocket motor thickness estimation/verification

The Ariane 5 EAP238 (also known as P230) solid rocket motor has a steel case (steel D6AC steel [Uhrig]). Case length and diameter is 24.77 m and 3.05 m, respectively. Case thickness is reported as 8 mm, (see figure). Maximum expected operating pressure of the booster is 65 bar [Uhrig]. The booster carries a total propellant mass of 238 metric ton, and its empty mass is 31,000 kg[8] (31t).

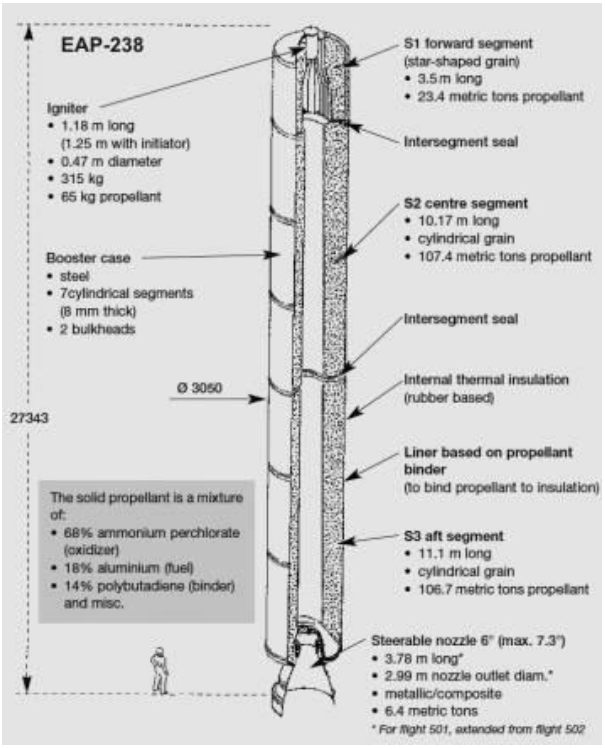

Figure M - 1: EAP238/P230 solid rocket motor [ESA], [CAPCOM]

For D6AC steel, the following properties can be found in open literature:

- UTS = 1480 MPa
- Mass density = 7850 kg/m^3
- Poisson ratio = 0.32
- Young's modulus = 200 GPa

Additionally, we select a Factor of Safety of 1.5 on ultimate strength, which gives an allowable stress of 1480/1.5 = 986.7 MPa.

Using the above material data, we can compute the thickness of the motor case using a thin-shell approximation.

We obtain:

$$t = \frac{p * R}{\sigma_{allowable}} = \frac{65E5\ Pa * 1.525\ m}{986.7\text{E}6\ \text{Pa}} = 10.05\ mm$$

The thickness of 10.05 mm that results is higher than the value of 8 mm as reported in figure. So, let's carefully explore what could explain this.

Option 1: Lower Safety Factor

Some typical values obtained from literature [ECSS] include:

Case	Safety Factor
Aerospace structure (primary load path)	1.25 – 1.5 (on UTS)
Aerospace pressure vessels (flight-tested, high-reliability materials)	As low as 1.25
Space systems in controlled failure mode (e.g. SRBs)	Possibly even lower locally

Let us determine the resulting factor of safety using the 8 mm wall thickness as a given while keeping UTS at 1480 MPa.

Using same formulas but now solving the occurring stress. Here, we again focus on Hoop stress as the determining stress:

$$\sigma_{\text{hoop}} = \frac{\text{p} \cdot \text{r}}{\text{t}} = \frac{(6.5 \times 10^6\ \text{Pa} \cdot 1.5250\ \text{m})}{0.008\ \text{m}} \approx 1.24 \times 10^9\ \text{Pa} = 1240\ \text{MPa}$$

[8] The motor dry mass (31t) is not to be confused with the booster dry mass (37t), as the latter also includes various other elements not considered to be part of the motor. These other elements include e.g. the nose section, booster attachments, and TVC controls.

Now:

$$FoS = \frac{UTS}{\sigma_{hoop}} = \frac{1480\ MPa}{1240\ MPa} = \sim 1.19$$

That's a safety factor of ~1.19 on hoop stress, slightly below 1.25 — and not unreasonable for a single-use structure like a solid rocket booster that is:

- Well-characterized
- Used with conservative testing
- Allowed to fail safely after burnout

Option 2: Higher-Strength D6AC Variant
D6AC is a very high-strength steel, but even stronger variants or heat treatments exist.

Variant/Treatment	UTS (MPa)
Standard D6AC	~1480
Peak-aged D6AC	1600–1800
D6AC with special heat treat	Up to 1900 MPa

Let's reverse-engineer what UTS would be needed for 8 mm wall and SF = 1.5:

$\sigma_{hoop} = (p \cdot r)/t = 1240$ MPa
UTS $= 1.5 \cdot \sigma_{hoop} = 1.5 \cdot 1240$ MPa = 1860MPa

So, to maintain SF = 1.5 with an 8 mm wall, you'd need a D6AC-type steel with UTS ≈ 1860 MPa. This is at the high end of what D6AC can achieve with specialized heat treatment, but it is not impossible.

Besides the above two factors, there may be still other factors. This we will leave for the reader to explore further upon.

Closure
The 8 mm reported in literature suggests at least that the structure is operating close to its material limits using high-strength D6AC and FoS of 1.2. This may be normal though for expendable launch vehicle components, like solid rocket boosters.

Based on the given thickness of the case (8 mm) and the case dimensions, we can estimate the case mass. Assuming flat heads with same thickness as the cylinder wall, it follows for the mass of the case:

$$M_{case} = \rho_{steel}\left(\pi * D_{case} * L_{case} * t_{case} + 2 * \frac{\pi}{4} * (D_{case})^2 * t_{case}\right)$$
$$= 7850\left(\pi * 3.05\ * 24.77\ * 8.0E-3 + 2 * \frac{\pi}{4} * (3.05)^2 * 8.0E-3\right)$$
$$M_{case} = 7850\ (1.899 + 0.117) = 15{,}825\ kg$$

Comparing this mass with a reported case mass of 19.1 ton, see Flugwerft Schleisheim, we find that there is a difference of a factor 1.2 between the estimated case mass and the reported case mass. This mass addition may be explained as of additional mass needed for:

- Actual heads are of an ellipsoidal design, which leads to a higher surface area and hence a higher mass.
- Intersegment structural rings[9].
- Load-bearing structures at the base (for thrust transfer), dome junctions, and top (nose) attachment.
- Bulkhead reinforcements, and weld beads.

[9] In [Uhrig], it is mentioned that changing from Clevis/Tang to welded connections of case segments will reduce the inert weight of the booster with 1900 kg.

To conclude we find that the reported case thickness of 8 mm is a value that can reasonably well explained from theory. A difficulty is in knowing the exact material data and FoS as used in the design.

References:

1. CAPCOM ESPACE website: http://www.capcomespace.net/dossiers/espace_europeen/ariane/ariane5/caracteristiques.htm, retrieved 2 May 2025.
2. ECSS, Space engineering: Structural design and verification of pressurized hardware, ECSS-E-ST-32-02C Rev.2 DIR1, 11 December 2024, retrieved from https://ecss.nl/wp-content/uploads/2024/12/ECSS-E-ST-32-02C_Rev.2-DIR(11December2024).pdf
3. Gonzalex-Blazquez A., Constanzo A., First Test Firing of an Ariane-5 Production Booster, ESA bulletin 104, November 2000.
4. Uhrig G., Boury D., Large Space Solid Rocket Motors in Europe – Past and Future Developments, SEP, SNECMA, France, AIAA-98-3980, 1998.